CORTICAL-SUBCORTICAL LOOPS IN SENSORY PROCESSING

EDITED BY: Max F. K. Happel, Livia de Hoz, Anita Luthi and Julio C. Hechavarría

PUBLISHED IN: Frontiers in Neural Circuits

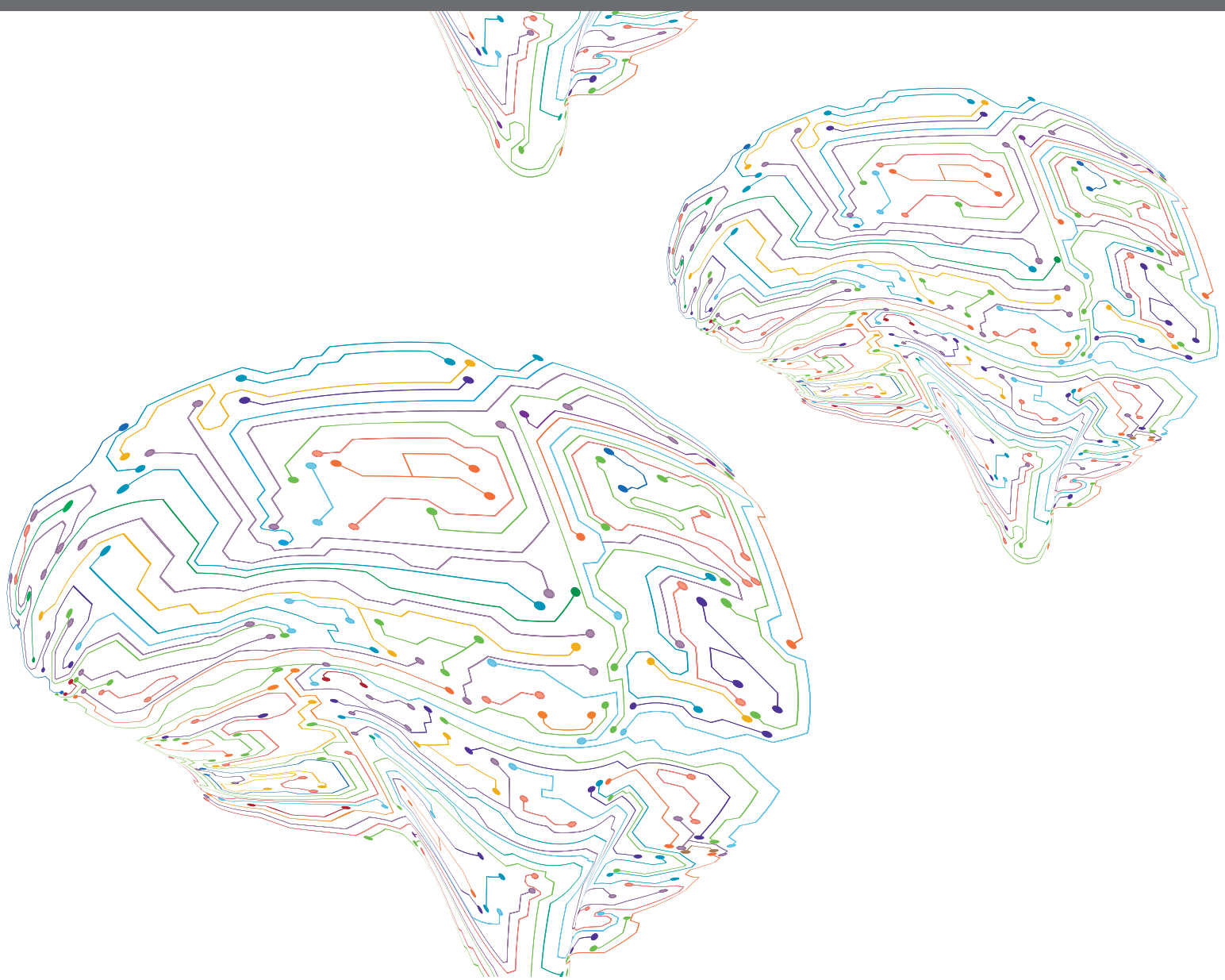

frontiers Research Topics

ISSN 1664-8714
ISBN 978-2-88974-585-2
DOI 10.3389/978-2-88974-585-2

About Frontiers

Frontiers is more than just an open-access publisher of scholarly articles: it is a pioneering approach to the world of academia, radically improving the way scholarly research is managed. The grand vision of Frontiers is a world where all people have an equal opportunity to seek, share and generate knowledge. Frontiers provides immediate and permanent online open access to all its publications, but this alone is not enough to realize our grand goals.

Frontiers Journal Series

The Frontiers Journal Series is a multi-tier and interdisciplinary set of open-access, online journals, promising a paradigm shift from the current review, selection and dissemination processes in academic publishing. All Frontiers journals are driven by researchers for researchers; therefore, they constitute a service to the scholarly community. At the same time, the Frontiers Journal Series operates on a revolutionary invention, the tiered publishing system, initially addressing specific communities of scholars, and gradually climbing up to broader public understanding, thus serving the interests of the lay society, too.

Dedication to Quality

Each Frontiers article is a landmark of the highest quality, thanks to genuinely collaborative interactions between authors and review editors, who include some of the world's best academicians. Research must be certified by peers before entering a stream of knowledge that may eventually reach the public - and shape society; therefore, Frontiers only applies the most rigorous and unbiased reviews.
Frontiers revolutionizes research publishing by freely delivering the most outstanding research, evaluated with no bias from both the academic and social point of view. By applying the most advanced information technologies, Frontiers is catapulting scholarly publishing into a new generation.

What are Frontiers Research Topics?

Frontiers Research Topics are very popular trademarks of the Frontiers Journals Series: they are collections of at least ten articles, all centered on a particular subject. With their unique mix of varied contributions from Original Research to Review Articles, Frontiers Research Topics unify the most influential researchers, the latest key findings and historical advances in a hot research area! Find out more on how to host your own Frontiers Research Topic or contribute to one as an author by contacting the Frontiers Editorial Office: frontiersin.org/about/contact

CORTICAL-SUBCORTICAL LOOPS IN SENSORY PROCESSING

Topic Editors:
Max F. K. Happel, Medical School Berlin, Germany
Livia de Hoz, Charité Universitätsmedizin Berlin, Germany
Anita Luthi, University of Lausanne, Switzerland
Julio C. Hechavarría, Goethe University Frankfurt, Germany

Citation: Happel, M. F. K., de Hoz, L., Luthi, A., Hechavarría, J. C., eds. (2022). Cortical-Subcortical Loops in Sensory Processing. Lausanne: Frontiers Media SA. doi: 10.3389/978-2-88974-585-2

Table of Contents

frontiers in Neural Circuits

EDITORIAL
published: 04 February 2022
doi: 10.3389/fncir.2022.851612

Editorial: Cortical-Subcortical Loops in Sensory Processing

Max F. K. Happel[1,2]*, *Julio C. Hechavarria*[3] *and Livia de Hoz*[4]

[1] *Medical Faculty, MSB Medical School Berlin, Berlin, Germany,* [2] *RG CortXplorer, Leibniz-Institute for Neurobiology, Magdeburg, Germany,* [3] *Institute for Cell Biology and Neuroscience, Goethe University, Frankfurt am Main, Germany,* [4] *Neuroscience Research Center, Charité Medical University, Berlin, Germany*

Keywords: corticothalamic, cortico-subcortical networks, sensory processing, behavior, neuronal loops, corticofugal, subcortico-cortical

Editorial on the Research Topic

Cortical-Subcortical Loops in Sensory Processing

Every organism faces a myriad of sensory stimuli, from which only a small subset is behaviorally relevant to each individual at a given moment. How do brains represent available sensory stimuli in spatiotemporal neuronal activity patterns on one hand, and on the other make the pivotal and immediate selection of information relevant for their individual behavioral responses? It is believed that the hierarchical organization of sensory pathways, from subcortical to cortical structures, allows reciprocal bottom-up and top-down processing of neuronal information *via* the presence of extensive feedback loops between their stations, to select and represent sensory stimuli during processes such as focused perception, attention, and learning (Carandini, 2012). How is this realized within and across different sensory modalities? What specific neural networks, cell-types and neuromodulatory systems play a role in information transmission and selection? In recent years, progress in systems neuroscience has been made, that has allowed us to begin answering some of these questions.

This Research Topic presents a collection of 15 articles that delineate current insights about the commonalities and differences in operational principles of subcortico-cortical loops across sensory modalities, different species, and basic and higher-cognitive functions and brain systems. The collection includes seven original research articles, seven reviews, and one opinion.

In her brief opinion article, Rocklands summarizes the multi-dimensionality of subtypes of corticothalamic neurons, the diversity of microcircuits within and across sensory and neuromodulatory systems, challenging the often-quoted idea of neuronal loops between two areas, or even two directly connected neurons lying significantly apart from each other.

In this line, Mease and Gonzalez aim to connect the predominant single-neuron view of cortico-thalamocortical connections into a broader framework of brain-wide network (dys)functions and their impact on cortical computation, like bursting, and synchronization of ensemble activity. They particularly discuss the interaction of circuits between first-order and higher-order thalamic and cortical regions with respect to function and dysfunction in pain, sensation and cognition.

In this line, Adeyelu et al. provide new evidence that the prevailing view of strictly unilateral thalamo-corticothalamic loops is incorrect. They used retrograde tracing and cre-lox mediated viral anterograde tracing strategies in insular cortex to reveal separate populations of ipsilateral and contralateral projecting corticothalamic layer 6 neurons. These populations also target topographically distinct thalamic subregions.

The topic of higher order thalamic nuclei is also covered by Castejon et al. Here, the authors investigated the function of the posterior medial (POm) nucleus of the thalamus in somatosensory processing. They found that POm is highly sensitive to bilateral multi-whisker

OPEN ACCESS

Edited and reviewed by:
Edward S. Ruthazer, McGill University, Canada

***Correspondence:**
Max F. K. Happel
mhappel@lin-magdeburg.de

Received: *10 January 2022*
Accepted: *11 January 2022*
Published: *04 February 2022*

Citation:
Happel MFK, Hechavarria JC and de Hoz L (2022) Editorial: Cortical-Subcortical Loops in Sensory Processing. Front. Neural Circuits 16:851612. doi: 10.3389/fncir.2022.851612

stimuli, a finding that challenges the notion of somatosensory thalamus computing only unilateral sensory information. The circuits involved in inter-hemispheric integration involve POm-POm loops formed by thalamocortical and corticothalamic interhemispheric projections. Using the same model but focusing on neuromodulation of feedback processing, Nersisyan et al. found both cholinergic and noradrenergic modulation of L6 projections to POm in rats with somewhat different consequences for repeated stimulation.

In the primary sensory pathways, the corticofugal feedback on subcortical nuclei forms direct cellular response properties of upstream sensory processing neurons. Qi et al. investigated the corticocollicular synaptic transmission from primary auditory cortex (A1) on neurons in the inferior colliculus (ICc). In a detailed study, they systematically mapped corticocollicular input in the ipsilateral ICc to be primarily excitatory and tonotopically mapped between corticocollicular neurons in AI and ICc neurons.

Feedback loops in the auditory system are one of the most studied loops in the brain. In this Research Topic, they are reviewed by Asilador and Llano, Tabas and von Kriegstein, and Antunes and Malmierca from different perspectives. Asilador and Llano provide a thorough review on feedback modulation and predictive coding in the auditory system of humans and animal models. They push forward the idea that corticofugal pathways contain the requisite circuitry to implement predictive coding mechanisms that facilitate the perception of complex sounds, and that different levels of top-down modulation, occurring at subcortical and cortical stages, complement one another. Tabas and von Kriegstein provide a more theoretical perspective on predictive coding. Focusing initially on auditory processing but including later evidence from other modalities across brain regions, they contrast the hypothesis that predictions are computed locally at each processing stage with the more favored hypothesis that predictions are computed globally at higher order stations and then conveyed through feedback projections to lower processing regions. The comprehensive review by Antunes and Malmierca discusses corticothalamic feedback pathways in auditory processing and other sensory modalities. They advance the idea that higher order thalamus could coordinate and contextualize hierarchical inference in cortical hierarchies *via* trans-thalamic pathways.

Loops in the auditory system are also the study topic of Jeschke et al. In this research article the authors developed a small cooling probe to manipulate corticofugal feedback in non-human primates and described changes in cortical and thalamic responses after cortical cooling. Cortical cooling altered spiking dynamics of cortical neurons (i.e., spontaneous activity, cortical spike width), and the temporal and spatial tuning of thalamic neurons.

The role of deep cortical projections in learning is explored by Paraouty and Mowery who found discrimination learning deficits in Mongolian gerbils upon chemogenetic inactivation of L5 auditory cortex projections to the striatum. They further showed that this plasticity is mediated by striatal local inhibition whose levels are tuned during early age, pointing to the likely calibration of subcortico-cortical loops' processing during early sensory experience.

Visual selection is ideal to study sensorimotor integration. A suited readout are eye movements, particularly microsaccades, which are generated by a network of cortical and subcortical neural circuits. Hafed et al. provide a framework on how microsaccades are influenced by peripheral visual cues and impact on visual representation in neurons of superior colliculus and the frontal eye field in primates. The emergent view from stimulation experiments, behavior and theoretical modelling is, that up to date, the visual-motor interactions in perception, attention, and visual acting must be explained by complex cortical and subcortical circuit interactions, which are not fully understood yet. Eye movement research, henceforth, provides an ideal testbed to further differentiate unaddressed reciprocal brain circuits and their impact on complex perceptual, cognitive, and behavioral readouts.

Feedback loops are not only important for information processing in the healthy brain but also mediate how the brain reacts in abnormal conditions, as reviewed by Ewall et al. The authors compiled cortical and subcortical mechanisms that can mediate plasticity upon loss of vision. They summarized potential cellular plasticity mechanisms involved in cross-modal recruitment and compensatory plasticity.

That cortico-subcortical loops exist also between architectonically more complex and diverse circuits than primary sensory circuits, is nicely documented in Lefevre et al., that reviews the reciprocal connectivity of oxytocin neurons in the hypothalamus on various cortical and subcortical structures constituting a brain-wide network to orchestrate social behaviors.

With this Research Topic we contribute to a better understanding of the diversity of these circuits. We should understand neuronal "loops" less as a direct bisynaptic connection between two neurons from different brain areas, but rather as a mutual influence of brain-wide networks, that allow to integrate multi-stranded information from basic sensation, attention, neuromodulation, and action-planning in order to guide adaptive behaviors (Steinmetz et al., 2021).

AUTHOR CONTRIBUTIONS

MH, JH, and LH prepared and discussed a list of guests-authors, invited them, revised their manuscripts, and handled their revisions. The Editorial was written by all authors. All authors contributed to the article and approved the submitted version.

REFERENCES

Carandini, M. (2012). From circuits to behavior: a bridge too far? *Nat. Neurosci.* 15, 507–509. doi: 10.1038/nn.3043

Steinmetz, N. A., Aydin, C., Lebedeva, A., Okun, M., Pachitariu, M., Bauza, M., et al. (2021). Neuropixels 2.0: a miniaturized high-density probe for stable, long-term brain recordings. *Science* 372:abf4588. doi: 10.1126/science.abf4588

Conflict of Interest: The authors declare that the research was conducted in the absence of any commercial or financial relationships that could be construed as a potential conflict of interest.

Publisher's Note: All claims expressed in this article are solely those of the authors and do not necessarily represent those of their affiliated organizations, or those of the publisher, the editors and the reviewers. Any product that may be evaluated in this article, or claim that may be made by its manufacturer, is not guaranteed or endorsed by the publisher.

frontiers in Neural Circuits

ORIGINAL RESEARCH
published: 26 October 2020
doi: 10.3389/fncir.2020.591986

Cortical Stimulation Induces Excitatory Postsynaptic Potentials of Inferior Colliculus Neurons in a Frequency-Specific Manner

*Jiyao Qi, Zizhen Zhang, Na He, Xiuping Liu, Caseng Zhang and Jun Yan**

Department of Physiology and Pharmacology, Hotchkiss Brain Institute, Cumming School of Medicine, University of Calgary, Calgary, AB, Canada

Corticofugal modulation of auditory responses in subcortical nuclei has been extensively studied whereas corticofugal synaptic transmission must still be characterized. This study examined postsynaptic potentials of the corticocollicular system, i.e., the projections from the primary auditory cortex (AI) to the central nucleus of the inferior colliculus (ICc) of the midbrain, in anesthetized C57 mice. We used focal electrical stimulation at the microampere level to activate the AI (ES_{AI}) and *in vivo* whole-cell current-clamp to record the membrane potentials of ICc neurons. Following the whole-cell patch-clamp recording of 88 ICc neurons, 42 ICc neurons showed ES_{AI}-evoked changes in the membrane potentials. We found that the ES_{AI} induced inhibitory postsynaptic potentials in 6 out of 42 ICc neurons but only when the stimulus current was 96 μA or higher. In the remaining 36 ICc neurons, excitatory postsynaptic potentials (EPSPs) were induced at a much lower stimulus current. The 36 ICc neurons exhibiting EPSPs were categorized into physiologically matched neurons (n = 12) when the characteristic frequencies of the stimulated AI and recorded ICc neurons were similar (≤1 kHz) and unmatched neurons (n = 24) when they were different (>1 kHz). Compared to unmatched neurons, matched neurons exhibited a significantly lower threshold of evoking noticeable EPSP, greater EPSP amplitude, and shorter EPSP latency. Our data allow us to propose that corticocollicular synaptic transmission is primarily excitatory and that synaptic efficacy is dependent on the relationship of the frequency tunings between AI and ICc neurons.

Keywords: auditory cortex, corticofugal system, postsynaptic potentials, inferior colliculus, mouse

OPEN ACCESS

Edited by:
Max F. K. Happel, Leibniz Institute for Neurobiology (LG), Germany

Reviewed by:
Miguel A. Merchán, University of Salamanca, Spain
Victoria M. Bajo Lorenzana, University of Oxford, United Kingdom

****Correspondence:***
Jun Yan
juyan@ucalgary.ca

Received: *05 August 2020*
Accepted: *24 September 2020*
Published: *26 October 2020*

Citation:
Qi J, Zhang Z, He N, Liu X, Zhang C and Yan J (2020) Cortical Stimulation Induces Excitatory Postsynaptic Potentials of Inferior Colliculus Neurons in a Frequency-Specific Manner. Front. Neural Circuits 14:591986. doi: 10.3389/fncir.2020.591986

INTRODUCTION

The auditory cortex sends large numbers of descending projections to most auditory nuclei in the thalamus, midbrain, and low brainstem (Weedman and Ryugo, 1996; Druga et al., 1997; Winer et al., 1998, 2001; Rouiller and Welker, 2000; Schofield and Coomes, 2005). These corticofugal projections comprise a feedback system that enables cortex-oriented modulation or control of the neural processing of incoming sound information (Syka and Popelár, 1984; Suga et al., 2000; Jen et al., 2002; Xiong et al., 2009; Bajo et al., 2010; Bajo and King, 2013; Terreros and Delano, 2015; Suga, 2020).

Following the pioneering work by Suga and his colleagues (Yan and Suga, 1996; Suga et al., 1997; Zhang et al., 1997), a surge of studies over the last quarter-century has established a highly specific corticofugal function. Specifically, cortical neurons implement differential modulation of the auditory responses of subcortical neurons depending on the functional relationship of cortical and subcortical neurons, facilitation when cortical and subcortical neurons have similar tunings, and suppression when they have different ones (Suga, 2020). This cortex-oriented modulation is seen across various domains i.e., frequency, amplitude, and time (Yan and Suga, 1996; Ma and Suga, 2001; Yan and Ehret, 2002; Zhou and Jen, 2007), various processing centers i.e., thalamus, midbrain, and cochlear nucleus (Zhang and Suga, 2000; Zhou and Jen, 2000; Luo et al., 2008; Liu et al., 2010) and various species i.e., bats, gerbils and mice (Zhang et al., 1997; Zhou and Jen, 2000; Sakai and Suga, 2002; Yan and Ehret, 2002). To date, little is known about the synaptic mechanism underlying the corticofugal system and its highly specific modulation.

Recognized as a convergence and/or integration center, the inferior colliculus (IC) of the midbrain is often chosen as the target for corticofugal studies (Druga et al., 1997; Zhang et al., 1997; Gao and Suga, 1998; Zhou and Jen, 2000, 2007; Yan and Ehret, 2002; Bajo and King, 2013). The direct projections from the primary auditory cortex (AI) to the central nucleus of the inferior colliculus (ICc) are tonotopically organized (Feliciano and Potashner, 1995; Saldaña et al., 1996; Bajo and Moore, 2005; Lim and Anderson, 2007; Markovitz et al., 2013), providing an anatomical basis of highly specific corticocollicular modulation, at least in the frequency domain. Physiological studies show that focal electrical stimulation of the AI (ES_{AI}) facilitates the responses of ICc neurons to the frequency that is tuned by the stimulated AI neurons, whereas it suppresses responses to the frequencies that are not tuned by the stimulated AI neurons (Zhang and Suga, 2000; Zhou and Jen, 2000; Yan and Ehret, 2002). Yet another consideration, inactivation of the entire auditory cortex with muscimol ($GABA_AR$ agonist) reduces the responses of ICc neurons to all frequencies in a non-specific manner (Zhang and Suga, 1997; Yan and Suga, 1999). This finding suggests that direct AI-to-ICc projections are likely excitatory in general, which allows tonic support of auditory responses in ICc neurons. A question raised here is which postsynaptic potential (PSP) can be induced by ES_{AI}: excitatory PSP (EPSP), inhibitory PSP (IPSP), or both. Another important issue is the possibility that ES_{AI}-evoked PSPs exhibit frequency specificity.

This study focusses on AI-to-ICc PSPs and examines the ES_{AI}-evoked changes in the membrane potentials of ICc neurons in anesthetized C57 mice. The membrane potentials of ICc neurons were recorded by whole-cell current-clamp. We found that the majority of ICc neurons exhibited EPSPs after ES_{AI}. ES_{AI} also induced IPSPs in a few ICc neurons, but only with the use of strong stimulus current. ES_{AI}-evoked EPSPs exhibited a lower threshold, shorter latency, and greater amplitude when the stimulated AI neurons and recorded ICc neurons had similar frequency tunings i.e., characteristic frequencies (CFs).

MATERIALS AND METHODS

Our study examined 46 female C57 mice aged 4–7 weeks and weighing 15–25 g. Animal use was following the Canadian Council on Animal Care, and our protocol (AC14–0215) was approved by the Animal Care Committee at the University of Calgary. A schematic diagram of our experimental approach is shown in **Figure 1A**.

Animal Preparations

Mice were anesthetized throughout the surgery and physiological experiments by intraperitoneal injection. We used a mixture of ketamine (85 mg/kg, Bimeda-MTC Animal Health Inc., Canada) and xylazine (15 mg/kg, Bimeda-MTC Animal Health Inc., Canada). Additional doses of ketamine and xylazine (17 and 3 mg/kg, respectively) were given to maintain anesthesia if the animals showed any response to tail pinching. A custom-made head holder was used to fix the mouse's head by clamping between the palate and nasal bones. The Bregma and lambda of the skull were aligned in the horizontal plane. The scalp, subcutaneous tissue, and muscle were then removed to expose the skull. Two holes measuring 2 mm in diameter were made with a dental drill to expose the left primary auditory cortex (AI, 2.2–3.6 mm posterior to the Bregma, 4.0–4.5 mm lateral to the midline) and the left central nucleus of the inferior colliculus (ICc, 0.5–2.0 mm posterior to the lambda, 0.5–2.0 mm left to the midline). The exposed dura was gently removed. A feedback-controlled heating pad was used to maintain the body temperature of the mouse at ∼37°C during surgery and all experiments. The electrophysiological studies were conducted in an echo-attenuated chamber with electromagnetic shielding and soundproofing.

Acoustic Stimulation

A 20 ms-long pure tone burst (5 ms for both rise- and fall-times) was used for acoustic stimulation. Tone bursts were digitally generated and converted to analog signals by an RZ6 MULTI I/O processor (Tucker-Davis Technologies, Inc., Gainesville, FL, USA). The analog signals were sent to a digital attenuator and then to a loudspeaker (MF1, Tucker-Davis Technologies., Gainesville, FL, USA) positioned at 45° and 15 cm away from the right ear of the mouse. The speaker output (tone amplitude) was calibrated at the same position using a condenser microphone (Model 2520, Larson-Davis Laboratories, USA) and a microphone preamplifier (Model 2200C, Larson-Davis Laboratories, USA). The tone amplitude was expressed as dB SPL (re. 20 μPa). Frequencies and amplitudes of tone bursts were changed manually or digitally *via* BrainWare data acquisition software (Tucker-Davis Technologies, Inc., Gainesville, FL, USA). A frequency-amplitude scan (FA-scan) was used to sample the receptive field (frequency tuning curve) of a recorded neuron. The frequency varied from 3 to 40 kHz with 1 kHz increments and the amplitude from 5 to 85 dB SPL with 5 dB increments. To sample a reliable frequency tuning curve of a

single ICc neuron, the FA-scan was repeated three times and the frequency/amplitude of tone for each FA-scan was randomly altered using BrainWare software.

Recording and Focal Electrical Stimulation of the AI

The responses of AI neurons were recorded using a tungsten electrode (∼2 MΩ impedance), which was placed perpendicularly to the surface of the left auditory cortex and connected to a recording system *via* a headstage (Tucker-Davis Technologies, Inc., Gainesville, FL, USA). During the electrode penetration, tone-evoked action potentials were commonly identified in layers III/IV of the cortex (approximately 300–600 μm below the brain surface). After 5–8 penetrations, the location of AI was identified according to the tone-evoked response properties. The frequency tuning curves of AI neurons were first sampled by using an FA-scan and stored using BrainWare software. The same electrode was then advanced to a depth of about 700–800 μm below the brain surface to layer V and its connection was switched from a recording system to a stimulating system. Since the AI is organized in columns, the CFs of the AI in layer V and layers III/IV are identical (Abeles and Goldstein, 1970; Shen et al., 1999; Moerel et al., 2018). An indifferent electrode was placed on the brain surface next to the stimulating electrode. Electrical pulses (0.2 ms long, negative, monophasic square wave), generated by a Grass S88 stimulator (Astro-Medical, Inc., West Warwick, RI, USA) and an A360 constant current isolator (WPI, Inc., Sarasota, FL, USA), were delivered to deep layers of the AI through the tungsten electrode (i.e., ES_{AI}).

Whole-Cell Patch-Clamp Recording in the ICc

Glass pipettes (Sutter Instrument, Novato, CA, USA) were pulled to construct a glass electrode with a tip diameter of ∼1 μm (7–12 MΩ in impedance) for patch-clamp recording. The electrodes were filled with an intracellular solution of 125 mM K-gluconate, 20 mM KCl, 10 mM Na_2 phosphocreatine, 4 mM MgATP, 0.3 mM Na_2GTP, 0.5 mM EGTA, and 10 mM HEPES (7.25 pH and 290 mOsm). A silver wire inserted into the electrode was connected to the MultiClamp 700B amplifier (Molecular Device, Sunnyvale, CA, USA) through a headstage. The bioelectrical signals from the electrode were filtered by a 4 kHz low-pass filter using a MultiClamp 700B amplifier and digitized using the DigiData1550 (Molecular Device, Sunnyvale, CA, USA) at a sampling rate of 10 kHz. They were recorded and stored using Clampex 10.4 data acquisition software (Molecular Device, Sunnyvale, CA, USA). BrainWare data acquisition software (Tucker-Davis Tech., Inc., Alachua, FL, USA) was also used to record these signals to tag the parameters of acoustic stimulation on to tone-evoked events.

For whole-cell patch-clamp recording, the interelectrode pressure of the glass pipette electrode was set at 200–300 mbar and the MultiClamp 700B was set to voltage-clamp mode. The electrode was first positioned perpendicularly in the left ICc at about 400 μm from the brain surface and then advanced 1 μm per step using a digital manipulator. During the stepped penetration, a positive square voltage pulse (amplitude of 10 mV and a duration of 10 ms) was continuously delivered to monitor the electrode tip impedance using the Clampex data acquisition software. Confirmation of the electrode tip contacting the membrane of a neuron was typically indicated by a sharp increase (∼20%) in tip impedance. Once contact was established, the interelectrode pressure was released. A successful seal of the electrode tip on the neuronal membrane as indicated by a giga-ohm tip impedance. A negative pressure (20–30 mbar) was then applied to break the cell membrane. When attaining whole-cell patch configuration, the whole-cell capacitance was compensated completely, and the series resistance (20–60 MΩ) was compensated by 50–80%. The MultiClamp 700B amplifier was then switched to the whole-cell current-clamp mode in which the electrode capacitance was neutralized, and the current holding was set to 0 pA mode (He et al., 2017).

Experimental Protocol and Data Acquisition

Once the tungsten electrode was positioned in the AI, the following procedures were performed. First, the responses of AI neurons to tones with various frequencies and amplitudes were recorded (FA-scan). This established the CF of AI neurons. Second, ICc neurons were patched. Third, resting membrane potentials of given ICc neurons were recorded. Fourth, changes in membrane potentials of given ICc neurons were recorded in response to the FA-scan and a repetitive tone at the CF (20 dB above the MT) and 50 ms intervals. The recording was allowed to continue when a neuron exhibited sharp tuning and no adaptation. Last, the membrane potentials of ICc neurons were recorded before and after the ES_{AI}. The stimulus current was set to 2^x μA. The value of x ranged from 1 to 10.

Data Processing and Statistics

The data acquired were processed and analyzed using a custom-made SoundCode program and a Clampfit 10.4 program (Molecular Device, Sunnyvale, FL, USA). The frequency tunings of AI and ICc neurons were measured using SoundCode software and the changes in membrane potential of ICc neurons in response to tone and ES_{AI} were measured using Clampfit software.

Based on the frequency tuning curves, the minimum threshold (MT) was defined as the lowest dB SPL that was able to induce noticeable responses to tone across various frequencies. The CF was the frequency at the MT. Based on the relationship between the CFs of the recorded ICc neurons and the stimulated AI neurons, the ICc neurons were sorted into two groups: physiologically matched and unmatched neurons. If the CFs of AI and ICc neurons were similar (≤1 kHz), the neurons were labeled matched neurons; if the CFs were >1 kHz, they were labeled unmatched neurons.

Stimulus-evoked events were determined by the change in the membrane potential that was 20% larger than the averaged fluctuation of the baseline. The EPSP was a positive-going wave and the IPSP was a negative-going wave. The EPSP waveforms of ICc neurons were characterized using amplitude, latency, 50% duration, and a rising slope. The amplitude of an EPSP waveform

was determined by the range between the baseline and the peak of the waveform. The latency was measured as the time from stimulus onset to the EPSP onset (the crossing point of the baseline to the upward slope line of the waveform). The 50% duration was the time when the membrane potential exceeded the 50% mark of the EPSP amplitude. The rising slope was defined as the EPSP amplitude divided by the time from the onset to the peak of a given EPSP waveform.

Data were expressed as means ± SD. The ANOVA test was used to compare the differences between groups of data, and a p-value of less than 0.05 was considered statistically significant.

RESULTS

Eighty-eight ICc neurons were successfully patched in 46 mice. The resting membrane potentials (RMPs) of these ICc neurons are shown in **Supplementary Table 1** and the CFs and MTs of sampled ICc neurons and corresponding AI neurons are shown in **Supplementary Table 2**. The CFs and MTs of these AI and ICc neurons fell within the central hearing range of C57 mice (Zhang et al., 2005; Heffner and Heffner, 2007; Luo et al., 2009). The ES_{AI} induced noticeable changes in membrane potential in 42 neurons as shown in **Figure 1B** (left and middle). The 40 neurons that had exhibited no membrane potential changes following the ES_{AI} up to 256 μA (**Figure 1B**, right). The RMPs of ICc neurons and frequency tunings (CFs and MTs) of both AI and ICc neurons were not significantly different between the "response" and "no response" groups (**Supplementary Tables 1, 2**). Two neurons experienced a loss of signal resulting in an interrupted recording. The data from the "no response" group as well as from the neurons with interrupted recordings were then excluded.

Out of 42 neurons showing changes in membrane potential, 36 ICc neurons exhibited depolarization (excitatory PSPs—EPSPs, **Figure 1B**, left), and six neurons exhibited hyperpolarization (inhibitory PSPs—IPSPs, **Figure 1B**, middle) following ES_{AI}. The frequency tunings between AI and ICc neurons were different based on these two samples. These samples (**Figure 1B**, left and middle) also show an important feature of EPSP/IPSP induction; the current for EPSP is far lower than that for IPSP. On average, the threshold current of the ES_{AI} for EPSP induction ranged from 6 to 64 μA (38.17 ± 17.90 μA, n = 36) while that for an IPSP ranged from 96 to 128 μA (106.67 ± 15.08 μA, n = 6). ES_{AI}-evoked IPSPs were not specific to the tuning relationship of AI and ICc neurons. These findings were different from the ES_{AI}-evoked EPSPs as presented below. Considering the small sample size of IPSP data, the discussion focuses mostly on ICc neurons exhibiting ES_{AI}-evoked EPSPs.

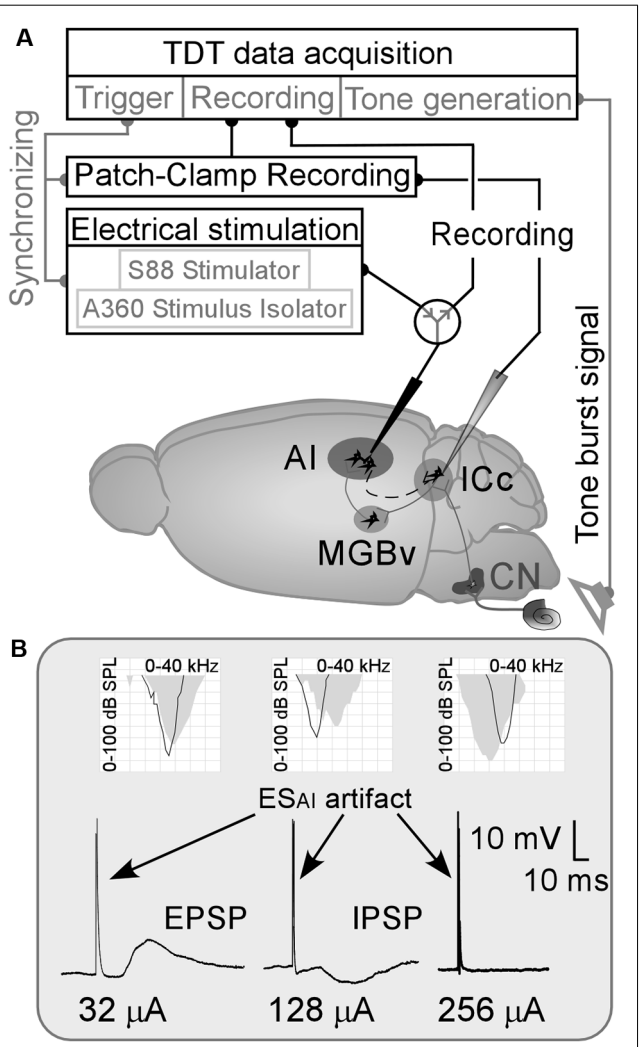

FIGURE 1 | (A) Schematic drawing of the experimental approach/mouse brain. AI, primary auditory cortex; CN, cochlear nucleus; ES_{AI}, focal electrical stimulation of the AI; ICc, central nucleus of the inferior colliculus; MGBv, ventral division of the medial geniculate body; ⓣ: a switch between recording system and stimulation system. **(B)** Examples of ES_{AI}-evoked changes in membrane potentials of ICc neurons and their frequency tunings (AI—gray areas and the ICc—black curves in the grid fields). EPSP and IPSP, excitatory and inhibitory postsynaptic potentials (PSPs).

Dynamic Range of ES_{AI}-Evoked EPSPs

The EPSP amplitudes of ICc neurons evoked by ES_{AI} were tested by a series of currents. As shown in **Figure 2A**, the ES_{AI} induced noticeable EPSPs in a neuron when the stimulus current was 8 μA or higher. EPSP amplitude gradually increased in response to increases in current. **Figure 2B** shows the EPSP amplitudes of ICc neurons as the function of ES_{AI} currents in a range from 4 to 128 μA. On average, the EPSP amplitude exhibited a sharper increase when the current of ES_{AI} ranged from 24 to 64 μA and rarely increased from 64 to 128 μA. **Figure 2C** shows the number of ICc neurons exhibiting EPSPs in responses to stimulus currents. Since the level of 64 μA evoked reliable EPSPs in all 36 ICc neurons, we used this data to characterize the ES_{AI}-evoked EPSPs.

Characterization of ES_{AI}-Evoked EPSPs of ICc Neurons

The amplitude, latency, rising slope, and 50% duration were measured for the ES_{AI}-evoked EPSPs of ICc neurons; the amplitude appeared to correlate with the latency, rising slope, and 50% duration. For example, a larger amplitude was associated with shorter latency, longer duration, and a

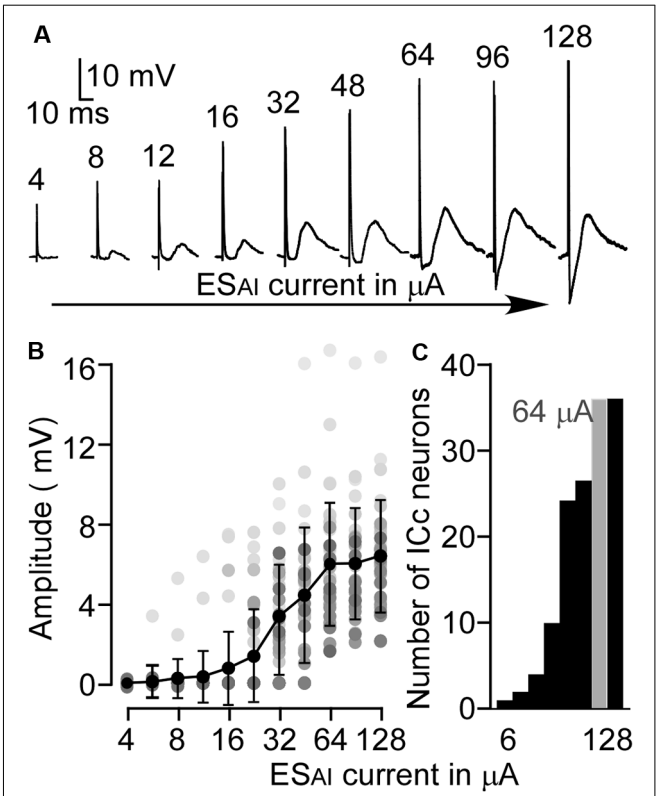

FIGURE 2 | The amplitude-to-intensity function of ES_{AI}-evoked EPSPs. **(A)** An example of the ES_{AI}-evoked EPSPs of an ICc neuron following ES_{AI} at a series of current levels. **(B)** Summarized amplitude-to-intensity function of ES_{AI}-evoked EPSPs (n = 36). Gray dots represent the sample distributions at different stimulus levels. **(C)** Histogram of the number of neurons showing EPSP in response to ES_{AI}. In this study, 64 μA (gray) was the lowest, optimal level because it enabled noticeable EPSP in all 36 ICc neurons.

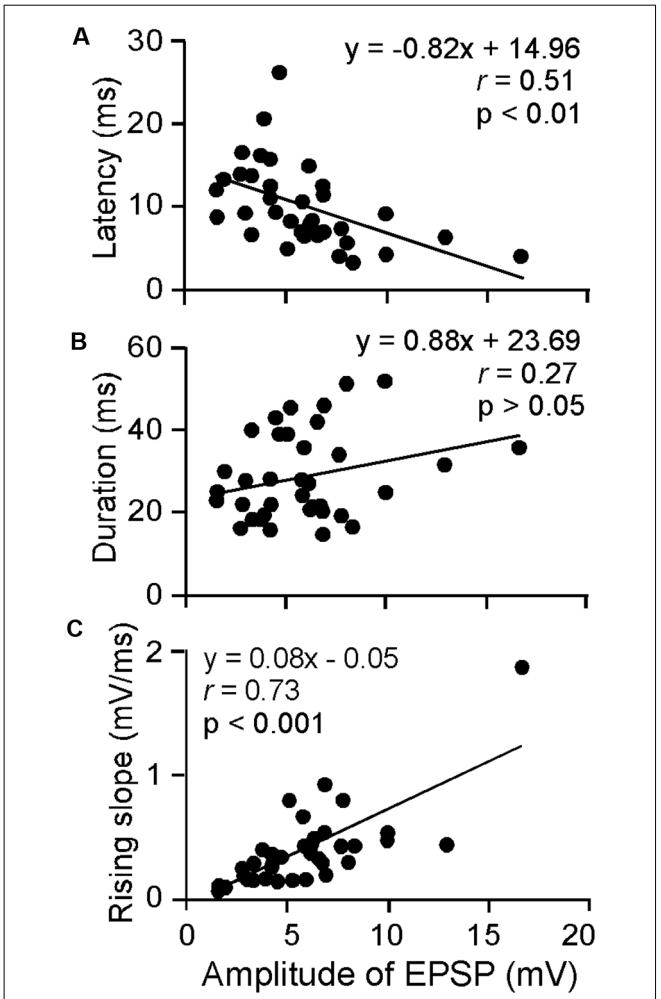

FIGURE 3 | Scatter plotting of latency **(A)**, 50% duration **(B)** and rising slope **(C)** as the function amplitude of ES_{AI}-evoked EPSPs of ICc neurons. At the 64 μA stimulation level, the latency and rising slope were significantly correlated to amplitude whereas duration was insignificant. The solid lines represent the regression.

larger rising slope. As shown in **Figure 3**, the latency and rising slope were significantly correlated to the amplitude ($r = -0.51$, $p < 0.01$, **Figure 3A** and $r = 0.73$, $p < 0.001$, **Figure 3C**). However, the 50% duration was poorly correlated to the amplitude ($r = 0.27$, $p > 0.05$, **Figure 3B**). At the level of 64 μA, the EPSP amplitude ranged from 1.59 to 16.66 mV (5.91 ± 3.05 mV, n = 36). The latency ranged from 3.30 to 26.30 ms (10.14 ± 4.92 ms, n = 36). The 50% duration ranged from 14.80 to 51.80 ms (28.92 ± 10.44 ms, n = 36). The rising slope ranged from 0.07 to 1.87 mV/ms (0.40 ± 0.32 mV/ms, n = 36).

ES_{AI}-Evoked EPSP vs. Frequency Tunings

As described above, ICc EPSPs evoked by ES_{AI} at the 64 μA level showed obvious variation from neuron to neuron. Previous studies using extracellular recording consistently demonstrate frequency-specific corticofugal modulation of the auditory responses of ICc neurons (Yan and Suga, 1998; Zhang and Suga, 2000; Jen et al., 2002; Yan and Ehret, 2002). ES_{AI} induces the facilitation of tone-evoked auditory responses when the difference in frequency tunings (CFs) between stimulated AI neurons and recorded ICc neurons is equal to or smaller than 1 kHz (physiologically matched neuron). Suppression is induced when the CF difference of stimulated AI neurons and recorded ICc neurons is larger than 1 kHz (physiologically unmatched neuron). We next analyzed if and how ES_{AI}-evoked EPSPs were associated with the frequency tunings (CFs) of AI and ICc neurons.

To be consistent with previous studies (Yan and Ehret, 2002; Wu and Yan, 2007; Luo et al., 2008; Liu et al., 2015), we sorted ICc neurons into two groups: a matched group when the CF difference between the recorded ICc neurons and stimulated AI neurons was 1 kHz or less (**Figure 4A**) and an unmatched group when the CF difference was larger than 1 kHz. Three examples are shown in **Figure 4A**. The ICc neuron in **Figure 4A** was tuned to 15 kHz and its corresponding AI neuron tuned to 21 kHz; the ICc CF was 6 kHz lower than AI CF. The ICc neuron in **Figure 4A** tuned to 22 kHz and its corresponding AI neuron tuned to 18 kHz; the ICc CF was 4 kHz higher than AI CF. These two neurons were sorted as physiologically unmatched neurons.

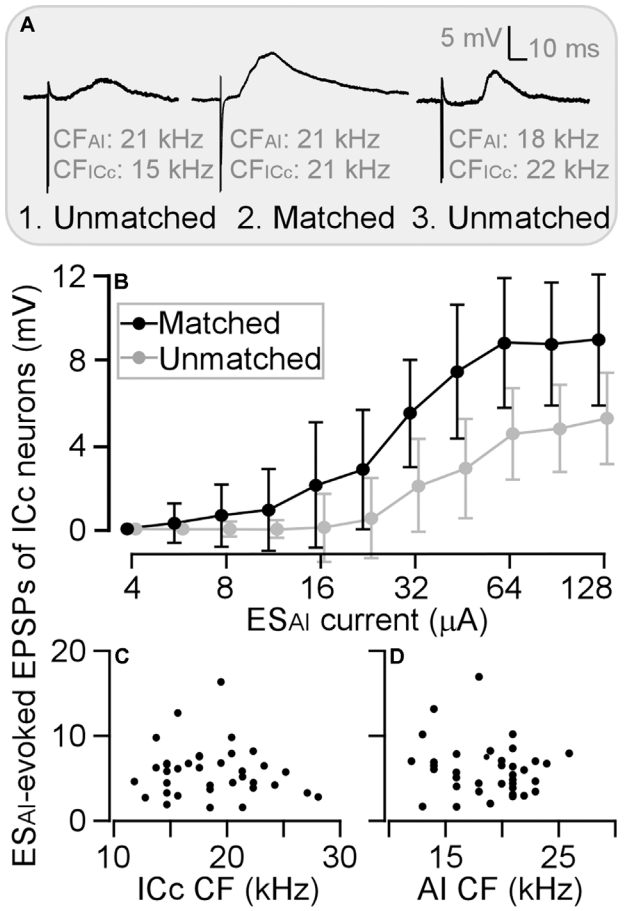

FIGURE 4 | Differences in the amplitude of ES_{AI}-evoked EPSPs between matched and unmatched ICc neurons. Three examples show greater EPSP of matched neurons compared with those of unmatched neurons at the stimulation level of 64 μA **(A)**. This difference is also shown by amplitude-to-intensity function **(B)**. However, the ES_{AI}-evoked EPSPs exhibit no relation to CFs of ICc neurons **(C)** or AI neurons **(D)**. AI, primary auditory cortex; CF, characteristic frequency; EPSP, excitatory postsynaptic potential; ES_{AI}, focal electrical stimulation of the AI; ICc, central nucleus of the inferior colliculus.

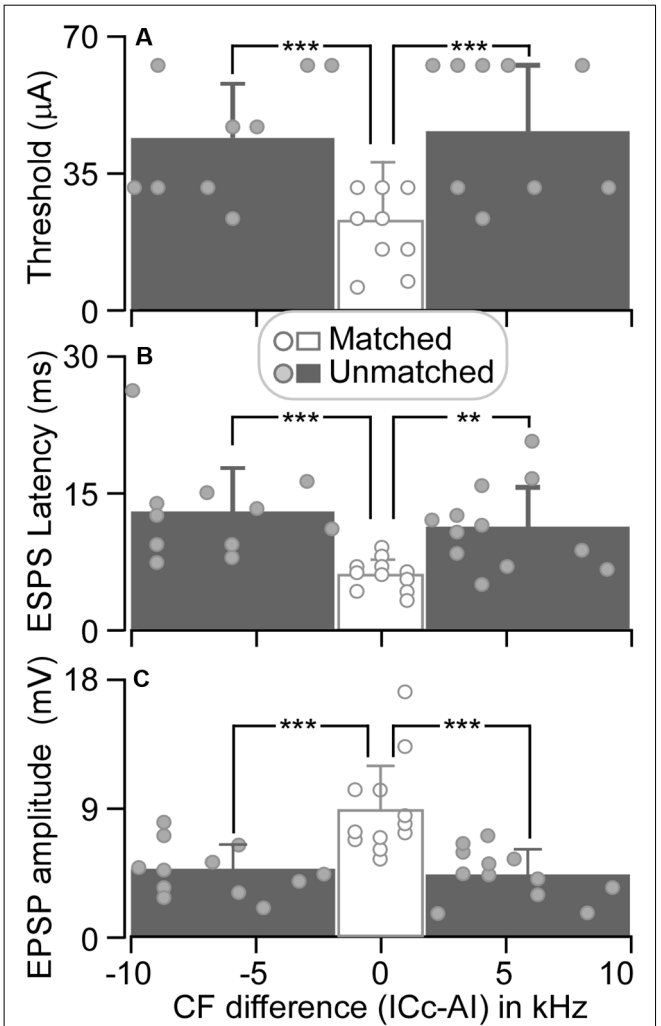

FIGURE 5 | The threshold induced EPSP **(A)**, EPSP latency **(B)**, and amplitude **(C)** are plotted as the function of CF difference between ICc and AI neurons. Histograms show the averaged values of ICc neurons that had similar CFs to (middle), lower than (left), and higher than (right) those of AI neurons. $^{**}p < 0.005$; $^{***}p < 0.001$.

In contrast, the CF of a neuron in **Figure 4A** was 21 kHz, identical to that of the corresponding AI neuron. This neuron was therefore sorted as a physiologically matched neuron. The EPSP amplitude of these ICc neurons exemplifies the efficacy of ES_{AI}. The ES_{AI}-evoked EPSP was greater in matched ICc neurons than in unmatched neurons. Examining the EPSP amplitude as the function of ES_{AI} current demonstrated that the matched neurons (n = 12) had a steeper slope than unmatched neurons (n = 24); ES_{AI} evoked larger EPSPs of ICc neurons at all current levels (**Figure 4B**). Similar to previous findings, ES_{AI}-evoked EPSPs were only associated with the CF difference between the recorded ICc and stimulated AI neurons; no correlation was observed between the ES_{AI}-evoked EPSPs and the CFs of either the recorded ICc (**Figure 4C**) or stimulated AI neurons (**Figure 4D**).

As illustrated in **Figure 4B**, ES_{AI}-evoked EPSPs were larger in matched than unmatched ICc neurons at all tested stimulus intensities. We further compared the threshold currents of evoking EPSPs induction, 64-μA-level EPSP latency, and 64-μA-level EPSP amplitude between matched and unmatched ICc neurons.

The threshold of matched ICc neurons ranged from 6 to 32 μA, with an average of 23.17 ± 9.22 μA (n = 12). For unmatched ICc neurons, the threshold ranged from 24 to 64 μA (44.67 ± 15.13 μA, n = 12) when AI CFs were higher than ICc CFs and from 24 to 64 μA (46.67 ± 17.54 μA, n = 12) when AI CFs were lower than ICc CFs (**Figure 5A**). The ES_{AI} threshold current in matched neurons was significantly lower than the threshold current in unmatched neurons, i.e., ICc CF < AI CF ($p < 0.001$) and ICc CF > AI CF ($p < 0.001$).

At a stimulus level of 64 μA, the latency and amplitude of ES_{AI}-evoked EPSPs of ICc matched neurons exhibited larger variation, whereas the latency and amplitude were different between matched and unmatched neurons (circles in **Figures 5B,C**). The EPSP latencies of matched neurons were shorter than those of unmatched neurons. On average, the latency of matched neurons was 6.03 ± 1.72 ms (n = 12). The latency of matched neurons was significantly shorter than 13.05 ± 4.83 ms (CF: ICc < AI, n = 12, $p < 0.001$) and 11.33 ± 4.41 ms (CF: ICc > AI, n = 12, $p < 0.005$) of unmatched neurons (columns in **Figure 5B**). Similarly, the EPSP amplitudes of matched neurons were different from those of unmatched neurons. The EPSP amplitude of matched neurons was 8.77 ± 3.12 mV (n = 12). This result was significantly greater than 4.62 ± 1.72 mV (CF: ICc < AI, n = 12, $p < 0.001$) and 4.33 ± 1.68 mV (CF: ICc > AI, n = 12, $p < 0.001$) of unmatched neurons (columns in **Figure 5C**).

DISCUSSION

The auditory cortex modulates the subcortical responses to sound stimulation in a frequency-specific manner (Zhang et al., 1997; Yan and Suga, 1998; Yan and Ehret, 2002; Zhou and Jen, 2007). As for the synaptic mechanism of such specific corticofugal modulation, this study substantiates three fundamental characteristics in the AI-to-ICc pathway, i.e., ES_{AI}-evoked PSPs of ICc neurons. First, AI-to-ICc synaptic transmission is primarily excitatory since the majority of ICc neurons exhibited EPSPs following ES_{AI} (**Figure 2**). Second, the inhibitory synaptic transmission may be involved in corticofugal modulation although the ES_{AI}-evoked IPSPs were limited to only a few ICc neurons and required a much larger stimulus intensity (high threshold, **Figure 1B**). Finally, corticofugal synaptic transmission appears to occur in a frequency-specific manner as the ES_{AI}-evoked EPSPs were significantly different between matched and unmatched ICc neurons (**Figures 4A,B**, **5**).

Corticofugal Excitation

The primary EPSP of the AI-to-ICc pathway is consistent with previous findings in several lines of study. Biochemical and immunochemical studies demonstrate that the neurotransmitter of corticocollicular synapses is glutamate (Feliciano and Potashner, 1995; Ito and Oliver, 2010). The *N*-methyl-D-aspartate receptor (NMDAR) and the metabotropic glutamate receptor (mGluR) that mediate corticofugal excitatory transmission have been demonstrated in different sensory systems and different species including rats (Malmierca and Nuñez, 2004), guinea pigs (McCormick and von Krosigk, 1992), cats (Scharfman et al., 1990; Rivadulla et al., 2002), and monkeys (Montero and Wenthold, 1989). Physiological studies show that the inactivation of the entire auditory cortex reduces the auditory responses of ICc neurons, suggesting excitatory effects in general (Zhang and Suga, 1997; Yan and Suga, 1999).

Previous findings, together with our data, allow us to glean an understanding of direct corticofugal pathways. Cortical neurons send direct glutamatergic projections to subcortical (i.e., ICc) neurons. When cortical neurons are active, corticofugal terminals release glutamate that acts on the postsynaptic NMDAR and mGluR, leading to postsynaptic depolarization and modulating the excitability of postsynaptic neurons.

One phenomenon of long ES_{AI}-evoked EPSP latency must be noted. The latency was related to stimulus intensity; the greater the stimulus intensity, the shorter the EPSP latency (**Figures 2B**, **3A**). At the 64 μA level, the ES_{AI}-evoked EPSP was about 6 ms in matched neurons, the latency reported here is far longer than previously reported (1–1.4 ms, Mitani et al., 1983). We assume that one explanation for this may be the difference in stimulus intensity although this information is not provided by the Mitani group. Yet another explanation might be the NMDAR that mediates the late EPSP component. Studies in different preparations show that the NMDAR-mediated latency can range from 3 to 6 ms (Shirokawa et al., 1989; Armstrong-James et al., 1993; Metherate and Ashe, 1994). Another consideration is multiple synaptic transmission; the AI-to-ICc pathway, even for matched neurons, may have multiple synaptic transmission as discussed below.

Corticofugal Inhibition

The neurotransmitter of corticofugal projections is glutamate, which acts on NMDAR and mGluR of postsynaptic neurons. Since GABAergic terminals are not found in the projections from the auditory cortex to the ICc (Feliciano and Potashner, 1995), the ES_{AI}-evoked ICc IPSP must have an indirect effect. In other words, AI neurons innervate local (collicular) GABAergic neurons that in turn innervate the neurons recorded in the ICc (Stebbings et al., 2014).

In the inferior colliculus (IC), GABAergic neurons are widely distributed; the percentage of GABAergic neurons in the ICc appears to be slightly larger than that in the external cortex of the IC (ICx), a non-lemniscal subdivision (Oliver et al., 1994; Merchán et al., 2005). Up to 25% of ICc neurons are GABAergic neurons that are large in soma size and evenly distributed across the tonotopic organization (Merchán et al., 2005; Wong and Borst, 2019), implicating that no less than 25% of ICc neurons recorded in this study could be GABAergic. These histological features support our findings that the ES_{AI} was also able to evoke the IPSP of ICc neurons. When compared to the ES_{AI}-evoked EPSP, two notable differences emerge. That is, IPSP was observed in fewer ICc neurons, and additionally, the threshold for inducing IPSP was much higher. Although a detailed analysis was not performed in this study due to limited sample size, ES_{AI}-evoked IPSPs favor the previous findings that ES_{AI} inhibits the tone-evoked responses of physiologically unmatched subcortical neurons (Yan and Ehret, 2002; Luo et al., 2008).

Frequency-Dependence of ES_{AI}-Evoked ICc EPSPs

Previous studies demonstrated that ES_{AI} induces highly frequency-specific modulation of the auditory responses of ICc neurons in the same species (Yan and Ehret, 2002; Yan et al., 2005) and in other species such as mustached bats, big brown bats, and gerbils (Gao and Suga, 1998; Yan and Suga, 1998; Sakai and Suga, 2002; Zhou and Jen, 2007; Bajo and King,

2013). The frequency-specificity appears to suggest a universal law of corticofugal modulation. In this study, an important finding is that the ES_{AI}-evoked ICc EPSPs also obey this law; EPSP induction was related to the CF difference between AI and ICc neurons (**Figure 5**). Our findings provide an initial understanding of a synaptic basis for the interpretation of frequency-specific corticofugal modulation of tone-evoked responses of ICc neurons.

Two themes derived from our findings of the ES_{AI}-evoked EPSPs are worthy of our attention. One is how the ES_{AI}-evoked EPSP is dependent on the difference in frequency tunings (i.e., CFs) between AI and ICc neurons. The other is how the frequency-specificity of ES_{AI}-evoked EPSPs can be converted into tone-evoked firing behavior of ICc neurons as observed in previous studies.

Concerning the frequency-dependency of the ES_{AI}-evoked EPSPs, three explanations are possible. The first relates to the damped propagation of electrical current within the brain. This means that AI neurons at a distance from the stimulus electrode (ref. to unmatched neurons) require a greater stimulus current to achieve a similar level of activation than those positioned near the electrode tip (ref. to matched neurons). Considering the tonotopic organization of the AI-to-ICc pathway (Huffman and Henson, 1990; Saldaña et al., 1996; Druga et al., 1997; Winer et al., 2001; Lim and Anderson, 2007; Bajo et al., 2010), the damped propagation of electrical current likely explains why the ES_{AI}-evoked EPSPs had a lower threshold (**Figure 5A**) and higher amplitude (**Figure 5C**) in matched than in unmatched ICc neurons. However, this interpretation may be flawed as the ES_{AI}-evoked EPSPs of matched neurons exhibited a shorter latency than those of unmatched neurons (**Figure 5B**). Also, we found that ES_{AI}-evoked EPSPs were similar between ICc neurons with CFs lower and higher than AI CF (**Figure 5**). With damped propagation, these EPSP properties should be different because the tonotopic organization of the auditory system is based on a logarithmical scale. For example, the affecting distance of 64 μA is about 500 μm (Ranck, 1975). If a stimulus electrode were placed at the 17 kHz area of the AI, we would expect that our stimulus current would affect the range from the 11 kHz area (low-frequency end) to the 28 kHz area (high-frequency end) according to the tonotopic organization in the AI of C57 mice (Zhang et al., 2005). A second explanation for the frequency-dependency may be the neural "spread" of the ES_{AI} effect due to intracortical excitatory projections (Sutter et al., 1999; Metherate et al., 2005). In other words, the AI neurons distant from the electrode tip may be activated or modulated by the neural inputs from the AI neurons in the vicinity of the electrode tip. This interpretation is also supported by our recent finding that ES_{AI} induces frequency-specific changes in auditory responses of other AI neurons in a linear scale under thalamic inactivation (Kong et al., 2018). A third explanation may involve intracollicular interactions, including the inhibitory projections from the ICx to ICc, as discussed above.

As for how ES_{AI}-evoked EPSPs can be converted to the frequency-specific changes in tone-evoked firing behavior of ICc neurons, the significance of postsynaptic glutamate receptor NMDAR and mGluR must be considered. It is well established that glutamate binding to NMDAR depolarizes postsynaptic neurons through cation influx and facilitates the input-specific responses (synaptic plasticity) of postsynaptic neurons (Furukawa et al., 2005; Li and Tsien, 2009). mGluR is a metabotropic receptor; it's binding with glutamate leads to changes in the excitability of postsynaptic neurons through the modulation of other ion channels (Chu and Hablitz, 2000; Gabriel et al., 2012). Our study suggests that corticofugal modulation of postsynaptic excitability through NMDAR/mGluR must have a significant impact on the responses of postsynaptic neurons to ascending inputs (i.e., tone-evoked inputs); greater corticofugal EPSP translates to a greater impact on the auditory responses of postsynaptic neurons (i.e., ICc neurons).

We propose that the ES_{AI}-evoked EPSP, through NMDAR and mGluR, facilitate the tone-evoked EPSP of ICc neurons, particularly when descending and ascending inputs are temporally close to each other. Furthermore, the strength of the corticofugal modulation depends on the amplitude of the ES_{AI}-evoked EPSP. Both proposals merit future investigation.

Possible Pathways of AI-to-ICc Transmission

Based on the above discussions, the AI-to-ICc transmission must involve both mono- and multi-synaptic transmission, and the pathways for matched neurons and unmatched neurons must be different.

In theory, the AI-to-ICc pathway can be mono-synaptic for matched neurons. However, the pathway should involve many multi-synaptic transmissions because the ES_{AI} at 64 μA can stimulate a group of neurons in the vicinity of the stimulus electrode through intracortical projections. In this scenario, the recorded EPSP of ICc neurons may consist of multiple synaptic inputs from a group of AI-to-ICc projections. Consequently, the EPSP properties should be dependent on the strength and timing of these inputs. This likely explains why the correlation of EPSP amplitude and duration is relatively poor (**Figure 3B**).

The significantly longer EPSP latency of unmatched ICc neurons suggests indirect (multi-synaptic) AI-to-ICc pathways. A possible pathway is that the stimulated AI neurons, *via* intracortical connections, activate other AI neurons that in turn act on collicular neurons through corticofugal projections. A well-tested pathway proposed by Jen and group (Jen et al., 1998) is an AI-ICx-ICc pathway; AI neurons activate ICx GABAergic neurons that in turn inhibit the ICc neurons. This pathway is supported by several important findings. First, corticofugal neurons more extensively innervate the ICx (Huffman and Henson, 1990). Second, ICx neurons send GABAergic fibers to the ICc (Merchán et al., 2005). Third, the ES_{AI} with a larger current increases the tone-evoked responses of ICx neurons but decreases those of ICc neurons in a non-frequency-specific manner (Jen et al., 1998). Fourth, the electrical stimulation of the ICx inhibits the tone-evoked responses of ICc neurons (Jen et al., 1998). Fifth, the ICx-inhibition of tone-evoked ICc responses can be eliminated by local application of bicuculline (an antagonist for $GABA_A$ receptor) to the ICc (Jen et al., 2001). Last, our

recorded data of the ES_{AI}-evoked IPSP was only observed with a strong current, i.e., 106.67 ± 15.08 μA.

CONCLUSION

This study reveals for the first time that ES_{AI} primarily evoked EPSPs of ICc neurons i.e., AI-to-ICc excitatory synaptic transmission, in a frequency-specific manner. Such frequency-specific effects may rely on intracortical and/or intracollicular circuits. Inhibitory circuits from ICx to ICc may also contribute to the frequency-specific variation of the ES_{AI}-evoked EPSPs. Our findings provide an initial understanding of the synaptic basis for frequency-specific corticofugal modulation of subcortical auditory information processing.

DATA AVAILABILITY STATEMENT

All datasets presented in this study are included in the article/**Supplementary Material**.

ETHICS STATEMENT

The animal study was reviewed and approved by Animal Care Committee at the University of Calgary.

AUTHOR CONTRIBUTIONS

JY supervised this study. JQ contributed to all experiments, data analysis, and manuscript writing. ZZ provided technical support. NH and XL contributed to the electrophysiological experiments. CZ contributed to data processing and manuscript editing. All authors contributed to the article and approved the submitted version.

FUNDING

This work was supported by grants from the Natural Science and Engineering Research Council of Canada (DG261338), and the Campbell McLaurin Chair for Hearing Deficiencies, the University of Calgary.

ACKNOWLEDGMENTS

We thank Dr. Jos J. Eggermont for his critical comments.

SUPPLEMENTARY MATERIAL

The Supplementary Material for this article can be found online at: https://www.frontiersin.org/articles/10.3389/fncir.2020.591986/full#supplementary-material.

REFERENCES

Abeles, M., and Goldstein, M. H. Jr. (1970). Functional architecture in cat primary auditory cortex: columnar organization and organization according to depth. *J. Neurophysiol.* 33, 172–187. doi: 10.1152/jn.1970.33.1.172

Armstrong-James, M., Welker, E., and Callahan, C. A. (1993). The contribution of NMDA and non-NMDA receptors to fast and slow transmission of sensory information in the rat SI barrel cortex . *J. Neurosci.* 13, 2149–2160. doi: 10.1523/JNEUROSCI.13-05-02149.1993

Bajo, V. M., and King, A. J. (2013). Cortical modulation of auditory processing in the midbrain. *Front. Neural Circuits* 6:114. doi: 10.3389/fncir.2012.00114

Bajo, V. M., and Moore, D. R. (2005). Descending projections from the auditory cortex to the inferior colliculus in the gerbil, Meriones unguiculatus. *J. Comp. Neurol.* 486, 101–116. doi: 10.1002/cne.20542

Bajo, V. M., Nodal, F. R., Moore, D. R., and King, A. J. (2010). The descending corticocollicular pathway mediates learning-induced auditory plasticity. *Nat. Neurosci.* 13, 253–260. doi: 10.1038/nn.2466

Chu, Z., and Hablitz, J. J. (2000). Quisqualate induces an inward current *via* mGluR activation in neocortical pyramidal neurons. *Brain Res.* 879, 88–92. doi: 10.1016/s0006-8993(00)02752-9

Druga, R., Syka, J., and Rajkowska, G. (1997). Projections of auditory cortex onto the inferior colliculus in the rat. *Physiol. Res.* 46, 215–222.

Feliciano, M., and Potashner, S. J. (1995). Evidence for a glutamatergic pathway from the guinea pig auditory cortex to the inferior colliculus. *J. Neurochem.* 65, 1348–1357. doi: 10.1046/j.1471-4159.1995.65031348.x

Furukawa, H., Singh, S. K., Mancusso, R., and Gouaux, E. (2005). Subunit arrangement and function in NMDA receptors. *Nature* 438, 185–192. doi: 10.1038/nature04089

Gabriel, L., Lvov, A., Orthodoxou, D., Rittenhouse, A. R., Kobertz, W. R., and Melikian, H. E. (2012). The acid-sensitive, anesthetic-activated potassium leak channel, KCNK3, is regulated by 14–3-3β-dependent, protein kinase C (PKC)-mediated endocytic trafficking. *J. Biol.* 287, 32354–32366. doi: 10.1074/jbc.M112.391458

Gao, E., and Suga, N. (1998). Experience-dependent corticofugal adjustment of midbrain frequency map in bat auditory system. *Proc. Natl. Acad. Sci. U S A* 95, 12663–12670. doi: 10.1073/pnas.95.21.12663

He, N., Kong, L., Lin, T., Wang, S., Liu, X., Qi, J., et al (2017). Diversity of bilateral synaptic assemblies for binaural computation in midbrain single neurons. *Hear. Res.* 355, 54–63. doi: 10.1016/j.heares.2017.09.007

Heffner, H. E., and Heffner, R. S. (2007). Hearing ranges of laboratory animals. *J. Am. Assoc. Lab. Anim. Sci.* 46, 20–22.

Huffman, R. F., and Henson, O. W. Jr. (1990). The descending auditory pathway and acousticomotor systems: connections with the inferior colliculus. *Brain Res.* 15, 295–323. doi: 10.1016/0165-0173(90)90005-9

Ito, T., and Oliver, D. L. (2010). Origins of glutamatergic terminals in the inferior colliculus identified by retrograde transport and expression of VGLUT1 and VGLUT2 genes. *Front. Neuroanat.* 4:135. doi: 10.3389/fnana.2010.00135

Jen, P. H.-S., Chen, Q. C., and Sun, X. D. (1998). Corticofugal regulation of auditory sensitivity in the bat inferior colliculus. *J. Comp. Physiol.* 183, 683–697. doi: 10.1007/s003590050291

Jen, P. H.-S., Sun, X., and Chen, Q. C. (2001). An electrophysiological study of neural pathways for corticofugally inhibited neurons in the central nucleus of the inferior colliculus of the big brown bat, *Eptesicus fuscus*. *Exp. Brain Res.* 137, 292–302. doi: 10.1007/s002210000637

Jen, P. H.-S., Zhou, X., Zhang, J., Chen, Q. C., and Sun, X. (2002). Brief and short-term corticofugal modulation of acoustic signal processing in the bat midbrain. *Hear. Res.* 168, 196–207. doi: 10.1016/s0378-5955(02)00358-1

Kong, L., Wang, S., Liu, X., Li, L., Zeeman, M., and Yan, J. (2018). Cortical frequency-specific plasticity is independently induced by intracortical circuitry. *Neurosci. Lett.* 668, 13–18. doi: 10.1016/j.neulet.2017.12.044

Li, F., and Tsien, J. Z. (2009). Memory and the NMDA receptors. *N. Engl. J. Med.* 361, 302–303. doi: 10.1056/NEJMcibr0902052

Lim, H. H., and Anderson, D. J. (2007). Antidromic activation reveals tonotopically organized projections from primary auditory cortex to the central nucleus of the inferior colliculus in guinea pig. *J. Neurophysiol.* 97, 1413–1427. doi: 10.1152/jn.00384.2006

Liu, X., Wang, C., Pan, C., and Yan, J. (2015). Physiological correspondence dictates cortical long-term potentiation and depression by thalamic induction. *Cereb. Cortex* 25, 545–553. doi: 10.1093/cercor/bht259

Liu, X., Yan, Y., Wang, Y., and Yan, J. (2010). Corticofugal modulation of initial neural processing of sound information from the ipsilateral ear in the mouse. *PLoS One* 5:e14038. doi: 10.1371/journal.pone.0014038

Luo, F., Wang, Q., Farid, N., Liu, X., and Yan, J. (2009). Three-dimensional tonotopic organization of the C57 mouse cochlear nucleus. *Hear. Res.* 257, 75–82. doi: 10.1016/j.heares.2009.08.002

Luo, F., Wang, Q., Kashani, A., and Yan, J. (2008). Corticofugal modulation of initial sound processing in the brain. *J. Neurosci.* 28, 11615–11621. doi: 10.1523/JNEUROSCI.3972-08.2008

Ma, X., and Suga, N. (2001). Corticofugal modulation of duration-tuned neurons in the midbrain auditory nucleus in bats. *Proc. Natl. Acad. Sci. U S A* 98, 14060–14065. doi: 10.1073/pnas.241517098

Malmierca, E., and Nuñez, A. (2004). Primary somatosensory cortex modulation of tactile responses in nucleus gracilis cells of rats. *Eur. J. Neurosci.* 19, 1572–1580. doi: 10.1111/j.1460-9568.2004.03256.x

Markovitz, C. D., Tang, T. T., and Lim, H. H. (2013). Tonotopic and localized pathways from primary auditory cortex to the central nucleus of the inferior colliculus. *Front. Neural Circuits* 7:77. doi: 10.3389/fncir.2013.00077

McCormick, D. A., and von Krosigk, M. (1992). Corticothalamic activation modulates thalamic firing through glutamate "metabotropic" receptors. *Proc. Natl. Acad. Sci. U S A* 89, 2774–2778. doi: 10.1073/pnas.89.7.2774

Merchán, M., Aguilar, L. A., Lopez-Poveda, E. A., and Malmierca, M. S. (2005). The inferior colliculus of the rat: quantitative immunocytochemical study of GABA and glycine. *Nat. Neurosci.* 136, 907–925. doi: 10.1016/j.neuroscience.2004.12.030

Metherate, R., and Ashe, J. H. (1994). Facilitation of an NMDA receptor-mediated EPSP by paired-pulse stimulation in rat neocortex *via* depression of GABAergic IPSPs. *J. Physiol.* 481, 331–348. doi: 10.1113/jphysiol.1994.sp020443

Metherate, R., Kaur, S., Kawai, H., Lazar, R., Liang, K., and Rose, H. J. (2005). Spectral integration in auditory cortex: mechanisms and modulation. *Hear. Res.* 206, 146–158. doi: 10.1016/j.heares.2005.01.014

Mitani, A., Shimokouchi, M., and Nomura, S. (1983). Effects of stimulation of the primary auditory cortex upon colliculogeniculate neurons in the inferior colliculus of the cat. *Neurosci. Lett.* 42, 185–189. doi: 10.1016/0304-3940(83)90404-4

Moerel, M., De Martino, F., Uğurbil, K., Formisano, E., and Yacoub, E. (2018). Evaluating the columnar stability of acoustic processing in the human auditory cortex. *J. Neurosci.* 38, 7822–7832. doi: 10.1523/JNEUROSCI.3576-17.2018

Montero, V. M., and Wenthold, R. J. (1989). Quantitative immunogold analysis reveals high glutamate levels in retinal and cortical synaptic terminals in the lateral geniculate nucleus of the macaque. *Nat. Neurosci.* 31, 639–647. doi: 10.1016/0306-4522(89)90429-6

Oliver, D. L., Winer, J., Beckius, G. E., and Saint Marie, R. L. (1994). Morphology of GABAergic neurons in the inferior colliculus of the cat. *J. Comp. Neurol.* 340, 27–42. doi: 10.1002/cne.903400104

Ranck, J. B. Jr. (1975). Which elements are axcited in electrical stimulation of mammalian central nervous system: a review. *Brain Res.* 98, 417–440. doi: 10.1016/0006-8993(75)90364-9

Rivadulla, C., Martínez, L. M., Varela, C., and Cudeiro, J. (2002). Completing the corticofugal loop: a visual role for the corticogeniculate type 1 metabotropic glutamate receptor. *J. Neurosci.* 22, 2956–2962. doi: 10.1523/JNEUROSCI.22-07-02956.2002

Rouiller, E. M., and Welker, E. (2000). A comparative analysis of the morphology of corticothalamic projections in mammals. *Brain Res. Bull.* 53, 727–741. doi: 10.1016/s0361-9230(00)00364-6

Sakai, M., and Suga, N. (2002). Centripetal and centrifugal reorganizations of frequency map of auditory cortex in gerbils. *Proc. Natl. Acad. Sci. U S A* 99, 7108–7112. doi: 10.1073/pnas.102165399

Saldaña, E., Feliciano, M., and Mugnaini, E. (1996). Distribution of descending projections from primary auditory neocortex to inferior colliculus mimics the topography of intracollicular projections. *J. Comp. Neurol.* 371, 15–40. doi: 10.1002/(SICI)1096-9861(19960715)371:1<15::AID-CNE2>3.0.CO;2-O

Scharfman, H. E., Lu, S. M., Guido, W., Adams, P. R., and Sherman, S. M. (1990). *N*-methyl-D-aspartate receptors contribute to excitatory postsynaptic potentials of cat lateral geniculate neurons recorded in thalamic slices. *Proc. Natl. Acad. Sci. U S A* 87, 4548–4552. doi: 10.1073/pnas.87.12.4548

Schofield, B. R., and Coomes, D. L. (2005). Auditory cortical projections to the cochlear nucleus in guinea pigs. *Hear. Res.* 199, 89–102. doi: 10.1016/j.heares.2004.08.003

Shen, J. X., Xu, Z. M., and Yao, Y. D. (1999). Evidence for columnar organization in the auditory cortex of the mouse. *Hear. Res.* 137, 174–177. doi: 10.1016/s0378-5955(99)00149-5

Shirokawa, T., Nishigori, A., Kimura, F., and Tsumoto, T. (1989). Actions of excitatory amino acid antagonists on synaptic potentials of layer II/III neurons of the cat's visual cortex. *Exp. Brain Res.* 78, 489–500. doi: 10.1007/BF00230237

Stebbings, K. A., Lesicko, A. M. H., and Llano, D. A. (2014). The auditory corticocollicular system: molecular and circuit level considerations. *Hear. Res.* 314, 51–59. doi: 10.1016/j.heares.2014.05.004

Suga, N. (2020). Plasticity of the adult auditory system based on corticocortical and corticofugal modulations. *Neurosci. Biobehav. Rev.* 113, 461–478. doi: 10.1016/j.neubiorev.2020.03.021

Suga, N., Gao, E., Zhang, Y., Ma, X., and Olsen, J. F. (2000). The corticofugal system for hearing: recent progress. *Proc. Natl. Acad. Sci. U S A* 97, 11807–11814. doi: 10.1073/pnas.97.22.11807

Suga, N., Yan, J., and Zhang, Y. (1997). Cortical maps for hearing and egocentric selection for self-organization. *Trends Cogn. Sci.* 1, 13–20. doi: 10.1016/S1364-6613(97)01002-4

Sutter, M. L., Schreiner, C. E., McLean, M., O'Connor, K. N., and Loftus, W. C. (1999). Organization of inhibitory frequency receptive fields in cat primary auditory cortex. *J. Neurophysiol.* 82, 2358–2371. doi: 10.1152/jn.1999.82.5.2358

Syka, J., and Popelár, J. (1984). Inferior colliculus in the rat: neuronal responses to stimulation of the auditory cortex. *Neurosci. Lett.* 51, 235–240. doi: 10.1016/0304-3940(84)90557-3

Terreros, G., and Delano, P. H. (2015). Corticofugal modulation of peripheral auditory responses. *Front. Syst. Neurosci.* 9:134. doi: 10.3389/fnsys.2015.00134

Weedman, D. L., and Ryugo, D. K. (1996). Projections from auditory cortex to the cochlear nucleus in rats: synapses on granule cell dendrites. *J. Comp. Neurol.* 371, 311–324. doi: 10.1002/(SICI)1096-9861(19960722)371:2<311::AID-CNE10s>3.0.CO;2-V

Winer, J. A., Diehl, J. J., and Larue, D. T. (2001). Projections of auditory cortex to the medial geniculate body of the cat. *J. Comp. Neurol.* 430, 27–55. doi: 10.1002/1096-9861(20010129)430:1<27::aid-cne1013>3.0.co;2-8

Winer, J. A., Larue, D. T., Diehl, J. J., and Hefti, B. J. (1998). Auditory cortical projections to the cat inferior colliculus. *J. Comp. Neurol.* 400, 147–174. doi: 10.1002/(sici)1096-9861(19981019)400:2<147::aid-cne1>3.0.co;2-9

Wong, A. B., and Borst, J. G. G. (2019). Tonotopic and non-auditory organization of the mouse dorsal inferior colliculus revealed by two-photon imaging. *eLife* 8:e49091. doi: 10.7554/eLife.49091

Wu, Y., and Yan, J. (2007). Modulation of the receptive fields of midbrain neurons elicited by thalamic electrical stimulation through corticofugal feedback. *J. Neurosci.* 27, 10651–10658. doi: 10.1523/JNEUROSCI.1320-07.2007

Xiong, Y., Zhang, Y., and Yan, J. (2009). The neurobiology of sound-specific auditory plasticity: a core neural circuit. *Neurosci. Biobehav. Rev.* 33, 1178–1184. doi: 10.1016/j.neubiorev.2008.10.006

Yan, J., and Ehret, G. (2002). Corticofugal modulation of midbrain sound processing in the house mouse. *Eur. J. Neurosci.* 16, 119–128. doi: 10.1046/j.1460-9568.2002.02046.x

Yan, J., and Suga, N. (1996). Corticofugal modulation of time-domain processing of biosonar information in bats. *Science* 273, 1100–1103. doi: 10.1126/science.273.5278.1100

Yan, W., and Suga, N. (1998). Corticofugal modulation of the midbrain frequency map in the bat auditory system. *Nat. Neurosci.* 1, 54–58. doi: 10.1038/255

Yan, J., and Suga, N. (1999). Corticofugal amplification of facilitative auditory responses of subcortical combination-sensitive neurons in the mustached bat. *J. Neurophysiol.* 81, 817–824. doi: 10.1152/jn.1999.81.2.817

Yan, J., Zhang, Y., and Ehret, G. (2005). Corticofugal shaping of frequency tuning curves in the central nucleus of the inferior colliculus of mice. *J. Neurophysiol.* 93, 71–83. doi: 10.1152/jn.00348.2004

Zhang, Y., Dyck, R. H., Hamilton, S. E., Nathanson, N. M., and Yan, J. (2005). Disrupted tonotopy of the auditory cortex in mice lacking M1 muscarinic

acetylcholine receptor. *Hear. Res.* 201, 145–155. doi: 10.1016/j.heares.2004.10.003

Zhang, Y., Suga, N., and Yan, J. (1997). Corticofugal modulation of frequency processing in bat auditory system. *Nature* 387, 900–903. doi: 10.1038/43180

Zhang, Y., and Suga, N. (1997). Corticofugal amplification of subcortical responses to single tone stimuli in the mustached bat. *J. Neurophysiol.* 78, 3489–3492. doi: 10.1152/jn.1997.78.6.3489

Zhang, Y., and Suga, N. (2000). Modulation of responses and frequency tuning of thalamic and collicular neurons by cortical activation in mustached bats. *J. Neurophysiol.* 84, 325–333. doi: 10.1152/jn.2000.84.1.325

Zhou, X., and Jen, P. H.-S. (2000). Brief and short-term corticofugal modulation of subcortical auditory responses in the big brown bat, Eptesicus Fuscus. *J. Neurophysiol.* 84, 3083–3087. doi: 10.1152/jn.2000.84.6.3083

Zhou, X., and Jen, P. H.-S. (2007). Corticofugal modulation of multi-parametric auditory selectivity in the midbrain of the big brown bat. *J. Neurophysiol.* 98, 2509–2516. doi: 10.1152/jn.00613.2007

Conflict of Interest: The authors declare that the research was conducted in the absence of any commercial or financial relationships that could be construed as a potential conflict of interest.

frontiers in Neural Circuits

REVIEW
published: 22 January 2021
doi: 10.3389/fncir.2020.615259

Top-Down Inference in the Auditory System: Potential Roles for Corticofugal Projections

Alexander Asilador[1,2] *and Daniel A. Llano*[1,2,3]*

[1]Neuroscience Program, The University of Illinois at Urbana-Champaign, Champaign, IL, United States, [2]Beckman Institute for Advanced Science and Technology, Urbana, IL, United States, [3]Molecular and Integrative Physiology, The University of Illinois at Urbana-Champaign, Champaign, IL, United States

It has become widely accepted that humans use contextual information to infer the meaning of ambiguous acoustic signals. In speech, for example, high-level semantic, syntactic, or lexical information shape our understanding of a phoneme buried in noise. Most current theories to explain this phenomenon rely on hierarchical predictive coding models involving a set of Bayesian priors emanating from high-level brain regions (e.g., prefrontal cortex) that are used to influence processing at lower-levels of the cortical sensory hierarchy (e.g., auditory cortex). As such, virtually all proposed models to explain top-down facilitation are focused on intracortical connections, and consequently, subcortical nuclei have scarcely been discussed in this context. However, subcortical auditory nuclei receive massive, heterogeneous, and cascading descending projections at every level of the sensory hierarchy, and activation of these systems has been shown to improve speech recognition. It is not yet clear whether or how top-down modulation to resolve ambiguous sounds calls upon these corticofugal projections. Here, we review the literature on top-down modulation in the auditory system, primarily focused on humans and cortical imaging/recording methods, and attempt to relate these findings to a growing animal literature, which has primarily been focused on corticofugal projections. We argue that corticofugal pathways contain the requisite circuitry to implement predictive coding mechanisms to facilitate perception of complex sounds and that top-down modulation at early (i.e., subcortical) stages of processing complement modulation at later (i.e., cortical) stages of processing. Finally, we suggest experimental approaches for future studies on this topic.

Keywords: auditory, cortex, thalamus, colliculus, top-down, speech perception, descending, medial geniculate body

OPEN ACCESS

Edited by:
Julio C. Hechavarría, Goethe University Frankfurt, Germany

Reviewed by:
Kirill Vadimovich Nourski, The University of Iowa, United States
Kasia M. Bieszczad, The State University of New Jersey, United States

***Correspondence:**
Daniel A. Llano
d-llano@illinois.edu

Received: *08 October 2020*
Accepted: *17 December 2020*
Published: *22 January 2021*

Citation:
Asilador A and Llano DA (2021) Top-Down Inference in the Auditory System: Potential Roles for Corticofugal Projections. Front. Neural Circuits 14:615259. doi: 10.3389/fncir.2020.615259

INTRODUCTION

We effortlessly navigate a world filled with complex sounds. Despite challenging listening environments, such as having a conversation on a windy day, talking over a poor cell phone connection, or presenting a poster at a busy scientific meeting, the auditory system routinely extracts the meaning of signals corrupted by noise. One type of cue that may be used to perform this operation is the linguistic or acoustic context within which a sound exists. For example, it has long been known that high-level information about the nature of ambiguous speech sounds

can dramatically enhance the ability to recognize these sounds (Miller et al., 1951; O'Neill, 1957; and reviewed in Davis and Johnsrude, 2007; Obleser, 2014). Also, acoustic perception and peripheral auditory responses in humans are strongly influenced by preceding non-speech acoustic stimuli (Lotto and Kluender, 1998; Skoe and Kraus, 2010), suggesting that contextual cueing may be a general mechanism used by the auditory system to deal with ambiguity. Contextual cueing is also of clinical importance as many individuals with language-related disorders, such as aphasia, autism, auditory processing disorder, and dyslexia, have difficulties using high-level contextual cues to disambiguate noisy or degraded sound stimuli (Tseng et al., 1993; Grindrod and Baum, 2002; Fink et al., 2006; Stewart and Ota, 2008; Chandrasekaran et al., 2009; Moore D. R., 2012).

The process of using prior knowledge to influence the processing of sensory information is referred to as "top-down modulation." Originally described as "unconscious influence" by Helmholz in the 1800s (Von Helmholtz, 1867), top-down modulation is a ubiquitous process that is seen across all sensory systems (Kobayashi et al., 2004; Haegens et al., 2011; Andersson et al., 2018). It is believed that the major roles of top-down modulation are to select certain sensory features over others in a cluttered sensory environment to favor encoding information that is more meaningful for the organism. On the latter point, meaningful information is often defined by the statistical regularity with which those features are encountered in the environment, a key point exploited by most of the experimental paradigms involving repetitive stimulation of a particular region of cortex (e.g., Gao and Suga, 2000; Yan and Ehret, 2002).

The neural substrates for top-down modulation are not well understood. Sensory systems are hierarchically organized such that sensory information ascends through a series of brain regions before reaching the primary sensory cortex (e.g., the primary auditory cortex). Canonically, the primary sensory cortex sends projections to secondary sensory cortical areas, which then project to areas outside of the sensory pathway, typically including areas of the prefrontal cortex. Also, virtually all of these "ascending" connections are associated with a returning "descending" connection, which in some cases contain axons that greatly outnumber the corresponding ascending connection. In some cases, the descending connections "skip" levels and send projections to areas that do not have a direct corresponding ascending connection (e.g., the projection from the cortex to the tectum or to the corpus striatum). Virtually all current models that describe the use of top-down modulation to facilitate auditory processing have focused on intracortical projections [e.g., from the frontal cortex to auditory cortex or from secondary auditory cortical fields to the primary auditory cortex (Zekveld et al., 2006; Hannemann et al., 2007; Sohoglu et al., 2012; Chennu et al., 2013, 2016; Hofmann-Shen et al., 2020)]. What is often left out of the discussion, however, are the massive and heterogeneous projections emanating from the auditory cortex that target virtually every level of the subcortical auditory system (herein "corticofugal projections") and, through cascading projections, impacting the most peripheral component: the cochlea (Xiao and Suga, 2002; León et al., 2012; Dragicevic et al., 2015; Jäger and Kössl, 2016).

This focus on cortical mechanisms of top-down modulation has existed despite the data demonstrating that descending influences can alter primary auditory input through the cochlear efferent system. For example, attentional tasks and prior linguistic knowledge modulate efferent projections to the cochlea (Collet et al., 1994; Marian et al., 2018), electrical stimulation of the human auditory cortex modulates cochlear activity (Perrot et al., 2006), and activation of subcortical auditory pathways to the cochlea facilitate speech recognition in challenging listening situations (De Boer and Thornton, 2008; Smith et al., 2012; Srinivasan et al., 2012; Mishra and Lutman, 2014; Shastri et al., 2014). As shown in **Figures 1A,B**, electrical stimulation of the human auditory cortex (but not non-auditory cortex) diminishes the mean amplitude and the variation in the amplitude of evoked otoacoustic emissions. Also, auditory attention leads to a decline in the amplitude of otoacoustic emissions, which are generated by the cochlea (**Figure 1C**). The projections from the auditory cortex that lead to modulation of the cochlea have been reviewed by Terreros and Délano (2015). They proposed a cascading model of multiple parallel pathways connecting the auditory cortex, inferior colliculus, cochlear nucleus, and superior olivary nuclei (including a direct projection from the auditory cortex to neurons making up the medial olivocochlear pathway; Mulders and Robertson, 2000) as potential neural substrates for these findings (**Figure 1D**; Terreros and Délano, 2015). Here, we attempt to link the bodies of literature on intracortical top-down modulation for processing of complex sounds (which has primarily been done in humans, with some notable exceptions; García-Rosales et al., 2020; Yin et al., 2020) and corticofugal modulation of subcortical auditory processing regions (which has primarily been done in animals), to develop a better understanding of the potential role of corticofugal projections in the disambiguation of corrupted acoustic signals.

EVIDENCE FOR TOP-DOWN MODULATION IN THE AUDITORY SYSTEM: HUMAN STUDIES

When engaged with acoustic stimuli, the goal at the behavioral level is the coherent perception of an object in its environment. In the auditory system, one of the earliest models used to describe perception was auditory scene analysis. The term was coined by Albert Bregman, a psychologist at McGill University (Bregman, 1994). He explored the idea that elements of a sound stimulus are grouped by the similarity of the components of a sound. These bottom-up features include the pitch, harmonicity, rhythmicity, similarity of sound, and timing of the sounds. Research in perceptual computing has shown some success in forming the foundation of scene analysis, where the computational model is capable of object detection, component extraction, and separation of sources in real-world situations (Smaragdis, 2001). However, when the level of ambiguity increases, object separation becomes much more difficult. Researchers have

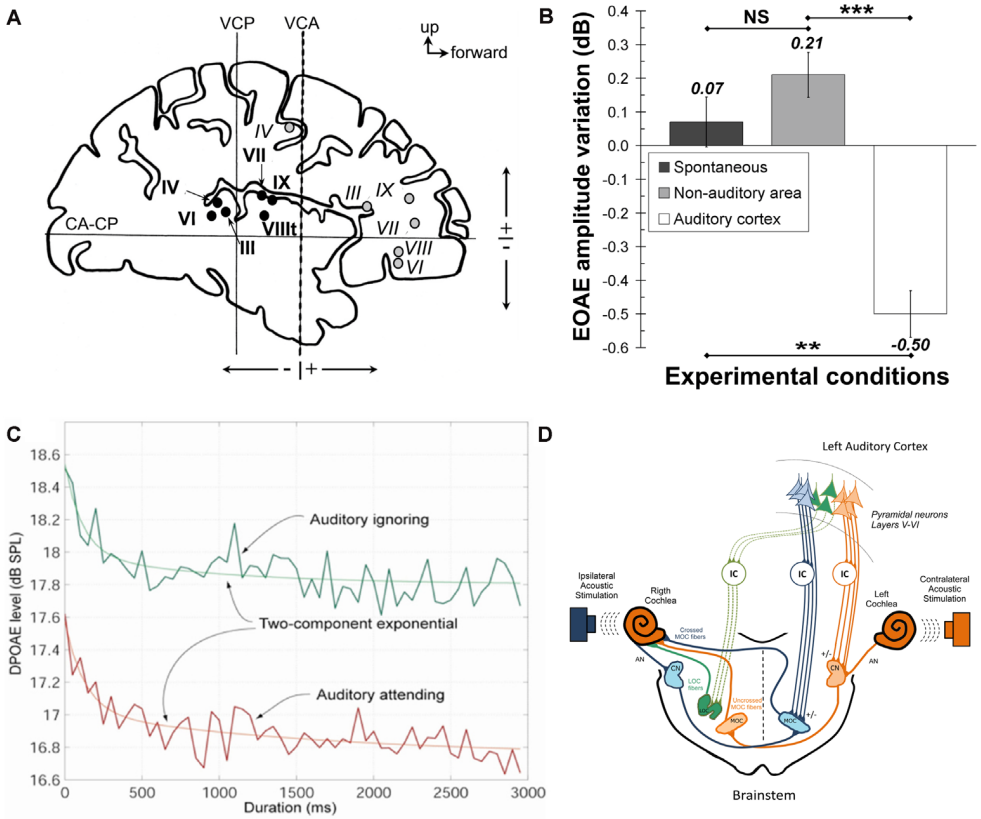

FIGURE 1 | (A,B) Illustration of the experiment by Perrot et al. (2006) showing electrical stimulation sites in the human auditory cortex in panel **(A)**. Black circles = auditory cortex stimulation sites, gray circles = non-auditory cortex stimulation sites, Roman numerals correspond to the individual patients. CA-CP, plane passing through the anterior and posterior commissures; VCA, vertical plane passing through the anterior commissure; VCP, vertical plane passing through the posterior commissure. Panel **(B)** shows the change in the variation in the amplitude of evoked otoacoustic emissions (EOAEs) under spontaneous conditions (dark bar), after stimulation in the non-auditory cortex (gray bar), and after stimulation in the auditory cortex (white bar). These data illustrate that human auditory cortical stimulation diminishes the variability of evoked otoacoustic emissions. $^{**}P < 0.01$; $^{***}P = 0.001$; NS, not significant using paired *t*-tests. Standard error of the mean is shown using error bars. Data obtained with permission from Perrot et al. (2006). Panel **(C)** Illustrates the impact of attending to an auditory stimulus on distortion product otoacoustic emissions (DPOAEs). As shown, attending to an acoustic stimulus diminishes the DPOAE amplitude (red trace), compared to ignoring that stimulus (green trace). Data obtained with permission from Smith et al. (2012). **(D)** Illustration of a model proposed by Terreros and Délano (2015) to explain the influence of the cortex on the cochlea. They propose multiple potential pathways from the auditory cortex, involving the inferior colliculus and the superior olivary nuclei, to impact the outer hair cells *via* the medial olivocochlear bundle. Figure obtained with permission from Terreros and Délano (2015).

investigated the effect of attention to resolve ambiguities, such as the separation of objects from distractors and noisy environments. For example, van Noorden (1971) examined stream segregation by presenting pure tones, tone A and tone B, to listeners. The stimulus was presented as a sequence of alternating A and B tones, but every second B tone was omitted. The two tones differed by a pitch for each experiment, and this difference was distinguished as either a denoted "small," "intermediate," or "large" difference. For small differences, the tones were perceived as a single rhythm and result in the perceptual fusion of the two tones. For large differences, the resulting perceived sound led to a separation of the two sounds, where the A tone was presented twice as fast as the B tone. For intermediate differences, the listeners either perceived either a fusion or fission of the two sounds based on the subject, however, the subjects can influence what type they hear based on the instructions given to the subjects. Thus, attentional bias can determine the nature of a percept when ambiguous signals are presented.

The effects of top-down modulation on bottom-up processing are particularly notable during speech perception. Any given speech unit is not represented solely by the instantaneous components of sound (frequency content and intensity) but is a time-varying cognitive construct whereby a combination of phonemes or acoustical patterns are used to represent a unit of speech. The same speech sounds vary from speaker to speaker and speech sounds may change based on their preceding or following sounds (coarticulation; Moore B. C., 2012). Yet, listeners can understand phrases and dialogue from different speakers without difficulty. As outlined by Davis and Johnsrude (2007), this form of perception is experience-driven and is demonstrated from an analysis by Fodor and Bever (1965) on the inclusion of clicks in a speech, as seen in speakers of Sub-Saharan languages. Such

psychoacoustic tests have revealed that the clicks are not perceptually heard in individuals who have not acquired this language. The argument here is that speech understanding is a perceptual process such that humans cognitively reorganize the acoustic input stream based on our experience with acoustic stimuli.

Several core perceptual processes are needed to effectuate speech perception in the face of widely varying sensory stimuli. One is categorical perception—the tendency to perceive acoustic stimuli as belonging to distinct categories despite having their stimulus properties vary on a continuum (e.g., perceiving a phoneme as either voiced vs. unvoiced despite having a gradual change in voice onset time). Another perceptual process that is key to understanding corrupted speech is a perceptual fill-in. In speech, this is typically referred to as the "phonemic restoration effect" (Warren, 1970) and describes the process of perceptually filling in noise-filled gaps in speech with the missing phoneme, analogous to filling in the contour of a partially obscured or partially-constructed visual object (e.g., Kanizsa objects). A third core perceptual process needed for speech processing is segmentation. That is, knowing the start and the stop of a meaningful acoustic signal. Generally, speech does not provide clear temporal demarcations between meaningful utterances, and these have to be inferred by the listener. Finally, stream segregation—the ability to perceptually separate different auditory objects whose waveforms are intermingled—is key to deciphering speech buried in noise. Although these core perceptual processes for speech understanding can potentially be explained solely *via* bottom-up processes (see Norris et al., 2000 for arguments in favor of a purely bottom-up approach to speech processing), as will be reviewed below, they are all strongly influenced by top-down factors.

Early evidence that lexical or semantic context could be used to facilitate the categorical perception of speech in noise was provided by Miller et al. (1951). They reported that the intelligibility of a word is enhanced when the appropriate context is provided. For example, the word "trees" buried in noise is more intelligible if it is preceded by the phrase "Apples grow on ____". Later work established that this effect is present at the lexical level (Ganong effect) such that preceding phonemes could increase the intelligibility of subsequent phonemes in words compared to nonwords (e.g., "task" vs. "dask"; Ganong, 1980).

Non-auditory cues can also be used to facilitate categorical perception. For example, observing the mouth movements of a speaker or seeing a written representation of a word before the obscured sound both facilitated perceptual performance (Sohoglu et al., 2012, 2014; Getz and Toscano, 2019; Pinto et al., 2019). For example, providing a written example of a semantically-associated word (e.g., "MASHED") before an acoustic representation of a word with ambiguous voice onset time (e.g., "potatoes"), facilitated the categorical perception of the initial consonant more than unrelated visual primes (Getz and Toscano, 2019). This use of cross-modal semantic priming modulated the earliest electroencephalography (EEG) peak examined by the investigators, the N1 peak, thought to be related to primary auditory cortex activation (Hillyard et al., 1973; Näätänen and Picton, 1987). Also, to compare the contributions of frontal vs. temporal cortex in a similar task, Sohoglu et al. found that use of written word prior information to disambiguate a vocoded speech sound was associated with inferior frontal gyrus activation using a combined EEG/magnetoencephalography (MEG) approach. In contrast, manipulations of the number of frequency bands available (thus increasing the bottom-up detail in the stimulus), activated auditory areas of the superior temporal gyrus (Sohoglu et al., 2012). These data are in line with a fronto-temporal hypothesis about descending control (Tzourio et al., 1997; Braga et al., 2013; Cope et al., 2017).

Concerning perceptual fill-in, the influence of context on phonemic restoration has been extensively examined, even from the earliest descriptions of the restoration phenomenon. For example, Marslen–Wilson demonstrated in 1975 that phonemic restoration was much more common when the target word was placed in the appropriate semantic and grammatical context and that the third syllable of a word was much more likely to be restored than the first syllable (Marslen–Wilson, 1975), suggesting that within-word context is an important cue. Expectation effects were also found by Samuel in 1981 who showed that words with a syllable replaced by noise were more likely to be reported as intact words if those words were incorporated into a sentence (Samuel, 1981). Samuel later (Samuel, 1997) showed that phonemic restoration introduced adaptation effects similar to those predicted by previous top-down models (e.g., the TRACE model; Mcclelland and Elman, 1986). More recently, it has been shown that the phonemic restoration effect remains intact despite voice discontinuities pre-and post-noise gap. That is, listeners were able to perceptually fill-in the gap despite the absence of spectral overlap between the pre-and post- gap voice, suggesting that other cues, such as linguistic context, are driving the filling-in phenomenon (Mcgettigan et al., 2013).

The third core perceptual process needed to disambiguate noisy speech is segmentation. Because most languages do not have clear acoustic demarcations separating meaningful utterances in speech, segmentation between words and sentences must be inferred (e.g., "mother's cold" vs. "mother scold"), and thus represents a key component of top-down speech perception (Davis and Johnsrude, 2007). Indeed a common complaint among most learners of a new language is not knowing where words start and end. Multiple potential cues can assist in this segmentation, such as loudness (stresses on particular syllables), word knowledge, semantic context, etc. Mattys et al. found that when multiple conflicting cues were available, listeners relied on higher-level cues (e.g., sentence context) rather than lower-level cues (e.g., word stress). They proposed a hierarchical organization with lexical knowledge occupying the highest level and what they referred to as "metrical prosody" (syllable stresses) at the bottom (Mattys et al., 2005). Supporting the idea that word knowledge plays a role in lexical segmentation is the finding by Cunillera et al. (2010) that knowing a small number of "anchor" words in a novel language facilitated the ability

to appropriately segment that language into meaningful units. Similar knowledge-based facilitation of segmentation of musical phrases has been observed, suggesting that top-down facilitation of segmentation may be a general property of the auditory system (Silva et al., 2019).

Another key requirement for inferring speech content under noisy conditions is the ability to separate competing sound streams. This process is multifaceted and involves both bottom-up cues (e.g., different pitch contours or spatial locations of different sources, as described above; Bregman, 1994) and top-down cues. Many investigators have established that bottom-up cues are sufficient to separate sound sources (often referred to as "sound streams") when the physical characteristics of the sound sources are distinct (Scholes et al., 2015). However, when there is substantial overlap between them, as is often the case in a sound-cluttered real-word environment, top-down cues become critical. Several studies have been done using such cluttered stimuli and have presented a priming stimulus containing the target and have observed a marked improvement in identifying the target (Freyman et al., 2004; Jones and Freyman, 2012; Wang et al., 2019). For example, Wang et al. examined the ability to separate two simultaneously-presented spectrally- and temporally- overlapping talkers without spatial cues. The presence of the target sound played before the simultaneously-presented sounds greatly facilitated the recognition of the target. This recognition was also associated with increased phase-locking of the superior temporal gyrus and sulcus MEG signals to the speech envelope (Wang et al., 2019). These data suggest that in the absence of bottom-up cues to separate sound sources, knowledge-based cues can be used and that this knowledge modulates processing in areas of the auditory cortex.

A common class of paradigms to study the various perceptual processes involved in auditory top-down modulation in humans is the oddball or omission paradigm. Such paradigms typically involve repetition of a particular sound, followed by an "oddball" (e.g., AAAAB), or the absence of sound (e.g., AAAA_). This paradigm or variations of it (e.g., presenting a global deviant such as AAAAA in the setting of a long series of AAAAB stimuli) have been heavily employed in the neuroscience literature. Oddballs typically evoke a voltage change measured at the scalp known as the mismatch negativity (MMN). The presence of the mismatch negativity has been taken as evidence of a core component of predictive coding—prediction error—and has thus been promoted as evidence for top-down modulation in the auditory system. The mapping of MMN onto top-down processing mechanisms is still not clear. The presence of some forms of MMN (sensitivity to local, rather than global deviants) in sleep or under anesthesia (Loewy et al., 2000; Nourski et al., 2018), which would be inconsistent with an active inferential process, suggests that bottom-up effects (such as habituation to repeated stimuli) may play a role. More modern instantiations of the oddball paradigm comparing responses to local vs. global deviants have shown that global deviants may be more vulnerable to anesthesia (Nourski et al., 2018), suggesting that this form of predictive error may better reflect active top-down control mechanisms.

COMPUTATIONAL PRINCIPLES OF TOP-DOWN MODULATION

Various models have been proposed to understand how contextual cues can influence sensory processing. Predictive coding is a general framework by which context, in the form of predictions about incoming data, can shape the properties of sensory-responsive neurons. Early instantiations of predictive coding algorithms were primarily focused on increasing the efficiency of the coding because of predictive coding's ability to reduce redundancies in data streams (Srinivasan et al., 1982), similar to bandwidth compression required to transmit large images. Notably, efficiency in terms of the number of neuronal connections does not appear to be a design principle of descending systems in the brain. These systems are massive and typically dwarf ascending projections, so it seems unlikely that they evolved to maximize the efficiency of coding in lower centers. It is more likely that these large, presumably energy-expensive systems, evolved to increase the accuracy of identifying causes of sensory inputs. To this end, approaches that have been shown to increase the accuracy of sensory estimation, such as Bayesian estimation, have been postulated to be of use. Such schemes involve the generation of a prediction about the outside world (a Bayesian prior) that, when combined with noisy or degraded sensory information, leads to an optimal estimate of the cause of the sensory signal (the posterior probability), see **Figure 2**. The Bayesian priors are based on previous experience with the world and thus are updated by experience. Several studies have shown that in the setting of sensory uncertainties, humans combine contextual information and sensory information in Bayes-optimal ways (Jacobs, 1999; Ernst and Banks, 2002; Battaglia et al., 2003). More general models that attempt to explain neural processing based on similar principles (e.g., the Free Energy Principle) have been proposed (Friston and Kiebel, 2009). In practice, most predictive coding models involve a prediction, which is compared to sensory input. When the two are unmatched, a "prediction error" occurs (increasing the Free Energy), which is used as a learning signal to modify the internal model. This scheme is consistent with the large body of work showing enhanced neural responses to unpredicted stimuli (e.g., the MMN, reviewed above). However, as described in "Neural Models of Top-Down Modulation," section this model has challenges both at the neural implementation level and at the level of linking neural responses to behavior.

Precisely how to link internal models with incoming information has been an open question. In modeling studies, the integration of predictive cues with incoming information has been implemented using several approaches. One approach has adapted linear systems theory and estimation theory into a model of the visual system. Rao and Ballard (1997) condensed the complexity of the visual system into a series of calculations that are inspired by work in minimum mean squared error estimation (MMSE): the Kalman filter (Kalman, 1960). The goal of MMSE is to estimate the internal (unknown) state of a system based on observation of noisy sensors to predict the next state. The Kalman filter is a linear estimator that assumes

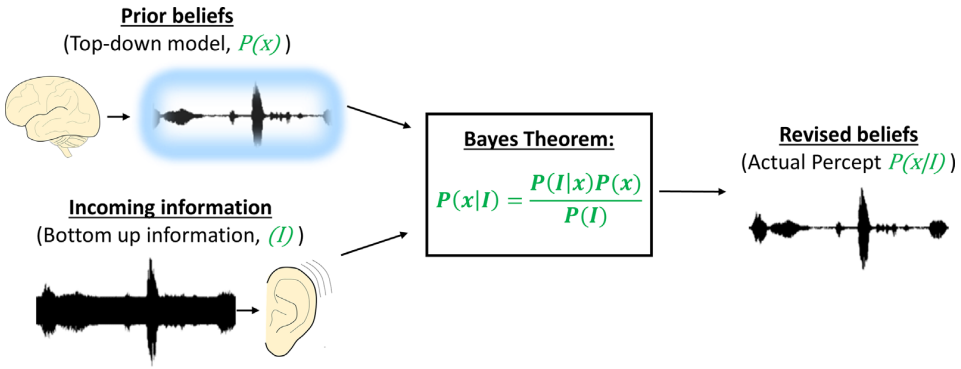

FIGURE 2 | Illustration of the principles of Bayesian inference in neuronal coding. Top-down pre-conceived notions about a sound (illustrated as a sound trace surrounded by a blue haze) are combined with noisy information from the periphery (illustrated as a noisy sound trace entering the ear). Bayes theorem (in the box) combines the pre-conceived notions with the noisy sensory information to recover the original signal (here represented as the posterior probability or the actual percept.

the noise from the environment is Gaussian. Further, any noise imparted by the internal state itself is pairwise uncorrelated to the noise of the sensor. This filter was used in an early model of hierarchical predictive coding in the visual system that, when trained on natural images, recapitulated some of the receptive field properties of early visual cortical neurons (Rao and Ballard, 1997). The model itself applies an extended form of the Kalman filter, capable of learning and prediction, with the learning rule obtained by the expectation-maximization (EM) algorithm formulated to mimic Hebbian learning. It can be shown that under Gaussian conditions that the Kalman filter is equivalent to the Bayes filter (Chen, 2003). A similar model to the extended Kalman filter initially proposed by Rao and Ballard (1997) has implemented a generative dynamical system in place of the Kalman filter to caputre nonlinearities of neural activation, and a learning scheme that takes into account the extra-classical effects experimentally observed in the visual system (Rao and Ballard, 1999).

Under non-Gaussian conditions, a more general implementation approach that has been used is the particle filter, as proposed by Lee and Mumford (2003). The calculations between the Kalman filter and particle filter are not similar, as the particle filter generates the likelihood weighting of states from the input and previous weights, followed by resampling of the input. While the Kalman filter is expressed by a linear operation, particle filters are constructed similarly to Markov chains to estimate the state of a given observation. The difference is that the dimensionality of the model is reduced by only looking at a weighted probability of being at a state instead of the total probability. This requires sampling a portion of the complete observation and estimating the weighted probability of the object being at some state. Subsequent re-sampling is performed with the weighted probabilities fed back into the model to more confidently estimate the state. In Lee and Mumford's influential 2003 article, the authors introduce a concept of a particle filter-based model that hypothesizes that cortical connections are responsible for the calculations but interact in a way where each neuron represents specific events in the external world (i.e., features of an object; Lee and Mumford, 2003). It is described as a generative model, calculating the likelihood of the state hierarchically. Single neuron activation indicates a specific event in the external environment. The external environment shows the co-activation of specific patterns, and the state of the hidden variable depends on the state at the previous time step. Synchronized activity in a population of neurons contributes to the image. Here, the activity of superficial pyramidal cells correspond to the bottom-up messages, and the deeper pyramidal cells reflect top-down messages. Current state is conditionally independent of other past states.

NEURAL MODELS OF TOP-DOWN MODULATION

Neural models employed in predictive coding algorithms have relied heavily on descending connections between cortical areas. For example, in an early large-scale iterative model of visual cortico-cortical interactions that implemented predictive coding, a hierarchical network was proposed, with the lowest level focusing on a small portion of the image (local image patches) at a short time scale, and each subsequent level in the hierarchy representing increasing feature complexity such as larger spatial and time scales (Rao and Ballard, 1999). In this model, it was argued that each level in the hierarchy first starts at the inputs from the visual thalamus to the primary visual cortex (V1). Similarly, the hierarchical structure proceeds from V1 into the secondary visual cortex (V2). Here, each level receives an input and estimates the object from its input. This estimate is calculated by a predictive estimator, learned from images the estimator is trained to, by a Kalman filter or generative system. It is argued in this model that this estimation is calculated *via* cortico-cortical connections in V1. Next, the model predicts the object at the next time step and conveys a predicted feature back to lower structures *via* descending cortical pathways. The usefulness of this hierarchical network model was established by its capacity to predict numerous types of neural and behavioral responses in the visual system. These include features such as: (1) distinguishing

a learned image from occluding objects (i.e., bottle partially occluding an image of a hand) and background noise added to the image; (2) predicting a sequence of images; (3) end stopping; and (4) other "extra-classical" receptive field effects (Rao and Ballard, 1999).

Establishing a neural implementation of predictive coding schemes has been challenging. At a minimum, one needs "prediction neurons" (or circuits) that provide a top-down signal and "prediction error neurons" (or circuits) that provide a bottom-up signal. In the context of the cerebral cortex, given the layer-specific directionality of cortical hierarchies (Rockland and Pandya, 1979; Felleman and Van Essen, 1991), prediction neurons would likely be found in the sources of descending connections: cells in layers 5 and 6. Since these cells project to layers 2 and 3 of areas lower in the sensory hierarchy, one would expect that supragranular layers would then contain prediction error neurons, as has been proposed previously (Bastos et al., 2012; Shipp, 2016). An important component of this basic circuit is the weighting of evidence from either bottom-up or top-down signals. For example, for highly reliable sensory signals, top-down predictions should carry less weight, while in situations of high sensory ambiguity (e.g., discerning a weak sound in noise), top-down signals should carry more weight. Most sensory systems do not have the luxury of repeatedly sampling the environment to determine the reliability of signals, but can estimate it based on saliency cues. It may be that neuromodulatory inputs (e.g., from cholinergic or monoaminergic fibers) can carry such a signal to dial up or down the reliance on top-down cues and thus adjust the "Kalman gain" of top-down modulation (**Figure 3**). Thus, sensory perception becomes a balance between reliance on top-down cues and bottom-up sensory saliency, as has recently been described human audition experiments (Huang and Elhilali, 2020). The over-reliance on top-down cues (possibly associated with disrupted neuromodulatory signals) may underlie pathophysiological states, such as the presence of delusions and hallucinations (Adams et al., 2014; Sterzer et al., 2018).

Physiological evidence for predictive coding at the single-neuron level has been observed in the visual cortex. Work in the late 1990s and early 2000s established that neurons in the early visual cortex of primates were sensitive to stimulus context and illusory signals (e.g., shape from shading or illusory contours in Kanizsa figures) and that these responses generally came after their response onsets (consistent with the time needed for feedback) and that the delayed responses were more characteristic of neurons from regions higher in the processing hierarchy (Lamme, 1995; Lee and Nguyen, 2001; Lee et al., 2002). Active silencing of descending connections from secondary visual areas can also eliminate surround suppressive effects, including end-stopping in V1 (Nassi et al., 2013), as proposed by Rao and Ballard (1999). More recent work has established similar patterns in the face-selective regions of the monkey temporal cortex (Schwiedrzik and Freiwald, 2017; Issa et al., 2018). In rodents, primary visual cortex neurons demonstrating responses to predictable stimuli, in advance of those stimuli, likely related to top-down signals from the cingulate cortex, have been identified

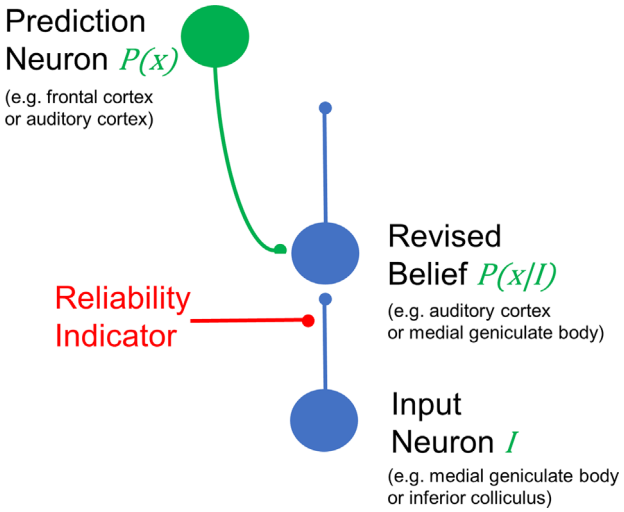

FIGURE 3 | Generic example of the simplest circuit to involve top-down modulation to implement Bayesian predictive coding. A top-down projection (in green) carries the predictive signal [$P(x)$] from **Figure 2**. Such a signal could be derived, for example, from the frontal cortex or auditory cortex. This descending input is combined with weighted information from the periphery (represented as I) at an intermediate structure, such as the auditory cortex or medial geniculate body, using the examples provided above. Using this same scheme, I would be derived from the medial geniculate body or inferior colliculus. The weighting is determined by the reliability of the signal, conceived as a presynaptic input onto the input terminals. Neurophysiologically, this reliability signal could be represented by cholinergic or monoaminergic inputs that scale with arousal or attention. Note that this generic model is not limited to the structures listed on the figure, which are given as examples.

(Fiser et al., 2016). These data all suggest that neurons in both the early- and late-visual cortex receive inputs from higher regions in the visual hierarchy that confer inferential properties upon those neurons.

However, applying these or other physiological data to a predictive coding model faces several challenges. First, as outlined above, cortical connectivity patterns in the primate brain imply that prediction neurons should be found infragranularly, and prediction error neurons should be found supragranularly (as has been proposed; Bastos et al., 2012; Shipp, 2016). Accepting the notion that we could recognize a "prediction neuron" when we see it (Kogo and Trengove, 2015), it is not clear from the physiological literature that there are differences in prediction error sensitivity in the upper vs. lower layers of the auditory cortex. For example, Atencio and Schreiner observed marked differences between granular and not-granular layers in terms of their representation of sound across multiple dimensions in the cat, but no indication that prediction-type neurons resided in infragranular layers or that prediction error was represented supragranularly (Atencio et al., 2009). Another study that observed suppression of motor-related prediction signals found that prediction error signals were found to be represented in the deep layers (Rummell et al., 2016), which is the opposite of that described by current canonical models of predictive coding (Bastos et al., 2012). Second, the

general approach of subtracting away predictions implies that top-down projections should synapse on inhibitory neurons primarily—an idea for which there is little evidence—and that neural responses are smaller for predicted stimuli than for unpredicted stimuli. Regarding the former point, most work has revealed that descending intracortical projections form synapses on excitatory neurons and predominantly produce excitation (Johnson and Burkhalter, 1996; Shao and Burkhalter, 1996). Regarding the latter point, behavioral studies suggest that when ambiguous stimuli are congruent with expectations, behavioral performance is enhanced. Taken to its logical extent, the subtractive formulation of predictive coding implies that perfect predictions, which produce optimal behavior, *are associated with no neural responses*.

Most predictive coding schemes postulate that top-down predictions subtract from lower-level processors, leaving behind that which is not predicted—the prediction error. This scheme suggests that peripheral neurons are primarily responding to prediction errors—that which we do not predict. However, our behavior is just the opposite—we tend to ignore sensory data that do not fit into our predictions about the world. Thus, although predictive coding schemes that rely on the concept of prediction error can reproduce the responses of peripheral neurons, they do a poor job of explaining perception. We note that motor prediction may be a special case where subtraction is needed to remove the expected sensory consequences of actions (e.g., to suppress acoustic responses to vocalizations; Eliades and Wang, 2003), and here top-down motor-auditory circuits have been found to synapse on inhibitory interneurons (Nelson et al., 2013). More recent formulations have modified predictive coding algorithms to not include the subtraction operation for this reason (discussed in Spratling, 2017). Finally, predictive coding models have virtually ignored the massive sets of descending connections from the cortex that target subcortical regions, which have a very natural hierarchical organization. In the following sections, we explore the degree to which predictive coding models may be applied to the auditory corticofugal system.

EARLY VS. LATE TOP-DOWN MODULATION

As described above, most previous work on predictive coding in the auditory system has focused on the cerebral cortex. Corticocentric views of predictive coding have been driven by the fact that most of the relevant work on top-down modulation has been done in humans, where the techniques that are commonly used, EEG, MEG, and functional magnetic resonance imaging (fMRI), are most suited to measure activity in the cortex. Even though activity in subcortical structures may be seen in fMRI studies, they require appropriate hemodynamic response functions and often motion-correction procedures not needed for cortex, leading to the general absence of analysis of the subcortical activity in speech and language studies, as we have argued previously (Llano, 2013; Esmaeeli et al., 2019). However, there are massive projections to subcortical structures at all levels of the auditory system and these have been documented for at least 100 years (Held, 1893). For example, in the visual system (the only system to our knowledge where such an analysis has been done) descending projections from the visual cortex outnumber ascending projections to the thalamus by at least 3-fold (Erişir et al., 1997). Beyond descending control to the thalamus, there are projections from the auditory cortex to the inferior colliculus (Fitzpatrick and Imig, 1978; Winer et al., 1998; Bajo and Moore, 2005; Bajo et al., 2007; Bajo and King, 2013; Torii et al., 2013; Stebbings et al., 2014), from the thalamus to the inferior colliculus (Kuwabara and Zook, 2000; Senatorov and Hu, 2002; Winer et al., 2002; Patel et al., 2017), from the inferior colliculus to the superior olive and cochlear nucleus (Conlee and Kane, 1982; Caicedo and Herbert, 1993; Saldaña, 1993; Vetter et al., 1993; Malmierca et al., 1996; Schofield, 2001; Groff and Liberman, 2003) and from the superior olive to the inner and outer hair cells in the cochlea (Liberman and Brown, 1986; Guinan, 2006). Thus, manipulations at the level of the auditory cortex, *via* these cascading descending projections, can, and have been shown to, substantially influence processing at the level of the cochlea (León et al., 2012). Indeed, early work established attentional effects at the level of single units in the cochlear nucleus in cats (Hernandez-Peon et al., 1956). Analogous projections from the sensory cortex to the sensory periphery have been identified in other sensory systems as well (see **Figure 4**), suggesting that early filtering in sensory systems may be a general principle for top-down modulation.

Other investigators have proposed potential advantages to the application of top-down modulation at the early (subcortical) processing stage, rather than later (cortical) processing stages (He, 2003a). For example, seminal work by Broadbent suggested an early filtering mechanism based on the apparent loss of information that was ignored during a dichotic listening task (Broadbent, 1958). Modifications to this theory to account for some retention of information filtered at an early stage were also proposed (Treisman, 1964). Most recently, a "new early filter model" was proposed by Marsh and Campbell (2016) which postulated that long-range corticofugal-corticopetal (ascending) loops may be responsible for early filtering of signals at the level of the brainstem (Marsh and Campbell, 2016) and that a tradeoff may exist between early and late filtering depending on task requirements. For example, very challenging attentional tasks or tasks that require very rapid processing of information may be better suited for an early filtering process (Giard et al., 2000). Also, tasks that require filtering based on features that are lost as information ascends the sensory hierarchy (e.g., fine temporal structure) may also be optimally filtered before those representations being lost (Marsh and Campbell, 2016). Importantly, however, top-down modulation in speech processing occurs at multiple levels of abstraction and at multiple time scales, some requiring higher-level filtering. For example, top-down information may come in the form of lexical cues (operating over ms) or prosodic cues (operating over ms to seconds) as well as other dimensions, such as using low-level cues such as voice familiarity vs. high-level pragmatic cues (Obleser, 2014). Thus, late (cortical) and early (subcortical) modulation may play complementary roles in top-down modulation during active listening.

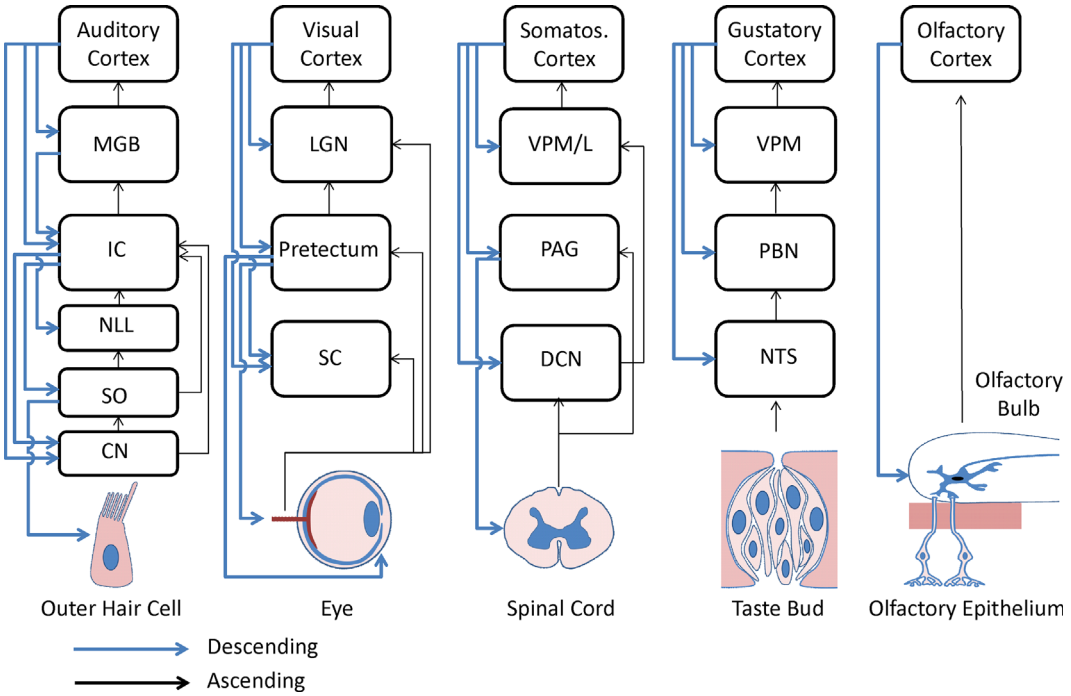

FIGURE 4 | Diagram of known corticofugal and other subcortical descending projections across sensory systems. Black arrows, bottom-up projections; Blue arrows; top-down projections; CN, cochlear nuclei; DCN, dorsal column nuclei; IC, inferior colliculus; LGN, lateral geniculate nucleus; MGB, medial geniculate body; NLL, nuclei of the lateral lemniscus; NTS, nucleus tractus solitarius; PAG, periaqueductal gray; PBN, parabrachial nuclei; SC, superior colliculus; SO, superior olive; VPL, ventral posterior lateral nucleus of the thalamus; VPM, ventral posterior medial nucleus of the thalamus. Taken with permission from Lesicko and Llano (2017).

METHODOLOGICAL ISSUES IN TOP-DOWN MODULATION IN THE SUBCORTICAL AUDITORY SYSTEM

Here we review methodological issues surrounding the study of descending projections from the auditory cortex to subcortical structures to effectuate top-down auditory control described above. It is worth noting that "descending projections" are not synonymous with top-down control. It is possible that lateral interactions within a brain structure (Srinivasan et al., 1982) can produce contextual modulation, as discussed in Rao and Ballard (1999) and Aitchison and Lengyel (2017). Here, we focus on corticofugal projections in keeping with the theme of this Special Issue on Cortical-Subcortical Loops in Sensory Processing.

Experimental paradigms for studying the corticofugal system have technical challenges that must be considered when analyzing the resulting data. Classical approaches include measuring response properties in a subcortical nucleus, then silencing the auditory cortex by cooling it or applying GABAergic agonists, and then re-measuring those properties. This paradigm is limited by: (1) incomplete recovery of cortical responses with certain GABAergic agents (Bäuerle et al., 2011); (2) lack of specificity of which layer (layer 5 or layer 6 corticofugal neurons) is silenced; (3) lack of specificity about which frequency ranges across the tonotopic axis of the auditory cortex are silenced; and (4) lack of knowledge if the effects of silencing are on the brain structure being studied (e.g., thalamus or inferior colliculus) or related to changes in the input to that structure from the cochlea, which is known to be impacted by cortical silencing (León et al., 2012). Regarding layer of origin, previous work has shown that both layers 5 and 6 project to the auditory thalamus and inferior colliculus (Games and Winer, 1988; Ojima, 1994; Künzle, 1995; Doucet et al., 2003; Bajo and Moore, 2005; Coomes et al., 2005; Llano and Sherman, 2008; Schofield, 2009; Slater et al., 2013, 2019), and that these projections have different physiological properties (Llano and Sherman, 2009; Slater et al., 2013) and likely different impacts on their target structures. Layer 5 cells have "driver"—type effects and layer 6 cells have "modulator"—type effects (for review see Lee and Sherman, 2010). Therefore bulk silencing is likely to homogenize the impacts of what could be quite different effects of these projections on their target structures. Likewise, work done using focal stimulation of the auditory cortex (reviewed in "Evidence That Auditory Corticofugal Systems Engage in Predictive Coding" section) suggests that corticofugal systems have markedly frequency-specific (in terms of the tonotopic axis) effects on their target structures, such that stimulation of neurons in certain frequency ranges can enhance, and others can suppress, subcortical responsiveness. Therefore, bulk silencing may produce a mixture of effects that are difficult to interpret. More modern approaches using viral-mediated delivery of optogenetic probes may solve some of these problems by permitting cell-type specific (Blackwell et al., 2020), layer-specific activation or silencing, and will permit activation

or silencing to occur at the level of terminals, diminishing the likelihood of indirect effects stemming from changes in cochlear function.

Activating corticofugal projections with electrical stimulation has also been used in many studies, but also has potential methodological pitfalls. Specific to the auditory thalamus, electrical stimulation may antidromically activate thalamocortical neurons, which may then activate other structures, such as the thalamic reticular nucleus, whose neurons project back to the dorsal thalamus, leading to indirect effects. Importantly, the specific protocol of electrical stimulation may make a large difference in the impact on subcortical neurons. Small changes in the relative timing of cortical vs. acoustic stimulation, relative amplitudes, pulse rates, etc, can change responses from excitatory to inhibitory, even with optogenetic stimulation (Guo et al., 2017; Vila et al., 2019). Also, many studies have used stimulation paradigms that are really perceptual learning paradigms. That is, by repeatedly stimulating the corticofugal fibers and observing a change in tuning in a target structure, one is no longer only studying on-line modulation of sensory responses based on prior knowledge, but instead is studying the impact of tetanic stimulation of corticofugal fibers on synaptic plasticity in the target structure. Finally, much of the early work done on corticofugal modulation has been done on anesthetized animals. We know from work in human subjects that top-down projections appear to be particularly vulnerable to anesthesia or other factors that alter consciousness (Boly et al., 2011; Raz et al., 2014; reviewed in Sikkens et al., 2019), and thus may not be adequately studied in an anesthetized animal.

EVIDENCE THAT AUDITORY CORTICOFUGAL SYSTEMS ENGAGE IN PREDICTIVE CODING

The auditory cortex sends massive projections to the auditory thalamus (and related thalamic reticular nucleus), the inferior colliculus, and the cochlear nucleus. The projections to the thalamus and inferior colliculus emanate from layers 5 and 6, while those to the cochlear nucleus appear to only emanate from layer 5. It is not yet known whether there is a single layer 5 system that projects to all subcortical nuclei, though evidence exists for the presence of individual layer 5 cells that branch to the auditory thalamus and inferior colliculus (Asokan et al., 2018). Early work suggests that the layer 5 projections to the inferior colliculus and cochlear nucleus are independent (Doucet et al., 2003), though it should be noted that the double-backlabel technique used in this study is prone to false negatives if the two tracers are not placed into physiologically-matched zones in each structure. The layer 6 projections to the auditory thalamus and inferior colliculus are likely at least partially independent since they are found in different sublayers of layer 6 (Llano and Sherman, 2008; Slater et al., 2013; Stebbings et al., 2014).

The auditory corticothalamic system is massive, develops early, before hearing onset (Torii et al., 2013), elicits responses in the majority of MGB neurons (Ryugo and Weinberger, 1976; Villa et al., 1991; He et al., 2002) that are strong enough to induce immediate-early gene expression (Guo et al., 2007; Sun et al., 2007), produces both short (2 ms) and long (hundreds of milliseconds) latency responses (Serkov et al., 1976) and elicits both excitation (the dominant response in the lemniscal ventral subdivision) and inhibition (likely mediated *via* the thalamic reticular nucleus; Amato et al., 1969; He, 1997, 2003b; He et al., 2002; Xiong et al., 2004; Yu et al., 2004; Zhang et al., 2008). Activation of corticothalamic fibers can adjust tuning and sensitivity of auditory thalamic neurons (Guo et al., 2017) and appears to be critical for performance in perceptually-challenging tasks (Happel et al., 2014; Homma et al., 2017), as well as for directing plastic changes that occur in the thalamus (Zhang and Yan, 2008; Nelson et al., 2015). Importantly from the predictive coding perspective, corticothalamic projections appear to be organized topographically (Takayanagi and Ojima, 2006), such that cortical and thalamic areas that are matched for best frequency tend to produce corticothalamic excitation, while those that are unmatched tend to produce inhibition (He, 1997; He et al., 2002). Also, auditory thalamic neurons have been shown to be strongly sensitive to local stimulus predictability (Anderson et al., 2009; Antunes et al., 2010; Richardson et al., 2013; Cai et al., 2016), suggesting that they play a role in the coding of expectancy.

Several key experiments have been done to investigate the potential for corticothalamic fibers to contribute to predictive coding. One commonly-employed paradigm has been to apply repetitive stimulation of the auditory cortex to simulate a repeated acoustic motif and then to measure tuning properties to various parameters (sound frequency, combination-sensitivity, et cetera) before and after cortical stimulation. A consistent finding in the thalamus (and indeed in the inferior colliculus and cochlear nucleus, as described in the following paragraphs) is that stimulation of corticofugal fibers induces a shift of tuning of thalamic neurons towards the tuning of the particular region of the auditory cortex (so-called "egocentric selection"; Yan and Suga, 1996; Zhang et al., 1997; Zhang and Suga, 2000). From a Bayesian perspective, these data suggest that corticothalamic fibers contain "priors" such that the presence of highly prevalent stimuli (simulated by electrical cortical stimulation) makes it more likely that more peripheral responses in the thalamus, midbrain, or cochlear nucleus (i.e., posterior probabilities) are biased to respond more strongly to stimuli that are more likely to exist in the environment. The repeated stimulus presentation may be utilized to expand the cortical representation of Bayesian priors (Köver and Bao, 2010). As outlined in the "Methodological Issues in Top-Down Modulation in the Subcortical Auditory System" section, this paradigm falls short of establishing that corticothalamic fibers provide predictive coding signals because of the myriad problems with electrical cortical stimulation of the cortex, and because of the lack of establishment that acoustic stimuli use corticothalamic fibers to implement a predictive coding in the thalamus. Conversely, although it is well-established that training to alter the salience of an acoustic stimulus will shift neuronal tuning curves to be more responsive to that stimulus (Fritz et al., 2003), it remains to be established that the shift in tuning is caused by corticofugal projections.

An alternative approach has been to implement "surprise" paradigms, similar to MMN described in humans. The analogous finding at the single-unit level is known as stimulus-specific adaptation (SSA). In SSA, neurons diminish their responsiveness to repeated stimuli but retain their responsiveness to unexpected stimuli (Ulanovsky et al., 2003). Although it has been argued whether SSA is the neuronal-level instantiation of MMN (Farley et al., 2010; Carbajal and Malmierca, 2018), for our purposes, it is sufficient to state that SSA clearly reflects a key component of predictive coding: suppression of responses to predicted, presumably irrelevant stimuli. SSA has been established to exist in MGB neurons (Anderson et al., 2009; Antunes et al., 2010; Richardson et al., 2013; as well as neurons in the nonlemniscal inferior colliculus, below). Reversible silencing of corticothalamic fibers does not eliminate thalamic SSA, though it does alter other basic properties, suggesting that corticothalamic fibers play a strong role in modulating the thalamus, but may not confer SSA-sensitivity upon the thalamus (Antunes and Malmierca, 2011). We note that more aggressive nonreversible suppression diminishes thalamic SSA (Bäuerle et al., 2011), however, the significance of this finding is uncertain in the absence of reversibility of the cortical lesion.

We also note that the findings of SSA, and the paradigm employed by Suga and colleagues showing egocentric selection, are essentially orthogonal findings. That is, SSA represents the elimination of a predictable (presumably irrelevant) signal while the Suga paradigm represents the enhancement of a repeated, presumably behaviorally-important, signal. Evidence for both repetition suppression and repetition enhancement have been seen in the human subcortical auditory system (May and Tiitinen, 2010; Skoe and Kraus, 2010), though the latter is more in line with Bayesian notions of predictive coding. Thus, the data demonstrating egocentric shifts in thalamic receptive field properties suggest that corticothalamic projections may play an important role in providing a set of priors to thalamic neurons to bias their response properties, but may not be involved in repetition suppression manifesting as SSA.

The corticocollicular system emanates primarily from layer 5 of the auditory cortex with a smaller component from layer 6 (Games and Winer, 1988; Künzle, 1995; Doucet et al., 2003; Bajo and Moore, 2005; Coomes et al., 2005; Schofield, 2009; Slater et al., 2013, 2019), and primarily targets the nonlemniscal portions of the inferior colliculus, grouped here as the lateral cortex and dorsal cortex (Saldaña et al., 1996; Winer et al., 1998). In the lateral cortex, the auditory projections interdigitate with somatosensory projections in a manner that is determined by neurochemical modules present in the lateral cortex (Lesicko et al., 2016). Electrical stimulation of the auditory cortex produces collicular responses with latencies as short as 1–2 ms (Mitani et al., 1983; Sun et al., 1989) and produces both excitation and inhibition (Mitani et al., 1983; Sun et al., 1989; Bledsoe et al., 2003; Markovitz et al., 2015). The projections are tonotopic (Lim and Anderson, 2007; Markovitz et al., 2013; Barnstedt et al., 2015) and the inhibition is presumably at least disynaptic because the corticocollicular system is thought to be excitatory (Feliciano and Potashner, 1995), and the suppression occurs in the later phases of the response (Popelář et al., 2015). Corticocollicular fibers are responsible for protean functions at the level of the inferior colliculus, including facilitating adaptive changes in inferior colliculus neurons (Zhang et al., 2005; Wu and Yan, 2007; Bajo et al., 2010; Robinson et al., 2016; Asokan et al., 2018), sharpening of frequency tuning (Blackwell et al., 2020) and elicitation of escape responses (Xiong et al., 2015).

In terms of predictive coding, similar experiments to those done in the corticothalamic system have been done in the corticocollicular system but, in some cases, with a broader range of stimulus manipulations. For example, electrical stimulation of the auditory cortex causes egocentric shifts across multiple stimulus parameters, including frequency, duration, combination-sensitivity, sound location, and sound threshold (Yan and Suga, 1996, 1998; Jen et al., 1998; Ma and Suga, 2001; Yan and Ehret, 2001, 2002; Jen and Zhou, 2003; Yan et al., 2005; Zhou and Jen, 2005, 2007). These data suggest that the auditory cortex actively adjusts the tuning of collicular neurons to bias the response property across multiple computed stimulus dimensions and is not just inherited as part of the basic tonotopic layout of the two structures. Thus, a whole family of Bayesian priors (not unlike the family of hypotheses employed in particle filtering) can be used to modify the inferior colliculus. One challenge in understanding the corticocollicular findings is that most of the studies have involved recordings in the central nucleus of the inferior colliculus, which receives a small number of corticocollicular projections compared to the nonlemniscal regions. One potential resolution is that corticocollicular projections to the lateral cortex may have cascading inhibitory projections to the central nucleus after providing glutamatergic inputs to the lateral cortex, thus leading to primary inhibition in the central nucleus (Jen et al., 2001).

SSA has been observed in the dorsal and lateral cortices of the inferior colliculus (Malmierca et al., 2009; Duque et al., 2012), and it is thought that this is the earliest level that SSA occurs in the auditory system (Duque et al., 2018). Similar to the thalamus, reversible deactivation of the auditory cortex did not eliminate SSA in the inferior colliculus (Anderson and Malmierca, 2013). Thus, corticocollicular projections provide a strong predictive signal, possibly corralling inhibition from the lateral cortex en route to the central nucleus, to shift the tuning of collicular neurons towards those of previously heard stimuli. In contrast, suppression of repetitive irrelevant stimuli used in SSA appears to not involve these projections.

The auditory cortex also projects to the nuclei of the caudal auditory brainstem: cochlear nucleus, nucleus sagulum, and superior olivary nuclei (Feliciano and Potashner, 1995; Doucet et al., 2002; Meltzer and Ryugo, 2006), reviewed in Saldaña (2015). Compared to thalamic and collicular projections, comparatively little work has been done on these projections concerning predictive coding and all of it has been done in the cochlear nucleus. That said, all of the studies that have been done that measure tuning properties before and after focal cortical stimulation have revealed the same egocentric selection process described above for corticothalamic and corticocollicular neurons (Luo et al., 2008; Liu et al., 2010; Kong et al., 2014).

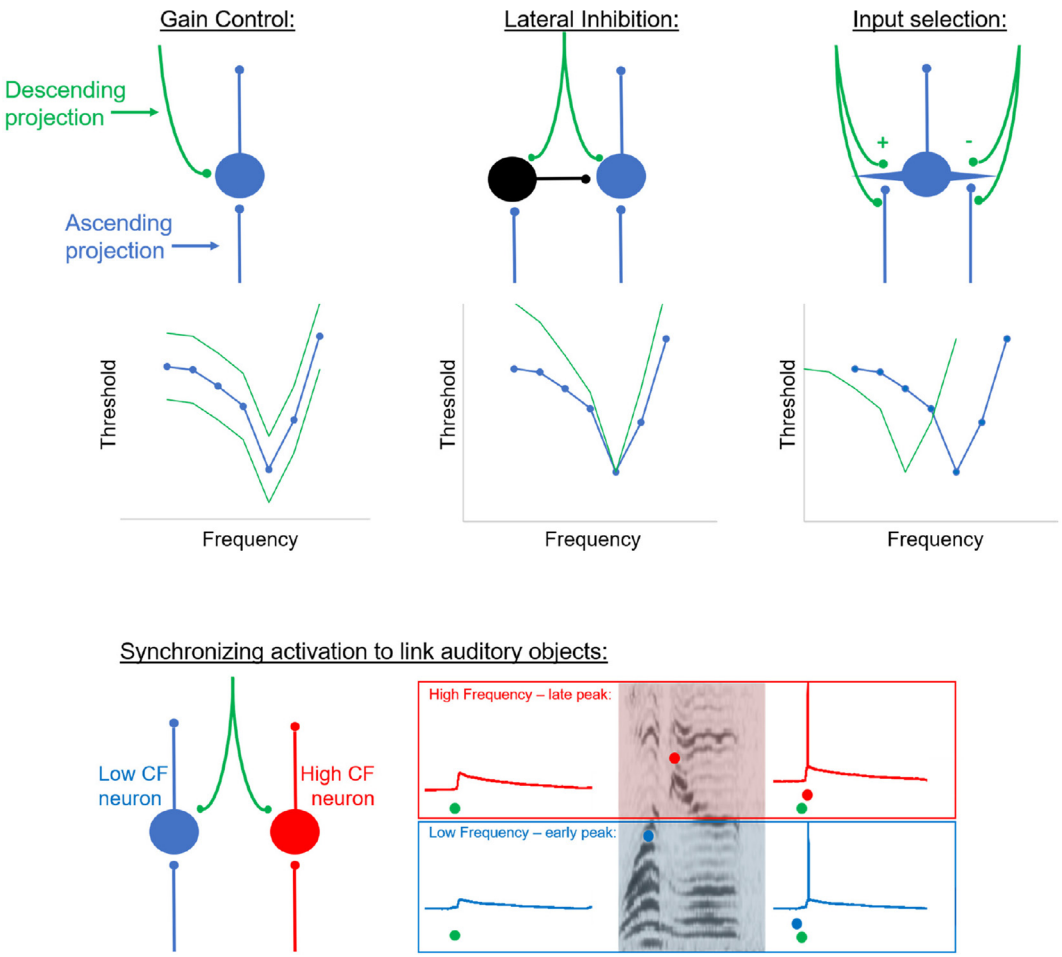

FIGURE 5 | Putative circuit motifs that can implement top-down modulation of frequency receptive fields using descending projections. Green tuning curves represent the modified tuning curves after descending projections were activated. Left, the simplest "gain control" motif whereby top-down projections dial the responsiveness of target cells up or down, thus shifting the frequency tuning curve up or down. Middle, a lateral inhibition motif, whereby descending input inhibits inputs representing frequencies other than the characteristic frequency. In this case, the tuning curve would sharpen. Right, an input selection motif, where top-down inputs would either enhance (denoted with a "+") or suppress (denoted with a "−") certain classes of inputs either pre-or post-synaptically. In doing so, the top-down projections could eliminate inputs from what was the previous characteristic frequency and thus shift the tuning curve laterally. Bottom corresponds to descending inputs synchronously eliciting excitatory post-synaptic potentials (EPSPs) in two neurons of different characteristic frequencies. If a sound object has multiple frequency components peaking at different times (e.g., an early low-frequency peak and a later high-frequency peak, marked with blue and red circles on the spectrogram, respectively), then when those bottom-up inputs arrive at neurons with synchronized EPSPs, they are more likely to fire synchronous spikes, thus linking them as part of one auditory object. CF, characteristic frequency.

Notably, much of the early work on corticofugal modulation in animal models was done on echolocating bats (Yan and Suga, 1996, 1998; Zhang et al., 1997; Jen et al., 1998, 2001; Gao and Suga, 2000; Zhang and Suga, 2000; Ma and Suga, 2001). Although these mechanisms may be specific to echolocating bats due to their specialized behavioral requirements (Kössl et al., 2015), much of the key findings of the egocentric section have been seen in corticofugal projections non-echolocating species (Yan and Ehret, 2001, 2002; Yan et al., 2005; Luo et al., 2008; Liu et al., 2010; Kong et al., 2014). These data suggest that the basic principle of shifting tuning towards highly stimulated cortical representations is shared amongst both echolocating and non-echolocating species.

CIRCUIT-LEVEL MECHANISMS OF CORTICOFUGAL TOP-DOWN CONTROL

Virtually all work to date on corticofugal modulation in the auditory system has been done at the level of phenomenology without circuit-level analysis. Interestingly, corticothalamic, corticocollicular, and corticobulbar projections all appear to have similar effects on their targets—they produce egocentric modifications of receptive fields after repetitive stimulation. This similarity suggests a common neural substrate may exist across these projections. The layer 5 corticofugal system is common to these projections, and thus may be a potential candidate. Layer 5 corticofugal neurons have similar properties across regions of the cortex. They are large pyramidal cells with long and

tufted apical dendrites that burst intrinsically when depolarized (Connors et al., 1982; Kasper et al., 1994; Hefti and Smith, 2000; Llano and Sherman, 2009) and receive direct inputs from the thalamus (Constantinople and Bruno, 2013; Slater et al., 2019). In the corticothalamic system, these axons end in large terminals that synapse on proximal dendrites, producing "driver" type responses (Reichova and Sherman, 2004; Prasad et al., 2020). As described above, auditory corticothalamic terminals branch to the inferior colliculus (Asokan et al., 2018), but corticocollicular axons apparently do not branch to the cochlear nucleus (Doucet et al., 2003). In this respect, the layer 5 auditory corticothalamic system may diverge from other corticofugal systems where widespread subcortical branching is seen (Bourassa et al., 1995; Deschenes et al., 1996; Kita and Kita, 2012), reviewed in Usrey and Sherman (2019). Future work with sensitive tracers will clarify the extent to which a single auditory layer 5 "broadcast" neurons exist that send similar training signals to auditory thalamus, inferior colliculus and cochlear nucleus. Alternatively, given the homogenous nature of the changes seen across these three auditory nuclei, and the potential for auditory cortex stimulation to alter ascending information flow from the cochlea (León et al., 2012), these changes may be, in part, caused by alterations in shared ascending auditory information. We note that layer 6 projections to the thalamus are more numerous than layer 5 projections but tend to have smaller and more distal terminals (Lee and Sherman, 2010), and relay inhibition through the thalamic reticular nucleus (Lam and Sherman, 2010). Layer 6 corticocollicular projections also emanate from smaller neurons than layer 5 and have thinner neuronal projections and end in smaller terminals (Yudintsev et al., 2019). These data suggest that the layer 6 system may operate on a slower time scale, and is more likely to engage inhibitory interneurons, and thus may have a different set of functions than the layer 5 system that has yet to be identified.

The synaptic mechanisms by which auditory corticofugal projections modulate response properties are unknown, but several limitations based on previous extracellular recording studies exist. For example, to effectuate a change in tuning to sound frequency, a significantly more sophisticated operation than "gain control" must take place. To induce a neuron to respond to a frequency of sound to which it was not previously responsive over a matter of minutes, there must have existed a population of latent (i.e., inactive) inputs that are responsive to those frequencies. Conversely, a population of synapses encoding previously-responsive sounds would need to be silenced. Although inhibitory/disinhibitory mechanisms may create these types of shifts and do appear to play a role in the corticocollicular system, a small fraction of the corticocollicular system (4%) synapses on inhibitory interneurons (Nakamoto et al., 2013). An alternative mechanism could be to strengthen or weaken synapses without the use of inhibition. Repetitive, tetanic stimulation of a focal area of the auditory cortex has been well-established to alter receptive field properties of that area of the cortex (Ohl and Scheich, 1997, 2005; Weinberger, 2004). Repetitive acoustic stimulation may also decrease the representation of that sound in the auditory cortex, depending on the behavioral salience of that sound (Condon and Weinberger, 1991). It is therefore possible that descending connections could strengthen synapses post-synaptically, though in the absence of an appropriately timed ascending signal would appear to be a non-Hebbian mechanism to induce a plastic change. Descending projections could also target presynaptic terminals to either activate them or diminish their strength, as suggested by early work in the visual system (Iwama et al., 1965), see **Figure 5**. However, at least in the auditory corticocollicular system, little evidence for presynaptic terminals exists in the corticocollicular or auditory corticothalamic system (Bartlett et al., 2000; Nakamoto et al., 2013). Beyond impacts at the level of individual cells, corticofugal projections may influence a population of cells to alter their likelihood of firing synchronously, as proposed previously (Gilbert and Li, 2013). Such a mechanism would be ideally suited to either integrate disparate pieces of information (as needed for contour integration, or phonemic restoration) or to segregate information (as needed during speech segmentation or stream segregation). For example, neural responses to a sound object with complex spectrotemporal properties with low and high-frequency peaks at different times may be linked into a singular perceptual object if descending projections synchronized subthreshold responses across an array of sensory neurons (**Figure 5**, bottom). Thus, unsynchronized responses from neurons with different characteristic frequencies at low levels of the hierarchy could be tagged as being derived from the same acoustic object by eliciting synchronized responses at higher levels of the hierarchy. Very little work of this type has been done, though it should be noted that inhibition of the corticothalamic system leads to greater synchrony of firing between thalamic neurons, suggesting that the corticothalamic system has the potential to enhance segregation between input streams (Villa et al., 1999). Similar findings were reported in the corticocollicular system by Nakamoto et al. (2010). Thus, multiple non-mutually exclusive synaptic motifs may help to explain the impact(s) of the corticofugal systems, and none have been systematically explored to date.

CONCLUSIONS AND FUTURE CHALLENGES

Top-down modulation is observed at the level of behavior and the level of the single neurons, and there is still much work left to be done to understand how these two levels of top-down modulation are linked. In our view, the weight of the evidence suggests that at least one role of descending projections is to modify receptive field properties to bias them towards frequently-occurring or highly salient stimuli. However, consistent with the anatomical and physiological heterogeneity of these systems, additional roles are possible. Complicating matters is the finding that these systems are often intermingled and individual projections may have more than one role. A challenge, then, in the field is how to design an experimental paradigm to identify the circuit motifs that produce top-down modulation and how they alter perceptual responses. The first step is to decide precisely what is being studied. The term "predictive coding" is broad enough to encompass many different types of processing. For example, the term is used to

describe both the "explaining away" of expected and ignored stimuli as well as the enhancement of expected but obscured stimuli. As described above, the computations underlying these two processes are not the same and do not appear to be handled by the same circuits. The other challenging experimental question is deciding which level of top-down modulation is to be studied.

There are many "descending systems" in the auditory system and many types of tasks that require top-down modulation. Descending projections extend from the frontal cortex to the auditory cortex and on to the cochlea, with a stop at every auditory subcortical structure along the way. Presumably, certain descending projections should be important for high-level modulation (e.g., using discourse cues to understand an ambiguous word) vs. low-level modulation (e.g., having a loud sound diminish the sensitivity of the cochlea to subsequent sounds). An additional dimension is task difficulty. That is, difficult tasks may require multiple descending projections to be involved, thereby altering the stimulus representation as soon as it enters the brain, and others may be less challenging, allowing later filtering, thus permitting several stimulus representations to "coexist" in the brain before one being selected. Therefore, engaging in a systematic process to identify which pathway is engaged during which task would be a starting point for future investigators.

Also, to facilitate comparisons across studies, it will be important for future experiments to specify the type and level of predictive coding being studied. Also, although electrical stimulation paradigms have provided insights about predictive coding by demonstrating that repetitive activation of a particular region of cortex can change the filtering properties of more peripheral sensory neurons (reviewed above), these changes typically have been found after long-term (minutes) tetanic stimulation of the corticofugal projections, which is a crude approximation to altering the statistical likelihood of a particular sound appearing in the environment. A more convincing demonstration would be to show that the tuning of a particular neuron changes dynamically, and under particular behavioral contexts (similar to that seen in Caras and Sanes, 2017) when the likelihood that a particular stimulus occurs changes. Besides, one would also anticipate that prediction neurons would have their strongest impact when peripheral signals are weak (i.e., the Kalman gain would be highest under these circumstances). Consistent with this idea, previous work has shown that top-down modulation tends to be strongest in broadly tuned neurons [presumably neurons with ambiguous frequency representations (Vila et al., 2019) or when acoustic stimulus amplitude is weak (Jen et al., 1998)]. It may be the case that neurons that are broadly tuned to isolated sounds may be more sharply tuned in other contexts. Also, future work should emphasize paradigms that alter stimulus expectancy without altering stimulus probability in awake animals [as used in Cai et al. (2016)], thus removing the bottom-up cue of stimulus probability. Finally, one experimentally pragmatic benefit of studying corticofugal systems is the physical separation between the descending system and the physical structure under study, allowing the examination of responses in putative "prediction axons" (presumably corticofugal) compared to bottom-up signals. This type of approach has been used in two-photon imaging of the visual system, where presumed prediction neurons in the anterior cingulate were labeled and their response properties appeared to carry prediction signals (Fiser et al., 2016). The use of this set of approaches would get us closer to understanding the unusual connectivity patterns described by Lorente de Nó almost 100 years ago (Lorente De Nó, 1933):

> *"The conception of the reflex arc as a unidirectional chain of neurons has neither anatomic nor functional basis. Histologic studies. . .show the universality of the existence of plural parallel connections and of recurrent, reciprocal connections."*

Thus, a deliberate approach using techniques to interrogate populations of neurons in awake animals will permit the understanding of the logic of highly recurrent systems whose roles have remained obscure for nearly a century.

AUTHOR CONTRIBUTIONS

AA and DL both wrote the manuscript together. All authors contributed to the article and approved the submitted version.

FUNDING

DL was supported by National Institutes of Health DC013073 and AG059103.

ACKNOWLEDGMENTS

We thank Drs. Donald Caspary, Manuel Malmierca, Tom Anastasio, Silvio Macias, and Brett Schofield for productive discussions about the contents of this review and Dr. Nathiya Vaithiyalingam Chandra Sekaran for translating assistance for the Held (1893) reference. We also thank Drs. Lionel Collet, Paul Délano, Xavier Perrot, and David Smith for permission and/or supplying high-resolution versions of their figures.

REFERENCES

Adams, R. A., Brown, H. R., and Friston, K. J. (2014). Bayesian inference, predictive coding and delusions. *Avant* 5, 51–88. doi: 10.26913/50302014.0112.0004

Aitchison, L., and Lengyel, M. (2017). With or without you: predictive coding and bayesian inference in the brain. *Curr. Opin. Neurobiol.* 46, 219–227. doi: 10.1016/j.conb.2017.08.010

Amato, G., La, V. G., and Enia, F. (1969). The control exerted by the auditory cortex on the activity of the medial geniculate body and inferior colliculus. *Arch. Sci. Biol.* 53, 291–313.

Anderson, L. A., Christianson, G. B., and Linden, J. F. (2009). Stimulus-specific adaptation occurs in the auditory thalamus. *J. Neurosci.* 29, 7359–7363. doi: 10.1523/JNEUROSCI.0793-09.2009

Anderson, L. A., and Malmierca, M. (2013). The effect of auditory cortex deactivation on stimulus-specific adaptation in the inferior colliculus of the rat. *Eur. J. Neurosci.* 37, 52–62. doi: 10.1111/ejn.12018

Andersson, L., Sandberg, P., Olofsson, J. K., and Nordin, S. (2018). Effects of task demands on olfactory, auditory and visual event-related potentials suggest similar top-down modulation across senses. *Chem. Senses* 43, 129–134. doi: 10.1093/chemse/bjx082

Antunes, F. M., and Malmierca, M. S. (2011). Effect of auditory cortex deactivation on stimulus-specific adaptation in the medial geniculate body. *J. Neurosci.* 31, 17306–17316. doi: 10.1523/JNEUROSCI.1915-11.2011

Antunes, F. M., Nelken, I., Covey, E., and Malmierca, M. S. (2010). Stimulus-specific adaptation in the auditory thalamus of the anesthetized rat. *PLoS One* 5:e14071. doi: 10.1371/journal.pone.0014071

Asokan, M. M., Williamson, R. S., Hancock, K. E., and Polley, D. B. (2018). Sensory overamplification in layer 5 auditory corticofugal projection neurons following cochlear nerve synaptic damage. *Nat. Commun.* 9:2468. doi: 10.1038/s41467-018-04852-y

Atencio, C. A., Sharpee, T. O., and Schreiner, C. E. (2009). Hierarchical computation in the canonical auditory cortical circuit. *Proc. Natl. Acad. Sci. U S A* 106, 21894–21899. doi: 10.1073/pnas.0908383106

Bajo, V. M., and King, A. J. (2013). Cortical modulation of auditory processing in the midbrain. *Front. Neural Circuits* 6:114. doi: 10.3389/fncir.2012.00114

Bajo, V. M., and Moore, D. R. (2005). Descending projections from the auditory cortex to the inferior colliculus in the gerbil, meriones unguiculatus. *J. Comp. Neurol.* 486, 101–116. doi: 10.1002/cne.20542

Bajo, V. M., Nodal, F. R., Bizley, J. K., Moore, D. R., and King, A. J. (2007). The ferret auditory cortex: descending projections to the inferior colliculus. *Cereb. Cortex* 17, 475–491. doi: 10.1093/cercor/bhj164

Bajo, V. M., Nodal, F. R., Moore, D. R., and King, A. J. (2010). The descending corticocollicular pathway mediates learning-induced auditory plasticity. *Nat. Neurosci.* 13, 253–260. doi: 10.1038/nn.2466

Barnstedt, O., Keating, P., Weissenberger, Y., King, A. J., and Dahmen, J. C. (2015). Functional microarchitecture of the mouse dorsal inferior colliculus revealed through *in vivo* two-photon calcium imaging. *J. Neurosci.* 35, 10927–10939. doi: 10.1523/JNEUROSCI.0103-15.2015

Bartlett, E. L., Stark, J. M., Guillery, R. W., and Smith, P. H. (2000). Comparison of the fine structure of cortical and collicular terminals in the rat medial geniculate body. *Neuroscience* 100, 811–828. doi: 10.1016/s0306-4522(00)00340-7

Bastos, A. M., Usrey, W. M., Adams, R. A., Mangun, G. R., Fries, P., and Friston, K. J. (2012). Canonical microcircuits for predictive coding. *Neuron* 76, 695–711. doi: 10.1016/j.neuron.2012.10.038

Battaglia, P. W., Jacobs, R. A., and Aslin, R. N. (2003). Bayesian integration of visual and auditory signals for spatial localization. *J. Opt. Soc. Am. A Opt. Image Sci. Vis.* 20, 1391–1397. doi: 10.1364/josaa.20.001391

Bäuerle, P., Von Der Behrens, W., Kössl, M., and Gaese, B. H. (2011). Stimulus-specific adaptation in the gerbil primary auditory thalamus is the result of a fast frequency-specific habituation and is regulated by the corticofugal system. *J. Neurosci.* 31, 9708–9722. doi: 10.1523/JNEUROSCI.5814-10.2011

Blackwell, J. M., Lesicko, A. M. H., Rao, W., De Biasi, M., and Geffen, M. N. (2020). Auditory cortex shapes sound responses in the inferior colliculus. *eLife* 9:e51890. doi: 10.7554/eLife.51890

Bledsoe, S., Shore, S. E., and Guitton, M. (2003). Spatial representation of corticofugal input in the inferior colliculus: a multicontact silicon probe approach. *Exp. Brain Res.* 153, 530–542. doi: 10.1007/s00221-003-1671-6

Boly, M., Garrido, M. I., Gosseries, O., Bruno, M.-A., Boveroux, P., Schnakers, C., et al. (2011). Preserved feedforward but impaired top-down processes in the vegetative state. *Science* 332, 858–862. doi: 10.1126/science.1202043

Bourassa, J., Pinault, D., and Deschênes, M. (1995). Corticothalamic projections from the cortical barrel field to the somatosensory thalamus in rats: a single-fibre study using biocytin as an anterograde tracer. *Eur. J. Neurosci.* 7, 19–30. doi: 10.1111/j.1460-9568.1995.tb01016.x

Braga, R. M., Wilson, L. R., Sharp, D. J., Wise, R. J., and Leech, R. (2013). Separable networks for top-down attention to auditory non-spatial and visuospatial modalities. *NeuroImage* 74, 77–86. doi: 10.1016/j.neuroimage.2013.02.023

Bregman, A. S. (1994). *Auditory Scene Analysis: The Perceptual Organization of Sound*. Cambridge, MA: MIT press.

Broadbent, D. (1958). *Perception and Communication*. Elmsford, NY: Pergamon Press.

Cai, R., Richardson, B. D., and Caspary, D. M. (2016). Responses to predictable versus random temporally complex stimuli from single units in auditory thalamus: impact of aging and anesthesia. *J. Neurosci.* 36, 10696–10706. doi: 10.1523/JNEUROSCI.1454-16.2016

Caicedo, A., and Herbert, H. (1993). Topography of descending projections from the inferior colliculus to auditory brainstem nuclei in the rat. *J. Comp. Neurol.* 328, 377–392. doi: 10.1002/cne.903280305

Caras, M. L., and Sanes, D. H. (2017). Top-down modulation of sensory cortex gates perceptual learning. *Proc. Natl. Acad. Sci. U S A* 114, 9972–9977. doi: 10.1073/pnas.1712305114

Carbajal, G. V., and Malmierca, M. S. (2018). The neuronal basis of predictive coding along the auditory pathway: from the subcortical roots to cortical deviance detection. *Trends Hear.* 22:2331216518784822. doi: 10.1177/2331216518784822

Chandrasekaran, B., Hornickel, J., Skoe, E., Nicol, T., and Kraus, N. (2009). Context-dependent encoding in the human auditory brainstem relates to hearing speech in noise: implications for developmental dyslexia. *Neuron* 64, 311–319. doi: 10.1016/j.neuron.2009.10.006

Chen, Z. (2003). Bayesian filtering: from kalman filters to particle filters and beyond. *Statistics* 182, 1–69. doi: 10.1080/02331880309257

Chennu, S., Noreika, V., Gueorguiev, D., Blenkmann, A., Kochen, S., Ibánez, A., et al. (2013). Expectation and attention in hierarchical auditory prediction. *J. Neurosci.* 33, 11194–11205. doi: 10.1523/JNEUROSCI.0114-13.2013

Chennu, S., Noreika, V., Gueorguiev, D., Shtyrov, Y., Bekinschtein, T. A., and Henson, R. (2016). Silent expectations: dynamic causal modeling of cortical prediction and attention to sounds that weren't. *J. Neurosci.* 36, 8305–8316. doi: 10.1523/JNEUROSCI.1125-16.2016

Collet, L., Bouchet, P., and Pernier, J. (1994). Auditory selective attention in the human cochlea. *Brain Res.* 633, 353–356. doi: 10.1016/0006-8993(94)91561-x

Condon, C. D., and Weinberger, N. M. (1991). Habituation produces frequency-specific plasticity of receptive fields in the auditory cortex. *Behav. Neurosci.* 105, 416–430. doi: 10.1037/0735-7044.105.3.416

Conlee, J., and Kane, E. (1982). Descending projections from the inferior colliculus to the dorsal cochlear nucleus in the cat: an autoradiographic study. *Neuroscience* 7, 161–178. doi: 10.1016/0306-4522(82)90158-0

Connors, B. W., Gutnick, M. J., and Prince, D. A. (1982). Electrophysiological properties of neocortical neurons *in vitro*. *J. Neurophysiol.* 48, 1302–1320. doi: 10.1152/jn.1982.48.6.1302

Constantinople, C. M., and Bruno, R. M. (2013). Deep cortical layers are activated directly by thalamus. *Science* 340, 1591–1594. doi: 10.1126/science.1236425

Coomes, D. L., Schofield, R. M., and Schofield, B. R. (2005). Unilateral and bilateral projections from cortical cells to the inferior colliculus in guinea pigs. *Brain Res.* 1042, 62–72. doi: 10.1016/j.brainres.2005.02.015

Cope, T. E., Sohoglu, E., Sedley, W., Patterson, K., Jones, P., Wiggins, J., et al. (2017). Evidence for causal top-down frontal contributions to predictive processes in speech perception. *Nat. Commun.* 8:2154. doi: 10.1038/s41467-017-01958-7

Cunillera, T., Càmara, E., Laine, M., and Rodríguez-Fornells, A. (2010). Words as anchors: known words facilitate statistical learning. *Exp. Psychol.* 57, 134–141. doi: 10.1027/1618-3169/a000017

Davis, M. H., and Johnsrude, I. S. (2007). Hearing speech sounds: top-down influences on the interface between audition and speech perception. *Hear. Res.* 229, 132–147. doi: 10.1016/j.heares.2007.01.014

De Boer, J., and Thornton, A. R. D. (2008). Neural correlates of perceptual learning in the auditory brainstem: efferent activity predicts and reflects improvement at a speech-in-noise discrimination task. *J. Neurosci.* 28, 4929–4937. doi: 10.1523/JNEUROSCI.0902-08.2008

Deschenes, M., Bourassa, J., Doan, V. D., and Parent, A. (1996). A single-cell study of the axonal projections arising from the posterior intralaminar thalamic nuclei in the rat. *Eur. J. Neurosci.* 8, 329–343. doi: 10.1111/j.1460-9568.1996.tb01217.x

Doucet, J., Molavi, D., and Ryugo, D. (2003). The source of corticocollicular and corticobulbar projections in area Te1 of the rat. *Exp. Brain Res.* 153, 461–466. doi: 10.1007/s00221-003-1604-4

Doucet, J. R., Rose, L., and Ryugo, D. K. (2002). The cellular origin of corticofugal projections to the superior olivary complex in the rat. *Brain Res.* 925, 28–41. doi: 10.1016/s0006-8993(01)03248-6

Dragicevic, C. D., Aedo, C., León, A., Bowen, M., Jara, N., Terreros, G., et al. (2015). The olivocochlear reflex strength and cochlear sensitivity are independently modulated by auditory cortex microstimulation. *J. Assoc. Res. Otolaryngol.* 16, 223–240. doi: 10.1007/s10162-015-0509-9

Duque, D., Pais, R., and Malmierca, M. S. (2018). Stimulus-specific adaptation in the anesthetized mouse revealed by brainstem auditory evoked potentials. *Hear. Res.* 370, 294–301. doi: 10.1016/j.heares.2018.08.011

Duque, D., Pérez-González, D., Ayala, Y. A., Palmer, A. R., and Malmierca, M. S. (2012). Topographic distribution, frequency and intensity dependence of stimulus-specific adaptation in the inferior colliculus of the rat. *J. Neurosci.* 32, 17762–17774. doi: 10.1523/JNEUROSCI.3190-12.2012

Eliades, S. J., and Wang, X. (2003). Sensory-motor interaction in the primate auditory cortex during self-initiated vocalizations. *J. Neurophysiol.* 89, 2194–2207. doi: 10.1152/jn.00627.2002

Erişir, A., Van Horn, S. C., and Sherman, S. M. (1997). Relative numbers of cortical and brainstem inputs to the lateral geniculate nucleus. *Proc. Natl. Acad. Sci. U S A* 94, 1517–1520. doi: 10.1073/pnas.94.4.1517

Ernst, M. O., and Banks, M. S. (2002). Humans integrate visual and haptic information in a statistically optimal fashion. *Nature* 415, 429–433. doi: 10.1038/415429a

Esmaeeli, S., Murphy, K., Swords, G. M., Ibrahim, B. A., Brown, J. W., and Llano, D. A. (2019). Visual hallucinations, thalamocortical physiology and Lewy body disease: a review. *Neurosci. Biobehav. Rev.* 103, 337–351. doi: 10.1016/j.neubiorev.2019.06.006

Farley, B. J., Quirk, M. C., Doherty, J. J., and Christian, E. P. (2010). Stimulus-specific adaptation in auditory cortex is an NMDA-independent process distinct from the sensory novelty encoded by the mismatch negativity. *J. Neurosci.* 30, 16475–16484. doi: 10.1523/JNEUROSCI.2793-10.2010

Feliciano, M., and Potashner, S. J. (1995). Evidence for a glutamatergic pathway from the guinea pig auditory cortex to the inferior colliculus. *J. Neurochem.* 65, 1348–1357. doi: 10.1046/j.1471-4159.1995.65031348.x

Felleman, D. J., and Van Essen, D. C. (1991). Distributed hierarchical processing in the primate cerebral cortex. *Cereb. Cortex* 1, 1–47. doi: 10.1093/cercor/1.1.1

Fink, M., Churan, J., and Wittmann, M. (2006). Temporal processing and context dependency of phoneme discrimination in patients with aphasia. *Brain Lang.* 98, 1–11. doi: 10.1016/j.bandl.2005.12.005

Fiser, A., Mahringer, D., Oyibo, H. K., Petersen, A. V., Leinweber, M., and Keller, G. B. (2016). Experience-dependent spatial expectations in mouse visual cortex. *Nat. Neurosci.* 19, 1658–1664. doi: 10.1038/nn.4385

Fitzpatrick, K. A., and Imig, T. J. (1978). Projections of auditory cortex upon the thalamus and midbrain in the owl monkey. *J. Comp. Neurol.* 177, 537–555. doi: 10.1002/cne.901770402

Fodor, J. A., and Bever, T. G. (1965). The psychological reality of linguistic segments. *J. Verbal Learning Verbal Behav.* 4, 414–420. doi: 10.1016/S0022-5371(65)80081-0

Freyman, R. L., Balakrishnan, U., and Helfer, K. S. (2004). Effect of number of masking talkers and auditory priming on informational masking in speech recognition. *J. Acoust. Soc. Am.* 115, 2246–2256. doi: 10.1121/1.1689343

Friston, K., and Kiebel, S. (2009). Predictive coding under the free-energy principle. *Philos. Trans. R. Soc. Lond. B Biol. Sci.* 364, 1211–1221. doi: 10.1098/rstb.2008.0300

Fritz, J., Shamma, S., Elhilali, M., and Klein, D. (2003). Rapid task-related plasticity of spectrotemporal receptive fields in primary auditory cortex. *Nat. Neurosci.* 6, 1216–1223. doi: 10.1038/nn1141

Games, K. D., and Winer, J. A. (1988). Layer V in rat auditory cortex: projections to the inferior colliculus and contralateral cortex. *Hear. Res.* 34, 1–25. doi: 10.1016/0378-5955(88)90047-0

Ganong, W. F. III (1980). Phonetic categorization in auditory word perception. *J. Exp. Psychol. Hum. Percept. Perform.* 6, 110–125. doi: 10.1037/0096-1523.6.1.110

Gao, E., and Suga, N. (2000). Experience-dependent plasticity in the auditory cortex and the inferior colliculus of bats: role of the corticofugal system. *Proc. Natl. Acad. Sci. U S A* 97, 8081–8086. doi: 10.1073/pnas.97.14.8081

García-Rosales, F., López-Jury, L., González-Palomares, E., Cabral-Calderín, Y., and Hechavarría, J. C. (2020). Fronto-temporal coupling dynamics during spontaneous activity and auditory processing in the bat *Carollia perspicillata*. *Front. Syst. Neurosci.* 14:14. doi: 10.1016/j.biologicals.2020.01.008

Getz, L. M., and Toscano, J. C. (2019). Electrophysiological evidence for top-down lexical influences on early speech perception. *Psychol. Sci.* 30, 830–841. doi: 10.1177/0956797619841813

Giard, M.-H., Fort, A., Mouchetant-Rostaing, Y., and Pernier, J. (2000). Neurophysiological mechanisms of auditory selective attention in humans. *Front. Biosci.* 5, D84–D94. doi: 10.2741/giard

Gilbert, C. D., and Li, W. (2013). Top-down influences on visual processing. *Nat. Rev. Neurosci.* 14, 350–363. doi: 10.1038/nrn3476

Grindrod, C. M., and Baum, S. R. (2002). Sentence context effects and the timecourse of lexical ambiguity resolution in nonfluent aphasia. *Brain Cogn.* 48, 381–385.

Groff, J. A., and Liberman, M. C. (2003). Modulation of cochlear afferent response by the lateral olivocochlear system: activation *via* electrical stimulation of the inferior colliculus. *J. Neurophysiol.* 90, 3178–3200. doi: 10.1152/jn.00537.2003

Guinan, J. J. Jr. (2006). Olivocochlear efferents: anatomy, physiology, function and the measurement of efferent effects in humans. *Ear Hear.* 27, 589–607. doi: 10.1097/01.aud.0000240507.83072.e7

Guo, W., Clause, A. R., Barth-Maron, A., and Polley, D. B. (2017). A corticothalamic circuit for dynamic switching between feature detection and discrimination. *Neuron* 95, 180.e5–194.e5. doi: 10.1016/j.neuron.2017.05.019

Guo, Y. P., Sun, X., Li, C., Wang, N. Q., Chan, Y.-S., and He, J. (2007). Corticothalamic synchronization leads to c-fos expression in the auditory thalamus. *Proc. Natl. Acad. Sci. U S A* 104, 11802–11807. doi: 10.1073/pnas.0701302104

Haegens, S., Händel, B. F., and Jensen, O. (2011). Top-down controlled alpha band activity in somatosensory areas determines behavioral performance in a discrimination task. *J. Neurosci.* 31, 5197–5204. doi: 10.1523/JNEUROSCI.5199-10.2011

Hannemann, R., Obleser, J., and Eulitz, C. (2007). Top-down knowledge supports the retrieval of lexical information from degraded speech. *Brain Res.* 1153, 134–143. doi: 10.1016/j.brainres.2007.03.069

Happel, M. F., Deliano, M., Handschuh, J., and Ohl, F. W. (2014). Dopamine-modulated recurrent corticoefferent feedback in primary sensory cortex promotes detection of behaviorally relevant stimuli. *J. Neurosci.* 34, 1234–1247. doi: 10.1523/JNEUROSCI.1990-13.2014

He, J. (1997). Modulatory effects of regional cortical activation on the onset responses of the cat medial geniculate neurons. *J. Neurophysiol.* 77, 896–908. doi: 10.1152/jn.1997.77.2.896

He, J. (2003a). Corticofugal modulation of the auditory thalamus. *Exp. Brain Res.* 153, 579–590. doi: 10.1007/s00221-003-1680-5

He, J. (2003b). Corticofugal modulation on both on andoff responses in the nonlemniscal auditory thalamus of the guinea pig. *J. Neurophysiol.* 89, 367–381. doi: 10.1152/jn.00593.2002

He, J., Yu, Y.-Q., Xiong, Y., Hashikawa, T., and Chan, Y.-S. (2002). Modulatory effect of cortical activation on the lemniscal auditory thalamus of the guinea pig. *J. Neurophysiol.* 88, 1040–1050. doi: 10.1152/jn.2002.88.2.1040

Hefti, B. J., and Smith, P. H. (2000). Anatomy, physiology and synaptic responses of rat layer V auditory cortical cells and effects of intracellular $GABA_A$ blockade. *J. Neurophysiol.* 83, 2626–2638. doi: 10.1152/jn.2000.83.5.2626

Held, H. (1893). Die centrale gehorleitung. *Arch. Anat. Physiol. Anat. Abt.* 201–248

Hernandez-Peon, R., Scherrer, H., and Jouvet, M. (1956). Modification of electric activity in cochlear nucleus during attention in unanesthetized cats. *Science* 123, 331–332. doi: 10.1126/science.123.3191.331

Hillyard, S. A., Hink, R. F., Schwent, V. L., and Picton, T. W. (1973). Electrical signs of selective attention in the human brain. *Science* 182, 177–180. doi: 10.1126/science.182.4108.177

Hofmann-Shen, C., Vogel, B. O., Kaffes, M., Rudolph, A., Brown, E. C., Tas, C., et al. (2020). Mapping adaptation, deviance detection and prediction error in auditory processing. *NeuroImage* 207:116432. doi: 10.1016/j.neuroimage.2019.116432

Homma, N. Y., Happel, M. F., Nodal, F. R., Ohl, F. W., King, A. J., and Bajo, V. M. (2017). A role for auditory corticothalamic feedback in the perception of

complex sounds. *J. Neurosci.* 37, 6149–6161. doi: 10.1523/JNEUROSCI.0397-17.2017

Huang, N., and Elhilali, M. (2020). Push-pull competition between bottom-up and top-down auditory attention to natural soundscapes. *eLife* 9:e52984. doi: 10.7554/eLife.52984

Issa, E. B., Cadieu, C. F., and Dicarlo, J. J. (2018). Neural dynamics at successive stages of the ventral visual stream are consistent with hierarchical error signals. *eLife* 7:e42870. doi: 10.7554/eLife.42870

Iwama, K., Sakajura, H., and Kasamatsu, T. (1965). Presynaptic inhibition in the lateral geniculate body induced by stimulation of the cerebral cortex. *Jap. J. Physiol.* 15, 310–322. doi: 10.2170/jjphysiol.15.310

Jacobs, R. A. (1999). Optimal integration of texture and motion cues to depth. *Vis. Res.* 39, 3621–3629. doi: 10.1016/s0042-6989(99)00088-7

Jäger, K., and Kössl, M. (2016). Corticofugal modulation of DPOAEs in gerbils. *Hear. Res.* 332, 61–72. doi: 10.3390/j3030024

Jen, P. H.-S., Chen, Q. C., and Sun, X. D. (1998). Corticofugal regulation of auditory sensitivity in the bat inferior colliculus. *J. Comp. Physiol. A* 183, 683–697. doi: 10.1007/s003590050291

Jen, P. H.-S., Sun, X. D., and Chen, Q. C. (2001). An electrophysiological study of neural pathways for corticofugally inhibited neurons in the central nucleus of the inferior colliculus of the big brown bat, *Eptesicus fuscus*. *Exp. Brain Res.* 137, 292–302. doi: 10.1007/s002210000637

Jen, P. H.-S., and Zhou, X. (2003). Corticofugal modulation of amplitude domain processing in the midbrain of the big brown bat, *Eptesicus fuscus*. *Hear. Res.* 184, 91–106. doi: 10.1016/s0378-5955(03)00237-5

Johnson, R. R., and Burkhalter, A. (1996). Microcircuitry of forward and feedback connections within rat visual cortex. *J. Comp. Neurol.* 368, 383–398. doi: 10.1002/(SICI)1096-9861(19960506)368:3<383::AID-CNE5>3.0.CO;2-1

Jones, J. A., and Freyman, R. L. (2012). Effect of priming on energetic and informational masking in a same-different task. *Ear Hear.* 33, 124–133. doi: 10.1097/AUD.0b013e31822b5bee

Kalman, R. E. (1960). A new approach to linear filtering and prediction problems. *J. Basic Eng.* 82, 35–45. doi: 10.1115/1.3662552

Kasper, E. M., Larkman, A. U., Lübke, J., and Blakemore, C. (1994). Pyramidal neurons in layer 5 of the rat visual cortex. I. Correlation among cell morphology, intrinsic electrophysiological properties and axon targets. *J. Comp. Neurol.* 339, 459–474. doi: 10.1002/cne.903390402

Kita, T., and Kita, H. (2012). The subthalamic nucleus is one of multiple innervation sites for long-range corticofugal axons: a single-axon tracing study in the rat. *J. Neurosci.* 32, 5990–5999. doi: 10.1523/JNEUROSCI.5717-11.2012

Kobayashi, M., Takeda, M., Hattori, N., Fukunaga, M., Sasabe, T., Inoue, N., et al. (2004). Functional imaging of gustatory perception and imagery: "top-down" processing of gustatory signals. *NeuroImage* 23, 1271–1282. doi: 10.1016/j.neuroimage.2004.08.002

Kogo, N., and Trengove, C. (2015). Is predictive coding theory articulated enough to be testable? *Front. Comput. Neurosci.* 9:111. doi: 10.3389/fncom.2015.00111

Kong, L., Xiong, C., Li, L., and Yan, J. (2014). Frequency-specific corticofugal modulation of the dorsal cochlear nucleus in mice. *Front. Syst. Neurosci.* 8:125. doi: 10.3389/fnsys.2014.00125

Kössl, M., Hechavarria, J., Voss, C., Schaefer, M., and Vater, M. (2015). Bat auditory cortex-model for general mammalian auditory computation or special design solution for active time perception? *Eur. J. Neurosci.* 41, 518–532. doi: 10.1111/ejn.12801

Köver, H., and Bao, S. (2010). Cortical plasticity as a mechanism for storing Bayesian priors in sensory perception. *PLoS One* 5:e10497. doi: 10.1371/journal.pone.0010497

Künzle, H. (1995). Regional and laminar distribution of cortical neurons projecting to either superior or inferior colliculus in the hedgehog tenrec. *Cereb. Cortex* 5, 338–352. doi: 10.1093/cercor/5.4.338

Kuwabara, N., and Zook, J. M. (2000). Geniculo-collicular descending projections in the gerbil. *Brain Res.* 878, 79–87. doi: 10.1016/s0006-8993(00)02695-0

Lam, Y.-W., and Sherman, S. M. (2010). Functional organization of the somatosensory cortical layer 6 feedback to the thalamus. *Cereb. Cortex* 20, 13–24. doi: 10.1093/cercor/bhp077

Lamme, V. A. F. (1995). The neurophysiology of figure-ground segregation in primary visual cortex. *J. Neurosci.* 15, 1605–1615. doi: 10.1523/JNEUROSCI.15-02-01605.1995

Lee, C. C., and Sherman, S. M. (2010). Drivers and modulators in the central auditory pathways. *Front. Neurosci.* 4:79. doi: 10.3389/neuro.01.014.2010

Lee, T. S., and Mumford, D. (2003). Hierarchical bayesian inference in the visual cortex. *J. Opt. Soc. Am. A. Opt. Image Sci. Vis.* 20, 1434–1448. doi: 10.1364/josaa.20.001434

Lee, T. S., and Nguyen, M. (2001). Dynamics of subjective contour formation in the early visual cortex. *Proc. Natl. Acad. Sci. U S A* 98, 1907–1911. doi: 10.1073/pnas.031579998

Lee, T. S., Yang, C. F., Romero, R. D., and Mumford, D. (2002). Neural activity in early visual cortex reflects behavioral experience and higher-order perceptual saliency. *Nat. Neurosci.* 5, 589–597. doi: 10.1038/nn0602-860

León, A., Elgueda, D., Silva, M. A., Hamamé, C. M., and Délano, P. H. (2012). Auditory cortex basal activity modulates cochlear responses in chinchillas. *PLoS One* 7:e36203. doi: 10.1371/journal.pone.0036203

Lesicko, A. M., Hristova, T., Maigler, K., and Llano, D. A. (2016). Connectional modularity of top-down and bottom-up multimodal inputs to the lateral cortex of the inferior colliculus. *J. Neurosci.* 36, 11037–11050. doi: 10.1523/JNEUROSCI.4134-15.2016

Lesicko, A. M., and Llano, D. A. (2017). Impact of peripheral hearing loss on top-down auditory processing. *Hear. Res.* 343, 4–13. doi: 10.1016/j.heares.2016.05.018

Liberman, M., and Brown, M. (1986). Physiology and anatomy of single olivocochlear neurons in the cat. *Hear. Res.* 24, 17–36. doi: 10.1016/0378-5955(86)90003-1

Lim, H. H., and Anderson, D. J. (2007). Antidromic activation reveals tonotopically organized projections from primary auditory cortex to the central nucleus of the inferior colliculus in guinea pig. *J. Neurophysiol.* 97, 1413–1427. doi: 10.1152/jn.00384.2006

Liu, X., Yan, Y., Wang, Y., and Yan, J. (2010). Corticofugal modulation of initial neural processing of sound information from the ipsilateral ear in the mouse. *PLoS One* 5:e14038. doi: 10.1371/journal.pone.0014038

Llano, D. (2013). Functional imaging of the thalamus in language. *Brain Lang.* 126, 62–72. doi: 10.1016/j.bandl.2012.06.004

Llano, D. A., and Sherman, S. M. (2008). Evidence for nonreciprocal organization of the mouse auditory thalamocortical-corticothalamic projection systems. *J. Comp. Neurol.* 507, 1209–1227. doi: 10.1002/cne.21602

Llano, D. A., and Sherman, S. M. (2009). Differences in intrinsic properties and local network connectivity of identified layer 5 and layer 6 adult mouse auditory corticothalamic neurons support a dual corticothalamic projection hypothesis. *Cereb. Cortex* 19, 2810–2826. doi: 10.1093/cercor/bhp050

Loewy, D. H., Campbell, K. B., De Lugt, D. R., Elton, M., and Kok, A. (2000). The mismatch negativity during natural sleep: intensity deviants. *Clin. Neurophysiol.* 111, 863–872. doi: 10.1016/s1388-2457(00)00256-x

Lorente De Nó, R. (1933). Vestibulo-ocular reflex arc. *Arch. Neurpsych.* 30, 245–291. doi: 10.1001/archneurpsyc.1933.02240140009001

Lotto, A. J., and Kluender, K. R. (1998). General contrast effects in speech perception: effect of preceding liquid on stop consonant identification. *Percept. Psychophys.* 60, 602–619. doi: 10.3758/bf03206049

Luo, F., Wang, Q., Kashani, A., and Yan, J. (2008). Corticofugal modulation of initial sound processing in the brain. *J. Neurosci.* 28, 11615–11621. doi: 10.1523/JNEUROSCI.3972-08.2008

Ma, X., and Suga, N. (2001). Corticofugal modulation of duration-tuned neurons in the midbrain auditory nucleus in bats. *Proc. Natl. Acad. Sci. U S A* 98, 14060–14065. doi: 10.1073/pnas.241517098

Malmierca, M. S., Cristaudo, S., Pérez-González, D., and Covey, E. (2009). Stimulus-specific adaptation in the inferior colliculus of the anesthetized rat. *J. Neurosci.* 29, 5483–5493. doi: 10.1523/JNEUROSCI.4153-08.2009

Malmierca, M. S., Le Beau, F. E. N., and Rees, A. (1996). The topographical organization of descending projections from the central nucleus of the inferior colliculus in guinea pig. *Hear. Res.* 93, 167–180. doi: 10.1016/0378-5955(95)00227-8

Marian, V., Lam, T. Q., Hayakawa, S., and Dhar, S. (2018). Top-down cognitive and linguistic influences on the suppression of spontaneous otoacoustic emissions. *Front. Neurosci.* 12:378. doi: 10.3389/fnins.2018.00378

Markovitz, C. D., Hogan, P. S., Wesen, K. A., and Lim, H. H. (2015). Pairing broadband noise with cortical stimulation induces extensive suppression of ascending sensory activity. *J. Neural Eng.* 12:026006. doi: 10.1088/1741-2560/12/2/026006

Markovitz, C. D., Tang, T. T., and Lim, H. H. (2013). Tonotopic and localized pathways from primary auditory cortex to the central nucleus of the inferior colliculus. *Front. Neural Circuits* 7:77. doi: 10.3389/fncir.2013.00077

Marsh, J. E., and Campbell, T. A. (2016). Processing complex sounds passing through the rostral brainstem: the new early filter model. *Front. Neurosci.* 10:136. doi: 10.3389/fnins.2016.00136

Marslen–Wilson, W. D. (1975). Sentence perception as an interactive parallel process. *Science* 189, 226–228. doi: 10.1126/science.189.4198.226

Mattys, S. L., White, L., and Melhorn, J. F. (2005). Integration of multiple speech segmentation cues: a hierarchical framework. *J. Exp. Psychol. Gen.* 134, 477–500. doi: 10.1037/0096-3445.134.4.477

May, P. J., and Tiitinen, H. (2010). Mismatch negativity (MMN), the deviance-elicited auditory deflection, explained. *Psychophysiology* 47, 66–122. doi: 10.1111/j.1469-8986.2009.00856.x

Mcclelland, J. L., and Elman, J. L. (1986). The TRACE model of speech perception. *Cogn. Psychol.* 18, 1–86. doi: 10.1016/0010-0285(86)90015-0

Mcgettigan, C., Eisner, F., Agnew, Z. K., Manly, T., Wisbey, D., and Scott, S. K. (2013). T'ain't what you say, it's the way that you say it—left insula and inferior frontal cortex work in interaction with superior temporal regions to control the performance of vocal impersonations. *J. Cogn. Neurosci.* 25, 1875–1886. doi: 10.1162/jocn_a_00427

Meltzer, N. E., and Ryugo, D. L. (2006). Projections from auditory cortex to cochlear nucleus: a comparative analysis of rat and mouse. *Anat. Rec. A Discov. Mol. Cell. Evol. Biol.* 288, 397–408. doi: 10.1002/ar.a.20300

Miller, G. A., Heise, G. A., and Lichten, W. (1951). The intelligibility of speech as a function of the context of the test materials. *J. Exp. Psychol.* 41, 329–335. doi: 10.1037/h0062491

Mishra, S. K., and Lutman, M. E. (2014). Top-down influences of the medial olivocochlear efferent system in speech perception in noise. *PLoS One* 9:e85756. doi: 10.1371/journal.pone.0085756

Mitani, A., Shimokouchi, M., and Nomura, S. (1983). Effects of stimulation of the primary auditory cortex upon colliculogeniculate neurons in the inferior colliculus of the cat. *Neurosci. Lett.* 42, 185–189. doi: 10.1016/0304-3940(83)90404-4

Moore, B. C. (2012). *An Introduction to the Psychology of Hearing*. Leiden: Brill.

Moore, D. R. (2012). Listening difficulties in children: bottom-up and top-down contributions. *J. Commun. Disord.* 45, 411–418. doi: 10.1016/j.jcomdis.2012.06.006

Mulders, W., and Robertson, D. (2000). Evidence for direct cortical innervation of medial olivocochlear neurones in rats. *Hear. Res.* 144, 65–72. doi: 10.1016/s0378-5955(00)00046-0

Näätänen, R., and Picton, T. (1987). The N1 wave of the human electric and magnetic response to sound: a review and an analysis of the component structure. *Psychophysiology* 24, 375–425. doi: 10.1111/j.1469-8986.1987.tb00311.x

Nakamoto, K. T., Mellott, J. G., Killius, J., Storey-Workley, M. E., Sowick, C. S., and Schofield, B. R. (2013). Ultrastructural examination of the corticocollicular pathway in the guinea pig: a study using electron microscopy, neural tracers and GABA immunocytochemistry. *Front. Neuroanat.* 7:13. doi: 10.3389/fnana.2013.00013

Nakamoto, K. T., Shackleton, T. M., and Palmer, A. R. (2010). Responses in the inferior colliculus of the guinea pig to concurrent harmonic series and the effect of inactivation of descending controls. *J. Neurophysiol.* 103, 2050–2061. doi: 10.1152/jn.00451.2009

Nassi, J. J., Lomber, S. G., and Born, R. T. (2013). Corticocortical feedback contributes to surround suppression in V1 of the alert primate. *J. Neurosci.* 33, 8504–8517. doi: 10.1523/JNEUROSCI.5124-12.2013

Nelson, A., Schneider, D. M., Takatoh, J., Sakurai, K., Wang, F., and Mooney, R. (2013). A circuit for motor cortical modulation of auditory cortical activity. *J. Neurosci.* 33, 14342–14353. doi: 10.1523/JNEUROSCI.2275-13.2013

Nelson, S. L., Kong, L., Liu, X., and Yan, J. (2015). Auditory cortex directs the input-specific remodeling of thalamus. *Hear. Res.* 328, 1–7. doi: 10.1016/j.heares.2015.06.016

Norris, D., Mcqueen, J. M., and Cutler, A. (2000). Merging information in speech recognition: feedback is never necessary. *Behav. Brain Sci.* 23, 299–325. doi: 10.1017/s0140525x00003241

Nourski, K. V., Steinschneider, M., Rhone, A. E., Kawasaki, H., Howard, M. A., and Banks, M. I. (2018). Auditory predictive coding across awareness states under anesthesia: an intracranial electrophysiology study. *J. Neurosci.* 38, 8441–8452. doi: 10.1523/JNEUROSCI.0967-18.2018

O'Neill, J. J. (1957). Recognition of intelligibility test materials in context and isolation. *J. Speech. Hear. Disord.* 22, 87–90. doi: 10.1044/jshd.2201.87

Obleser, J. (2014). Putting the listening brain in context. *Lang. Linguist. Compass* 8, 646–658. doi: 10.1111/lnc3.12098

Ohl, F. W., and Scheich, H. (1997). Learning-induced dynamic receptive field changes in primary auditory cortex of the unanaesthetized Mongolian gerbil. *J. Comp. Physiol. A* 181, 685–696. doi: 10.1007/s003590050150

Ohl, F. W., and Scheich, H. (2005). Learning-induced plasticity in animal and human auditory cortex. *Curr. Opin. Neurobiol.* 15, 470–477. doi: 10.1016/j.conb.2005.07.002

Ojima, H. (1994). Terminal morphology and distribution of corticothalamic fibers originating from layers 5 and 6 of cat primary auditory cortex. *Cereb. Cortex* 4, 646–663. doi: 10.1093/cercor/4.6.646

Patel, M., Sons, S., Yudintsev, G., Lesicko, A. M., Yang, L., Taha, G., et al. (2017). Anatomical characterization of subcortical descending projections to the inferior colliculus in mouse. *J. Comp. Neurol.* 525, 885–900. doi: 10.1002/cne.24106

Perrot, X., Ryvlin, P., Isnard, J., Guènot, M., Catenoix, H., Fischer, C., et al. (2006). Evidence for corticofugal modulation of peripheral auditory activity in humans. *Cereb. Cortex* 16, 941–948. doi: 10.1093/cercor/bhj035

Pinto, S., Tremblay, P., Basirat, A., and Sato, M. (2019). The impact of when, what and how predictions on auditory speech perception. *Exp. Brain Res.* 237, 3143–3153. doi: 10.1007/s00221-019-05661-5

Popelář, J., Šuta, D., Lindovský, J., Bureš, Z., Pysanenko, K., Chumak, T., et al. (2015). Cooling of the auditory cortex modifies neuronal activity in the inferior colliculus in rats. *Hear. Res.* 332, 7–16. doi: 10.1016/j.heares.2015.10.021

Prasad, J. A., Carroll, B. J., and Sherman, S. M. (2020). Layer 5 corticofugal projections from diverse cortical areas: variations on a pattern of thalamic and extrathalamic targets. *J. Neurosci.* 40, 5785–5796. doi: 10.1523/JNEUROSCI.0529-20.2020

Rao, R. P., and Ballard, D. H. (1997). Dynamic model of visual recognition predicts neural response properties in the visual cortex. *Neural Comput.* 9, 721–763. doi: 10.1162/neco.1997.9.4.721

Rao, R. P., and Ballard, D. H. (1999). Predictive coding in the visual cortex: a functional interpretation of some extra-classical receptive-field effects. *Nat. Neurosci.* 2, 79–87. doi: 10.1038/4580

Raz, A., Grady, S. M., Krause, B. M., Uhlrich, D. J., Manning, K. A., and Banks, M. I. (2014). Preferential effect of isoflurane on top-down vs. bottom-up pathways in sensory cortex. *Front. Syst. Neurosci.* 8:191. doi: 10.3389/fnsys.2014.00191

Reichova, I., and Sherman, S. M. (2004). Somatosensory corticothalamic projections: distinguishing drivers from modulators. *J. Neurophysiol.* 92, 2185–2197. doi: 10.1152/jn.00322.2004

Richardson, B. D., Hancock, K. E., and Caspary, D. M. (2013). Stimulus-specific adaptation in auditory thalamus of young and aged awake rats. *J. Neurophysiol.* 110, 1892–1902. doi: 10.1152/jn.00403.2013

Robinson, B. L., Harper, N. S., and Mcalpine, D. (2016). Meta-adaptation in the auditory midbrain under cortical influence. *Nat. Commun.* 7:13442. doi: 10.1038/ncomms13442

Rockland, K. S., and Pandya, D. N. (1979). Laminar origins and terminations of cortical connections of the occipital lobe in the rhesus monkey. *Brain Res.* 179, 3–20. doi: 10.1016/0006-8993(79)90485-2

Rummell, B. P., Klee, J. L., and Sigurdsson, T. (2016). Attenuation of responses to self-generated sounds in auditory cortical neurons. *J. Neurosci.* 36, 12010–12026. doi: 10.1523/JNEUROSCI.1564-16.2016

Ryugo, D. K., and Weinberger, N. M. (1976). Corticofugal modulation of the medial geniculate body. *Exp. Neurol.* 51, 377–391. doi: 10.1016/0014-4886(76)90262-4

Saldaña, E. (1993). "Descending projections from the inferior colliculus to the cochlear nuclei in mammals," in *The Mammalian Cochlear Nuclei. NATO ASI Series (Series A, Life Sciences)*, eds M. A. Merchán, J. M. Juiz, D. A. Godfrey and E. Mugnaini (Boston, MA: Springer), 153–165.

Saldaña, E. (2015). All the way from the cortex: a review of auditory corticosubcollicular pathways. *Cerebellum* 14, 584–596. doi: 10.1007/s12311-015-0694-4

Saldaña, E., Feliciano, M., and Mugnaini, E. (1996). Distribution of descending projections from primary auditory neocortex to inferior colliculus mimics the topography of intracollicular projections. *J. Comp. Neurol.* 371, 15–40. doi: 10.1002/(SICI)1096-9861(19960715)371:1<15::AID-CNE2>3.0.CO;2-O

Samuel, A. G. (1981). Phonemic restoration: insights from a new methodology. *J. Exp. Psychol. Gen.* 110, 474–494. doi: 10.1037/0096-3445.110.4.474

Samuel, A. G. (1997). Lexical activation produces potent phonemic percepts. *Cogn. Psychol.* 32, 97–127. doi: 10.1006/cogp.1997.0646

Schofield, B. R. (2001). Origins of projections from the inferior colliculus to the cochlear nucleus in guinea pigs. *J. Comp. Neurol.* 429, 206–220. doi: 10.1002/1096-9861(20000108)429:2<206::aid-cne3>3.0.co;2-x

Schofield, B. R. (2009). Projections to the inferior colliculus from layer VI cells of auditory cortex. *Neuroscience* 159, 246–258. doi: 10.1016/j.neuroscience.2008.11.013

Scholes, C., Palmer, A. R., and Sumner, C. J. (2015). Stream segregation in the anesthetized auditory cortex. *Hear. Res.* 328, 48–58. doi: 10.1016/j.heares.2015.07.004

Schwiedrzik, C. M., and Freiwald, W. A. (2017). High-level prediction signals in a low-level area of the macaque face-processing hierarchy. *Neuron* 96, 89.e4–97.e4. doi: 10.1016/j.neuron.2017.09.007

Senatorov, V., and Hu, B. (2002). Extracortical descending projections to the rat inferior colliculus. *Neuroscience* 115, 243–250. doi: 10.1016/s0306-4522(02)00316-0

Serkov, F., Kienko, V., and Limanskaya, L. (1976). Responses of medial geniculate body neurons to auditory cortical stimulation. *Neurophysiology* 8, 3–9. doi: 10.1007/BF01065232

Shao, Z., and Burkhalter, A. (1996). Different balance of excitation and inhibition in forward and feedback circuits of rat visual cortex. *J. Neurosci.* 16, 7353–7365. doi: 10.1523/JNEUROSCI.16-22-07353.1996

Shastri, U., Mythri, H., and Kumar, U. A. (2014). Descending auditory pathway and identification of phonetic contrast by native listeners. *J. Acoust. Soc. Am.* 135, 896–905. doi: 10.1121/1.4861350

Shipp, S. (2016). Neural elements for predictive coding. *Front. Psychol.* 7:1792. doi: 10.3389/fpsyg.2016.01792

Sikkens, T., Bosman, C. A., and Olcese, U. (2019). The role of top-down modulation in shaping sensory processing across brain states: implications for consciousness. *Front. Syst. Neurosci.* 13:31. doi: 10.3389/fnsys.2019.00031

Silva, S., Dias, C., and Castro, S. L. (2019). Domain-specific expectations in music segmentation. *Brain Sci.* 9:169. doi: 10.3390/brainsci9070169

Skoe, E., and Kraus, N. (2010). Hearing it again and again: on-line subcortical plasticity in humans. *PLoS One* 5:e13645. doi: 10.1371/journal.pone.0013645

Slater, B. J., Sons, S. K., Yudintsev, G., Lee, C. M., and Llano, D. A. (2019). Thalamocortical and intracortical inputs differentiate layer-specific mouse auditory corticocollicular neurons. *J. Neurosci.* 39, 256–270. doi: 10.1523/JNEUROSCI.3352-17.2018

Slater, B. J., Willis, A. M., and Llano, D. A. (2013). Evidence for layer-specific differences in auditory corticocollicular neurons. *Neuroscience* 229, 144–154. doi: 10.1016/j.neuroscience.2012.10.053

Smaragdis, P. J. (2001). *Redundancy Reduction for Computational Audition, a Unifying Approach.* Cambridge, MA: Massachusetts Institute of Technology.

Smith, D., Aouad, R., and Keil, A. (2012). Cognitive task demands modulate the sensitivity of the human cochlea. *Front. Psychol.* 3:30. doi: 10.3389/fpsyg.2012.00030

Sohoglu, E., Peelle, J. E., Carlyon, R. P., and Davis, M. H. (2012). Predictive top-down integration of prior knowledge during speech perception. *J. Neurosci.* 32, 8443–8453. doi: 10.1523/JNEUROSCI.5069-11.2012

Sohoglu, E., Peelle, J. E., Carlyon, R. P., and Davis, M. H. (2014). Top-down influences of written text on perceived clarity of degraded speech. *J. Exp. Psychol. Hum. Percept. Perform.* 40, 186–199. doi: 10.1037/a0033206

Spratling, M. W. (2017). A review of predictive coding algorithms. *Brain Cogn.* 112, 92–97. doi: 10.1016/j.bandc.2015.11.003

Srinivasan, M. V., Laughlin, S. B., and Dubs, A. (1982). Predictive coding: a fresh view of inhibition in the retina. *Proc. R. Soc. Lond. B* 216, 427–459. doi: 10.1098/rspb.1982.0085

Srinivasan, S., Keil, A., Stratis, K., Woodruff Carr, K. L., and Smith, D. W. (2012). Effects of cross-modal selective attention on the sensory periphery: cochlear sensitivity is altered by selective attention. *Neuroscience* 223, 325–332. doi: 10.1016/j.neuroscience.2012.07.062

Stebbings, K. A., Lesicko, A. M., and Llano, D. A. (2014). The auditory corticocollicular system: molecular and circuit-level considerations. *Hear. Res.* 314, 51–59. doi: 10.1016/j.heares.2014.05.004

Sterzer, P., Adams, R. A., Fletcher, P., Frith, C., Lawrie, S. M., Muckli, L., et al. (2018). The predictive coding account of psychosis. *Biol. Psychiatry* 84, 634–643. doi: 10.1016/j.biopsych.2018.05.015

Stewart, M. E., and Ota, M. (2008). Lexical effects on speech perception in individuals with "autistic" traits. *Cognition* 109, 157–162. doi: 10.1016/j.cognition.2008.07.010

Sun, X., Jen, P. H.-S., Sun, D., and Zhang, S. (1989). Corticofugal influences on the responses of bat inferior collicular neurons to sound stimulation. *Brain Res.* 495, 1–8. doi: 10.1016/0006-8993(89)91212-2

Sun, X., Xia, Q., Lai, C. H., Shum, D. K. Y., Chan, Y. S., and He, J. (2007). Corticofugal modulation of acoustically induced Fos expression in the rat auditory pathway. *J. Comp. Neurol.* 501, 509–525. doi: 10.1002/cne.21249

Takayanagi, M., and Ojima, H. (2006). Microtopography of the dual corticothalamic projections originating from domains along the frequency axis of the cat primary auditory cortex. *Neuroscience* 142, 769–780. doi: 10.1016/j.neuroscience.2006.06.048

Terreros, G., and Délano, P. H. (2015). Corticofugal modulation of peripheral auditory responses. *Front. Syst. Neurosci.* 9:134. doi: 10.3389/fnsys.2015.00134

Torii, M., Hackett, T. A., Rakic, P., Levitt, P., and Polley, D. B. (2013). EphA signaling impacts development of topographic connectivity in auditory corticofugal systems. *Cereb. Cortex* 23, 775–785. doi: 10.1093/cercor/bhs066

Treisman, A. M. (1964). Selective attention in man. *Br. Med. Bull.* 20, 12–16. doi: 10.1093/oxfordjournals.bmb.a070274

Tseng, C. H., Mcneil, M. R., and Milenkovic, P. (1993). An investigation of attention allocation deficits in aphasia. *Brain Lang.* 45, 276–296. doi: 10.1006/brln.1993.1046

Tzourio, N., El Massioui, F., Crivello, F., Joliot, M., Renault, B., and Mazoyer, B. (1997). Functional anatomy of human auditory attention studied with PET. *NeuroImage* 5, 63–77. doi: 10.1006/nimg.1996.0252

Ulanovsky, N., Las, L., and Nelken, I. (2003). Processing of low-probability sounds by cortical neurons. *Nat. Neurosci.* 6, 391–398. doi: 10.1038/nn1032

Usrey, W. M., and Sherman, S. M. (2019). Corticofugal circuits: communication lines from the cortex to the rest of the brain. *J. Comp. Neurol.* 527, 640–650. doi: 10.1002/cne.24423

van Noorden, L. P. (1971). Rhythmic fission as a function of tone rate. *IPO Ann. Prog. Rep.* 6, 9–12.

Vetter, D. E., Saldaña, E., and Mugnaini, E. (1993). Input from the inferior colliculus to medial olivocochlear neurons in the rat: a double label study with PHA-L and cholera toxin. *Hear. Res.* 70, 173–186. doi: 10.1016/0378-5955(93)90156-u

Villa, A. E. P., Rouiller, E., Simm, G., Zurita, P., De Ribaupierre, Y., and De Ribaupierre, F. (1991). Corticofugal modulation of the information processing in the auditory thalamus of the cat. *Exp. Brain Res.* 86, 506–517. doi: 10.1007/BF00230524

Villa, A. E. P., Tetko, I. V., Dutoit, P., De Ribaupierre, Y., and De Ribaupierre, F. (1999). Corticofugal modulation of functional connectivity within the auditory thalamus of rat, guinea pig and cat revealed by cooling deactivation. *J. Neurosci. Methods* 86, 161–178. doi: 10.1016/s0165-0270(98)00164-2

Vila, C.-H., Williamson, R. S., Hancock, K. E., and Polley, D. B. (2019). Optimizing optogenetic stimulation protocols in auditory corticofugal neurons based on closed-loop spike feedback. *J. Neural Eng.* 16:066023. doi: 10.1088/1741-2552/ab39cf

Von Helmholtz, H. (1867). *Handbuch Der Physiologischen Optik*. Leipzig: Voss.

Wang, Y., Zhang, J., Zou, J., Luo, H., and Ding, N. (2019). Prior knowledge guides speech segregation in human auditory cortex. *Cereb. Cortex* 29, 1561–1571. doi: 10.1093/cercor/bhy052

Warren, R. M. (1970). Perceptual restoration of missing speech sounds. *Science* 167, 392–393. doi: 10.1126/science.167.3917.392

Weinberger, N. M. (2004). Specific long-term memory traces in primary auditory cortex. *Nat. Rev. Neurosci.* 5, 279–290. doi: 10.1038/nrn1366

Winer, J. A., Chernock, M. L., Larue, D. T., and Cheung, S. W. (2002). Descending projections to the inferior colliculus from the posterior thalamus

and the auditory cortex in rat, cat and monkey. *Hear. Res.* 168, 181–195. doi: 10.1016/s0378-5955(02)00489-6

Winer, J. A., Larue, D. T., Diehl, J. J., and Hefti, B. J. (1998). Auditory cortical projections to the cat inferior colliculus. *J. Comp. Neurol.* 400, 147–174.

Wu, Y., and Yan, J. (2007). Modulation of the receptive fields of midbrain neurons elicited by thalamic electrical stimulation through corticofugal feedback. *J. Neurosci.* 27, 10651–10658. doi: 10.1523/JNEUROSCI.1320-07.2007

Xiao, Z., and Suga, N. (2002). Modulation of cochlear hair cells by the auditory cortex in the mustached bat. *Nat. Neurosci.* 5, 57–63. doi: 10.1038/nn786

Xiong, X. R., Liang, F., Zingg, B., Ji, X.-Y., Ibrahim, L. A., Tao, H. W., et al. (2015). Auditory cortex controls sound-driven innate defense behaviour through corticofugal projections to inferior colliculus. *Nat. Commun.* 6:7224. doi: 10.1038/ncomms8224

Xiong, Y., Yu, Y. Q., Chan, Y. S., and He, J. (2004). Effects of cortical stimulation on auditory-responsive thalamic neurones in anaesthetized guinea pigs. *J. Physiol.* 560, 207–217. doi: 10.1113/jphysiol.2004.067686

Yan, J., and Ehret, G. (2001). Corticofugal reorganization of the midbrain tonotopic map in mice. *Neuroreport* 12, 3313–3316. doi: 10.1097/00001756-200110290-00033

Yan, J., and Ehret, G. (2002). Corticofugal modulation of midbrain sound processing in the house mouse. *Eur. J. Neurosci.* 16, 119–128. doi: 10.1046/j.1460-9568.2002.02046.x

Yan, J., and Suga, N. (1996). Corticofugal modulation of time-domain processing of biosonar information in bats. *Science* 273, 1100–1103. doi: 10.1126/science.273.5278.1100

Yan, J., Zhang, Y., and Ehret, G. (2005). Corticofugal shaping of frequency tuning curves in the central nucleus of the inferior colliculus of mice. *J. Neurophysiol.* 93, 71–83. doi: 10.1152/jn.00348.2004

Yan, W., and Suga, N. (1998). Corticofugal modulation of the midbrain frequency map in the bat auditory system. *Nat. Neurosci.* 1, 54–58. doi: 10.1038/255

Yin, P., Strait, D. L., Radtke-Schuller, S., Fritz, J. B., and Shamma, S. A. (2020). Dynamics and hierarchical encoding of non-compact acoustic categories in auditory and frontal cortex. *Curr. Biol.* 30, 1649.e5–1663.e5. doi: 10.1016/j.cub.2020.02.047

Yu, Y.-Q., Xiong, Y., Chan, Y.-S., and He, J. (2004). Corticofugal gating of auditory information in the thalamus: an *in vivo* intracellular recording study. *J. Neurosci.* 24, 3060–3069. doi: 10.1523/JNEUROSCI.4897-03.2004

Yudintsev, G., Asilador, A., Coppinger, M., Nair, K., Prasad, M., and Llano, D. A. (2019). Connectional heterogeneity in the mouse auditory corticocollicular system. *BioRxiv* [Preprint]. doi: 10.1101/571711

Zekveld, A. A., Heslenfeld, D. J., Festen, J. M., and Schoonhoven, R. (2006). Top-down and bottom-up processes in speech comprehension. *NeuroImage* 32, 1826–1836. doi: 10.1016/j.neuroimage.2006.04.199

Zhang, Y., Hakes, J. J., Bonfield, S. P., and Yan, J. (2005). Corticofugal feedback for auditory midbrain plasticity elicited by tones and electrical stimulation of basal forebrain in mice. *Eur. J. Neurosci.* 22, 871–879. doi: 10.1111/j.1460-9568.2005.04276.x

Zhang, Y., and Suga, N. (2000). Modulation of responses and frequency tuning of thalamic and collicular neurons by cortical activation in mustached bats. *J. Neurophysiol.* 84, 325–333. doi: 10.1152/jn.2000.84.1.325

Zhang, Y., Suga, N., and Yan, J. (1997). Corticofugal modulation of frequency processing in bat auditory system. *Nature* 387, 900–903. doi: 10.1038/43180

Zhang, Y., and Yan, J. (2008). Corticothalamic feedback for sound-specific plasticity of auditory thalamic neurons elicited by tones paired with basal forebrain stimulation. *Cereb. Cortex* 18, 1521–1528. doi: 10.1093/cercor/bhm188

Zhang, Z., Liu, C.-H., Yu, Y.-Q., Fujimoto, K., Chan, Y.-S., and He, J. (2008). Corticofugal projection inhibits the auditory thalamus through the thalamic reticular nucleus. *J. Neurophysiol.* 99, 2938–2945. doi: 10.1152/jn.00002.2008

Zhou, X., and Jen, P. H.-S. (2005). Corticofugal modulation of directional sensitivity in the midbrain of the big brown bat, *Eptesicus fuscus*. *Hear. Res.* 203, 201–215. doi: 10.1016/j.heares.2004.12.008

Zhou, X., and Jen, P. H.-S. (2007). Corticofugal modulation of multi-parametric auditory selectivity in the midbrain of the big brown bat. *J. Neurophysiol.* 98, 2509–2516. doi: 10.1152/jn.00613.2007

Conflict of Interest: The authors declare that the research was conducted in the absence of any commercial or financial relationships that could be construed as a potential conflict of interest.

frontiers in Neural Circuits

OPINION
published: 02 February 2021
doi: 10.3389/fncir.2021.632668

A Closer Look at Corticothalamic "Loops"

*Kathleen S. Rockland**

Department of Anatomy & Neurobiology, Boston University School of Medicine, Boston, MA, United States

Keywords: corticogeniculate, heterogeneity, layer 6, reciprocity, cortical cell types

A defining feature of primary sensory cortical areas has been that they receive and reciprocate thalamic "relays" of external events. The interactions of sensory input, autonomous cortical processes, and more cognitive functions, however, remain under active investigation; and continuing work is bringing into better focus the fuller spatial, temporal, and dynamic complexity of the cortical-subcortical sensory pathways, conveniently described as "loops." There are reports that corticothalamic (CT) connections regulate the mode of thalamic activity and can exert a flexible control of thalamocortical (TC) inputs (mouse cortex: Mease et al., 2014; Crandall et al., 2015; Guo et al., 2017; Kirchgessner et al., 2020). Auditory CT feedback to the medial geniculate body is found to contribute to the detection of harmonicity, an important grouping cue in the perception of complex sounds (ferrets: Homma et al., 2017). Arousal related modulation can already be demonstrated at retinal inputs to the thalamus (mouse: Liang et al., 2020); and brainwide recordings of multiple structures suggest "an ubiquitous mixing of sensory and motor information," happening as early as primary sensory cortex (mouse: Stringer et al., 2019).

In this Opinion, I briefly bring together several anatomical features of CT connections, relevant to an emerging view of cognitive-sensory processes; namely, (1) cell type diversity, which may only partly be related to segregated parallel processing; (2) reciprocity, which may not be monosynaptic cell-to-cell and may not be strictly topographic; and (3) the massive convergence of multiple intrinsic cortical and multiple direct and indirect extrinsic connections beyond the primary thalamus. This Topic asks: do feedback circuits perform common functions, and are feedback mechanisms unique or shared across sensory modalities? Overall, the evidence supports a multilevel diversity; and I would like to propose that this diversity, not unlike that of cell types (e.g., Cembrowski and Spruston, 2019), is central to brain organization and connectivity, and thus an important perspective in the context of cortico-subcortical sensory processing (CT projections from layers 5 or 6 to higher order thalamic nuclei will not be covered here; but see discussion and references in e.g., Rockland, 2019; Usrey and Sherman, 2019; Vanni et al., 2020).

CT PROJECTION NEURONS: LAYER 6

Across species and across modalities, CT projections to primary sensory thalamus originate from excitatory neurons in layer 6. However, the proportion of CT neurons within layer 6 is variable by species. Corticogeniculate (CG) neurons are reported to comprise about 15% in primates but 50% in carnivores [reviewed in Hasse and Briggs (2017), Vanni et al. (2020)]. Whether this proportion also varies within an area (e.g., foveal vs. peripheral visual field for area V1) is not known.

CT neurons in layer 6 are heterogeneous according to multiple criteria (Baker et al., 2018). First, physiological recordings have established that stimulus driven conduction times are variable,

OPEN ACCESS

Edited by:
Max F. K. Happel,
Leibniz Institute for Neurobiology (LG), Germany

Reviewed by:
Patrik Krieger,
Ruhr University Bochum, Germany
Markus Rothermel,
RWTH Aachen University, Germany

***Correspondence:**
Kathleen S. Rockland
krock@bu.edu

Received: *23 November 2020*
Accepted: *13 January 2021*
Published: *02 February 2021*

Citation:
Rockland KS (2021) A Closer Look at Corticothalamic "Loops". Front. Neural Circuits 15:632668. doi: 10.3389/fncir.2021.632668

ranging from short to extremely long (<2 to 40–50 ms), probably due to presence or absence of myelin [reviewed in Hasse and Briggs (2017), Stoelzel et al. (2017)]. In rabbit visual cortex, fast CG neurons are preferentially situated in the superficial stratum of layer 6 (Stoelzel et al., 2017). Of the CG neurons characterized as slow, "many of the slowest are silent and [sensory stimulus] unresponsive," perhaps arguing for a multimodal or more complex role (or, "plastic reduction," Stoelzel et al., 2017).

Second, multiple groups of CT neurons have been distinguished on the basis of apical dendritic morphology. For macaque visual cortex (V1 and the smaller population in V2), broad categories of CG neurons are distinguished on the basis of long or short apical dendrites, respectively, extending toward layer 1 or terminating in layer 3 (Hasse and Briggs, 2017; or two classes, with subtypes: Wiser and Callaway, 1996). Unlike pyramidal neurons in layers 5, which typically extend to and ramify in layer 1, the computationally significant apical tuft is often absent or poorly developed (Ledergerber and Larkum, 2010; Thomson, 2010; Baker et al., 2018).

Third, in macaque primary visual cortex, six main functional clusters have been reported based on responsiveness to visual stimuli (i.e., achromatic gratings, with varying parameters; Hawken et al., 2020). Transcriptomic identity was not determined, nor the actual connectional identity of the neurons (i.e., whether these project to the LGN, or the claustrum, or are solely intrinsic); but these data might be expected from continuing work, as in other reports in mouse (e.g., Tasic et al., 2018; Cembrowski and Spruston, 2019).

A fourth differentiating factor is the number, identity, and arrangement of inputs to individual CT neurons. Complete input maps are so far not available at the single neuron level; but the conspicuous difference in apical dendritic extent clearly implies differences of input number and identity, and thus in the integrative capacity of the individual neurons. TC inputs, for example, can contact CT neurons directly in layer 4 (on apical dendrites) and/or in layer 6 (on basal dendrites), in addition to the polysynaptic input from cortical neurons in layer 4. In the macaque, layer 6 inputs can occur as collaterals of TC axons continuing to layer 4 (area V1: Blasdel and Lund, 1983; Freund et al., 1989; somatosensory cortex: Garraghty and Sur, 1990). In the rodent, direct layer 6 terminations, although less dense than those to layer 4, have been demonstrated in rat barrel cortex (Constantinople and Bruno, 2013; Crandall et al., 2017), where the postsynaptic targets have been identified (proportion unknown) as neurons in layer 5B, corticocortical neurons (CC) in layer 6, and CT neurons in layer 6 (Constantinople and Bruno, 2013). The latter receive only weak direct inputs from VPm (Crandall et al., 2017).

Other inputs to CT neurons are more numerous than the TC inputs and include a range of intrinsic excitatory, intrinsic inhibitory, and some excitatory cortical feedback inputs (to layer 6 or, in macaque visual cortex, layer 4B for the neurons with longer apical dendrites). Of these, several potentially convey multi-sensory information. Macaque V1 receives input from auditory (Falchier et al., 2002; Rockland and Ojima, 2003) and parietal association areas (Borra and Rockland, 2011), particularly in the representation of the peripheral visual field. In the mouse area V1, layer 6 neurons receive a widespread head-motion signal from retrosplenial cortex (Velez-Fort et al., 2018).

Fifth, CT neurons in layer 6 may receive differential neuromodulatory inputs. These are known to have multiple effects, which in part depend on receptor distributions and substance concentration, likely to vary across neurons. Acetylcholine, for example, preferentially contributes to a facilitation of CT layer 6 neurons by an interaction of muscarinic and nicotinic receptors (in rats: Yang et al., 2020; and for recent reviews of neuromodulators: Coppola and Disney, 2018; Jacob and Nienborg, 2018; Radnikow and Feldmeyer, 2018). In primary somatosensory and visual cortices (but also non-primary sensory areas), orexin, a peptide associated with wakefulness and attention, excites cortical neurons in layer 6B by a direct postsynaptic action (rats: Bayer et al., 2004).

A common interpretation of CT neuron subtypes has been that these are related to segregated, parallel submodality processing. Transcriptional results, however, are tending to support a continuous variation and more textured heterogeneity within cell types as classically defined (Cembrowski and Menon, 2018; Cembrowski and Spruston, 2019). In mouse barrel cortex, for example, single gene expression profiles are preferentially associated with the two broad classes of layer 6 CT neurons, as defined by distinctive targeting by VPm alone or by VPm and POm (Chevee et al., 2018). Further, altering the neuronal activity state, by partial removal of whiskers, not only resulted in asynchronous gene expression between the two subtypes, but also in variation among neurons of the same subtype. This was discussed as a byproduct of regulatory redundancy, a temporal snapshot of dynamic processes, or as an inherent molecular variability in some ways essential to population-level function [Dueck et al., 2015, in Chevee et al. (2018)].

CT AND TC CONNECTIONS ARE ONLY APPROXIMATELY RECIPROCAL

Reciprocity of CT and TC connections is basic to the idea of a recursive loop; and zonal topographic reciprocity has been repeatedly demonstrated, by target and origin correspondence of cortical and thalamic projections. Visualization of single CG axons in cats, however, demonstrates a finer organization, consisting of a central region of dense terminations (400–500 μm across) and a larger, sparser surround zone (maximum spread of 500–1,500 μm; $n = 14$ axons, in cat: Murphy and Sillito, 1996). The smaller central region is consistent with a retinotopic correspondence; but the larger surround implies more global, not necessarily retinotopic processes, perhaps related to stimulus context over longer distances (Murphy and Sillito, 1996; and related, Darian-Smith et al., 1999). Comparably detailed data are lacking for other species and modalities, although whole brain imaging offers a promising new resource

for investigating these questions (in rodent: Winnubst et al., 2019).

Does reciprocity apply at the single cellular level ("looped" reciprocity)? Potentially, the several TC neurons postsynaptic to a layer 6 CT neuron could contact the same CT neuron, by direct monosynaptic terminations in layer 6 and/or indirect polysynaptic input via terminations in layer 4. If monosynaptic reciprocity actually occurs is unknown, but if so, it would be only a small percentage of the total synaptic input for the respective cortical and thalamic neurons. As reference, we can consider what is known of convergence and divergence of retinogeniculate axons, where a given LGN neuron (in cat) is estimated to receive input from 10 or more retinal axons, and each retinal axon diverges to innervate more than 20 relay thalamic cells. For four thalamic relay neurons, the proportion of retinal input from a single identified retinogeniculate axon varied from 2 to 100% [reviewed in Bickford (2019), and related Guo et al. (2020)].

For the more experimentally accessible visual cortical connections, information about global contours in a cluttered background is reported to emerge initially in "upstream" area V4 and only 40 ms later in V1, and then to develop in parallel in both areas. This has been interpreted as an incremental mechanism, drawing on both bottom-up and reentrant processes (Chen et al., 2014).

DIVERGENCE/CONVERGENCE

CT and TC connections are often discussed as if a segregated two-way ("loop") network. CT layer 6 neurons in the sensory areas, however, project not only to thalamus, but also to the reticular nucleus (RT), source of inhibitory inputs to the same thalamic nucleus (and potentially to the same, cortically-recipient thalamic neurons?). This connectivity motif is all the more compelling, since layer 5 CT projections (to association thalamus) tend to avoid giving collaterals to RT (e.g., Usrey and Sherman, 2019). The quantitative and spatial synaptic relationships have not been investigated in detail; and the degree of variability across CT neurons is unknown as concerns synaptic numbers and distribution. Recent results demonstrate that many, but not all the RT neurons exert a graded, frequency dependent inhibition of LGN relay cells (in mice: Campbell et al., 2020).

In the macaque visual system, secondary (i.e., less dense) CT projections originate from layer 6 of extrastriate area V2 (Briggs et al., 2016). It is currently unknown whether these extrastriate CT terminations converge on the same thalamic neurons as the denser projections from V1, or whether these CT neurons in V2 have feedback branches to V1 and/or to the pulvinar. There are of course multiple potential polysynaptic interconnections across the striatum, colliculus, pulvinar, and claustrum with both sensory thalamus and sensory cortex ("recurrent and highly interactive": Kravitz et al., 2013, for visual pathways).

The action of CT projections is not necessarily uniform across a thalamic nucleus (as, source and target specificity). Sensory thalamic nuclei are not homogeneous, but have nucleus-specific terminal configurations. In the LGN, for example, synaptic organization differs in encapsulated (glomerular) vs. interstitial zones, each having a differential juxtaposition of retinogeniculate, CG terminations, and local inhibitory neurons in relation to TC relay cell dendrites. The central visual representation of the LGN contains more encapsulated zones than regions receiving input from the peripheral retina. CT synapses (and inhibitory synapses from the reticular nucleus) predominate in the non-encapsulated, interstitial zones (Bickford, 2016, 2019). Here, also, talking about a two-way "loop" overly simplifies, and thereby limits progress.

COMMON SENSORY CORTICAL CALCULATION?

The classical anatomical terminology recognized primary sensory cortices as "heterotypical," with specialized architectonic features. Thus, area V1 in the visually dominant macaque has an elaborate laminar and modular organization; and in mice and rats, there is the intricate barrel/septum architecture in the somatosensory cortex. Intra-modal architectural features, however, differ even across related species (layer 4A in humans and non-human primates: Preuss and Coleman, 2002) and across individuals (size and number of ocular dominance columns in macaque: Horton and Hocking, 1996). The basic pattern of CT connections is recognizable across modalities and, with variations, phylogenetically conserved (summarized for rodents, cats, and monkeys: Rouiller and Welker, 2000); but it is not stereotyped: functionally significant quantitative parameters and microcircuitry vary by area and species. From the perspective of anatomical circuitry and architectural specializations, the idea of "common cortical calculation" seems hard to endorse.

In summary, the characterization of CT connections as "loops" is best seen as provisional. Both conceptually and methodologically, research is moving rapidly to a finer granularity and multi-dimensionality, taking account of subtypes of CT neurons, diversity of microcircuits, a plurality of physiological effects, and abundant and intricate interactions across systems, including neuromodulatory (i.e., the loop is multi-stranded). CT connections are not an isolated silo, but are components of large interacting networks (confluence of loops). This is in no way a new observation (Tantirigama et al., 2020 among others), but worth repeating, especially since the technical tools now available offer new opportunities for probing activity dependent interactions over whole brain networks, an essential approach for further investigations of basic elements of CT processing.

AUTHOR CONTRIBUTIONS

KR is responsible for content and presentation.

ACKNOWLEDGMENTS

I thank Drs. Giorgio Innocenti and Jennifer Luebke for constructive discussion and comments on the manuscript.

REFERENCES

Baker, A., Kalmbach, B., Morishima, M., Kim, J., Juavinett, A., Li, N., et al. (2018). Specialized subpopulations of deep-layer pyramidal neurons in the neocortex: bridging cellular properties to functional consequences. *J. Neurosci.* 38, 5441–5455. doi: 10.1523/JNEUROSCI.0150-18.2018

Bayer, L., Serafin, M., Eggermann, E., Saint-Mleux, B., Machard, D., Jones, B. E., et al. (2004). Exclusive postsynaptic action of hypocretin-orexin on sublayer 6b cortical neurons. *J. Neurosci.* 24, 6760–6764. doi: 10.1523/JNEUROSCI.1783-04.2004

Bickford, M. E. (2016). Thalamic circuit diversity: modulation of the driver/modulator framework. *Front. Neural Circuits* 9:86. doi: 10.3389/fncir.2015.00086

Bickford, M. E. (2019). Synaptic organization of the dorsal lateral geniculate nucleus. *Eur. J. Neurosci.* 49, 938–947. doi: 10.1111/ejn.13917

Blasdel, G. G., and Lund, J. S. (1983). Termination of afferent axons in macaque striate cortex. *J. Neurosci.* 3, 1389–1413. doi: 10.1523/JNEUROSCI.03-07-01389.1983

Borra, E., and Rockland, K. S. (2011). Projections to early visual areas v1 and v2 in the calcarine fissure from parietal association areas in the macaque. *Front. Neuroanat.* 5:35. doi: 10.3389/fnana.2011.00035

Briggs, F., Kiley, C. W., Callaway, E. M., and Usrey, W. M. (2016). Morphological substrates for parallel streams of corticogeniculate feedback originating in both V1 and V2 of the macaque monkey. *Neuron* 90, 388–399. doi: 10.1016/j.neuron.2016.02.038

Campbell, P. W., Govindaiah, G., Masterton, S. P., Bickford, M. E., and Guido, W. (2020). Synaptic properties of thefeedback connections from the thalamic reticular nucleus to the lateral geniculate nucleus. *J. Neurophysiol.* 124, 404–417. doi: 10.1152/jn.00757.2019

Cembrowski, M. S., and Menon, V. (2018). Continuous variation within cell types of the nervous system. *Trends Neurosci.* 41, 337–348. doi: 10.1016/j.tins.2018.02.010

Cembrowski, M. S., and Spruston, N. (2019). Heterogeneity within classical cell types is the rule: lessons from hippocampal pyramidal neurons. *Nat. Rev. Neurosci.* 20, 193–204. doi: 10.1038/s41583-019-0125-5

Chen, M., Yan, Y., Gong, X., Gilbery, C. D., Liang, H., and Li, W. (2014). Incremental integration of global contours through interplay between visual areas. *Neuron* 82, 682–694. doi: 10.1016/j.neuron.2014.03.023

Chevee, M., De Jong Robertson, J., Cannon, G. H., Brown, S. P., and Goff, L. A. (2018). Variation in activity state, axonal projection, and position define the transcriptional identity of individual neocortical projection neurons. *Cell Rep.* 22, 441–455. doi: 10.1016/j.celrep.2017.12.046

Constantinople, C. M., and Bruno, R. M. (2013). Deep cortical layers are activated directly by thalamus. *Science* 340, 1591–1594. doi: 10.1126/science.1236425

Coppola, J. J., and Disney, A. A. (2018). Is there a canonical circuit for the cholinergic system? Anatomical differences across common model systems. *Front. Neural Circuits* 12:8. doi: 10.3389/fncir.2018.00008

Crandall, S. R., Cruikshank, S. J., and Connors, B. W. (2015). A Corticothalamic switch: controlling the thalamus with dynamic synapses. *Neuron* 86, 768–782. doi: 10.1016/j.neuron.2015.03.040

Crandall, S. R., Patrick, S. L., Cruikshank, S. J., and Connors, B. W. (2017). Infrabarrels are layer 6 circuit modules in the barrel cortex that link long-range inputs and outputs. *Cell Rep.* 21, 3065–3078. doi: 10.1016/j.celrep.2017.11.049

Darian-Smith, C., Tan, A., and Edwards, S. (1999). Comparing thalamocortical and corticothalamic microstructure and spatial reciprocity in the macaque ventral posterolateral nucleus (VPLc) and medial pulvinar. *J. Comp. Neurol.* 410, 211–234. doi: 10.1002/(SICI)1096-9861(19990726)410:2<211::AID-CNE4>3.0.CO;2-X

Dueck, H., Eberwine, J., and Kim, J. (2015). Variation is function: are single cell differences functionally important? *Bioessays* 38, 172–180. doi: 10.1002/bies.201500124

Falchier, A., Clavagnier, S., Barone, P., and Kennedy, H. (2002). Anatomical evidence of multimodal integration in primate striate cortex. *J. Neurosci.* 22, 5749–5759. doi: 10.1523/JNEUROSCI.22-13-05749.2002

Freund, T. F., Martin, K. A., Soltesz, I., Somogyi, P., and Whitteridge, D. (1989). Arborisation pattern and postsynaptic targets of physiologically identified thalamocortical afferents in striate cortex of the macaque monkey. *J. Comp. Neurol.* 289, 315–336. doi: 10.1002/cne.902890211

Garraghty, P. E., and Sur, M. (1990). Morphology of single intracellularly stained axons terminating in area 3b of macaque monkeys. *J. Comp. Neurol.* 294, 583–592. doi: 10.1002/cne.902940406

Guo, K., Yamawaki, N., Barrett, J. M., Tapies, M., and Shepherd, G. M. G. (2020). Cortico-thalamo-cortical circuits of mouse forelimb S1 are organized primarily as recurrent loops. *J. Neurosci.* 40, 2849–2858. doi: 10.1523/JNEUROSCI.2277-19.2020

Guo, W., Clause, A. R., Barth-Maron, A., and Polley, D. B. (2017). A Corticothalamic circuit for dynamic switching between feature detection and discrimination. *Neuron* 95, 180–194. doi: 10.1016/j.neuron.2017.05.019

Hasse, J. M., and Briggs, F. (2017). A cross-species comparison of corticogeniculate structure and function. *Vis. Neurosci.* 34:E016. doi: 10.1017/S095252381700013X

Hawken, M. J., Shapley, R. M., Disney, A. A., Garcia-Marin, V., Henrie, A., Henry, C. A., et al. (2020). Functional clusters of neurons in layer 6 of macaque V1. *J. Neurosci.* 40, 2445–2457. doi: 10.1523/JNEUROSCI.1394-19.2020

Homma, N. Y., Happel, M. F. K., Nodal, F. R., Ohl, F. W., King, A. J., and Bajo, V. M. (2017). A Role for auditory corticothalamic feedback in the perception of complex sounds. *J. Neurosci.* 37, 6149–6161. doi: 10.1523/JNEUROSCI.0397-17.2017

Horton, J. C., and Hocking, D. R. (1996), Intrinsic variability of ocular dominance column periodicity in normal macaque monkeys. *J. Neurosci.* 16, 7228–7339. doi: 10.1523/JNEUROSCI.16-22-07228.1996

Jacob, S. N., and Nienborg, H. (2018). Monoaminergic neuromodulation of sensory processing. *Front. Neural Circuits* 12:51. doi: 10.3389/fncir.2018.00051

Kirchgessner, M. A., Franklin, A. D., and Callaway, E. M. (2020). Context-dependent and dynamic functional influence of corticothalamic pathways to first- and higher-order visual thalamus. *Proc. Natl. Acad. Sci. U.S.A.* 117, 13066–13077. doi: 10.1073/pnas.2002080117

Kravitz, D. J., Saleem, K. S., Baker, C. I., Ungerleider, L. G., and Mishkin, M. (2013). The ventral visual pathway: an expanded neural framework for the processing of object quality. *Trends Cogn. Sci.* 17, 26–49. doi: 10.1016/j.tics.2012.10.011

Ledergerber, L., and Larkum, M. E. (2010). Properties of layer 6 pyramidal neuron apical dendrites. *J. Neurosci.* 30, 13031–13044. doi: 10.1523/JNEUROSCI.2254-10.2010

Liang, L., Fratzl, A., Reggiani, J. D. S., Mansour, O. E., Chen, C., and Andermann, M. L. (2020). Retinal inputs to the thalamus are selectively gated by arousal. *Curr. Biol.* 30, 3923–3934.e9. doi: 10.1016/j.cub.2020.07.065

Mease, R. A., Krieger, P., and Groh, A. (2014). Cortical control of adaptation and sensory relay mode in the thalamus. *Proc. Natl. Acad. Sci. U.S.A.* 111, 6798–6803. doi: 10.1073/pnas.1318665111

Murphy, P. C., and Sillito, A. M. (1996). Functional morphology of the feedback pathway from area 17 of the cat visual cortex to the lateral geniculate nucleus. *J. Neurosci.* 16, 1180–1192. doi: 10.1523/JNEUROSCI.16-03-01180.1996

Preuss, T. M., and Coleman, G. Q. (2002). Human-specific organization of primary visual cortex: Alternating compartments of dense Cat-301 and calbindin immunoreactivity in layer 4A. *Cereb. Cortex* 12, 671–691. doi: 10.1093/cercor/12.7.671

Radnikow, G., and Feldmeyer, D. (2018). Layer- and cell type-specific modulation of excitatory neuronal activity in the neocortex. *Front. Neuroanat.* 12:1. doi: 10.3389/fnana.2018.00001

Rockland, K. S. (2019). Corticothalamic axon morphologies and network architecture. *Eur. J. Neurosci.* 49, 969–977. doi: 10.1111/ejn.13910

Rockland, K. S., and Ojima, H. (2003). Multisensory convergence in calcarine visual areas in macaque monkey. *Int. J. Psychophysiol.* 50, 19–26. doi: 10.1016/S0167-8760(03)00121-1

Rouiller, E. M., and Welker, E. (2000). Comparative analysis of the morphology of corticothalamic projections in mammals. *Brain Res. Bull.* 53, 727–741. doi: 10.1016/S0361-9230(00)00364-6

Stoelzel, C. R., Bereshpolova, Y., Alonso, J. M., and Swadlow, H. A. (2017). Axonal conduction delays, brain state, and corticogeniculate communication. *J. Neurosci.* 37, 6342–6358. doi: 10.1523/JNEUROSCI.0444-17.2017

Stringer, C., Pachitariu, M., Steinmetz, N., Reddy, C. B., Carandini, M., and Harris, K. D. (2019). Spontaneous behaviors drive multidimensional, brainwide activity. *Science* 364:255. doi: 10.1126/science.aav7893

Tantirigama, M. L. S., Zolnik, T., Judkewitz, B., Larkum, M. E., and Sachdev, R. N. S. (2020). Perspective on the multiple pathways to changing brain states. *Front. Syst. Neurosci.* 14:23. doi: 10.3389/fnsys.2020.00023

Tasic, B., Yao, Z., Graybuck, L. T., Smith, K. A., Nguyen, T. N., Bertagnolli, D., et al. (2018). Shared and distinct transcriptomic cell types across neocortical areas. *Nature* 563, 72–78. doi: 10.1038/s41586-018-0654-5

Thomson, A. M. (2010). Neocortical layer 6, a review. *Front. Neuroanat.* 4:13. doi: 10.3389/fnana.2010.00013

Usrey, W. M., and Sherman, S. M. (2019). Corticofugal circuits: communication lines from the cortex to the rest of the brain. *J. Comp. Neurol.* 527, 640–650. doi: 10.1002/cne.24423

Vanni, S., Hokkanen, H., Werner, F., and Angelucci, A. (2020). Anatomy and physiology of macaque visual cortical areas V1, V2, and V5/MT: bases for biologically realistic models. *Cereb. Cortex* 30, 3483–3517. doi: 10.1093/cercor/bhz322

Velez-Fort, M., Bracey, E. F., Keshavarzi, S., Rousseau, C. V., Cossell, L., Lenzi, S. C., et al. (2018). A circuit for integration of head- and visual-motion signals in layer 6 of mouse primary visual cortex. *Neuron* 98, 179–191. doi: 10.1016/j.neuron.2018.02.023

Winnubst, J., Bas, E., Ferreira, T. A., Wu, Z., Economo, M. N., Edson, P., et al. (2019). Reconstruction of 1,000 projection neurons reveals new cell types and organization of long-range connectivity in the mouse brain. *Cell* 179, 268–281. doi: 10.1016/j.cell.2019.07.042

Wiser, A. K., and Callaway, E. M. (1996). Contributions of individual layer 6 pyramidal neurons to local circuitry in macaque primary visual cortex. *J. Neurosci.* 16, 2724–2739. doi: 10.1523/JNEUROSCI.16-08-02724.1996

Yang, D., Gunter, R., Qi, G., Radnikow, G., and Feldmeyer, D. (2020). Muscarinic and nicotinic modulation of neocortical layer 6A synaptic microcircuits is cooperative and cell-specific. *Cereb. Cortex* 30, 3528–3542. doi: 10.1093/cercor/bhz324

Conflict of Interest: The author declares that the research was conducted in the absence of any commercial or financial relationships that could be construed as a potential conflict of interest.

frontiers in Neural Circuits

REVIEW
published: 11 March 2021
doi: 10.3389/fncir.2021.638429

Dissociable Cortical and Subcortical Mechanisms for Mediating the Influences of Visual Cues on Microsaccadic Eye Movements

Ziad M. Hafed[1,2], Masatoshi Yoshida[3], Xiaoguang Tian[4], Antimo Buonocore[1,2] and Tatiana Malevich[1,2,5]*

[1] Physiology of Active Vision Laboratory, Werner Reichardt Centre for Integrative Neuroscience, Tübingen University, Tübingen, Germany, [2] Hertie Institute for Clinical Brain Research, Tübingen University, Tübingen, Germany, [3] Center for Human Nature, Artificial Intelligence, and Neuroscience, Hokkaido University, Sapporo, Japan, [4] Department of Neurobiology, University of Pittsburgh Brain Institute, University of Pittsburgh, Pittsburgh, PA, United States, [5] Graduate School of Neural and Behavioural Sciences, International Max-Planck Research School, Tübingen University, Tübingen, Germany

Visual selection in primates is intricately linked to eye movements, which are generated by a network of cortical and subcortical neural circuits. When visual selection is performed covertly, without foveating eye movements toward the selected targets, a class of fixational eye movements, called microsaccades, is still involved. Microsaccades are small saccades that occur when maintaining precise gaze fixation on a stationary point, and they exhibit robust modulations in peripheral cueing paradigms used to investigate covert visual selection mechanisms. These modulations consist of changes in both microsaccade directions and frequencies after cue onsets. Over the past two decades, the properties and functional implications of these modulations have been heavily studied, revealing a potentially important role for microsaccades in mediating covert visual selection effects. However, the neural mechanisms underlying cueing effects on microsaccades are only beginning to be investigated. Here we review the available causal manipulation evidence for these effects' cortical and subcortical substrates. In the superior colliculus (SC), activity representing peripheral visual cues strongly influences microsaccade direction, but not frequency, modulations. In the cortical frontal eye fields (FEF), activity only compensates for early reflexive effects of cues on microsaccades. Using evidence from behavior, theoretical modeling, and preliminary lesion data from the primary visual cortex and microstimulation data from the lower brainstem, we argue that the early reflexive microsaccade effects arise subcortically, downstream of the SC. Overall, studying cueing effects on microsaccades in primates represents an important opportunity to link perception, cognition, and action through unaddressed cortical-subcortical neural interactions. These interactions are also likely relevant in other sensory and motor modalities during other active behaviors.

Keywords: superior colliculus, frontal eye fields, primary visual cortex, brainstem omnipause neurons, visual attention, microsaccades, fixational eye movements, visual selection

OPEN ACCESS

Edited by:
Max F. K. Happel, Leibniz Institute for Neurobiology (LG), Germany

Reviewed by:
Ken-ichi Amemori, Kyoto University, Japan
Jeffrey C. Erlich, New York University Shanghai, China

****Correspondence:***
Ziad M. Hafed
ziad.m.hafed@cin.uni-tuebingen.de

Received: *06 December 2020*
Accepted: *22 February 2021*
Published: *11 March 2021*

Citation:
Hafed ZM, Yoshida M, Tian X, Buonocore A and Malevich T (2021) Dissociable Cortical and Subcortical Mechanisms for Mediating the Influences of Visual Cues on Microsaccadic Eye Movements. Front. Neural Circuits 15:638429. doi: 10.3389/fncir.2021.638429

INTRODUCTION

Vision is a particularly important sensory modality for primates, and it is processed in early visual brain areas by magnifying the neural representation of the tiny foveal region of the retinal image (Rovamo et al., 1978; Dow et al., 1981; Perry and Cowey, 1985; Azzopardi and Cowey, 1996; Chen et al., 2019). This form of neural specialization creates a need to closely coordinate vision and eye movements, the latter being particularly important to sequentially align the foveal retinal image with different salient and/or behaviorally-relevant targets. As a result, foveating eye movements (most typically, saccades) represent one of the most obvious forms of visual selection mechanisms, and a plethora of behavioral evidence confirms an almost-obligatory link between visual selection and foveating eye movements (Schneider and Deubel, 1995; Deubel and Schneider, 1996; Awh et al., 2006). Mirroring such a close relationship, cortical and subcortical brain areas that are critical for eye movement generation, such as the frontal eye fields (FEF) (Bruce and Goldberg, 1985; Bruce et al., 1985; Schall, 1991a, 2002; Schall and Hanes, 1993; Schall et al., 1995; Tehovnik et al., 2000), lateral intraparietal area (LIP) (Andersen et al., 1987, 1992; Barash et al., 1991a,b; Mazzoni et al., 1996), and superior colliculus (SC) (Cynader and Berman, 1972; Updyke, 1974; Wurtz and Albano, 1980; Sparks and Nelson, 1987; Munoz and Wurtz, 1995), all exhibit visual sensory responses as well movement-related discharge.

The need for visual selection also extends to cases in which we proactively attempt to dissociate our gaze position from the retinal image region that we wish to preferentially process. In this covert form of selection, visual processing capabilities of peripheral image regions can be enhanced or suppressed, depending on a variety of factors related to task demands. For example, a highly predictive cue presented at an upcoming peripheral target location may result in perception at that "cued" location being momentarily better than perception at competing image locations, in a so-called "cueing effect" (Posner, 1980; Nakayama and Mackeben, 1989; Cameron et al., 2002; Solomon, 2004; Pestilli and Carrasco, 2005; Carrasco, 2011). Historically, such covert orienting was studied exclusively under gaze fixation, with the assumption that small fixational eye movements do not influence peripheral visual sensitivity. There have been numerous reviews on the behavioral and neural properties of covert visual selection with this assumption (Bisley, 2011; Carrasco, 2011; Petersen and Posner, 2012; Anton-Erxleben and Carrasco, 2013; Krauzlis et al., 2013; Veale et al., 2017; Fiebelkorn and Kastner, 2019).

However, during gaze fixation, small saccades still occur, and it is now evident that they are functionally important for both vision and cognition. These eye movements, commonly called microsaccades, optimize eye position at the foveal target (Ko et al., 2010; Poletti et al., 2013; Intoy and Rucci, 2020), and they are also associated with foveal target selection processes (Poletti et al., 2017). This makes microsaccades functionally similar to larger saccades, in the sense that they serve the purpose of scanning visual image regions; in the case of microsaccades, the image regions just happen to be foveal. Interestingly, microsaccades also influence peripheral visual processing in intriguing manners. For example, microsaccades contribute to visual "refreshing" of retinal images whenever they occur (Martinez-Conde et al., 2000; Khademi et al., 2020). And, perhaps more importantly, microsaccades can alter peripheral visual sensitivity (Hafed, 2013; Chen et al., 2015; Tian et al., 2016; Lowet et al., 2018), in a manner similar to how visual sensitivity is affected during covert cueing paradigms. It is this last functional role of microsaccades that is particularly relevant for the present article: if microsaccades can influence peripheral visual sensitivity, are they systematically modulated in covert visual cueing paradigms? At the turn of the current century, two human behavioral studies were instrumental in answering this question (Hafed and Clark, 2002; Engbert and Kliegl, 2003). These studies uncovered a clear correlation between both the rate and direction of microsaccades and the onset and loci of peripheral events being covertly processed; there was also a relationship to behavioral performance improvements or impairments associated with cueing. These two studies contributed, at least in part, to a much renewed interest in microsaccades over the ensuing two decades. The net result was that a long lasting segregation between investigating covert visual selective mechanisms and ever-present fixational microsaccades had ended.

Nonetheless, strong debates quickly emerged, especially when it came to assessing a potential causal role for microsaccades in influencing peripheral visual performance (Hafed, 2013; Chen et al., 2015; Hafed et al., 2015; Tian et al., 2016; Lowet et al., 2018). Such debates can only be resolved, in our view, if sufficient knowledge about the neural mechanisms linking visual cueing and microsaccadic modulations is acquired. In this article, we describe the current state of the art concerning such mechanisms, and we hypothesize about the future directions that will likely develop. The picture that is emerging is one of an interesting dissociation between contributions of cortical and subcortical visual and motor circuits. Most intriguingly, the evidence so far points to the importance of visual sensory processing even in classically-viewed motor areas deep in the brainstem, and this idea, in our opinion, has the potential to significantly advance our understanding of the physiology of active vision in primates.

Scope of This Article

We focus on causal perturbation experiments investigating how the onsets of peripheral visual cues can modulate microsaccades. As a result, the main emphasis will be on non-human primate studies. This emphasis exploits the remarkable repeatability of cueing effects on microsaccades in these animals (Hafed et al., 2011; Hafed and Ignashchenkova, 2013), thus enabling neurophysiological experiments. We also relate the findings to computational models, which were also motivated by non-human primate studies (Engbert et al., 2011; Engbert, 2012; Hafed and Ignashchenkova, 2013; Peel et al., 2016; Tian et al., 2016).

In all of the evidence that we review, we emphasize what is perhaps the most intriguing aspect of the links between microsaccades and visual selection: the large spatial dissociation between microsaccadic eye movement endpoints, which are tiny and foveal, and the peripheral loci of cues, cue-induced neural activity, and/or cue-influenced perceptual performance, which are all much farther out in eccentricity. This dissociation

can clarify interesting properties of visual-motor interactions in cortical and subcortical circuits, especially with respect to how readout of oculomotor maps may be realized for eye movements in general.

MICROSACCADES AND VISUAL CUES

Even though microsaccades were known to exist for many decades (Rolfs, 2009; Hafed, 2011), the impacts of peripheral visual cues on them only became documented in the present century. It is now known that the sudden onset of peripheral visual cues causes predictable microsaccadic modulations like those summarized in **Figures 1A,B**, based on data from rhesus macaque monkeys (Hafed and Ignashchenkova, 2013); very similar modulations also take place in humans (**Figure 1C**; Engbert and Kliegl, 2003; Galfano et al., 2004; Laubrock et al., 2005; Betta et al., 2007; Pastukhov and Braun, 2010; Engbert et al., 2011; Engbert, 2012; Tian et al., 2016).

In terms of microsaccade rate, the first modulation to occur is an abrupt cessation of microsaccade generation <100 ms after cue onset. This cessation is called microsaccadic inhibition (**Figure 1A**), and it is robust whether cues are behaviorally relevant or irrelevant, and whether cues are peripheral or foveal (Galfano et al., 2004; Laubrock et al., 2005; Betta et al., 2007; Rolfs et al., 2008; Hafed et al., 2011; Hafed and Ignashchenkova, 2013; Tian et al., 2016; White and Rolfs, 2016; Buonocore et al., 2017; Meyberg et al., 2017; Tian et al., 2018; Malevich et al., 2020). This inhibition also occurs with auditory stimuli (Rolfs et al., 2005, 2008), and it is generally similar to inhibition of larger saccades after abrupt visual onsets, in the phenomenon called saccadic inhibition (Reingold and Stampe, 1999, 2000, 2002; Buonocore and McIntosh, 2008; Edelman and Xu, 2009).

After a short microsaccadic inhibition interval of <100 ms, the second characteristic cue-induced modulation in microsaccade rate occurs. In this case, microsaccade rate increases to levels above the baseline pre-cue rate. This phenomenon is sometimes referred to as microsaccadic rebound, reflecting a rebound effect from the prior inhibition. In all cases with peripheral cues, the microsaccades are, by definition, too small to cause foveation of the visual onsets. Rather, they reflect an interaction between peripheral cue-induced visual activity and tiny microsaccade generation. Given the fact that many brain areas exhibit early stimulus-induced visual activity (and at approximately the same time as the onset of microsaccadic inhibition), the real question becomes which of these areas is causally most relevant for microsaccadic rate modulations.

In terms of microsaccade directions, even though the movements are not sufficiently large to foveate the appearing stimuli, their directions are still systematically related to them. Movements right before microsaccadic inhibition have directions that are highly congruent with the direction of the peripheral cues (**Figures 1B,C**). On the other hand, movements during the microsaccadic rebound phase are primarily directed in the opposite, cue-incongruent, direction (**Figures 1B,C**).

Thus, there is a microsaccadic direction oscillation (**Figures 1B,C**) that is unmasked by cue onset. The reason that we use the term "unmasked" is that behavioral and theoretical accounts have revealed that microsaccades tend to have temporal structure in terms of when they occur, and that such rhythmicity is associated with a general anti-correlation in direction between successive movements (Hafed and Clark, 2002; Abadi and Gowen, 2004; Gowen et al., 2007; Bosman et al., 2009; Hafed and Ignashchenkova, 2013; Tian et al., 2016). The role of peripheral visual cues in these accounts is, thus, akin to a phase resetting of the ongoing rhythms (**Figure 1D**), thus unmasking the direction oscillations (Engbert et al., 2011; Engbert, 2012; Hafed and Ignashchenkova, 2013; Tian et al., 2016; Bellet et al., 2017). Interestingly, phase resetting helps explain, at least partially, the strong microsaccadic rebound after microsaccadic inhibition: resetting results in a re-initiation of microsaccade generation processes; therefore, because it takes time to eventually trigger the movements after re-initiation, there will necessarily be a brief period of no microsaccades followed by a peak (**Figure 1D**). The peak time of the rebound reflects the approximate period of the microsaccadic rhythms, and subsequent peaks are washed out due to variability of inter-microsaccadic intervals.

We next describe the role of key cortical and subcortical brain structures that have been investigated with respect to such theoretical accounts. What one finds are dissociable impacts of different brain circuits to explain different aspects of the modulations. Perhaps most surprisingly, it is quite clear that microsaccadic inhibition, in particular, is not mediated by the most obvious candidate area repeatedly mentioned for it, the SC, as we now demonstrate. After demonstrating this, we will then relate the SC effects to effects mediated by other brain regions like the FEF, the primary visual cortex (V1), and the lower brainstem. By the end of the article, we will provide an integrative view of how we think all of the discussed brain areas complement each other in mediating the effects of **Figure 1**. This will provide a solid foundation for further exploring the functional role of microsaccades in covert visual selection mechanisms in the future.

THE SUPERIOR COLLICULUS (SC)

The SC and Microsaccade Generation

The first investigations linking SC neural activity to microsaccades were not concerned with studying cue-induced microsaccadic modulations. However, these modulations, and the original two human studies (Hafed and Clark, 2002; Engbert and Kliegl, 2003), provided strong motivation to search for a potential causal role for the SC in microsaccade generation (Hafed et al., 2009, 2021; Hafed, 2011; Hafed and Krauzlis, 2012). Recordings in the rostral portion of the SC, in which small retinotopic eccentricities are represented (Cynader and Berman, 1972; Robinson, 1972; Krauzlis et al., 1997, 2000; Hafed et al., 2008; Hafed and Krauzlis, 2008; Chen et al., 2019), revealed microsaccade-related discharge (Hafed et al., 2009; Hafed and Krauzlis, 2012). Specifically, for a given subset of microsaccade directions and amplitudes, constituting a given rostral SC neuron's movement field, the neuron emitted a strong burst

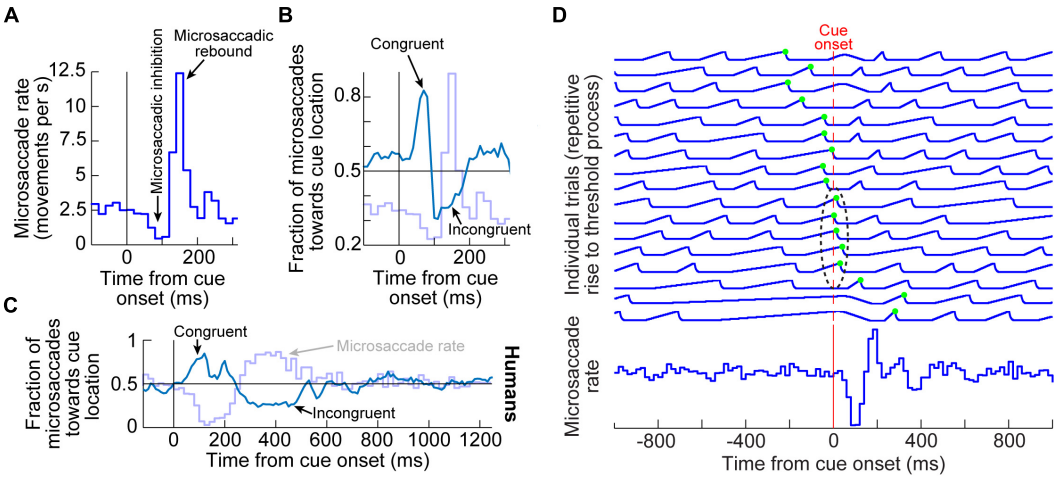

FIGURE 1 | Systematic modulation of microsaccades after peripheral cue onsets. **(A)** Microsaccade rate from one monkey as a function of time from cue onset. In a baseline interval (e.g. before the cue), microsaccades come at a steady rate. Less than 100 ms after cue onset, microsaccade rate abruptly decreases (microsaccadic inhibition). A later rebound above baseline microsaccade rate then occurs, before a subsequent return to steady-state frequency. **(B)** The distribution of microsaccade directions relative to peripheral cue onset location is also time varying, and in a manner that is related to the microsaccadic rate modulations [the faint curve shows microsaccade frequency from **(A)** as a reference]. At the onset of microsaccadic inhibition, microsaccade directions are strongly biased toward the cue location (congruent microsaccades). Shortly afterward, at the onset of the rebound phase, microsaccades are strongly biased opposite the cue direction (incongruent microsaccades). **(C)** Human microsaccades show very similar modulations, but with slower temporal dynamics. **(D)** Mechanistically, the effects in **(A–C)** may reflect a resetting of ongoing microsaccade generation rhythms. Each fixation trial may be viewed as a repetitive rise-to-threshold process; a microsaccade is triggered at every threshold crossing (green dots indicate the time of the nearest microsaccade to stimulus onset). Cue onset resets the rise-to-threshold process, such that across trials, the modulations in **(A–C)** can emerge (bottom histogram for the case of microsaccade rate). Note how the trials highlighted with the black oval are trials in which cue onset comes too late to successfully reset the currently ongoing microsaccade rise-to-threshold process, resulting in very early microsaccades after cue onset. This theoretical framework suggests that cued-induced microsaccadic modulations depend on specific sensory and motor structures contributing specific components of the modulations in **(A–C)**, as we review in this article. **(A,B,D)** adapted with permission from Hafed and Ignashchenkova (2013); **(C)** adapted with permission from Tian et al. (2016).

of spikes starting right before microsaccade onset and peaking during the movement itself (Hafed et al., 2009; Hafed and Krauzlis, 2012). Moreover, reversible inactivation of the rostral region of the SC significantly reduced microsaccade likelihood (Hafed et al., 2009; Goffart et al., 2012).

Subsequent results related these motor properties of SC discharge to visual activity in the same rostral SC region (Chen et al., 2019). It was found that superficial neurons have foveal visual response fields and deeper neurons exhibit microsaccade-related movement fields (Chen et al., 2019). Interestingly, there are also visual-movement SC neurons for microsaccades (Willeke et al., 2019). Therefore, in the decidedly small realm of microsaccades, all of the classic properties of the SC in saccade generation were observed (e.g., visual responses in the superficial layers, and visual-motor and motor responses in the deeper layers). This represents an important development because it demonstrates a continuum between microsaccades and larger saccades (Hafed and Krauzlis, 2012), and a similar continuum between representing foveal and peripheral visual eccentricities (Chen et al., 2019). Such continua provide a good reason for investigating how peripheral SC activity during cueing may influence microsaccades.

In the past few years, discovering the role of the rostral SC in microsaccade generation became even more relevant for the context of the current article. Specifically, the similarity between microsaccades and saccades at the level of the SC led to a natural question (Hafed, 2011) on whether known peri-saccadic changes in visual perception, such as saccadic suppression of visual sensitivity (Zuber and Stark, 1966; Beeler, 1967; Riggs and Manning, 1982; Thiele et al., 2002; Lee et al., 2007; Bremmer et al., 2009; Krekelberg, 2010; Idrees et al., 2020) and saccadic distortion of visual space (Ross et al., 1997, 2001; Tolias et al., 2001; Zirnsak et al., 2014; Hartmann et al., 2017; Grujic et al., 2018), also take place around microsaccades. This was indeed the case. Around microsaccades, it was found that neural visual sensitivity can be enhanced or suppressed in several areas, including the SC and FEF (Bosman et al., 2009; Herrington et al., 2009; Hafed and Krauzlis, 2010; Chen et al., 2015; Bellet et al., 2017; Chen and Hafed, 2017). Most interestingly, sensitivity enhancement or suppression could occur at eccentricities far from the microsaccade endpoints (Hafed and Krauzlis, 2010; Chen et al., 2015). Because covert visual selection also involves alterations in sensitivity at eccentricities away from the fovea, this led to the intriguing possibility of linking peri-microsaccadic changes in perception (at far eccentricities) with changes that are normally attributed to covert visual selection. In other words, if microsaccades are not random during visual cueing (Hafed and Clark, 2002; Engbert and Kliegl, 2003; Laubrock et al., 2005), and if they are associated with changes in (foveal and peripheral) visual perception and neural activity when they do occur (Hafed, 2013; Chen et al., 2015), then could it be that performance changes in classic covert cueing paradigms are simply mediated

by peri-microsaccadic changes in vision (Hafed, 2013; Hafed et al., 2015; Tian et al., 2016)? Such a hypothesis turned out to be entirely sufficient to account for some of the most classic cueing effects in the literature (Tian et al., 2016), but it was naturally controversial. To best assess how far such a suggestion could go in accounting for covert visual selection mechanisms, it became necessary to investigate the neural bases for cue-induced microsaccadic modulations, and the SC was the first natural place to look.

The SC and Cueing Effects on Microsaccades

The key aspect of peripheral cueing effects on microsaccades is the spatial dissociation between cue locations and movement endpoints: small microsaccades are influenced by visual onsets having eccentricities that can be more than an order of magnitude larger than the movement amplitudes (**Figure 1**). Therefore, to understand the impacts of peripheral cueing on microsaccades, it was important to consider peripheral, rather than foveal, SC activity. The question, therefore, became whether peripheral SC activity that is induced by cue onsets (e.g., cue-driven visual bursts) is causally necessary for influencing cue-induced microsaccadic modulations.

To answer this question, Hafed et al. (2011) first relied on an established attentional cueing task used previously with monkeys (Lovejoy and Krauzlis, 2010). The task involved four placeholder rings appearing around the fixated point, in each of the four display quadrants. One of these rings was a color singleton, acting as the cue to covertly select a location for a subsequent perceptual discrimination. Since color singletons pop out in the SC representation of the visual image, resulting in higher activity at the singleton's location (White et al., 2017a,b, 2019), it was expected that the onset of the color singleton was associated with differential peripheral spatial activation in the SC topographic map. It was, therefore, expected that microsaccades would be modulated after cue onset in this task (in a manner similar to **Figure 1**), and this was indeed the case (Hafed et al., 2011).

The authors then reversibly inactivated a portion of the SC topographic map by injecting muscimol, a GABA agonist (**Figure 2A**; Hafed et al., 2013). The goal was to inactivate the SC representation of either the attended visual quadrant or the diametrically opposite one, but without affecting the rostral SC region where microsaccade generation commands are originated (Hafed et al., 2009; Chen et al., 2019). Once a portion of the SC map was rendered inactive, the same cueing task was run again with the peripheral cue (color singleton) being placed either inside the affected visual quadrant or in the diametrically opposite, unaffected, location.

Surprisingly, microsaccadic rate modulations after cue onset were unaltered by SC inactivation. For example, **Figure 2B** (top) shows microsaccade rate from an example session's baseline data collected before muscimol injection. There was clear microsaccadic inhibition after cue onset, followed by a rebound. The very same modulation happened when the cue appeared in the affected quadrant (**Figure 2B**, bottom). Therefore, peripheral SC inactivation of cue-induced visual activity had no impact on the microsaccadic rate signature (**Figure 1A**). This conclusion was rendered even more concrete by inspecting the results from all inactivation sessions together (**Figure 2C**): whether the cue was placed inside the affected region of the display, in which cue-induced visual bursts were inactivated, or outside, the microsaccadic rate signature was the same. These results indicate that, contrary to expectations from models of microsaccadic and saccadic inhibition (Engbert, 2006; Rolfs et al., 2008; Bompas and Sumner, 2011; Engbert, 2012; Bompas et al., 2020), the SC is actually not causally involved in microsaccadic (or saccadic) inhibition.

Where the SC was indeed causally relevant was in the cue-induced direction oscillations; these were strongly disrupted. In the same example monkey of **Figure 2**, a large array of behavioral trials from the same task had previously shown cue-induced microsaccade direction oscillations (**Figure 3**, top; Hafed et al., 2011). There was an initial period of microsaccades being congruent in direction with the cue location (blue curve) followed by a subsequent period of incongruent microsaccades (red curve; **Figure 3**, top); this is similar to the direction oscillations shown in **Figures 1B,C**. When the SC was now inactivated and the cue was placed inside the affected region of the display, the initial biasing of microsaccade directions toward the cued location disappeared (**Figure 3**, middle), and it was replaced by an earlier biasing of cue-incongruent movements. Thus, elimination of peripheral cue-induced visual bursts in the SC did not affect microsaccade rate modulations (**Figure 2**), but it did result in an imbalance of peripheral SC representations, which reduced the propensity to generate cue-congruent microsaccades in the early phase after cue onset. This result was the first causal evidence that microsaccade directions can be strongly influenced by peripheral neural activity, despite the fact that the microsaccade endpoints are much smaller than the eccentricities associated with such activity. It was now finally possible to pinpoint a clear mechanism for the directional effects of cueing on microsaccades. It was also possible to confirm a related hypothesis on peripheral cueing motivated by rostral SC investigations of microsaccade generation (Hafed et al., 2009).

Most interestingly, when the peripheral singleton cue was now placed opposite the inactivated visual field region (that is, in a portion of the SC map that was intact), the cue-driven microsaccade direction oscillations were largely unaffected (**Figure 3**, bottom). This result is particularly intriguing when one considers the late population of microsaccades directed opposite the cue (after microsaccadic inhibition had ended; see **Figure 1**). With the cue placed outside of the affected region, these late microsaccades were actually directed toward the region inactivated by muscimol, but they still happened as if the entire SC map was intact (Hafed et al., 2013). This suggests that the impairment of microsaccade directions with the cue being placed in the affected region (**Figure 3**, middle) was specific to cue-induced visual bursts occurring near the onset time of microsaccadic inhibition. When microsaccades happened later in time, microsaccades could still be generated in the direction of the affected SC region without any clear impairments (we demonstrate later how the FEF may be critical

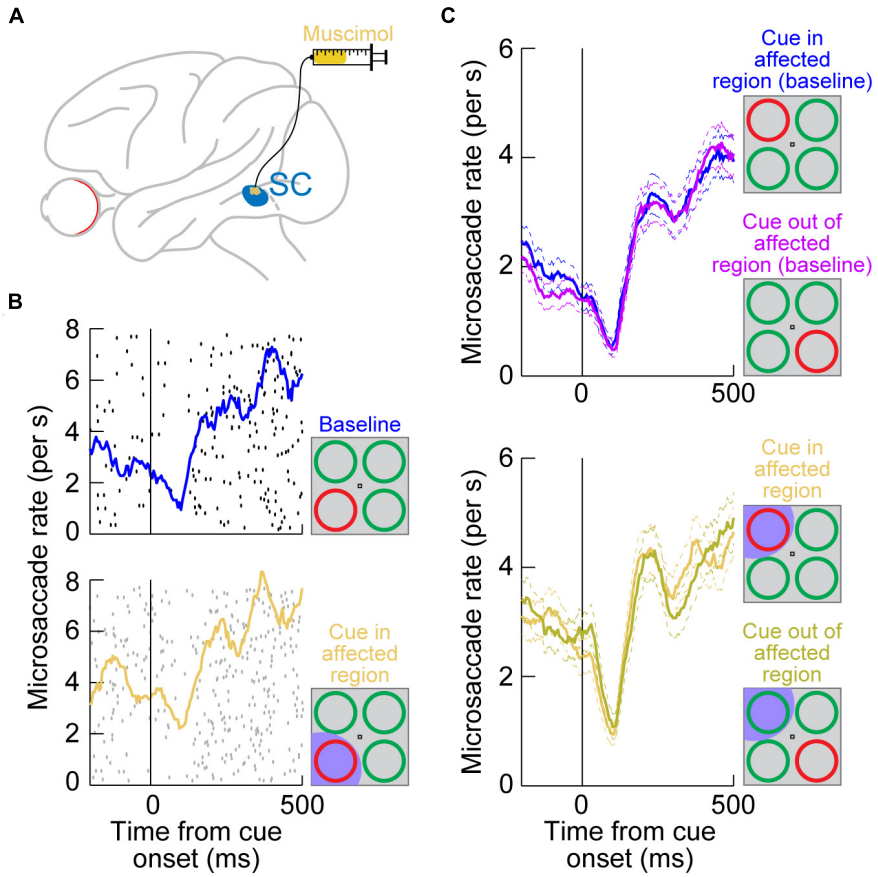

FIGURE 2 | Reversible inactivation of the SC does not influence microsaccadic rate modulations after peripheral cue onsets. **(A)** Injection of the GABA agonist muscimol into a restricted region of the SC topographic map. The injection was intended to affect only an extra-foveal representation of the SC, such that microsaccade-related neurons in the foveal zone (Hafed et al., 2009; Hafed and Krauzlis, 2012; Chen et al., 2019; Willeke et al., 2019) were largely not affected. Rather, it was the representation of the location of a peripheral visual cue that was targeted [see the bottom schematic in **(B)**] (Hafed et al., 2013). **(B)** Microsaccade rate in a cueing task from a sample session before SC inactivation (top) and after inactivation (bottom). The task consisted of the onset of a color singleton ring as the cue in an attentional task (Lovejoy and Krauzlis, 2010); see schematics on the right. In this session, the cue appeared in the bottom left quadrant of the display relative to fixation position. Each black or gray dot indicates the onset time of a microsaccade relative to cue onset (different rows represent different trials), and all microsaccades toward or opposite the cue quadrant are shown. The colored curves show microsaccade rate estimates in each block. In the bottom panel, the SC representation of the lower left quadrant of the display was inactivated (shaded in the bottom schematic); that is, it was the representation of the singleton cue that was affected. Microsaccadic inhibition happened regardless of SC inactivation, and the overall rate modulation was similar with or without SC inactivation (Hafed et al., 2013). **(C)** Microsaccade rate from the same monkey across all sessions. The top panel shows rate modulations without SC inactivation when the cue was either in or outside of the region to be targeted by muscimol (opposite quadrants; see schematic insets on the right). Microsaccade rate modulations were identical, with strong microsaccadic inhibition shortly after cue onset. In the bottom panel, data from the same sessions are shown, but now with the SC inactivated in one quadrant of the visual display. Whether the cue was placed in the affected quadrant or opposite from it (see schematic insets on the right), microsaccadic rate modulations were similar. **(B,C)** Adapted with permission from Hafed et al. (2013).

for these later microsaccades, explaining the lack of deficit with SC inactivation).

An interesting additional implication of the results in **Figure 3** is that they suggest that microsaccadic endpoint variance should be sensitive to the visual configuration of peripheral cues. That is, even though microsaccades never foveate the appearing peripheral cues, the early cue-congruent movements should still be sensitive to the spatial distribution of visual activation caused by the cues. Consider, for example, the two cue configurations in **Figures 4A,B**. In both cases, a peripheral stimulus appears to the right of fixation. However, in one case, the stimulus is a horizontal line (that is, with parallel visual activation to the axis connecting the line's center to fixation), and in the other case, it is a vertical line (that is, with orthogonal visual activation to the axis connecting the line's center to fixation). If peripheral visual bursts matter, then early cue-congruent microsaccades should exhibit endpoint variability that is parallel to the line's orientation in both cases. This means that in the orthogonal case, early cue-congruent microsaccades would not only be directed toward the cue (**Figures 1B,C**), but their orthogonal endpoint variability should also now reflect the orthogonal orientation of the stimulus. Indeed, microsaccade endpoint variability turned out to be sensitive to such spatial stimulus manipulations (**Figures 4D,E**). In the extreme case,

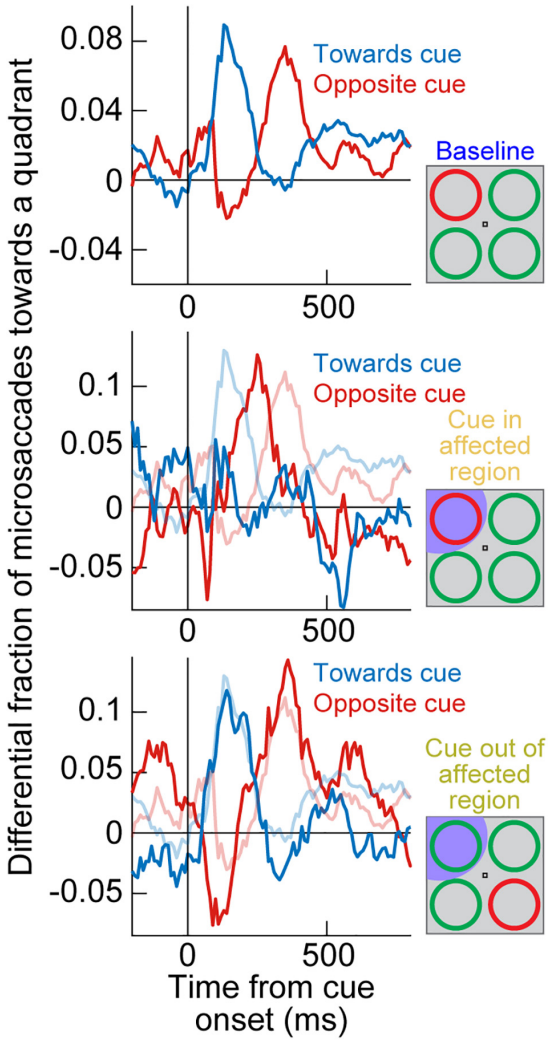

FIGURE 3 | Reversible inactivation of the SC strongly influences cue-induced microsaccade direction oscillations by impairing the propensity for early cue-directed movements. Each panel shows a measure of propensity to generate microsaccades in a certain direction. In the top panel, the singleton cue onset, without SC inactivation, caused a clear microsaccade direction oscillation in the same monkey as in **Figure 2**. First, there was an increased likelihood of microsaccades toward the visual quadrant of the cue (blue curve), and then there was an increased likelihood of microsaccades toward the opposite quadrant (red curve). For simplicity, movements to the other two visual display quadrants (the least modulated by the cue) are not shown. This panel was adapted with permission from Hafed et al. (2011). In the middle panel, the cue appeared in the quadrant affected by SC inactivation (see shading in the schematic inset on the right). The early cue-directed microsaccades were massively reduced relative to baseline (blue curve), and oppositely directed microsaccades (red curve) came earlier than in baseline. The baseline curves from the top panel are shown in faint colors for comparison. When the cue was placed opposite the affected region (bottom panel), the direction oscillations were normal again, and very similar to the baseline data without any SC inactivation (faint colors). Therefore, cue-incongruent microsaccades after microsaccadic inhibition (e.g., **Figure 1**) are not affected by SC inactivation (even when they are still directed toward the affected quadrant, as in the bottom panel); only the earlier cue-congruent microsaccades are affected when the cue is in the impaired display region. The middle and bottom panels are adapted with permission from Hafed et al. (2013).

when the cue onset consisted of a simultaneous onset of two spatially segregated stimuli (**Figure 4C**), a prediction out of these results was that early cue-induced microsaccades should be directed toward neither stimulus, but toward the vector average location. This was again the case (**Figures 4F,G**; Hafed and Ignashchenkova, 2013), lending further credence to the notion that cue-induced microsaccade directions are particularly influenced by SC activity: even for large saccades (Findlay, 1982), readout of SC activity by the oculomotor system is known to result in vector averaging saccades when multiple simultaneous loci of neural activation exist on the SC topographic map (Lee et al., 1988; Glimcher and Sparks, 1993; McPeek et al., 2003; Port and Wurtz, 2003; Katnani et al., 2012; Vokoun et al., 2014).

A further implication of the results of SC inactivation on early cue-influenced microsaccade directions (**Figure 3**) is that one can now attempt to establish a quantitative link between microsaccade endpoint variability and SC cue-induced visual bursts. Specifically, the timing of early cue-congruent microsaccades in **Figures 1–3** is consistent with the timing of SC visual bursts (Buonocore et al., 2017, 2020b). If eliminating such visual bursts via SC inactivation diminishes the likelihood of cue-congruent microsaccades (**Figure 3**; Hafed et al., 2013), then this might suggest that these cue-congruent microsaccades reflect readout of the SC map under a very specific simultaneity condition: a microsaccade burst in the direction of the appearing cue in the rostral SC region, and a simultaneous visual burst in the periphery at the site representing the cue's location (**Figure 5A**). If true, then there should be a measurable number of cue-induced visual spikes that are "injected" onto the SC map (when the cue appears) at the same time as the triggering of microsaccades (Buonocore et al., 2017, 2020b). This should "add" to the triggered movements and alter their size.

This idea was validated by measuring early cue-congruent microsaccade metrics: cue-congruent microsaccades were significantly larger in size than other microsaccades (Hafed and Ignashchenkova, 2013; Tian et al., 2016; Buonocore et al., 2020b). Importantly, there was also a quantitatively predictable relationship between the number of cue-induced visual spikes in the peripheral SC and the cue-congruent microsaccade amplitudes. To demonstrate this, Buonocore et al. (2020b) counted the number of visual spikes emitted by individually recorded peripheral SC neurons at the time of microsaccade triggering (**Figure 5A**). There was a linear relationship between the number of peripheral "visual" spikes and cue-congruent microsaccade amplitudes (**Figures 5B,C**): every single spike of every single visually-driven neuron contributed to the trajectory of early cue-congruent microsaccades (Buonocore et al., 2020b). Therefore, we now had a detailed mechanistic account of why early microsaccades after cue onset, near microsaccadic inhibition, are both directed toward the cue (**Figure 1**) and also larger in size (**Figure 5**).

Summary and Outlook

The SC does not cause microsaccadic inhibition, unlike in previous modeling assumptions (Engbert, 2006; Bompas and Sumner, 2011; Bompas et al., 2020). However, cue-induced SC visual bursts do alter both the directions (**Figures 3**, **4**) and

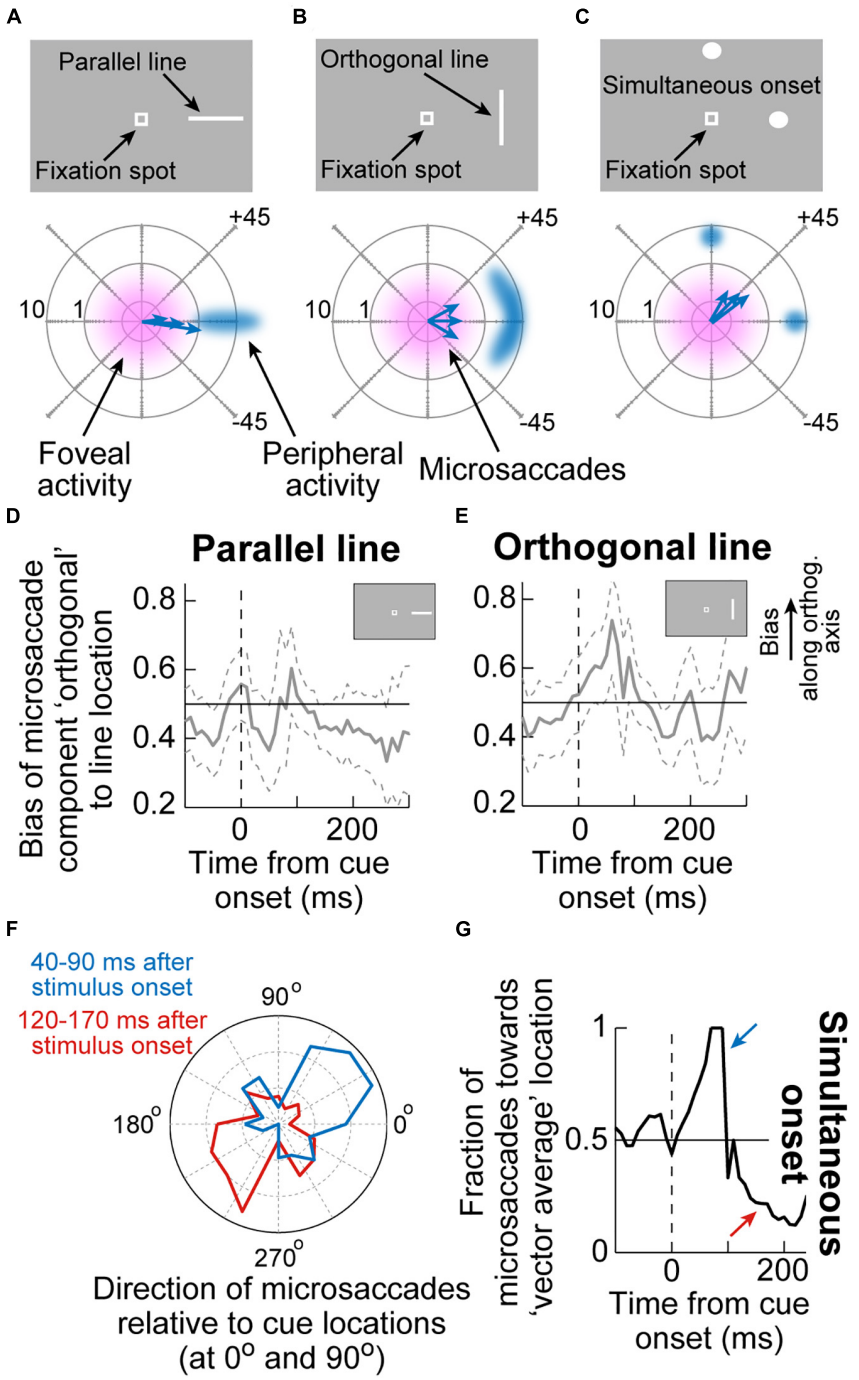

FIGURE 4 | Sensitivity of cue-induced microsaccade direction distributions to the spatial layout of peripheral cue configuration. **(A)** If the peripheral cue is spatially distributed as a parallel line relative to cue direction (top), as opposed to just a spot, then early cue-congruent microsaccades would exhibit endpoint variance along the axis of the appearing line. The bottom schematic shows how microsaccade endpoints, despite being foveal and not reaching the peripheral stimulus location, are still cue-directed, but exhibit variance along the orientation of the line. Eccentricity in the bottom schematic is plotted on a logarithmic scale to visually magnify the small amplitudes. **(B)** If the peripheral cue is at the same peripheral location but is oriented as an orthogonal line instead, then early cue-congruent microsaccades (bottom schematic) would have vertical variance reflecting the spatial extent of the peripheral stimulus. **(C)** In the extreme of two simultaneous onsets, spatial readout from a map like that of the SC for saccades would predict microsaccades to neither of the stimuli (bottom schematic). **(D,E)** The time course of microsaccade orthogonal bias for the configurations in **(A,B)**. For a parallel line **(D)**, there is no orthogonal bias. However, for an orthogonal line **(E)**, early cue-induced microsaccades directed toward the peripheral stimulus have increased orthogonal variance, as in **(B)**. **(F)** For a simultaneous stimulus onset, like in **(C)**, early cue-induced microsaccades (40–90 ms) are directed toward the vector average direction of the two stimulus locations, consistent with saccadic readout of SC map activity (Lee et al., 1988; Glimcher and Sparks, 1993; Port and Wurtz, 2003; Katnani et al., 2012). Later microsaccades (120–170 ms) are opposite the vector average location. **(G)** Time course of the effects in **(F)**. Adapted with permission from Hafed and Ignashchenkova (2013).

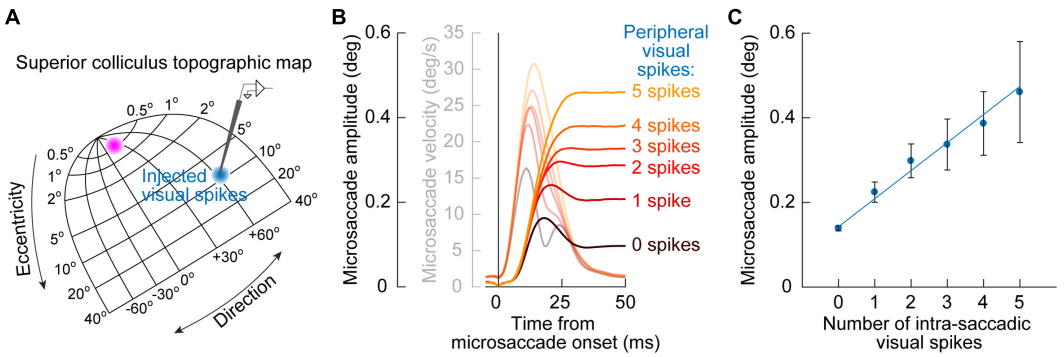

FIGURE 5 | Quantitative link between microsaccade endpoint variability for early cue-induced microsaccades and the number of peripheral cue-induced SC visual spikes. **(A)** After cue onset, a visual burst is emitted in the peripheral SC representation (blue population of neurons on the SC topographic map). The timing of these visual burst spikes coincides with the timing of early cue-congruent microsaccades (e.g., **Figure 1B**). This might suggest that the impact of the SC on early microsaccade directions (as predicted from **Figure 3**) is mediated by readout, by downstream structures, of cue-induced visual spikes in the SC as if they were part of the simultaneously occurring movement spikes in the rostral SC (magenta population). **(B)** Consistent with this, cue-congruent microsaccades are larger in size than baseline microsaccades (Hafed and Ignashchenkova, 2013; Tian et al., 2016). More critically, the increase in size is deterministically related to the number of peripheral cue-induced SC spikes. The more "visual" spikes in a recorded peripheral SC neuron at the cued location, the larger the microsaccade. Faint colors also show microsaccade velocity profiles. **(C)** This relationship between cue-induced visual spikes in the SC and early cue-induced microsaccade amplitudes is linear for movements toward the cue (the great majority of movements shortly after cue onset). Thus, every spike of every active cue-driven SC neuron contributes to microsaccade endpoint variability. Adapted with permission from Buonocore et al. (2020b).

amplitudes (**Figure 5**) of early cue-congruent microsaccades. Later cue-incongruent movements (i.e., during the microsaccadic rebound phase in **Figure 1**) are unaffected by SC inactivation (**Figure 3**, bottom). What, then, controls post-inhibition microsaccades? According to phase resetting hypotheses (**Figure 1D**; Hafed and Ignashchenkova, 2013; Tian et al., 2016, 2018), rebound microsaccades represent deliberate responses to the recently appearing and cognitively processed visual stimuli. From that perspective, cue incongruence would result from a willful attempt to avoid "breaking fixation" and overtly looking toward the cue (Tian et al., 2016, 2018). Indeed, with simultaneous stimulus onsets (**Figures 4C,F,G**), post-inhibition microsaccades were also directed opposite the vector average direction rather than toward or opposite either of the two stimulus locations, again suggesting compensation for an earlier reflexive tendency to look. In what follows, we describe how post-inhibition microsaccades are, therefore, particularly sensitive to FEF activity. This suggests a division of labor between cortical and subcortical influences on cue-induced microsaccades, and it paves the way for further discussions of V1 and lower brainstem involvements.

THE FRONTAL EYE FIELDS (FEF)

The FEF and Microsaccade Generation

Unlike in the SC, there are currently no physiological recording data in the FEF demonstrating microsaccade-related neural discharge. However, the FEF is an important structure for mediating saccadic eye movements in general (Bruce and Goldberg, 1985; Schall, 1991b, 2002; Schall et al., 1995; Tehovnik et al., 2000; Sommer and Wurtz, 2001). Also, large-volume inactivations of the FEF, using cryogenic techniques (**Figure 6A**), significantly altered microsaccades (Peel et al., 2016). Specifically, unilateral inactivation of the FEF resulted in microsaccades becoming larger than normal. This effect was larger for contraversive microsaccades (that is, directed toward the visual hemifield affected by FEF inactivation) than for ipsiversive movements (Peel et al., 2016). Moreover, microsaccade kinematics were also altered, with both unilateral and bilateral FEF inactivation resulting in abnormally slower and longer-duration movements (Peel et al., 2016). In other words, the known main sequence relationship of peak velocity vs. amplitude (Zuber et al., 1965; Bahill et al., 1975) was shifted downwards by FEF inactivation. Interestingly, unlike in the rostral SC (Hafed et al., 2009; Goffart et al., 2012), unilateral FEF inactivation did not reduce baseline microsaccade rate in the absence of cueing (Peel et al., 2016). Only with bilateral FEF cooling was the overall microsaccade rate reduced.

These results were the first causal demonstration that FEF neural activity can influence microsaccades, likely by affecting both the SC and downstream brainstem oculomotor control circuitry. This is also consistent with the fact that unilateral FEF inactivation using the same cryogenic techniques also reduced the peak velocities of large saccades (Peel et al., 2014); also see related lidocaine and muscimol inactivation results in Sommer and Tehovnik (1997) and Dias and Segraves (1999). However, a causal impact of the FEF on microsaccades was also very interesting from the perspective of cueing effects on these eye movements, as we describe next.

The FEF and Cueing Effects on Microsaccades

With unilateral large-volume FEF inactivation, microsaccadic rate modulations after the onset of a peripheral visual target still showed intact microsaccadic inhibition (Peel et al., 2016).

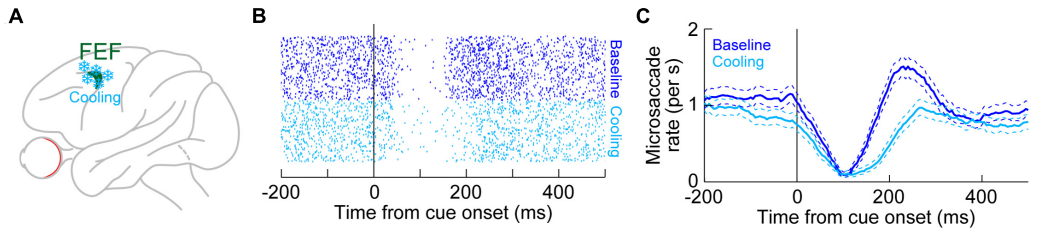

FIGURE 6 | Reversible inactivation of the FEF, through cryogenic techniques, strongly influences microsaccade rate in the post-inhibition rebound phase. **(A)** Large portions of the FEF (either unilaterally or bilaterally) were reversibly inactivated by cooling of neural tissue. **(B)** Microsaccade onset times across trials (each row of rasters represents an individual trial) in baseline (blue) or with unilateral FEF inactivation (light blue). The task consisted of fixation with the onset of a peripheral spot in the affected hemifield. In baseline, there was expected microsaccadic inhibition shortly after cue onset, followed by a rebound in microsaccade likelihood. With FEF inactivation, microsaccadic inhibition still occurred, and with similar latency to baseline. However, the post-inhibition rebound was strongly impaired, resulting in an appearance of prolonged microsaccadic inhibition. **(C)** Microsaccade rate estimates for the data in **(B)**. Microsaccadic inhibition still clearly happened with or without FEF inactivation. However, microsaccadic rebound only happened when the FEF was intact (baseline). **(B,C)** Adapted with permission from Peel et al. (2016).

In fact, even with bilateral FEF inactivation, microsaccadic inhibition was still largely unaffected. Therefore, like in the SC, the early microsaccadic inhibition phase of the microsaccadic rate signature (**Figure 1A**) was strongly resilient to impaired FEF activity.

However, unlike with the SC, FEF inactivation had a strong effect on microsaccadic rebound rate, and particularly with bilateral inactivation. For example, **Figure 6B** shows microsaccade times after cue onset in the absence of FEF inactivation (blue dots, top half of the panel) or during unilateral FEF inactivation (light blue dots, bottom half of the panel). The microsaccade rasters were very similar except during the rebound phase. This is also evident in **Figure 6C**, plotting the rate curves for the same data. Microsaccadic inhibition was unaltered by unilateral FEF inactivation, but there was an impairment in the generation of post-inhibition rebound microsaccades (Peel et al., 2016). This effect was almost doubled in size when the FEF was inactivated bilaterally (Peel et al., 2016), and bilateral inactivation also reduced overall microsaccade rates even in the baseline pre-cue interval as well (Peel et al., 2016). Once again, microsaccadic inhibition was largely unchanged by bilateral inactivation.

The effect of FEF inactivation on microsaccade rate during the microsaccadic rebound phase (**Figure 6**) is additionally interesting from the perspective of cue location. With unilateral inactivation, the cue could either appear in the affected hemifield (contralesional) or in the unaffected one (ipsilesional). In both cases, the rebound rate was reduced. This could reflect the fact that each of the right and left FEF might still contain a small component of ipsilateral visual field representation, and it is also consistent with the kinematic effects described above (Peel et al., 2016). Naturally, bilateral FEF inactivation also affected the rebound rate in both the right and left hemifields (Peel et al., 2016). Nonetheless, one could wonder whether the presence of a rate effect in **Figure 6** and its absence in **Figure 2** for the case of SC inactivation could reflect methodological differences between techniques. For example, the volume of tissue affected by cooling was putatively larger than that affected by muscimol injection (Hafed et al., 2013; Peel et al., 2016). Moreover, the SC (Chen et al., 2019) is more topographically organized than the FEF (Bruce et al., 1985; Sommer and Wurtz, 2000), allowing the authors of Hafed et al. (2013) to avoid, as much as experimentally possible, injection of muscimol into the rostral region where microsaccade-related discharge is found. Were the results of **Figure 6**, then, a technique artifact?

The authors of Peel et al. (2016) concluded that it is unlikely that methodological differences provided the full explanation for the microsaccade rate differences between SC and FEF inactivation. In fact, both of the above-mentioned methodological differences (which are inherent in the FEF experiments) should be expected to cause massive, non-specific effects on microsaccade rate. Rather, the effect of FEF inactivation was temporally specific (**Figure 6**), only affecting microsaccade rate in the rebound phase (Peel et al., 2016). Therefore, it is safe to conclude that the role of the FEF in cue-induced microsaccadic modulations is indeed critical for mediating the microsaccadic rebound modulation of **Figure 1**.

In terms of microsaccade directions, the overall results were slightly harder to interpret, especially because of a small offset in eye position caused by the FEF inactivation, and because of idiosyncratic biases of the monkeys even without inactivation (Peel et al., 2016). Nonetheless, there was a sufficiently clear pattern for the microsaccades occurring late after cue onset, in the microsaccadic rebound phase: the directions of these movements were affected the most by unilateral FEF inactivation. The specific effect was to temper the expected strong bias away from the cue. In other words, impairing the FEF also impaired the ability to bias late microsaccades away from the cue. Interestingly, this result was strongest when the cue had appeared in the affected hemifield, suggesting that the intact FEF somehow tags cue location for dealing with the microsaccades that come after microsaccadic inhibition, even when these microsaccades are cue-incongruent (Peel et al., 2016). Thus, the primary effect of FEF inactivation was to control the timing of microsaccadic deployment after microsaccadic inhibition, through modulation of the rebound phase (Peel et al., 2016). This is almost the opposite of the role of the SC in mediating cue-induced microsaccadic modulations, in which it was direction (and not rate) that was most affected, and earlier in time (Hafed et al., 2013).

Consistent with the above, changing a single parameter in the same theoretical model described in **Figure 1D** (Hafed and Ignashchenkova, 2013) could account for the influences of unilateral FEF inactivation. Specifically, after successful microsaccadic inhibition, these models (developed well before the FEF inactivation experiments) invoked a top-down facilitation factor for programming the first rebound microsaccade (that is, an increase in the slope of the rise-to-threshold process in **Figure 1D**). A conceptually similar top-down facilitation factor was also invoked in other models of cueing effects on microsaccades (Engbert, 2012). To model unilateral FEF inactivation, simply reducing this top-down facilitation factor was sufficient to replicate the results in **Figure 6** (Peel et al., 2016). Interestingly, adding just an overall sluggishness for all microsaccades (that is, just reduced global drive) was also sufficient to account for the bilateral FEF inactivation effects of both reduced rebound but also reduced overall microsaccade rate in general (Peel et al., 2016).

Summary and Outlook

A significant component of microsaccadic modulations after cue onsets is now relatively well understood in terms of dissociable causal contributions of the cortical FEF and the subcortical SC (**Figures 2–6**). What remains is to understand why microsaccadic inhibition is so resilient in the face of large perturbations of two key candidate areas for mediating it (the SC and FEF), and also to link the microsaccadic modulations to the bigger question of why microsaccades happen at all in the first place during cueing tasks. Answering the first question will complete the story of explaining all key components of the now-classic modulations seen in **Figure 1**, and answering the second question can help clarify the functional role of cue-induced microsaccadic modulations, particularly with respect to the hypotheses associated with peri-microsaccadic changes in covert visual selection performance that we alluded to earlier (Hafed et al., 2015).

A CAUSAL BEHAVIORAL MANIPULATION FOR ISOLATING PUTATIVE SC AND FEF CONTRIBUTIONS TO CUEING EFFECTS ON MICROSACCADES

We will address the first question above shortly. For the latter, significant insight can be made when considering perturbation experiments that are not neural, but behavioral. Specifically, microsaccades, like other eye movements, ultimately alter the visual image impinging on the retina. Thus, even the simple act of fixating a tiny spot is an active visual-motor process, with microsaccades and ocular position drifts continuously shifting the visual position of the spot in the fovea. It therefore stands to reason that a visual error in the fovea (that is, a difference between where gaze is directed and where the target for fixation is in the retinal image) should be an important visual driver for microsaccades (Ko et al., 2010; Poletti et al., 2013). Indeed, microsaccades correct tiny foveal position errors, even during cueing tasks (Tian et al., 2016, 2018). In that regard, experimentally perturbing the natural active vision cycle for microsaccades, by experimentally eliminating expected modulations of foveal visual error as a result of microsaccade occurrence, should magnify and isolate the putative impacts of the SC (mediating reflexive cue-directed microsaccades) and FEF (mediating subsequent deliberate movements). Thus, so-called retinal-image stabilization experiments may be viewed as a behavioral test of the results and interpretations of **Figures 3–6**.

This approach was adopted by Tian et al. (2016, 2018). In their experiments, monkeys fixated, and a peripheral visual stimulus appeared and persisted on the display (**Figure 7A**). In control trials (**Figure 7A**, left), the normal visual-motor loop was active because the stimuli were stable on the display; therefore, whenever an eye movement happened, the visual error at the fixation spot was altered due to movement of the retinal image. On the other hand, in retinal-image stabilization experiments (**Figure 7A**, right), both the fixation spot and peripheral stimulus were presented in a gaze-contingent manner. Thus, the fixation spot and peripheral stimulus were rendered much more stable on the retina. Moreover, the fixation spot was stabilized as close as possible to the current gaze position, thus resulting in minimal visual error for most of the time (Tian et al., 2016).

In the control trials, oscillations in microsaccade directions after stimulus onset were evident (**Figure 7B**, left), as expected from **Figure 1**. However, with retinal-image stabilization, two key results emerged. First, the early cue-directed bias in microsaccade directions was still present, but it was amplified relative to control trials (blue upward arrow). This supports the mechanisms laid out in **Figure 5**. Specifically, without retinal image stabilization, the microsaccade goal (magenta location in **Figure 5A**) could either be congruent with the upcoming peripheral stimulus location (the situation depicted in **Figure 5A**) or it could be incongruent. This was simply uncontrollable because the peripheral stimulus always came asynchronously to ongoing state. Therefore, if it happened that the peripheral bursts occurred with a microsaccade goal being in the opposite direction, then there would have been a conflict between the need of the oculomotor system to correct the foveal error (by implementing the microsaccade burst) and the impact of peripheral visual bursts in the other direction. This is a condition that makes it harder for the peripheral cue to "attract" microsaccades (Tian et al., 2016, 2018). If the microsaccade goal happened to be congruent with the peripheral visual bursts, then cue-directed microsaccades were easier to trigger. As a result, on average, the effect was muted when compared to the retinal-image stabilization condition, in which the visual error at the fixation spot was experimentally minimized and controlled on every single trial (**Figure 7B**, blue upward arrow). Thus, not only does the SC contribute to modifying early microsaccade metrics in a seemingly reflexive manner (**Figures 3–5**), but this is functionally related to what the oculomotor system is anyway trying to achieve when gaze fixation is required: minimize visual errors at fixation (Tian et al., 2016).

The second effect that happened with retinal-image stabilization was the observation that subsequent microsaccades (after the initial cue-congruent movements) became much

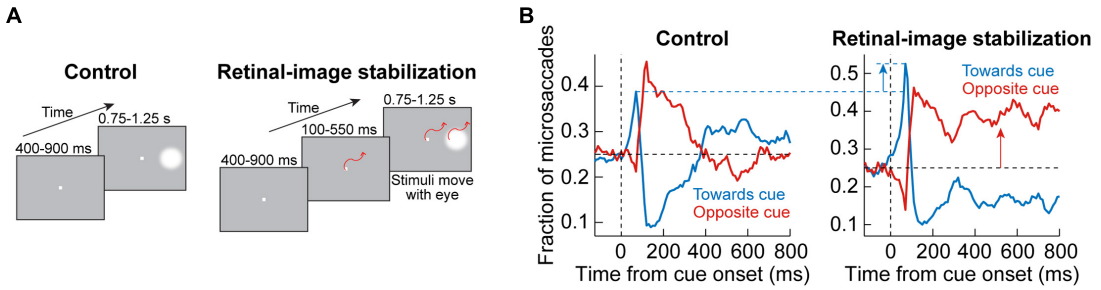

FIGURE 7 | Behavioral causal manipulation to isolate the influences of SC and FEF activity on cue-induced microsaccades. **(A)** Behavioral task to experimentally control the spatial landscape of visual and oculomotor activity (Tian et al., 2016). In control (left), a peripheral cue appeared during fixation and was maintained throughout trial duration. With real-time retinal-image stabilization, the fixation spot and cue were experimentally pegged on the retina (that is, moved with the eye). Thus, a cue-induced early microsaccade did not generate a foveal position error at fixation that needed to be corrected; on the other hand, it could move the peripheral stimulus even farther out on the display (potentially rendering it invisible beyond the display edge if there was no top-down compensation that is implemented). **(B)** In control (left panel), a plot of microsaccade direction distributions reveals a similar oscillation to **Figure 1**: first, there was a bias of movements toward the cue (blue curve elevating above the horizontal black dashed line), and then there was a bias of opposite movements (red curve elevating above the horizontal black dashed line). With retinal-image stabilization (right panel), the early cue-induced effect was amplified. This was because the spatial layout of the peripheral stimulus onset was no longer competing with other factors like foveal position error at the fixation spot, which was uncontrolled in the control condition. Moreover, for subsequent microsaccades, there was a strong bias opposite the cue. Without such a bias, the peripheral stimulus could eventually have moved out of the display if all microsaccades continued to be toward the cue. Therefore, this causal manipulation further highlights the notion that post-inhibition microsaccades require top down strategic control, whereas early cue-induced microsaccades (during microsaccadic inhibition) are more reflexive (and likely subcortically mediated). Adapted with permission from Tian et al. (2016).

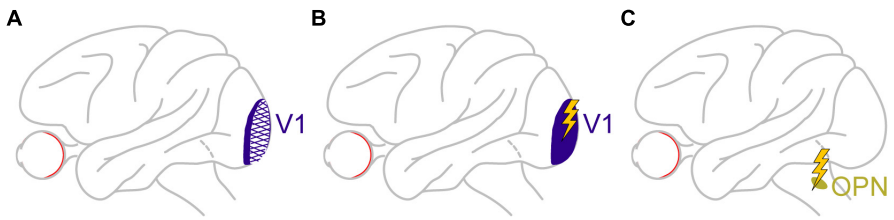

FIGURE 8 | Causal manipulations in V1 and also downstream of the SC provide additional insights on the dissociable roles of cortical and subcortical pathways in mediating cue-induced influences on microsaccades. **(A)** Monkeys with large V1 lesions can perform cueing tasks (Yoshida et al., 2017), and how microsaccades in them are affected will provide a rich source of information on cortical routes for affecting cue-induced microsaccades. The available evidence so far suggests that, for at least some type of cues, V1 is not necessary for microsaccadic inhibition to occur (Yoshida and Hafed, 2017). **(B)** In monkeys with an intact V1, brief microstimulation pulses mimicking the brief visual bursts caused by cue onsets also provide hints on the role of V1 visual bursts in microsaccadic rate and direction modulations. In this case, V1 is sufficient for inhibition to occur (Buonocore et al., 2020a), likely through the generation of visual phosphenes that eventually propagate into the oculomotor system. **(C)** Finally, brief microstimulation pulses mimicking brief visual bursts (Buonocore et al., 2020a) in omnipause neurons (OPN's), downstream of the SC, are isolating a role for these neurons, which constitute the final gating point for saccade generation, in implementing microsaccadic inhibition. The lack of influence of SC and FEF inactivation on microsaccadic inhibition (**Figures 2**, **6**), as well as the persistence of inhibition even with V1 lesions (for at least the types of cues tested so far), might mean that it is indeed OPN's that are the most critical structure for implementing microsaccadic inhibition.

more strongly biased away from the persistent stimulus (**Figure 7B**, right; red upward arrow). Therefore, unlike the earlier cue-directed microsaccades, which were minimally affected, subsequent microsaccades became very different with a different kind of behavioral context (this time, the retinal-image stabilization context). Again, this supports the notion that post-inhibition microsaccades are a deliberate act relying on frontal cortical control (**Figure 6**), and therefore dependent on behavioral task. Indeed, if the eyes were to reflexively follow the cue continuously under retinal-image stabilization, then the peripheral target would end up moving beyond the extent of the visual display; success in the task required a purposeful strategy to bias microsaccades in the opposite direction to maintain view of the peripheral target on the display until trial end (Tian et al., 2016). If post-inhibition microsaccades were not under top-down control, then such contextual modification of the directional bias of these subsequent microsaccades would not be possible.

Summary and Outlook

Microsaccadic modulations after peripheral cue onsets are stereotypical (**Figure 1**), but they have dissociable components in terms of their underlying mechanisms. Certain components of the modulations, such as microsaccadic inhibition, are unaccounted for by large perturbations of both the SC (**Figure 2**) and FEF (**Figure 6**). On the other hand, other components, such as directional biases, are separated based on when they happen: early biases are mediated by the SC and seem to be reflexive (**Figures 3–5**); later biases are mediated by the FEF (**Figure 6**) and seem to be deliberate. Functionally, all

components of cue-induced microsaccadic modulations aim to optimize eye position at the fixation spot, despite momentary reflexive tendencies to be attracted by the suddenly appearing peripheral cues (**Figure 7**). This leaves a final unanswered question about the cue-induced microsaccadic modulations studied in the current article: why is microsaccadic inhibition so resilient to large inactivations of the SC and FEF, and what mediates it?

THE PRIMARY VISUAL CORTEX (V1)

Microsaccadic inhibition must have an inherently sensory component associated with it. First, it arrives at the time of cue-induced visual bursts (e.g., **Figures 1**, **5**). Second, microsaccadic inhibition timing and strength depend on various stimulus properties, such as cue contrast, spatial frequency, and luminance contrast polarity (Rolfs et al., 2008; Bonneh et al., 2015; Scholes et al., 2015; Malevich et al., 2020). The inhibition is also correlated with subjective stimulus visibility (White and Rolfs, 2016). Therefore, even though the inhibition itself is a motor action, it must clearly be sensitive to visual sensory signals. This might suggest that an early sensory area, like V1, can contribute to microsaccadic inhibition, by virtue of its obvious sensory capabilities.

In another large perturbation experiment, large portions of unilateral V1 were lesioned in monkeys (**Figure 8A**), in order to generate an animal model of blindsight (Yoshida et al., 2008, 2012; Isa and Yoshida, 2009; Ikeda et al., 2011; Kato et al., 2011; Takaura et al., 2011). In addition to all of the characterizations of visual and oculomotor capabilities of these animals in the above studies, it was recently found that these "blindsight monkeys" could also still perform covert cueing tasks, albeit with altered performance (Yoshida et al., 2017). This finding was important because it represented an excellent opportunity to test for a causal role of V1 in microsaccadic inhibition (and other modulations). Therefore, the authors analyzed microsaccades in these animals during cueing tasks. Preliminary results so far (Yoshida and Hafed, 2017) reveal that microsaccadic inhibition still took place, despite the large V1 lesions, although the analyses were made with foveal cues (foveal V1 was largely spared by the lesions). It therefore remains to be seen how microsaccadic inhibition in these animals behaved when peripheral cues, like in the tasks of Peel et al. (2016), were used. It is highly likely, in our opinion, that microsaccadic inhibition will still be seen, suggesting that an intact V1 is not necessary for microsaccadic inhibition to occur. Interestingly, there were other asymmetries in microsaccade generation that resulted from V1 lesions, but these are beyond the scope of this exposition.

The fact that V1 might not be necessary for microsaccadic inhibition does not mean that V1 cannot still contribute, at least indirectly. After all, cue onsets are expected to cause short-lived visual bursts in V1, and at roughly similar times to the visual bursts in the SC (e.g., **Figure 5**). Moreover, signals from V1 bursts can then propagate, with short latencies, to areas that can ultimately influence the oculomotor system. To test for this idea, in yet additional preliminary perturbation results (Buonocore et al., 2020a), Buonocore et al. recently electrically microstimulated V1 neurons with very brief bursts of pulses (**Figure 8B**). These brief pulse trains were intended to simulate the occurrence of visually-driven neural bursts after visual stimulus onsets. The monkeys simply fixated a spot, and brief bursts of microstimulation pulses were injected into V1. Shortly after microstimulation onset, microsaccade rate was indeed modulated in a manner very similar to that in **Figure 1A**. The primary difference was that the inhibition started even earlier than in **Figure 1A**, and the rebound also came earlier (Buonocore et al., 2020a). This is consistent with V1 microstimulation inducing a visual phosphene (Tehovnik et al., 2005; Schiller et al., 2011; Chen et al., 2020) that essentially bypassed the delay of the retino-cortical pathway associated with a normal visual stimulus impinging on the retina. Therefore, the whole curve of **Figure 1A** was just shifted backwards in time. This means that even though V1 is not necessary for microsaccadic inhibition to occur, based on the preliminary lesion data of Yoshida and Hafed (2017), it is sufficient for the inhibition to be seen, as evident from the preliminary microstimulation data (Buonocore et al., 2020a). Such sufficiency is probably mediated by signal propagation of V1-induced phosphenes to normal pathways eventually affecting the oculomotor system.

We are thus back to square one with respect to discovering the primary source for microsaccadic inhibition in **Figure 1A**: even with large V1 perturbation through lesioning, microsaccadic inhibition seems to be still intact.

THE NEED FOR ADDITIONAL SUBCORTICAL MECHANISMS IN MEDIATING CUE-INDUCED MODULATIONS OF MICROSACCADES

To complete the search for a potential brain area that is both necessary and sufficient for microsaccadic inhibition, it was necessary to start explicitly testing an earlier hypothesis (Hafed and Ignashchenkova, 2013; Buonocore et al., 2017) that microsaccadic inhibition needs to be mediated by a brain region that is both sensitive to visual inputs and also capable of rapidly changing the likelihood to generate a saccade. This hypothesis has directly motivated studying a class of neurons in the nucleus raphe interpositus (rip) in the lower brainstem, and downstream of the SC. These neurons are called omnipause neurons (OPN's), and they derive their name from a very distinctive property: the neurons are tonically active, and they only completely pause their activity during any saccade of any size and any direction (Cohen and Henn, 1972; Luschei and Fuchs, 1972; Keller, 1974; Missal and Keller, 2002). OPN's are thus thought to act as the final gating point to allow saccades to happen (Cohen and Henn, 1972; Luschei and Fuchs, 1972; Keller, 1974; Gandhi and Keller, 1999; Missal and Keller, 2002), and electrically microstimulating OPN's in the middle of saccades is sufficient to interrupt the movements mid-flight (Keller et al., 1996; Gandhi and Keller, 1999). These neurons thus satisfy one of the two criteria for successfully implementing microsaccadic inhibition: the neurons

should be capable of changing the likelihood of microsaccades by changing whether they remain tonically active or pause.

However, as stated above, microsaccadic inhibition must also be sensitive to sensory stimuli, and it was not known, so far, whether OPN's can exhibit sophisticated sensory tuning properties to image characteristics like contrast, spatial frequency, and orientation, which are all characteristics that can influence microsaccadic inhibition. It, therefore, became necessary to investigate whether OPN's exhibit sophisticated visual pattern analysis capabilities, despite being the final motor gate for triggering saccades. Surprisingly, preliminary data revealed exactly such visual pattern analysis capabilities (Buonocore et al., 2020a). Thus, OPN's satisfy the two criteria for mediating rapid microsaccadic inhibition: sensitivity to visual stimuli of different patterns from the outside world, and an ability to gate saccades (and microsaccades) with very short latencies.

To further test this hypothesis, Buonocore et al. then started electrically microstimulating OPN's during steady-state fixation (**Figure 8C**), much like they did in V1. Brief pulse trains were introduced to mimic short-lived visual bursts by these neurons. Microsaccade rate was reduced with even shorter latencies than with V1 microstimulation, and there was no appreciable microsaccadic rebound afterward (Buonocore et al., 2020a). Interestingly, brief pulse trains in the SC, to mimic SC visual bursts, instead increased microsaccade likelihood rather than decreased it, and there was a strong directional and amplitude component as well (directly consistent with the results of **Figure 5**).

Therefore, in all likelihood, microsaccadic inhibition was so resilient to inactivation of the SC and FEF (and lesioning of V1) simply because it is a phenomenon that is critically dependent on yet another brain area, even more downstream of the SC. In our opinion, this area is the rip, containing OPN's.

AN INTEGRATIVE VIEW OF CURRENTLY KNOWN CORTICAL AND SUBCORTICAL CIRCUITS MEDIATING THE INFLUENCES OF VISUAL CUES ON MICROSACCADES

Taking all of the above evidence together, one can now develop an integrative view of the currently known cortical and subcortical circuits responsible for the stereotypical cue-induced microsaccadic modulations of **Figure 1**. The SC may be viewed as critical for reflexive orienting responses by early cue-induced microsaccades, whereas the FEF serves a re-orienting purpose to influence subsequent deliberate movements (**Figure 9A**). In terms of microsaccade timing, V1 senses peripheral stimuli, but it only influences microsaccadic inhibition indirectly, or at least less directly than OPN's, which can help to coordinate microsaccade timing much more precisely (by rapidly inhibiting movements after cue onsets). Finally, in terms of the actual modulations of microsaccade rates and directions, **Figures 9B,C** now adds labels of the mechanisms associated with the brain areas in **Figure 9A** for the specific components of the so-called microsaccadic rate signature after cue onsets (**Figure 9B**) and the related time course of microsaccade direction oscillations (**Figure 9C**). While further investigations of V1 and OPN's are needed in order to solidify the emerging picture, the scheme laid out in **Figure 9** provides an important foundation for understanding the functional implications of microsaccades in covert visual selection tasks. Additional investigations of other

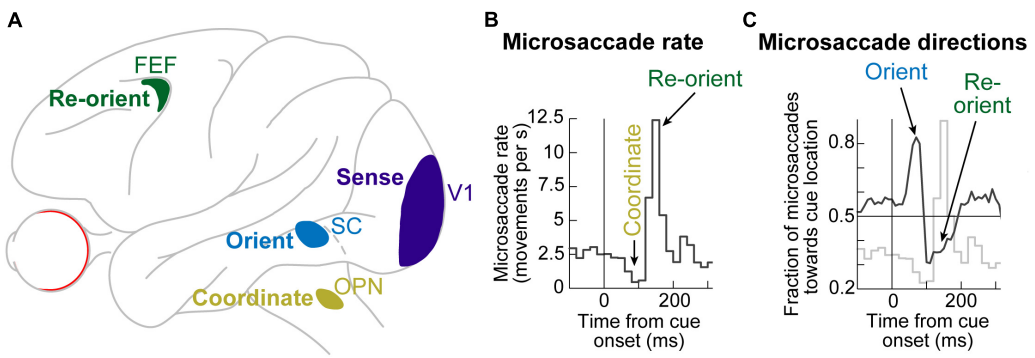

FIGURE 9 | An integrative view of the cortical and subcortical contributions to modulations of microsaccades after visual cues. **(A)** Cue onsets are essentially "sensed" by all shown areas. However, the visual bursts occurring in the different areas contribute differential roles. Visual bursts in V1 likely serve visual detection in general. However, those in the SC at very similar times influence microsaccade directions, and those in OPN's (again at similar times) influence coordination of microsaccade timing to result in microsaccadic inhibition. Such early cue-induced visual bursts in all of these areas likely trump the influences of early visual bursts in FEF, because the FEF seems to be least critical for early cue-induced microsaccades (**Figure 6**). Rather, FEF activity matters much more after the initial reflexive influences mediated subcortically. Thus, FEF activity serves to re-orient microsaccades after the initial cue-induced reflexes. **(B)** The integrative view in **(A)** allows explicitly interpreting the individual components of known modulations in microsaccades after cue onset (e.g., **Figure 1**). In terms of microsaccade rate, visual bursts in OPN's allow coordination of microsaccade timing, resulting in microsaccadic inhibition. Subsequent microsaccades (during the post-inhibition rebound phase) are mediated by FEF re-orienting. **(C)** In terms of microsaccade direction oscillations, SC visual bursts after cue onset are read out in a way to influence microsaccade directions toward the appearing cues. Subsequent microsaccades are deliberate efforts to maintain the eye at the fixated target despite the peripherally appearing cue. Therefore, microsaccade direction oscillations reflect an initial reflexive orientation mediated by the SC followed by a deliberate re-orientation mediated by the FEF.

visual patterns for the cues, as well as additional visual, cognitive, and motor pathways, will become necessary to develop an even more complete picture, for example, with respect to other cognitive factors that can influence microsaccades (such as memory, reward, motivation, and fatigue).

CONCLUSION

In this work, we reviewed the causal perturbation evidence for explaining highly robust modulations of microsaccadic eye movements after peripheral cueing. We particularly described dissociable contributions to both microsaccade likelihood and microsaccade direction from different cortical and subcortical regions, like the SC, FEF, and V1. In the future, additional insights can be gleaned when combining behavioral perturbation manipulations, such as in **Figure 7**, with either neurophysiological recordings or neurophysiological perturbation manipulations. In all, we believe that studying the neural mechanisms for the influences of cues on microsaccades can illuminate broader questions on the links between perception, cognition, and action, and in multiple species as well. The links between microsaccades and covert visual selective mechanisms remain to be a highly interesting topic of investigation.

AUTHOR CONTRIBUTIONS

All authors listed have made a substantial, direct and intellectual contribution to the work, and approved it for publication.

FUNDING

ZH, XT, AB, and TM were funded by the Werner Reichardt Centre for Integrative Neuroscience (CIN), an excellence cluster (EXC307) of the Deutsche Forschungsgemeinschaft (DFG). ZH and AB were additionally funded by the DFG-funded Research Unit FOR1847 (project A6: HA6749/2-1). ZH and TM were also funded by an intramural funding program of the CIN (CIN Mini_GK 2017-04). MY was funded by a Brain/MINDS grant from AMED (19dm0207069h0001) and by JSPS KAKENHI Grant Number 20H05487.

ACKNOWLEDGMENTS

We acknowledge financial support to cover publication costs from the Open Access Publishing Fund of the University of Tübingen.

REFERENCES

Abadi, R. V., and Gowen, E. (2004). Characteristics of saccadic intrusions. *Vision Res.* 44, 2675–2690. doi: 10.1016/j.visres.2004.05.009

Andersen, R. A., Brotchie, P. R., and Mazzoni, P. (1992). Evidence for the lateral intraparietal area as the parietal eye field. *Curr. Opin. Neurobiol.* 2, 840–846. doi: 10.1016/0959-4388(92)90143-9

Andersen, R. A., Essick, G. K., and Siegel, R. M. (1987). Neurons of area 7 activated by both visual stimuli and oculomotor behavior. *Exp. Brain Res.* 67, 316–322. doi: 10.1007/BF00248552

Anton-Erxleben, K., and Carrasco, M. (2013). Attentional enhancement of spatial resolution: linking behavioural and neurophysiological evidence. *Nat. Rev. Neurosci.* 14, 188–200. doi: 10.1038/nrn3443

Awh, E., Armstrong, K. M., and Moore, T. (2006). Visual and oculomotor selection: links, causes and implications for spatial attention. *Trends Cogn. Sci.* 10, 124–130. doi: 10.1016/j.tics.2006.01.001

Azzopardi, P., and Cowey, A. (1996). The overrepresentation of the fovea and adjacent retina in the striate cortex and dorsal lateral geniculate nucleus of the macaque monkey. *Neuroscience* 72, 627–639.

Bahill, A. T., Clark, M. R., and Stark, L. (1975). The main sequence, a tool for studying human eye movements. *Mathematical Biosci.* 24, 191–204.

Barash, S., Bracewell, R. M., Fogassi, L., Gnadt, J. W., and Andersen, R. A. (1991a). Saccade-related activity in the lateral intraparietal area. I. Temporal properties; comparison with area 7a. *J. Neurophysiol.* 66, 1095–1108. doi: 10.1152/jn.1991.66.3.1095

Barash, S., Bracewell, R. M., Fogassi, L., Gnadt, J. W., and Andersen, R. A. (1991b). Saccade-related activity in the lateral intraparietal area. II. Spatial properties. *J. Neurophysiol.* 66, 1109–1124. doi: 10.1152/jn.1991.66.3.1109

Beeler, G. W. Jr. (1967). Visual threshold changes resulting from spontaneous saccadic eye movements. *Vision Res.* 7, 769–775.

Bellet, J., Chen, C. Y., and Hafed, Z. M. (2017). Sequential hemifield gating of alpha- and beta-behavioral performance oscillations after microsaccades. *J. Neurophysiol.* 118, 2789–2805. doi: 10.1152/jn.00253.2017

Betta, E., Galfano, G., and Turatto, M. (2007). Microsaccadic response during inhibition of return in a target-target paradigm. *Vision Res.* 47, 428–436. doi: 10.1016/j.visres.2006.09.010

Bisley, J. W. (2011). The neural basis of visual attention. *J. Physiol.* 589(Pt 1), 49–57. doi: 10.1113/jphysiol.2010.192666

Bompas, A., Campbell, A. E., and Sumner, P. (2020). Cognitive control and automatic interference in mind and brain: a unified model of saccadic inhibition and countermanding. *Psychol. Rev.* 127, 524–561. doi: 10.1037/rev0000181

Bompas, A., and Sumner, P. (2011). Saccadic inhibition reveals the timing of automatic and voluntary signals in the human brain. *J. Neurosci.* 31, 12501–12512. doi: 10.1523/JNEUROSCI.2234-11.2011

Bonneh, Y. S., Adini, Y., and Polat, U. (2015). Contrast sensitivity revealed by microsaccades. *J. Vis.* 15:11. doi: 10.1167/15.9.11

Bosman, C. A., Womelsdorf, T., Desimone, R., and Fries, P. (2009). A microsaccadic rhythm modulates gamma-band synchronization and behavior. *J. Neurosci.* 29, 9471–9480. doi: 10.1523/JNEUROSCI.1193-09.2009

Bremmer, F., Kubischik, M., Hoffmann, K. P., and Krekelberg, B. (2009). Neural dynamics of saccadic suppression. *J. Neurosci.* 29, 12374–12383. doi: 10.1523/JNEUROSCI.2908-09.2009

Bruce, C. J., and Goldberg, M. E. (1985).). Primate frontal eye fields. I. Single neurons discharging before saccades. *J. Neurophysiol.* 53, 603–635.

Bruce, C. J., Goldberg, M. E., Bushnell, M. C., and Stanton, G. B. (1985). Primate frontal eye fields. II. Physiological and anatomical correlates of electrically evoked eye movements. *J. Neurophysiol.* 54, 714–734.

Buonocore, A., Baumann, M. P., and Hafed, Z. M. (2020a). "Visual pattern analysis by motor neurons (Abstract)," in *Proceedings of the Computational and Systems Neuroscience (Cosyne) 2020 Conference* (Denver), 147.

Buonocore, A., Chen, C. Y., Tian, X., Idrees, S., Munch, T. A., and Hafed, Z. M. (2017). Alteration of the microsaccadic velocity-amplitude main sequence relationship after visual transients: implications for models of saccade control. *J. Neurophysiol.* 117, 1894–1910. doi: 10.1152/jn.00811.2016

Buonocore, A., and McIntosh, R. D. (2008). Saccadic inhibition underlies the remote distractor effect. *Exp. Brain Res.* 191, 117–122. doi: 10.1007/s00221-008-1558-7

Buonocore, A., Tian, X., Khademi, F., and Hafed, Z. M. (2020b). Instantaneous movement-unrelated midbrain activity modifies ongoing eye movements. *bioRxiv* [Preprint]. doi: 10.1101/2020.05.31.126359

Cameron, E. L., Tai, J. C., and Carrasco, M. (2002). Covert attention affects the psychometric function of contrast sensitivity. *Vision Res.* 42, 949–967.

Carrasco, M. (2011). Visual attention: the past 25 years. *Vision Res.* 51, 1484–1525. doi: 10.1016/j.visres.2011.04.012

Chen, C. Y., and Hafed, Z. M. (2017). A neural locus for spatial-frequency specific saccadic suppression in visual-motor neurons of the primate superior colliculus. *J. Neurophysiol.* 117, 1657–1673. doi: 10.1152/jn.00911.2016

Chen, C. Y., Hoffmann, K. P., Distler, C., and Hafed, Z. M. (2019). The foveal visual representation of the primate superior colliculus. *Curr. Biol.* 29, 2109–2119.e2107. doi: 10.1016/j.cub.2019.05.040

Chen, C. Y., Ignashchenkova, A., Thier, P., and Hafed, Z. M. (2015). Neuronal response gain enhancement prior to microsaccades. *Curr. Biol.* 25, 2065–2074. doi: 10.1016/j.cub.2015.06.022

Chen, X., Wang, F., Fernandez, E., and Roelfsema, P. R. (2020). Shape perception via a high-channel-count neuroprosthesis in monkey visual cortex. *Science* 370, 1191–1196. doi: 10.1126/science.abd7435

Cohen, B., and Henn, V. (1972). Unit activity in the pontine reticular formation associated with eye movements. *Brain Res.* 46, 403–410. doi: 10.1016/0006-8993(72)90030-3

Cynader, M., and Berman, N. (1972). Receptive-field organization of monkey superior colliculus. *J. Neurophysiol.* 35, 187–201.

Deubel, H., and Schneider, W. X. (1996). Saccade target selection and object recognition: evidence for a common attentional mechanism. *Vision Res.* 36, 1827–1837.

Dias, E. C., and Segraves, M. A. (1999). Muscimol-induced inactivation of monkey frontal eye field: effects on visually and memory-guided saccades. *J. Neurophysiol.* 81, 2191–2214. doi: 10.1152/jn.1999.81.5.2191

Dow, B. M., Snyder, A. Z., Vautin, R. G., and Bauer, R. (1981). Magnification factor and receptive field size in foveal striate cortex of the monkey. *Exp. Brain Res.* 44, 213–228.

Edelman, J. A., and Xu, K. Z. (2009). Inhibition of voluntary saccadic eye movement commands by abrupt visual onsets. *J. Neurophysiol.* 101, 1222–1234. doi: 10.1152/jn.90708.2008

Engbert, R. (2006). Microsaccades: a microcosm for research on oculomotor control, attention, and visual perception. *Prog. Brain Res.* 154, 177–192. doi: 10.1016/S0079-6123(06)54009-9

Engbert, R. (2012). Computational modeling of collicular integration of perceptual responses and attention in microsaccades. *J. Neurosci.* 32, 8035–8039. doi: 10.1523/JNEUROSCI.0808-12.2012

Engbert, R., and Kliegl, R. (2003). Microsaccades uncover the orientation of covert attention. *Vision Res.* 43, 1035–1045.

Engbert, R., Mergenthaler, K., Sinn, P., and Pikovsky, A. (2011). An integrated model of fixational eye movements and microsaccades. *Proc. Natl. Acad. Sci. U.S.A.* 108, E765–E770. doi: 10.1073/pnas.1102730108

Fiebelkorn, I. C., and Kastner, S. (2019). A rhythmic theory of attention. *Trends Cogn. Sci.* 23, 87–101. doi: 10.1016/j.tics.2018.11.009

Findlay, J. M. (1982). Global visual processing for saccadic eye movements. *Vision Res.* 22, 1033–1045.

Galfano, G., Betta, E., and Turatto, M. (2004). Inhibition of return in microsaccades. *Exp. Brain Res.* 159, 400–404. doi: 10.1007/s00221-004-2111-y

Gandhi, N. J., and Keller, E. L. (1999). Comparison of saccades perturbed by stimulation of the rostral superior colliculus, the caudal superior colliculus, and the omnipause neuron region. *J. Neurophysiol.* 82, 3236–3253.

Glimcher, P. W., and Sparks, D. L. (1993). Representation of averaging saccades in the superior colliculus of the monkey. *Exp. Brain Res.* 95, 429–435. doi: 10.1007/BF00227135

Goffart, L., Hafed, Z. M., and Krauzlis, R. J. (2012). Visual fixation as equilibrium: evidence from superior colliculus inactivation. *J. Neurosci.* 32, 10627–10636. doi: 10.1523/JNEUROSCI.0696-12.2012

Gowen, E., Abadi, R. V., Poliakoff, E., Hansen, P. C., and Miall, R. C. (2007). Modulation of saccadic intrusions by exogenous and endogenous attention. *Brain Res.* 1141, 154–167. doi: 10.1016/j.brainres.2007.01.047

Grujic, N., Brehm, N., Gloge, C., Zhuo, W., and Hafed, Z. M. (2018). Peri-saccadic perceptual mislocalization is different for upward saccades. *J. Neurophysiol.* 120, 3198–3216. doi: 10.1152/jn.00350.2018

Hafed, Z. M. (2011). Mechanisms for generating and compensating for the smallest possible saccades. *Eur. J. Neurosci.* 33, 2101–2113. doi: 10.1111/j.1460-9568.2011.07694.x

Hafed, Z. M. (2013). Alteration of visual perception prior to microsaccades. *Neuron* 77, 775–786. doi: 10.1016/j.neuron.2012.12.014

Hafed, Z. M., Chen, C.-Y., and Tian, X. (2015). Vision, perception, and attention through the lens of microsaccades: mechanisms and implications. *Front. Syst. Neurosci.* 9:167. doi: 10.3389/fnsys.2015.00167

Hafed, Z. M., Chen, C. Y., Tian, X., Baumann, M., and Zhang, T. (2021). Active vision at the foveal scale in the primate superior colliculus. *J. Neurophysiol.* doi: 10.1152/jn.00724.2020

Hafed, Z. M., and Clark, J. J. (2002). Microsaccades as an overt measure of covert attention shifts. *Vision Res.* 42, 2533–2545.

Hafed, Z. M., Goffart, L., and Krauzlis, R. J. (2008). Superior colliculus inactivation causes stable offsets in eye position during tracking. *J. Neurosci.* 28, 8124–8137. doi: 10.1523/JNEUROSCI.1317-08.2008

Hafed, Z. M., Goffart, L., and Krauzlis, R. J. (2009). A neural mechanism for microsaccade generation in the primate superior colliculus. *Science* 323, 940–943. doi: 10.1126/science.1166112

Hafed, Z. M., and Ignashchenkova, A. (2013). On the dissociation between microsaccade rate and direction after peripheral cues: microsaccadic inhibition revisited. *J. Neurosci.* 33, 16220–16235. doi: 10.1523/JNEUROSCI.2240-13.2013

Hafed, Z. M., and Krauzlis, R. J. (2008). Goal representations dominate superior colliculus activity during extrafoveal tracking. *J. Neurosci.* 28, 9426–9439. doi: 10.1523/JNEUROSCI.1313-08.2008

Hafed, Z. M., and Krauzlis, R. J. (2010). Microsaccadic suppression of visual bursts in the primate superior colliculus. *J. Neurosci.* 30, 9542–9547. doi: 10.1523/JNEUROSCI.1137-10.2010

Hafed, Z. M., and Krauzlis, R. J. (2012). Similarity of superior colliculus involvement in microsaccade and saccade generation. *J. Neurophysiol.* 107, 1904–1916. doi: 10.1152/jn.01125.2011

Hafed, Z. M., Lovejoy, L. P., and Krauzlis, R. J. (2011). Modulation of microsaccades in monkey during a covert visual attention task. *J. Neurosci.* 31, 15219–15230. doi: 10.1523/JNEUROSCI.3106-11.2011

Hafed, Z. M., Lovejoy, L. P., and Krauzlis, R. J. (2013). Superior colliculus inactivation alters the relationship between covert visual attention and microsaccades. *Eur. J. Neurosci.* 37, 1169–1181. doi: 10.1111/ejn.12127

Hartmann, T. S., Zirnsak, M., Marquis, M., Hamker, F. H., and Moore, T. (2017). Two types of receptive field dynamics in area v4 at the time of eye movements? *Front. Syst. Neurosci.* 11:13. doi: 10.3389/fnsys.2017.00013

Herrington, T. M., Masse, N. Y., Hachmeh, K. J., Smith, J. E., Assad, J. A., and Cook, E. P. (2009). The effect of microsaccades on the correlation between neural activity and behavior in middle temporal, ventral intraparietal, and lateral intraparietal areas. *J. Neurosci.* 29, 5793–5805. doi: 10.1523/JNEUROSCI.4412-08.2009

Idrees, S., Baumann, M. P., Franke, F., Munch, T. A., and Hafed, Z. M. (2020). Perceptual saccadic suppression starts in the retina. *Nat. Commun.* 11:1977. doi: 10.1038/s41467-020-15890-w

Ikeda, T., Yoshida, M., and Isa, T. (2011). Lesion of primary visual cortex in monkey impairs the inhibitory but not the facilitatory cueing effect on saccade. *J. Cogn. Neurosci.* 23, 1160–1169. doi: 10.1162/jocn.2010.21529

Intoy, J., and Rucci, M. (2020). Finely tuned eye movements enhance visual acuity. *Nat. Commun.* 11:795. doi: 10.1038/s41467-020-14616-2

Isa, T., and Yoshida, M. (2009). Saccade control after V1 lesion revisited. *Curr. Opin. Neurobiol.* 19, 608–614. doi: 10.1016/j.conb.2009.10.014

Katnani, H. A., Van Opstal, A. J., and Gandhi, N. J. (2012). A test of spatial temporal decoding mechanisms in the superior colliculus. *J. Neurophysiol.* 107, 2442–2452. doi: 10.1152/jn.00992.2011

Kato, R., Takaura, K., Ikeda, T., Yoshida, M., and Isa, T. (2011). Contribution of the retino-tectal pathway to visually guided saccades after lesion of the primary visual cortex in monkeys. *Eur. J. Neurosci.* 33, 1952–1960. doi: 10.1111/j.1460-9568.2011.07729.x

Keller, E. L. (1974). Participation of medial pontine reticular formation in eye movement generation in monkey. *J. Neurophysiol.* 37, 316–332.

Keller, E. L., Gandhi, N. J., and Shieh, J. M. (1996). Endpoint accuracy in saccades interrupted by stimulation in the omnipause region in monkey. *Visual Neurosci.* 13, 1059–1067.

Khademi, F., Chen, C.-Y., and Hafed, Z. M. (2020). Visual feature tuning of superior colliculus neural reafferent responses after fixational microsaccades. *J. Neurophysiol.* 123, 2136–2153. doi: 10.1152/jn.00077.2020

Ko, H. K., Poletti, M., and Rucci, M. (2010). Microsaccades precisely relocate gaze in a high visual acuity task. *Nat. Neurosci.* 13, 1549–1553. doi: 10.1038/nn.2663

Krauzlis, R. J., Basso, M. A., and Wurtz, R. H. (1997). Shared motor error for multiple eye movements. *Science* 276, 1693–1695.

Krauzlis, R. J., Basso, M. A., and Wurtz, R. H. (2000). Discharge properties of neurons in the rostral superior colliculus of the monkey during smooth-pursuit eye movements. *J. Neurophysiol.* 84, 876–891.

Krauzlis, R. J., Lovejoy, L. P., and Zenon, A. (2013). Superior colliculus and visual spatial attention. *Annu. Rev. Neurosci.* 36, 165–182. doi: 10.1146/annurev-neuro-062012-170249

Krekelberg, B. (2010). Saccadic suppression. *Curr. Biol.* 20, R228–R229. doi: 10.1016/j.cub.2009.12.018

Laubrock, J., Engbert, R., and Kliegl, R. (2005). Microsaccade dynamics during covert attention. *Vision Res.* 45, 721–730. doi: 10.1016/j.visres.2004.09.029

Lee, C., Rohrer, W. H., and Sparks, D. L. (1988). Population coding of saccadic eye movements by neurons in the superior colliculus. *Nature* 332, 357–360. doi: 10.1038/332357a0

Lee, P. H., Sooksawate, T., Yanagawa, Y., Isa, K., Isa, T., and Hall, W. C. (2007). Identity of a pathway for saccadic suppression. *Proc. Natl. Acad. Sci. U.S.A.* 104, 6824–6827. doi: 10.1073/pnas.0701934104

Lovejoy, L. P., and Krauzlis, R. J. (2010). Inactivation of primate superior colliculus impairs covert selection of signals for perceptual judgments. *Nat. Neurosci.* 13, 261–266. doi: 10.1038/nn.2470

Lowet, E., Gomes, B., Srinivasan, K., Zhou, H., Schafer, R. J., and Desimone, R. (2018). Enhanced neural processing by covert attention only during microsaccades directed toward the attended stimulus. *Neuron* 99, 207–214.e203. doi: 10.1016/j.neuron.2018.05.041

Luschei, E. S., and Fuchs, A. F. (1972). Activity of brain stem neurons during eye movements of alert monkeys. *J. Neurophysiol.* 35, 445–461. doi: 10.1152/jn.1972.35.4.445

Malevich, T., Buonocore, A., and Hafed, Z. M. (2020). Dependence of the stimulus-driven microsaccade rate signature in rhesus macaque monkeys on visual stimulus size and polarity. *J. Neurophysiol.* 125, 282–295. doi: 10.1152/jn.00304.2020

Martinez-Conde, S., Macknik, S. L., and Hubel, D. H. (2000). Microsaccadic eye movements and firing of single cells in the striate cortex of macaque monkeys. *Nat. Neurosci.* 3, 251–258. doi: 10.1038/72961

Mazzoni, P., Bracewell, R. M., Barash, S., and Andersen, R. A. (1996). Motor intention activity in the macaque's lateral intraparietal area. I. Dissociation of motor plan from sensory memory. *J. Neurophysiol.* 76, 1439–1456. doi: 10.1152/jn.1996.76.3.1439

McPeek, R. M., Han, J. H., and Keller, E. L. (2003). Competition between saccade goals in the superior colliculus produces saccade curvature. *J. Neurophysiol.* 89, 2577–2590. doi: 10.1152/jn.00657.2002

Meyberg, S., Sinn, P., Engbert, R., and Sommer, W. (2017). Revising the link between microsaccades and the spatial cueing of voluntary attention. *Vision Res.* 133, 47–60. doi: 10.1016/j.visres.2017.01.001

Missal, M., and Keller, E. L. (2002). Common inhibitory mechanism for saccades and smooth-pursuit eye movements. *J. Neurophysiol.* 88, 1880–1892.

Munoz, D. P., and Wurtz, R. H. (1995). Saccade-related activity in monkey superior colliculus. I. Characteristics of burst and buildup cells. *J. Neurophysiol.* 73, 2313–2333.

Nakayama, K., and Mackeben, M. (1989). Sustained and transient components of focal visual attention. *Vision Res.* 29, 1631–1647.

Pastukhov, A., and Braun, J. (2010). Rare but precious: microsaccades are highly informative about attentional allocation. *Vision Res.* 50, 1173–1184. doi: 10.1016/j.visres.2010.04.007

Peel, T. R., Hafed, Z. M., Dash, S., Lomber, S. G., and Corneil, B. D. (2016). A causal role for the cortical frontal eye fields in microsaccade deployment. *PLoS Biol.* 14:e1002531. doi: 10.1371/journal.pbio.1002531

Peel, T. R., Johnston, K., Lomber, S. G., and Corneil, B. D. (2014). Bilateral saccadic deficits following large and reversible inactivation of unilateral frontal eye field. *J. Neurophysiol.* 111, 415–433. doi: 10.1152/jn.00398.2013

Perry, V. H., and Cowey, A. (1985). The ganglion cell and cone distributions in the monkey's retina: implications for central magnification factors. *Vision Res.* 25, 1795–1810.

Pestilli, F., and Carrasco, M. (2005). Attention enhances contrast sensitivity at cued and impairs it at uncued locations. *Vision Res.* 45, 1867–1875. doi: 10.1016/j.visres.2005.01.019

Petersen, S. E., and Posner, M. I. (2012). The attention system of the human brain: 20 years after. *Annu. Rev. Neurosci.* 35, 73–89. doi: 10.1146/annurev-neuro-062111-150525

Poletti, M., Listorti, C., and Rucci, M. (2013). Microscopic eye movements compensate for nonhomogeneous vision within the fovea. *Curr. Biol.* 23, 1691–1695. doi: 10.1016/j.cub.2013.07.007

Poletti, M., Rucci, M., and Carrasco, M. (2017). Selective attention within the foveola. *Nat. Neurosci.* 20, 1413–1417. doi: 10.1038/nn.4622

Port, N. L., and Wurtz, R. H. (2003). Sequential activity of simultaneously recorded neurons in the superior colliculus during curved saccades. *J. Neurophysiol.* 90, 1887–1903. doi: 10.1152/jn.01151.2002

Posner, M. I. (1980). Orienting of attention. *Q. J. Exp. Psychol.* 32, 3–25.

Reingold, E. M., and Stampe, D. M. (1999). "Saccadic inhibition in complex visual tasks," in *Current Oculomotor Research*, eds W. Becker, H. Deubel, and T. Mergner, (Boston: Springer), 249–255.

Reingold, E. M., and Stampe, D. M. (2000). "Saccadic inhibition and gaze contingent research paradigms," in *Reading as a Perceptual Process*, eds A. Kennedy, R. Radach, D. Heller, and J. Pynte, (Amsterdam: North-Holland), 119–145.

Reingold, E. M., and Stampe, D. M. (2002). Saccadic inhibition in voluntary and reflexive saccades. *J. Cogn. Neurosci.* 14, 371–388. doi: 10.1162/089892902317361903

Riggs, L. A., and Manning, K. A. (1982). Saccadic suppression under conditions of whiteout. *Invest. Ophthalmol. Vis. Sci.* 23, 138–143.

Robinson, D. A. (1972). Eye movements evoked by collicular stimulation in the alert monkey. *Vision Res.* 12, 1795–1808.

Rolfs, M. (2009). Microsaccades: small steps on a long way. *Vision Res.* 49, 2415–2441. doi: 10.1016/j.visres.2009.08.010

Rolfs, M., Engbert, R., and Kliegl, R. (2005). Crossmodal coupling of oculomotor control and spatial attention in vision and audition. *Exp. Brain Res.* 166, 427–439. doi: 10.1007/s00221-005-2382-y

Rolfs, M., Kliegl, R., and Engbert, R. (2008). Toward a model of microsaccade generation: the case of microsaccadic inhibition. *J. Vis.* 8, 1–23. doi: 10.1167/8.11.5

Ross, J., Morrone, M. C., and Burr, D. C. (1997). Compression of visual space before saccades. *Nature* 386, 598–601. doi: 10.1038/386598a0

Ross, J., Morrone, M. C., Goldberg, M. E., and Burr, D. C. (2001). Changes in visual perception at the time of saccades. *Trends Neurosci.* 24, 113–121.

Rovamo, J., Virsu, V., and Nasanen, R. (1978). Cortical magnification factor predicts the photopic contrast sensitivity of peripheral vision. *Nature* 271, 54–56.

Schall, J. D. (1991a). Neuronal activity related to visually guided saccades in the frontal eye fields of rhesus monkeys: comparison with supplementary eye fields. *J. Neurophysiol.* 66, 559–579.

Schall, J. D. (1991b). Neuronal activity related to visually guided saccadic eye movements in the supplementary motor area of rhesus monkeys. *J. Neurophysiol.* 66, 530–558.

Schall, J. D. (2002). The neural selection and control of saccades by the frontal eye field. *Philos. Trans. R. Soc. Lond. B Biol. Sci.* 357, 1073–1082. doi: 10.1098/rstb.2002.1098

Schall, J. D., and Hanes, D. P. (1993). Neural basis of saccade target selection in frontal eye field during visual search. *Nature* 366, 467–469. doi: 10.1038/366467a0

Schall, J. D., Hanes, D. P., Thompson, K. G., and King, D. J. (1995). Saccade target selection in frontal eye field of macaque. I. Visual and premovement activation. *J. Neurosci.* 15, 6905–6918.

Schiller, P. H., Slocum, W. M., Kwak, M. C., Kendall, G. L., and Tehovnik, E. J. (2011). New methods devised specify the size and color of the spots monkeys see when striate cortex (area V1) is electrically stimulated. *Proc. Natl. Acad. Sci. U.S.A.* 108, 17809–17814. doi: 10.1073/pnas.1108337108

Schneider, W. X., and Deubel, H. (1995). "Visual attention and saccadic eye movements: evidence for obligatory and selective spatial coupling," in *Studies in Visual Information Processing 6. Eye Movement Research: Mechanisms, Processes and Applications*, eds J. M. Findlay, R. Walker, and R. W. Kentridge, (Amsterdam: Elsevier Science), 317–324.

Scholes, C., McGraw, P. V., Nystrom, M., and Roach, N. W. (2015). Fixational eye movements predict visual sensitivity. *Proc. Biol. Sci.* 282:20151568. doi: 10.1098/rspb.2015.1568

Solomon, J. A. (2004). The effect of spatial cues on visual sensitivity. *Vision Res.* 44, 1209–1216. doi: 10.1016/j.visres.2003.12.003

Sommer, M. A., and Tehovnik, E. J. (1997). Reversible inactivation of macaque frontal eye field. *Exp. Brain Res.* 116, 229–249. doi: 10.1007/pl00005752

Sommer, M. A., and Wurtz, R. H. (2000). Composition and topographic organization of signals sent from the frontal eye field to the superior colliculus. *J. Neurophysiol.* 83, 1979–2001.

Sommer, M. A., and Wurtz, R. H. (2001). Frontal eye field sends delay activity related to movement, memory, and vision to the superior colliculus. *J. Neurophysiol.* 85, 1673–1685.

Sparks, D., and Nelson, J. (1987). Sensory and motor maps in the mammalian superior colliculus. *Trends Neurosci.* 10, 312–317.

Takaura, K., Yoshida, M., and Isa, T. (2011). Neural substrate of spatial memory in the superior colliculus after damage to the primary visual cortex. *J. Neurosci.* 31, 4233–4241. doi: 10.1523/JNEUROSCI.5143-10.2011

Tehovnik, E. J., Slocum, W. M., Carvey, C. E., and Schiller, P. H. (2005). Phosphene induction and the generation of saccadic eye movements by striate cortex. *J. Neurophysiol.* 93, 1–19. doi: 10.1152/jn.00736.2004

Tehovnik, E. J., Sommer, M. A., Chou, I. H., Slocum, W. M., and Schiller, P. H. (2000). Eye fields in the frontal lobes of primates. *Brain Res. Brain Res. Rev.* 32, 413–448. doi: 10.1016/s0165-0173(99)00092-2

Thiele, A., Henning, P., Kubischik, M., and Hoffmann, K. P. (2002). Neural mechanisms of saccadic suppression. *Science* 295, 2460–2462. doi: 10.1126/science.1068788

Tian, X., Yoshida, M., and Hafed, Z. M. (2016). A microsaccadic account of attentional capture and inhibition of return in posner cueing. *Front. Syst. Neurosci.* 10:23. doi: 10.3389/fnsys.2016.00023

Tian, X., Yoshida, M., and Hafed, Z. M. (2018). Dynamics of fixational eye position and microsaccades during spatial cueing: the case of express microsaccades. *J. Neurophysiol.* 119, 1962–1980. doi: 10.1152/jn.00752.2017

Tolias, A. S., Moore, T., Smirnakis, S. M., Tehovnik, E. J., Siapas, A. G., and Schiller, P. H. (2001). Eye movements modulate visual receptive fields of V4 neurons. *Neuron* 29, 757–767.

Updyke, B. V. (1974). Characteristics of unit responses in superior colliculus of the Cebus monkey. *J. Neurophysiol.* 37, 896–909. doi: 10.1152/jn.1974.37.5.896

Veale, R., Hafed, Z. M., and Yoshida, M. (2017). How is visual salience computed in the brain? Insights from behaviour, neurobiology and modelling. *Philos. Trans. R. Soc. Lond. B Biol. Sci.* 372:20160113. doi: 10.1098/rstb.2016.0113

Vokoun, C. R., Huang, X., Jackson, M. B., and Basso, M. A. (2014). Response normalization in the superficial layers of the superior colliculus as a possible mechanism for saccadic averaging. *J. Neurosci.* 34, 7976–7987. doi: 10.1523/JNEUROSCI.3022-13.2014

White, A. L., and Rolfs, M. (2016). Oculomotor inhibition covaries with conscious detection. *J. Neurophysiol.* 116, 1507–1521. doi: 10.1152/jn.00268.2016

White, B. J., Berg, D. J., Kan, J. Y., Marino, R. A., Itti, L., and Munoz, D. P. (2017a). Superior colliculus neurons encode a visual saliency map during free viewing of natural dynamic video. *Nat. Commun.* 8:14263. doi: 10.1038/ncomms14263

White, B. J., Itti, L., and Munoz, D. P. (2019). Superior colliculus encodes visual saliency during smooth pursuit eye movements. *Eur. J. Neurosci.* doi: 10.1111/ejn.14432

White, B. J., Kan, J. Y., Levy, R., Itti, L., and Munoz, D. P. (2017b). Superior colliculus encodes visual saliency before the primary visual cortex. *Proc. Natl. Acad. Sci. U.S.A.* 114, 9451–9456. doi: 10.1073/pnas.1701003114

Willeke, K. F., Tian, X., Buonocore, A., Bellet, J., Ramirez-Cardenas, A., and Hafed, Z. M. (2019). Memory-guided microsaccades. *Nat. Commun.* 10:3710. doi: 10.1038/s41467-019-11711-x

Wurtz, R. H., and Albano, J. E. (1980). Visual-motor function of the primate superior colliculus. *Annu. Rev. Neurosci.* 3, 189–226. doi: 10.1146/annurev.ne.03.030180.001201

Yoshida, M., and Hafed, Z. M. (2017). Microsaccades in blindsight monkeys (Abstract). *J. Vision* 17:896. doi: 10.1167/17.10.896

Yoshida, M., Hafed, Z. M., and Isa, T. (2017). Informative cues facilitate saccadic localization in blindsight monkeys. *Front. Syst. Neurosci.* 11:5. doi: 10.3389/fnsys.2017.00005

Yoshida, M., Itti, L., Berg, D. J., Ikeda, T., Kato, R., Takaura, K., et al. (2012). Residual attention guidance in blindsight monkeys watching complex natural scenes. *Curr. Biol.* 22, 1429–1434. doi: 10.1016/j.cub.2012.05.046

Yoshida, M., Takaura, K., Kato, R., Ikeda, T., and Isa, T. (2008). Striate cortical lesions affect deliberate decision and control of saccade: implication for blindsight. *J. Neurosci.* 28, 10517–10530. doi: 10.1523/JNEUROSCI.1973-08.2008

Zirnsak, M., Steinmetz, N. A., Noudoost, B., Xu, K. Z., and Moore, T. (2014). Visual space is compressed in prefrontal cortex before eye movements. *Nature* 507, 504–507. doi: 10.1038/nature13149

Zuber, B. L., and Stark, L. (1966). Saccadic suppression: elevation of visual threshold associated with saccadic eye movements. *Exp. Neurol.* 16, 65–79.

Zuber, B. L., Stark, L., and Cook, G. (1965). Microsaccades and the velocity-amplitude relationship for saccadic eye movements. *Science* 150, 1459–1460.

Conflict of Interest: The authors declare that the research was conducted in the absence of any commercial or financial relationships that could be construed as a potential conflict of interest.

frontiers in Neural Circuits

REVIEW
published: 12 March 2021
doi: 10.3389/fncir.2021.644743

Adjudicating Between Local and Global Architectures of Predictive Processing in the Subcortical Auditory Pathway

Alejandro Tabas[1,2]* *and Katharina von Kriegstein*[1,2]

[1] *Chair of Cognitive and Clinical Neuroscience, Faculty of Psychology, Technische Universität Dresden, Dresden, Germany,*
[2] *Max Planck Institute for Human Cognitive and Brain Sciences, Leipzig, Germany*

Predictive processing, a leading theoretical framework for sensory processing, suggests that the brain constantly generates predictions on the sensory world and that perception emerges from the comparison between these predictions and the actual sensory input. This requires two distinct neural elements: generative units, which encode the model of the sensory world; and prediction error units, which compare these predictions against the sensory input. Although predictive processing is generally portrayed as a theory of cerebral cortex function, animal and human studies over the last decade have robustly shown the ubiquitous presence of prediction error responses in several nuclei of the auditory, somatosensory, and visual subcortical pathways. In the auditory modality, prediction error is typically elicited using so-called oddball paradigms, where sequences of repeated pure tones with the same pitch are at unpredictable intervals substituted by a tone of deviant frequency. Repeated sounds become predictable promptly and elicit decreasing prediction error; deviant tones break these predictions and elicit large prediction errors. The simplicity of the rules inducing predictability make oddball paradigms agnostic about the origin of the predictions. Here, we introduce two possible models of the organizational topology of the predictive processing auditory network: (1) the global view, that assumes that predictions on the sensory input are generated at high-order levels of the cerebral cortex and transmitted in a cascade of generative models to the subcortical sensory pathways; and (2) the local view, that assumes that independent local models, computed using local information, are used to perform predictions at each processing stage. In the global view information encoding is optimized globally but biases sensory representations along the entire brain according to the subjective views of the observer. The local view results in a diminished coding efficiency, but guarantees in return a robust encoding of the features of sensory input at each processing stage. Although most experimental results to-date are ambiguous in this respect, recent evidence favors the global model.

Keywords: predictive coding, medial geniculate body, inferior colliculus, abstract processing, sensory coding, auditory processing, subcortical sensory pathway

OPEN ACCESS

Edited by:
Livia de Hoz,
Charité - Universitätsmedizin Berlin, Germany

Reviewed by:
Manuel S. Malmierca,
University of Salamanca, Spain
Kasia M. Bieszczad,
Rutgers, The State University of New Jersey, United States

***Correspondence:**
Alejandro Tabas
alejandro.tabas@tu-dresden.de

Received: *21 December 2020*
Accepted: *16 February 2021*
Published: *12 March 2021*

Citation:
Tabas A and von Kriegstein K (2021) Adjudicating Between Local and Global Architectures of Predictive Processing in the Subcortical Auditory Pathway. Front. Neural Circuits 15:644743. doi: 10.3389/fncir.2021.644743

1. INTRODUCTION

The massive bundle of corticofugal fibers stemming from auditory cortex and targeting nuclei of the subcortical auditory pathway (Winer, 1984, 2005b; Schofield, 2011) have posed a puzzling problem to the auditory neuroscience community for decades (Syka et al., 1988; Winer, 2005a; Robinson and McAlpine, 2009; He and Yu, 2010). Sensory processing is classically understood as a bottom up problem, where increasingly complex features are read-out in a hierarchical constructive manner (Epstein, 1993; Martin, 1994; DeCharms and Zador, 2000). But then, what is the corticofugal system good for, and why is it that massive?

One possibility is that sensory processing is not a purely bottom-up process, but that top-down information is used proactively to encode sensory input (Mumford, 1992; Rao and Ballard, 1999; Friston, 2003, 2005). This is the thesis of the predictive processing framework (PPF) (Heeger, 2017; Spratling, 2017; Keller and Mrsic-Flogel, 2018; Walsh et al., 2020): that higher-level regions of the cerebral cortex keep and update a model of the sensory world that is used to predict, in a generative manner, the sensory input at lower-level regions of the cerebral cortex; and that neurons at those lower-level regions encode *prediction error*: the difference between the predictions and the actual input. Prediction error is further conveyed to the higher-level representation and used there to adjust the generative model. Extending this role to the corticofugal system between cerebral cortex and subcortical sensory pathway nuclei suggests that predictions drawn by generative models in cerebral cortex are conveyed to subcortical sensory neurons that encode prediction error (Von Kriegstein et al., 2008; Diaz et al., 2012; Malmierca et al., 2015). Many authors have argued that the PPF might underlay cognitive processes beyond perception including (e.g.,): vocalization in humans (Okada et al., 2018) and birds (Yildiz and Kiebel, 2011), learning in cognitive development (Nagai, 2019), episodic memory (Barron et al., 2020), abstract cognition and reasoning (Spratling, 2016), inculturation (Fabry, 2018), and even the emergence of faith (Andersen, 2019). Here we focus on sensory processing and, in particular, on auditory perception.

Over the last decade the auditory neuroscience community has robustly shown the predominance of neurons encoding prediction error neurons in subcortical sensory pathway nuclei (Anderson et al., 2009; Malmierca et al., 2009, 2014, 2019; Grimm et al., 2016; Parras et al., 2017; Carbajal and Malmierca, 2018). Although these results are often taken as proof that the corticofugal system is indeed transmitting predictions, most experimental paradigms control predictability using simple rules that can be readily encoded at the same processing stage as the prediction error (Eytan et al., 2003; Mill et al., 2011; Wang et al., 2014; May et al., 2015); i.e., without needing a top-down system. We will call this the 'local model' of predictive coding in the following. Conversely, we refer to predictive coding as a 'global model' if a generative model at higher-levels of the processing hierarchy generates predictions for the lower levels. The distinction between local and global models of predictive coding is important for understanding the function of the corticofugal pathway. It is also important for the understanding of the nature of sensory processing: if predictions are computed at higher stages of the processing hierarchy and transmitted downwards, that would mean that the auditory system can only make sense of stimuli that are conceivable at these higher-level representations.

Predictability plays an important role in sensory processing: there are many benefits of predictability on behavioral performance in the neurotypical brain (e.g., Davis and Johnsrude, 2007; Jaramillo and Zador, 2011; Sohoglu and Davis, 2016; Mazzucato et al., 2019). If using such predictability for understanding the world is not possible, this likely results in dysfunction. Deficits in the predictive elements of the PPF have already been suggested to explain a number of symptoms in neuropsychiatric conditions, including in schizophrenia (Horga et al., 2014; Sterzer et al., 2018, 2019), autism-spectrum disorders (van de Cruys et al., 2014; van Schalkwyk et al., 2017), attention deficit and hyperactivity (Gonzalez-Gadea et al., 2015), and mood and eating disorders (Frank et al., 2016; Clark et al., 2018). Deficits in the predictive elements of the PPF have also been directly linked to dysfunction of cortico-thalamic pathways and sensory auditory thalamus in developmental dyslexia (Diaz et al., 2012; Müller-Axt et al., 2017; Tschentscher et al., 2019). Understanding the computational mechanism for encoding predictability and the role of the corticofugal system in predictive sensory processing is a necessary prerequisite for a mechanistic understanding of these disorders.

In the following, we review the existing literature on predictive processing in the auditory sensory system with a special focus on the potential role of the corticofugal pathway. We focus on audition because it is the modality where subcortical predictive processing has been explored the most in the last decade (Nelken and Ulanovsky, 2007; Garrido et al., 2009; Grimm et al., 2011; Escera and Malmierca, 2014; Malmierca et al., 2015; Heilbron and Chait, 2017; Carbajal and Malmierca, 2018).

2. GLOBAL AND LOCAL MODELS OF THE PREDICTIVE PROCESSING FRAMEWORK

A longstanding question on sensory processing is whether perception is purely exploratory or rather a process of inference (Von Helmholtz, 1867; Atick, 1992; Bejjanki et al., 2011; Lochmann and Deneve, 2011; Purves et al., 2015; de Lange et al., 2018). In the exploratory view, observers passively receive information from their senses and construct a representation of their sensory surrounds based on a lump of perceptual objects (Epstein, 1993; Martin, 1994; Quiroga et al., 2005; Chechik et al., 2006; Wood et al., 2019). The exploratory view is implemented by the so-called *representational framework* of sensory processing (Epstein, 1993; DeCharms and Zador, 2000; DiCarlo et al., 2012). The representational framework sees perception as a constructive process carried out by a cascade of *feature detectors*: neurons that analyse neural activity at the immediately lower hierarchical stage and respond selectively to certain activation patterns (**Figure 1A**). For instance, a neuron that responds selectively to the word *percept* integrates inputs from neurons

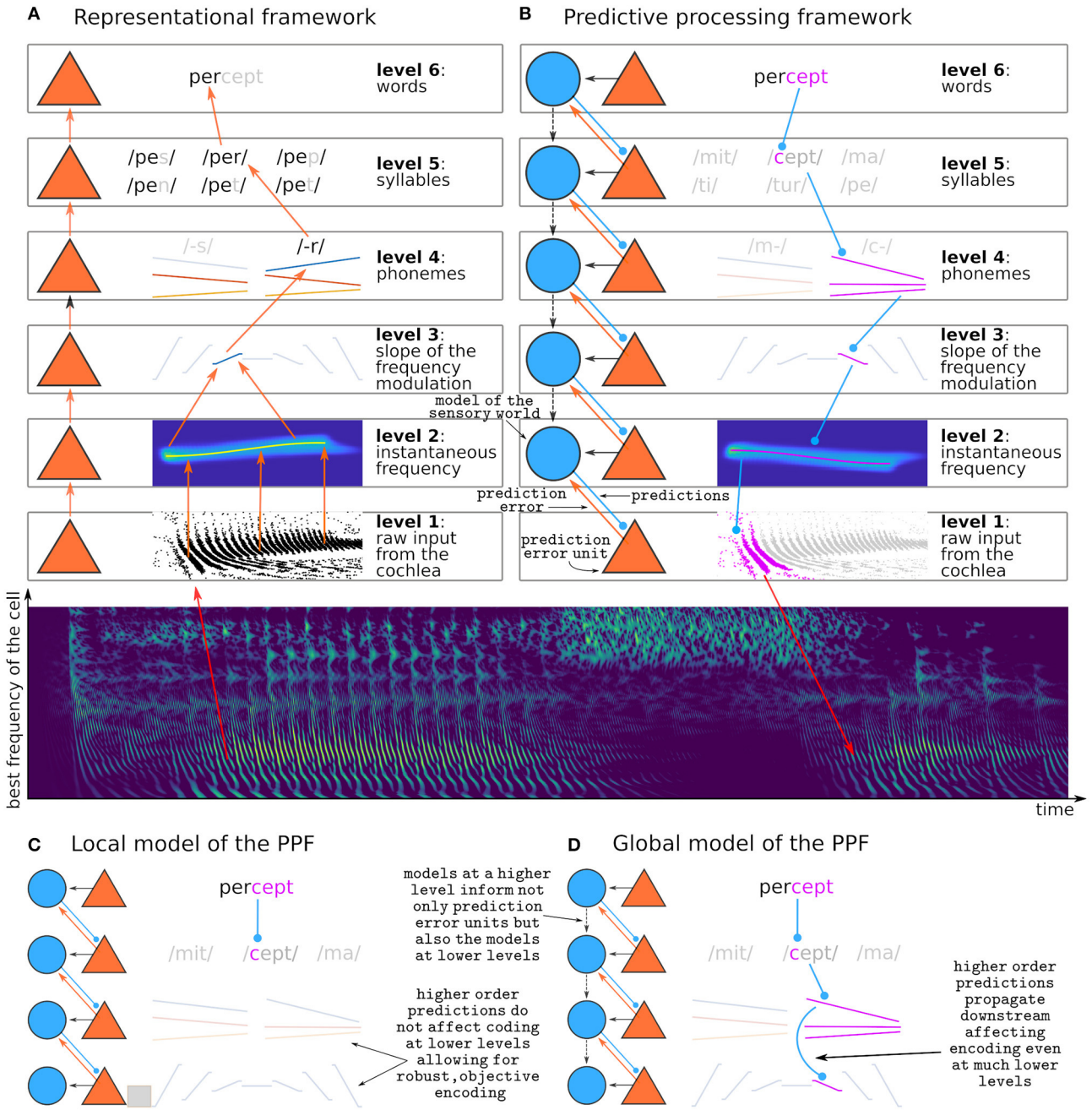

FIGURE 1 | Representational and predictive processing frameworks. **(A)** Schematic view of a possible implementation of the representational framework during the decoding of the syllable */per-/*. **(B)** Schematic view of a possible implementation of the predictive processing framework while performing predictions on the incoming syllable */-cept/*. Purple features are predictions. The middle panel depicts a simulation of the neural activity in the auditory nerve across the tonotopic axis (*y*-axis) elicited by the spoken word *percept*. **(C)** Example implementation of the local model: whereas predictions at the word level are used to encode prediction error at the immediately lower level as formulated by the PPF, predictions are not used to calculate the predictive model of the lower stages, and thus the remaining levels depend on bottom-up information only. **(D)** Example implementation of the global model: predictions at the word level propagate downwards affecting the predictive model of all stages (dashed descending arrows), so that prediction error at the lowest level is encoded with respect to a model that is ultimately defined in the highest level. Intermediate implementations where interactions between the models exist up to a certain level only are also possible but not displayed here. Note that **(B)** depicts the global model.

encoding the syllables *per* and *cept*; the neuron encoding *per* receives inputs from neurons encoding *p-*, *e*, and *-r*; and, if the word is decoded from the auditory modality, the neuron encoding *p-* receives inputs from the neurons encoding each of the formant transitions (frequency-modulated sweeps) that characterize the consonant.

The PPF (Heeger, 2017; Spratling, 2017; Keller and Mrsic-Flogel, 2018; Walsh et al., 2020) presents the same hierarchical organization as the representational framework, but the feature detectors are used for inference rather than exploration. In the PPF, a feature detector needs two ingredients: a *(generative) model* that builds hypotheses about the sensory world, and a *prediction error* unit that tests these hypotheses against the actual sensory input. The PPF is intimately linked with Bayesian inference (Friston, 2005; Kiebel et al., 2008), where the posterior conclusions drawn from the data are amplifications or reductions of a prior belief. This means that according to the PPF we are more likely to perceive what we expect. In an extreme interpretation of the framework, it implies that if we do not have an implicit prior belief that a perceptual object might exist, we cannot perceive its existence at all. Today, evidence from psychophysics (de Lange et al., 2018), human neuroimaging (Siman-Tov et al., 2019; Walsh et al., 2020), animal neurophysiology (Bendixen et al., 2012; Carbajal and Malmierca, 2018; Pakan et al., 2018), and theoretical neuroscience (Brenner et al., 2000; Fairhall et al., 2001; Huang and Rao, 2011; Badcock et al., 2019), converges in the idea that predictions on the sensory world are constantly used to encode sensory input.

To-date there are at least three different algorithms describing how the PPF could be implemented in the brain (for a review, see Spratling, 2017). All of them hypothesize the existence of two kinds of sensory neurons: those that encode the generative model, and those that encode prediction error. A neuron encoding the generative model at a certain stage of the processing hierarchy k receives inputs from its associated prediction error units, that signal if the model is correct or incorrect. It also receives input from generative models at higher stages $l > k$, that guide the generation of predictions at level k. A prediction error unit at stage k compares the predictions of its associated generative model at stage $k + 1$ with the sensory inputs incoming from the immediately lower processing stage (**Figure 1B**).

Although the PPF was first formulated as a theory on sensory processing in the cerebral cortex (Rao and Ballard, 1999; Friston, 2005; Shipp, 2016), the existence of potential prediction error units in the subcortical auditory pathway has been reported widely during the last decade (Anderson et al., 2009; Malmierca et al., 2009, 2014, 2019; Grimm et al., 2016; Parras et al., 2017; Carbajal and Malmierca, 2018). Whether this prediction error is, as proposed by the PPF, a signature of active inference, is still unclear (Carbajal and Malmierca, 2018). If that was the case, prediction error in subcortical sensory structures should signal error with respect to global hypotheses of the sensory world. This means that, if after hearing *per-* we expect the word to be completed with a *-cept* (**Figure 1B**), an auditory signal breaking such prediction (like, for instance, *-meable*) should elicit prediction errors in those neurons encoding the syllable *-cept*, but also errors on the neurons encoding the *-c-* and its corresponding spectrotemporal properties such as formant transitions. This schema assumes that predictions are transmitted downwards through an inverse hierarchical structure (**Figure 1D**). We call this the *global model*, because it assumes that predictions at the highest stage in the processing hierarchy are used to inform generative models globally across the brain (Kiebel et al., 2008; Malmierca et al., 2015; Siman-Tov et al., 2019; Casado-Román et al., 2020).

An alternative possibility is that predictions and its associated errors are computed locally (Eytan et al., 2003; Mill et al., 2011; Wang et al., 2014; May et al., 2015). We call this scenario the *local model*. Predictions at each stage are performed accordingly to the level of abstraction of the local representation and its local time constant of integration. In this scenario, violations to the prediction *-cept* would elicit prediction error in the populations encoding the syllable *-cept*, but not in the populations encoding the formant transitions of the syllable *-c-* (**Figure 1C**). Although not strictly adherent to the principles of the PPF, this local strategy presents its own advantages. First, it still optimizes the neural code by encoding only those parts of the stimulus that are not predictable. Second, it keeps robust representations of the stimuli that are independent of each other across stages of the processing hierarchy - this has the advantage that it could be used to simultaneously test multiple hypotheses. Third, it does not require a constant top-down transmission of expectations.

3. PREDICTION ERROR RESPONSES ARE UBIQUITOUS IN THE AUDITORY THALAMUS AND MIDBRAIN

Prediction error responses in the mammal subcortical auditory pathway (Malmierca et al., 2015; Parras et al., 2017) have been mostly investigated through stimulus-specific adaptation (SSA). SSA is a phenomenon where individual sensory neurons adapt to specific stimulus properties (Ulanovsky et al., 2003, 2004). SSA is typically shown in passive listening conditions (and often in anesthetized animals) using some variation of the classical oddball paradigm: sequences of several repetitions of a standard tone that are interrupted by rarely occurring deviants. Deviants typically differ from the standards only in the tone frequency. In oddball sequences, pure tones are separated by fixed inter-stimulus-intervals (ISI), so that the onset of the next tone in the sequence is always predictable. By repetition of the standard tones, oddball paradigms induce predictions on the frequency of the next tone. The experimenter can control the amount of prediction error elicited by the deviants with two variables: the frequency difference between deviant and standard (which controls the amount of error of the prediction with respect to the actual sensory input) and the probability of occurrence of the deviant (which controls how certain the model is about the prediction that the next stimulus will be a standard). SSA to frequency deviants has been consistently found in the auditory thalamus (medial geniculate body, MGB) (Anderson et al., 2009; Antunes et al., 2010; Richardson et al., 2013; Duque et al., 2014; Parras et al., 2017) and midbrain (inferior colliculus, IC) (Malmierca et al., 2009; Zhao et al., 2011; Duque et al., 2012; Pérez-González et al., 2012; Ayala et al., 2013, 2015, 2016; Ayala and Malmierca, 2015, 2018; Duque and Malmierca, 2015; Parras et al., 2017; Valdés-Baizabal et al., 2017, 2020) of non-human mammals, as well as in the human IC and MGB (Cacciaglia et al., 2015; Tabas et al., 2020). Several studies have failed to detect any SSA in neurons or populations of the first stage of the

auditory subcortical pathway: the auditory brainstem (cochlear nucleus, CN) (Duque et al., 2012, 2018; Ayala et al., 2013, 2015; Parras et al., 2017). Although SSA has been mostly investigated using frequency deviants, similar adaptation dynamics have been demonstrated to amplitude modulation deviants (Gao et al., 2014) and, in bats, to frequency modulation deviants (Thomas et al., 2012). However, there seems to be no SSA to loudness deviants (Duque et al., 2016). The SSA magnitude is typically measured with the SSA index, a ratio that compares the neuronal responses to a tone when used as a standard with the responses to the same tone when used as a deviant.

Although positive SSA indices are often taken as an indication that the neuron encodes prediction error (i.e., surprise to the violation of a prediction), positive SSA indices could also result from simple repetition suppression to the standard (Taaseh et al., 2011; Parras et al., 2017; Carbajal and Malmierca, 2018). Parras et al. developed a novel approach to disentangle repetition suppression from prediction error by comparing the responses to deviants in classical oddball sequences with the responses to the same sounds when embedded in control sequences that contain varying non-predictable stimuli. They argued that, if the responses to deviants encoded prediction error, these responses should be stronger when a precise prediction on the incoming stimuli is available (as in oddball sequences) than when predictions are broad (as in the control sequences, where all control stimuli have the same likelihood of occurrence). They termed the difference of the responses to the deviant tone in oddball and control sequences the *index of prediction error* (iPE), and demonstrated that neurons showing SSA do typically show positive iPEs. However, $iPE > 0$ is not a sufficient indication of prediction error because, as modeling studies have shown (Eytan et al., 2003; Mill et al., 2011, 2012), positive iPEs can also arise due to simple repetition suppression due to suppressed inhibition. In any case, it is useful to consider SSA as an aggregation of two separate phenomena: the suppression of the responses to the standards, and the recovery of the responses to the deviant.

The IC, MGB, and also auditory cortex are typically subdivided in primary and secondary subdivisions. The bulk of primary subdivisions, consisting of the entire CN, the central nucleus of the IC (cIC), and the ventral section of the MGB (vMGB), constitute the so-called *lemniscal* pathway, characterized by narrow frequency tuning bands and faithful encoding of the stimulus properties (Lee and Sherman, 2011).

The bulk of secondary subdivisions, consisting of the cortex of the IC (xIC), and the medial (mMGB) and dorsal (dMGB) sections of the MGB, constitute the *non-lemniscal* pathway, characterized by wider or absent frequency tuning and stronger corticofugal projections (Lee and Sherman, 2011). While the primary or lemniscal subdivision is attributed with the task of transmitting sensory information directly to the cerebral cortex, the secondary or non-lemniscal subvidision is thought to play a secondary role (Lee and Sherman, 2011). If the PPF is the main mechanism for sensory processing, it should govern sensory coding in the lemniscal pathway.

Animal studies seem to converge in that SSA is more prevalent (i.e., present in a larger fraction of neurons) and stronger (i.e., showing larger SSA indices) in non-lemniscal sections of IC and MGB (Anderson et al., 2009; Ayala et al., 2016; Parras et al., 2017). SSA neurons in the non-lemniscal pathways also show larger iPEs than their lemniscal counterparts. This finding is, however, not backed by studies in humans, which found no topological organization of SSA across IC or MGB (Cacciaglia et al., 2015; Tabas et al., 2020), or even reported comparable SSA indices in lemniscal and non-lemniscal MGB (Tabas et al., 2020).

SSA is elicited in IC and MGB in both, awake and anesthetized animals (Richardson et al., 2013; Duque and Malmierca, 2015; Parras et al., 2017), and under passive and active listening in humans (Cacciaglia et al., 2015; Tabas et al., 2020). One study reported higher SSA indices under anesthesia due to a global reduction of spontaneous activity (Duque and Malmierca, 2015); another study reported generally higher iPEs in the awake condition (Parras et al., 2017). Therefore, although SSA might be modulated by awareness, it is also present in states of reduced consciousness. This is fully in line with the principles of the PPF, where inference on the sensory world is computed autonomously as a coding strategy, rather than as a conscious inference effort.

In IC and MGB, the SSA index always increases with increasing frequency difference between deviant and standard, with decreasing ISI, and with decreasing probability of occurrence of the deviant. This phenomenology seems to indicate that neurons showing SSA do encode prediction error with respect to the hypothesis that the next tone will be a standard, and that this error is larger when there is a precise hypothesis than when there is none. Whether this model is computed locally (in the IC or the MGB) or globally and projected across the hierarchy (see **Figures 1C,D**) is still unclear. Early studies interpreted the fact that SSA is more prominent in non-lemniscal subdivisions of the rodent auditory pathway as evidence of global computation (Malmierca et al., 2015; Ayala et al., 2016). Later, evidence that both SSA indices and iPE increase along the rodent ascending auditory pathway led to the interpretation that prediction error is also computed locally at each stage (Parras et al., 2017; Carbajal and Malmierca, 2018). Functional MRI (fMRI) studies in humans also indicated that IC and MGB showed stronger responses to sounds that broke the predictions than to sounds for which predictions were not available. They did, however, not find that these effects were more prominent in the non-lemniscal subdivisions (Cacciaglia et al., 2015; Tabas et al., 2020).

4. ENCODING FIDELITY IN THE AUDITORY BRAINSTEM IS ENHANCED BY REPETITION AND PREDICTABILITY

Electroencephalographic (EEG) methods present a much higher temporal resolution than fMRI (Buxton, 2009), allowing to measure directly the responses to each individual tone in the sequence. However, fine temporal resolution is offered at the expense of spatial precision: triangulating the origin of the evoked potentials in the brain is generally an ill-posed problem. This difficulty makes measuring responses from subcortical nuclei, particularly because they are located centrally in the brain, especially challenging (Boston and Moller, 1985; Coffey et al., 2019).

To-date, the only non-invasive measurements of subcortical auditory evoked activity are the auditory brainstem response (ABR) and the frequency-following response (FFR). The ABR (Jewett et al., 1970; Parkkonen et al., 2009) consist of a series of short transient auditory evoked potentials peaking within 8 ms after tone onset with sources ranging from the auditory nerve up to the MGB. Human ABRs do not seem to show SSA to broadband spectrum deviants (Slabu et al., 2010) nor loudness deviants (Althen et al., 2011).

The FFR (Gerken et al., 1975; Boston and Moller, 1985; Chandrasekaran and Kraus, 2010) is a component of the auditory evoked fields that is synchronized to the acoustical signal. Although the FFR partially stems from sources in cerebral cortex (Coffey et al., 2016), most generators seem to be subcortical (Bidelman, 2018; Coffey et al., 2019), especially when it is synchronized to stimulus frequencies above the cortical limit for phase-locking (estimated to be between 50 and 250 Hz).

Two studies have shown SSA of the absolute power of the FFR in a neighborhood of the frequencies characterizing the stimuli (Shiga et al., 2015; Alho et al., 2019). However, the entrainment of the FFR to the stimulus waveform seems to follow the exact opposite trend than SSA: an increased entrainment to standards as compared to deviants (Chandrasekaran et al., 2009; Strait et al., 2011; Slabu et al., 2012; Skoe et al., 2014; Lau et al., 2017; Font-Alaminos et al., 2020). We call this phenomenology *repetition entrainment enhancement*. The repetition entrainment enhancement of the FFR seems independent of stimulus class: it has been shown for syllables (Chandrasekaran et al., 2009; Strait et al., 2011; Slabu et al., 2012; Gorina-Careta et al., 2016; Lau et al., 2017; Alho et al., 2019), amplitude modulated tones (Shiga et al., 2015), pitch contours in Mandarin syllables (Skoe et al., 2014), and pure tones (Font-Alaminos et al., 2020). One of these studies showed that the repetition entrainment enhancement is present even when the onset of the sounds is not predictable (i.e., with jittered ISIs) (Slabu et al., 2012), although predictable onsets do result in lower FFR power and higher FFR entrainment (Gorina-Careta et al., 2016). Moreover, two studies showed that the magnitude of the repetition entrainment enhancement correlates with the ability of the subjects to recognize speech in noise (Chandrasekaran et al., 2009; Strait et al., 2011). The fact that the FFR adapts its properties to the stimulation history is contrary to the predictions of a representational framework. The FFR repetition entrainment enhancement is, however, also not straightforward to interpret within the PPF. If the FFR represented prediction error, we would expect a gradual decay of the signal (and with it its SNR and quality of the entrainment) with each repetition of a standard. Another possibility is that the FFR encodes the generative model of the sensory input, which becomes more and more precise with each repetition. However, if that was the case the FFR would always represent expectations, which means that we would expect an FFR tuned to the standard during the presentation of a deviant. It is possible that the generative model corrects itself quickly after detecting that the stimulus is not a standard, which would result in a reduction of the FFR entrainment to the deviant. If that was the case the entrainment to the deviants would be much weaker than to the first standards in the sequence; however, the literature reports that the deviant and first standard elicit the same FFR entrainment (Font-Alaminos et al., 2020). A last possibility is that the FFR has contributions from both, prediction error and generative model units, and that the balance between the contribution of one and the other results in the observed phenomenology.

5. MIXED EVIDENCE ON THE GLOBAL MODEL BASED ON DEACTIVATION OF HIGH-ORDER PROCESSING STRUCTURES

Studies reviewed so far have established that sensory processing in the auditory pathway cannot be explained by a representational framework. The studies suggested that computation of expectations and prediction error is common to many mammals, and that it occurs even during sleep and anesthesia. However, all these studies use paradigms that have as a core feature repetition to induce predictions on the sensory input. This means that prediction error is computed with respect to a model of the sensory world that could have been generated locally, at the level of the IC and MGB, or globally, at a higher level of the processing hierarchy. Thus, results reviewed so far are ambivalent with respect to the actual organization of the PPF and are compatible with both, the local and global models. The next sections of this review focus on studies that tried to disentangle between these two possibilities.

Neural populations encoding higher levels of abstraction are thought to be encoded at successively higher stages in the processing hierarchy (Kiebel et al., 2008). This hierarchical organization is exquisitely presented in the auditory system, where the CN encodes a faithful representation of raw sensory input (Rhode and Smith, 1986), the IC and MGB encode intermediate features like formant transitions (Kuo and Wu, 2012), and auditory cortex encodes the identity of sounds as complex auditory objects (Chechik and Nelken, 2012). One way to test whether expectations are computed globally and transmitted downwards through the auditory hierarchy is to study whether SSA in IC and MGB depends on the cerebral cortex.

Three animal studies have compared SSA in subcortical sensory pathway nuclei before and during reversible deactivation of the ipsilateral auditory cortex. Two of the studies used a cryoloop to temporarily deactivate rat's auditory cortex, and measured SSA in neurons of the IC (Anderson and Malmierca, 2013) and MGB (Antunes and Malmierca, 2011). Both studies reported that SSA in single neurons was affected by deactivation of the cerebral cortex. The overall averaged amount of SSA in IC and MGB did, however, not significantly change during deactivation. The authors concluded that although cerebral cortex may modulate subcortical SSA, it does not generate it. This means that SSA cannot be solely driven by the global model of the PPF. In contrast, a third study (Bauerle et al., 2011) used muscimol to deactivate auditory cortex and measured SSA in neurons of vMGB (i.e., in the lemniscal section) in gerbils. The authors found that SSA was completely abolished after muscimol

application, concluding that SSA indeed depends on cerebral cortex function, supporting the global model.

Divergences between the three studies could be caused by: (1) different deactivation methods, (2) different species, or (3) differences between the lemniscal and non-lemniscal pathways. Whereas deactivation by cryoloop allowed the investigators to show recovered responses after cortical inactivation, the longer recovery periods and possible diffusion of muscimol (Lomber, 1999) prevented Bauerle et al. from recording post-inactivation responses. Thus, Bauerle et al. could not completely rule out that the abolition of SSA after drug administration was due to irreversible damages induced during the application of the drug or diffusion of the drug into thalamus (Bauerle et al., 2011). Although the authors claim that side effects of muscimol were unlikely, reproduction of the results are needed to confirm that deactivation of auditory cortex abolishes SSA in vMGB.

Although the studies using the cryoloop (Antunes and Malmierca, 2011; Anderson and Malmierca, 2013) do not report whether neurons belong to the lemniscal or non-lemniscal subdivisions of the IC and MGB, the relatively elevated SSA indices [$SSAi > 0.18$ in IC (Anderson and Malmierca, 2013) and average $SSAi \sim 0.31$ in MGB (Antunes and Malmierca, 2011)] indicate that most recorded neurons in the cryoloop experiments belonged to the non-lemniscal subdivisions. In comparison, SSA indices from the vMGB in Bauerle et al. (2011) were around $SSAi = 0.07$, even though they used shorter ISIs and higher intensity levels than the cryoloop studies, which potentially elicits higher levels of SSA. One possibility is that the cerebral cortex triggers SSA only in the lemniscal pathway. This would be surprising, given that most corticofugal fibers target neurons in the non-lemniscal subdivisions of the IC and MGB (Lee and Sherman, 2011). Another possibility is that cortical control of non-lemniscal areas depends on the stimuli used and the specific experimental task and that the conditions used in the animal experiments so far do not elicit top-down control of SSA.

The thalamic reticular nucleus (TRN) is a laminar GABAergic nucleus that covers large parts of the thalamus and serves as interface to the cerebral cortex (Ohara and Lieberman, 1985; Pinault, 2004). TRN neurons show even stronger SSA than nuclei of the auditory sensory pathway, with SSA indices that double those of the (non-lemniscal) MGB (Yu et al., 2009). Moreover, TRN deactivation has been shown to affect the responses on MGB after (not during) the presentation of a deviant (Yu et al., 2009). This suggests that the deactivation does not influence the prediction error component of MGB responses, but potentially rather the encoding of the generative model of the sensory world. However, Yu et al. measured the effect of TRN deactivation in just one MGB neuron so these results should be interpreted with caution until replications are available.

In summary, there are only very few studies investigating corticofugal influences on presumed prediction error responses in IC and MGB. Only two studies show that SSA in IC and MGB is driven by top-down control (Yu et al., 2009; Bauerle et al., 2011).

6. FAVORING EVIDENCE FOR THE GLOBAL MODEL BASED ON MANIPULATION OF HIGH-ORDER EXPECTATIONS

An alternative approach to study the computational principles of the subcortical sensory pathway nuclei is to measure adaptation in subcortical sensory nuclei while manipulating predictions that are unlikely to stem directly from subcortical processing. Such predictions can be derived either from complex statistical regularities that are unlikely to be encoded in subcortical sensory structures or from cognitive representations that are characterized by high levels of abstraction.

One first step toward such an approach is to use paradigms that tap into so-called *meta-adaptation*. Meta-adaptation is a phenomenon where adaptation dynamics themselves adapt depending on changes in the context in which the adaptation dynamics occur (Robinson et al., 2016): Robinson and colleagues exposed Guinea pigs to repeated switches between quiet and loud environments. They observed that the adjustment in the dynamic range of neurons in IC accelerated after repeated exposure to the two different environments. Thus, the adaptation of the dynamic range adapted to the novel but familiar environmental context. This meta-adaptation effect largely attenuated after the experimenters deactivated auditory cortex using a cryoloop. Under the light of the PPF, the faster adaptation dynamics would result from the prediction that switches occur often. The result that meta-adaptation on IC depends on the integrity of the cerebral cortex can thus be interpreted as evidence that the generative model is encoded in auditory cortex, favoring the global model.

Malmierca et al. (2019) used an elegant paradigm with complex statistical regularities to investigate responses in the anesthetized rat's IC. The authors used as predictable entity a pattern of two tones that was presented in a repetitive manner (i.e., A-B-A-B-A-B…). To elicit prediction error, the pattern was rarely violated by a repetition of one of the tones (…A-B-A-B-B). The rationale was that the representation of the tone dyad A-B is putatively encoded at higher processing levels than the representation of a single tone typically exploited in SSA experiments. Neurons encoding prediction error in IC would therefore only respond to violations of the pattern if predictions encoded in higher levels are used to predict sensory input in the IC. The authors reported that only 14 of 281 measured samples of IC neurons, located in both lemniscal and non-lemniscal subdivisions of the nucleus, showed statistically significant prediction errors to violation of the patterns. The study was the first to investigate SSA in the subcortical sensory pathway with a paradigm that it likely represented in complex generative models in the brain. However, since the fraction of neurons with significant prediction error reported in the study ($14/281 \simeq 4.98\%$) was close to the false-discovery rate of the study ($\alpha = 0.05$), replications would need to confirm this effect unequivocally.

Yu et al. (2009) used a different approach to control predictability: They used a light to cue the onset of the auditory stimuli while recording from neurons of the anesthetized rat's

MGB. They found that the visual cue resulted in significantly suppressed responses in 20 of 118 ($\simeq$ 17%) measured neurons and significantly enhanced responses in 23 of them ($\simeq$ 19.5%), both way above the false discovery rate of the study. Assuming that the causal link connecting the visual cue to the expectations on the auditory input is computed at a processing stage other than the MGB, we interpret these results as evidence for the global model. Favoring this interpretation, the authors show that deactivation of the TRN suppresses the effects of cuing in both directions; however, this result is once again shown in a single neuron and should be interpreted with caution until replications are available.

Lau et al. (2017) showed entrainment enhancement of the FFR in humans driven by high-order predictability using pitch contours of Mandarin syllables. The authors presented a target syllable in three different contexts: an unpredictable context, where the likelihood of the target was 1/3; a repetitive context, where all stimuli were repetitions of the target; and a patterned context, where the target was presented in a pattern of three syllables that was repeated over and over. The results demonstrated that the FFR entrainment was enhanced by predictability (i.e., that the FFR was more correlated to the stimulus waveform in the two predictable contexts than in the unpredictable context). In addition, the entrainment was stronger for the high-order predictability (i.e., in the patterned context) than when predictability was dictated by repetition. Although *predictability enhancement* cannot be interpreted as prediction error dynamics within the PPF, the result that predictability stemming from a higher level of abstraction has a stronger weight than predictability stemming from repetition in the strength of the FFR supports the global model.

The most recent evidence for the global model comes from a study in humans from our lab (Tabas et al., 2020) where we manipulated high-order predictions while preserving local stimulus statistics. We used fMRI to measure responses in the IC and MGB to a variation of the classical oddball sequence where the predictability of the deviants was manipulated using abstract rules. We disclosed to the participants that in each oddball sequence one of the standards at positions 4, 5, or 6 will be substituted by a deviant (**Figure 2A**). Since each position was equally likely across the experiment, after 3 repetitions of the standard subjects expect a deviant in position 4 with a likelihood of $p = 1/3$, after hearing 4 standards they expect a deviant in position 5 with $p = 1/2$, and after 5 standards subjects fully expect a deviant in position 6. According to the local model of the PPF, only the ratio between deviants and standards will have an effect on the strength of the responses to the deviant tones (**Figure 2A**, blue); according to the global model of the PPF, the responses will be the weaker the higher the likelihood of the tone according to the abstract rules (**Figure 2A**, red).

Using Bayesian Model comparison, we showed that responses in the IC and MGB (**Figure 2B**) were far more likely to be produced by a mechanism following the principles of the global model (where the magnitude of the response decreased with predictability) than by a mechanism following the principles of the local model (where the magnitude of the responses decreased with the number of times the stimulus has been repeated before). The global model was similarly prominent in both lemniscal and non-lemniscal sections of the MGB, revealing once again no particular functional organization of the human auditory pathway in respect of the PPF.

7. SUBCORTICAL PREDICTIVE PROCESSING IN OTHER SENSORY MODALITIES

Although here we have focused on the auditory modality, it is likely that the processing architecture of other sensory modalities follows similar principles. Indeed, analogous functional and anatomical organizations have been found between the auditory and visual (Rauschecker, 2015), and visual and somatosensory (Pack and Bensmaia, 2015) systems. Moreover, if the auditory pathway is organized according to a global PPF, this organization should necessarily extend to other sensory modalities: otherwise the predictive potential of the global model would be largely under-exploited. There is indeed plenty of evidence that information across modalities is integrated and applied to sensory coding according to the principles of the PPF (see reviews, von Kriegstein, 2012; van Wassenhove, 2013; Talsma, 2015). In this section, we describe a few examples of predictive processing in the visual and somatosensory subcortical pathways.

Predictive coding was originally enunciated as a visual theory (Rao and Ballard, 1999). Most literature on visual predictive processing is concerned with the problem of extra-classical receptive field properties in response to concurrent stimulation (e.g., Aitchison and Lengyel, 2017). Some studies have, however, also considered how predictions on future events are used during the encoding of visual information in the subcortical visual pathway. Evidence for predictive processing of this kind has been reported in the retina (Hosoya et al., 2005; Kastner and Baccus, 2013; Howlett et al., 2017; Johnston et al., 2019; Kastner et al., 2019), including a study demonstrating SSA to movement in retinal bipolar cells (Ölveczky et al., 2007); in the superior colliculus, in the form of SSA to Gabor patterns (Jin and Glickfeld, 2020) and luminance (Boehnke et al., 2011); and in visual thalamus to location and polarity of light bars (Dhruv and Carandini, 2014). In the visual thalamus, predictive feedback has been suggested to stem from corticofugal efferents from primary visual cortex (Jehee and Ballard, 2009; Zabbah et al., 2014), but has yet not been demonstrated empirically. Thus, evidence to-date in the visual subcortical pathway is compatible with both, the global and local models of the PPF.

Adaptation to local stimulus statistics has also been reported in the mammal (Khatri et al., 2004; Mohar et al., 2013; Liu et al., 2017) and human somatosensory thalamus (Allen et al., 2016), but results are compatible with both, the local and global models of the PPF. One of these studies (Mohar et al., 2013) found a functional subdivision of the somatosensory thalamus similar to that of the animal literature in the auditory modality: non-lemniscal subdivisions showed stronger adaptation dynamics than their lemniscal counterparts. Evidence for the global model was provided by a study (Pais-Vieira et al., 2013) that considered the effect of anticipation on somatosensory thalamus during the

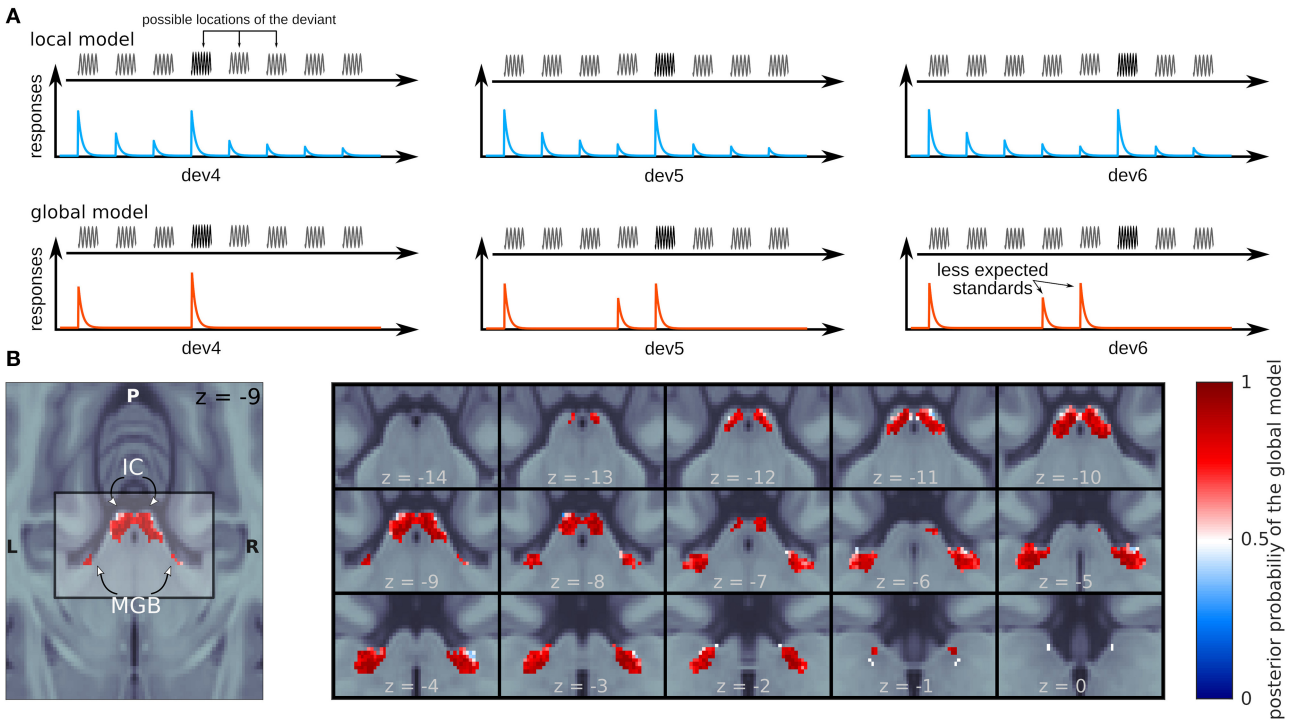

FIGURE 2 | Evidence for the global model in the human IC and MGB. **(A)** Schematic view of the expected responses for the different trials by the local (blue) and the global (red) models. **(B)** Posterior probability map of the global (red) and local (blue) models. *z*-coordinates correspond to the MNI space.

activation of the facial whiskers of the rat. Pais-Vieira et al. found that effects of anticipation clearly present in somatosensory thalamus vanished after deactivation of the somatosensory cortex with muscimol. Perhaps the most compelling demonstration that the somatosensory pathway is organized according to the PPF is the common placebo effect, described by the PPF as a drastic reduction of pain sensation by the imposition of a strong analgesic prior (Büchel et al., 2014). Favoring the global model, reduction of activity to painful stimulation after the administration of a placebo has been found in the medulla (Matre et al., 2006; Eippert et al., 2009).

8. CONCLUSION

Converging evidence indicates that hierarchical predictive processing is a key feature, if not the principal encoding strategy, of subcortical sensory pathways. In the auditory modality, it is clear that encoding in the IC and MGB are strongly driven by expectations on the incoming stimuli. There is, however, still mixed evidence about the underlying mechanism of these expectations. We have summarized the two extreme possible architectures of the predictive processing network in two opposing views: a local model, where each stage in the hierarchy encodes its own representation of the stimulus and performs predictions on the representation of the immediately lower stage; and the global model, where a global prediction, encoded at higher processing stages, propagates downwards generating local predictions at all subsequent cortical and subcortical stages. In our review of the literature we have found a few studies favoring the local model, several studies favoring the global model, and a large number of studies whose results are agnostic to the architecture of the predictive processing network.

One possibility is that the feedback propagation of the global model is adapted according to the specific context. Electrophysiological experiments in animals are typically performed under anesthesia. This work has impressively shown that SSA is a fundamental automatic reaction of sensory systems rather than a phenomenon triggered by particular cognitive actions or arousal. In anesthesia, however, animals experience sounds under the same context: that of drug-induced coma. The two studies that investigated pure tone SSA on awake animals (Duque and Malmierca, 2015; Parras et al., 2017) demonstrated that SSA is pervasive in alert states, but used passive listening conditions. Whether the cognitive context and behavioral relevance of the stimuli might have deeper repercussions when more complex models of the sensory world are necessary in order to compute expectations has not being investigated yet. This possibility could explain why evidence for the global model in the IC of anesthesized rats was inconclusive (Malmierca et al., 2019), while there was strong evidence for the global model in awake human participants (Tabas et al., 2020). It is also possible that not all processing stages conform under the same context to the same model: different stages of the processing hierarchy might depend to a greater or smaller degree on high-level expectations. Differences between the two studies could, however, also be explained by the many methodological differences between

animal and human studies and by potential species-specific differences in rodent and human sensory systems.

An important open question is exactly where the neural units that encode the model of the sensory world used to compute prediction error in the subcortical nuclei are located. Although in theory there is no reason why prediction error units could not encode the generative model in a multiplexed code, prediction error and the model are usually argued to be encoded in distinct populations (e.g., Friston, 2003, 2005; Bastos et al., 2012; Spratling, 2017; Keller and Mrsic-Flogel, 2018). However, in comparison with the evidence for the ubiquity of prediction error units, evidence for the existence of the generative model units is scarce in the cerebral cortex (Bell et al., 2016; Fiser et al., 2016; Walsh et al., 2020), and practically non-existent in subcortical areas. There is weak evidence that TRN neurons might have an active role on applying these models in MGB (Yu et al., 2009), but the fact that TRN neurons themselves show SSA render this hypothesis unlikely. According to the existing formulations of the PPF (Kiebel et al., 2008; Spratling, 2017; Keller and Mrsic-Flogel, 2018), each representational level should have a corresponding local model (see **Figure 1B**). This means that, if we accept that the IC and MGB encode different stages of the processing hierarchy, the MGB should have a local population of neurons encoding predictions that are transferred to the IC. Some algorithms actually locate the predictive model at the same processing stage, meaning that the populations encoding the model would actually reside in the IC (Spratling, 2017). There is, however, still no evidence for the encoding of these models in subcortical stages. Direct corticofugal connections exist all the way down to the cochlear nucleus (Winer, 2005a), so it is theoretically possible that all subcortical nuclei are located at the same hierarchical stage with respect to the PPF and that their corresponding model is located in primary auditory cortex. However, the presence of thalamo-collicular, thalamo-cochlear, and colliculo-cochlear efferents (Schofield, 2011) indicate that predictions are most likely also conveyed across different subcortical stages.

Another key ingredient necessary to understand the architecture of the PPF is the exact mechanism underlying the computation of prediction error and generation of predictions at each stage. Some PPF algorithms have suggested that prediction error might be computed by subtracting the predictions from the sensory input via inhibition (Wacongne et al., 2012). However, predictability leads to behavioral benefits and wrong predictions can sometime bias perception toward incorrect percepts (de Lange et al., 2018); an inhibitory account of the computation of prediction error would not be able to account for any of these effects. Moreover, the dependence of the repetition entrainment enhancement of the FFR on predictability and the enhancement of the responses in the MGB by visual cues (Yu et al., 2009) seem to indicate that predictions can enhance the sensory representation, rather than inhibiting it. Future models of the PPF face the challenge of reconciling these findings with the repetition/predictability suppression characteristic of prediction error.

Understanding the neural mechanisms underlying sensory processing is the only robust approach to understand perception. If, as enunciated by the global PPF model, sensory processing is a process of inference, we should remove all claims of perceptual objectivity, pay close attention to our priors and our internal models of the world, and question ourselves about the realities we cannot perceive just because they are not part of our model space. Although absolute inference is an unlikely scenario, since we must have formed our current models based on empirical experiences, it is possible that our reliance on inference grows more and more as we age (Lucas et al., 2014; Sherratt and Morand-Ferron, 2018; Cohen et al., 2020). SSA and the discovery of the encoding of prediction in subcortical sensory pathways have opened the gates to a deep exploration on sensory organization that might have strong philosophical repercussions on the way we understand what we call reality. If future work departs from paradigms that are unspecific about the underlying model of the sensory world, research on the PPF could lead us to the roots of the mechanisms that make us see, hear, and feel.

AUTHOR CONTRIBUTIONS

AT and KK reviewed the literature and wrote the manuscript. Both authors contributed to the article and approved the submitted version.

FUNDING

This study was funded by the European Research Council ERC Consolidator Grant SENSOCOM (647051).

REFERENCES

Aitchison, L., and Lengyel, M. (2017). With or without you: predictive coding and Bayesian inference in the brain. *Curr. Opin. Neurobiol.* 46, 219–227. doi: 10.1016/j.conb.2017.08.010

Alho, K., Żarnowiec, K., Gorina-Careta, N., and Escera, C. (2019). Phonological task enhances the frequency-following response to deviant task-irrelevant speech sounds. *Front. Hum. Neurosci.* 13:245. doi: 10.3389/fnhum.2019.00245

Allen, M., Fardo, F., Dietz, M. J., Hillebrandt, H., Friston, K. J., Rees, G., et al. (2016). Anterior insula coordinates hierarchical processing of tactile mismatch responses. *Neuroimage* 127, 34–43. doi: 10.1016/j.neuroimage.2015.11.030

Althen, H., Grimm, S., and Escera, C. (2011). Fast detection of unexpected sound intensity decrements as revealed by human evoked potentials. *PLoS ONE* 6:e28522. doi: 10.1371/journal.pone.0028522

Andersen, M. (2019). Predictive coding in agency detection. *Religion Brain Behav.* 9, 65–84. doi: 10.1080/2153599X.2017.1387170

Anderson, L. A., Christianson, G. B., and Linden, J. F. (2009). Stimulus-specific adaptation occurs in the auditory thalamus. *J. Neurosci.* 29, 7359–7363. doi: 10.1523/JNEUROSCI.0793-09.2009

Anderson, L. A., and Malmierca, M. S. (2013). The effect of auditory cortex deactivation on stimulus-specific adaptation in the inferior colliculus of the rat. *Eur. J. Neurosci.* 37, 52–62. doi: 10.1111/ejn.12018

Antunes, F. M., and Malmierca, M. S. (2011). Effect of auditory cortex deactivation on stimulus-specific adaptation in the medial geniculate body. *J. Neurosci.* 31, 17306–17316. doi: 10.1523/JNEUROSCI.1915-11.2011

Antunes, F. M., Nelken, I., Covey, E., and Malmierca, M. S. (2010). Stimulus-specific adaptation in the auditory thalamus of the anesthetized rat. *PLoS ONE* 5:e14071. doi: 10.1371/journal.pone.0014071

Atick, J. J. (1992). Could information theory provide an ecological theory of sensory processing? *Network Comput. Neural Syst.* 3, 213–251. doi: 10.1088/0954-898X_3_2_009

Ayala, Y. A., and Malmierca, M. S. (2015). Cholinergic modulation of stimulus-specific adaptation in the inferior colliculus. *J. Neurosci.* 35, 12261–12272. doi: 10.1523/JNEUROSCI.0909-15.2015

Ayala, Y. A., and Malmierca, M. S. (2018). The effect of inhibition on stimulus-specific adaptation in the inferior colliculus. *Brain Struct. Funct.* 223, 1391–1407. doi: 10.1007/s00429-017-1546-4

Ayala, Y. A., Pérez-gonzález, D., Duque, D., Nelken, I., and Malmierca, M. S. (2013). Frequency discrimination and stimulus deviance in the inferior colliculus and cochlear nucleus. *Front. Neural Circ.* 6:119. doi: 10.3389/fncir.2012.00119

Ayala, Y. A., Pérez-González, D., and Malmierca, M. S. (2016). Stimulus-specific adaptation in the inferior colliculus: the role of excitatory, inhibitory and modulatory inputs. *Biol. Psychol.* 116, 10–22. doi: 10.1016/j.biopsycho.2015.06.016

Ayala, Y. A., Udeh, A., Dutta, K., Bishop, D., Malmierca, M. S., and Oliver, D. L. (2015). Differences in the strength of cortical and brainstem inputs to SSA and non-SSA neurons in the inferior colliculus. *Sci. Rep.* 5:10383. doi: 10.1038/srep10383

Badcock, P. B., Friston, K. J., and Ramstead, M. J. (2019). The hierarchically mechanistic mind: a free-energy formulation of the human psyche. *Phys. Life Rev.* 31, 104–121. doi: 10.1016/j.plrev.2018.10.002

Barron, H. C., Auksztulewicz, R., and Friston, K. (2020). Prediction and memory: a predictive coding account. *Prog. Neurobiol.* 192:101821. doi: 10.1016/j.pneurobio.2020.101821

Bastos, A. M., Usrey, W. M., Adams, R., a., Mangun, G. R., Fries, P., et al. (2012). Canonical microcircuits for predictive coding. *Neuron* 76, 695–711. doi: 10.1016/j.neuron.2012.10.038

Bauerle, P., von der Behrens, W., Kossl, M., and Gaese, B. H. (2011). Stimulus-specific adaptation in the gerbil primary auditory thalamus is the result of a fast frequency-specific habituation and is regulated by the corticofugal system. *J. Neurosci.* 31, 9708–9722. doi: 10.1523/JNEUROSCI.5814-10.2011

Bejjanki, V. R., Beck, J. M., Lu, Z. L., and Pouget, A. (2011). Perceptual learning as improved probabilistic inference in early sensory areas. *Nat. Neurosci.* 14, 642–650. doi: 10.1038/nn.2796

Bell, A. H., Summerfield, C., Morin, E. L., Malecek, N. J., and Ungerleider, L. G. (2016). Encoding of stimulus probability in macaque inferior temporal cortex. *Curr. Biol.* 26, 2280–2290. doi: 10.1016/j.cub.2016.07.007

Bendixen, A., SanMiguel, I., and Schröger, E. (2012). Early electrophysiological indicators for predictive processing in audition: a review. *Int. J. Psychophysiol.* 83, 120–131. doi: 10.1016/j.ijpsycho.2011.08.003

Bidelman, G. M. (2018). Subcortical sources dominate the neuroelectric auditory frequency-following response to speech. *Neuroimage* 175, 56–69. doi: 10.1016/j.neuroimage.2018.03.060

Boehnke, S. E., Berg, D. J., Marino, R. A., Baldi, P. F., Itti, L., and Munoz, D. P. (2011). Visual adaptation and novelty responses in the superior colliculus. *Eur. J. Neurosci.* 34, 766–779. doi: 10.1111/j.1460-9568.2011.07805.x

Boston, J. R., and Moller, A. R. (1985). Brainstem auditory-evoked potentials. *Crit. Rev. Biomed. Eng.* 13, 97–123.

Brenner, N., Bialek, W., and de Ruyter van Steveninck, R. (2000). Adaptive rescaling maximizes information transmission. *Neuron* 26, 695–702. doi: 10.1016/S0896-6273(00)81205-2

Büchel, C., Geuter, S., Sprenger, C., and Eippert, F. (2014). Placebo analgesia: a predictive coding perspective. *Neuron* 81, 1223–1239. doi: 10.1016/j.neuron.2014.02.042

Buxton, R. B. (2009). *Introduction to Functional Magnetic Resonance Imaging*. Cambridge: Cambridge University Press. doi: 10.1017/CBO9780511605505

Cacciaglia, R., Escera, C., Slabu, L., Grimm, S., Sanjuán, A., Ventura-Campos, N., et al. (2015). Involvement of the human midbrain and thalamus in auditory deviance detection. *Neuropsychologia* 68, 51–58. doi: 10.1016/j.neuropsychologia.2015.01.001

Carbajal, G. V., and Malmierca, M. S. (2018). The neuronal basis of predictive coding along the auditory pathway: from the subcortical roots to cortical deviance detection. *Trends Hear.* 22:233121651878482. doi: 10.1177/2331216518784822

Casado-Román, L., Carbajal, G. V., Pérez-González, D., and Malmierca, M. S. (2020). Prediction error signaling explains neuronal mismatch responses in the medial prefrontal cortex. *PLoS Biol.* 18:e3001019. doi: 10.1371/journal.pbio.3001019

Chandrasekaran, B., Hornickel, J., Skoe, E., Nicol, T., and Kraus, N. (2009). Context-dependent encoding in the human auditory brainstem relates to hearing speech in noise: implications for developmental dyslexia. *Neuron* 64, 311–319. doi: 10.1016/j.neuron.2009.10.006

Chandrasekaran, B., and Kraus, N. (2010). The scalp-recorded brainstem response to speech: neural origins and plasticity. *Psychophysiology* 47, 236–246. doi: 10.1111/j.1469-8986.2009.00928.x

Chechik, G., Anderson, M. J., Bar-Yosef, O., Young, E. D., Tishby, N., and Nelken, I. (2006). Reduction of information redundancy in the ascending auditory pathway. *Neuron* 51, 359–368. doi: 10.1016/j.neuron.2006.06.030

Chechik, G., and Nelken, I. (2012). Auditory abstraction from spectro-temporal features to coding auditory entities. *Proc. Natl. Acad. Sci. U.S.A.* 109, 18968–18973. doi: 10.1073/pnas.1111242109

Clark, J. E., Watson, S., and Friston, K. J. (2018). What is mood? A computational perspective. *Psychol. Med.* 48, 2277–2284. doi: 10.1017/S0033291718000430

Coffey, E. B., Nicol, T., White-Schwoch, T., Chandrasekaran, B., Krizman, J., Skoe, E., et al. (2019). Evolving perspectives on the sources of the frequency-following response. *Nat. Commun.* 10, 1–10. doi: 10.1038/s41467-019-13003-w

Coffey, E. B. J., Herholz, S. C., Chepesiuk, A. M. P., Baillet, S., and Zatorre, R. J. (2016). Cortical contributions to the auditory frequency-following response revealed by MEG. *Nat. Commun.* 7:11070. doi: 10.1038/ncomms11070

Cohen, A. O., Nussenbaum, K., Dorfman, H. M., Gershman, S. J., and Hartley, C. A. (2020). The rational use of causal inference to guide reinforcement learning strengthens with age. *NPJ Sci. Learn.* 5, 1–9. doi: 10.1038/s41539-020-00075-3

Davis, M. H., and Johnsrude, I. S. (2007). Hearing speech sounds: Top-down influences on the interface between audition and speech perception. *Hear. Res.* 229, 132–147. doi: 10.1016/j.heares.2007.01.014

de Lange, F. P., Heilbron, M., and Kok, P. (2018). How do expectations shape perception? *Trends Cogn. Sci.* 22, 764–779. doi: 10.1016/j.tics.2018.06.002

DeCharms, C., and Zador, A. (2000). Neural representation andthe cordical code. *Annu. Rev. Neurosci.* 23, 613–647. doi: 10.1146/annurev.neuro.23.1.613

Dhruv, N. T., and Carandini, M. (2014). Report cascaded effects of spatial adaptation in the early visual system. *Neuron* 81, 529–535. doi: 10.1016/j.neuron.2013.11.025

Diaz, B., Hintz, F., Kiebel, S. J., and von Kriegstein, K. (2012). Dysfunction of the auditory thalamus in developmental dyslexia. *Proc. Natl. Acad. Sci. U.S.A.* 109, 13841–13846. doi: 10.1073/pnas.1119828109

DiCarlo, J. J., Zoccolan, D., and Rust, N. C. (2012). How does the brain solve visual object recognition? *Neuron* 73, 415–434. doi: 10.1016/j.neuron.2012.01.010

Duque, D., and Malmierca, M. S. (2015). Stimulus-specific adaptation in the inferior colliculus of the mouse: anesthesia and spontaneous activity effects. *Brain Struct. Funct.* 220, 3385–3398. doi: 10.1007/s00429-014-0862-1

Duque, D., Malmierca, M. S., and Caspary, D. M. (2014). Modulation of stimulus-specific adaptation by GABA(A) receptor activation or blockade in the medial geniculate body of the anaesthetized rat. *J. Physiol.* 592(Pt 4), 729–743. doi: 10.1113/jphysiol.2013.261941

Duque, D., Pais, R., and Malmierca, M. S. (2018). Stimulus-specific adaptation in the anesthetized mouse revealed by brainstem auditory evoked potentials. *Hear. Res.* 370, 294–301. doi: 10.1016/j.heares.2018.08.011

Duque, D., Pérez-González, D., Ayala, Y. A., Palmer, A. R., and Malmierca, M. S. (2012). Topographic distribution, frequency, and intensity dependence of stimulus-specific adaptation in the inferior colliculus of the rat. *J. Neurosci.* 32, 17762–17774. doi: 10.1523/JNEUROSCI.3190-12.2012

Duque, D., Wang, X., Nieto-Diego, J., Krumbholz, K., and Malmierca, M. S. (2016). Neurons in the inferior colliculus of the rat show stimulus-specific adaptation for frequency, but not for intensity. *Sci. Rep.* 6, 1–15. doi: 10.1038/srep24114

Eippert, F., Finsterbusch, J., Bingel, U., and Büchel, C. (2009). Direct evidence for spinal cord involvement in Placebo Analgesia. *Science* 326:404. doi: 10.1126/science.1180142

Epstein, W. (1993). The representational framework in perceptual theory. *Percept. Psychophys.* 53, 704–709. doi: 10.3758/BF03211747

Escera, C., and Malmierca, M. S. (2014). The auditory novelty system: an attempt to integrate human and animal research. *Psychophysiology* 51, 111–123. doi: 10.1111/psyp.12156

Eytan, D., Brenner, N., and Marom, S. (2003). Selective adaptation in networks of cortical neurons. *J. Neurosci.* 23, 9349–9356. doi: 10.1523/JNEUROSCI.23-28-09349.2003

Fabry, R. E. (2018). Betwixt and between: the enculturated predictive processing approach to cognition. *Synthese* 195, 2483–2518. doi: 10.1007/s11229-017-1334-y

Fairhall, A. L., Lewen, G. D., Bialek, W., and de Ruyter van Steveninck, R. R. (2001). Efficiency and ambiguity in an adaptive neural code. *Nature* 412, 787–792. doi: 10.1038/35090500

Fiser, A., Mahringer, D., Oyibo, H. K., Petersen, A. V., Leinweber, M., and Keller, G. B. (2016). Experience-dependent spatial expectations in mouse visual cortex. *Nat. Neurosci.* 19, 1658–1664. doi: 10.1038/nn.4385

Font-Alaminos, M., Ribas-Prats, T., Gorina-Careta, N., and Escera, C. (2020). Emergence of prediction error along the human auditory hierarchy. *Hear. Res.* 399:107954. doi: 10.1016/j.heares.2020.107954

Frank, G. K., Collier, S., Shott, M. E., and O'Reilly, R. C. (2016). Prediction error and somatosensory insula activation in women recovered from anorexia nervosa. *J. Psychiatry Neurosci.* 41, 304–311. doi: 10.1503/jpn.150103

Friston, K. (2003). Learning and inference in the brain. *Neural Netw.* 16, 1325–1352. doi: 10.1016/j.neunet.2003.06.005

Friston, K. (2005). A theory of cortical responses. *Philos. Trans. R. Soc. Lond. Ser. B Biol. Sci.* 360, 815–836. doi: 10.1098/rstb.2005.1622

Gao, P. P., Zhang, J. W., Cheng, J. S., Zhou, I. Y., and Wu, E. X. (2014). The inferior colliculus is involved in deviant sound detection as revealed by BOLD fMRI. *Neuroimage* 91, 220–227. doi: 10.1016/j.neuroimage.2014.01.043

Garrido, M. I., Kilner, J. M., Stephan, K. E., and Friston, K. J. (2009). The mismatch negativity: a review of underlying mechanisms. *Clin. Neurophysiol.* 120, 453–463. doi: 10.1016/j.clinph.2008.11.029

Gerken, G. M., Moushegian, G., Stillman, R. D., and Rupert, A. L. (1975). Human frequency-following responses to monaural and binaural stimuli. *Electroencephalogr. Clin. Neurophysiol.* 38, 379–386. doi: 10.1016/0013-4694(75)90262-X

Gonzalez-Gadea, M. L., Chennu, S., Bekinschtein, T. A., Rattazzi, A., Beraudi, A., Tripicchio, P., et al. (2015). Predictive coding in autism spectrum disorder and attention deficit hyperactivity disorder. *J. Neurophysiol.* 114, 2625–2636. doi: 10.1152/jn.00543.2015

Gorina-Careta, N., Zarnowiec, K., Costa-Faidella, J., and Escera, C. (2016). Timing predictability enhances regularity encoding in the human subcortical auditory pathway. *Sci. Rep.* 6, 1–9. doi: 10.1038/srep37405

Grimm, S., Escera, C., and Nelken, I. (2016). Early indices of deviance detection in humans and animal models. *Biol. Psychol.* 116, 23–27. doi: 10.1016/j.biopsycho.2015.11.017

Grimm, S., Escera, C., Slabu, L., and Costa-Faidella, J. (2011). Electrophysiological evidence for the hierarchical organization of auditory change detection in the human brain. *Psychophysiology* 48, 377–384. doi: 10.1111/j.1469-8986.2010.01073.x

He, J., and Yu, Y. (2010). Role of descending control in the auditory pathway. *Oxford Handb. Audit. Neurosci.* 2, 247–268. doi: 10.1093/oxfordhb/9780199233281.013.0011

Heeger, D. J. (2017). Theory of cortical function. *Proc. Natl. Acad. Sci. U.S.A.* 114, 1773–1782. doi: 10.1073/pnas.1619788114

Heilbron, M., and Chait, M. (2017). Great expectations: Is there evidence for predictive coding in auditory cortex? *Neuroscience.* 389, 54–73. doi: 10.1016/j.neuroscience.2017.07.061

Horga, G., Schatz, K. C., Abi-Dargham, A., and Peterson, B. S. (2014). Deficits in predictive coding underlie hallucinations in schizophrenia. *J. Neurosci.* 34, 8072–8082. doi: 10.1523/JNEUROSCI.0200-14.2014

Hosoya, T., Baccus, S. A., and Meister, M. (2005). Dynamic predictive coding by the retina. *Nature* 436, 71–77. doi: 10.1038/nature03689

Howlett, M. H., Smith, R. G., and Kamermans, M. (2017). A novel mechanism of cone photoreceptor adaptation. *PLoS Biol.* 15:e2001210. doi: 10.1371/journal.pbio.2001210

Huang, Y., and Rao, R. P. N. (2011). Predictive coding. *WIREs Cogn. Sci.* 2, 580–593. doi: 10.1002/wcs.142

Jaramillo, S., and Zador, A. M. (2011). The auditory cortex mediates the perceptual effects of acoustic temporal expectation. *Nat. Neurosci.* 14, 246–253. doi: 10.1038/nn.2688

Jehee, J. F., and Ballard, D. H. (2009). Predictive feedback can account for biphasic responses in the lateral geniculate nucleus. *PLoS Comput. Biol.* 5:e1000373. doi: 10.1371/journal.pcbi.1000373

Jewett, D. L., Romano, M. N., and Williston, J. S. (1970). Human auditory evoked potentials: possible brain stem components detected on the scalp. *Science* 167, 1517–1518. doi: 10.1126/science.167.3924.1517

Jin, M., and Glickfeld, L. L. (2020). Magnitude, time course, and specificity of rapid adaptation across mouse visual areas. *J. Neurophysiol.* 124, 245–258. doi: 10.1152/jn.00758.2019

Johnston, J., Seibel, S. H., Darnet, L. S. A., Renninger, S., Orger, M., and Lagnado, L. (2019). A retinal circuit generating a dynamic predictive code for oriented features. *Neuron* 102, 1211.e3–1222.e3. doi: 10.1016/j.neuron.2019.04.002

Kastner, D. B., and Baccus, S. A. (2013). Spatial segregation of adaptation and predictive sensitization in retinal ganglion cells. *Neuron* 79, 541–554. doi: 10.1016/j.neuron.2013.06.011

Kastner, D. B., Ozuysal, Y., Panagiotakos, G., and Baccus, S. A. (2019). Adaptation of inhibition mediates retinal sensitization. *Curr. Biol.* 29, 2640.e4–2651.e4. doi: 10.1016/j.cub.2019.06.081

Keller, G. B., and Mrsic-Flogel, T. D. (2018). Predictive processing: a canonical cortical computation. *Neuron* 100, 424–435. doi: 10.1016/j.neuron.2018.10.003

Khatri, V., Hartings, J. A., and Simons, D. J. (2004). Adaptation in thalamic barreloid and cortical barrel neurons to periodic whisker deflections varying in frequency and velocity. *J. Neurophysiol.* 92, 3244–3254. doi: 10.1152/jn.00257.2004

Kiebel, S. J., Garrido, M. I., Moran, R. J., and Friston, K. J. (2008). Dynamic causal modelling for EEG and MEG. *Cogn. Neurodyn.* 2, 121–136. doi: 10.1007/s11571-008-9038-0

Kuo, R. I., and Wu, G. K. (2012). The generation of direction selectivity in the auditory system. *Neuron* 73, 1016–1027. doi: 10.1016/j.neuron.2011.11.035

Lau, J. C., Wong, P. C., and Chandrasekaran, B. (2017). Context-dependent plasticity in the subcortical encoding of linguistic pitch patterns. *J. Neurophysiol.* 117, 594–603. doi: 10.1152/jn.00656.2016

Lee, C. C., and Sherman, S. M. (2011). On the classification of pathways in the auditory midbrain, thalamus, and cortex. *Hear. Res.* 276, 79–87. doi: 10.1016/j.heares.2010.12.012

Liu, C., Foffani, G., Scaglione, A., Aguilar, J., and Moxon, K. A. (2017). Adaptation of thalamic neurons provides information about the spatiotemporal context of stimulus history. *J. Neurosci.* 37, 10012–10021. doi: 10.1523/JNEUROSCI.0637-17.2017

Lochmann, T., and Deneve, S. (2011). Neural processing as causal inference. *Curr. Opin. Neurobiol.* 21, 774–781. doi: 10.1016/j.conb.2011.05.018

Lomber, S. G. (1999). The advantages and limitations of permanent or reversible deactivation techniques in the assessment of neural function. *J. Neurosci. Methods* 86, 109–117. doi: 10.1016/S0165-0270(98)00160-5

Lucas, C. G., Bridgers, S., Griffiths, T. L., and Gopnik, A. (2014). When children are better (or at least more open-minded) learners than adults: developmental differences in learning the forms of causal relationships. *Cognition* 131, 284–299. doi: 10.1016/j.cognition.2013.12.010

Malmierca, M. S., Anderson, L. A., and Antunes, F. M. (2015). The cortical modulation of stimulus-specific adaptation in the auditory midbrain and thalamus: a potential neuronal correlate for predictive coding. *Front. Syst. Neurosci.* 9:19. doi: 10.3389/fnsys.2015.00019

Malmierca, M. S., Cristaudo, S., Pérez-González, D., and Covey, E. (2009). Stimulus-specific adaptation in the inferior colliculus of the anesthetized rat. *J. Neurosci.* 29, 5483–5493. doi: 10.1523/JNEUROSCI.4153-08.2009

Malmierca, M. S., Ni no-Aguillón, B. E., Nieto-Diego, J., Porteros, Á., Pérez-González, D., and Escera, C. (2019). Pattern-sensitive neurons reveal encoding of complex auditory regularities in the rat inferior colliculus. *Neuroimage* 184, 889–900. doi: 10.1016/j.neuroimage.2018.10.012

Malmierca, M. S., Sanchez-Vives, M. V., Escera, C., and Bendixen, A. (2014). Neuronal adaptation, novelty detection and regularity encoding in audition. *Front. Syst. Neurosci.* 8:111. doi: 10.3389/fnsys.2014.00111

Martin, K. A. (1994). A brief history of the "feature detector". *Cereb. Cortex* 4, 1–7. doi: 10.1093/cercor/4.1.1

Matre, D., Casey, K. L., and Knardahl, S. (2006). Placebo-induced changes in spinal cord pain processing. *J. Neurosci.* 26, 559–563. doi: 10.1523/JNEUROSCI.4218-05.2006

May, P. J., Westö, J., and Tiitinen, H. (2015). Computational modelling suggests that temporal integration results from synaptic adaptation in auditory cortex. *Eur. J. Neurosci.* 41, 615–630. doi: 10.1111/ejn.12820

Mazzucato, L., Camera, G., and Fontanini, A. (2019). Expectation-induced modulation of metastable activity underlies faster coding of sensory stimuli. *Nat. Neurosci.* 22, 787–796. doi: 10.1038/s41593-019-0364-9

Mill, R., Coath, M., Wennekers, T., and Denham, S. L. (2011). A neurocomputational model of stimulus-specific adaptation to oddball and Markov sequences. *PLoS Comput. Biol.* 7:e1002117. doi: 10.1371/journal.pcbi.1002117

Mill, R., Coath, M., Wennekers, T., and Denham, S. L. (2012). Characterising stimulus-specific adaptation using a multi-layer field model. *Brain Res.* 1434, 178–188. doi: 10.1016/j.brainres.2011.08.063

Mohar, B., Katz, Y., and Lampl, I. (2013). Opposite adaptive processing of stimulus intensity in two major nuclei of the somatosensory brainstem. *J. Neurosci.* 33, 15394–15400. doi: 10.1523/JNEUROSCI.1886-13.2013

Müller-Axt, C., Anwander, A., and von Kriegstein, K. (2017). Altered structural connectivity of the left visual thalamus in developmental dyslexia. *Curr. Biol.* 27, 3692.e4–3698.e4. doi: 10.1016/j.cub.2017.10.034

Mumford, D. (1992). On the computational architecture of the neocortex II: The role o f cortico-cortical loops. *Biol. Cybernet.* 66, 241–251. doi: 10.1007/BF00198477

Nagai, Y. (2019). Predictive learning: its key role in early cognitive development. *Philos. Trans. R. Soc. B Biol. Sci.* 374:20180030. doi: 10.1098/rstb.2018.0030

Nelken, I., and Ulanovsky, N. (2007). Mismatch negativity and stimulus-specific adaptation in animal models. *J. Psychophysiol.* 21, 214–223. doi: 10.1027/0269-8803.21.34.214

Ohara, P. T., and Lieberman, A. R. (1985). The thalamic reticular nucleus of the adult rat: experimental anatomical studies. *J. Neurocytol.* 14, 365–411. doi: 10.1007/BF01217752

Okada, K., Matchin, W., and Hickok, G. (2018). Neural evidence for predictive coding in auditory cortex during speech production. *Psychon. Bull. Rev.* 25, 423–430. doi: 10.3758/s13423-017-1284-x

Ölveczky, B. P., Baccus, S. A., and Meister, M. (2007). Retinal adaptation to object motion. *Neuron* 56, 689–700. doi: 10.1016/j.neuron.2007.09.030

Pack, C. C., and Bensmaia, S. J. (2015). Seeing and feeling motion: canonical computations in vision and touch. *PLoS Biol.* 13:e1002271. doi: 10.1371/journal.pbio.1002271

Pais-Vieira, M., Lebedev, M. A., Wiest, M. C., and Nicolelis, M. A. (2013). Simultaneous top-down modulation of the primary somatosensory cortex and thalamic nuclei during active tactile discrimination. *J. Neurosci.* 33, 4076–4093. doi: 10.1523/JNEUROSCI.1659-12.2013

Pakan, J. M., Francioni, V., and Rochefort, N. L. (2018). Action and learning shape the activity of neuronal circuits in the visual cortex. *Curr. Opin. Neurobiol.* 52, 88–97. doi: 10.1016/j.conb.2018.04.020

Parkkonen, L., Fujiki, N., and Mäkelä, J. P. (2009). Sources of auditory brainstem responses revisited: contribution by magnetoencephalography. *Hum. Brain Mapp.* 30, 1772–1782. doi: 10.1002/hbm.20788

Parras, G. G., Nieto-Diego, J., Carbajal, G. V., Valdés-Baizabal, C., Escera, C., and Malmierca, M. S. (2017). Neurons along the auditory pathway exhibit a hierarchical organization of prediction error. *Nat. Commun.* 8:2148. doi: 10.1038/s41467-017-02038-6

Pérez-González, D., Hernández, O., Covey, E., and Malmierca, M. S. (2012). GABA A-mediated inhibition modulates stimulus-specific adaptation in the inferior colliculus. *PLoS ONE* 7:e34297. doi: 10.1371/journal.pone.0034297

Pinault, D. (2004). The thalamic reticular nucleus: structure, function and concept. *Brain Res. Rev.* 46, 1–31. doi: 10.1016/j.brainresrev.2004.04.008

Purves, D., Morgenstern, Y., and Wojtach, W. T. (2015). Perception and reality: Why a wholly empirical paradigm is needed to understand vision. *Front. Syst. Neurosci.* 9:156. doi: 10.3389/fnsys.2015.00156

Quiroga, R. Q., Reddy, L., Kreiman, G., Koch, C., and Fried, I. (2005). Invariant visual representation by single neurons in the human brain. *Nature* 435, 1102–1107. doi: 10.1038/nature03687

Rao, R. P. N., and Ballard, D. H. (1999). Predictive coding in the visual cortex: a functional interpretation of some extra-classical receptive-field effects. *Nat. Neurosci.* 2, 79–87. doi: 10.1038/4580

Rauschecker, J. P. (2015). Auditory and visual cortex of primates: a comparison of two sensory systems. *Eur. J. Neurosci.* 41, 579–585. doi: 10.1111/ejn.12844

Rhode, W. S., and Smith, P. H. (1986). Encoding timing and intensity in the ventral cochlear nucleus of the cat. *J. Neurophysiol.* 56, 261–286. doi: 10.1152/jn.1986.56.2.261

Richardson, B. D., Hancock, K. E., and Caspary, D. M. (2013). Stimulus-specific adaptation in auditory thalamus of young and aged awake rats. *J. Neurophysiol.* 110, 1892–1902. doi: 10.1152/jn.00403.2013

Robinson, B. L., Harper, N. S., and McAlpine, D. (2016). Meta-adaptation in the auditory midbrain under cortical influence. *Nat. Commun.* 7:13442. doi: 10.1038/ncomms13442

Robinson, B. L., and McAlpine, D. (2009). Gain control mechanisms in the auditory pathway. *Curr. Opin. Neurobiol.* 19, 402–407. doi: 10.1016/j.conb.2009.07.006

Schofield, B. R. (2011). "Central descending auditory pathways," in *Auditory and Vestibular Efferents*, eds D. Ryugo and R. Fay (New York, NY: Springer), 261–290. doi: 10.1007/978-1-4419-7070-1_9

Sherratt, T. N., and Morand-Ferron, J. (2018). The adaptive significance of age-dependent changes in the tendency of individuals to explore. *Anim. Behav.* 138, 59–67. doi: 10.1016/j.anbehav.2018.01.025

Shiga, T., Althen, H., Cornella, M., Zarnowiec, K., Yabe, H., and Escera, C. (2015). Deviance-related responses along the auditory hierarchy: combined FFR, MLR and MMN evidence. *PLoS ONE* 10:e0136794. doi: 10.1371/journal.pone.0136794

Shipp, S. (2016). Neural elements for predictive coding. *Front. Psychol.* 7:1792. doi: 10.3389/fpsyg.2016.01792

Siman-Tov, T., Granot, R. Y., Shany, O., Singer, N., Hendler, T., and Gordon, C. R. (2019). Is there a prediction network? Meta-analytic evidence for a cortical-subcortical network likely subserving prediction. *Neurosci. Biobehav. Rev.* 105, 262–275. doi: 10.1016/j.neubiorev.2019.08.012

Skoe, E., Chandrasekaran, B., Spitzer, E. R., Wong, P. C., and Kraus, N. (2014). Human brainstem plasticity: the interaction of stimulus probability and auditory learning. *Neurobiol. Learn. Mem.* 109, 82–93. doi: 10.1016/j.nlm.2013.11.011

Slabu, L., Escera, C., Grimm, S., and Costa-Faidella, J. (2010). Early change detection in humans as revealed by auditory brainstem and middle-latency evoked potentials. *Eur. J. Neurosci.* 32, 859–865. doi: 10.1111/j.1460-9568.2010.07324.x

Slabu, L., Grimm, S., and Escera, C. (2012). Novelty detection in the human auditory brainstem. *J. Neurosci.* 32, 1447–1452. doi: 10.1523/JNEUROSCI.2557-11.2012

Sohoglu, E., and Davis, M. H. (2016). Perceptual learning of degraded speech by minimizing prediction error. *Proc. Natl. Acad. Sci. U.S.A.* 113, E1747ï£¡E1756. doi: 10.1073/pnas.1523266113

Spratling, M. W. (2016). Predictive coding as a model of cognition. *Cogn. Process.* 17, 279–305. doi: 10.1007/s10339-016-0765-6

Spratling, M. W. (2017). A review of predictive coding algorithms. *Brain Cogn.* 112, 92–97. doi: 10.1016/j.bandc.2015.11.003

Sterzer, P., Adams, R. A., Fletcher, P., Frith, C., Lawrie, S. M., Muckli, L., et al. (2018). The predictive coding account of psychosis. *Biol. Psychiatry* 84, 634–643. doi: 10.1016/j.biopsych.2018.05.015

Sterzer, P., Voss, M., Schlagenhauf, F., and Heinz, A. (2019). Decision-making in schizophrenia: a predictive-coding perspective. *Neuroimage* 190, 133–143. doi: 10.1016/j.neuroimage.2018.05.074

Strait, D. L., Hornickel, J., and Kraus, N. (2011). Subcortical processing of speech regularities underlies reading and music aptitude in children. *Behav. Brain Funct.* 7, 1–11. doi: 10.1186/1744-9081-7-44

Syka, J., Popelá, J., Druga, R., and Vlková, A. (1988). Descending central auditory pathway - structure and function. *Audit. Pathway* 279–292. doi: 10.1007/978-1-4684-1300-7

Taaseh, N., Yaron, A., and Nelken, I. (2011). Stimulus-specific adaptation and deviance detection in the rat auditory cortex. *PLoS ONE* 6:e23369. doi: 10.1371/journal.pone.0023369

Tabas, A., Mihai, G., Kiebel, S., Trampel, R., and von Kriegstein, K. (2020). Predictive coding underlies adaptation in the subcortical sensory pathway. *arXiv preprint arXiv:2003.11328*. doi: 10.7554/eLife.64501

Talsma, D. (2015). Predictive coding and multisensory integration: an attentional account of the multisensory mind. *Front. Integr. Neurosci.* 9:19. doi: 10.3389/fnint.2015.00019

Thomas, J. M., Morse, C., Kishline, L., O'Brien-Lambert, A., Simonton, A., Miller, K. E., et al. (2012). Stimulus-specific adaptation in specialized neurons in the inferior colliculus of the big brown bat, *Eptesicus fuscus*. *Hear. Res.* 291, 34–40. doi: 10.1016/j.heares.2012.06.004

Tschentscher, N., Ruisinger, A., Blank, H., Diaz, B., and von Kriegstein, K. (2019). Reduced structural connectivity between left auditory thalamus and the motion-sensitive planum temporale in developmental dyslexia. *J Neurosci.* 27, 1720–1732. doi: 10.1523/JNEUROSCI.1435-18.2018

Ulanovsky, N., Las, L., Farkas, D., and Nelken, I. (2004). Multiple time scales of adaptation in auditory cortex neurons. *J. Neurosci.* 24, 10440–10453. doi: 10.1523/JNEUROSCI.1905-04.2004

Ulanovsky, N., Las, L., and Nelken, I. (2003). Processing of low-probability sounds by cortical neurons. *Nat. Neurosci.* 6, 391–398. doi: 10.1038/nn1032

Valdés-Baizabal, C., Carbajal, G. V., Pérez-González, D., and Malmierca, M. S. (2020). Dopamine modulates subcortical responses to surprising sounds. *PLoS Biol.* 18:e3000744. doi: 10.1371/journal.pbio.3000744

Valdés-Baizabal, C., Parras, G. G., Ayala, Y. A., and Malmierca, M. S. (2017). Endocannabinoid modulation of stimulus-specific adaptation in inferior colliculus neurons of the rat. *Sci. Rep.* 7:6997. doi: 10.1038/s41598-017-07460-w

van de Cruys, S., Evers, K., van der Hallen, R., van Eylen, L., Boets, B., De-Wit, L., et al. (2014). Precise minds in uncertain worlds: Predictive coding in autism. *Psychol. Rev.* 121, 649–675. doi: 10.1037/a0037665

van Schalkwyk, G. I., Volkmar, F. R., and Corlett, P. R. (2017). A predictive coding account of psychotic symptoms in autism spectrum disorder. *J. Autism Dev. Disord.* 47, 1323–1340. doi: 10.1007/s10803-017-3065-9

van Wassenhove, V. (2013). Speech through ears and eyes: interfacing the senses with the supramodal brain. *Front. Psychol.* 4:388. doi: 10.3389/fpsyg.2013.00388

Von Helmholtz, H. (1867). *Handbuch der physiologischen Optik: mit 213 in den Text eingedruckten Holzschnitten und 11 Tafeln*. Leipzig: Voss.

von Kriegstein, K. (2012). "A multisensory perspective on human auditory communication," in *The Neural Bases of Multisensory Processes*, eds M. M. Murray and M. T. Wallace (Boca Raton, FL: CRC Press), 683–700. doi: 10.1201/9781439812174-43

Von Kriegstein, K., Dogan, Ö., Grüter, M., Giraud, A. L., Kell, C. A., Grüter, T., et al. (2008). Simulation of talking faces in the human brain improves auditory speech recognition. *Proc. Natl. Acad. Sci. U.S.A.* 105, 6747–6752. doi: 10.1073/pnas.0710826105

Wacongne, C., Changeux, J.-P., and Dehaene, S. (2012). A neuronal model of predictive coding accounting for the mismatch negativity. *J. Neurosci.* 32, 3665–3678. doi: 10.1523/JNEUROSCI.5003-11.2012

Walsh, K. S., McGovern, D. P., Clark, A., and O'Connell, R. G. (2020). Evaluating the neurophysiological evidence for predictive processing as a model of perception. *Ann. N. Y. Acad. Sci.* 1464, 242–268. doi: 10.1111/nyas.14321

Wang, H., Han, Y. F., Chan, Y. S., and He, J. (2014). Stimulus-specific adaptation at the synapse level *in vitro*. *PLoS ONE* 9:e114537. doi: 10.1371/journal.pone.0114537

Winer, J. A. (1984). The human medial geniculate body. *Hear. Res.* 15, 225–280. doi: 10.1016/0378-5955(84)90031-5

Winer, J. A. (2005a). Decoding the auditory corticofugal systems. *Hear. Res.* 207, 1–9. doi: 10.1016/j.heares.2005.06.007

Winer, J. A. (2005b). "Three systems of descending projections to the inferior colliculus," in *The Inferior Colliculus*, eds J. A. Winer and C. E. Schreiner (New York, NY: Springer-Verlag), 231–247. doi: 10.1007/0-387-27083-3_8

Wood, K. C., Town, S. M., and Bizley, J. K. (2019). Neurons in primary auditory cortex represent sound source location in a cue-invariant manner. *Nat. Commun.* 10, 1–15. doi: 10.1038/s41467-019-10868-9

Yildiz, I. B., and Kiebel, S. J. (2011). A hierarchical neuronal model for generation and online recognition of birdsongs. *PLoS Comput. Biol.* 7:e1002303. doi: 10.1371/journal.pcbi.1002303

Yu, X.-J., Xu, X.-X., He, S., and He, J. (2009). Change detection by thalamic reticular neurons. *Nat. Neurosci.* 12, 1165–1170. doi: 10.1038/nn.2373

Zabbah, S., Rajaei, K., Mirzaei, A., Ebrahimpour, R., and Khaligh-Razavi, S. M. (2014). The impact of the lateral geniculate nucleus and corticogeniculate interactions on efficient coding and higher-order visual object processing. *Vis. Res.* 101, 82–93. doi: 10.1016/j.visres.2014.05.006

Zhao, L., Liu, Y., Shen, L., Feng, L., and Hong, B. (2011). Stimulus-specific adaptation and its dynamics in the inferior colliculus of rat. *Neuroscience* 181, 163–174. doi: 10.1016/j.neuroscience.2011.01.060

Conflict of Interest: The authors declare that the research was conducted in the absence of any commercial or financial relationships that could be construed as a potential conflict of interest.

frontiers in Neural Circuits

ORIGINAL RESEARCH
published: 26 April 2021
doi: 10.3389/fncir.2021.624381

Cholinergic and Noradrenergic Modulation of Corticothalamic Synaptic Input From Layer 6 to the Posteromedial Thalamic Nucleus in the Rat

*Syune Nersisyan[1,2], Marek Bekisz[1], Ewa Kublik[1], Björn Granseth[2] and Andrzej Wróbel[1,3]**

[1] Nencki Institute of Experimental Biology, Polish Academy of Sciences, Warsaw, Poland, [2] Department of Clinical and Experimental Medicine, Linköping University, Linköping, Sweden, [3] Faculty of Philosophy, University of Warsaw, Warsaw, Poland

Cholinergic and noradrenergic neuromodulation of the synaptic transmission from cortical layer 6 of the primary somatosensory cortex to neurons in the posteromedial thalamic nucleus (PoM) was studied using an *in vitro* slice preparation from young rats. Cholinergic agonist carbachol substantially decreased the amplitudes of consecutive excitatory postsynaptic potentials (EPSPs) evoked by a 20 Hz five pulse train. The decreased amplitude effect was counteracted by a parallel increase of synaptic frequency-dependent facilitation. We found this modulation to be mediated by muscarinic acetylcholine receptors. In the presence of carbachol the amplitudes of the postsynaptic potentials showed a higher trial-to-trial coefficient of variation (CV), which suggested a presynaptic site of action for the modulation. To substantiate this finding, we measured the failure rate of the excitatory postsynaptic currents in PoM cells evoked by "pseudominimal" stimulation of corticothalamic input. A higher failure-rate in the presence of carbachol indicated decreased probability of transmitter release at the synapse. Activation of the noradrenergic modulatory system that was mimicked by application of norepinephrine did not affect the amplitude of the first EPSP evoked in the five-pulse train, but later EPSPs were diminished. This indicated a decrease of the synaptic frequency-dependent facilitation. Treatment with noradrenergic α-2 agonist clonidine, α-1 agonist phenylephrine, or β-receptor agonist isoproterenol showed that the modulation may partly rely on α-2 adrenergic receptors. CV analysis did not suggest a presynaptic action of norepinephrine. We conclude that cholinergic and noradrenergic modulation act as different variable dynamic controls for the corticothalamic mechanism of the frequency-dependent facilitation in PoM.

Keywords: gain control, *in vitro*, intracellular recordings, frequency-dependent facilitation, cholinergic and noradrenergic modulation

OPEN ACCESS

Edited by:
Livia de Hoz, Charité – Universitätsmedizin Berlin, Germany

Reviewed by:
Veronica Egger, University of Regensburg, Germany
Daniel Llano, University of Illinois at Urbana–Champaign, United States

***Correspondence:**
Andrzej Wróbel
a.wrobel@nencki.edu.pl

Received: *31 October 2020*
Accepted: *22 March 2021*
Published: *26 April 2021*

Citation:
Nersisyan S, Bekisz M, Kublik E, Granseth B and Wróbel A (2021) Cholinergic and Noradrenergic Modulation of Corticothalamic Synaptic Input From Layer 6 to the Posteromedial Thalamic Nucleus in the Rat. Front. Neural Circuits 15:624381. doi: 10.3389/fncir.2021.624381

INTRODUCTION

In addition to afferent sensory thalamocortical fibers, the thalamic cells of mammals are reached by feedback corticothalamic axons that outnumber the peripheral projection (Rouiller and Welker, 2000). The major source of this descending feedback input to the thalamus originates in the pyramidal neurons of the cortical layer 6 (Erisir et al., 1997; Alitto and Usrey, 2003;

Sherman and Guillery, 2006; Van Horn and Sherman, 2007). The layer 6 input evokes direct depolarization of the thalamic relay cells (Lindström and Wróbel, 1990; Reichova and Sherman, 2004) or indirect hyperpolarization via recurrent interneurons in the thalamic reticular nucleus (Lam and Sherman, 2010). One hypothesis regarding the layer 6 input to the thalamus posits its functional role as a variable gain regulator for sensory relay at the thalamus. This mechanism would control the flow of ascending sensory information from the periphery to the cortex depending on the behavioral state of the animal (Ahlsen et al., 1985; Lindström and Wróbel, 1990; Granseth et al., 2002; Granseth, 2004; Lam and Sherman, 2010).

In the rat somatosensory system both the first-order ventrobasal nucleus (VB) and the higher-order posteromedial nucleus (PoM) receive cortical input from layer 6. PoM, however, receives an additional driver input from cortical layer 5. Accordingly, PoM is thought to be involved in cortico-cortical transmission via a cortico-thalamo-cortical route (Theyel et al., 2010).

Sensory thalamus and sensory cortex are extensively innervated by rich cholinergic and noradrenergic neuromodulatory inputs from the brainstem and basal forebrain. Most of the studies on these modulatory systems demonstrate their role in setting different vigilance levels from awakening to arousal (Steriade et al., 1993). While their role in sleep-wake cycles is well recognized, much less is known about the mechanisms underlying the neuromodulatory action at sensory relays. Specifically, we are not aware of any research investigating the modulation of synaptic integration at higher-order thalamic nuclei, even though they receive denser modulatory projections than the first-order nuclei (Van Horn and Sherman, 2007). Sensory thalamus receives powerful modulatory projections from the brainstem and from layer 6 of the primary sensory cortex (Erisir et al., 1997). Importantly, the cortical layer 6 synaptic input to the thalamic neurons is also efficiently regulated by projections from the brainstem (Steriade, 2000; Castro-Alamancos and Calcagnotto, 2001). The interplay between the cortical and brainstem modulatory inputs may constitute a complex functional control system of the thalamic cells. Therefore, our study aimed to investigate the influence of cholinergic and noradrenergic modulatory systems on the synaptic transmission from cortical layer 6 to the higher-order somatosensory posteromedial thalamic nucleus, with special focus on facilitation at the corticothalamic synapse.

MATERIALS AND METHODS

Preparation of Slices

All experiments were performed with the approval of the first Local Ethic Commission in Warsaw and Committee for Ethics in Animal Research of Linköping in accordance with Polish, Swedish and EU legislations.

Three- to four-week old Wistar rats were decapitated under deep isoflurane anesthesia. Brains were quickly removed and immersed in cold (between −1°C and +0.5°C) artificial cerebrospinal fluid (ACSF) with NaCl substituted with sucrose, having the following composition (in mM): KCl 3, NaH_2PO_4 1.25, $NaHCO_3$ 24, $MgSO_4$ 4, $CaCl_2$ 0.5, D-glucose 10, sucrose 219 (300–308 mOsm). Thalamocortical slices (350 μm) (Agmon and Connors, 1991; Land and Kandler, 2002), ideally suitable for selective studies of synapses formed on PoM cells by axons from cortical layer 6 (Landisman and Connors, 2007) were prepared using a Leica VT1000S vibrating blade microtome. Slices were incubated at 31°C for 30 min and then at room temperature for at least 1 h. ACSF in the incubation chamber contained (in mM): NaCl 126, KCl 3, NaH_2PO_4 1.25, $NaHCO_3$ 24, $MgSO_4$ 3, $CaCl_2$ 1, D-glucose 10. Individual slices were transferred to the recording chamber, with circulating (2–2.5 ml/min), warm (31–32°C) ACSF of a similar composition to the incubation solution except for $MgSO_4$ and $CaCl_2$ which concentrations were changed to 2 mM. All solutions were saturated with 95% O_2–5% CO_2. The recording chamber was mounted under the nosepiece of an Olympus BX61WI microscope equipped with a C7500 near infrared CCD video camera (Hamamatsu, Hamamatsu City, Japan). In most of the slices, the cortex was cut-off to prevent activation of the thalamo-cortico-thalamic loop. In the thalamocortical slices, the PoM nucleus was readily distinguished from the VB, TRN, and the internal capsule when using a low-magnification (4x) objective with an additional 0.35x magnification changer (1.4 × final magnification; **Figure 1A**).

Pharmacology

Activation of cholinergic or noradrenergic modulatory system was mimicked by bath application of a non-specific cholinergic agonist carbamoylcholine chloride (carbachol) (6–8 μM) or norepinephrine hydrochloride (100 μM), accordingly. All drugs were added to the ACSF that perfused the slices and 3–5 min was allowed for complete solution-exchange in the recording chamber. This time period was determined from preliminary experiments with drugs that depolarized the neurons. Incubation with the drug lasted usually 5–25 min.

Bicuculline methiodide (10 μM) was used to block $GABA_A$ receptors. For complete elimination of the recurrent inhibitory influence from the thalamic reticular nucleus (TRN) the $GABA_B$ receptor antagonist CGP 55845 hydrochloride (2 μM) was also used in most of the experiments. The GABA receptor inhibitors were present during both the control period and periods of the application of cholinergic or adrenergic agents. To investigate the role of different subtypes of cholinergic and adrenergic receptors in the observed effects, the following specific receptor agonists and antagonists were used: nicotinic agonist DMPP (dimethylphenylpiperazinium, 10 μM); muscarinic receptor antagonist scopolamine (1 μM); adrenergic α-2 receptors agonist clonidine hydrochloride (40 μM), α-1 adrenergic receptors agonist phenylephrine hydrochloride (100 μM) and β adrenergic receptors agonist isoproterenol hydrochloride (100 μM). All chemicals were obtained from Sigma (St Louis, MO, United States), except for CGP 55845 hydrochloride which was purchased from Tocris (Bristol, United Kingdom). To prevent oxidation of adrenergic agonists, in the experiments where adrenergic agents were used, sodium ascorbate (40 μM) was present in the ACSF during both the control period and incubation with the drugs.

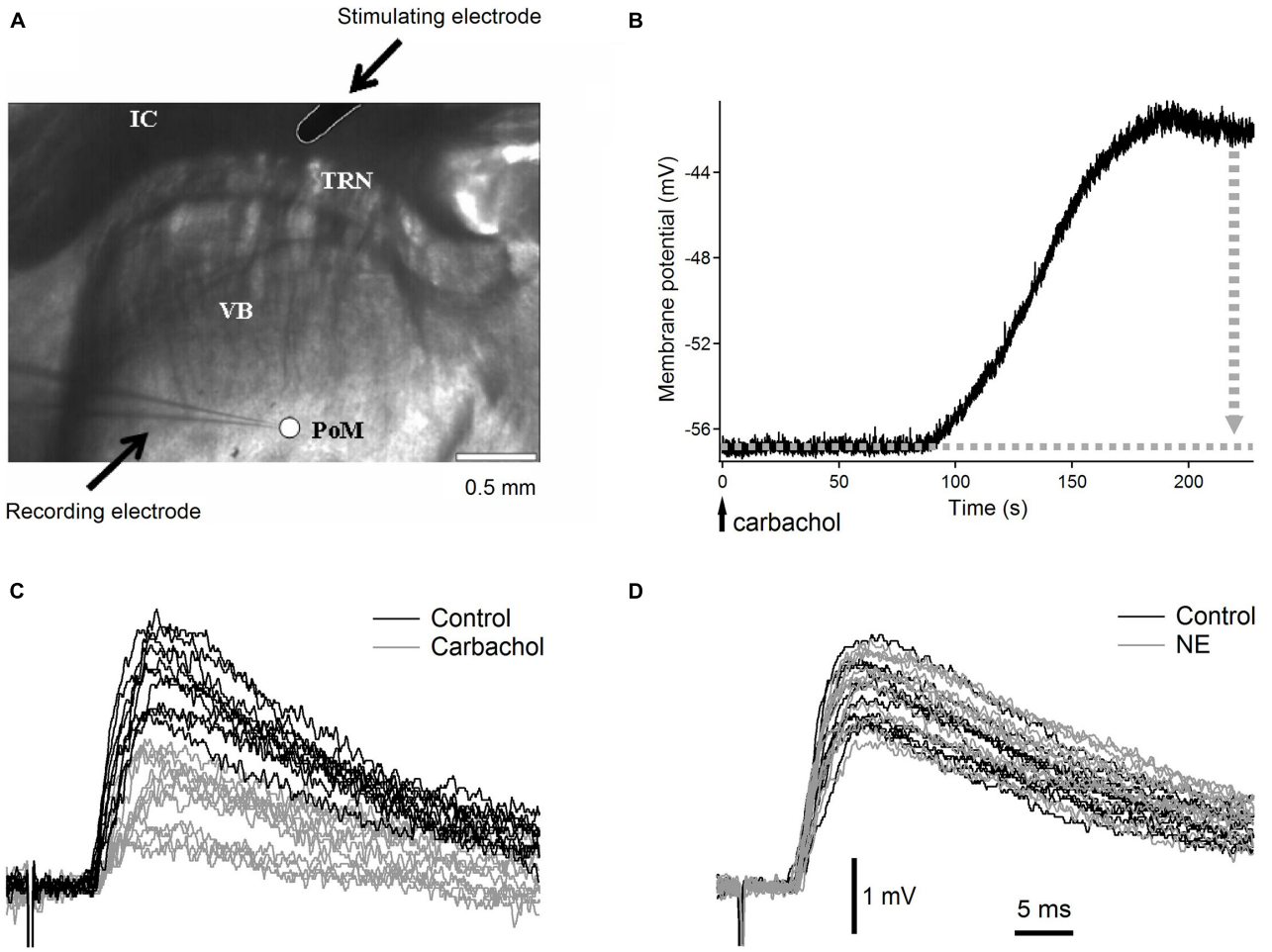

FIGURE 1 | Raw experimental data. **(A)** Low magnification (1.4×) image of the somatosensory thalamic area with recording electrode in posteromedial nucleus and stimulation electrode in the internal capsule. VB, ventrobasal nucleus with characteristic stripes of dense fibers; PoM, posteromedial nucleus recognized as uniform, brighter area; IC, internal capsule; TRN, thalamic reticular nucleus; arrows point to recording and stimulating electrodes. Scale bar is 0.5 mm. **(B)** Typical depolarization of a PoM cell after application of cholinergic agonist carbachol. The vertical dotted gray arrow indicates the manual compensation of membrane potential shift by adding negative DC current. **(C)** Examples of raw EPSPs evoked in a PoM cell by the 1st impulse of the five-pulse train (0.033 Hz train repetition rate) stimulating cortico-thalamic axons in the internal capsule. Black traces show EPSPs in the control condition (with the ACSF containing both $GABA_A$ and $GABA_B$ inhibitors – 10 μM bicuculline and 2 μM CGP55845 respectively). Gray traces show EPSPs after adding carbachol (7 μM) to the ACSF. **(D)** Raw EPSPs evoked by the 1st stimulation pulse in the control condition (black traces) and after adding norepinephrine (100 μM) to the ACSF (gray traces). In this case, as with the study of each noradrenergic substance in this work, both control and test ACSFs contained in addition to $GABA_A$ and $GABA_B$ inhibitors also an antioxidant – 40 μM sodium ascorbate. In **(C,D)** all EPSPs were recorded at similar membrane potential between –56 and –57 mV but their individual baselines varied within about 1 mV range. To better show inter-trial fluctuations of EPSPs amplitude, all EPSP traces were adjusted in **(C,D)** to the same baseline. Vertical and horizontal scales for **(C,D)** are indicated by black bars at the bottom of **(D)**.

Recording and Stimulation

Whole-cell patch-clamp recordings were performed from PoM neurons using electrodes (3–6 MΩ) pulled from standard-wall (1.2 mm outer diameter) borosilicate glass capillaries. In most of the experiments, electrodes were filled with (in mM): potassium gluconate 120, HEPES 10, EGTA 0.1, KCl 4, NaCl 2, Mg-ATP 4, Na_2-GTP 0.5, phosphocreatine (Tris salt) 10; pH was adjusted to 7.25 with KOH and osmolarity to 285–290 mOsm with sucrose.

To improve the space constancy of the maintained membrane potential in the voltage clamp method during the experiments with the pseudominimal stimulation (see below), a Cs-based electrode solution was used with the following composition (in mM): Cs-gluconate 100, NaCl 10, HEPES 10, TEA-Cl 20, QX-314 5, EGTA 0.1 and Mg-ATP 1; pH = 7.3, osmolarity adjusted to 300 mOsm.

In most experiments, the membrane potential was recorded in fast current-clamp mode with Axopatch 200B amplifier and pCLAMP software (Molecular Devices, United States). In "pseudominimal stimulation" experiments the thalamus and PoM cells were visualized using Axioskop FS microscope (Carl Zeiss, Jena, Germany) with Hamamatsu C7500 camera and membrane current was recorded in voltage-clamp mode using Heka EPC9 (HEKA Elektronik, Lambrecht, Germany) amplifier and Pulse software. In current clamp, the recorded

membrane potential values were not corrected for the junction potential. In voltage clamp, the holding membrane potential was corrected for the measured 8 mV junction potential. To evoke excitatory postsynaptic potentials (EPSPs) or currents (EPSCs), repetitive trains of five electrical pulses (200 μs duration) at 20 Hz frequency were applied through a concentric stimulating electrode placed at the corticothalamic fiber tract in the internal capsule (**Figure 1A**). Individual trains were repeated at 30 s interval. Stimulation current ranged from 90 to 500 μA. The electrical train stimuli were repeated 8–30 times in control condition and 16–50 times after corresponding cholinergic or noradrenergic drug application (see below).

Typically, after application of most cholinergic or noradrenergic agonists to the ACSF, the neurons started to depolarize after about 60–90 s and reached a steady state after 100 s. For instance, application of carbachol and norepinephrine depolarized PoM neurons by 9.1 ± 1.3 mV and 11.8 ± 0.7 mV (mean ± SEM; $n = 16$ and $n = 15$, correspondingly) (**Figure 1B**). If necessary, the depolarization induced by cholinergic or noradrenergic agents was compensated by manual injection of a negative DC current through the recording electrode which brought the membrane potential back to a more negative value. This compensation was done in order to have the same driving force for the ions responsible for the generation of the EPSPs in the control condition and after application of the appropriate drug. To avoid the appearance of low-threshold calcium spikes during the stimulation train, EPSPs were recorded in all situations at adjusted manually membrane potential of –56 mV (with an accuracy of ±1 mV). The membrane resistance was measured always at resting potential from the initial recording period prior to administration of the agonists.

During the voltage-clamp pseudominimal stimulation experiments, the stimulation intensities were adjusted to activate a sufficiently low number of corticothalamic axons so that the initial postsynaptic responses had a failure rate of ∼50%. These EPSC recordings were made at a holding potential of –58 mV. In this kind of experiment, the stimulation train was repeated 35–68 times in control and 47–158 times after drug application.

Analysis and Statistics

Excitatory postsynaptic potentials amplitudes were measured from the baseline to the peak amplitude (in pCLAMP). In case of temporal overlap during train stimulation, the decay of the preceding EPSP was exponentially extrapolated and used as a baseline for measuring the amplitude of the consecutive EPSPs. In order to examine facilitation of consecutive responses in trains EPSP amplitudes were normalized to the first EPSP amplitude ($EPSP_n/EPSP_1$; "normalized amplitudes"). Ratios between amplitudes of successive EPSPs ($EPSP_n/EPSP_{n-1}$) were also calculated to illustrate the temporal (instantaneous) changes of facilitation during stimulation trains.

The coefficients of variations (CVs) of the noise-free inter-trial amplitude fluctuations of the consecutive postsynaptic potentials were estimated from the data as the square root of the noise-free variance of the EPSP amplitude distribution, divided by the mean EPSP amplitude (Clements, 1990). An exemplary inter-trial variation of the amplitudes of the 1st EPSP in various experimental conditions can be traced in **Figures 1C,D**. In the noise-free variance calculation, the variance of the noise was subtracted from the variance of the individual EPSP amplitudes. Consequently, CV values were calculated according to the following equation:

$$CV = (\mathrm{Var}(EPSP) - \mathrm{Var}(noise))^{1/2}/\mathrm{Mean}(EPSP) \quad \text{(Eq. 1)}$$

The CV values calculated in the control condition were compared to the CVs during drug exposure. Large differences between CVs in these two conditions strongly implicated a presynaptic site of modulation (Clements, 1990; Nagumo et al., 2011).

Analysis of EPSCs recorded in voltage-clamp was performed with IgorPro (Wavemetrics Inc., United States). The EPSC amplitudes were measured as the difference between the mean membrane current over 1.5 ms at the peak of the EPSC and the preceding 1.5 ms baseline. Noise distribution was obtained by similar measurements during the baseline period. EPSC amplitudes smaller than 2SD of the noise distribution were considered to be EPSC failures (Granseth and Lindström, 2003). The SD at the noisiest condition for each cell was used for this classification whether it was recorded from control condition or with carbachol. The EPSC failure (or response success) rates were calculated as the number of failures (or responses) divided by the total number of stimulation trains ($N_{failures}/N_{trains}$ or $N_{responses}/N_{trains}$) for each pulse in each cell individually. EPSC amplitude histograms were constructed using a bin size of 0.5 pA and accumulated across cells. To determine the quantal size (Q) of the corticothalamic EPSCs, the averaged amplitude probability histograms obtained for the first impulse were fitted with a double Gaussian function with two peaks separated from zero with Q and 2Q and the same standard deviation (del Castillo and Katz, 1954).

Throughout the text, the averaged data were presented as means ± SEM. Student *t*-test for paired comparisons was used throughout the text, unless otherwise indicated and $P \leq 0.05$ was considered to be significant. In case of multiple comparisons, significance of P values was additionally checked with Benjamini–Hochberg (B-H) false discovery rate (FDR) procedure at level 0.05 (Benjamini and Hochberg, 1995). According to a suggestion given by McDonald (2014) we did not present B-H FDR corrected *P*-values. Instead, we show the original *P*-values and describe which remain significant after using B-H FDR procedure.

Histological Staining

Some slices were subjected to cytochrome oxidase histochemistry to visualize the somatosensory thalamic nuclei, i.e., to highlight the border between VB and PoM. For this purpose, slices were fixed in 4% formalin, washed with phosphate buffer (0.05M, pH = 7.4) and incubated in DAB solution (100 ml of which contained: sucrose 1 g, DAB 25 mg, cytochrome C 15 mg, catalase 10 mg, imidazole 250 μl, nickel ammonium sulfate 50 mg) on a shaker at 30–40°C for about 2–3 h until specific staining appeared. Finally, slices were rinsed in a phosphate buffer three times, 5 min each. After the staining, images of the stained and

non-stained slices were compared to confirm the localization of the recorded cells.

RESULTS

Basic Electrophysiological Properties of PoM Cells

In the vast majority (≈90%, $n = 74$) of the investigated cells the membrane potential was recorded in current-clamp mode. The average resting membrane potential was –61.92 ± 0.31 mV and the membrane resistance was 84.90 ± 3.36 MΩ, which slightly differ from those described earlier (Landisman and Connors, 2007). In particular, a little less negative membrane potential and a little larger membrane resistance was reported by these authors. This discrepancy may result from the age difference of the experimental animals (3–4-week-old in our experiments versus 2–3-week-old used by Landisman and Connors).

In response to the injection of 500 ms rectangular depolarizing or hyperpolarizing current pulses, the firing pattern of PoM neurons exhibited tonic and burst modes typical for thalamic cells (Jahnsen and Llinas, 1984). In the tonic mode, the response during a +300 pA depolarizing pulse was characterized by mean firing rate of 39.5 ± 6.7 Hz and in burst mode the response to a –200 pA hyperpolarizing current was characterized by mean burst frequency of 265 ± 17.3 Hz. This burst firing frequency is similar to the one reported for PoM neurons by Landisman and Connors (2007), however much lower than the value obtained for VPM cells by the same authors. This fact additionally supports the notion that the cells recorded in our experiments were located in PoM.

Facilitation of the EPSP amplitudes is a typical feature of corticothalamic synapses formed by axons descending from layer 6 pyramids to thalamic relay cells (Lindström and Wróbel, 1990; Granseth et al., 2002; Granseth, 2004). That is, with high frequency (i.e., 20 Hz) stimulation train the first impulse evokes an EPSP of a small amplitude while the amplitudes of the EPSPs evoked by the following pulses in the train are progressively enhanced. The opposite effect characterizes layer 5 input when the first impulse evokes a large EPSP while following responses in a high-frequency train are progressively decreased (Reichova and Sherman, 2004; Groh et al., 2008). We observed synaptic facilitation in response to a 20 Hz stimulation in all recorded PoM cells. This proved that "classical" thalamocortical slices (Agmon and Connors, 1991; Land and Kandler, 2002) used by us were well suited for selective studies of the synapses formed on PoM cells by the axons from cortical layer 6 (Landisman and Connors, 2007), as in such preparation the corticothalamic fibers from layer 5 appeared to be mostly cut.

Cholinergic and Noradrenergic Systems Differentially Modulate Corticothalamic Synaptic Transmission in PoM

Compared to the control condition, carbachol substantially decreased the amplitudes of all postsynaptic responses evoked by five impulses of a 20 Hz electrical stimulation of the corticothalamic axons. The amplitude reduction (about threefold) was most pronounced for the first EPSP in the train (**Figure 2A**, gray trace; and raw, non-averaged potential waveforms in **Figure 1C**). The following postsynaptic potentials were affected progressively less than the first one. Consequently, the amplitude of the last EPSP in the presence of carbachol was less than two times smaller than the one recorded in the control condition. Apparently, in parallel to the reduction of the EPSP amplitudes, carbachol increased the facilitation of the EPSPs during the 5-pulse train stimulation (see normalized amplitudes in **Figure 2A**).

For the group of the studied cells ($n = 16$), the mean amplitude of the first EPSP was 3.4 times smaller after application of carbachol (**Figure 2B** – gray vs. black trace). Much weaker responses were also evoked by the subsequent pulses in the train. The relative reduction of the 2nd, 3rd, 4th, and 5th EPSP became progressively smaller (for appropriate numerical values see **Table 1**A), supporting the idea that despite the reduction of the amplitudes of all EPSPs in the train the application of carbachol increased the facilitation of consecutive responses.

Facilitation of consecutive EPSPs in the control condition and in the presence of carbachol was in addition analyzed by calculating normalized amplitudes (each EPSP amplitude in the train divided by the first one – $EPSP_N/EPSP_1$) (**Figure 2C**). In the presence of carbachol normalized amplitude of the 2nd EPSP was 1.42 times larger than the one obtained during the control condition. Normalized amplitudes of the 3rd, 4th, and 5th EPSPs obtained for carbachol were accordingly 1.73; 2.05 and 2.27 times larger than in control (**Figure 2C**, see also **Table 1**B). These results indicate that carbachol induced a consistent and instantaneous increase of facilitation along the train of consecutive EPSPs. In the presence of carbachol the 5th EPSP had about 20 times larger amplitude than the 1st EPSP. This ratio (2.27 times larger than for the control situation) demonstrates the potency by which carbachol enhances the global facilitation of EPSP amplitudes during the 5 impulses/20 Hz stimulation train.

The examination of the momentary changes in facilitation along the train (calculated by $EPSP_N/EPSP_{N-1}$ ratio and plotted in **Figure 2C** as dashed lines against the right vertical axis) revealed that although the largest increase of the $EPSP_N/EPSP_{N-1}$ ratio occurred for the first two EPSPs (2nd/1st = 1.42) the carbachol-induced enhancement of momentary facilitation affected also the subsequent responses in the train (the 3rd/2nd ratio was 1.20 times larger than in control condition; 4th/3rd by 1.18; 5th/4th by 1.10; $P < 0.001$ for each pair of comparisons, all significant using FDR procedure at level 0.05; see also **Table 1**C).

In contrast to carbachol, norepinephrine did not change the amplitude of the first EPSP in the train (**Figures 1D**, **2D**), however, it did reduce the amplitudes of later EPSPs (**Figure 2D**). Similar to a single cell observation, norepinephrine did not change the mean amplitude of the 1st EPSP for a group of PoM cells studied with this drug ($n = 15$), but reduced amplitudes of the 2nd, 3rd, 4th, and 5th EPSPs (**Figure 2E** and **Table 2**A).

In general, the amplitude reduction caused by norepinephrine suggests a moderate decrease in facilitation during the train.

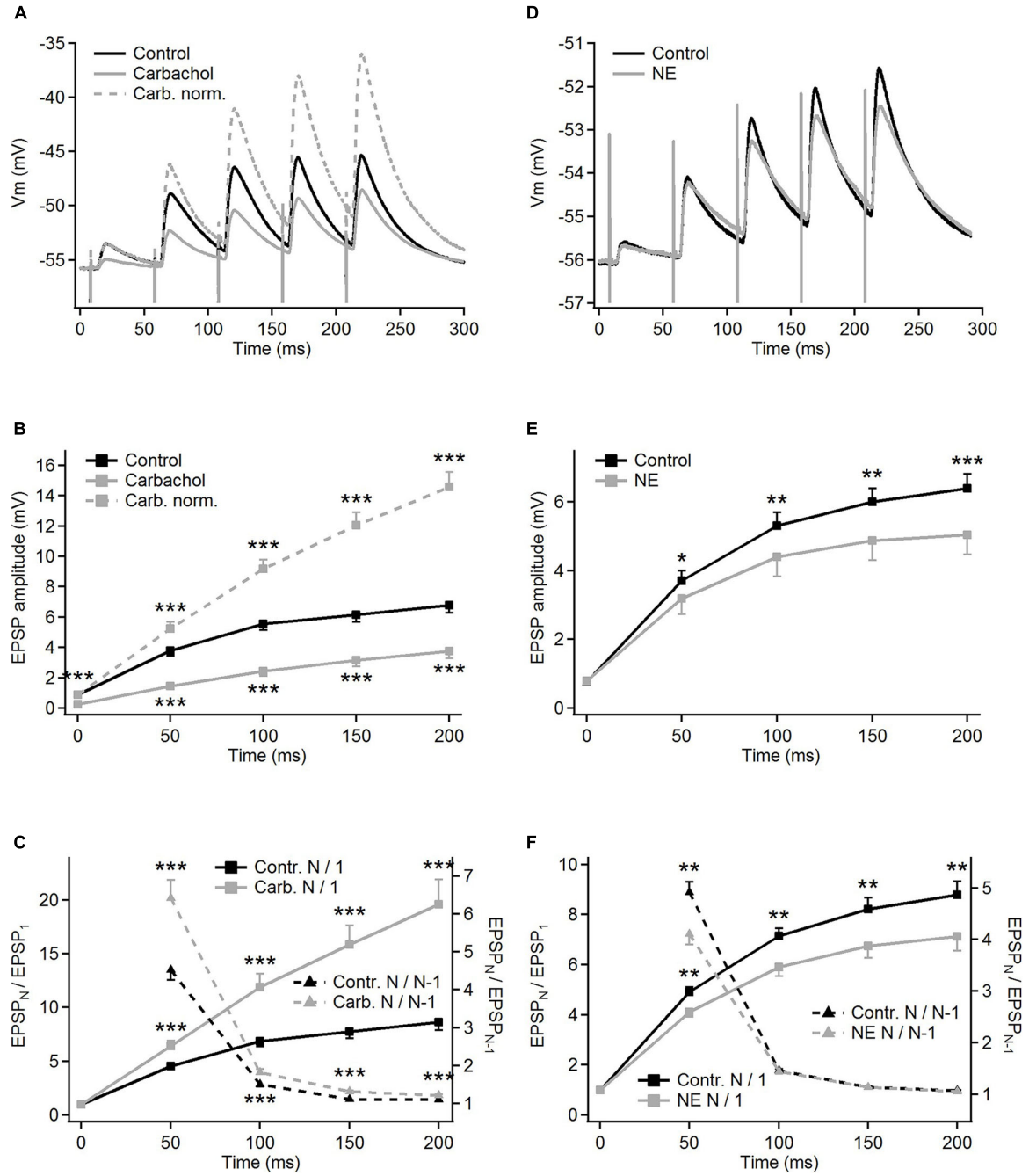

FIGURE 2 | Modulation of frequency-dependent facilitation of the cortico-thalamic synapse in PoM by cholinergic and noradrenergic agents. **(A)** Examples of facilitating synaptic responses of a single PoM cell to the electrical stimulation of the cortico-thalamic axons in control condition with ACSF containing GABA inhibitors (black trace, average of 11 trials), and after adding 6–8 μM carbachol (solid gray trace, average of 33 trials). Dashed gray trace shows the data with carbachol after normalization to the first control EPSP. **(B)** Average amplitudes of the consecutive EPSPs in the train, measured for a group of 16 cells studied with carbachol. Mean amplitudes obtained for "carbachol" (solid gray line) conditions were significantly lower than in "control" (black line) for each EPSP in the train. **(C)** Left *Y* axis: normalized amplitudes ($EPSP_N/EPSP_1$, the same $n = 16$ cells) in control conditions (solid black trace) and in the presence of carbachol [solid gray line; note that the same data are included in **(B)** as gray dashed line]. Right *Y* axis: momentary facilitation, i.e., ratios of the consecutive EPSP amplitudes ($EPSP_N/EPSP_{N-1}$) in control conditions and after application of carbachol (dashed lines). Both measures were significantly different from control values for all EPSP in the train. **(D)** Examples of the averages of single cell postsynaptic responses to stimulation of the corticothalamic axons in the control condition with GABA inhibitors and ascorbic acid (black trace, 22 repetitions) and after adding 100 μM norepinephrine (NE, gray trace, 32 repetitions). **(E)** Average amplitudes of the consecutive EPSPs measured for a whole group of cells ($n = 15$) studied with norepinephrine. Black trace shows EPSP amplitudes in control condition, gray trace – after adding norepinephrine. **(F)** Left *Y* axis: average normalized EPSP amplitudes ($EPSP_N/EPSP_1$) in the control condition (black trace) and after application of norepinephrine (gray trace). Right *Y* axis: average ratios of the neighboring EPSP amplitudes ($EPSP_N/EPSP_{N-1}$) in the control condition and after application of norepinephrine (black and gray dashed lines, respectively). Data are expressed as mean ± SEM, $^*P \leq 0.05$, $^{**}P \leq 0.01$, $^{***}P \leq 0.001$.

Indeed, the average values of the normalized amplitudes ($EPSP_N/EPSP_1$) (**Figure 2F** and **Table 2**B), were consistently larger in the control condition than in the presence of norepinephrine indicating a decrease of the facilitation after application of the drug. Normalized amplitudes obtained for the 2nd, 3rd, 4th, and 5th EPSP were by 16.3, 17.4, 17.9, and 19% smaller in the presence of norepinephrine. Trend for a higher reduction for late EPSPs was, however, weak and the observed decrease of facilitation was solely due to the difference in ratios between the amplitudes of the 2nd and the 1st EPSPs. The momentary facilitation ($EPSP_N/EPSP_{N-1}$) differed only for the first pair of the postsynaptic responses ($EPSP_2/EPSP_1$, $P = 0.008$) (**Figure 2F**). The following ratios (3rd/2nd, 4th/3rd, 5th/4th EPSP) measured in control condition and after application of norepinephrine were similar (see **Table 2**C).

To sum up, activation of cholinergic receptors by carbachol significantly reduced the amplitudes of all EPSPs evoked in PoM cells by train stimulation of descending fibers from the cortical layer 6, simultaneously enhancing the frequency-dependent facilitation at this synapse. Instead, activation of noradrenergic receptors via application of norepinephrine decreased the amplitudes of all but the first EPSP evoked by train stimuli, indicating a reduction of the facilitation.

Muscarinic Receptors Are Responsible for Cholinergic Modulation of Corticothalamic EPSPs

The addition of carbachol to the ACSF already containing the selective muscarinic receptor antagonist scopolamine (1 μM) resulted in only a very weak but still consistent and significant ($P < 0.001$, single group t-test) depolarization of 0.98 ± 0.12 mV ($n = 9$). Moreover, the presence of scopolamine prevented the EPSP amplitude reduction caused by carbachol. Instead, a weak increase in EPSPs amplitudes (**Figure 3A**, gray trace) was observed (see also **Table 1**A).

In the presence of scopolamine, application of carbachol did not change the facilitation of synaptic responses (**Figure 3B** and **Table 1**B). Similarly, data comparisons did not reveal any changes in the momentary facilitation ($EPSP_N/EPSP_{N-1}$) during the train (**Table 1**C). Thus, blocking muscarinic receptors reversed the carbachol-induced pronounced reduction of EPSP amplitudes to a moderate enhancement as well as eliminated all

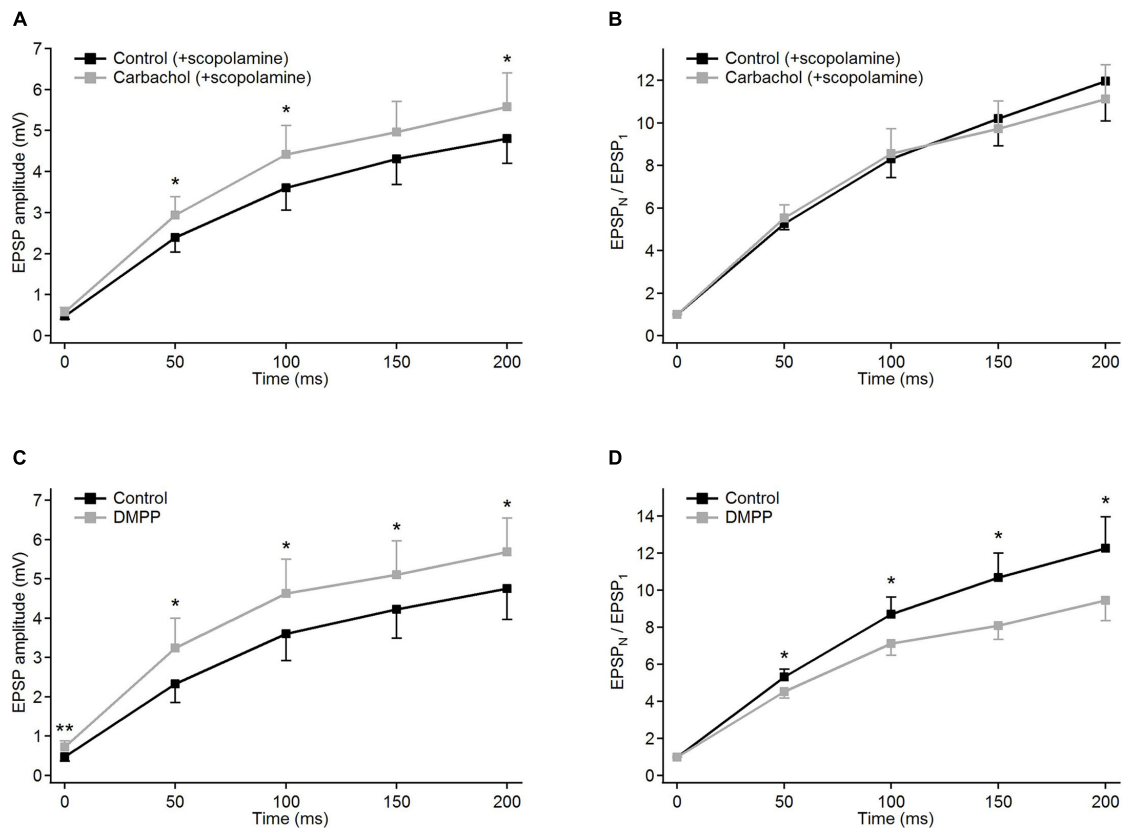

FIGURE 3 | Modulatory effects of different cholinergic agents on EPSP trains in PoM cells. **(A,B)** Blockade of muscarinic receptors by scopolamine: **(A)** EPSP amplitudes and **(B)** corresponding normalized EPSP amplitudes averaged for nine cells in the control condition (ACSF containing GABA inhibitors and 1 μM scopolamine, black traces), and after adding 6–8 μM carbachol (gray traces). **(C,D)** Blockade of nicotinic receptors by an agonist DMPP: **(C)** average EPSP amplitudes and **(D)** corresponding normalized EPSP amplitudes in control conditions with ACSF (black traces) and after application of 10 μM DMPP (gray traces). Data are expressed as mean ± SEM, $^*P \leq 0.05$, $^{**}P \leq 0.01$.

changes in facilitation followed by the application of this general cholinergic agonist.

The weak increase in the amplitudes observed after application of carbachol, when muscarinic receptors had been blocked by scopolamine, could have been a result of the activation of nicotinic receptors. To verify this, another group of experiments using specific nicotinic agonist DMPP (10 μM) was performed. Activation of nicotinic receptors by DMPP led to a moderate depolarization in all investigated cells (n = 9) – on average by 3.78 ± 0.43 mV. In all cells treated with DMPP, amplitudes of the EPSPs became significantly larger (**Figure 3C** and **Table 1**A). The largest increase in the amplitude after application of DMPP was observed for the first EPSP (to, on average, 148% of control value). The 2nd, 3rd, 4th, and 5th EPSPs increased progressively less to 139, 129, 121, and 119% of control values.

Facilitation estimated from consecutive normalized amplitudes ($EPSP_N/EPSP_1$ – **Figure 3D**) decreased in the presence of DMPP (**Table 1**B). Thus, 10 μM DMPP increased EPSP amplitudes and at the same time reduced frequency-dependent facilitation of EPSPs in the train. The instantaneous facilitation ($EPSP_N/EPSP_{N-1}$) decreased only between the first two postsynaptic responses.

Thus, selective activation of nicotinic receptors by 10 μM DMPP, moderately increasing EPSP amplitudes and decreasing their facilitation, seemed to have an opposite effect on corticothalamic synaptic transmission compared to carbachol. Since application of DMPP and application of carbachol after blocking muscarinic receptors by scopolamine had similar effects, we concluded that carbachol-induced reduction of EPSP amplitudes and enhancement of their facilitation are mediated by activation of muscarinic cholinergic receptors. The additional decrease of facilitation after specific nicotinic activation by DMPP may be due to the different strength by which 10 μM DMPP and 6–8 μM carbachol activate individual subtypes of nicotinic receptors. Application of 10 μM DMPP had in fact a larger depolarizing effect (3.78 ± 0.43 mV) than carbachol with blocked muscarinic receptors (0.98 ± 0.12 mV, $P < 0.001$).

Carbachol-Induced Reduction of Corticothalamic EPSP Amplitudes and a Parallel Increase of Their Facilitation Are Associated With a Decreased Transmitter Release Probability

The coexistence of two effects caused by the application of carbachol, i.e., the depression of corticothalamic EPSP amplitudes and enhancement of their frequency-dependent facilitation suggests a presynaptic process underlying this general cholinergic modulatory action (Zucker and Regehr, 2002). To substantiate this finding, we used the "coefficient of variation (CV)" analysis of EPSP amplitudes (Clements, 1990). The CV method is based on the mathematical model describing the process of the neurotransmitter release formulated by del Castillo and Katz (1954). According to this model CV of postsynaptic response amplitudes depend only on two presynaptic factors: the probability of release of a neurotransmitter quantum – q, and the number of available units (quanta) – n, which has been correlated with the number of morphologically identified release sites or active zones (Korn et al., 1981, 1982; Korn and Faber, 1991). As both CV factors (q and n) characterize solely presynaptic mechanisms, any drug-related modulation of the postsynaptic site should not change the CV values of EPSP amplitudes (Clements, 1990). In contrast, a big difference in CV values before and after application of the tested drug strongly implicates a presynaptic site of the modulation.

For the group of cells studied with carbachol (n = 16), we calculated the noise-free inter-trial CV values for consecutive EPSPs in the train (see section "Materials and Methods" for details) before and after application of the drug (**Figure 4A**). The average CV values became much higher after application of carbachol. The largest increase of CV value (2.8 times) was found for the 1st EPSP. The CV values calculated for the following EPSPs were about two times larger compared to the control condition (**Figure 4A** and **Table 1**A). Such a large increase of the CVs in the presence of carbachol strongly points to a presynaptic site of action of this drug (Clements, 1990; Nagumo et al., 2011).

To verify if the presynaptic mechanism of the cholinergic modulation relies on the decreased probability of transmitter release, PoM cells (n = 6) were studied during so-called "pseudominimal stimulation" of the corticothalamic fibers (see "Materials and Methods" for details). An increased failure rate of postsynaptic responses after application of carbachol would indicate reduced transmitter release probability caused

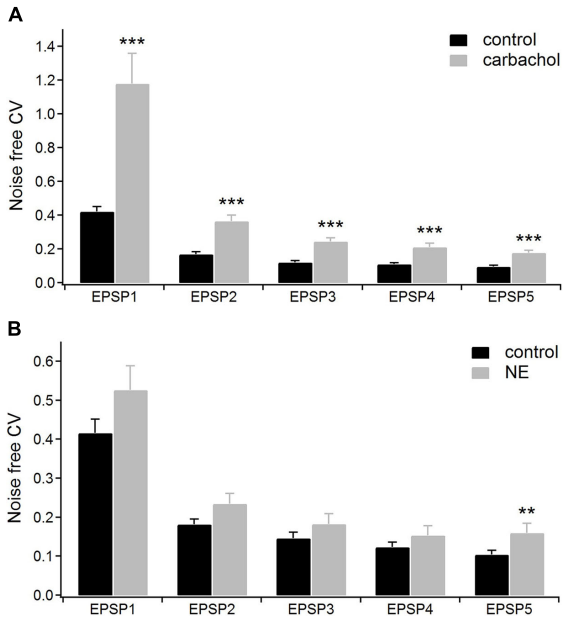

FIGURE 4 | The coefficients of variations (CV) analysis. **(A)** Mean CV values (n = 16) for consecutive EPSPs of the train in the control condition (with ACSF containing GABA inhibitors) and after application of 6–8 μM carbachol. **(B)** Mean CV values (n = 15) for the consecutive EPSPs in the control condition (with ACSF containing GABA inhibitors plus ascorbic acid) and after application of 100 μM norepinephrine. Data are expressed as mean ± SEM, $^{***}P \leq 0.001$, $^{**}P \leq 0.01$.

by the drug and further support the presynaptic site of cholinergic modulation.

Representative time courses of membrane currents recorded in a single cell during five consecutive stimulations in the control condition and after application of carbachol are shown in **Figure 5A**. Note, that the number of evoked EPSCs (marked by asterisks) was about two times higher (19 synaptic events in response to 25 stimulation pulses) in control conditions than during the recordings with the presence of cholinergic agent (10 events). Accordingly, the number of the failures was much smaller in the control state (6 vs. 15 in the presence of carbachol). Note that some spontaneous responses with amplitudes similar to evoked EPSCs were also recorded (**Figure 5A**, indicated by "S"). This observation indicated that only a small number of corticothalamic axons were stimulated. The average EPSC failure rate (i.e., number of failures divided by the number of stimulation trains and multiplied by 100%) for the 1st, 2nd, 3rd, and 4th EPSCs (**Figure 5B**) was substantially higher after application of carbachol (see also **Table 1**A). The failure rate of the 5th EPSC in the presence of carbachol was low and did not differ from the value in the control condition. In fact, the last (5th) stimulation pulse in the train typically produced the strongest and most reliable postsynaptic response.

We also investigated how carbachol affected the amplitude distribution of EPSCs (**Figure 5C**). The bimodal nature of the uppermost histograms for the 1st EPSC indicates that the first impulse in the train evoked EPSCs caused by the release of primarily two quanta. Comparison of amplitude histograms obtained for the 1st EPSC before and after application of carbachol suggests that the released quantal size was not affected by adding the drug. Although carbachol markedly reduced the total amount of EPSC responses (i.e., in control situation the probability of evoking an EPSC by the 1st impulse in the train was much larger) it did not change the positions of the two peaks of the histogram. To determine more precisely the quantal size of corticothalamic EPSCs, the histograms of amplitude probabilities obtained for the 1st impulse were fitted with a double Gaussian function (del Castillo and Katz, 1954; see section "Materials and Methods"). The fitting procedure returned the following quantal size values ± 95% confidence intervals: –5.9 ± 0.2 pA for the control situation and –5.6 ± 0.2 pA after addition of carbachol. As 95% confidence limits overlap, we can state that the obtained two quantal amplitudes are similar. This suggests that carbachol did not change the postsynaptic response size to the release of a single vesicle. This was most apparent for the first EPSC in the train but was also seen for the later EPSCs.

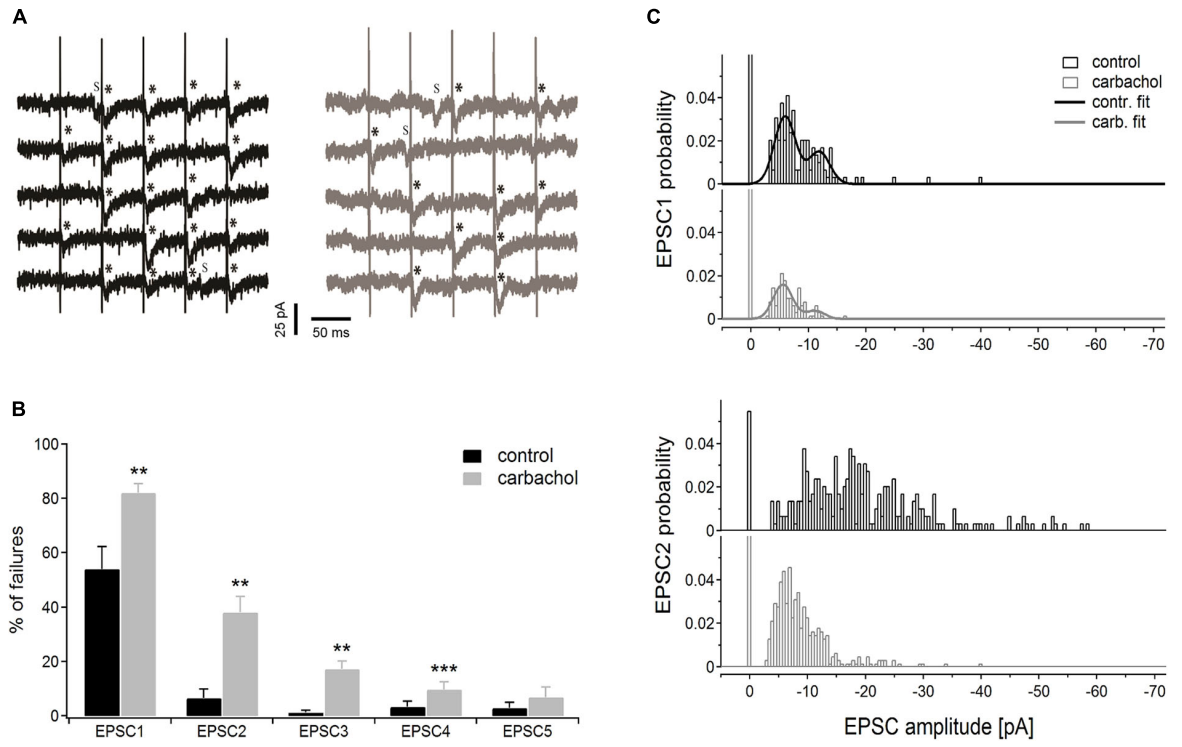

FIGURE 5 | Pseudominimal stimulation experiment (n = 6 PoM cells). **(A)** Examples of the unitary excitatory postsynaptic currents (EPSCs) evoked in a single cell by trains of five pseudominimal stimulation of the corticothalamic fibers in the control condition (with ACSF containing GABA inhibitors, black traces on the left) and after application of 6–8 μM carbachol (gray traces on the right). Successively evoked EPSCs are marked with asterisks (*), letter "s" indicates the spontaneous EPSCs. **(B)** Percentage of the failures averaged for a group of cells in the control condition and after adding carbachol. **(C)** Histograms showing amplitude distribution for 1st (upper panel) and 2nd (lower panel) EPSCs in the train, in control conditions and with the addition of carbachol. Bars drawn at zero of the abscissa axes indicate probabilities of failures. Continuous black and gray curves on EPSC1 histograms show the appropriate double Gaussian fits. Data are expressed as mean ± SEM, $^{**}P \leq 0.01$, $^{***}P \leq 0.001$.

To conclude, results obtained during the pseudominimal stimulation directly indicated that cholinergic modulation of corticothalamic synapse formed by the axons from layer 6 on PoM neurons is presynaptic and relies on a decreased probability of transmitter release.

Multiple Types of Adrenergic Receptors Mediate the Changes Caused by Application of Norepinephrine

In the presence of noradrenergic agonist norepinephrine, a significant increase of the CV value was found only for the 5th EPSP (**Figure 4B** and **Table 2**A). These results do not distinctly support the hypothesis of the presynaptic mechanism of noradrenergic modulation. We suspected that this could be due to various effects exerted by different groups of norepinephrine receptors. Therefore, in the following experiments we investigated to what extent α-2, α-1, and β receptors were involved in noradrenergic modulation of the corticothalamic synapse from layer 6 to the PoM (**Figure 6**).

To check the involvement of α-2 receptors we studied the effect of clonidine on the amplitudes of evoked EPSPs. In contrast to norepinephrine, application of clonidine did not change the resting membrane potential of the investigated cells – the average change in the membrane potential was −0.58 ± 0.62 mV (not different from zero, $P = 0.4$, single group Student t-test). The plot of the average EPSP amplitudes obtained from a group of cells ($n = 5$) indicated that activation of α-2-adrenergic receptors increased amplitudes of the EPSPs (**Figure 6A** and **Table 2**A). On average, compared to the control values, clonidine increased the EPSP amplitudes by 1.89, 1.51, 1.43, 1.28, and 1.19 times respectively. Interestingly, the largest increase in the presence of clonidine was noted for the amplitude of the 1st EPSP. Hence, clonidine seemed to reduce the facilitation of the consecutive responses in the train. This is shown by the normalized amplitudes ($EPSP_N/EPSP_1$; **Figure 6B** and **Table 2**B) which had significantly larger values in control conditions than

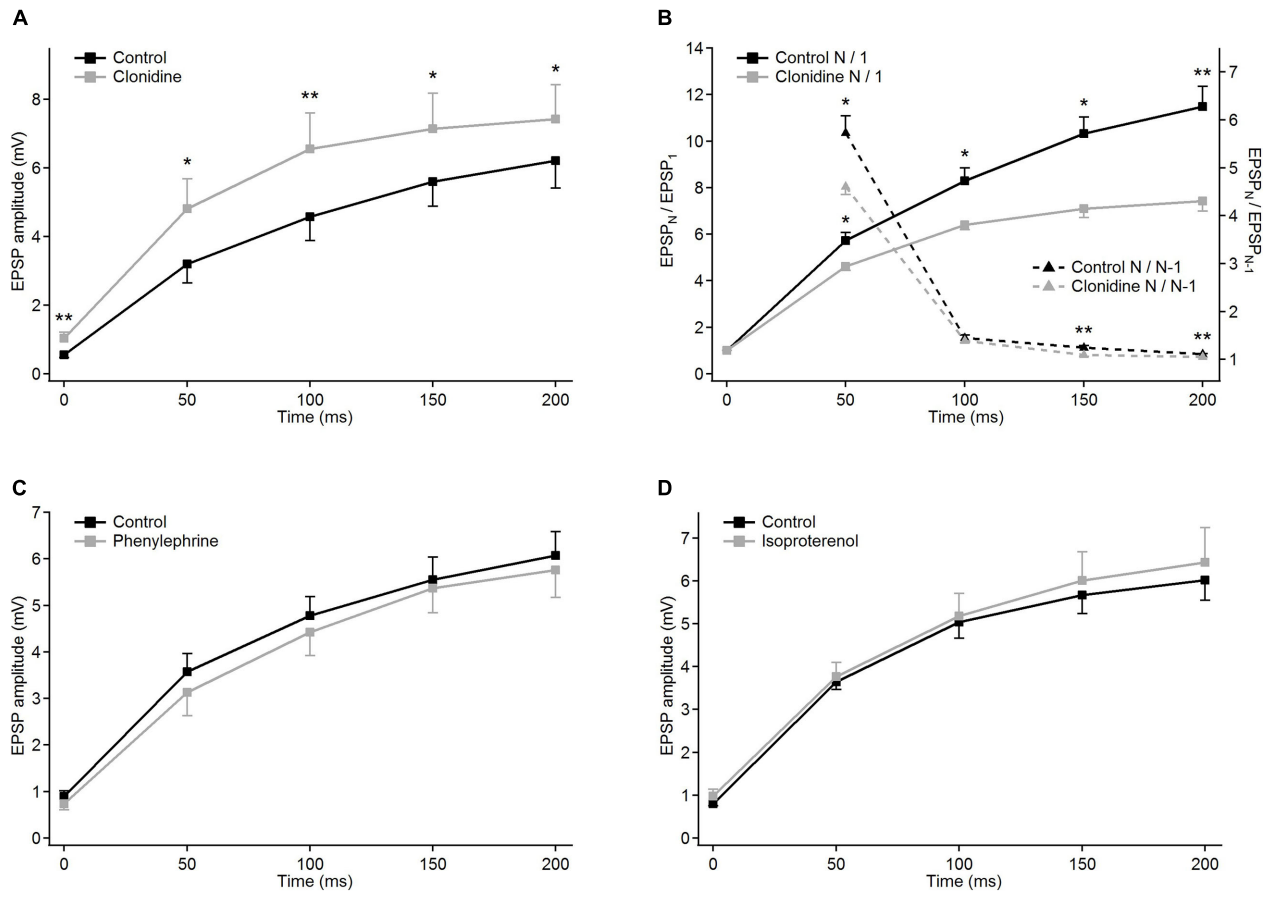

FIGURE 6 | Modulatory effects of different noradrenergic agents on EPSP trains in PoM cells. Group average of EPSP amplitudes in the control condition (black traces) and after application of the drugs (gray traces): **(A)** 40 μM clonidine ($n = 6$); **(C)** 100 μM phenylephrine ($n = 6$) and **(D)** 100 μM isoproterenol ($n = 7$). **(B)** Clonidine effects on normalized EPSP amplitudes and momentary facilitation. Left Y axis: average normalized amplitudes ($EPSP_N/EPSP_1$) in the control condition (solid black trace) and in the presence of clonidine (solid gray line). Right Y axis: average ratios of the consecutive EPSP amplitudes ($EPSP_N/EPSP_{N-1}$) in the control condition and after application of clonidine (black and gray dashed lines, respectively). For all NE drugs, control bath solution contained GABA inhibitors plus sodium ascorbate. Data are expressed as mean ± SEM, $^*P \leq 0.05$ and $^{**}P \leq 0.01$.

after application of clonidine. Ratios between amplitudes of neighboring EPSPs (see dashed lines on **Figure 6B**) were smaller in the presence of clonidine also for the 3rd ($EPSP_{4/3}$) and 4th ($EPSP_{5/4}$) pairs (**Table 2**C).

Summing up, the application of clonidine, similar to norepinephrine, decreased the frequency-dependent facilitation of the EPSPs evoked by the stimulation train. Thus, activation of α-2 adrenergic receptors replicated a part of the effects caused by norepinephrine. Moreover, the lack of membrane potential changes with application of clonidine suggested presynaptic action of α-2 receptors.

The difference between results obtained with the general adrenergic agonist norepinephrine (moderate decrease of EPSP amplitudes) and specific alpha-2 agonist clonidine (moderate increase of EPSP amplitudes) suggested that yet another class of adrenergic receptors, having a decreasing effect on EPSP amplitudes, should also be involved in the noradrenergic modulation of the corticothalamic synapses to the PoM.

Selective activation of α-1 receptors by phenylephrine led to the depolarization of the thalamic cells ($n = 6$) by 7.22 ± 1.11 mV on average. Phenylephrine did not cause any changes in the average EPSP amplitude values (**Figure 6C** and **Table 2**A). Consequently, the normalized amplitudes did not differ before and after α-1 adrenergic activation. Neither, phenylephrine changed the consecutive EPSP ratios. Thus, selective activation of α-1 adrenergic receptors did not affect EPSP amplitudes of PoM cells after activation of cortical layer 6 axons nor did it change the frequency-dependent facilitation, what suggested that α-1 receptors were not involved in noradrenergic modulation of the corticothalamic synapses. However, these receptors were partly responsible for the membrane potential shift caused by norepinephrine.

Finally, the role of the β receptors in the noradrenergic modulation was studied by application of a non-selective β-adrenoreceptor agonist isoproterenol. Activation of β adrenergic receptors depolarized the ($n = 7$) PoM cells on average by 7.34 ± 0.57 mV, but similarly to phenylephrine did not affect the amplitudes of the EPSPs in the train (**Figure 6D**). Similarly, the normalized amplitude values after β adrenergic activation did not change compared to the corresponding control values (**Table 2**B). Thus, selective activation of the β-adrenergic receptors did not affect the EPSP amplitudes in the train neither it changed their frequency-dependent facilitation. However, activation of this group of receptors resulted in the membrane potential shift which was about half of that seen after norepinephrine application.

DISCUSSION

This study provides the first data concerning cholinergic and noradrenergic modulation of the corticothalamic synaptic transmission from the cortical layer 6 to the cells in the higher-order posteromedial nucleus (PoM) of the somatosensory thalamus in mammals. We have characterized these modulations in rats PoM cells and showed that they substantially differ from each other.

Cholinergic modulation (induced by application of the general cholinergic agonist carbachol) led to a substantial decrease in PSPs amplitudes but at the same time enhanced frequency-dependent facilitation. This cholinergic modulation was caused by activation of muscarinic receptors, as it was reliably eliminated by muscarinic receptor blockage and did not appear in the presence of the agonists selective for nicotinic acetylcholine receptors. With cholinergic modulation, the amplitudes of consecutive EPSPs in the five pulse trains had a much higher trial-to-trial CV (SD/mean), suggesting a presynaptic change in the transmitter release probability rather than a postsynaptic change in the EPSP scaling. This was confirmed by increased failure rates to "pseudominimal" stimulation of the corticothalamic axons.

Noradrenergic modulation of the same synapse (mimicked by the application of general agonist norepinephrine) was different in all these respects. The amplitude of the first EPSP in the train was unchanged whereas amplitudes of the 2nd, 3rd, 4th, and 5th EPSPs decreased. In contrast to the cholinergic effect, the adrenergic activation decreased the frequency-dependent facilitation at the corticothalamic synapse. Norepinephrine did not change the coefficients of variation of consecutive EPSPs in the train in any consistent way. Thus, we could not find a support for either presynaptic or postsynaptic site of noradrenaline action.

Receptors Regulating Cholinergic Modulation of Corticothalamic Transmission From Layer 6 to the PoM

In order to reveal what type of receptors are responsible for the cholinergic modulation of the corticothalamic transmission, we used drugs with selective pharmacological profiles. Application of carbachol after the pre-incubation with 1 μM scopolamine (a selective and powerful muscarinic antagonist) did not reduce the EPSPs and did not change the frequency-dependent facilitation. Instead, the responses were slightly increased in amplitude compared to the control condition. Therefore, we concluded that the modulatory action of carbachol on corticothalamic transmission in PoM was due to activation of muscarinic receptors and did not involve nicotinic receptors.

This conclusion was further supported by experiments with selective activation of nicotinic receptors by DMPP. There is a great diversity of nicotinic receptor subtypes depending on the α- and β-subunits composition, with DMPP affinities ranging from nanomolar to micromolar range (Parker et al., 2001; Romanelli et al., 2001). We decided to perform experiments with 10 μM concentration of DMPP as it should activate most of the nicotinic receptors and was comparable to the concentration of carbachol in the experiments with muscarinic receptors blocked by scopolamine. The effect of nicotinic receptors activation was, however, completely different than that of muscarinic receptors – the EPSP amplitudes were enhanced and frequency-dependent facilitation was reduced. The changes induced by DMPP were also small compared to those induced by carbachol. Our data were not sufficient to suggest the postsynaptic or presynaptic site of DMPP action. A possible presynaptic mechanism could rely on an increase of the probability of transmitter release.

However, we do not exclude that any postsynaptic mechanisms could also be involved in the observed modulation (Blitz et al., 2004; Sun and Beierlein, 2011), although it should not depend on changes of the membrane resistance, as it did not change after incubation with the drug.

Thus, our results indicate that carbachol-induced depression of the EPSPs and simultaneous enhancement of the frequency-dependent facilitation of the corticothalamic input from the layer 6 to the PoM are caused by activation of muscarinic receptors. These effects are accompanied by smaller nicotinic modulation acting in the opposite direction. This smaller modulation was not visible after general cholinergic activation, presumably being hidden by an overwhelming muscarinic effect. More extensive studies are needed to reveal the role and mechanism of this weaker nicotinic effect.

Our study provides the first data concerning the cholinergic modulation of the corticothalamic synaptic input to the mammalian higher-order sensory thalamic nuclei. Similar experiments have been conducted in the first order ventrobasal (VB) nucleus of mouse. In general, these results were similar: postsynaptic responses were decreased and simultaneously, the frequency-dependent facilitation was enhanced (Castro-Alamancos and Calcagnotto, 2001; Nagumo et al., 2011). In addition, these studies showed that types of receptors involved in such modulatory effects depend on the age of the animals. In young adult (>7-week old) mice these effects were mediated by muscarinic receptors (Castro-Alamancos and Calcagnotto, 2001), while in neonatal (14–19 days old) mice they were mediated by nicotinic receptors, particularly by those containing the α-5 subunit (Nagumo et al., 2011). Nagumo et al. (2011) proposed that this age-dependent difference may be caused by developmental changes in the expression of acetylcholine receptors during the postnatal development. In particular, nicotinic receptor expression usually decreases, and muscarinic receptor expression increases during the postnatal development in mice (Fiedler et al., 1987). The rats we used were in the middle of this age range (3–4 weeks old, i.e., weaning age) but the postnatal development of the cholinergic receptors may slightly differ between rats and mice or between first order and second order thalamic nuclei. These observations should be taken into account when accepting the major muscarinic nature of the cholinergic modulation found in our study.

Despite similar effects (depression of the postsynaptic responses and enhancement of facilitation) induced by cholinergic agents in the primary and secondary relay nuclei in both young and adult rodents, the subtypes of the receptors (muscarinic or nicotinic) involved in these processes might differ. We did not examine the involvement of particular subtypes of muscarinic receptors (M1–M5), mainly because of the lack of highly specific agonists and antagonists. We suppose, however, that M2 receptors could be involved in the cholinergic modulation. First of all, the affinity of carbachol to M2 receptors is higher than to other muscarinic receptor types (Peralta et al., 1987; Jakubik et al., 1997; Cheng et al., 2002) and these receptors are located on the presynaptic terminals (Guo et al., 2012). Moreover, higher-order nuclei in adult rats contain more muscarinic M2 receptors compared to the first-order nuclei (Barthó et al., 2002). However, one cannot exclude either that more than one subtype of muscarinic receptors may be involved in the processes of cholinergic modulation in PoM.

Mechanism of Cholinergic Modulation of Corticothalamic Transmission From Layer 6 to the PoM

We also aimed to study whether cholinergic modulation is supported by pre- or postsynaptic mechanism. Simultaneous decrease of the EPSP amplitudes and enhancement of the frequency-dependent facilitation induced by carbachol are consistent with a presynaptic mechanism related to the decrease of the neurotransmitter release probability (Zucker, 1989; Zucker and Regehr, 2002). This hypothesis posits that a low initial release probability initiates stronger facilitation of the postsynaptic responses (Manabe et al., 1993). To solve this issue, we used an analysis based on the CV which has been used previously to study the site of the action of a modulatory drug (Clements, 1990; Faber and Korn, 1991; Hannay et al., 1993; Sjöström et al., 2003). As the inter-trial, noise-free CV values for all EPSPs in the train were much larger after cholinergic activation we assumed that a presynaptic mechanism was responsible for the carbachol-induced cholinergic modulation.

Direct experimental evidence for such presynaptic modulatory action of carbachol was obtained by measuring the unitary EPSCs using a pseudominimal stimulation of the corticothalamic tract. Activation of only one corticothalamic axon (Hanse and Gustafsson, 2001; Granseth and Lindström, 2003) is very difficult since the synaptic transmitter release probability is exceedingly small (<10%; Granseth and Lindström, 2003). However, for establishing if a drug effect is pre- or postsynaptic, an EPSC failure rate analysis can be performed with less strict experimental conditions. EPSC failures are seen in the postsynaptic cell when the action potential does not release neurotransmitter and is related to the transmitter release probability (p) and the number of release sites (n) as ($1–p^n$). An increase in the number of EPSC failures would consequently represent a reduction in the transmitter release and *vice versa*. Thus, the most sensitive way to probe for a change in presynaptic transmitter release was to adjust the stimulation pulse intensity to have 50% of EPSCs failures. We called this "pseudominimal" stimulation since more than one axon was recruited by the stimulation pulses. Our results showed that for each of four first impulses in the train carbachol caused a substantial increase in the number of failures which clearly indicated a decrease of transmitter release probability. The facilitation mechanism of the studied synapse substantially increased the probability of transmitter release during the train and carbachol-induced reduction of the failures was not significant for the 5th EPSC. This did not necessarily mean that carbachol did not reduce the release probability for the last stimulus (for which the averaged EPSP amplitude still remained lower under carbachol). The EPSC amplitude histograms showed, in addition, that carbachol did not change the unitary size of the postsynaptic responses caused by

a single synaptic vesicle and provided a further support for the presynaptic site of modulatory action.

Taken together our data demonstrate that carbachol exerts presynaptic modulatory action on corticothalamic synaptic transmission from layer 6 of area S1 to PoM neurons by decreasing the probability of transmitter release. There is no evidence that cholinergic synapses are located directly on the corticothalamic connections, but acetylcholine could activate presynaptic muscarinic cholinergic receptors located at the synapses by means of volume transmission. It was previously established that a decrease of the initial release probability led to an enhanced facilitation (Manabe et al., 1993). Such a mechanism might explain the increase of carbachol-induced facilitation of the subsequent corticothalamic responses if the spikes arrive sufficiently close to each other.

Suppression of the glutamate release by activation of muscarinic receptors was previously suggested for many other synaptic connections (Williams and Johnston, 1990; Sim and Griffith, 1996; de Sevilla et al., 2002; Zhang and Warren, 2002; Guo et al., 2012). It is also known that presynaptic action of cholinergic agents decreases excitatory transmission in various other structures such as hippocampus (Scanziani et al., 1995), ventral striatum (Pennartz and Lopes da Silva, 1994) and, interestingly, inhibitory transmission in the thalamus (Masri et al., 2006). Other experiments suggest (by indirect effect of the enhanced frequency-dependent facilitation) that carbachol decreases the transmitter release probability at the corticothalamic synapses also in the first order VB complex (Castro-Alamancos and Calcagnotto, 2001; Nagumo et al., 2011).

Although our data strongly supports the involvement of presynaptic muscarinic receptors in cholinergic modulation of corticothalamic transmission to the PoM, we do not know which elements from the cascade of the events leading to the release of the neurotransmitter are actually affected by this modulatory process. In general, two types of events at the corticothalamic terminal can be regulated: calcium entry through voltage-gated calcium channels and the factors responsible for the preparation of the release-ready vesicles and their final exocytosis. For example, in case of presynaptic muscarinic inhibition of the excitatory synaptic transmission in CA3 area of hippocampus (Scanziani et al., 1995) the results suggested direct interference in the neurotransmitter release process at some point subsequent to calcium influx. It remains an intriguing question whether this might also be true also in the rat's PoM.

It is important to mention that we cannot exclude other postsynaptic mechanisms like receptor saturation or desensitization to be involved in muscarinic modulation in PoM. It has been shown that postsynaptic mechanisms can affect the frequency-dependent facilitation of postsynaptic responses (Blitz et al., 2004; Sun and Beierlein, 2011) and one of these processes – receptor saturation was acknowledged in corticothalamic synapses in the first order VB complex of mice (Sun and Beierlein, 2011). It is likely that such a postsynaptic mechanism can additionally shape the muscarinic modulation. Following synaptic depression, the smaller amounts of neurotransmitter released into the synaptic cleft will have less chance to saturate the postsynaptic receptors. As a consequence, less saturation would additionally raise the facilitation enhancement at the presynaptic site. Further experiments are needed to investigate other postsynaptic mechanisms that may also be involved in the cholinergic modulation of the corticothalamic synapses in PoM.

Mechanism Underlying the Noradrenergic Modulation of the Corticothalamic Transmission From Layer 6 to the PoM

Activation of noradrenergic receptors by noradrenaline led to the depression of the later EPSP amplitudes with an unchanged magnitude of the 1st EPSP and reduced frequency-dependent facilitation during the EPSP train. Closer inspection of the ratios between the amplitudes of the consecutive postsynaptic responses showed that the decreased facilitation resulted solely from the difference between the first two EPSPs (**Figure 2F**). The observed effects of noradrenergic modulation of synaptic transmission from layer 6 to the PoM were surprising for us. Assuming that a presynaptic mechanism is at work, i.e., by changing the initial transmitter release probability, a decreased facilitation should have led to a larger amplitude of the 1st EPSP (Zucker, 1989; Zucker and Regehr, 2002). However, the 1st EPSP in the presence of norepinephrine was not changed. One should, therefore, consider a possible mixture of the effects caused by different subtypes of adrenergic receptors or that both pre- and postsynaptic sites may be involved in the noradrenergic modulation or a direct effect on the facilitation mechanism *per se*.

A similar conclusion can be drawn from the analysis of coefficients of variation. In contrast to the cholinergic modulation, where CVs for all the EPSPs were much larger after application of carbachol, norepinephrine did not cause a consistent change in CV values. Such a result does not support to any change in the transmitter release probability.

To better understand the process of noradrenergic modulation in PoM, we selectively activated the α-2 adrenergic receptors using specific agonist clonidine. The reason for performing this experiment was that α-2 receptors were shown to be involved in noradrenergic modulation of the corticothalamic transmission to VB in mice (Castro-Alamancos and Calcagnotto, 2001). In our experiments, clonidine did not depolarize PoM cells, which was in accordance with their putative presynaptic localization. Moreover, activation of α-2 receptors increased the amplitudes of all EPSPs, including first, and lowered the frequency-dependent facilitation during the train. This fits the classical picture observed after an increase in transmitter release probability.

It should be noted that clonidine appeared to increase the EPSP amplitudes, which is opposite to the effect of the general agonist norepinephrine. Most probably, another group of adrenergic receptors (α-1 or β) substantially depressed the corticothalamic postsynaptic responses in PoM and the reduction with noradrenergic effect is the net effect of all these receptors being activated together. However, activation of α-1 adrenoceptors by application of phenylephrine had no effect on the EPSP amplitudes or the frequency-dependent facilitation at the corticothalamic synapse. This data indicates that these receptors are not involved in the modulation of

the corticothalamic synaptic transmission to the PoM by norepinephrine despite the fact that they had a consistent depolarizing postsynaptic effect on all studied PoM cells.

It was previously found that β adrenergic receptors can affect short term synaptic properties (Pu et al., 2009). However, we did not find experimental proof that β-adrenoceptors are responsible for the noradrenergic modulation of corticothalamic synaptic transmission in PoM. Although isoproterenol, a general β-receptor agonist (Baker et al., 1991) similar to phenylephrine, consistently depolarized the cells it had no effect on the response amplitudes neither it affected their frequency-dependent facilitation. Differences between the affinities of isoproterenol and norepinephrine to different subclasses of adrenergic β receptors might, to some extent, explain this discrepancy. Namely, isoproterenol has a greater affinity to both β-1 and β-2 adrenergic receptors as compared to norepinephrine (Sillence et al., 2005). This compound was also found to be equally potent on β-1 and β-2 adrenergic receptors, while norepinephrine is 10-fold more selective for β-1 than for β-2 receptors (Michel, 1991; Hoffmann et al., 2004). Thus, further experiments with the use of more selective β-1 and β-2 receptor agonists might finally reveal the receptors underlying the noradrenergic modulation of the corticothalamic synapses to the PoM. Finally, the modulatory effect of norepinephrine might be not a simple summation of the separate actions produced by more specific agonists. When activated simultaneously, different adrenergic receptor subtypes could interact to shape the response in different ways.

Noradrenergic modulation of corticothalamic synaptic transmission was investigated before by Castro-Alamancos and Calcagnotto (2001) in the first order ventrobasal (VB) nucleus of mice. These authors revealed that both noradrenergic and cholinergic activation decreased the postsynaptic responses with a simultaneous increase of the frequency-dependent facilitation at the synapse. The noradrenergic modulation was shown to be mediated by α2-adrenergic receptors and the authors proposed that the mechanism of this synaptic regulation was presynaptic. Our results also show that α2-adrenergic receptors modulate layer 6 input to higher-order PoM nucleus of the rat, but in the opposite direction – as compared to the VB of mice - by enhancing synaptic responses and decreasing their frequency-dependent facilitation. The difference may be related to different species used, different nuclei which were investigated or different ages of experimental animals (adult, older than 7 weeks mice versus 3–4 weeks old rats). Age-related differences in the noradrenergic modulation would be possible because of temporal differences in the postnatal development of adrenergic receptors (Happe et al., 2004) and could resemble age-related differences in the cholinergic modulation in VPM of mice (Castro-Alamancos and Calcagnotto, 2001 vs. Nagumo et al., 2011).

TABLE 1 | Cholinergic effects.

					A					B				C		
					No of EPSP in the train					Normalized amplitudes (EPSPn/EPSP1)				Momentary facilitation (EPSP n /EPSP n-1)		
	Drug	No of cells	Measure	Drug condition	1st	2nd	3rd	4th	5th	2nd/1st	3rd/1st	4th/1st	5th/1st	3rd/2nd	4th/3rd	4th/5th
Mean values ± SEM	Carbachol	16	EPSP amplitude	Control	**0.89 ± 0.12**	**3.80 ± 0.34**	**5.54 ± 0.41**	**6.16 ± 0.47**	**6.78 ± 0.52**	**4.52 ± 0.26**	**6.85 ± 0.48**	**7.2 ± 0.81**	**7.73 ± 0.61**	**1.51 ± 0.06**	**1.12 ± 0.03**	**1.11 ± 0.02**
				Carbachol	**0.26 ± 0.05**	**1.44 ± 0.22**	**2.44 ± 0.32**	**3.15 ± 0.42**	**3.74 ± 0.46**	**6.42 ± 0.48**	**11.89 ± 1.23**	**15.87 ± 1.78**	**19.57 ± 2.30**	**1.82 ± 0.09**	**1.32 ± 0.03**	**1.22 ± 0.03**
			CV	Control	**0.42 ± 0.03**	**0.17 ± 0.02**	**0.12 ± 0.01**	**0.11 ± 0.01**	**0.09 ± 0.01**	–	–	–	–	–	–	–
				Carbachol	**1.18 ± 0.18**	**0.36 ± 0.04**	**0.24 ± 0.02**	**0.21 ± 0.02**	**0.18 ± 0.01**	–	–	–	–	–	–	–
		6	Failures	Control	**54.1 ± 8.20**	**6.5 ± 3.30**	**1.2 ± 0.90**	**3.3 ± 2.10**	*2.9 ± 2.00*	–	–	–	–	–	–	–
				Carbachol	**82.1 ± 3.40**	**38.0 ± 5.80**	**17.2 ± 2.90**	**9.8 ± 2.70**	*6.8 ± 3.70*	–	–	–	–	–	–	–
	Scopolamine	9	EPSP amplitude	Scopolamine	*0.47 ± 0.08*	**2.39 ± 0.35**	**3.61 ± 0.55**	*4.31 ± 0.63*	**4.81 ± 0.61**	*5.27 ± 0.29*	*8.3 0 ± 0.89*	*10.2 ± 1.28*	*11.97 ± 1.88*	*1.55 ± 0.10*	*1.21 ± 0.03*	*1.15 ± 0.05*
				Scopolamine + Carbachol	*0.58 ± 0.11*	**2.94 ± 0.45**	**4.42 ± 0.71**	*4.96 ± 0.74*	**5.58 ± 0.82**	*5.53 ± 0.61*	*8.56 ± 1.17*	*9.73 ± 1.3*	*11.13 ± 1.62*	*1.52 ± 0.08*	*1.14 ± 0.04*	*1.13 ± 0.03*
	DMPP	9	EPSP amplitude	Control	**0.48 ± 0.11**	**2.33 ± 0.48**	**3.60 ± 0.68**	**4.22 ± 0.73**	**4.75 ± 0.79**	**5.31 ± 0.41**	**8.70 ± 0.93**	**10.68 ± 1.33**	**12.26 ± 1.69**	*1.62 ± 0.07*	*1.21 ± 0.03*	*1.13 ± 0.02*
				DMPP	**0.72 ± 0.16**	**3.24 ± 0.76**	**4.63 ± 0.87**	**5.11 ± 0.86**	**5.68 ± 0.86**	**4.54 ± 0.36**	**7.13 ± 0.64**	**8.09 ± 0.75**	**9.46 ± 1.11**	*1.58 ± 0.09*	*1.14 ± 0.03*	*1.15 ± 0.04*
P-values	Carbachol	16	EPSP ampl	Carbachol – Control	**0.001**	**0.001**	**0.001**	**0.001**	**0.001**	**0.001**	**0.001**	**0.001**	**0.001**	**0.001**	**0.001**	**0.001**
			CV	Carbachol – Control	**0.0003**	**0.0001**	**0.0001**	**0.0001**	**0.0001**	–	–	–	–	–	–	–
		6	Failures	Carbachol – Control	**0.01**	**0.002**	**0.002**	**0.00099**	*0.1*	–	–	–	–	–	–	–
	Scop	9	EPSP ampl	Scop – (Scop + Carbachol)	*0.48*	**0.019**	**0.021**	*0.085*	**0.024**	*0.54*	*0.73*	*0.52*	*0.32*	*0.68*	*0.27*	*0.77*
	DMPP	9	EPSP ampl	DMPP – Control	**0.003**	**0.019**	**0.017**	**0.02**	**0.037**	**0.037**	**0.024**	**0.014**	**0.015**	*0.55*	*0.11*	0.69

Measured values and their corresponding p-values that were significant are written in bold, nonsignificant in faint italic. Abbreviations: ampl – amplitude; Scop – Scopolamine.

TABLE 2 | Noradrenergic effects.

					A					B				C		
					No of EPSP in the train					Normalized amplitudes (EPSPn/EPSP1)				Momentary facilitation (EPSP n /EPSP n-1)		
	Drug	No of cells	Measure	Drug condition	1st	2nd	3rd	4th	5th	2nd/1st	3rd/1st	4th/1st	5th/1st	3rd/2nd	4th/3rd	4th/5th
Mean values ± SEM	Norepinephrine	15	EPSP amplitude	Control	*0.77 ± 0.07*	**3.70 ± 0.29**	**5.30 ± 0.38**	**6.00 ± 0.39**	**6.39 ± 0.42**	**4.91 ± 0.20**	**7.14 ± 0.31**	**8.21 ± 0.45**	**8.79 ± 0.53**	*1.46 ± 0.03.*	*1.14 ± 0.02*	*1.07 ± 0.01*
				Norepinephrine	*0.8 ± 0.12*	**3.18 ± 0.46**	**4.39 ± 0.57**	**4.87 ± 0.57**	**5.04 ± 0.56**	**4.11 ± 0.20**	**5.90 ± 0.36**	**6.74 ± 0.47**	**7.12 ± 0.57**	*1.44 ± 0.05*	*1.14 ± 0.02*	*1.05 ± 0.01*
			CV	Control	*0.42 ± 0.04*	*0.18 ± 0.01*	*0.15 ± 0.02*	*0.12 ± 0.01*	0.1 ± 0.01	–	–	–	–	–	–	–
				Norepinephrine	*0.53 ± 0.06*	*0.23 ± 0.03*	*0.18 ± 0.03*	*0.15 ± 0.02*	0.16 ± 0.02	–	–	–	–	–	–	–
	Clonidine	5	EPSP amplitude	Control	**0.55 ± 0.08**	**3.20 ± 0.55**	**4.58 ± 0.69**	**5.6 ± 0.72**	**6.22 ± 0.80**	**5.73 ± 0.35**	**8.30 ± 0.55**	**10.33 ± 0.71**	**11.48 ± 0.86**	*1.45 ± 0.06*	**1.25 ± 0.04**	**1.11 ± 0.01**
				Clonidine	**1.04 ± 0.18**	**4.81 ± 0.87**	**6.56 ± 1.05**	**7.15 ± 1.04**	**7.43 ± 1.00**	**4.61 ± 0.17**	**6.41 ± 0.20**	**7.09 ± 0.38**	**7.42 ± 0.43**	*1.39 ± 0.04*	**1.10 ± 0.03**	**1.05 ± 0.02**
	Phenylephrine	6	EPSP amplitude	Control	*0.89 ± 0.12*	*3.57 ± 0.39*	*4.78 ± 0.5*	*5.55 ± 0.49*	*6.07 ± 0.51*	*4.25 ± 0.49*	*5.83 ± 0.94*	*6.87 ± 1.34*	*7.54 ± 1.44*	*1.35 ± 0.05*	*1.16 ± 0.03*	*1.10 ± 0.03*
				Phenylephrine	*0.74 ± 0.13*	*3.13 ± 0.5*	*4.42 ± 0.5*	*5.37 ± 0.53*	*5.76 ± 0.59*	*4.57 ± 0.49*	*6.65 ± 0.93*	*8.06 ± 1.05*	*8.69 ± 1.22*	*1.43 ± 0.06*	*1.23 ± 0.06*	*1.07 ± 0.02*
	Isoproterenol	7	EPSP amplitude	Control	*0.80 ± 0.05*	*3.64 ± 0.18*	*5.04 ± 0.38*	*5.67 ± 0.43*	*6.02 ± 0.47*	*4.65 ± 0.40*	*6.41 ± 0.59*	*7.21 ± 0.69*	*7.66 ± 0.72*	*1.38 ± 0.05*	*1.13 ± 0.04*	*1.06 ± 0.01*
				Isoproterenol	*0.98 ± 0.16*	*3.77 ± 0.33*	*5.18 ± 0.53*	*6.01 ± 0.67*	*6.43 ± 0.81*	*4.02 ± 0.33*	*5.49 ± 0.42*	*6.43 ± 0.70*	*6.81 ± 0.66*	*1.38 ± 0.07*	*1.16 ± 0.05*	*1.06 ± 0.03*
P-values	Norepinephrine	15	EPSP ampl	Norepinephrine – Control	*0.69*	**0.04**	**0.004**	**0.001**	**0.009**	**0.008**	**0.006**	**0.007**	**0.009**	*0.63*	*0.88*	*0.28*
			CV	Norepinephrine – Control	*0.096*	*0.027*	*0.64*	*0.63*	**0.008**	–	–	–	–	–	–	–
	Clon	5	EPSP ampl	Clonidine – Control	**0.009**	**0.033**	**0.001**	**0.019**	**0.021**	**0.046**	**0.036**	**0.013**	**0.01**	*0.46*	**0.002**	**0.005**
	Phenyl	6	EPSP ampl	Phenylephrine – Control	*0.12*	*0.07*	*0.13*	*0.3*	*0.17*	*0.17*	*0.17*	*0.17*	*0.17*	*0.26*	*0.40*	*0.36*
	Isop	7	EPSP ampl	Isoproterenol – Control	*0.18*	*0.61*	*0.47*	*0.17*	*0.19*	*0.13*	*0.14*	*0.27*	*0.24*	*0.88*	*0.86*	*0.46*

Measured values and their corresponding p-values that were significant are written in bold, nonsignificant in faint italic. Abbreviations: ampl – amplitude; Clon – Clonidine, Phenyl – Phenylephrine; Isop – Isoproterenol.

Interestingly, some developmental changes in noradrenergic modulation occur also within the cortex in the case of the layer 5 corticothalamic neurons. Such cells in juvenile rats (3–4 weeks old, as in our study) have almost exclusively regular spiking firing pattern, while in adults predominantly show a bursting activity (Llano and Sherman, 2009). In parallel, norepinephrine enhances synaptically driven responses in regularly spiking layer 5 cells but depresses them in bursting neurons (Waterhouse et al., 2000). In consequence, synaptic responses of layer 5 corticothalamic cells can be enhanced in juvenile but depressed in adult rats. The maturation of noradrenergic modulation of layer 6 synaptic input to the PoM could go hand in hand with age-related noradrenergic effect within the layer 5.

Taken together, our data provide an evidence that noradrenergic modulation of layer 6 corticothalamic transmission in PoM acts (at least partly) via the α-2 receptors. Additional experiments are needed to reveal all the receptors and mechanisms involved in this process.

Functional Role of Cholinergic and Noradrenergic Modulation of Corticothalamic Transmission From Layer 6 to the PoM

Cholinergic and noradrenergic connections in the brain form rich, complex, and mutually linked neuromodulatory system playing an important role in the transition from sleep to arousal, setting different levels of vigilance, attentive behavior or executive function. The classical experiment by Livingstone and Hubel (1981) showed that the activity of cells in the cortical layer 6 is profoundly depressed during sleep and activated during arousal evoked by brainstem stimulation. The regulation of arousal is provided by cholinergic afferents from the brainstem pedunculopontine and laterodorsal tegmental nuclei to the thalamo-cortical system (Steriade et al., 1993; Pita-Almenar et al., 2014; Trofimova and Robbins, 2016) whereas the afferents from the basal forebrain to cortical and some thalamic sites (Varela, 2014) participate in the regulation of attentive processes induced by a novel, salient or "emotionally charged" stimuli (Klinkenberg et al., 2011; Unal et al., 2012). In parallel, noradrenergic afferents from the locus coeruleus have strong reciprocal connections with the prefrontal cortex, are activated by important, salient stimuli, and initiate attentive processing (for reviews see: Sarter and Bruno, 2000; Samuels and Szabadi, 2008; Sara, 2009).

We have previously proposed that the functional role of the frequency-dependent facilitation at the corticothalamic synapse might be to provide a dynamic gain control of the transmission of the sensory information through the thalamus (Lindström and Wróbel, 1990; Granseth et al., 2002; Granseth, 2004). Later results carried out in our laboratory (Bekisz and Wróbel, 1993; Wróbel et al., 2007) showed that this gain enhancement operates in the beta frequency band (12–30 Hz) and may

be utilized as an attentional mechanism. It was hypothesized that short-lasting (200–300 ms) beta oscillatory bursts in the corticothalamic pathway can depolarize the thalamic neurons by means of frequency-dependent facilitation and thus change the gain for the information stream from the periphery to the cortex (Wróbel, 2000, 2014). Activation of the cholinergic (and/or noradrenergic) system could provide further control of this gain mechanism (Wróbel and Kublik, 2001).

It has been previously shown that activation of both cholinergic and noradrenergic systems increases the frequency-dependent facilitation in the first order, VPM nucleus (Castro-Alamancos and Calcagnotto, 2001). However, *in vivo* cholinergic activation increases the spontaneous firing and enlarges the VPM receptive fields, whereas noradrenergic activation decreases spontaneous activity and focuses the receptive fields (Hirata et al., 2006). It was proposed that the two modulatory systems play different roles in information processing at the first order somatosensory thalamus, with noradrenergic modulation being more specific/focused than cholinergic (Hirata et al., 2006).

Our data extends the notion, that in the higher-order PoM nucleus these two systems act differently – the cholinergic system enhances the frequency-dependent facilitation, while noradrenergic system reduces it. Interaction between the two systems is not yet understood. One has to take into consideration the complicated modulatory network acting on the secondary order nuclei. For example, it has been shown that cholinergic activation of *zona incerta* (Masri et al., 2006) increases the gain of information flow through the PoM. It is possible that reduction of the corticothalamic facilitation by noradrenaline counteracts this gain increase to keep the necessary balance of the activation in PoM. Whether this hypothesis survives the experimental investigation remains to be checked. Our experiment allows, however, to conclude that both cholinergic and noradrenergic modulation act as a variable dynamic control for the corticothalamic mechanism of the frequency-dependent facilitation in PoM.

DATA AVAILABILITY STATEMENT

The original contributions presented in the study are included in the article, further inquiries can be directed to the corresponding author/s.

ETHICS STATEMENT

The animal study was reviewed and approved by 1st Local Ethic Commission in Warsaw and Committee for Ethics in Animal Research of Linköping in accordance with Polish, Swedish and EU legislations.

AUTHOR CONTRIBUTIONS

AW, MB, and BG conceived and designed the experiments. SN and MB performed the experiments in the Laboratory of Visual Neurobiology at the Nencki Institute of Experimental Biology of PAS. SN and BG carried on the experiments in the Department of Clinical and Experimental Medicine of Linköping University. SN, MB, and BG analyzed the data. SN, MB, EK, AW, and BG participated in the discussion of results and wrote the manuscript. All the authors approved the final version of the manuscript.

FUNDING

This research was supported by the European Union Regional Development Fund through the Foundation for Polish Science within the frames of the International Ph.D. Program in Neurobiology and by a grant from the National Science Center (2013/08/W/NZ4/00691).

REFERENCES

Agmon, A., and Connors, B. (1991). Thalamocortical responses of mouse somatosensory (barrel) cortex in vitro. *Neuroscience* 41, 365–379. doi: 10.1016/0306-4522(91)90333-j

Ahlsen, G., Lindstrom, S., and Lo, F. (1985). Interaction between inhibitory pathways to principal cells in the lateral geniculate nucleus of the cat. *Exp. Brain Res.* 58, 134–143. doi: 10.1007/BF00238961

Alitto, H., and Usrey, M. (2003). Corticothalamic feedback and sensory processing. *Curr. Opin. Neurobiol.* 13, 440–445. doi: 10.1016/s0959-4388(03)00096-5

Baker, D. M., Watson, S. P., and Santer, R. M. (1991). Evidence for a decrease in sympathetic control of intestinal function in the aged rat. *Neurobiol. Aging* 12, 363–365. doi: 10.1016/0197-4580(91)90023-d

Barthó, P., Freund, T., and Acsady, L. (2002). Selective GABAergic innervation of thalamic nuclei from zona incerta. *Eur. J. Neurosci.* 16, 999–1014. doi: 10.1046/j.1460-9568.2002.02157.x

Bekisz, M., and Wróbel, A. (1993). 20 Hz rhythm of activity in visual system of perceiving cat. *Acta Neurobiol. Exp.* 53, 175–182.

Benjamini, Y., and Hochberg, Y. (1995). Controlling the false discovery rate: a practical and powerful approach to multiple testing. *J.R. Stat. Soc. Ser. B* 57, 289–300. doi: 10.1111/j.2517-6161.1995.tb02031.x

Blitz, D. M., Foster, K. A., and Regehr, W. G. (2004). Short-term synaptic plasticity: a comparison of two synapses. *Nat. Rev. Neurosci.* 5, 630–640. doi: 10.1038/nrn1475

Castro-Alamancos, M., and Calcagnotto, M. (2001). High-pass filtering of corticothalamic activity by neuromodulators released in the thalamus during arousal: in vitro and in vivo. *J. Neurophysiol.* 85, 1489–1497. doi: 10.1152/jn.2001.85.4.1489

Cheng, K., Khurana, S., Chen, Y., Kennedy, R., Zimniak, P., and Raufman, J. (2002). Lithocholylcholine, a bile acid/acetylcholine hybrid, is a muscarinic receptor antagonist. *J. Pharmacol. Exp. Ther.* 303, 29–35. doi: 10.1124/jpet.102.036376

Clements, J. (1990). A statistical test for demonstrating a presynaptic site of action for a modulator for synaptic amplitude. *J. Neurosci. Methods* 31, 75–88. doi: 10.1016/0165-0270(90)90012-5

de Sevilla, D. F., Cabezas, C., de Prada, A. N. O., Sanchez-Jimenez, A., and Buno, W. (2002). Selective muscarinic regulation of functional glutamatergic Schaffer collateral synapses in rat CA1 pyramidal neurons. *J. Physiol.* 545, 51–63.

del Castillo, J., and Katz, B. (1954). Quantal components of the end-plate potential. *J. Physiol.* 124, 560–573. doi: 10.1113/jphysiol.1954.sp005129

Erisir, A., van Horn, S., and Sherman, M. (1997). Relative numbers of cortical and brainstem inputs to the lateral geniculate nucleus. *Proc. Natl. Acad. Sci. U. S. A.* 94, 1517–1520. doi: 10.1073/pnas.94.4.1517

Faber, D., and Korn, H. (1991). Applicability of the coefficient of variation method for analyzing synaptic plasticity. *Biophys. J.* 60, 1288–1294. doi: 10.1016/S0006-3495(91)82162-2

Fiedler, E., Marks, M., and Collins, A. (1987). Postnatal Development of Cholinergic Enzymes and Receptors in Mouse Brain. *J. Neurochem.* 49, 983–990. doi: 10.1111/j.1471-4159.1987.tb00990.x

Granseth, B. (2004). Dynamic properties of corticogeniculate excitatory transmission in the rat dorsal lateral geniculate nucleus in vitro. *J. Physiol.* 556, 135–146. doi: 10.1113/jphysiol.2003.052720

Granseth, B., Ahlstrand, E., and Lindstrom, S. (2002). Paired pulse facilitation of corticogeniculate EPSCs in the dorsal lateral geniculate nucleus of the rat investigated in vitro. *J. Physiol.* 544, 477–486. doi: 10.1113/jphysiol.2002.024703

Granseth, B., and Lindström, S. (2003). Unitary EPSCs of cortico-geniculate fibers in the rat dorsal lateral geniculate nucleus in vitro. *J. Neurophysiol.* 89, 2952–2960. doi: 10.1152/jn.01160.2002

Groh, A., de Kock, C. P. J., Wimmer, V. C., Sakmann, B., and Kuner, T. (2008). Driver or coincidence detector: modal switch of a corticothalamic giant synapse controlled by spontaneous activity and short-term depression. *J. Neurosci.* 28, 9652–9663. doi: 10.1523/JNEUROSCI.1554-08.2008

Guo, J. D., Hazra, R., Dabrowska, J., Muly, E. C., Wess, J., and Rainnie, D. G. (2012). Presynaptic muscarinic M2 receptors modulate glutamatergic transmission in the bed nucleus of the stria terminalis. *Neuropharmacology* 62, 1671–1683. doi: 10.1016/j.neuropharm.2011.11.013

Hannay, T., Larkman, A., Stratford, K., and Jack, J. (1993). A common rule governs the synaptic locus of both short-term and long-term potentiation. *Cell Biol.* 3, 832–841. doi: 10.1016/0960-9822(93)90217

Hanse, E., and Gustafsson, B. (2001). Vesicle release probability and pre-primed pool at glutamatergic synapses in area CA1 of the rat neonatal hippocampus. *J. Physiol.* 531, 481–493. doi: 10.1111/j.1469-7793.2001.0481i.x

Happe, H. K., Coulter, C. L., Gerety, M. E., Sanders, J. D., O'Rourke, M., Bylund, D. B., et al. (2004). Alpha-2 adrenergicreceptordevelopment in rat CNS: an autoradiographic study. *Neuroscience* 123, 167–178. doi: 10.1016/j.neuroscience.2003.09.004

Hirata, A., Aguilar, J., and Castro Alamancos, M. (2006). Noradrenergic activation amplifies bottom up and top down signal to noise ratios in sensory thalamus. *J. Neurosci.* 26, 4426–4436. doi: 10.1523/JNEUROSCI.5298-05.2006

Hoffmann, C., Leitz, M. R., Oberdorf-Maass, S., Lohse, M. J., and Klotz, K. N. (2004). Comparative pharmacology of human beta-adrenergic receptor subtypes–characterization of stably transfected receptors in CHO cells. *Naunyn Schmiedebergs Arch. Pharmacol.* 369, 151–159. doi: 10.1007/s00210-003-0860-y

Jahnsen, H., and Llinas, R. (1984). Electrophysiological properties of guinea pig thalamic neurons an in vitro study. *J. Physiol.* 349, 205–226. doi: 10.1113/jphysiol.1984.sp015153

Jakubik, J., Bacakova, L., El-Fakahany, E., and Tucek, S. (1997). Positive cooperativity of acetylcholine and other agonists with allosteric ligands on muscarinic acetylcholine receptors. *Mol. Pharmacol.* 52, 172–179. doi: 10.1124/mol.52.1.172

Klinkenberg, I., Sambeth, A., and Blokland, A. (2011). Acetylcholine and attention. *Behav. Brain Res.* 221, 430–442. doi: 10.1016/j.bbr.2010.11.033

Korn, H., and Faber, D. S. (1991). Quantal analysis and synaptic efficacy in the CNS. *Trends Neurosci.* 14, 439–445. doi: 10.1016/0166-2236(91)90042-s

Korn, H., Mallet, A., Triller, A., and Faber, D. (1982). Transmission at a central inhibitory synapse. Quantal description of release with a physical correlate of binomial n. *J. Neurophysiol.* 48, 679–707. doi: 10.1152/jn.1982.48.3.679

Korn, H., Triller, A., Mallet, A., and Faber, D. (1981). Fluctuating responses at a central synapse: n of binomial fit predicts number of stained presynaptic boutons. *Science* 213, 898–901. doi: 10.1126/science.6266015

Lam, Y., and Sherman, M. (2010). Functional organization of the somatosensory cortical layer 6 feedback to the thalamus. *Cereb. Cortex* 20, 13–24. doi: 10.1093/cercor/bhp077

Land, P., and Kandler, K. (2002). Somatotopic organization of rat thalamocortical slices. *J. Neurosci. Methods* 119, 15–21. doi: 10.1016/s0165-0270(02)00150-4

Landisman, C., and Connors, B. (2007). VPM and PoM nuclei of the rat somatosensory thalamus: intrinsic neuronal properties and corticothalamic feedback. *Cereb. Cortex* 17, 2853–2865. doi: 10.1093/cercor/bhm025

Lindström, S., and Wróbel, A. (1990). Frequency dependent corticofugal excitation of principal cells in the cat's dorsal lateral geniculate nucleus. *Exp. Brain Res.* 79, 313–318. doi: 10.1007/BF00608240

Livingstone, M. S., and Hubel, D. H. (1981). Effects of sleep and arousal on the processing of visual information in the cat. *Nature* 291, 554–561.

Llano, D. A., and Sherman, S. M. (2009). Differences in intrinsic Properties and local network connectivity of identified layer 5 and layer 6 adult mouse auditory corticothalamic neurons support a dual corticothalamic projection hypothesis. *Cereb. Cortex* 19, 2810–2826. doi: 10.1093/cercor/bhp050

Manabe, T., Wyllie, D., Perkel, D., and Nicoll, R. (1993). Modulation of synaptic transmission and long-term potentiation: effects on paired pulse facilitation and EPSC variance in the CA1 region of the hippocampus. *J. Neurophysiol* 70, 1451–1459. doi: 10.1152/jn.1993.70.4.1451

Masri, R., Trageser, J., Bezdudnaya, T., Li, Y., and Keller, A. (2006). Cholinergic regulation of the posterior medial thalamic nucleus. *J. Neurophysiol.* 96, 2265–2273. doi: 10.1152/jn.00476.2006

McDonald, J. H. (2014). *Handbook of biological statistics. Third edition*. Baltimore, MD: Sparky House Publishing, 299.

Michel, M. C. (1991). Receptors for neuropeptide Y: multiple subtypes and multiple second messengers. *Trends Pharmacol. Sci.* 12, 389–394. doi: 10.1016/0165-6147(91)90610-5

Nagumo, Y., Takeuchi, Y., Imoto, K., and Miyata, M. (2011). Synapse- and subtype-specific modulation of synaptic transmission by nicotinic acetylcholine receptors in the ventrobasal thalamus. *Neurosci. Res.* 69, 203–213.

Parker, M., Harvey, S., and Luetje, C. (2001). Determinants of agonist binding affinity on neuronal nicotinic receptor beta subunits. *J. Pharmacol. Exp. Ther.* 299, 385–391.

Pennartz, C. M., and Lopes da Silva, F. H. (1994). Muscarinic modulation of synaptic transmission in slices of the rat ventral striatum is dependent on the frequency of afferent stimulation. *Brain Res.* 645, 231–239. doi: 10.1016/0006-8993(94)91656-x

Peralta, E., Ashkenazi, A., Winslowl, J., Smith, D., Ramachandran, J., and Capon, D. (1987). Distinct primary structures, ligand-binding properties and tissue specific expression of four human muscarinic acetylcholine receptors. *EMBO J.* 6, 3923–3929.

Pita-Almenar, J., Yu, D., Lu, H., and Beierlein, M. (2014). Mechanisms underlying desynchronization of cholinergic-evoked thalamic network activity. *J. Neurosci.* 34, 14463–14474. doi: 10.1523/JNEUROSCI.2321-14.2014

Pu, Z., Krugers, H. J., and Joëls, M. (2009). β-adrenergic facilitation of synaptic plasticity in the rat basolateral amygdala in vitro is gradually reversed by corticosterone. *Learn. Mem.* 16, 155–160. doi: 10.1101/lm.1272409

Reichova, I., and Sherman, M. (2004). Somatosensory corticothalamic projections: distinguishing drivers from modulators. *J. Neurophysiol.* 92, 2185–2197. doi: 10.1152/jn.00322.2004

Romanelli, M., Manetti, D., Scapecchi, S., Borea, P., Dei, S., and Bartolini, A. (2001). Structure-Affinity Relationships of a Unique Nicotinic Ligand:N1-Dimethyl-N4-phenylpiperazinium Iodide (DMPP). *J. Med. Chem.* 44, 3946–3955. doi: 10.1021/jm010901y

Rouiller, E., and Welker, E. (2000). A comparative analysis of the morphology of corticothalamic projections in mammals. *Brain Res. Bull.* 53, 727–741. doi: 10.1016/s0361-9230(00)00364-6

Samuels, E., and Szabadi, E. (2008). Functional neuroanatomy of the noradrenergic locus coeruleus: its roles in the regulation of arousal and autonomic function part II: physiological and pharmacological manipulations and pathological alterations of locus coeruleus activity in humans. *Curr. Neuropharmacol.* 6, 254–285. doi: 10.2174/157015908785777193

Sara, S. (2009). The locus coeruleus and noradrenergic modulation of cognition. *Nat. Rev. Neurosci.* 10, 211–223. doi: 10.1038/nrn2573

Sarter, M., and Bruno, P. (2000). Cortical cholinergic inputs mediating arousal attentional processing and dreaming: differential afferent regulation of the basal forebrain by telencephalic and brainstem afferents. *Neuroscience* 95, 933–952. doi: 10.1016/s0306-4522(99)00487-x

Scanziani, M., Gahwiler, B., and Thomson, S. (1995). Presynaptic inhibition of excitatory synaptic transmission by muscarinic and metabotropic glutamate receptor activation in the hippocampus: are Ca2+ vhannels involved? *Neuropharmacol* 34, 1549–1557. doi: 10.1016/0028-3908(95)00119-q

Sherman, M., and Guillery, R. (2006). *Exploring the Thalamus and its Role in Cortical Function*. Cambridge, MA: MIT Press.

Sillence, M. N., Hooper, J., Zhou, G. H., Liu, Q., and Munn, K. J. (2005). Characterization of porcine beta1- and beta2-adrenergic receptors in heart, skeletal muscle, and adipose tissue, and the identification of an atypical beta-adrenergic binding site. *J. Anim. Sci.* 83, 2339–2348. doi: 10.2527/2005.83102339x

Sim, J., and Griffith, W. (1996). Muscarinic inhibition of glutamatergic transmissions onto rat magnocellular basal forebrain neurons in a thin-slice preparation. *Eur. J. Neurosci.* 8, 880–891. doi: 10.1111/j.1460-9568.1996.tb01575.x

Sjöström, P. J., Turrigiano, G., and Nelson, S. (2003). Neocortical LTD via Coincident Activation of Presynaptic NMDA and Cannabinoid Receptors. *Neuron* 39, 641–654. doi: 10.1016/s0896-6273(03)00476-8

Steriade, M. (2000). Corticothalamic resonance, states of vigilance and mentation. *Neuroscience* 101, 243–276. doi: 10.1016/s0306-4522(00)00353-5

Steriade, M., McCormick, D., and Sejnowski, T. (1993). Thalamocortical oscillations in the sleeping and arousal brain. *Science* 262, 679–685. doi: 10.1126/science.8235588

Sun, Y., and Beierlein, M. (2011). Receptor saturation controls short-term synaptic plasticity at corticothalamic synapses. *J. Neurophysiol.* 105, 2319–2329. doi: 10.1152/jn.00942.2010

Theyel, B., Llano, D., and Sherman, M. (2010). The corticothalamocortical circuit drives higher-order cortex in the mouse. *Nat. Neurosci.* 13, 84–88. doi: 10.1038/nn.2449

Trofimova, I., and Robbins, T. (2016). Temperament and arousal systems: a new synthesis of differential psychology and functional neurochemistry. *Neurosci. Behav. Rev.* 64, 382–402. doi: 10.1016/j.neubiorev.2016.03.008

Unal, A. B., Steg, L., and Epstude, K. (2012). The influence of music on mental effort and driving performance. *Accid. Anal. Prev.* 48, 271–278. doi: 10.1016/j.aap.2012.01.022

Van Horn, S., and Sherman, M. (2007). Fewer driver synapses in higher order than in first order thalamic relays. *Neuroscience* 146, 463–470. doi: 10.1016/j.neuroscience.2007.01.026

Varela, C. (2014). Thalamic neuromodulation and its implications for executive networks. *Front. Neural Circuits* 8:69. doi: 10.3389/fncir.2014.00069

Waterhouse, B. D., Mouradian, R., Sessler, F. M., and Lin, R. C. S. (2000). Differential modulatory effects of norepinephrine on synaptically driven responses of layer V barrel field cortical neurons. *Brain Res.* 868, 39–47. doi: 10.1016/S0006-8993(00)02261-7

Williams, S., and Johnston, D. (1990). Muscarinic depression of synaptic transmission at the hippocampal mossy fiber synapse. *J. Neurophysiol.* 64, 1089–1097. doi: 10.1152/jn.1990.64.4.1089

Wróbel, A. (2000). Beta activity: a carrier for visual attention. *Acta Neurobiol. Exp.* 60, 247–260.

Wróbel, A. (2014). "Attentional activation in cortico-thalamic loops of the visual system," in *New Visual Neurosciences*, eds J. S. Werner and L. M. Chalupa (Massachusetts: MIT Press).

Wróbel, A., Ghazaryan, A., Bekisz, M., Bogdan, W., and Kamiński, J. (2007). Two streams of attention-dependent beta activity in the striate recipient zone of cat's lateral posterior-pulvinar complex. *J. Neurosci.* 27, 2230–2240. doi: 10.1523/JNEUROSCI.4004-06.2007

Wróbel, A., and Kublik, E. (2001). "Modification of evoked potentials in the rat's barrel cortex induced by conditioning stimuli," in *Plasticity of Adult Barrel Cortex*, ed. M. Kossut (Johnson City, TN: Graham Publ. Corp).

Zhang, L., and Warren, R. (2002). Muscarinic and nicotinic presynaptic modulation of EPSCs in the nucleus accumbens during postnatal development. *J. Neurophysiol.* 88, 3315–3330. doi: 10.1152/jn.01025.2001

Zucker, R., and Regehr, W. (2002). Short term synaptic plasticity. *Annu. Rev. Physiol.* 64, 355–405. doi: 10.1146/annurev.physiol.64.092501.114547

Zucker, R. S. (1989). Short-term synaptic plasticity. *Ann. Rev. Neurosci.* 12, 13–31.

Conflict of Interest: The authors declare that the research was conducted in the absence of any commercial or financial relationships that could be construed as a potential conflict of interest.

frontiers in Neural Circuits

REVIEW
published: 25 May 2021
doi: 10.3389/fncir.2021.665009

Cortical and Subcortical Circuits for Cross-Modal Plasticity Induced by Loss of Vision

*Gabrielle Ewall[1†], Samuel Parkins[2†], Amy Lin[1], Yanis Jaoui[1] and Hey-Kyoung Lee[1,2,3]**

[1]Solomon H. Snyder Department of Neuroscience, Zanvyl-Krieger Mind/Brain Institute, Johns Hopkins School of Medicine, Baltimore, MD, United States, [2]Cell, Molecular, Developmental Biology and Biophysics (CMDB) Graduate Program, Johns Hopkins University, Baltimore, MD, United States, [3]Kavli Neuroscience Discovery Institute, Johns Hopkins University, Baltimore, MD, United States

Cortical areas are highly interconnected both via cortical and subcortical pathways, and primary sensory cortices are not isolated from this general structure. In primary sensory cortical areas, these pre-existing functional connections serve to provide contextual information for sensory processing and can mediate adaptation when a sensory modality is lost. Cross-modal plasticity in broad terms refers to widespread plasticity across the brain in response to losing a sensory modality, and largely involves two distinct changes: cross-modal recruitment and compensatory plasticity. The former involves recruitment of the deprived sensory area, which includes the deprived primary sensory cortex, for processing the remaining senses. Compensatory plasticity refers to plasticity in the remaining sensory areas, including the spared primary sensory cortices, to enhance the processing of its own sensory inputs. Here, we will summarize potential cellular plasticity mechanisms involved in cross-modal recruitment and compensatory plasticity, and review cortical and subcortical circuits to the primary sensory cortices which can mediate cross-modal plasticity upon loss of vision.

Keywords: cross-modal plasticity, cortical plasticity, cortical circuits, subcortical circuits, sensory loss, multi-sensory interaction, metaplasticity, functional connectivity

OPEN ACCESS

Edited by:
Julio C. Hechavarría, Goethe University Frankfurt, Germany

Reviewed by:
Lutgarde Arckens, KU Leuven, Belgium
Kai-Wen He, Interdisciplinary Research Center on Biology and Chemistry (CAS), China

****Correspondence:***
Hey-Kyoung Lee
heykyounglee@jhu.edu

†These authors have contributed equally to this work and share first authorship

Received: *06 February 2021*
Accepted: *14 April 2021*
Published: *25 May 2021*

Citation:
Ewall G, Parkins S, Lin A, Jaoui Y and Lee H-K (2021) Cortical and Subcortical Circuits for Cross-Modal Plasticity Induced by Loss of Vision. Front. Neural Circuits 15:665009. doi: 10.3389/fncir.2021.665009

Abbreviations: 5HT, 5-hydroxytryptamine; A1, primary auditory cortex; ACg, anterior cingulate cortex; AChR, acetylcholine receptor; AL, anterolateral area; aLP, anterior-ventral lateral posterior nucleus; AM, anteromedial area; AMPA, α-amino-3-hydroxy-5-methyl-4-isoxazolepropionic acid; BCM, Bienenstock-Cooper-Monroe; cAMP, cyclic adenosine 3, 5-monophosphate; dLGN, dorsal lateral geniculate nucleus; EEG, electroencephalogram; EPSC, excitatory postsynaptic current; fMRI, functional magnetic resonance imaging, GAD65, glutamic acid decarboxylase 65; GluN2B, glutamate receptor N-methyl-D-aspartate receptor subunit 2B; HVA, higher order visual areas; IC, intracortical; IPSC, inhibitory postsynaptic current; L1, layer 1; L2/3, layer 2/3; L4, layer 4; L5, layer 5; L6, layer 6; LD, lateral dorsal nucleus; LI, laterointermediate area; LM, lateromedial area; LP, lateral posterior nucleus; LSD, lysergic acid diethylamide; LTD, long-term depression; LTP, long-term potentiation; mAChR, muscarinic acetylcholine receptor; MD, mediodorsal nucleus; mEPSC, miniature excitatory postsynaptic current; mIPSC, miniature inhibitory postsynaptic current; MGBv, ventral division of medial geniculate body; mLP, medial lateral posterior nucleus; nAChR, nicotinic acetylcholine receptor; NMDAR, N-methyl-D-aspartate receptor; NTSR1, neurotensin receptor 1; ODP, ocular dominance plasticity; PFC, prefrontal cortex; PLC, phospholipase C; pLP, posterior-dorsal lateral posterior nucleus; PM, posteromedial area; PO, posterior thalamic nucleus; POm, posterior medial thalamic nucleus; POR, postrhinal area; PV, parvalbumin; RL, rostolateral area; RSP, retrosplenial cortex; S1, primary somatosensory cortex; SC, superior colliculus; SOM, somatostatin; STDP, spike timing dependent plasticity; TMS, transcranial magnetic stimulation; TRN, thalamic reticular nucleus; TTX, tetrodotoxin; V1, primary visual cortex; V2, secondary visual cortex; V2L, lateral secondary visual cortex; VEPs, visually evoked potentials; VIP, vasoactive intestinal peptide; VPM, ventral posteromedial nucleus.

INTRODUCTION

It is well established that sensory experience can alter cortical and subcortical circuits, especially during early development. In addition, proper sensory experience is crucial for interacting with our environment. Upon loss of a sensory modality, for example, vision, an individual has to rely on the remaining senses to navigate the world. It has been documented that blind individuals show enhanced ability to discriminate auditory (Lessard et al., 1998; Röder et al., 1999; Gougoux et al., 2004; Voss et al., 2004), tactile (Grant et al., 2000; Van Boven et al., 2000) or olfactory (Cuevas et al., 2009; Renier et al., 2013) information. Plastic changes involved can be robust and long–lasting. For example, individuals with congenital bilateral cataracts demonstrate heightened reaction times to auditory stimuli even in adulthood long after surgical removal of cataracts (De Heering et al., 2016). Experimental evidence suggests that there is a rather widespread functional plasticity in the adult sensory cortices upon loss of a sensory modality (Lee and Whitt, 2015), which could constitute the neural basis for cross-modal plasticity (Bavelier and Neville, 2002; Merabet and Pascual-Leone, 2010). Here we use the terminology "cross-modal plasticity" in a broad context to refer to plasticity triggered across sensory modalities to allow adaptation to the loss of sensory input. Changes associated with cross-modal plasticity are often attributed to two distinct plasticity mechanisms that take place across various sensory cortices, some of which manifest at the level of primary sensory cortices (**Figure 1**). One process is functional adaptation of the primary sensory cortex deprived of its own inputs, which is referred to as "cross-modal recruitment" (Lee and Whitt, 2015) or as "cross-modal plasticity" in its narrower definition (Bavelier and Neville, 2002; Merabet and Pascual-Leone, 2010). The other process, manifested as changes in the functional circuit of the spared sensory cortices, is termed "compensatory plasticity" (Rauschecker, 1995; Lee and Whitt, 2015). A dramatic example of cross-modal recruitment is the activation of visual cortical areas, including the primary visual cortex, when blind individuals are reading braille (Sadato et al., 1996; Buchel et al., 1998; Burton and McLaren, 2006). Compensatory plasticity is observed as functional changes in the circuits of primary auditory and somatosensory cortices of blind individuals (Pascual-Leone and Torres, 1993; Sterr et al., 1998a,b; Elbert et al., 2002). The former is thought to enhance the processing of the remaining senses by recruiting the deprived sensory cortex for increasing the capacity of processing the remaining senses, while the latter is thought to allow refinement of the ability of the spared cortices to process the remaining sensory inputs.

At the neural level, depriving vision leads to specific adaptation of functional circuits within the primary visual cortex (V1), and a distinct set of changes in the primary auditory (A1) and the primary somatosensory (S1) cortices (**Figure 2**). As will be discussed in more detail in the subsequent sections, the former involves potentiation of lateral intracortical connections to the principal neurons in the superficial layers of V1 (Petrus et al., 2015; Chokshi et al., 2019), and the latter manifests as potentiation of the feedforward inputs that convey sensory inputs to the cortex (Petrus et al., 2014, 2015; Rodríguez et al., 2018) as well as functional refinement of the cortical circuits (Meng et al., 2015, 2017; Solarana et al., 2019). Cellular mechanisms underlying these two distinct plasticity modes involve both Hebbian and homeostatic metaplasticity as we will describe below, and are thought to be the plasticity of pre-existing functional circuits.

Central to understanding the phenomenon of cross-modal plasticity is the question of what functional circuits allow multisensory information to influence cross-modal recruitment and compensatory changes in primary sensory cortices. The focus of this review will be identifying these potential cortical and subcortical circuits. Most of our discussion will be focused on studies from rodents, which recently have generated cell-type specific data on functional and anatomical connections.

CROSS-MODAL RECRUITMENT

Cross-modal recruitment describes the co-opting of a cortical area deprived of its own sensory input by the spared sensory modalities, so that those spared modalities may better guide behavior. While earlier studies have shown such cross-modal recruitment in early-onset blind individuals (Sadato et al., 1996; Buchel et al., 1998; Röder et al., 1999), a more recent study suggests that this can also manifest more acutely in adults. For example, temporarily blindfolding adults while training on braille leads to activation of V1 within a week as visualized in functional magnetic resonance imaging (fMRI; Merabet et al., 2008). Furthermore, this study demonstrated that V1 activity was essential for enhanced learning of braille reading in blindfolded individuals by showing that transcranial magnetic stimulation (TMS) of V1 removes this advantage in blindfolded adults. Cross-modal recruitment is not only restricted to the recruitment of V1 for other senses in blind but has been observed as activation of the auditory cortex by visual stimulation in deaf individuals (Sandmann et al., 2012). Hence such plasticity is thought to be a general principle across sensory cortices. While cross-modal recruitment is viewed as providing adaptive benefits to an individual, it has also been shown to restrict functional recovery of a deprived sense. For example, the success of restoring speech perception in deaf individuals using cochlear implants is inversely correlated with the degree of cross-modal recruitment of A1 by visual inputs (Sandmann et al., 2012).

Cellular and circuit-level plasticity related to cross-modal recruitment can be inferred from studies using various experimental paradigms designed to examine how the deprived cortices change following the loss of their respective sensory modalities. Sensory deprivation paradigms have been traditionally used to examine how sensory experience sculpts the developing sensory cortices. Starting from the initial pioneering work of Hubel and Wiesel, various visual deprivation studies have established the essential role of early visual experience in the proper development of both subcortical and cortical circuits serving visual processing (Hooks and Chen, 2020). While such studies demonstrate that visual cortical plasticity, i.e., ocular dominance plasticity (ODP), is limited to early development

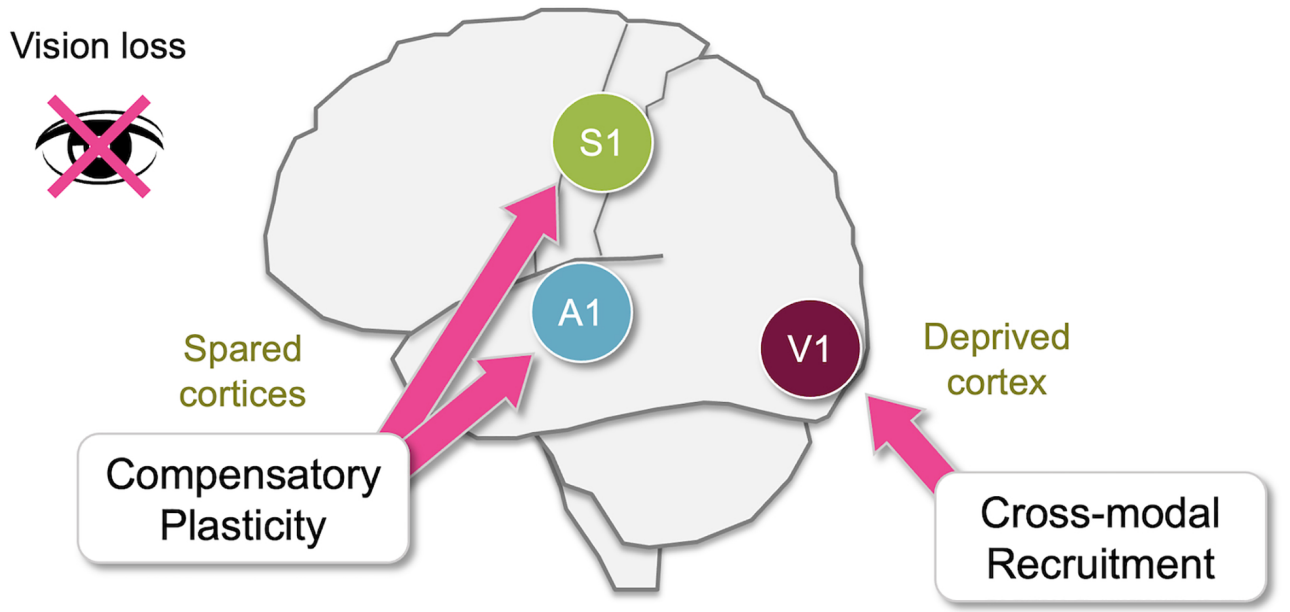

FIGURE 1 | Overview of cross-modal plasticity. Loss of a sensory modality, such as vision, triggers widespread adaptation across different brain areas referred to as cross-modal plasticity. Largely there are two distinct aspects of cross-modal plasticity: cross-modal recruitment and compensatory plasticity. The former involves recruitment of the deprived sensory cortex by the remaining senses, and the latter is manifested as a functional refinement of the spared sensory cortices. While many brain areas are involved in cross-modal plasticity, some of these changes manifest as plasticity at the level of the primary sensory cortices. In this review, we will discuss various cortical and subcortical pathways that are potentially involved in cross-modal plasticity of primary sensory cortices following loss of vision primarily focusing on functional connectivity of the mouse brain.

termed the "critical period," the adult visual cortex is not devoid of plasticity. In particular, total deprivation of vision, for example in the form of dark-rearing, has been shown to extend the critical period for ODP (Cynader and Mitchell, 1980; Mower et al., 1981), and the current model is that such deprivation paradigm triggers homeostatic metaplasticity or changes in cortical inhibition to promote Hebbian plasticity involved in ODP (Cooke and Bear, 2014; Hooks and Chen, 2020). Furthermore, total deprivation of vision later in life, in the form of dark-exposure, has been shown to restore ODP in the adult visual cortex (He et al., 2007). At a cellular level, the ability to induce long-term synaptic plasticity, such as long-term potentiation (LTP) and long-term depression (LTD), in sensory cortices is critically dependent on the lamina location of these synapses. For example, across primary sensory cortices, thalamocortical synapses to layer 4 (L4) has an early critical period for plasticity (Crair and Malenka, 1995; Feldman et al., 1998; Jiang et al., 2007; Barkat et al., 2011), but synapses from L4 to L2/3 undergo plasticity through adulthood (Jiang et al., 2007). Interestingly, L2/3 is considered a location where top-down contextual information is provided for sensory processing and has been shown to exhibit modulation of activity by other sensory modalities (Lakatos et al., 2007; Iurilli et al., 2012; Ibrahim et al., 2016; Chou et al., 2020). L2/3 is a logical substrate for cross-modal recruitment because of its susceptibility to adult plasticity and its role in integrating top-down multisensory inputs.

Plasticity of V1 Circuit That Can Support Cross-modal Recruitment

Vision loss alters the strength of both excitatory and inhibitory synaptic transmission on V1 L2/3 principal neurons. Experiments in rodents have demonstrated that even as little as 2 days of visual deprivation leads to the strengthening of excitatory synapses observed as increases in the average amplitude of miniature excitatory postsynaptic currents (mEPSCs; Desai et al., 2002; Goel and Lee, 2007; Maffei and Turrigiano, 2008; Gao et al., 2010; He et al., 2012; Chokshi et al., 2019). This plasticity, which was initially interpreted as a form of *in vivo* synaptic scaling (Desai et al., 2002; Goel and Lee, 2007), is observed around the 3rd postnatal week (Desai et al., 2002; Goel and Lee, 2007) and persists through adulthood (Goel and Lee, 2007; Petrus et al., 2015). However, strengthening of excitatory synapses by visual deprivation is dependent on the mode of visual deprivation, such that total loss of vision is necessary, and it is not observed with bilateral lid-suture (He et al., 2012). Lid-suture is different from other modes of visual deprivation, such as dark-exposure, enucleation, or intraocular tetrodotoxin (TTX) injection, in that visual stimuli through the closed eyelids can elicit visually evoked potentials (VEPs) in V1

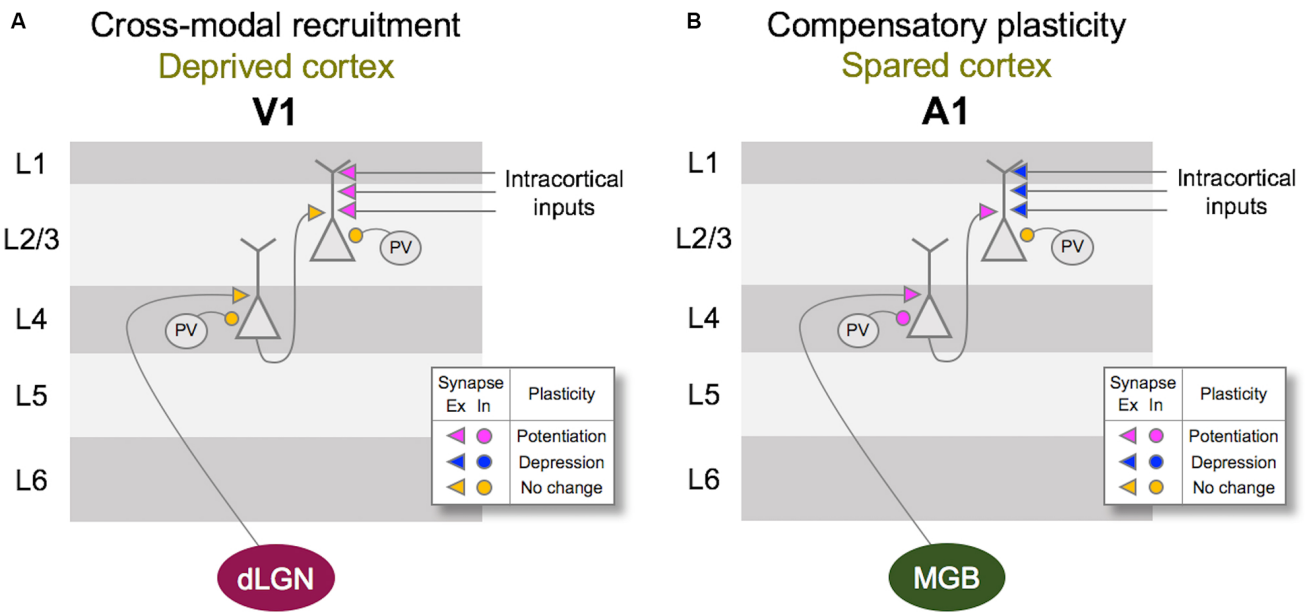

FIGURE 2 | Vision loss triggers cross-modal recruitment and compensatory plasticity across primary sensory cortices. **(A)** Summary of synaptic plasticity observed in V1 following the loss of vision. Synaptic connections that are examined are shown color-coded for potentiation (magenta), depression (dark blue), and no change (yellow) in synaptic strength. Excitatory (Ex) synapses are shown as arrowheads and inhibition (In) synapses are shown as circles. Vision loss does not alter the strength of excitatory feedforward connections from dLGN to Layer 4 (L4) or L4 to L2/3. There is no change in the inhibitory synaptic strength from PV interneurons to L4 or L2/3 principal neurons. In contrast, intracortical synapses onto L2/3 principal neurons potentiate. Based on the fact that L2/3 principal neurons receive multisensory information through long-range intracortical inputs, such adaptation is expected to allow cross-modal recruitment of V1 in the absence of vision. **(B)** Summary of synaptic plasticity observed in the spared A1. Feedforward excitatory synapses from MGBv to L4 as well as L4 to L2/3 potentiate following a week of visual deprivation. This is accompanied by a potentiation of PV inhibition to L4 principal neurons, but not to L2/3 principal neurons. In addition, intracortical excitatory synapses onto L2/3 principal neurons depress. Such synaptic changes are predicted to favor feedforward processing of information at the expense of intracortical influences, and may underlie lowered auditory threshold and refined frequency tuning of A1 L4 neurons following visual deprivation (Petrus et al., 2014).

(Blais et al., 2008). This suggests that residual vision through the closed eyelids is sufficient to prevent visual deprivation-induced synaptic scaling. Sensory deprivation-induced strengthening of excitatory synapses is not restricted to V1 L2/3 but is observed in A1 L2/3 following a conductive hearing loss (Kotak et al., 2005). Interestingly, whisker deprivation is typically unable to increase the strength of excitatory synapses in barrel cortex L2/3 neurons (Bender et al., 2006; He et al., 2012; Li et al., 2014; see Glazewski et al., 2017 for exception) which suggests that whisker deprivation may be similar to lid-suture in that it may not completely remove all inputs to the barrel cortex.

In addition to the plasticity of the excitatory synapses, inhibitory synapses on principal neurons in V1 also undergo lamina-specific adaptation to visual deprivation, which differs depending on the developmental age. In V1 L4 of rodents, monocular deprivation before the critical period leads to a reduction of inhibition, measured as a decrease in both spontaneous and evoked inhibitory postsynaptic currents (IPSCs) in the deprived monocular zone of V1 (Maffei et al., 2004), whereas monocular deprivation during the critical period leads to an increase in inhibition (Maffei et al., 2006; Nahmani and Turrigiano, 2014). With L4 serving as the main thalamorecipient layer, this increase in inhibition within L4 later in development could serve to lower the recurrent activity and reduce the propagation of sensory information in V1. In L2/3, a few days of visual deprivation during the critical period leads to a reduction in the frequency of miniature inhibitory postsynaptic currents (mIPSCs; Gao et al., 2010, 2014). This decrease in mIPSC frequency correlated with a reduction in the density of perisomatic GAD65 punta (Gao et al., 2014) suggesting a decrease in the number of inhibitory synaptic contacts likely from local parvalbumin-positive (PV) interneurons. However, visual deprivation-induced plasticity of inhibitory synapses in the adult V1 L2/3 is different in that it is specific to action potential-independent inhibitory synaptic transmission (Barnes et al., 2015; Gao et al., 2017), which suggests that it is not likely due to changes in the number of inhibitory synapses. The selective plasticity of action potential independent mIPSCs is thought to benefit sensory processing in the mature cortex by maintaining temporal coding while providing homeostasis of overall neural activity (Gao et al., 2017).

In terms of the mode of plasticity, initial studies have interpreted the overall increase in mEPSC amplitudes following visual deprivation in the framework of synaptic scaling (Desai et al., 2002; Goel and Lee, 2007). However, recent data suggest that the changes are not global across all synapses but are input-specific and restricted mainly to intracortical synapses without changes in the feedforward input from L4 (Petrus et al., 2015; **Figure 2A**). Furthermore, the increase in mEPSC amplitudes with visual deprivation requires NMDA receptor (NMDAR)

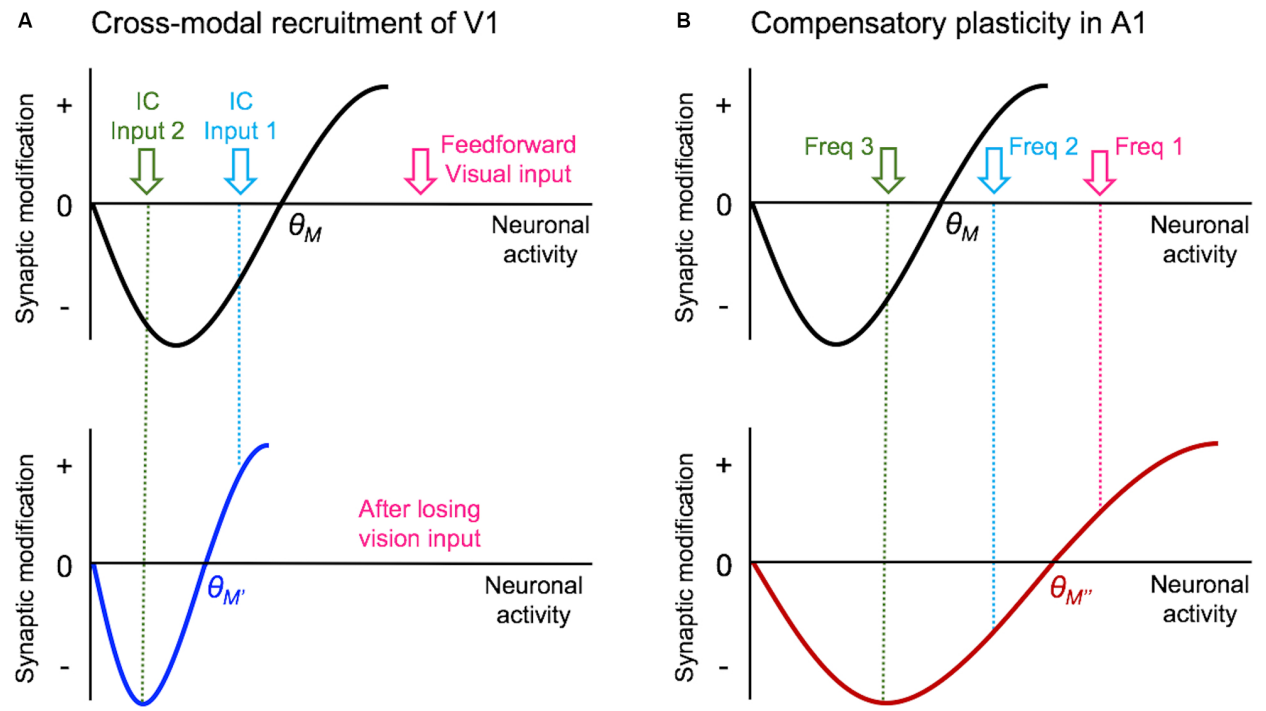

FIGURE 3 | Metaplasticity model for cross-modal synaptic plasticity induced by vision loss. The sliding threshold (or BCM) model of metaplasticity posits that the synaptic modification threshold (θ_M) for Long-term potentiation (LTP) and Long-term depression (LTD) slides as a function of past activity (Cooper and Bear, 2012). **(A)** In V1, loss of vision is expected to reduce the θ_M to a new value ($\theta_{M'}$), which will favor LTP induction. This will allow some of the stronger intracortical inputs (IC Input 1) to cross the threshold and potentiate. However, the weaker intracortical inputs (IC Input 2) will still fall below the $\theta_{M'}$ value and remain weaker. Such plasticity is expected to allow V1 neurons to preferentially respond to IC Input 1 in the absence of vision. As many of these intracortical inputs are multisensory, such as feedback projections from HVAs and other cortico-cortical connections, selective potentiation of intracortical synapses could allow V1 to process non-visual contextual information. **(B)** In the spared primary sensory cortex, as given an example of A1, loss of vision is thought to increase the synaptic modification threshold ($\theta_{M''}$) based on the observation that there is potentiation of feedforward excitatory inputs originating from MGBv. The resulting metaplasticity is expected to sharpen the response properties of A1 neurons, such that the strength of inputs carrying two close sound frequencies (Freq 1 and Freq 2) will separate further by a preferential strengthening of the most dominant frequency (Freq 1).

activation (Rodríguez et al., 2018), which distinguishes it from synaptic scaling which has been shown not to require the activity of NMDARs (O'Brien et al., 1998; Turrigiano et al., 1998). On the contrary, experimental evidence suggests that synaptic scaling induced by inactivity is accelerated when blocking NMDARs (Sutton et al., 2006). The observation that visual deprivation-induced potentiation of excitatory synapses in V1 L2/3 is input-specific and dependent on NMDAR activity suggests that it is likely a manifestation of Hebbian LTP following metaplasticity as proposed by the Bienenstock-Cooper-Monroe (BCM) model (Bienenstock et al., 1982; Bear et al., 1987; Cooper and Bear, 2012; Lee and Kirkwood, 2019; **Figure 3**). The BCM model, often referred to as the "sliding threshold" model, posits that the synaptic modification threshold for LTP/LTD induction "slides" is a function of the past history of neural activity. An overall reduction in neural activity, as would occur in V1 following visual deprivation, is expected to lower the synaptic modification threshold to promote LTP induction. Indeed, studies have demonstrated that visual deprivation can lower the LTP induction threshold in V1 L2/3 (Kirkwood et al., 1996; Guo et al., 2012). However, to induce LTP with the lowered synaptic modification threshold, synaptic activity is required. While visual deprivation reduces the overall activity in V1, a recent study reported that spontaneous activity is increased following a few days of visual deprivation in the form of dark exposure (Bridi et al., 2018). In addition, the study demonstrated that this increase in spontaneous activity is critical for strengthening excitatory synapses on V1 L2/3 neurons dependent on the activity of the GluN2B subunit of NMDARs (Bridi et al., 2018). It is possible that visual deprivation-induced reduction in the inhibitory synaptic transmission (Gao et al., 2010, 2014; Barnes et al., 2015) may contribute to enhance spontaneous activity or help facilitate the induction of LTP. Collectively, these studies suggest a novel model in which visual deprivation reduces the threshold for LTP induction, and the increase in spontaneous activity acts on NMDARs to trigger potentiation of excitatory synapses, which tend to be of intracortical origin. Therefore, understanding the potential source of these intracortical synapses to V1 L2/3 will provide insights into how V1 may undergo cross-modal recruitment in the absence of vision.

In the following sections, we will review potential cortical and subcortical structures that can mediate cross-modal plasticity observed with vision loss. The anatomical locations of these structures are highlighted in **Figure 4**. First, we will provide

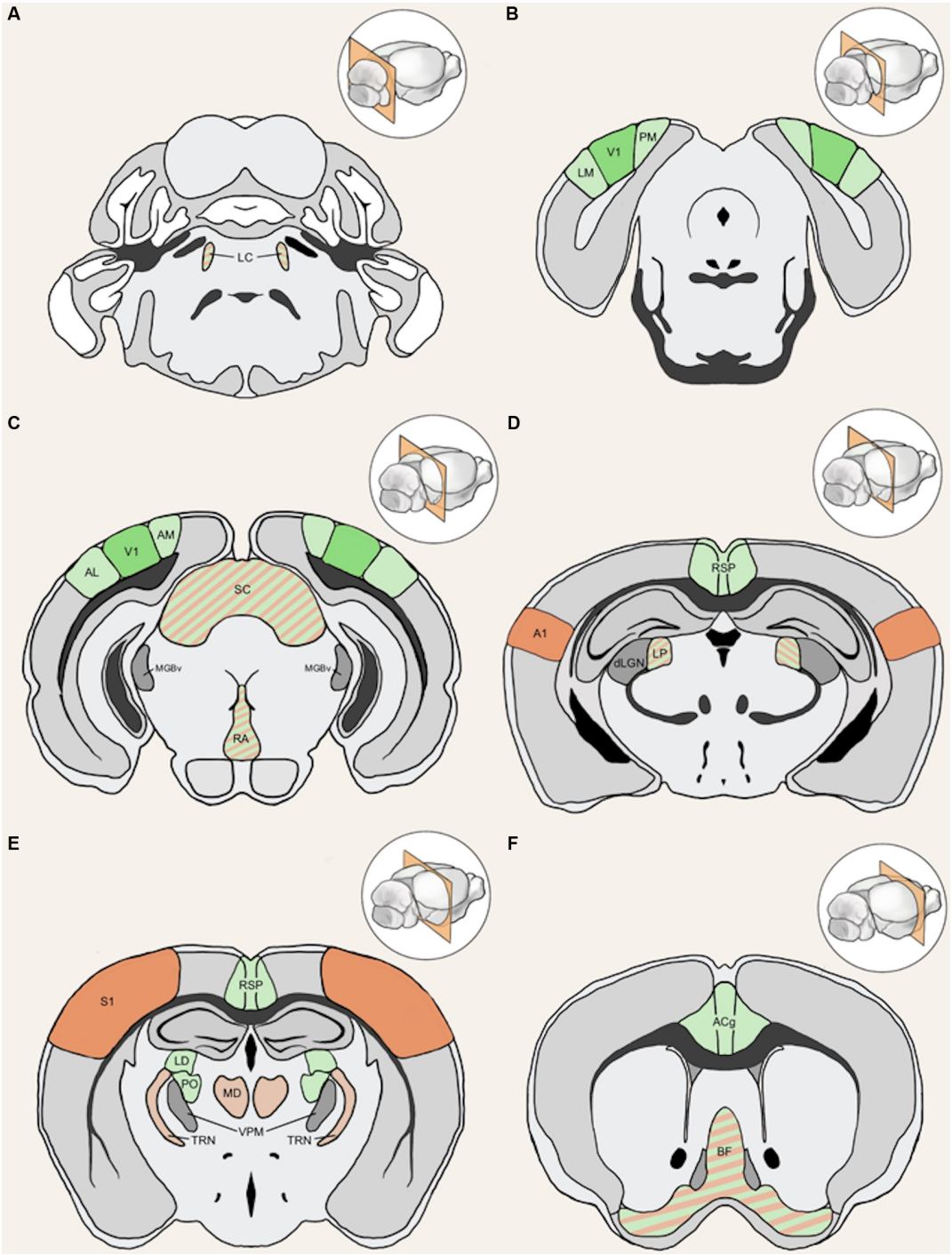

FIGURE 4 | Anatomical structures implicated in cross-modal plasticity induced by vision loss. Six coronal sections of a mouse brain are listed in order from posterior to anterior. Structures involved in cross-modal recruitment are labeled in green (V1, LM, PM, AM, AL, RSP, ACg, LD, PO), structures involved in compensatory plasticity are labeled in orange (A1, S1, MD, TRN), and those involved in both are labeled with stripes of green and orange (LC, superior colliculus (SC), RA, LP, BF). Darker shades (V1, A1, S1) represent cortical structures that have been experimentally demonstrated to undergo plasticity with visual deprivation, while lighter shades are tentative structures implicated in the plasticity. Primary sensory thalamic nuclei are labeled in gray (dLGN, MGBv, VPM). Inset in each panel shows the location of the coronal section plane. **(A)** The locus coeruleus (LC) contains the cell bodies of most norepinephrine expressing neurons. These cells send vast projections across cortical areas and are involved in both attention and arousal. Following vision loss, the increased salience of auditory and somatosensory cues might be conveyed through norepinephrine projections, facilitating potentiation in spared sensory cortices (compensatory plasticity) as well as potentiation of spared inputs into V1 (cross-modal recruitment). The relative concentration of norepinephrine is thought to play a role in determining the polarity spike-timing-dependent

(*Continued*)

FIGURE 4 | Continued
of plasticity (STDP; Seol et al., 2007). **(B)** The lateral medial visual area (LM) and the posteromedial visual area (PM) are both HVAs, which flank V1. HVAs process higher-order visual information and provide feedback connections to V1 which modulate V1 activity. Visual deprivation leads to plasticity specifically of intracortical inputs in L2/3 pyramidal neurons without changes in the strength of feedforward inputs from the thalamus to L4 or from L4 to L2/3 (Petrus et al., 2014, 2015; Chokshi et al., 2019; see **Figure 2A**). **(C)** This section shows V1 in addition to the anterolateral visual area (AL) and the anteromedial visual area (AM), which are both a part of the HVA. The section also includes the SC, the primary auditory thalamus (MGBv), and the raphe nuclei (RA). SC is an area of the brain that is in charge of processing sensory input and is involved in the integration of visual, auditory, and tactile stimuli, hence could play a role in cross-modal plasticity. MGBv transmits auditory information to A1. Visual deprivation induces potentiation of MGBv synapses to A1 L4 principal neurons (Petrus et al., 2014; see **Figure 2B**). RA is found in the brain stem and contains serotonergic neurons. Serotonin is implicated in cross-modal recruitment of V1 (Lombaert et al., 2018) and compensatory plasticity of S1 (Jitsuki et al., 2011) following visual deprivation. **(D)** This section contains the lateral posterior thalamic nucleus (LP), the retrosplenial cortex (RSP), the primary visual thalamus (dLGN), and the primary auditory cortex (A1). LP is a higher-order visual thalamus in rodents, which is equivalent to the pulvinar in primates. LP receives input from SC and influences V1, and it has been shown to reduce background noise to enhance visual responses (Fang et al., 2020). SC to LP circuit mainly targets inhibitory neurons in L1 of V1 (Fang et al., 2020). RSP is interconnected with the lateral dorsal nucleus of thalamus (LD; Shibata, 2000). LD is a higher-order thalamic nucleus that plays a part in learning and memory and may transmit somatosensory information to V1. A1 processes auditory information and undergoes compensatory plasticity in the absence of vision (Goel et al., 2006; Petrus et al., 2014, 2015; Meng et al., 2015, 2017; Solarana et al., 2019; see **Figure 2B**). **(E)** The retrosplenial cortex (RSP) along with the mediodorsal nucleus of the thalamus (MD), the thalamic reticular nucleus (TRN), and the primary somatosensory cortex (S1) are highlighted. RSP is a multisensory cortical area that sends projections to V1 (see **Figure 5**). MD is a higher-order thalamic nucleus that is reciprocally connected with the prefrontal cortex and projects to TRN. MD is involved in attention and learning by gating sensory inputs. TRN is a band of inhibitory neurons that provides the major corticothalamic feedback inhibition to the primary sensory thalamic nuclei. Hence, TRN is in an ideal position to regulate feedforward excitatory thalamocortical input to A1 and S1 to mediate compensatory plasticity. S1 processes tactile information and undergoes compensatory plasticity in the absence of vision (Goel et al., 2006; Jitsuki et al., 2011; He et al., 2012). **(F)** The basal forebrain (BF) and the anterior cingulate cortex (ACg) are highlighted in this section. BF includes structures involved in the production of acetylcholine, including the nucleus basalis and medial septum, which affects attention and plasticity. ACg is a multisensory cortex that has direct and indirect functional connections to V1 (see **Figure 5**).

information on potential functional circuits involved in cross-modal recruitment of V1, which involve cortico-cortical connections from multisensory or spared sensory cortices. Some of these cortical interactions involve indirect functional circuits mediated by subcortical structures. In addition, we will outline various neuromodulatory systems, which can enhance or enable plasticity of these intracortical and subcortical inputs to V1.

Cortical Inputs to V1 L2/3 That Can Mediate Cross-modal Recruitment

V1 L2/3 cells are a probable substrate for multimodal recruitment of V1 due to their extensive and varied inputs. Intracortical inputs onto L2/3 of V1 originate from various sources, including local connections from within V1, feedback projections from higher-order visual areas (HVAs), other sensory cortices, as well as other cortical areas (e.g., Wertz et al., 2015; **Figure 5**). A recent monosynaptic tracing of presynaptic partners of a single V1 L2/3 pyramidal neuron showed that these neurons receive inputs from 70 to 800 neurons across many brain regions with the majority of them (50–700 neurons) situated within V1 (Wertz et al., 2015). In addition to these local inputs, V1 L2/3 neurons receive multisensory information from other cortical areas via direct long-range intracortical connections, as well as indirectly via subcortical structures (**Figure 5**; "Subcortical Sources of Inputs to V1 L2/3 That Can Mediate Cross-modal Recruitment" section). Therefore, V1 L2/3 could mediate a role in cross-modal recruitment in the absence of vision.

Cortical inputs that reside locally within V1 serve as the major source of excitatory inputs onto L2/3 neurons with local L2/3 inputs being the most numerous (Binzegger et al., 2004; Wertz et al., 2015) with connections heavily favored between neurons showing similar functional properties (Ko et al., 2011; Wertz et al., 2015; Lee et al., 2016). Neurons across the various layers are interconnected to allow for the efficient processing of information. Visual information is transmitted from the primary visual thalamus (dLGN), which densely projects onto V1 L4 neurons. L4 principal neurons relay this information across V1, but most prominently onto L2/3 neurons (Binzegger et al., 2004; Wertz et al., 2015). L5 is mainly an output layer, projecting to HVAs, the contralateral cortex, the striatum, the higher-order thalamus, and other subcortical targets, but it also projects locally within V1 to L2/3 (Binzegger et al., 2004; Kim et al., 2015; Ramaswamy and Markram, 2015; Wertz et al., 2015). L5 neurons integrate inputs from a variety of sources, including local inputs from L4 and L2/3 (Binzegger et al., 2004; Wertz et al., 2015) as well as feedback projections from HVAs and multisensory cortical areas such as the retrosplenial cortex (Kim et al., 2015). The output from lower L5 (L5b) to higher-order visual thalamus (lateral posterior nucleus, LP; Kim et al., 2015; Roth et al., 2016) allows indirect communication from V1 to HVA forming a transthalamic or cortico-thalamo-cortical loop (Sherman, 2016). L6 is a thalamorecipient layer, like L4, and also receives local inputs from L2/3, L4, and L5 as well as feedback projections from HVAs (Thomson, 2010). A subset of L6 neurons, which are identified by the marker NTSR1 (Gong et al., 2007), project back to the dLGN to provide corticothalamic feedback (Olsen et al., 2012; Bortone et al., 2014; Sundberg et al., 2018), which also involves disynaptic inhibition through the thalamic reticular nucleus (TRN; Olsen et al., 2012). Corticothalamic L6 neurons also project locally within V1, and it has been observed that they may provide net inhibition to the other layers (Olsen et al., 2012; Bortone et al., 2014) *via* recruitment of L6 fast-spiking interneurons with translaminar projections (Bortone et al., 2014). While local connectivity within V1 serves to process visual information, it can also convey multisensory information to L2/3. In particular, infragranular layers receive multisensory information from other cortical and subcortical areas (Thomson, 2010; Kim et al., 2015).

A second major source of cortical inputs to V1 L2/3 is feedback connections from HVAs (Wertz et al., 2015). In higher mammals, including humans and primates, HVAs integrate and process higher-order visual information, such as form and

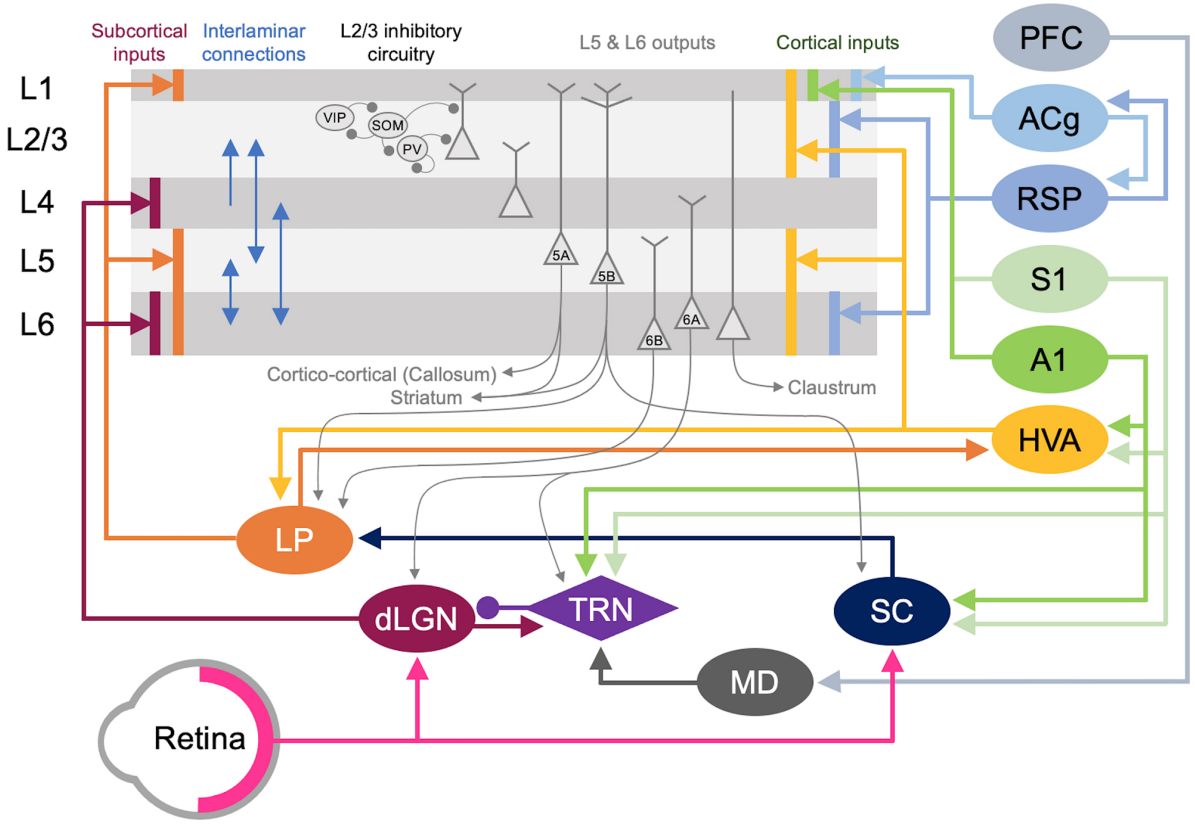

FIGURE 5 | Cortical and subcortical circuits for multisensory influence on V1. The laminar profile of subcortical inputs from dLGN and LP to V1 is shown on the left. Major interlaminar excitatory connections are shown next in blue arrows followed by the inhibitory local circuit in L2/3. Next, the major outputs of L5 and L6 neurons are shown. At the rightmost side, the origins and laminar profiles of cortical inputs to V1 are shown. Subcortical structures are shown below V1 and cortical structures are listed on the right side. Arrows (→) depict excitatory inputs and inputs ending in a round circle (—•) show inhibitory connections. The extent of the spread of inputs to V1 that span different laminae are depicted as vertical bars. V1 L2/3 and L5A neurons form reciprocal connections with HVA neurons (Kim et al., 2015; Glickfeld and Olsen, 2017), which is omitted in the figure for clarity. Direct cortico-cortical connections that can provide multisensory information to V1 originate from HVA, A1, S1, RSP, and ACg. In addition, as depicted in the figure many of the subcortical and cortical structures form cortico-thalamo-cortical loops that can provide multisensory influence on V1: for example, HVA–LP–V1, PFC–MD–TRN–dLGN–V1, S1/A1–TRN–dLGN–V1, and S1/A1–SC–LP–V1.

movement of objects (Orban, 2008). In rodents, 10 HVAs are anatomically identified, using intrinsic signal imaging, surrounding V1 (Garrett et al., 2014; Glickfeld and Olsen, 2017). While in primates and carnivores, HVAs are mostly hierarchically organized such that the main feedback to V1 is from the secondary visual cortex (V2, area 18; Felleman and Van Essen, 1991), in rodents each HVA is highly interconnected with V1 and send direct feedback projections to V1 (Glickfeld and Olsen, 2017). Direct cortico-cortical feedback connections from HVAs originate in L2/3 and L5 and arrive through L1, L2/3 as well as L5/6 of V1 (Glickfeld and Olsen, 2017). These feedback connections from HVAs have been shown to synapse onto pyramidal neurons as well as PV interneurons (Johnson and Burkhalter, 1996; Yang et al., 2013; Lu et al., 2014), thereby recruiting both the excitatory and inhibitory networks in V1 with a functional bias towards excitation (Shao and Burkhalter, 1996). In rodents, HVA neurons that provide feedback to V1 are reciprocally connected to HVA projecting V1 neurons in L2/3 (Johnson and Burkhalter, 1997), forming a closed-loop circuit which may amplify the feedback control of V1 (Glickfeld and Olsen, 2017). In addition to direct cortico-cortical connections, HVAs and V1 are indirectly connected via the higher-order thalamus. For example, HVAs send feedforward projections to the pulvinar (lateral posterior nucleus, LP, in rodents), a higher-order visual thalamus, which then sends projections to L1 and deeper layers of V1 (Roth et al., 2016; Zhou et al., 2017; Fang et al., 2020). Hence, HVAs can influence V1 processing via both cortico-cortical and indirect cortico-thalamo-cortical feedback loops.

The influence of HVA feedback connections in V1 is highlighted by a phenomenon called the perceptual "filling-in" effect (Weil and Rees, 2011). Individuals with a focal scotoma will perceive the missing visual space as being "filled-in" such that the person is often unaware of the scotoma (Bender and Teuber, 1946). Because this "filled-in" percept contains higher-order visual features, such as texture, the information is thought to originate from HVAs (Ramachandran and Gregory, 1991; Zur and Ullman, 2003). Recent studies using rodents also have shown that V1 neurons can respond to higher-order visual features in awake preparations and that these

responses are dependent on feedback connections from HVAs as demonstrated using optogenetic silencing (Keller et al., 2020; Pak et al., 2020). In addition to feedforward information originating from V1, HVAs receive multisensory information *via* connections from other sensory cortices (Gamanut et al., 2018). For example, V2L, which is an HVA lateral to V1 corresponding to anterolateral area (AL; Meijer et al., 2020) and lateromedial (LM; Sanderson et al., 1991), receive connections from both V1 and A1 (Laramee et al., 2011). A1 projections to V2L mainly terminate in supra- and infragranular layers (Laramee et al., 2011). L5 neurons in V2L provide major feedback to V1 (Bai et al., 2004) and receive direct inputs from A1 on their apical and basal dendrites (Laramee et al., 2011), thus demonstrating an A1-V2L-V1 pathway. The rostrolateral area (RL), another HVA in rodents, has been shown to receive tactile information from S1 as verified through whole-cell recordings and tracing studies (Olcese et al., 2013). Therefore, feedback projections from HVAs can relay other sensory information to V1.

In addition to the indirect route through HVAs, other sensory modalities can also gain access to V1 via direct connections (**Figure 5**). Anatomical tracing studies have demonstrated direct cortico-cortical projections from A1 (Iurilli et al., 2012; Wertz et al., 2015; Ibrahim et al., 2016; Deneux et al., 2019) and S1 (Wertz et al., 2015), especially to the superficial layers of V1. Recent studies showed that these projections are functional and can influence V1 processing (Iurilli et al., 2012; Ibrahim et al., 2016; Deneux et al., 2019). Ibrahim and colleagues (2016) found that sound increases the spike rate and sharpens orientation selectivity of V1 L2/3 neurons. This study further demonstrated that sound activates a disinhibitory circuit in L1 and L2/3 involving vasoactive intestinal peptide-positive (VIP) and somatostatin-positive (SOM) interneurons, which is mediated by a direct functional connection from A1 L5 that arrives through V1 L1 (Ibrahim et al., 2016). A1 neurons also have been shown to project directly to PV interneurons in V1 (Lu et al., 2014; Ibrahim et al., 2016), however, PV neuronal responses are not effectively altered by sound (Ibrahim et al., 2016). Interestingly, the influence of A1 on V1 appears to be context-dependent. A1 projections to V1 have a net excitatory effect in the presence of visual stimuli but a net inhibitory effect in the absence of visual stimuli (Deneux et al., 2019). These projections predominantly originate from A1 L5 neurons encoding loud sound (Deneux et al., 2019). The role of SOM inhibitory circuit in cross-modal recruitment is also evident with monocular enucleation paradigm (Scheyltjens et al., 2018), where the deprived monocular zone of V1 becomes reactivated by whisker inputs (Van Brussel et al., 2011). In addition to the inhibitory circuit within L2/3 of V1, L1 inhibitory neurons can also provide multisensory influence on V1 functionality. For example, L1 inhibitory neurons contain a subpopulation of neurons that respond to whisker touch (Mesik et al., 2019). Multisensory influence on neural activity is not limited to V1: whisker stimulation and visual stimulation produce subthreshold responses in A1, and likewise, auditory stimulation and visual stimulation produce subthreshold responses in S1 (Iurilli et al., 2012; Maruyama and Komai, 2018). Subthreshold influence on primary sensory cortical activity by other sensory modalities is not just restricted to rodents but has also been reported in awake primates (Lakatos et al., 2007). While there are direct anatomical pathways between primary sensory cortices in primates (Falchier et al., 2002; Cappe and Barone, 2005), the somatosensory evoked oscillations in L2/3 of A1 are thought to occur via subcortical inputs based on their short latency (Lakatos et al., 2007). Such subcortical sources will be discussed in the next section. Overall, cross-modal influence seems to be a general property of primary sensory cortices across species.

Multisensory cortical regions serve as another source through which V1 can be recruited by other sensory modalities after the loss of vision (**Figure 5**). One such region is the anterior cingulate cortex (ACg). Using tracing methods, it was shown that ACg neurons contain two distinct populations, L2/3, and L5 neurons that project directly to V1 and neurons primarily in L5 that project to the superior colliculus (SC; Zhang et al., 2016). Consistent with this anatomy, ACg has been shown to directly (Zhang et al., 2016) and indirectly (Hu et al., 2019) modulate the activity of V1 neurons. Optogenetic activation of ACg axons elicits a short latency monosynaptic EPSC and a longer latency disynaptic IPSC in V1 L2/3 neurons (Zhang et al., 2014), which illustrates recruitment of both excitatory and inhibitory networks. There are two indirect routes through which the ACg exerts its modulatory activity on V1 neurons. The first is through the SC and the posterior lateral posterior nucleus of the thalamus (pLP; ACg-SC-pLP-V1) and the second via the anterior LP (ACg-aLP-V1; Hu et al., 2019). Activating both pathways enhances visual behavior as well as responses in V1 neurons (Hu et al., 2019). While LP receives inputs from ACg and projects to V1, whether the ACg recipient LP neurons are the ones projecting to V1 is unclear. A recent study suggests that ACg projects to medial LP (mLP), which does not project directly to V1, but to HVAs (AL, RL, AM, PM; Bennett et al., 2019). Since the HVAs project to V1, this suggests a more indirect pathway in which ACg could influence V1 function.

The retrosplenial cortex (RSP) is another multisensory area directly linked to V1. Neurons from the RSP were shown to directly synapse unto V1 L2/3 neurons (Wertz et al., 2015) and L6 cortico-thalamic neurons (Vélez-Fort et al., 2014). These V1 projecting RSP neurons were also shown to be responsive to rotation implicating them as a potential source of head-related motion signals to V1 (Vélez-Fort et al., 2014). The RSP also received inputs directly from A1 and indirectly from S1 through the claustrum (Todd et al., 2019). RSP also forms reciprocal cortico-cortical connections between ACg and V1 (ACg–RSP–V1; Zhang et al., 2016). The influence of multisensory cortex on sensory processing is not limited to V1. Pairing of a tone with the activation of the frontal cortex leads to enhanced frequency selectivity and functional organization in A1 neurons (Winkowski et al., 2018).

Recently, posterior parietal cortex (PPC) has been suggested to play a role in cross-modal recruitment (Gilissen and Arckens, 2021). This is based on the multisensory nature of PPC and its functional modulation of V1 (Hishida et al., 2018). Recent studies demonstrated that PPC is involved in resolving sensory conflict

during auditory-visual discrimination tasks (Song et al., 2017) and is involved in transferring sensory-specific signals to higher order association areas (Gallero-Salas et al., 2021). RL and AM, two HVAs, are considered part of the PPC because they display connectivity patterns similar to other components of the PPC (Gilissen et al., 2021).

Subcortical Sources of Inputs to V1 L2/3 That Can Mediate Cross-modal Recruitment

In addition to inputs from cortical areas, V1 also receives multimodal information from various subcortical regions (**Figure 5**). The lateral posterior nucleus (LP), posterior thalamic nucleus (PO), and lateral dorsal nucleus of the thalamus (LD) all project directly to V1 and might be potential sources of multimodal input subserving cross-modal recruitment.

The higher-order visual thalamus, called the lateral posterior nucleus (LP) in rodents, is equivalent to the pulvinar in primates (Baldwin et al., 2017; Zhou et al., 2017). A recent study suggests that LP can be subdivided into three portions based on connectivity: (1) posterior-dorsal LP (pLP) receives input primarily from SC and HVAs which are considered the "ventral stream" equivalent in rodents (LI, POR); (2) anterior-ventral LP (aLP) receives input primarily from V1 and HVAs considered the "dorsal stream" (AL, RL, AM, PM); and (3) mLP with inputs from frontal cortical areas (ACg and orbitofrontal; Bennett et al., 2019). Most of the projections to LP are reciprocal, but they also form a cortico-thalamo-cortical loop (Sherman, 2016) to connect different cortical areas. Cortical inputs to LP originate from L5/6 of the cortical areas (Roth et al., 2016). The major subcortical input to LP is from the SC (Ibrahim et al., 2016; Roth et al., 2016; Zingg et al., 2017), which integrates multisensory information and is implicated in spatial attention (Krauzlis et al., 2013). Superficial layers of SC receive visual information from both V1 and retina (Krauzlis et al., 2013; Zingg et al., 2017; Cang et al., 2018), while intermediate and deep layers receive multimodal inputs (Krauzlis et al., 2013; Cang et al., 2018) and inputs from HVAs (Krauzlis et al., 2013). LP projects to L4 of HVAs and predominantly to L1 and deep layers of V1 (Roth et al., 2016; Zhou et al., 2017; Bennett et al., 2019). Hence, LP is in a position to influence V1 processing either directly or indirectly through HVAs. It was recently demonstrated in rodents that LP provides contextual information to V1, especially pertaining to distinguishing self-generated motion, and information from a wider visual field from that of local V1 neurons (Roth et al., 2016). In addition, it was reported that LP acts to enhance V1 L2/3 responses by subtracting "noisy" background information from visual stimuli (Fang et al., 2020). This effect was shown to occur *via* a bottom-up alternative pathway originating from the retina that routes through SC to LP, which then makes functional connections to inhibitory neurons in V1 L1 (Fang et al., 2020). Based on the multisensory information it receives *via* SC, it is possible that LP inputs may provide other sensory information to V1 in the absence of vision. In support of this idea, a recent study demonstrated that LP conveys visual information arising from SC to A1 (Chou et al., 2020). In particular, it was shown that this subcortical circuit allows a visual looming stimulus, which produces an innate fear response in mice (Yilmaz and Meister, 2013), to sharpen frequency tuning and increase the signal to noise ratio of auditory responses in L2/3 of A1 (Chou et al., 2020). It was demonstrated that SC-LP input to A1 activates inhibitory neurons in L1 as well as PV interneurons in L2/3 (Chou et al., 2020). It is interesting to contrast this with the previously discussed enhancement of tuning and signal-to-noise ratio in V1 L2/3 with sound, which involved direct input from A1 L5 (Ibrahim et al., 2016). Whether similar indirect influence through LP can provide cross-modal modulation of V1 responses remains to be determined.

The posterior thalamic nucleus (PO) and lateral dorsal nucleus of thalamus (LD) also project directly to V1 (van Groen and Wyss, 1992; Charbonneau et al., 2012). PO is a higher-order somatosensory relay nucleus, hence its direct projection to V1 could become a channel for providing somatosensory information and form the basis for cross-modal recruitment following vision loss. In addition, PO has direct projections to several HVAs (Sanderson et al., 1991; Olcese et al., 2013), which might mediate indirect influence on V1. LD is extensively interconnected with RSP (Shibata, 2000) and the hippocampal formation (Todd et al., 2019), and LD contains head direction cells that require visual inputs (Mizumori and Williams, 1993). These findings have led to the characterization of LD as a higher-order thalamic nucleus involved in learning and memory. More recently, the finding that neurons in LD respond to whisker stimulation (Bezdudnaya and Keller, 2008) suggests that LD might relay somatosensory information to V1.

Neuromodulatory Influences on Cross-modal Recruitment

As described above, there are numerous sources of cortical and subcortical input to V1 that could serve as substrates for allowing other sensory systems to recruit V1. One key plasticity mechanism that can aid in the cross-modal recruitment is the potentiation of the lateral intracortical inputs to V1 L2/3 observed following several days of total visual deprivation (Petrus et al., 2015). This particular study did not identify the source of these glutamatergic intracortical inputs, and these synapses were defined as intracortical based on exclusion criteria that they were not from L4 (Petrus et al., 2015). Hence, in addition to "true" intracortical inputs carrying multisensory information, they could also include subcortical excitatory synapses described above. The functional consequence of potentiating these intracortical excitatory synapses is that it would allow the normally subthreshold multisensory influences to potentially cross the action potential threshold to recruit the dormant V1 for processing information from the intact senses. As discussed in a previous section ("Plasticity of V1 Circuit That Can Support Cross-modal Recruitment" section), the synaptic plasticity mechanism that is thought to allow potentiation of these intracortical synapses is likely a reduction in the synaptic modification threshold via metaplasticity triggered by the loss of visually evoked activity in V1. As intracortical inputs would retain activity driven from the intact senses, it is possible that their activity would

cross the lowered synaptic modification threshold to produce NMDAR-dependent LTP (**Figure 3A**). However, in addition to the lowered synaptic modification threshold, other factors might be at play to enhance the plasticity of the intracortical inputs.

Neuromodulators such as acetylcholine, norepinephrine, and serotonin play a key role in facilitating plasticity (Gu, 2002). In V1 L2/3, norepinephrine and acetylcholine are involved in sharpening spike timing-dependent plasticity (STDP), and their relative concentrations are thought to determine the polarity of STDP (Seol et al., 2007; Huang et al., 2012). While the initial studies showed that activation of beta-adrenergic receptors and muscarinic acetylcholine receptors (mAchRs) are respectively critical for LTP and LTD, it is now clear that this effect is due to the differential coupling of these receptors to downstream second messenger signaling. Regardless of the neuromodulators, activation of cAMP-coupled receptors is critical for LTP while phospholipase C (PLC)-coupled receptors are involved in LTD (Huang et al., 2012). Both norepinephrine and acetylcholine have been shown critical for *in vivo* sensory experience-dependent plasticity, as they are necessary for (Bear and Singer, 1986; Imamura and Kasamatsu, 1989) and can accelerate (Hong et al., 2020), ocular dominance plasticity in V1. Norepinephrine and acetylcholine are associated with arousal and attention, hence if they are involved in cross-modal plasticity, it would suggest that behavioral state would be a variable in engaging the cellular mechanisms of plasticity.

Serotonin has received some attention as promoting plasticity in the adult brain. The role of serotonin in sensory perception has been historically revealed through studies of hallucinogenic serotonin receptor agonists such as LSD and psilocybin, but recent studies highlight its role in adult cortical plasticity. For example, administration of a serotonin reuptake inhibitor, fluoxetine, was found to reinstate ODP in adult V1 of rats (Maya Vetencourt et al., 2008). This suggests that juvenile forms of plasticity could be enabled in the adult brain by serotonin. Of interest, serotonin has also been specifically implicated in cross-modal recruitment in adults. Lombaert et al. (2018) found evidence that serotonin tone is higher in the deprived V1 using a monocular enucleation paradigm, and that serotonin facilitates recruitment of the deprived V1 by whisker stimulation (Lombaert et al., 2018). In particular, long–term cross-modal recruitment was dependent on activation of 5HT-2A and 5HT-3A receptors as determined by specific antagonists.

At the circuit level, neuromodulators, in particular serotonin and acetylcholine, act through VIP interneurons in the superficial layers of V1 (Tremblay et al., 2016), which is the same circuit element that allows cross-modal modulated of V1 by sound (Ibrahim et al., 2016). Coincidently, VIP interneurons are a subset of 5HT-3A receptor expressing inhibitory interneurons (Tremblay et al., 2016), which may explain the dependence of cross-modal recruitment on 5HT-3A receptors (Lombaert et al., 2018). Collectively, these findings suggest that VIP interneuron-mediated disinhibitory circuit may be a common element for gating cross-modal information flow into L2/3 of V1 to mediate cross-modal recruitment.

COMPENSATORY PLASTICITY

In addition to cross-modal recruitment of V1, which may add capacity to the processing of the remaining senses, there is evidence that the cortical areas serving the spared senses also undergo their own unique adaptation to enhance the processing of their sensory inputs. This phenomenon is referred to as "compensatory plasticity" (Rauschecker, 1995; Lee and Whitt, 2015; **Figure 1**). Such compensatory changes are seen in parts of the cortex serving both somatosensation and audition. Blind individuals who use a single finger to read Braille exhibit increased representation of that reading finger in the sensorimotor cortex compared to nonreading fingers and compared to sighted controls (Pascual-Leone and Torres, 1993). The auditory cortex likewise undergoes expansion as measured by magnetic source imaging (Elbert et al., 2002). In early blind subjects, the response levels of auditory cortical neurons differ from sighted controls, and these changes are interpreted as supporting more efficient processing of auditory information (Stevens and Weaver, 2009).

Cortical Plasticity of Spared Sensory Cortices

In animal models, vision loss leads to plasticity within A1 and S1. Mice deprived of vision since birth have enlarged whisker representations in S1 (Rauschecker et al., 1992). Visual deprivation from birth also results in decreased amplitude of mEPSCs in L2/3 of A1 and S1 in rodents (Goel et al., 2006), which as discussed later, may reflect a shift in processing of information from intracortical towards feedforward sources (Petrus et al., 2015). In an animal model, where visual deprivation can be done before the development of retinogeniculate connections, anatomical changes in cortical and subcortical inputs to S1 have been observed (Dooley and Krubitzer, 2019). Plasticity is not restricted to early-onset vision loss. At least in rodents, the adaptation of neural circuits in A1 and S1 has been observed even with a few days of dark exposure or bilateral lid suture (Goel et al., 2006; Jitsuki et al., 2011; He et al., 2012; Petrus et al., 2014, 2015; Meng et al., 2015, 2017; Solarana et al., 2019). Even in adult mice, a short duration of visual deprivation has been shown to trigger functional enhancement of feedforward inputs and refinement of functional circuits within A1 (Petrus et al., 2014, 2015; Meng et al., 2015, 2017). Specifically, when adult mice are subjected to 7 days of dark exposure, potentiation of synapses serving the feedforward pathway, thalamocortical inputs to L4, and subsequent L4 to L2/3 inputs, is observed in A1 (Petrus et al., 2014, 2015; **Figure 2B**). Potentiation of the feedforward connections is accompanied by a weakening of intracortical synapses onto L2/3 neurons of A1 (Petrus et al., 2015; **Figure 2B**), which manifests as a decrease in the average amplitude of mEPSCs (Goel et al., 2006; Petrus et al., 2015). Similarly, visual deprivation leads to a reduction in the average amplitude of mEPSCs in L2/3 of barrel cortex (Goel et al., 2006; He et al., 2012) but not in the frontal cortex (Goel et al., 2006), which suggests that this type of adaptation is common across the spared primary sensory cortices. The shift in synaptic strength to favor

feedforward synapses in A1 with visual deprivation correlated with heightened sensitivity to sound, observed as a decrease in the threshold of A1 L4 neurons to sound (Petrus et al., 2014). In addition, a few days of visual deprivation-induced sharpening of tuning of A1 L4 neurons to sound frequency (Petrus et al., 2014), which is likely a reflection of increased inhibition from PV-interneurons to L4 principal neurons (Petrus et al., 2015). Furthermore, the short duration of visual deprivation leads to refinement of the spatial extent of connectivity within L4 and L2/3 of A1 (Meng et al., 2015, 2017), as well as sparsification of population-level coding of sound in L2/3 of A1 (Solarana et al., 2019). These adaptations involving circuit refinement are likely to maximize the coding capacity of A1 as demonstrated by computational modeling (Meng et al., 2015). Collectively, the compensatory plasticity observed in A1 with visual deprivation is consistent with the notion that A1 would be better at processing sound, which could underlie enhanced auditory discrimination abilities often observed in blind individuals (Lessard et al., 1998; Röder et al., 1999; Gougoux et al., 2004; Voss et al., 2004).

Improvement in auditory or tactile discrimination abilities reported in blind human subjects is, however, not universal and may depend on perceptual learning (Grant et al., 2000; Wong et al., 2011). This may stem from the fact that compensatory changes observed in the spared sensory cortices are dependent on their own sensory inputs (He et al., 2012; Petrus et al., 2014). Removing whiskers or deafening mice that are undergoing visual deprivation prevents synaptic plasticity changes observed in S1 barrel cortex (He et al., 2012) and A1 (Petrus et al., 2014), respectively. These findings suggest that the potentiation of feedforward inputs to the spared primary sensory cortices is likely driven by an experience-dependent synaptic plasticity mechanism, such as LTP. Consistent with this idea, deafening normal sighted mice recover LTP of thalamocortical inputs to L4 in V1 of adult mice (Rodriguez et al., 2019). Potentiation of feedforward connections is then expected to induce metaplasticity to compensate for the increased overall input activity, which would slide the synaptic modification threshold up to promote LTD (**Figure 3B**). This shift in the synaptic modification threshold would preferentially weaken intracortical synapses via LTD to provide homeostasis in neural activity.

One interesting aspect of compensatory synaptic plasticity observed in the spared primary sensory cortices is that it requires a less drastic loss in vision than is required for cross-modal recruitment. As discussed earlier, V1 plasticity induced by vision loss requires a complete loss of retinal inputs and is not observed with bilateral lid-suture (He et al., 2012). However, lid-suture is sufficient to induce compensatory synaptic plasticity in the spared cortex (He et al., 2012). This suggests that total loss of retinal input is required for cross-modal recruitment of V1, while a milder degradation of vision that would hinder using vision to guide behavior may trigger compensatory plasticity in the spared cortical areas. This also indicates that cross-modal recruitment and compensatory plasticity are likely induced independently. Another difference between the two plasticity mechanisms is the duration of visual deprivation required: V1 plasticity can be triggered by a shorter duration (i.e., 2 days is sufficient) of visual deprivation (Goel and Lee, 2007; Gao et al., 2010; He et al., 2012; Chokshi et al., 2019) than that required to observe plasticity in A1 and S1 (Goel et al., 2006; He et al., 2012).

While compensatory plasticity observed in A1 and S1 following vision loss is not critically tied to the plasticity in V1, it nonetheless needs to be triggered by the loss of vision. Therefore, there must be functional circuits that carry information or convey the state of visual experience to A1 and S1 to gate compensatory plasticity. There are several possible functional circuits that can provide information on vision to A1 and S1. One is via direct or indirect (*via* higher-order sensory cortices or through higher-order thalamic nucleus) functional projections between V1 and A1/S1. This may involve gating inhibition in the target A1/S1 circuit to enable plasticity. A second possibility is through neuromodulatory systems since the loss of vision would likely change the global arousal or attentional state of an individual to the spared sensory stimuli. A third possibility is via a bottom-up "spot-light" attentional control within each spared modality.

Intracortical Circuits That Can Mediate Compensatory Plasticity

As mentioned in a previous section (section 2.2), there are direct cortico-cortical connections between the primary sensory cortices, and there is evidence that this functional pathway can gate plasticity. In gerbils, a direct connection from V1 gates the critical period plasticity in A1, where early eye-opening leads to termination of the critical period for A1 plasticity while delayed eye opening extends it (Mowery et al., 2016). While this study did not determine how the direct functional input from V1 gates plasticity of the feedforward circuit in A1, the observation that visual deprivation can extend the critical period is consistent with other studies demonstrating recovery of thalamocortical plasticity in the adult primary sensory cortices with cross-modal sensory deprivation (Petrus et al., 2014; Rodríguez et al., 2018).

In addition to the direct projections, feedback from higher-order sensory cortices or multisensory cortical areas also can provide information on visual experience to the spared primary sensory cortices either through direct cortico-cortical connections or indirect connections via the higher-order thalamus. As explained previously, both cortico-cortical and trans-thalamic connections arrive through L1 and influence the inhibitory circuits present in L2/3 (Ibrahim et al., 2016; Roth et al., 2016; Zhou et al., 2017). It is well documented that inhibitory circuits are well poised to gate cortical plasticity (Jiang et al., 2005). In the S1 barrel cortex, input from POm, a higher-order somatosensory thalamus, is critical for gating potentiation of whisker inputs to L2/3 (Gambino et al., 2014). In particular, POm activation generates NMDAR-mediated dendritic plateau potentials in the principal neurons in L2/3, which are necessary for the observed LTP (Gambino et al., 2014). A follow-up study demonstrated that POm gating of L4 to L2/3 LTP in the S1 barrel cortex is due to disinhibition of L2/3 principal neurons *via* activation of VIP- and PV-interneurons and a concomitant decrease in SOM-interneuron activity (Williams and Holtmaat, 2019). These studies suggest that POm activity stimulates VIP-interneurons, which in turn inhibit SOM-interneurons.

SOM-interneurons are known to target inhibition to dendrites (Tremblay et al., 2016). Hence, reduced SOM-interneuron activity would cause disinhibition of dendrites of L2/3 principal neurons, which could support the activation of NMDAR-mediated dendritic plateau potentials to induce LTP of the feedforward synapses from L4. As mentioned before (see "Subcortical Sources of Inputs to V1 L2/3 That Can Mediate Cross-modal Recruitment" section), trans-thalamic connections through higher-order thalamic nuclei can transmit multisensory information to primary sensory cortices. In particular, we discussed evidence on how LP conveys visual information to A1 to modulate auditory responses (Chou et al., 2020). Whether such a functional circuit involving higher-order thalamic nuclei could mediate compensatory plasticity upon loss of vision will need to be examined.

Thalamic Circuits That May Gate Compensatory Plasticity

Considering that compensatory plasticity of feedforward circuits in A1 and S1 depends on their respective sensory inputs (He et al., 2012; Petrus et al., 2014), there is also a possibility that gating of this plasticity could occur at the level of the thalamus. The TRN is a thin band of inhibitory neurons that surrounds and projects to the primary sensory thalamic nuclei, controlling information flow to the primary sensory cortex (Halassa and Acsády, 2016; Crabtree, 2018). Although TRN is divided roughly according to modality, about 25% of TRN cells receive multimodal input from multiple relay centers in the thalamus (Lam and Sherman, 2011; Kimura, 2014). These multisensory TRN neurons could play a role in regulating feedforward excitatory thalamocortical input to A1 and S1 based on visual experience. There is potential for multisensory TRN neurons to fire less upon vision loss, which leads to disinhibition of auditory (MGBv) and somatosensory (VPM) thalamic nuclei. This would increase feedforward activity propagation to A1 and S1, which could be the basis for driving potentiation of thalamocortical synapses in L4 as observed following visual deprivation (Petrus et al., 2014).

Another potential mode by which TRN can gate activity through the spared primary thalamic nucleus is *via* feedback projections from the respective spared primary sensory cortex. Corticothalamic L6 neurons provide feedback control of their respective primary sensory thalamic nuclei via direct excitation and disynaptic inhibition through the TRN. It was demonstrated in the somatosensory system of rodents that the feedback control is activity-dependent, such that low-frequency activation of L6 neurons in the barrel cortex predominantly inhibits VPM while higher frequency stimulation leads to activation (Crandall et al., 2015). This effect was due to the difference in short-term dynamics of excitation vs. inhibition; excitatory synaptic transmission displays facilitation while inhibitory synaptic transmission undergoes depression with a train of stimulation (Crandall et al., 2015). As mentioned previously ("Cortical Plasticity of Spared Sensory Cortices" section), one of the main adaptations of the spared cortical circuit is the potentiation of feedforward synapses (Petrus et al., 2014, 2015; Rodríguez et al., 2018; **Figure 2B**). Therefore, there is potential for L6 to convey the heightened cortical activity, which can result in further amplification of the spared sensory input at the level of the primary sensory thalamus.

It is important to note that increasing activity of thalamocortical inputs alone cannot support potentiation. It is known that stimulation of thalamocortical inputs to L4 in cortical slices is unable to induce LTP beyond the early critical period (Crair and Malenka, 1995; Jiang et al., 2007; Barkat et al., 2011; Rodríguez et al., 2018). In contrast, electrically stimulating dLGN *in vivo* can produce LTP in adult V1 (Heynen and Bear, 2001), which suggests that there may be additional factors present in an intact *in vivo* circuitry that may allow LTP at thalamocortical synapses in the adult cortex.

Neuromodulatory Control of Compensatory Plasticity

As discussed in the context of cross-modal recruitment, neuromodulators play a critical role in enabling plasticity in the primary sensory cortices, even in adults. There are reports that the levels of serotonin and norepinephrine are relatively higher in spared cortices than deprived cortex following visual deprivation (Qu et al., 2000; Jitsuki et al., 2011). As will be discussed in more detail below, VIP-interneuron mediated disinhibitory circuit seems a key circuit component that can be recruited for neuromodulatory control of compensatory plasticity, in addition to cortical and subcortical control, following the loss of vision.

Loss of vision could increase the behavioral relevance or salience of the remaining sensory inputs (De Heering et al., 2016). This suggests that auditory or somatosensory inputs may be more likely to be paired with acetylcholine or norepinephrine release based on the heightened attention and/or arousal to these sensory inputs in the absence of vision. Acetylcholine is particularly interesting as a candidate for mediating compensatory plasticity because it has been observed to facilitate potentiation of feedforward thalamocortical inputs especially in adult primary sensory cortices (Dringenberg et al., 2007; Chun et al., 2013). Furthermore, there is evidence that acetylcholine can differentially alter the strength of thalamocortical and intracortical synapses, such that only the former is potentiated by nicotinic acetylcholine receptor (nAChR) activation while both inputs depress when muscarinic acetylcholine receptors (mAChRs) are activated (Gil et al., 1997). Such dual action of acetylcholine is proposed to refine A1 tuning by enhancing responses from the feedforward thalamocortical receptive field while suppressing lateral intracortical inputs (Metherate, 2011). Therefore, acetylcholine could in principle coordinate potentiation of thalamocortical synapses and depression of intracortical synapses, as well as refinement of tuning properties, observed in A1 following visual deprivation (Petrus et al., 2014, 2015). Acetylcholine is widely viewed as setting the arousal level because the activity of acetylcholine neurons in nucleus basalis is associated with a desynchronized electroencephalogram (EEG) pattern, generally accepted to indicate heightened attention (Metherate et al., 1992). It is interesting to note that during strongly desynchronized EEG activity, acetylcholine preferentially activates L1 interneurons and VIP cells by acting on nAChRs expressed on these neurons

(Alitto and Dan, 2012). This would disinhibit principal neurons, potentially allowing for plasticity. On the other hand, lower levels of cortical desynchronization preferentially activate PV interneurons *via* mAChRs (Alitto and Dan, 2012), which would enhance inhibition in the circuit. This observation suggests that the degree of attention or behavioral alertness may factor into how cortical circuits undergo plasticity.

The norepinephrine system has been shown to impact network activity and plasticity in sensory cortices (Salgado et al., 2016). For example, iontophoretic application of norepinephrine to A1 of awake rodents causes A1 neurons to exhibit a greater degree of frequency selectivity (Manunta and Edeline, 1997, 1999). This is reminiscent of the sharpened frequency selectivity of A1 L4 neurons following visual deprivation (Petrus et al., 2014). It has been shown that norepinephrine acting through beta-adrenergic receptors facilitates the induction of LTP and suppresses LTD (Seol et al., 2007; Huang et al., 2012). Beta-adrenergic receptors have a lower affinity to norepinephrine compared to alpha-adrenergic receptors (Salgado et al., 2016). Therefore, higher noradrenergic tone in the spared cortical area accompanying visual deprivation (Qu et al., 2000) could activate these receptors and encourage potentiation of feedforward circuits in A1.

Among the neuromodulators discussed here, serotonin has the most concrete evidence to support a role in compensatory plasticity. As mentioned in a previous section, serotonin is critical for recovering adult cortical plasticity (Maya Vetencourt et al., 2008) and cross-modal recruitment (Lombaert et al., 2018). Of relevance to compensatory plasticity, which involves recovering thalamocortical LTP in adults (Rodríguez et al., 2018), certain serotonin receptor antagonists can block thalamocortical LTP in anesthetized rats (Lee et al., 2018). Furthermore, there is direct evidence that serotonin is specifically involved in the cross-modal compensatory plasticity of the feedforward circuit. In rats that were visually deprived via bilateral lid suture, serotonin levels were elevated in the barrel cortex, but not in V1 (Jitsuki et al., 2011). Elevated serotonin levels triggered the insertion of AMPA receptors into the synapse between L4 and L2/3 cells, enhancing feedforward processing of whisker information after visual deprivation (Jitsuki et al., 2011). How serotonin levels increase specifically in deprived (Lombaert et al., 2018) vs. spared sensory cortices (Qu et al., 2000; Jitsuki et al., 2011) is unclear, but could be due to differences in the visual deprivation paradigm. Lombaert and colleagues used monocular enucleation, while Jitsuki and colleagues performed bilateral lid-suture. As mentioned previously, lid-suture is ineffective at driving changes in V1 but induces plasticity in S1 (He et al., 2012). In any case, these studies highlight the importance of the serotonergic system in coordinating cross-modal plasticity in adults.

Functional Circuits for Bottom-Up "Spotlight" Attentional Control of Compensatory Plasticity

A great deal of interest has been devoted recently to the concept of an attentional spotlight, also referred to as selective attention or feature-based attention. The attentional spotlight, which in higher mammals has been described as a neocortical attribute, also heavily relies on subcortical mechanisms for directing attention and cognitive resources towards one salient stimulus or modality, while de-emphasizing others (Saalmann and Kastner, 2011; Halassa and Kastner, 2017; Krauzlis et al., 2018). Global neuromodulatory systems are likely enabling factors for compensatory plasticity, while continued sensory input and spotlight attentional mechanisms may play an instructive role to shape the plasticity in the spared sensory cortices. Spotlight attention is thought to act at a subcortical level to gate the information ascending to the cortex, hence controlling the flow of activity necessary for inducing activity-dependent plasticity. Therefore, turning the attentional spotlight towards auditory and somatosensory inputs in response to visual deprivation would heighten or alter the pattern of activity reaching A1 and S1 in such a way as to drive plasticity. As mentioned before, instructive mechanisms, such as increased sensory gating, cannot alone result in plasticity at synapses that have a defined critical period for plasticity, such as the thalamocortical synapses (Crair and Malenka, 1995; Jiang et al., 2007; Barkat et al., 2011; Rodríguez et al., 2018). Therefore, especially in adults, we believe attentional spotlight mechanisms would need to work together with enabling factors, such as neuromodulators, to reopen plasticity. Indeed, prior work examining adult plasticity has noted the importance of attention and behavioral relevance in enabling plasticity (e.g., Polley et al., 2006). Here, we will highlight two potential substrates for attentional spotlight regulation of feedforward circuit plasticity involved in compensatory plasticity: superior colliculus (SC) and mediodorsal nucleus (MD). TRN is another candidate to gate sensory input, as was discussed earlier ("Thalamic Circuits That May Gate Compensatory Plasticity" section).

Superior colliculus (SC) is an evolutionarily old part of the brain which processes sensory input and computes a saliency map of the environment (Krauzlis et al., 2013). As discussed above (see "Subcortical Sources of Inputs to V1 L2/3 That Can Mediate Cross-modal Recruitment" section), SC has long been appreciated to participate in visual processing but also harbors multimodal cells in the deeper layers which integrate tactile, visual, and auditory stimuli (Krauzlis et al., 2013; Cang et al., 2018). These multimodal cells in deep layers of SC account for the majority of output neurons (Cang et al., 2018), sending collaterals to many structures, including higher-order thalamic nuclei as well as TRN (Krauzlis et al., 2013). SC input to POm, a higher-order somatosensory thalamus, has been shown to allow attentional enhancement of somatosensory stimuli in the cortex, as observed by enhanced S1 responses to weaker whisker stimulation upon activation of SC neurons (Gharaei et al., 2020). This effect may be mediated by the aforementioned disinhibition of L2/3 principal neurons upon POm activation (Williams and Holtmaat, 2019) (see "Intracortical Circuits That Can Mediate Compensatory Plasticity" section). SC also has been shown to sharpen A1 processing *via* its connections to LP (Chou et al., 2020; see "Subcortical Sources of Inputs to V1 L2/3 That Can Mediate Cross-modal Recruitment" section). Therefore, SC is in a prime position to provide multisensory information to a

key circuit motif involving higher-order thalamic nuclei that can mediate localized enhancement of response properties in primary sensory cortices.

The mediodorsal nucleus (MD) is a higher-order thalamic nucleus considered to be important in attention and learning (Mitchell and Chakraborty, 2013; Mitchell, 2015), in part due to its extensive and reciprocal connections with the prefrontal cortex (Zikopoulos and Barbas, 2007; Mitchell and Chakraborty, 2013; Mitchell, 2015). In addition, MD projects to all parts of the TRN, which differs from primary thalamic nuclei which have projections mainly limited to a subregion of TRN (Zikopoulos and Barbas, 2007; Mitchell, 2015). These features suggest that MD may provide a functional connection between prefrontal cortical networks involved in the attentional selection and TRN to gate sensory input (Zikopoulos and Barbas, 2007; Mitchell, 2015). The prefrontal cortex has been shown to modulate performance on a multimodal attentional task via its effect on TRN activity (Wimmer et al., 2015). The close connection between MD and TRN thus offers a potential substrate for attentional regulation of input from the thalamus to primary sensory cortices.

CONCLUSIONS

Primary sensory cortices are highly interconnected to multisensory cortical and subcortical structures, which under normal circumstances provide contextual and saliency information needed for proper sensory processing. We suggest that these cortical and subcortical functional connections play a critical role in mediating cross-modal plasticity when a sensory modality is lost, such that an organism can effectively navigate its environment based on the remaining senses. As summarized in this review, these functional connections will allow cross-modal recruitment of the deprived sensory cortex for processing the spared sensory information, as well as enabling and instructing plasticity needed for refining sensory processing of the spared sensory cortices. Visual-deprivation studies highlight the involvement of Hebbian and homeostatic metaplasticity in sculpting the cortical circuits for cross-modal plasticity, which involves not only the plasticity of excitatory synapses, but also that of inhibitory synapses. Cross-modal plasticity across sensory cortices is likely coordinated globally via direct connection across sensory cortices, indirect connectivity through cortico-thalamo-cortical loops or indirect cortical connections through multisensory cortical areas. It is likely that global neuromodulatory systems are engaged to enable plasticity across the sensory cortices. In parallel, multisensory functional inputs that target cortical inhibitory circuits could also gate plasticity within each cortical area. Instructive signals for plasticity likely arise through activity from cortical and subcortical multisensory inputs to V1 and feedforward inputs to the spared cortices. The latter may involve subcortical structures that provide "spotlight" attention to sculpt the spared cortices to better process the most relevant information. While future studies are needed to clarify the role of these diverse functional circuits in cross-modal plasticity, this extensive network of functional connectivity highlights the rich array of contextual information that can influence sensory processing even at the level of primary sensory cortices.

AUTHOR CONTRIBUTIONS

GE, SP, and H-KL wrote the manuscript. AL and YJ compiled information used for the text and generated the figures with the help of GE, SP, and H-KL. All authors contributed to the article and approved the submitted version.

FUNDING

This work was supported by National Institutes of Health (NIH) grant R01-EY014882 to H-KL and NRSA F31-EY031946 to SP.

ACKNOWLEDGMENTS

We would like to thank Dr. Alfredo Kirkwood for helpful discussions.

REFERENCES

Alitto, H. J., and Dan, Y. (2012). Cell-type-specific modulation of neocortical activity by basal forebrain input. *Front. Syst. Neurosci.* 6:79. doi: 10.3389/fnsys.2012.00079

Bai, W.-Z., Ishida, M., and Arimatsu, Y. (2004). Chemically defined feedback connections from infragranular layers of sensory association cortices in the rat. *Neuroscience* 123, 257–267. doi: 10.1016/j.neuroscience.2003.08.056

Baldwin, M. K. L., Balaram, P., and Kaas, J. H. (2017). The evolution and functions of nuclei of the visual pulvinar in primates. *J. Comp. Neurol.* 525, 3207–3226. doi: 10.1002/cne.24272

Barkat, T. R., Polley, D. B., and Hensch, T. K. (2011). A critical period for auditory thalamocortical connectivity. *Nat. Neurosci.* 14, 1189–1194. doi: 10.1038/nn.2882

Barnes, S. J., Sammons, R. P., Jacobsen, R. I., Mackie, J., Keller, G. B., and Keck, T. (2015). Subnetwork-specific homeostatic plasticity in mouse visual cortex *in vivo*. *Neuron* 86, 1290–1303. doi: 10.1016/j.neuron.2015.05.010

Bavelier, D., and Neville, H. J. (2002). Cross-modal plasticity: where and how? *Nat. Rev. Neurosci.* 3, 443–452. doi: 10.1038/nrn848

Bear, M. F., Cooper, L. N., and Ebner, F. F. (1987). A physiological basis for a theory of synapse modification. *Science* 237, 42–48. doi: 10.1126/science.3037696

Bear, M. F., and Singer, W. (1986). Modulation of visual cortical plasticity by acetylcholine and noradrenaline. *Nature* 320, 172–176. doi: 10.1038/320172a0

Bender, K. J., Allen, C. B., Bender, V. A., and Feldman, D. E. (2006). Synaptic basis for whisker deprivation-induced synaptic depression in rat somatosensory cortex. *J. Neurosci.* 26, 4155–4165. doi: 10.1523/JNEUROSCI.0175-06.2006

Bender, M. B., and Teuber, H. L. (1946). Phenomena of fluctuation, extinction and completion in visual perception. *Arch. Neurol. Psychiatry* 55, 627–658. doi: 10.1001/archneurpsyc.1946.02300170075008

Bennett, C., Gale, S. D., Garrett, M. E., Newton, M. L., Callaway, E. M., Murphy, G. J., et al. (2019). Higher-order thalamic circuits channel parallel streams of visual information in mice. *Neuron* 102, 477.e5–492.e5. doi: 10.1016/j.neuron.2019.02.010

Bezdudnaya, T., and Keller, A. (2008). Laterodorsal nucleus of the thalamus: a processor of somatosensory inputs. *J. Comp. Neurol.* 507, 1979–1989. doi: 10.1002/cne.21664

Bienenstock, E. L., Cooper, L. N., and Munro, P. W. (1982). Theory for the development of neuron selectivity: orientation specificity and binocular interaction in visual cortex. *J. Neurosci.* 2, 32–48. doi: 10.1523/JNEUROSCI.02-01-00032.1982

Binzegger, T., Douglas, R. J., and Martin, K. A. (2004). A quantitative map of the circuit of cat primary visual cortex. *J. Neurosci.* 24, 8441–8453. doi: 10.1523/JNEUROSCI.1400-04.2004

Blais, B. S., Frenkel, M. Y., Kuindersma, S. R., Muhammad, R., Shouval, H. Z., Cooper, L. N., et al. (2008). Recovery from monocular deprivation using binocular deprivation. *J. Neurophysiol.* 100, 2217–2224. doi: 10.1152/jn.90411.2008

Bortone, D. S., Olsen, S. R., and Scanziani, M. (2014). Translaminar inhibitory cells recruited by layer 6 corticothalamic neurons suppress visual cortex. *Neuron* 82, 474–485. doi: 10.1016/j.neuron.2014.02.021

Bridi, M. C. D., De Pasquale, R., Lantz, C. L., Gu, Y., Borrell, A., Choi, S. Y., et al. (2018). Two distinct mechanisms for experience-dependent homeostasis. *Nat. Neurosci.* 21, 843–850. doi: 10.1038/s41593-018-0150-0

Buchel, C., Price, C., Frackowiak, R. S., and Friston, K. (1998). Different activation patterns in the visual cortex of late and congenitally blind subjects. *Brain* 121, 409–419. doi: 10.1093/brain/121.3.409

Burton, H., and McLaren, D. G. (2006). Visual cortex activation in late-onset, Braille naive blind individuals: an fMRI study during semantic and phonological tasks with heard words. *Neurosci. Lett.* 392, 38–42. doi: 10.1016/j.neulet.2005.09.015

Cang, J., Savier, E., Barchini, J., and Liu, X. (2018). Visual function, organization, and development of the mouse superior colliculus. *Annu. Rev. Vis. Sci.* 4, 239–262. doi: 10.1146/annurev-vision-091517-034142

Cappe, C., and Barone, P. (2005). Heteromodal connections supporting multisensory integration at low levels of cortical processing in the monkey. *Eur. J. Neurosci.* 22, 2886–2902. doi: 10.1111/j.1460-9568.2005.04462.x

Charbonneau, V., Laramée, M.-E., Boucher, V., Bronchti, G., and Boire, D. (2012). Cortical and subcortical projections to primary visual cortex in anophthalmic, enucleated and sighted mice. *Eur. J. Neurosci.* 36, 2949–2963. doi: 10.1111/j.1460-9568.2012.08215.x

Chokshi, V., Gao, M., Grier, B. D., Owens, A., Wang, H., Worley, P. F., et al. (2019). Input-specific metaplasticity in the visual cortex requires homer1a-mediated mGluR5 signaling. *Neuron* 104, 736.e6–748.e6.doi: 10.1016/j.neuron.2019.08.017

Chou, X.-L., Fang, Q., Yan, L., Zhong, W., Peng, B., Li, H., et al. (2020). Contextual and cross-modality modulation of auditory cortical processing through pulvinar mediated suppression. *eLife* 9:e54157. doi: 10.7554/eLife.54157

Chun, S., Bayazitov, I. T., Blundon, J. A., and Zakharenko, S. S. (2013). Thalamocortical long-term potentiation becomes gated after the early critical period in the auditory cortex. *J. Neurosci.* 33, 7345–7357. doi: 10.1523/JNEUROSCI.4500-12.2013

Cooke, S. F., and Bear, M. F. (2014). How the mechanisms of long-term synaptic potentiation and depression serve experience-dependent plasticity in primary visual cortex. *Philos. Trans. R. Soc. Lond. B Biol. Sci.* 369:20130284. doi: 10.1098/rstb.2013.0284

Cooper, L. N., and Bear, M. F. (2012). The BCM theory of synapse modification at 30: interaction of theory with experiment. *Nat. Rev. Neurosci.* 13, 798–810. doi: 10.1038/nrn3353

Crabtree, J. W. (2018). Functional diversity of thalamic reticular subnetworks. *Front. Syst. Neurosci.* 12:41. doi: 10.3389/fnsys.2018.00041

Crair, M. C., and Malenka, R. C. (1995). A critical period for long-term potentiation at thalamocortical synapses. *Nature* 375, 325–328. doi: 10.1038/375325a0

Crandall, S. R., Cruikshank, S. J., and Connors, B. W. (2015). A corticothalamic switch: controlling the thalamus with dynamic synapses. *Neuron* 86, 768–782. doi: 10.1016/j.neuron.2015.03.040

Cuevas, I., Plaza, P., Rombaux, P., De Volder, A. G., and Renier, L. (2009). Odour discrimination and identification are improved in early blindness. *Neuropsychologia* 47, 3079–3083. doi: 10.1016/j.neuropsychologia.2009.07.004

Cynader, M., and Mitchell, D. E. (1980). Prolonged sensitivity to monocular deprivation in dark-reared cats. *J. Neurophysiol.* 43, 1026–1040. doi: 10.1152/jn.1980.43.4.1026

De Heering, A., Dormal, G., Pelland, M., Lewis, T., Maurer, D., and Collignon, O. (2016). A brief period of postnatal visual deprivation alters the balance between auditory and visual attention. *Curr. Biol.* 26, 3101–3105. doi: 10.1016/j.cub.2016.10.014

Deneux, T., Harrell, E. R., Kempf, A., Ceballo, S., Filipchuk, A., and Bathellier, B. (2019). Context-dependent signaling of coincident auditory and visual events in primary visual cortex. *eLife* 8:e44006. doi: 10.7554/eLife.44006

Desai, N. S., Cudmore, R. H., Nelson, S. B., and Turrigiano, G. G. (2002). Critical periods for experience-dependent synaptic scaling in visual cortex. *Nat. Neurosci.* 5, 783–789. doi: 10.1038/nn878

Dooley, J. C., and Krubitzer, L. A. (2019). Alterations in cortical and thalamic connections of somatosensory cortex following early loss of vision. *J. Comp. Neurol.* 527, 1675–1688. doi: 10.1002/cne.24582

Dringenberg, H. C., Hamze, B., Wilson, A., Speechley, W., and Kuo, M. C. (2007). Heterosynaptic facilitation of *in vivo* thalamocortical long-term potentiation in the adult rat visual cortex by acetylcholine. *Cereb. Cortex* 17, 839–848. doi: 10.1093/cercor/bhk038

Elbert, T., Sterr, A., Rockstroh, B., Pantev, C., Muller, M. M., and Taub, E. (2002). Expansion of the tonotopic area in the auditory cortex of the blind. *J. Neurosci.* 22, 9941–9944. doi: 10.1523/JNEUROSCI.22-22-09941.2002

Falchier, A., Clavagnier, S., Barone, P., and Kennedy, H. (2002). Anatomical evidence of multimodal integration in primate striate cortex. *J. Neurosci.* 22, 5749–5759. doi: 10.1523/JNEUROSCI.22-13-05749.2002

Fang, Q., Chou, X.-L., Peng, B., Zhong, W., Zhang, L. I., and Tao, H. W. (2020). A differential circuit *via* retino-colliculo-pulvinar pathway enhances feature selectivity in visual cortex through surround suppression. *Neuron* 105, 355.e6–369.e6. doi: 10.1016/j.neuron.2019.10.027

Feldman, D. E., Nicoll, R. A., Malenka, R. C., and Isaac, J. T. (1998). Long-term depression at thalamocortical synapses in developing rat somatosensory cortex. *Neuron* 21, 347–357. doi: 10.1016/s0896-6273(00)80544-9

Felleman, D. J., and Van Essen, D. C. (1991). Distributed hierarchical processing in the primate cerebral cortex. *Cereb. Cortex* 1, 1–47. doi: 10.1093/cercor/1.1.1

Gallero-Salas, Y., Han, S., Sych, Y., Voigt, F. F., Laurenczy, B., Gilad, A., et al. (2021). Sensory and behavioral components of neocortical signal flow in discrimination tasks with short-term memory. *Neuron* 109, 135.e6–148.e6. doi: 10.1016/j.neuron.2020.10.017

Gamanut, R., Kennedy, H., Toroczkai, Z., Ercsey-Ravasz, M., Van Essen, D. C., Knoblauch, K., et al. (2018). The mouse cortical connectome, characterized by an ultra-dense cortical graph, maintains specificity by distinct connectivity profiles. *Neuron* 97, 698.e10–715.e10. doi: 10.1016/j.neuron.2017.12.037

Gambino, F., Pagès, S., Kehayas, V., Baptista, D., Tatti, R., Carleton, A., et al. (2014). Sensory-evoked LTP driven by dendritic plateau potentials *in vivo*. *Nature* 515, 116–119. doi: 10.1038/nature13664

Gao, M., Maynard, K. R., Chokshi, V., Song, L., Jacobs, C., Wang, H., et al. (2014). Rebound potentiation of inhibition in juvenile visual cortex requires vision-induced BDNF expression. *J. Neurosci.* 34, 10770–10779. doi: 10.1523/JNEUROSCI.5454-13.2014

Gao, M., Sossa, K., Song, L., Errington, L., Cummings, L., Hwang, H., et al. (2010). A specific requirement of Arc/Arg3.1 for visual experience-induced homeostatic synaptic plasticity in mouse primary visual cortex. *J. Neurosci.* 30, 7168–7178. doi: 10.1523/JNEUROSCI.1067-10.2010

Gao, M., Whitt, J. L., Huang, S., Lee, A., Mihalas, S., Kirkwood, A., et al. (2017). Experience-dependent homeostasis of 'noise' at inhibitory synapses preserves information coding in adult visual cortex. *Philos. Trans. R. Soc. Lond. B Biol. Sci.* 372:20160156. doi: 10.1098/rstb.2016.0156

Garrett, M. E., Nauhaus, I., Marshel, J. H., and Callaway, E. M. (2014). Topography and areal organization of mouse visual cortex. *J. Neurosci.* 34, 12587–12600. doi: 10.1523/JNEUROSCI.1124-14.2014

Gharaei, S., Honnuraiah, S., Arabzadeh, E., and Stuart, G. J. (2020). Superior colliculus modulates cortical coding of somatosensory information. *Nat. Commun.* 11:1693. doi: 10.1038/s41467-020-15443-1

Gil, Z., Connors, B. W., and Amitai, Y. (1997). Differential regulation of neocortical synapses by neuromodulators and activity. *Neuron* 19, 679–686. doi: 10.1016/s0896-6273(00)80380-3

Gilissen, S., and Arckens, L. (2021). Posterior parietal cortex contributions to cross-modal brain plasticity upon sensory loss. *Curr. Opin. Neurobiol.* 67, 16–25. doi: 10.1016/j.conb.2020.07.001

Gilissen, S. R. J., Farrow, K., Bonin, V., and Arckens, L. (2021). Reconsidering the border between the visual and posterior parietal cortex of mice. *Cereb. Cortex* 31, 1675–1692. doi: 10.1093/cercor/bhaa318

Glazewski, S., Greenhill, S., and Fox, K. (2017). Time-course and mechanisms of homeostatic plasticity in layers 2/3 and 5 of the barrel cortex. *Philos. Trans. R. Soc. Lond. B Biol. Sci.* 372:20160150. doi: 10.1098/rstb.2016.0150

Glickfeld, L. L., and Olsen, S. R. (2017). Higher-order areas of the mouse visual cortex. *Annu. Rev. Vis. Sci.* 3, 251–273. doi: 10.1146/annurev-vision-102016-061331

Goel, A., Jiang, B., Xu, L. W., Song, L., Kirkwood, A., and Lee, H. K. (2006). Cross-modal regulation of synaptic AMPA receptors in primary sensory cortices by visual experience. *Nat. Neurosci.* 9, 1001–1003. doi: 10.1038/nn1725

Goel, A., and Lee, H.-K. (2007). Persistence of experience-induced homeostatic synaptic plasticity through adulthood in superficial layers of mouse visual cortex. *J. Neurosci.* 27, 6692–6700. doi: 10.1523/JNEUROSCI.5038-06.2007

Gong, S., Doughty, M., Harbaugh, C. R., Cummins, A., Hatten, M. E., Heintz, N., et al. (2007). Targeting Cre recombinase to specific neuron populations with bacterial artificial chromosome constructs. *J. Neurosci.* 27, 9817–9823. doi: 10.1523/JNEUROSCI.2707-07.2007

Gougoux, F., Lepore, F., Lassonde, M., Voss, P., Zatorre, R. J., and Belin, P. (2004). Neuropsychology: pitch discrimination in the early blind. *Nature* 430:309. doi: 10.1038/430309a

Grant, A. C., Thiagarajah, M. C., and Sathian, K. (2000). Tactile perception in blind Braille readers: a psychophysical study of acuity and hyperacuity using gratings and dot patterns. *Percept. Psychophys.* 62, 301–312. doi: 10.3758/bf03205550

Gu, Q. (2002). Neuromodulatory transmitter systems in the cortex and their role in cortical plasticity. *Neuroscience* 111, 815–835. doi: 10.1016/s0306-4522(02)00026-x

Guo, Y., Huang, S., De Pasquale, R., McGehrin, K., Lee, H.-K., Zhao, K., et al. (2012). Dark exposure extends the integration window for spike-timing-dependent plasticity. *J. Neurosci.* 32, 15027–15035. doi: 10.1523/JNEUROSCI.2545-12.2012

Halassa, M. M., and Acsády, L. (2016). Thalamic inhibition: diverse sources, diverse scales. *Trends Neurosci.* 39, 680–693. doi: 10.1016/j.tins.2016.08.001

Halassa, M. M., and Kastner, S. (2017). Thalamic functions in distributed cognitive control. *Nat. Neurosci.* 20, 1669–1679. doi: 10.1038/s41593-017-0020-1

He, K., Petrus, E., Gammon, N., and Lee, H. K. (2012). Distinct sensory requirements for unimodal and cross-modal homeostatic synaptic plasticity. *J. Neurosci.* 32, 8469–8474. doi: 10.1523/JNEUROSCI.1424-12.2012

He, H.-Y., Ray, B., Dennis, K., and Quinlan, E. M. (2007). Experience-dependent recovery of vision following chronic deprivation amblyopia. *Nat. Neurosci.* 10, 1134–1136. doi: 10.1038/nn1965

Heynen, A. J., and Bear, M. F. (2001). Long-term potentiation of thalamocortical transmission in the adult visual cortex *in vivo*. *J. Neurosci.* 21, 9801–9813. doi: 10.1523/JNEUROSCI.21-24-09801.2001

Hishida, R., Horie, M., Tsukano, H., Tohmi, M., Yoshitake, K., Meguro, R., et al. (2018). Feedback inhibition derived from the posterior parietal cortex regulates the neural properties of the mouse visual cortex. *Eur. J. Neurosci.* 50, 2970–2987. doi: 10.1111/ejn.14424

Hong, S. Z., Huang, S., Severin, D., and Kirkwood, A. (2020). Pull-push neuromodulation of cortical plasticity enables rapid bi-directional shifts in ocular dominance. *eLife* 9:e54455. doi: 10.7554/eLife.54455

Hooks, B. M., and Chen, C. (2020). Circuitry underlying experience-dependent plasticity in the mouse visual system. *Neuron* 106, 21–36. doi: 10.1016/j.neuron.2020.01.031

Hu, F., Kamigaki, T., Zhang, Z., Zhang, S., Dan, U., and Dan, Y. (2019). Prefrontal corticotectal neurons enhance visual processing through the superior colliculus and pulvinar thalamus. *Neuron* 104, 1141.e4–1152.e4. doi: 10.1016/j.neuron.2019.09.019

Huang, S., Treviño, M., He, K., Ardiles, A., Pasquale, R., Guo, Y., et al. (2012). Pull-push neuromodulation of LTP and LTD enables bidirectional experience-induced synaptic scaling in visual cortex. *Neuron* 73, 497–510. doi: 10.1016/j.neuron.2011.11.023

Ibrahim, L. A., Mesik, L., Ji, X. Y., Fang, Q., Li, H. F., Li, Y. T., et al. (2016). Cross-modality sharpening of visual cortical processing through layer-1-mediated inhibition and disinhibition. *Neuron* 89, 1031–1045. doi: 10.1016/j.neuron.2016.01.027

Imamura, K., and Kasamatsu, T. (1989). Interaction of noradrenergic and cholinergic systems in regulation of ocular dominance plasticity. *Neurosci. Res.* 6, 519–536. doi: 10.1016/0168-0102(89)90042-4

Iurilli, G., Ghezzi, D., Olcese, U., Lassi, G., Nazzaro, C., Tonini, R., et al. (2012). Sound-driven synaptic inhibition in primary visual cortex. *Neuron* 73, 814–828. doi: 10.1016/j.neuron.2011.12.026

Jiang, B., Huang, Z. J., Morales, B., and Kirkwood, A. (2005). Maturation of GABAergic transmission and the timing of plasticity in visual cortex. *Brain Res. Rev.* 50, 126–133. doi: 10.1016/j.brainresrev.2005.05.007

Jiang, B., Treviño, M., and Kirkwood, A. (2007). Sequential development of long-term potentiation and depression in different layers of the mouse visual cortex. *J. Neurosci.* 27, 9648–9652. doi: 10.1523/JNEUROSCI.2655-07.2007

Jitsuki, S., Takemoto, K., Kawasaki, T., Tada, H., Takahashi, A., Becamel, C., et al. (2011). Serotonin mediates cross-modal reorganization of cortical circuits. *Neuron* 69, 780–792. doi: 10.1016/j.neuron.2011.01.016

Johnson, R. R., and Burkhalter, A. (1996). Microcircuitry of forward and feedback connections within rat visual cortex. *J. Comp. Neurol.* 368, 383–398. doi: 10.1002/(SICI)1096-9861(19960506)368:3<383::AID-CNE5>3.0.CO;2-1

Johnson, R. R., and Burkhalter, A. (1997). A polysynaptic feedback circuit in rat visual cortex. *J. Neurosci.* 17, 7129–7140. doi: 10.1523/JNEUROSCI.17-18-07129.1997

Keller, A. J., Roth, M. M., and Scanziani, M. (2020). Feedback generates a second receptive field in neurons of the visual cortex. *Nature* 582, 545–549. doi: 10.1038/s41586-020-2319-4

Kim, E. J., Juavinett, A. L., Kyubwa, E. M., Jacobs, M. W., and Callaway, E. M. (2015). Three types of cortical layer 5 neurons that differ in brain-wide connectivity and function. *Neuron* 88, 1253–1267. doi: 10.1016/j.neuron.2015.11.002

Kimura, A. (2014). Diverse subthreshold cross-modal sensory interactions in the thalamic reticular nucleus: implications for new pathways of cross-modal attentional gating function. *Eur. J. Neurosci.* 39, 1405–1418. doi: 10.1111/ejn.12545

Kirkwood, A., Rioult, M. C., and Bear, M. F. (1996). Experience-dependent modification of synaptic plasticity in visual cortex. *Nature* 381, 526–528. doi: 10.1038/381526a0

Ko, H., Hofer, S. B., Pichler, B., Buchanan, K. A., Sjostrom, P. J., and Mrsic-Flogel, T. D. (2011). Functional specificity of local synaptic connections in neocortical networks. *Nature* 473, 87–91. doi: 10.1038/nature09880

Kotak, V. C., Fujisawa, S., Lee, F. A., Karthikeyan, O., Aoki, C., and Sanes, D. H. (2005). Hearing loss raises excitability in the auditory cortex. *J. Neurosci.* 25, 3908–3918. doi: 10.1523/JNEUROSCI.5169-04.2005

Krauzlis, R. J., Bogadhi, A. R., Herman, J. P., and Bollimunta, A. (2018). Selective attention without a neocortex. *Cortex* 102, 161–175. doi: 10.1016/j.cortex.2017.08.026

Krauzlis, R. J., Lovejoy, L. P., and Zénon, A. (2013). Superior colliculus and visual spatial attention. *Annu. Rev. Neurosci.* 36, 165–182. doi: 10.1146/annurev-neuro-062012-170249

Lakatos, P., Chen, C.-M., O'Connell, M. N., Mills, A., and Schroeder, C. E. (2007). Neuronal oscillations and multisensory interaction in primary auditory cortex. *Neuron* 53, 279–292. doi: 10.1016/j.neuron.2006.12.011

Lam, Y.-W., and Sherman, S. M. (2011). Functional organization of the thalamic input to the thalamic reticular nucleus. *J. Neurosci.* 31, 6791–6799. doi: 10.1523/JNEUROSCI.3073-10.2011

Laramee, M. E., Kurotani, T., Rockland, K. S., Bronchti, G., and Boire, D. (2011). Indirect pathway between the primary auditory and visual cortices through layer V pyramidal neurons in V2L in mouse and the effects of bilateral enucleation. *Eur. J. Neurosci.* 34, 65–78. doi: 10.1111/j.1460-9568.2011.07732.x

Lee, W.-C. A., Bonin, V., Reed, M., Graham, B. J., Hood, G., Glattfelder, K., et al. (2016). Anatomy and function of an excitatory network in the visual cortex. *Nature* 532, 370–374. doi: 10.1038/nature17192

Lee, H.-K., and Kirkwood, A. (2019). Mechanisms of homeostatic synaptic plasticity *in vivo*. *Front. Cell. Neurosci.* 13:520. doi: 10.3389/fncel.2019.00520

Lee, K. K. Y., Soutar, C. N., and Dringenberg, H. C. (2018). Gating of long-term potentiation (LTP) in the thalamocortical auditory system of rats by serotonergic (5-HT) receptors. *Brain Res.* 1683, 1–11. doi: 10.1016/j.brainres.2018.01.004

Lee, H.-K., and Whitt, J. L. (2015). Cross-modal synaptic plasticity in adult primary sensory cortices. *Curr. Opin. Neurobiol.* 35, 119–126. doi: 10.1016/j.conb.2015.08.002

Lessard, N., Paré, M., Lepore, F., and Lassonde, M. (1998). Early-blind human subjects localize sound sources better than sighted subjects. *Nature* 395, 278–280. doi: 10.1038/26228

Li, L., Gainey, M. A., Goldbeck, J. E., and Feldman, D. E. (2014). Rapid homeostasis by disinhibition during whisker map plasticity. *Proc. Natl. Acad. Sci. U S A* 111, 1616–1621. doi: 10.1073/pnas.1312455111

Lombaert, N., Hennes, M., Gilissen, S., Schevenels, G., Aerts, L., Vanlaer, R., et al. (2018). 5-HTR_{2A} and 5-HTR_{3A} but not 5-HTR_{1A} antagonism impairs the cross-modal reactivation of deprived visual cortex in adulthood. *Mol. Brain* 11:65. doi: 10.1186/s13041-018-0404-5

Lu, J., Tucciarone, J., Lin, Y., and Huang, Z. J. (2014). Input-specific maturation of synaptic dynamics of parvalbumin interneurons in primary visual cortex. *Proc. Natl. Acad. Sci. U S A* 111, 16895–16900. doi: 10.1073/pnas.1400694111

Maffei, A., Nataraj, K., Nelson, S. B., and Turrigiano, G. G. (2006). Potentiation of cortical inhibition by visual deprivation. *Nature* 443, 81–84. doi: 10.1038/nature05079

Maffei, A., Nelson, S. B., and Turrigiano, G. G. (2004). Selective reconfiguration of layer 4 visual cortical circuitry by visual deprivation. *Nat. Neurosci.* 7, 1353–1359. doi: 10.1038/nn1351

Maffei, A., and Turrigiano, G. G. (2008). Multiple modes of network homeostasis in visual cortical layer 2/3. *J. Neurosci.* 28, 4377–4384. doi: 10.1523/JNEUROSCI.5298-07.2008

Manunta, Y., and Edeline, J. M. (1997). Effects of noradrenaline on frequency tuning of rat auditory cortex neurons. *Eur. J. Neurosci.* 9, 833–847. doi: 10.1111/j.1460-9568.1997.tb01433.x

Manunta, Y., and Edeline, J. M. (1999). Effects of noradrenaline on frequency tuning of auditory cortex neurons during wakefulness and slow-wave sleep. *Eur. J. Neurosci.* 11, 2134–2150. doi: 10.1046/j.1460-9568.1999.00633.x

Maruyama, A. T., and Komai, S. (2018). Auditory-induced response in the primary sensory cortex of rodents. *PLoS One* 13:e0209266. doi: 10.1371/journal.pone.0209266

Maya Vetencourt, J. F., Sale, A., Viegi, A., Baroncelli, L., De Pasquale, R., O'Leary, O. F., et al. (2008). The antidepressant fluoxetine restores plasticity in the adult visual cortex. *Science* 320, 385–388. doi: 10.1126/science.1150516

Meijer, G. T., Marchesi, P., Mejias, J. F., Montijn, J. S., Lansink, C. S., and Pennartz, C. M. A. (2020). Neural correlates of multisensory detection behavior: comparison of primary and higher-order visual cortex. *Cell Rep.* 31:107636. doi: 10.1016/j.celrep.2020.107636

Meng, X., Kao, J. P., Lee, H.-K., and Kanold, P. O. (2015). Visual deprivation causes refinement of intracortical circuits in the auditory cortex. *Cell Rep.* 12, 955–964. doi: 10.1016/j.celrep.2015.07.018

Meng, X., Kao, J. P., Lee, H. K., and Kanold, P. O. (2017). Intracortical circuits in thalamorecipient layers of auditory cortex refine after visual deprivation. *eNeuro* 4:ENEURO.0092-17.2017. doi: 10.1523/ENEURO.0092-17.2017

Merabet, L. B., Hamilton, R., Schlaug, G., Swisher, J. D., Kiriakopoulos, E. T., Pitskel, N. B., et al. (2008). Rapid and reversible recruitment of early visual cortex for touch. *PLoS One* 3:e3046. doi: 10.1371/journal.pone.0003046

Merabet, L. B., and Pascual-Leone, A. (2010). Neural reorganization following sensory loss: the opportunity of change. *Nat. Rev. Neurosci.* 11, 44–52. doi: 10.1038/nrn2758

Mesik, L., Huang, J. J., Zhang, L. I., and Tao, H. W. (2019). Sensory- and motor-related responses of layer 1 neurons in the mouse visual cortex. *J. Neurosci.* 39, 10060–10070. doi: 10.1523/JNEUROSCI.1722-19.2019

Metherate, R. (2011). Functional connectivity and cholinergic modulation in auditory cortex. *Neurosci. Biobehav. Rev.* 35, 2058–2063. doi: 10.1016/j.neubiorev.2010.11.010

Metherate, R., Cox, C. L., and Ashe, J. H. (1992). Cellular bases of neocortical activation: modulation of neural oscillations by the nucleus basalis and endogenous acetylcholine. *J. Neurosci.* 12, 4701–4711. doi: 10.1523/JNEUROSCI.12-12-04701.1992

Mitchell, A. S. (2015). The mediodorsal thalamus as a higher order thalamic relay nucleus important for learning and decision-making. *Neurosci. Biobehav. Rev.* 54, 76–88. doi: 10.1016/j.neubiorev.2015.03.001

Mitchell, A. S., and Chakraborty, S. (2013). What does the mediodorsal thalamus do? *Front. Syst. Neurosci.* 7:37. doi: 10.3389/fnsys.2013.00037

Mizumori, S. J., and Williams, J. D. (1993). Directionally selective mnemonic properties of neurons in the lateral dorsal nucleus of the thalamus of rats. *J. Neurosci.* 13, 4015–4028. doi: 10.1523/JNEUROSCI.13-09-04015.1993

Mower, G. D., Berry, D., Burchfiel, J. L., and Duffy, F. H. (1981). Comparison of the effects of dark rearing and binocular suture on development and plasticity of cat visual cortex. *Brain Res.* 220, 255–267. doi: 10.1016/0006-8993(81)91216-6

Mowery, T. M., Kotak, V. C., and Sanes, D. H. (2016). The onset of visual experience gates auditory cortex critical periods. *Nat. Commun.* 7:10416. doi: 10.1038/ncomms10416

Nahmani, M., and Turrigiano, G. G. (2014). Deprivation-induced strengthening of presynaptic and postsynaptic inhibitory transmission in layer 4 of visual cortex during the critical period. *J. Neurosci.* 34, 2571–2582. doi: 10.1523/JNEUROSCI.4600-13.2014

O'Brien, R. J., Kamboj, S., Ehlers, M. D., Rosen, K. R., Fischbach, G. D., and Huganir, R. L. (1998). Activity-dependent modulation of synaptic AMPA receptor accumulation. *Neuron* 21, 1067–1078. doi: 10.1016/s0896-6273(00)80624-8

Olcese, U., Iurilli, G., and Medini, P. (2013). Cellular and synaptic architecture of multisensory integration in the mouse neocortex. *Neuron* 79, 579–593. doi: 10.1016/j.neuron.2013.06.010

Olsen, S. R., Bortone, D. S., Adesnik, H., and Scanziani, M. (2012). Gain control by layer six in cortical circuits of vision. *Nature* 483, 47–52. doi: 10.1038/nature10835

Orban, G. A. (2008). Higher order visual processing in macaque extrastriate cortex. *Physiol. Rev.* 88, 59–89. doi: 10.1152/physrev.00008.2007

Pak, A., Ryu, E., Li, C., and Chubykin, A. A. (2020). Top-down feedback controls the cortical representation of illusory contours in mouse primary visual cortex. *J. Neurosci.* 40, 648–660. doi: 10.1523/JNEUROSCI.1998-19.2019

Pascual-Leone, A., and Torres, F. (1993). Plasticity of the sensorimotor cortex representation of the reading finger in Braille readers. *Brain* 116, 39–52. doi: 10.1093/brain/116.1.39

Petrus, E., Isaiah, A., Jones, A. P., Li, D., Wang, H., Lee, H. K., et al. (2014). Crossmodal induction of thalamocortical potentiation leads to enhanced information processing in the auditory cortex. *Neuron* 81, 664–673. doi: 10.1016/j.neuron.2013.11.023

Petrus, E., Rodriguez, G., Patterson, R., Connor, B., Kanold, P. O., and Lee, H. K. (2015). Vision loss shifts the balance of feedforward and intracortical circuits in opposite directions in mouse primary auditory and visual cortices. *J. Neurosci.* 35, 8790–8801. doi: 10.1523/JNEUROSCI.4975-14.2015

Polley, D. B., Steinberg, E. E., and Merzenich, M. M. (2006). Perceptual learning directs auditory cortical map reorganization through top-down influences. *J. Neurosci.* 26, 4970–4982. doi: 10.1523/JNEUROSCI.3771-05.2006

Qu, Y., Eysel, U. T., Vandesande, F., and Arckens, L. (2000). Effect of partial sensory deprivation on monoaminergic neuromodulators in striate cortex of adult cat. *Neuroscience* 101, 863–868. doi: 10.1016/s0306-4522(00)00441-3

Ramachandran, V. S., and Gregory, R. L. (1991). Perceptual filling in of artificially induced scotomas in human vision. *Nature* 350, 699–702. doi: 10.1038/350699a0

Ramaswamy, S., and Markram, H. (2015). Anatomy and physiology of the thick-tufted layer 5 pyramidal neuron. *Front. Cell. Neurosci.* 9:233. doi: 10.3389/fncel.2015.00233

Rauschecker, J. P. (1995). Compensatory plasticity and sensory substitution in the cerebral cortex. *Trends Neurosci.* 18, 36–43. doi: 10.1016/0166-2236(95)93948-w

Rauschecker, J. P., Tian, B., Korte, M., and Egert, U. (1992). Crossmodal changes in the somatosensory vibrissa/barrel system of visually deprived animals. *Proc. Natl. Acad. Sci. U S A* 89, 5063–5067. doi: 10.1073/pnas.89.11.5063

Renier, L., Cuévas, I., Grandin, C. B., Dricot, L., Plaza, P., Lerens, E., et al. (2013). Right occipital cortex activation correlates with superior odor processing performance in the early blind. *PLoS One* 8:e71907. doi: 10.1371/journal.pone.0071907

Röder, B., Teder-Sälejärvi, W., Sterr, A., Rösler, F., Hillyard, S. A., and Neville, H. J. (1999). Improved auditory spatial tuning in blind humans. *Nature* 400, 162–166. doi: 10.1038/22106

Rodríguez, G., Chakraborty, D., Schrode, K. M., Saha, R., Uribe, I., Lauer, A. M., et al. (2018). Cross-modal reinstatement of thalamocortical plasticity accelerates ocular dominance plasticity in adult mice. *Cell Rep.* 24, 3433.e4–3440.e4. doi: 10.1016/j.celrep.2018.08.072

Rodriguez, G., Mesik, L., Gao, M., Parkins, S., Saha, R., and Lee, H. K. (2019). Disruption of NMDA receptor function prevents normal experience-dependent homeostatic synaptic plasticity in mouse primary visual cortex. *J. Neurosci.* 39, 7664–7673. doi: 10.1523/JNEUROSCI.2117-18.2019

Roth, M. M., Dahmen, J. C., Muir, D. R., Imhof, F., Martini, F. J., and Hofer, S. B. (2016). Thalamic nuclei convey diverse contextual information to layer 1 of visual cortex. *Nat. Neurosci.* 19, 299–307. doi: 10.1038/nn.4197

Saalmann, Y. B., and Kastner, S. (2011). Cognitive and perceptual functions of the visual thalamus. *Neuron* 71, 209–223. doi: 10.1016/j.neuron.2011.06.027

Sadato, N., Pascual-Leone, A., Grafman, J., Ibañez, V., Deiber, M. P., Dold, G., et al. (1996). Activation of the primary visual cortex by Braille reading in blind subjects. *Nature* 380, 526–528. doi: 10.1038/380526a0

Salgado, H., Treviño, M., and Atzori, M. (2016). Layer- and area-specific actions of norepinephrine on cortical synaptic transmission. *Brain Res.* 1641, 163–176. doi: 10.1016/j.brainres.2016.01.033

Sanderson, K. J., Dreher, B., and Gayer, N. (1991). Prosencephalic connections of striate and extrastriate areas of rat visual cortex. *Exp. Brain Res.* 85, 324–334. doi: 10.1007/BF00229410

Sandmann, P., Dillier, N., Eichele, T., Meyer, M., Kegel, A., Pascual-Marqui, R. D., et al. (2012). Visual activation of auditory cortex reflects maladaptive plasticity in cochlear implant users. *Brain* 135, 555–568. doi: 10.1093/brain/awr329

Scheyltjens, I., Vreysen, S., Van den Haute, C., Sabanov, V., Balschun, D., Baekelandt, V., et al. (2018). Transient and localized optogenetic activation of somatostatin-interneurons in mouse visual cortex abolishes long-term cortical plasticity due to vision loss. *Brain Struct. Funct.* 223, 2073–2095. doi: 10.1007/s00429-018-1611-7

Seol, G. H., Ziburkus, J., Huang, S., Song, L., Kim, I. T., Takamiya, K., et al. (2007). Neuromodulators control the polarity of spike-timing-dependent synaptic plasticity. *Neuron* 55, 919–929. doi: 10.1016/j.neuron.2007.08.013

Shao, Z., and Burkhalter, A. (1996). Different balance of excitation and inhibition in forward and feedback circuits of rat visual cortex. *J. Neurosci.* 16, 7353–7365. doi: 10.1523/JNEUROSCI.16-22-07353.1996

Sherman, S. M. (2016). Thalamus plays a central role in ongoing cortical functioning. *Nat. Neurosci.* 19, 533–541. doi: 10.1038/nn.4269

Shibata, H. (2000). Organization of retrosplenial cortical projections to the laterodorsal thalamic nucleus in the rat. *Neurosci. Res.* 38, 303–311. doi: 10.1016/s0168-0102(00)00174-7

Solarana, K., Liu, J., Bowen, Z., Lee, H. K., and Kanold, P. O. (2019). Temporary visual deprivation causes decorrelation of spatiotemporal population responses in adult mouse auditory cortex. *eNeuro* 6:ENEURO.0269-19.2019. doi: 10.1523/ENEURO.0269-19.2019

Song, Y.-H., Kim, J.-H., Jeong, H.-W., Choi, I., Jeong, D., Kim, K., et al. (2017). A neural circuit for auditory dominance over visual perception. *Neuron* 93, 1236–1237. doi: 10.1016/j.neuron.2017.02.026

Sterr, A., Müller, M. M., Elbert, T., Rockstroh, B., Pantev, C., and Taub, E. (1998a). Changed perceptions in Braille readers. *Nature* 391, 134–135. doi: 10.1038/34322

Sterr, A., Müller, M. M., Elbert, T., Rockstroh, B., Pantev, C., and Taub, E. (1998b). Perceptual correlates of changes in cortical representation of fingers in blind multifinger Braille readers. *J. Neurosci.* 18, 4417–4423. doi: 10.1523/JNEUROSCI.18-11-04417.1998

Stevens, A. A., and Weaver, K. E. (2009). Functional characteristics of auditory cortex in the blind. *Behav. Brain Res.* 196, 134–138. doi: 10.1016/j.bbr.2008.07.041

Sundberg, S. C., Lindstrom, S. H., Sanchez, G. M., and Granseth, B. (2018). Cre-expressing neurons in visual cortex of Ntsr1-Cre GN220 mice are corticothalamic and are depolarized by acetylcholine. *J. Comp. Neurol.* 526, 120–132. doi: 10.1002/cne.24323

Sutton, M. A., Ito, H. T., Cressy, P., Kempf, C., Woo, J. C., and Schuman, E. M. (2006). Miniature neurotransmission stabilizes synaptic function *via* tonic suppression of local dendritic protein synthesis. *Cell* 125, 785–799. doi: 10.1016/j.cell.2006.03.040

Thomson, A. M. (2010). Neocortical layer 6, a review. *Front. Neuroanat.* 4:13. doi: 10.3389/fnana.2010.00013

Todd, T. P., Fournier, D. I., and Bucci, D. J. (2019). Retrosplenial cortex and its role in cue-specific learning and memory. *Neurosci. Biobehav. Rev.* 107, 713–728. doi: 10.1016/j.neubiorev.2019.04.016

Tremblay, R., Lee, S., and Rudy, B. (2016). GABAergic interneurons in the neocortex: from cellular properties to circuits. *Neuron* 91, 260–292. doi: 10.1016/j.neuron.2016.06.033

Turrigiano, G. G., Leslie, K. R., Desai, N. S., Rutherford, L. C., and Nelson, S. B. (1998). Activity-dependent scaling of quantal amplitude in neocortical neurons. *Nature* 391, 892–896. doi: 10.1038/36103

Van Boven, R. W., Hamilton, R. H., Kauffman, T., Keenan, J. P., and Pascual-Leone, A. (2000). Tactile spatial resolution in blind braille readers. *Neurology* 54, 2230–2236. doi: 10.1212/wnl.54.12.2230

Van Brussel, L., Gerits, A., and Arckens, L. (2011). Evidence for cross-modal plasticity in adult mouse visual cortex following monocular enucleation. *Cereb. Cortex* 21, 2133–2146. doi: 10.1093/cercor/bhq286

van Groen, T., and Wyss, J. M. (1992). Projections from the laterodorsal nucleus of the thalamus to the limbic and visual cortices in the rat. *J. Comp. Neurol.* 324, 427–448. doi: 10.1002/cne.903240310

Vélez-Fort, M., Rousseau, C. V., Niedworok, C. J., Wickersham, I. R., Rancz, E. A., Brown, A. P., et al. (2014). The stimulus selectivity and connectivity of layer six principal cells reveals cortical microcircuits underlying visual processing. *Neuron* 83, 1431–1443. doi: 10.1016/j.neuron.2014.08.001

Voss, P., Lassonde, M., Gougoux, F., Fortin, M., Guillemot, J. P., and Lepore, F. (2004). Early- and late-onset blind individuals show supra-normal auditory abilities in far-space. *Curr. Biol.* 14, 1734–1738. doi: 10.1016/j.cub.2004.09.051

Weil, R. S., and Rees, G. (2011). A new taxonomy for perceptual filling-in. *Brain Res. Rev.* 67, 40–55. doi: 10.1016/j.brainresrev.2010.10.004

Wertz, A., Trenholm, S., Yonehara, K., Hillier, D., Raics, Z., Leinweber, M., et al. (2015). Single-cell-initiated monosynaptic tracing reveals layer-specific cortical network modules. *Science* 349, 70–74. doi: 10.1126/science.aab1687

Williams, L. E., and Holtmaat, A. (2019). Higher-order thalamocortical inputs gate synaptic long-term potentiation *via* disinhibition. *Neuron* 101, 91.e4–102.e4. doi: 10.1016/j.neuron.2018.10.049

Wimmer, R. D., Schmitt, L. I., Davidson, T. J., Nakajima, M., Deisseroth, K., and Halassa, M. M. (2015). Thalamic control of sensory selection in divided attention. *Nature* 526, 705–709. doi: 10.1038/nature15398

Winkowski, D. E., Nagode, D. A., Donaldson, K. J., Yin, P., Shamma, S. A., Fritz, J. B., et al. (2018). Orbitofrontal cortex neurons respond to sound and activate primary auditory cortex neurons. *Cereb. Cortex* 28, 868–879. doi: 10.1093/cercor/bhw409

Wong, M., Gnanakumaran, V., and Goldreich, D. (2011). Tactile spatial acuity enhancement in blindness: evidence for experience-dependent mechanisms. *J. Neurosci.* 31, 7028–7037. doi: 10.1523/JNEUROSCI.6461-10.2011

Yang, W., Carrasquillo, Y., Hooks, B. M., Nerbonne, J. M., and Burkhalter, A. (2013). Distinct balance of excitation and inhibition in an interareal feedforward and feedback circuit of mouse visual cortex. *J. Neurosci.* 33, 17373–17384. doi: 10.1523/JNEUROSCI.2515-13.2013

Yilmaz, M., and Meister, M. (2013). Rapid innate defensive responses of mice to looming visual stimuli. *Curr. Biol.* 23, 2011–2015. doi: 10.1016/j.cub.2013.08.015

Zhang, S., Xu, M., Chang, W.-C., Ma, C., Hoang Do, J. P., Jeong, D., et al. (2016). Organization of long-range inputs and outputs of frontal cortex for top-down control. *Nat. Neurosci.* 19, 1733–1742. doi: 10.1038/nn.4417

Zhang, S., Xu, M., Kamigaki, T., Hoang Do, J. P., Chang, W. C., Jenvay, S., et al. (2014). Selective attention. Long-range and local circuits for

top-down modulation of visual cortex processing. *Science* 345, 660–665. doi: 10.1126/science.1254126

Zhou, N. A., Maire, P. S., Masterson, S. P., and Bickford, M. E. (2017). The mouse pulvinar nucleus: organization of the tectorecipient zones. *Vis. Neurosci.* 34:E011. doi: 10.1017/S0952523817000050

Zikopoulos, B., and Barbas, H. (2007). Circuits formultisensory integration and attentional modulation through the prefrontal cortex and the thalamic reticular nucleus in primates. *Rev. Neurosci.* 18, 417–438. doi: 10.1515/revneuro.2007.18.6.417

Zingg, B., Chou, X.-L., Zhang, Z.-G., Mesik, L., Liang, F., Tao, H. W., et al. (2017). AAV-mediated anterograde transsynaptic tagging: mapping corticocollicular input-defined neural pathways for defense behaviors. *Neuron* 93, 33–47. doi: 10.1016/j.neuron.2016.11.045

Zur, D., and Ullman, S. (2003). Filling-in of retinal scotomas. *Vis. Res.* 43, 971–982. doi: 10.1016/s0042-6989(03)00038-5

Conflict of Interest: The authors declare that the research was conducted in the absence of any commercial or financial relationships that could be construed as a potential conflict of interest.

frontiers in Neural Circuits

ORIGINAL RESEARCH
published: 28 May 2021
doi: 10.3389/fncir.2021.670858

Early Sensory Deprivation Leads to Differential Inhibitory Changes in the Striatum During Learning

Nihaad Paraouty[1]* *and Todd M. Mowery*[2,3]

[1]Center for Neural Science, New York University, New York, NY, United States, [2]Department of Otolaryngology, Head and Neck Surgery, Rutgers Robert Wood Johnson Medical School, New Brunswick, NJ, United States, [3]Rutgers Brain Health Institute, Rutgers University, New Brunswick, NJ, United States

The corticostriatal circuit has been identified as a vital pathway for associative learning. However, how learning is implemented when the sensory striatum is permanently impaired remains unclear. Using chemogenetic techniques to suppress layer five auditory cortex (AC) input to the auditory striatum, learning of a sound discrimination task was significantly impacted in freely moving Mongolian gerbils, in particular when this suppression occurs early on during learning. Whole-cell recordings sampled throughout learning revealed a transient reduction in postsynaptic (GABAA) inhibition in both striatal D1 and D2 cells in normal-hearing gerbils during task acquisition. In contrast, when the baseline striatal inhibitory strengths and firing rates were permanently reduced by a transient period of developmental sensory deprivation, learning was accompanied by augmented inhibition and increased firing rates. Direct manipulation of striatal inhibition *in vivo* and *in vitro* revealed a key role of the transient inhibitory changes in task acquisition. Together, these results reveal a flexible corticostriatal inhibitory synaptic plasticity mechanism that accompanies associative auditory learning.

Keywords: corticostriatal pathway, associative learning, auditory discrimination, medium spiny neuron, layer 5 neurons, synaptic inhibition, hearing loss

OPEN ACCESS

Edited by:
Livia de Hoz, Charité—Universitätsmedizin Berlin, Germany

Reviewed by:
Qiaojie Xiong, Stony Brook University, United States
Yulia Dembitskaya, Collège de France, France

***Correspondence:**
Nihaad Paraouty
np64@nyu.edu

Received: *22 February 2021*
Accepted: *29 April 2021*
Published: *28 May 2021*

Citation:
Paraouty N and Mowery TM (2021) Early Sensory Deprivation Leads to Differential Inhibitory Changes in the Striatum During Learning. Front. Neural Circuits 15:670858. doi: 10.3389/fncir.2021.670858

INTRODUCTION

The ability of an organism to associate different stimuli from the environment with specific sets of actions is fundamental to survival. Evidence from a range of species suggests that the corticostriatal network governs the acquisition of goal-directed behaviors (Balleine et al., 2007; Balleine and O'Doherty, 2010; Dolan and Dayan, 2013; Reig and Silberberg, 2014; Sippy et al., 2015; Yartsev et al., 2018; Cox and Witten, 2019), and reward-based learning in general (Wickens et al., 2003, 2007; Calabresi et al., 2007; Thorn et al., 2010; Humphries et al., 2012; Kupferschmidt et al., 2017). Degeneration in the corticostriatal network is linked to a spectrum of neurological and neuropsychiatric disorders, such as autism spectrum, Huntington's, schizophrenia, Parkinson's, amyotrophic lateral sclerosis, and obsessive-compulsive disorder (Shepherd, 2013), which are often accompanied by various impairments in action control and reward-related processes.

Abbreviations: AM, amplitude modulation; AC, auditory cortex; DREADD, Designer Receptors Exclusively Activated by Designer Drug; EP, earplugged-reared; EPSP, excitatory postsynaptic strengths; IPSP, inhibitory postsynaptic strength; IT, intratelencephalic neurons; eLTP, long-term excitatory plasticity; MSN, medium spiny neuron; PT, pyramidal tract neurons.

The posterior tail of the dorsal striatum, termed the auditory striatum plays a key role in sound-action associations (Znamenskiy and Zador, 2013; Xiong et al., 2015; Chen et al., 2019; Guo et al., 2019). In fact, the auditory striatum receives a majority of its excitatory inputs from the auditory cortex (AC; McGeorge and Faull, 1989; Voorn et al., 2004; Budinger et al., 2008; Hackett, 2011; Mowery et al., 2017). More precisely, the AC-auditory striatum circuit has been shown to be critical for sound discrimination (Znamenskiy and Zador, 2013), and optogenetic activation or silencing of auditory striatal neurons can bias discrimination performances (Guo et al., 2018). Like the rest of the basal ganglia, the auditory striatum includes two distinct populations of medium spiny neurons (MSNs), defined in part by the expression of dopamine receptor type: D1-receptor expressing (direct pathway) and D2-receptor expressing cells (indirect pathway). These MSNs receive, in majority excitatory input from AC layer 5 intratelencephalic neurons (IT) and pyramidal tract neurons (PT), respectively (Reiner et al., 2010; Cui et al., 2013; Freeze et al., 2013; Kress et al., 2013; Calabresi et al., 2014; Cazorla et al., 2014; Rock et al., 2016). In the classical model, the direct pathway is associated with reinforcing movement and locomotion, while the indirect pathway is linked to freezing and movement suppression (Cox and Witten, 2019). However, their respective roles in learning an auditory discrimination task remain unclear, especially when the auditory striatum is permanently impaired.

At a cellular level, learning is often associated with a transient downregulation in GABAergic inhibition that facilitates long–term excitatory plasticity (eLTP) in cortical processing (Wigström and Gustafsson, 1986; Steward et al., 1990; Mott and Lewis, 1991; Bilkey, 1996; Brucato et al., 1996; Cho et al., 2000; Ziakopoulos et al., 2000; Kreitzer and Malenka, 2008; Ormond and Woodin, 2011; Perugini et al., 2012). Similarly, auditory learning and eLTP in normal hearing models have been linked to transient decreases in inhibitory synaptic gain in layer 2/3 AC cells (Letzkus et al., 2011; Sarro et al., 2015), and in the perirhinal cortex (Kotak et al., 2017). However, the baseline inhibition in striatal cells is permanently disturbed with a transient period of developmental sensory deprivation (Mowery et al., 2017). Here, we asked whether auditory learning was accompanied by similar reductions in inhibition in such an impaired model of the corticostriatal pathway. Thus, using a combination of *in vivo* behavioral measures and *in vitro* recordings, we examined the changes in cellular and synaptic properties of layer 5 AC cells and their auditory recipient striatal D1 and D2 cells throughout learning of a Go-Nogo auditory discrimination task in control and developmental sensory-deprived Mongolian gerbils.

We first demonstrated the necessity of the corticostriatal pathway in learning a sound discrimination task by chemogenetically suppressing excitatory cortical input to auditory striatal D1 and D2 cells. As control animals transitioned from a naïve stage of poor discrimination performances to better discrimination performances, *in vitro* whole-cell recordings revealed a local and transient decrease in inhibitory post-synaptic strengths in D1 and D2 striatal cells. In contrast, we found that learning was accompanied by augmented inhibition in D1 and D2 striatal cells of developmental sensory-deprived animals. By direct manipulation of inhibitory levels during task acquisition, we found that learning could be suppressed in control animals when inhibition was maintained at a high level through local infusions of a GABAA-α2/3 subunit receptor agonist. Together, these results bridge the gap between control and pathological corticostriatal networks by showing that reduced inhibition might not be the only facilitating factor for auditory associative learning in the corticostriatal network. Our results suggest that transient changes to the inhibitory tone in striatal D1 and D2 cells may be required for learning-related plasticity to occur. Such transient and flexible inhibitory shifts in both striatal D1 and D2 cells may be key for reward-based auditory learning.

MATERIALS AND METHODS

Experimental Animals

Gerbil (*Meriones unguiculatus*) pups were weaned at postnatal day (P) 30 from commercial breeding pairs (Charles River). Littermates were caged together, but separated by sex, and maintained in a 12 h light/dark cycle. All procedures related to the maintenance and use of animals were approved by the University Animal Welfare Committee at New York University. Both male and female gerbils were tested (n = 109 gerbils, 67 female).

Reversible Auditory Deprivation

Mild auditory deprivation was induced by inserting a malleable plug (BlueStik Adhesive Putty, RPM International Inc.) into the opening of each ear canal at P11 (Mowery et al., 2014, 2017; Caras and Sanes, 2015). Animals were checked daily, and earplugs were adjusted to accommodate growth. Earplugs were removed at P35. Earplugs attenuate auditory brainstem responses and perceptual thresholds by approximately 15–50 dB, depending on frequency, and the attenuation is completely reversible (Mowery et al., 2014; Caras and Sanes, 2015).

Behavioral Setup

Gerbils were placed in a plastic test cage (dimensions: 0.25 × 0.25 × 0.4 m for 62 animals and 0.4 × 0.4 × 0.4 m for 42 animals) that was housed in a sound attenuation booth (Industrial Acoustics; internal dimensions: 2.2 × 2 × 2 m), and observed *via* a closed-circuit monitor. Auditory stimuli were delivered from a calibrated free-field tweeter (DX25TG0504; Vifa) positioned 1 m above the test cage. Sound calibration measurements were made with 1/4 inch free-field condenser recording microphone (Bruel and Kjaer). A pellet dispenser (Med Associates Inc., 20 mg) was connected to a food tray placed within the test cage, and a nose port was placed on the opposite side. Stimuli, food reward delivery, and behavioral data acquisition were controlled by a personal computer through custom MATLAB scripts and an RZ6 multifunction processor (Tucker-Davis Technologies).

Sound Stimuli

The Go stimulus consisted of amplitude modulated (AM) frozen broadband noise tokens (25 dB roll-off at 3.5 kHz and 20 kHz) with a modulation rate of 12 Hz and a modulation depth of 100%.

The Nogo stimulus was similar to the Go stimulus, except for the modulation rate which was 4 Hz. Both Go and Nogo stimuli had a 200 ms onset ramp, followed by an unmodulated period of 200 ms which then transitioned to an AM stimuli. The sound level used was 66 dB SPL.

Behavioral Training

Animals were placed on controlled food access and trained using an appetitive reinforcement operant conditioning procedure. When introduced to the test cage, animals first learned to eat food pellets (Bio Serv) placed in the food tray. After this phase, the Go stimulus (12 Hz AM, 100% modulation depth) was delivered whenever animals were at the food tray. Animals were then trained to respond to the Go stimulus by approaching the food tray. After this sound-food association phase, the nose port was placed in the testing cage. During the first day of nose port training, the experimenter triggered trials whenever animals were in close proximity to the port. This maximized exploration of the nose port and facilitated poking behavior. Within 1 to 2 training sessions, animals were shaped to reliably initiate Go trials by placing their nose in the port, without any experimenter intervention. During the nose port training sessions, only Go stimuli were presented. Once animals reached a hit rate >80% and were performing a minimum of 80 Go trials, Nogo trials were introduced and the Go-Nogo phase began.

At this point, animals were run once per day until they performed at least 80 Go trials and at least 20 Nogo trials. Typically, a session lasted on average 30 min (min-max: 20–50 min). During Go trials, responses were scored as a Hit when animals approached the food tray and broke a light beam to obtain a food reward. If animals re-poked or did not respond during the 5-s time window following a Go stimulus, then it was scored a Miss. During Nogo trials, responses were scored as a False Alarm when animals incorrectly approached the food tray and broke the light beam. If animals re-poked or did not respond during the 5-s time window following a Nogo stimulus, then it was scored a Correct Reject. On the second day of Nogo training, False Alarm trials were paired with a 2-s time out, during which the house lights were extinguished and the animal could not initiate a new trial. From day 3 onwards, a 4-s time out was used when animals False Alarmed. The presentation of Go and Nogo trials was randomized to avoid animals developing a predictive strategy. Hit and False Alarm rates were constrained to floor (0.05) and ceiling (0.95) values. A performance metric, d prime (d′) was calculated for each session by performing a z-transform of both Hit rate and False Alarm rate: $d' = z(\text{Hit rate}) - z(\text{False Alarm rate})$ (Green and Swets, 1966).

Three different phases of learning were described, based on the results from **Figure 1**. First, a *naïve phase* was described as d′ criteria values <1 as the iDREADD + c21 animals (**Figure 1C**, purple line) showed a d′ below 1 across the eight tested days. Next, an *acquisition phase* was described based on the results from **Figure 1D** (late c21 group). Once those animals were performing with a d′ > 1, c21 infusions did not decrease their performance below 1. Thus the acquisition phase was defined here for d′ values comprised between 1 and 2. Last, a *mastery phase* was defined as the range of values closest to the highest d′ value, which is limited by the Hit and False Alarm rates. The latter was constrained to the floor (0.05) and ceiling (0.95) values. In order to account for variance between sessions, the mastery phase was defined for all d′ values >2.

Designer Receptors Exclusively Activated by Designer Drug Transfection

Gerbils were anesthetized (isoflurane 2%) and placed in a stereotaxic frame. The left and right temporal bone was exposed. A craniotomy was made in the temporal bone at the level of core AC (∼3.9–3.2 mm rostral from lambda), and a durotomy was made around 3.5 and 3.3 mm rostral from lambda. A glass pipette was loaded with adenovirus containing a CaMKII promotor that transfects pyramidal neurons with the inhibitory DREADDs receptor HM4D (pAAV-CaMKIIa-hM4D(Gi)-mCherry, Plasmid #50477). A Nanoject (Drummond) was then used to deliver 350 nL of the virus at a depth of 800–900 microns from the pial surface. Injections were made bilaterally. Histological feedback from our animals confirmed that the injection sites were consistently in Layer 5, although spread to other laminar layers did occur. Note that DREADDs activation occurred downstream through cannula perfusion of the activating drug. Finally, the craniotomy was covered with sterile bone wax, and the surgical site was closed with sutures.

Cannula Implantation

Gerbils were anesthetized (isoflurane 2%), placed in a stereotaxic frame, and the parietal, occipital, and frontal bones were exposed. The skin overlying these bones was removed and sinew were removed from the surface of the skull. Two anchor screws were placed over the frontal cortex and secured in place with dental acrylic (Hereaus). Two craniotomies were made for bilateral cannula insertion into striatal areas designated to receive dense input from AC layer 5 (∼4.7 mm lateral and 3.7 mm rostral of lambda, see Mowery et al., 2017). Cannulae (Plastics One) were lowered to a depth of 3 mm from the skull surface and secured in place with dental acrylic (Hereaus). Dummy guide cannulae were inserted and protective caps were locked in place. Animals were allowed to recover for 1 week.

Cannula Infusions

Prior to all infusions, animals were anesthetized (∼2% isoflurane). The concentration of the inhibitory-DREADD activating drug: Compound 21 (c21, HelloBio) was 5 mg/ml. Physiological saline (0.9% NaCl) was infused as indicated. The concentration of $GABA_A$-α2/3 subunit agonist: TPA023 (Sigma) was 5 mg/ml. The dose of drugs and saline infused was 2 μl at a rate of 1 μl per minute. The dose remained unchanged for all animals across testing days. Following infusions, animals were allowed to fully recover in a recovery cage (for 15 min on average) before behavioral testing began. Higher doses of c21 produced noted behavioral, motor effects (like thigmotaxis and lethargy) suggesting both the effectiveness of the drugs

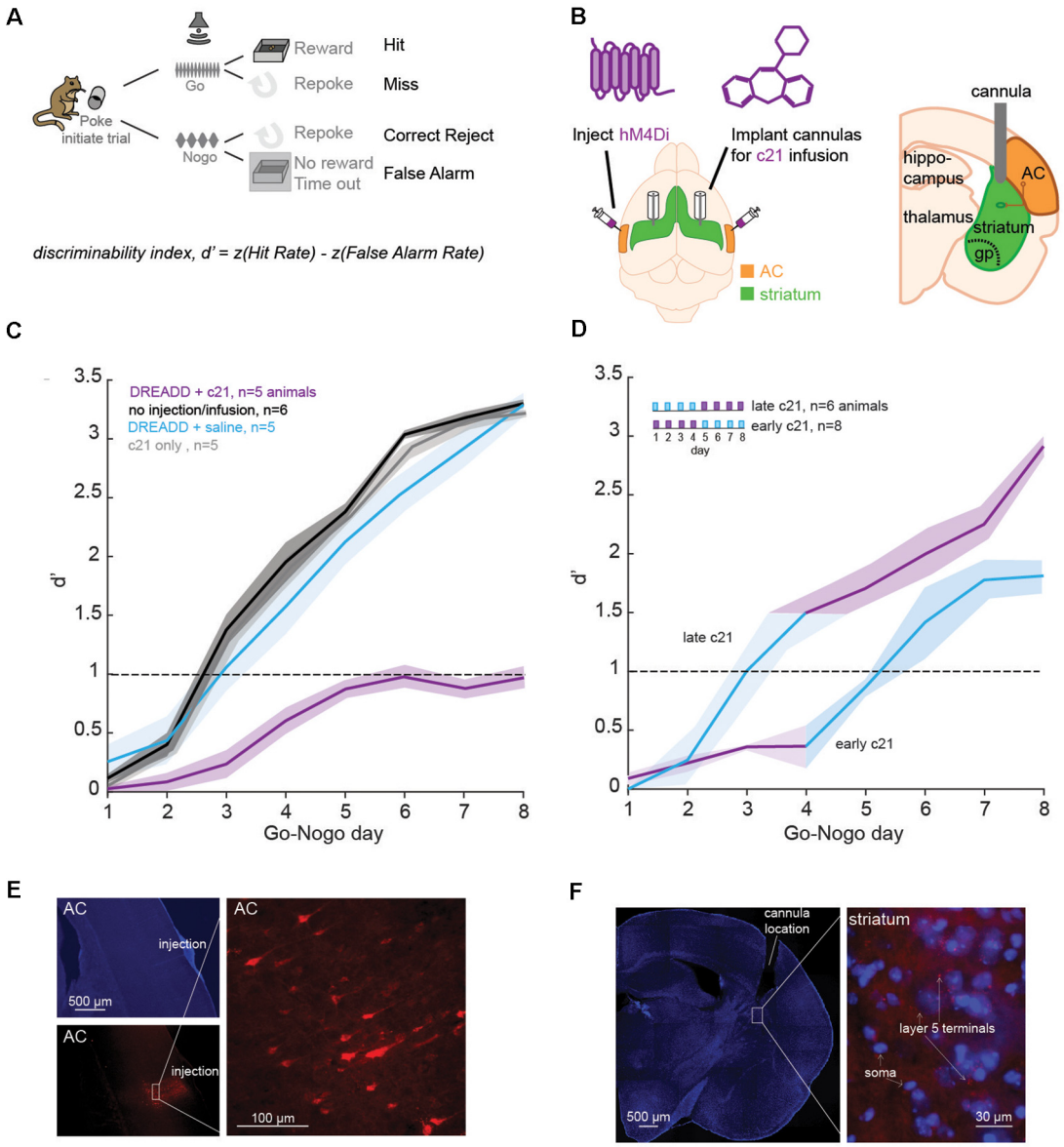

FIGURE 1 | Suppression of the corticostriatal pathway impacts learning. **(A)** Go-Nogo discrimination task. A performance measure, d′ is computed for each animal and for each Go-Nogo session. **(B)** Illustration of the surgical procedure in which bilateral injections of iDREADD are performed in the auditory cortex (AC), followed by cannulae insertions in the auditory striatum. Local infusions of the activating agent, c21, or saline were carried out prior to behavioral testing. **(C)** Mean (±SEM) d′ measures across Go-Nogo days for different groups tested: (1) in purple, animals with iDREADD injections and c21 infusions, (2) in black, animals without iDREADD injections and without any infusion, (3) in blue, animals with iDREADD injections and saline infusions, and (4) in gray, animals without iDREADD injections but with c21 infusions. **(D)** Mean (±SEM) d′ measures for two additional groups: (1) late c21 animals with iDREADD injections and saline infusions on days 1–4, followed by c21 infusions on days 5–8, and (2) early c21 animals with iDREADD injections and c21 infusions on days 1–4, followed by saline infusions on days 5–8. **(E)** Photomicrographs confirming the injection site of iDREADD with labeled AC cells (mCherry). **(F)** Confirmation of the position of implanted cannulae in the dorsolateral striatum with an overlay of MSNs (in blue, DAPI) and AC projections (in red, mCherry).

and volumetric spread thresholds into the sensorimotor areas of the striatum.

Corticostriatal Brain Slice Preparation

Brain slices were obtained within 3 h after a training/testing session. The details for corticostriatal brain slice preparation have been previously described (see Mowery et al., 2017). Animals were deeply anesthetized (chloral hydrate, 400 mg/kg, IP) and brains dissected into 4°C oxygenated artificial cerebrospinal fluid (ACSF, in mM: 125 NaCl, 4 KCl, 1.2 KH_2PO_4, 1.3 $MgSO_4$, 26 $NaHCO_3$, 15 glucose, 2.4 $CaCl_2$, and 0.4 L-ascorbic acid; and bubbled with 95%O_2-5%CO_2 to a pH = 7.4). A 25° cut was made through the right hemisphere and the brains were vibratome-sectioned through the left hemisphere to obtain 300–400 µm

perihorizontal auditory corticostriatal slices. To validate the thalamo-recipient AC, a bipolar stimulating electrode (FHC) was placed at the rostral border of the medial geniculate (MG), and MG-evoked field responses were recorded in the AC. To validate cortico-recipient striatum, a bipolar stimulating electrode was placed in layer 5 AC and AC-evoked field responses were recorded in the striatum. Whole-cell current clamp recordings were obtained (Warner PC-501A) from striatal MSNs at 32°C in oxygenated ACSF. Recording electrodes were fabricated from borosilicate glass (1.5 mm OD; Sutter P-97). The internal recording solution contained (in mM): 5 KCl, 127.5 K-gluconate, 10 HEPES, 2 $MgCl_2$, 0.6 EGTA, 2 ATP, 0.3 GTP, and 5 phosphocreatine (pH 7.2 with KOH). The resistance of patch electrodes filled with an internal solution was between 5 and 10 MΩ. Access resistance was 15–30 MΩ, and was compensated by about 70%.

Recordings were digitized at 10 kHz and analyzed offline using custom Igor-based macros (IGOR, WaveMetrics, Lake Oswego, OR, USA). All recorded neurons had a resting potential ≤−50 mV and overshooting action potentials. Frequency-current (F-I) curves were constructed from the responses to 1,500 ms current pulses, in steps of 100 pA (Mowery et al., 2014). Inhibitory postsynaptic potentials (IPSP) were evoked *via* biphasic stimulation of local fast-spiking interneurons for striatal neurons (1–10 mV, 10 s interstimulus interval) in the presence of ionotropic glutamate receptor antagonists (6,7-Dinitroquinoxaline-2,3-dione, DNQX, 20 μM; 2-amino-5-phosphonopentanoate, AP-5, 50 μM). The drugs were applied for a minimum of 8 min before recording IPSPs. Importantly, all recordings were systematically carried out at 200–300 microns from the right shank of the biphasic stimulator. In addition, the depth of recordings were carried out in the first 15–25 microns of tissue as visibility quickly decreases in striatal tissue under IRDIC illumination. To control for differences in stimulation strengths, we systematically employed 0.3–0.4 mA of stimulation to obtain a plateau in IPSP amplitudes. Once this maximum was reached, increasing stimulation did not lead to further increases in amplitude or duration for both GABA-A/B potentials. In addition, pilot studies demonstrated that higher stimulation levels tend to damage the surrounding tissue and lead to local circuit changes (results not shown here). Peak amplitudes of the short latency hyperpolarization (putative GABAA component) were measured from each response at a holding potential (V_{hold}) of −50 mV. In a subset of experiments (n = 10), we verified that the short-latency IPSP components were selectively blocked by a GABAA antagonist (20 μM bicuculline), thereby suggesting that the IPSPs reported in this study are related to GABAA receptor potentials.

Assessing the Suppression Effect of hM4Di-DREADD Activating Drug

Proof of principle experiments for inhibitory DREADD inhibitory action were conducted in animals (n = 2) that had received unilateral injections of iDREADD 2–3 weeks prior to corticostriatal slice preparation (see **Supplementary Figure 2**). For these experiments, whole cell recordings were made from medium spiny cells (current clamp: −80 mV hold). Excitatory postsynaptic potentials were evoked by stimulating layer 5 AC pyramidal cells with a biphasic stimulating electrode. Cells were held at −80 mV to isolate AMPA receptor potentials. After establishing a baseline, cells were exposed to 30 min of ACSF containing the iDREADD activating drug: Compound 21 (50 uM, HelloBio). Excitatory post synaptic potentials (EPSPs) were collected up to an hour after drug exposure prior to washout.

Histology

At the end of experiments all implanted animals were deeply anesthetized with an intraperitoneal injection of sodium pentobarbital (150 mg/kg) and perfused with phosphate-buffered saline and 4% paraformaldehyde. Brains were extracted, post-fixed, and sectioned at 50 μm on a benchtop vibratome (Leica). Sections were stained for DAPI (4′,6-diamidino-2-phenylindole), and coverslipped for imaging. DAPI images were acquired at 2×, 10× and 40× using a revolve microscope (Echo) and locations of cannulae were verified and compared to a gerbil brain atlas (Radtke-Schuller et al., 2016). For the animals which received both iDREADD injections and bilateral cannulae implants, both brightfield and fluorescent images were acquired to confirm virus expression in AC and projections to the auditory striatum.

Statistical Analyses

Statistical tests for distribution and significance were performed using the SAS-based package JMP. Normality was determined using the Shapiro–Wilk Test. Groups with normally distributed data were analyzed using a mixed-model ANOVA, as indicated. Tukey's HSD comparisons were used as indicated for pairwise comparisons. Nonparametric statistical tests were used when data was not normally distributed (Wilcoxon tests).

RESULTS

Necessity of the Corticostriatal Pathway in Learning a Sound Discrimination Task

We first assessed the necessity of the corticostriatal pathway in learning a Go-Nogo sound discrimination task in freely-moving Mongolian gerbils (**Figure 1A**). Specifically, we chemogenetically suppressed the excitatory input from layer 5 AC to the auditory striatum with an inhibitory Designer Receptors Exclusively Activated by Designer Drug (iDREADD; **Supplementary Figure 1**). To suppress both D1 and D2 pathways, we bilaterally injected hM4Di-mCherry, an inhibitory DREADD into AC layer 5 to express hM4Di receptor in IT and PT neurons (**Figure 1B**). The hM4Di receptor hyperpolarizes the cell (i.e., increases potassium influx), and decreases the presynaptic excitability, thereby reducing the probability of presynaptic glutamatergic release (see **Supplementary Figure 2**). To limit iDREADD activation to different projecting sites of IT and PT cells, we implanted bilateral cannulae in the auditory striatum for local infusions of the activating agent, compound 21 (c21, **Figure 1B**). After a week of recovery, animals began the behavioral task. Briefly, animals were trained to initiate each

trial by entering a nose-port which triggered the presentation of the Go stimulus: a 12-Hz amplitude-modulated noise (AM), signaling the availability of a food pellet. Once animals were performing >80 Go trials, with a hit rate above 80%, we proceeded to the Go-Nogo phase of the task (**Figure 1A**). The Go stimulus (12-Hz AM noise) remained unchanged and indicated the presence of a food reward, while the Nogo stimulus (4-Hz AM noise) signaled the absence of a food reward. A discrimination performance metric, d-prime (d′) was calculated for each session as d′ = z(hit rate) − z(false alarm rate).

In order to suppress the corticostriatal circuit, animals received bilateral injections of iDREADD in AC layer 5 and infusions of c21 in the auditory striatum on all Go-Nogo days (n = 5; **Figure 1C**, purple line). Three control conditions were run, the first one consisted of animals without iDREADD injections nor c21 infusions (n = 6; black line). The second control group was composed of animals which received bilateral injections of iDREADD and infusions of saline on all Go-Nogo days (n = 5; blue line). Finally, the third control group was composed of animals which only received infusions of c21 (n = 5; gray line). A significant group effect was found (mixed model ANOVA, $F_{(3,16)} = 36.76$, $p < 0.001$), with the iDREADD + c21 group (purple line) showing significantly poorer task acquisition as compared to the three control groups (all Bonferroni corrected *post hoc* comparisons, $p < 0.001$). In contrast, the three control groups were not significantly different from one another ($p > 0.05$ for all *post hoc* comparisons).

To further identify the necessity of the corticostriatal pathway at different stages of the learning process, we ran two additional groups of animals. In the first condition, animals received bilateral injections of iDREADD and infusions of c21 on the first 4 days of Go-Nogo, followed by saline infusion on the last 4 days (*early c21*, n = 8; **Figure 1D**). In parallel, animals in the second condition received bilateral injections of iDREADD and infusions of saline on the first 4 days of Go-Nogo, followed by c21 infusion on the last 4 days (*late c21*, n = 4; **Figure 1D**). Early c21 infusions caused a significant learning delay as compared to the three control groups from **Figure 1C** (mixed model ANOVA, all Bonferroni corrected *post hoc* group comparisons, $p < 0.001$). In contrast, late c21 infusions resulted in no significant group difference as compared to the three control groups from **Figure 1C** ($p > 0.05$ for all *post hoc* comparisons). Once c21 infusions were replaced by saline infusions in the early c21 group, the mean d′ measure increased above 1.0, showing that c21 infusions early on did not permanently inhibit learning.

Comparison of all groups tested showed no significant difference in terms of latency of response (one-way ANOVA, Kruskal–Wallis H test: $X^2_{(5)} = 1.45$, $p = 0.919$) nor in terms of the total number of trials performed during each session (one-way ANOVA, Kruskal–Wallis H test: $X^2_{(5)} = 2.97$, $p = 0.704$), suggesting that the learning differences reported above could not be explained by a motor deficit. Transfection and cannulae positions were confirmed for each animal at the end of each experiment (**Figures 1E,F**). Together, these results suggest that suppressing the corticostriatal pathway, in particular early on during learning prevented the acquisition of an auditory discrimination task (i.e., behavioral d′ remained below 1).

Learning Is Accompanied by a Transient Change in Inhibition in Control Animals

As the corticostriatal pathway is crucial for auditory associative learning, it is likely that such learning is supported by changes in cellular and synaptic properties of layer 5 AC cells and striatal D1 and D2 MSNs in the control (i.e., normal-hearing) model. More precisely, excitatory long-term potentiation (eLTP) associated with auditory learning has been shown to be facilitated by GABAergic inhibition in many brain regions (Cho et al., 2000; Letzkus et al., 2011; Perugini et al., 2012; Sarro et al., 2015; Kotak et al., 2017). Here, we applied a cross-sectional approach to investigate how synaptic inhibitory strengths (GABAA receptor potentials, see "Materials and Methods" section) along the direct and indirect pathways change as a function of learning. Following each day of behavioral Go-Nogo testing, an animal (n = 23) was randomly selected to undergo corticostriatal functional slice preparation, followed by whole cell current-clamp recordings of both AC layer 5 IT and PT cells, as well as their respective MSN targets, D1 and D2 cells (**Figure 2**). As described in Mowery et al. (2017), the cells were clustered using their electrophysiological properties (Kawaguchi, 1993; Cepeda et al., 2008; Gertler et al., 2008; Mowery et al., 2017; Goodliffe et al., 2018; see **Supplementary Figure 3**). The AC cell phenotype was characterized by cell type-specific discharge properties (Hattox and Nelson, 2007; Mowery et al., 2017; see **Supplementary Figure 3**). The results are presented in **Figure 2** for both AC IT and PT cells and auditory striatal D1 and D2 cells during three phases of learning characterized by different d′ criteria values based on the results from **Figures 1C,D** (see "Materials and Methods" section): a naïve phase: d′ < 1, an acquisition phase: d′ between 1 and 2, and mastery phase: d′ > 2.

Both IT (n = 26) and PT (n = 75) cells showed significant increases in their inhibitory postsynaptic strengths (IPSP amplitude, **Figure 2B**) when comparing the naïve phase with the acquisition phase, and a return to baseline during the mastery phase (IT naïve vs. acquisition, Tukey's HSD comparisons, $p = 0.034$; IT acquisition vs. mastery, $p < 0.005$; PT naïve vs. acquisition, $p < 0.001$; PT acquisition vs. mastery, $p = 0.0003$). In contrast, for the striatal D1 (n = 39) and D2 cells (n = 66; **Figure 2C**), there was a significant decrease of IPSP amplitudes from the naïve phase to the acquisition phase, and a return to baseline during the mastery phase (D1 naïve vs. acquisition, $p = 0.0023$; D1 acquisition vs. mastery, $p = 0.0108$; D2 naïve vs. acquisition, $p = 0.0003$; D2 acquisition vs. mastery, $p < 0.0001$).

Unlike IPSP strength, there were no changes to the input-output functions, i.e., evoked firing rate patterns, during task acquisition (**Figures 2D,E**). For layer 5 AC, both IT and PT cells retained similar patterns of evoked firing rate throughout learning (IT naïve vs. acquisition, $p = 0.61$; IT acquisition vs. mastery, $p = 0.67$; PT naïve vs. acquisition, $p = 0.51$; PT acquisition vs. mastery, $p = 0.81$). Similarly, no change was found for firing rate patterns in D1 and D2 cells (D1 naïve vs. acquisition, $p = 0.82$; D1 acquisition vs. mastery, $p = 0.264$;

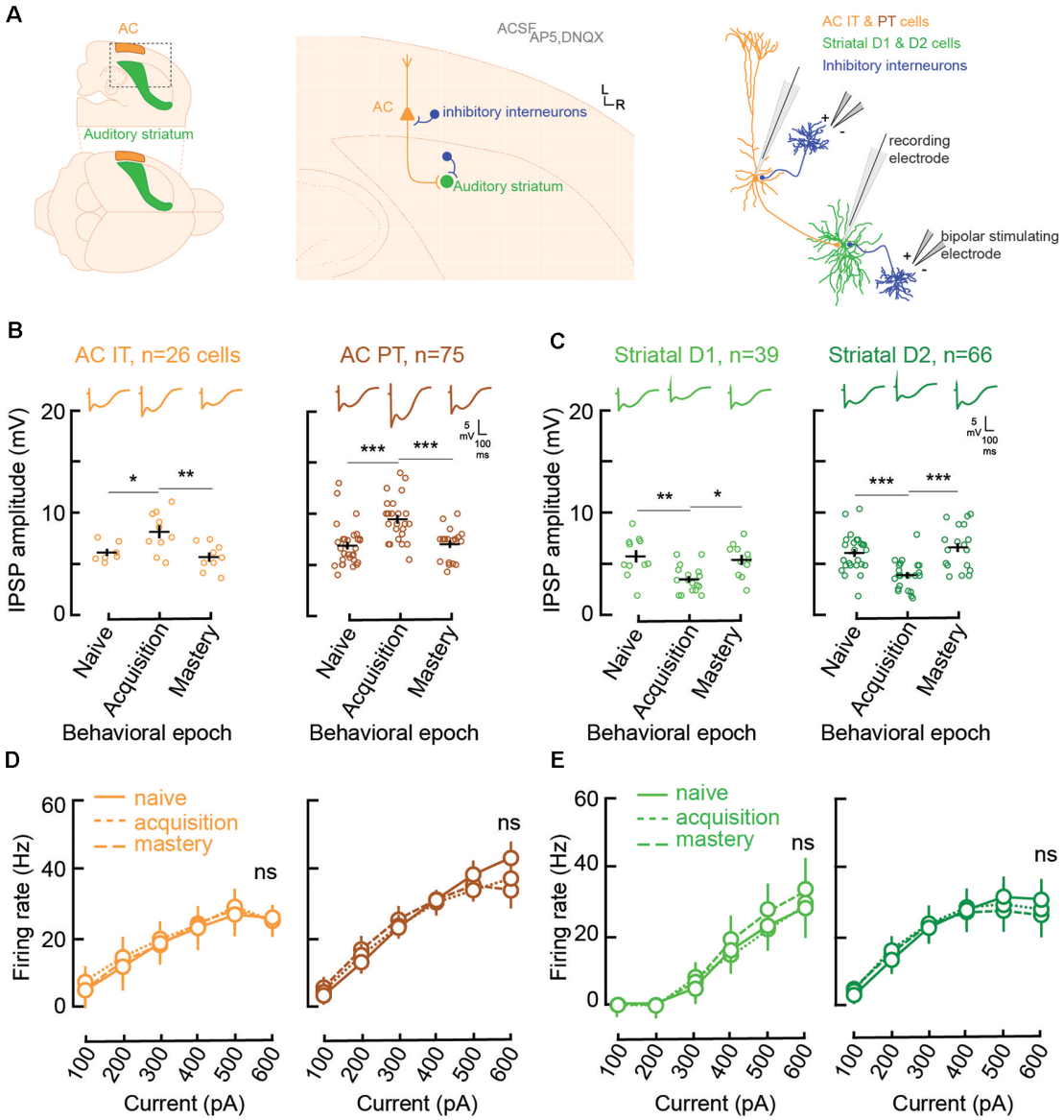

FIGURE 2 | Learning is accompanied by changes in both AC and striatal GABAA inhibitory strengths. **(A)** Illustration of slice preparation for recordings in AC layer 5 IT and PT cells, and striatal D1 and D2 MSNs. Whole-cell current was used to measure inhibitory postsynaptic strength (IPSP) amplitudes and evoked firing rates (see "Materials and Methods" section). **(B)** Individual (open circles) and mean (±SEM, black lines) maximum evoked IPSP amplitudes in AC layer 5 IT and PT cells from normal-hearing gerbils (n = 23) previously trained until their performance matched one of three behavioral epochs: naïve (d′ < 1), acquisition (d′ between 1 and 2), and mastery phase (d′ > 2). Representative traces are shown at the top. **(C)** Individual and mean (±SEM) IPSP amplitudes in striatal D1 and D2 cells as a function of behavioral epochs. **(D)** Input-output functions (firing rate patterns; mean ± SEM) for IT and PT cells as a function of behavioral epochs. **(E)** Input-output functions for striatal D1 and D2 cells as a function of behavioral epochs. Asterisks denote statistically significant differences at the following levels: *$p < 0.05$, **$p < 0.01$, ***$p < 0.001$, and ns = not significant.

D2 naïve vs. acquisition, p = 0.94; D2 acquisition vs. mastery, p = 0.61). Overall, normal auditory discrimination learning was not accompanied by changes in firing rate patterns of AC layer 5 cells nor auditory striatal cells. Conversely, auditory discrimination learning was accompanied by significant synaptic inhibitory changes, with a transient increase in IPSP strength in layer 5 AC and a transient decrease in IPSP strengths in both striatal D1 and D2 cells.

Augmented Inhibition Accompanies Learning in an Impaired Corticostriatal Model

Striatal function is permanently impacted by a transient period of sensory deprivation during development (Mowery et al., 2017). Precisely, when we compared cellular and synaptic properties of MSNs in a group of adult gerbils that received bilateral earplugs (to induce a conductive hearing

loss) early during development, permanent physiological changes were found in terms of baseline firing rates and IPSP strengths, as compared to a control population (Mowery et al., 2014, 2017; Caras and Sanes, 2015). Given those permanent shifts in inhibition, we tested whether such an impaired corticostriatal circuit was accompanied by similar changes in inhibition during learning as the control animals.

To achieve this, a group of gerbils received bilateral earplugs from the day of ear canal opening (postnatal day, P11) until the beginning of the juvenile phase of development (P35). As from P36, the earplugged reared animals (EP, n = 24) were allowed to recover under normal-hearing conditions (**Figure 3A**). The EP animals were trained in a similar manner as the control animals to perform the Go-Nogo sound discrimination task. The individual and mean performance of both groups of animals are shown in **Figure 3B** (control animals in gray and EP animals in red). The performance of both groups of animals was not statistically different (mixed model ANOVA, group effect: $F_{(1,25)}$ = 0.253, p = 0.62). No significant difference was found in terms of age (one-way ANOVA, Kruskal–Wallis H test: $X^2_{(1)}$ = 3.16, p = 0.075), or the number of trials performed per day in each group ($X^2_{(1)}$ = 1.32, p = 0.250). Similarly, no significant group difference was found in terms of response latency ($X^2_{(1)}$ = 0.05, p = 0.823).

As learning was not impacted by a transient developmental hearing loss, we asked whether similar inhibitory synaptic changes in AC and auditory striatal cells accompanied learning in the EP animals as the control ones. Hence, whole cell recordings of AC layer 5 IT (n = 26) and PT cells (n = 76), as well as their projection target D1 (n = 36) and D2 cells (n = 59) were also carried out for the EP animals at the three different phases of learning: naïve, acquisition, and mastery.

In line with Mowery et al. (2017), significant changes induced by the transient developmental auditory deprivation were present in *adult* striatal D1 and D2 cells. More precisely, there were significant reductions in baseline inhibitory strength for striatal D1, and D2 cells (**Figures 2C**, **3D**, naïve stage; baseline control vs. baseline EP, p = 0.0006 and $p < 0.0001$, respectively). In addition, significant changes in baseline evoked firing rate patterns in D1 and D2 cells were present more than 30 days after hearing was restored (**Figures 2E**, **3F**, naïve stage; baseline control vs. baseline EP, p = 0.0231 and $p < 0.0001$, respectively).

During the course of learning, in contrast to the control population, no significant changes in IPSP amplitudes were found for AC IT and PT cells in the EP group (**Figure 3C**; IT naïve vs. acquisition, Tukey's HSD corrected *post hoc* comparisons, p = 0.760; IT acquisition vs. mastery, p = 0.093; PT naïve vs. acquisition, p = 0.736; PT acquisition vs. mastery, p = 1.000). While transient decreases in IPSP amplitudes were found for control striatal cells during learning, in the EP group, significant increases in inhibitory strength were observed for both D1 and D2 cells during task acquisition (**Figure 3D**; D1 naïve vs. acquisition, p = 0.029; D2 naïve vs. acquisition, p = 0.0106). Once the EP animals mastered the task, the IPSP amplitudes returned to baseline (D1 acquisition vs. mastery, p = 0.0007; D2 acquisition vs. mastery, p = 0.0034).

Moreover, there were no significant firing rate changes in AC with learning in the EP animals (**Figure 3E**; IT naïve vs. acquisition, p = 0.820; IT acquisition vs. mastery, p = 0.468; PT naïve vs. acquisition, p = 0.232; PT acquisition vs. mastery, p = 0.130). Conversely, significant changes in the evoked firing rate patterns of EP striatal D1 and D2 cells were found with learning (**Figure 3F**). More specifically, a significant increase in firing rate was observed during the acquisition phase for both D1 and D2 cells, and a return to baseline once the EP animals mastered the task (**Figure 3F**; D1 naïve vs. acquisition, p = 0.0018; D1 acquisition vs. mastery, p = 0.0032; D2 naïve vs. acquisition, p = 0.0003; D2 acquisition vs. mastery, p = 0.0015).

Overall, in comparison to control animals, no changes in inhibitory strengths of layer 5 AC cells were found in EP animals (**Figure 4A**). However, significant changes were found in D1 and D2 cells, both in terms of IPSP amplitudes and firing rate patterns (**Figures 4A,B**). Furthermore, those transient changes both in IPSP amplitudes and firing rate patterns for D1 and D2 cells during learning move towards values close to the control population at the same stage (**Supplementary Figures 4F–H**).

Those results can be further explained by phenotype-dependent changes in the underlying cellular physiology of the EP animals. For D1 cells, a significant increase in adaptation ratio was found during task acquisition (**Supplementary Figure 5D**, D1 naïve vs. acquisition for EP, p = 0.0026; D1 acquisition vs. mastery, p = 0.0027). On the other hand, for D2 cells, significant changes in both resting membrane potential (more depolarized) and membrane resistance (higher) were observed (**Supplementary Figure 5E**, D2 naïve vs. acquisition for EP, p = 0.0042 and $p < 0.0001$; D2 acquisition vs. mastery, p = 0.0095 and p = 0.0019, respectively). In contrast, the underlying cellular physiology in control striatal D1 and D2 cells did not show any significant changes in resting membrane potential, membrane resistance, nor in sensory adaptation ratios throughout learning (**Supplementary Figures 5A–C**). Those transient shifts in the striatal cellular physiology of EP animals temporarily matched the cellular physiology of control animals during the task acquisition phase (comparison of control vs. EP for adaptation ratio in D1 cells, p = 0.5311; for resting membrane potential in D2 cells, p = 0.08; for membrane resistance in D2 cells, p = 0.538). Thus, through transient changes in adaptation ratios for D1 cells, and resting membrane potential and membrane resistance for D2 cells, the EP striatal MSNs seem to compensate for their phenotype-specific deficits and approach control values during learning. Together, these results suggest how plasticity could potentially be supported by the corticostriatal pathway when the baseline physiology is impaired.

Learning Is Causally Linked to Changes in Striatal Inhibition

In order to test whether the change in inhibition is causally related to behavioral task acquisition and learning, we used local infusions of selective GABAA agonists in the auditory striatum *in vivo*, prior to each Go-Nogo session. As we found a transient

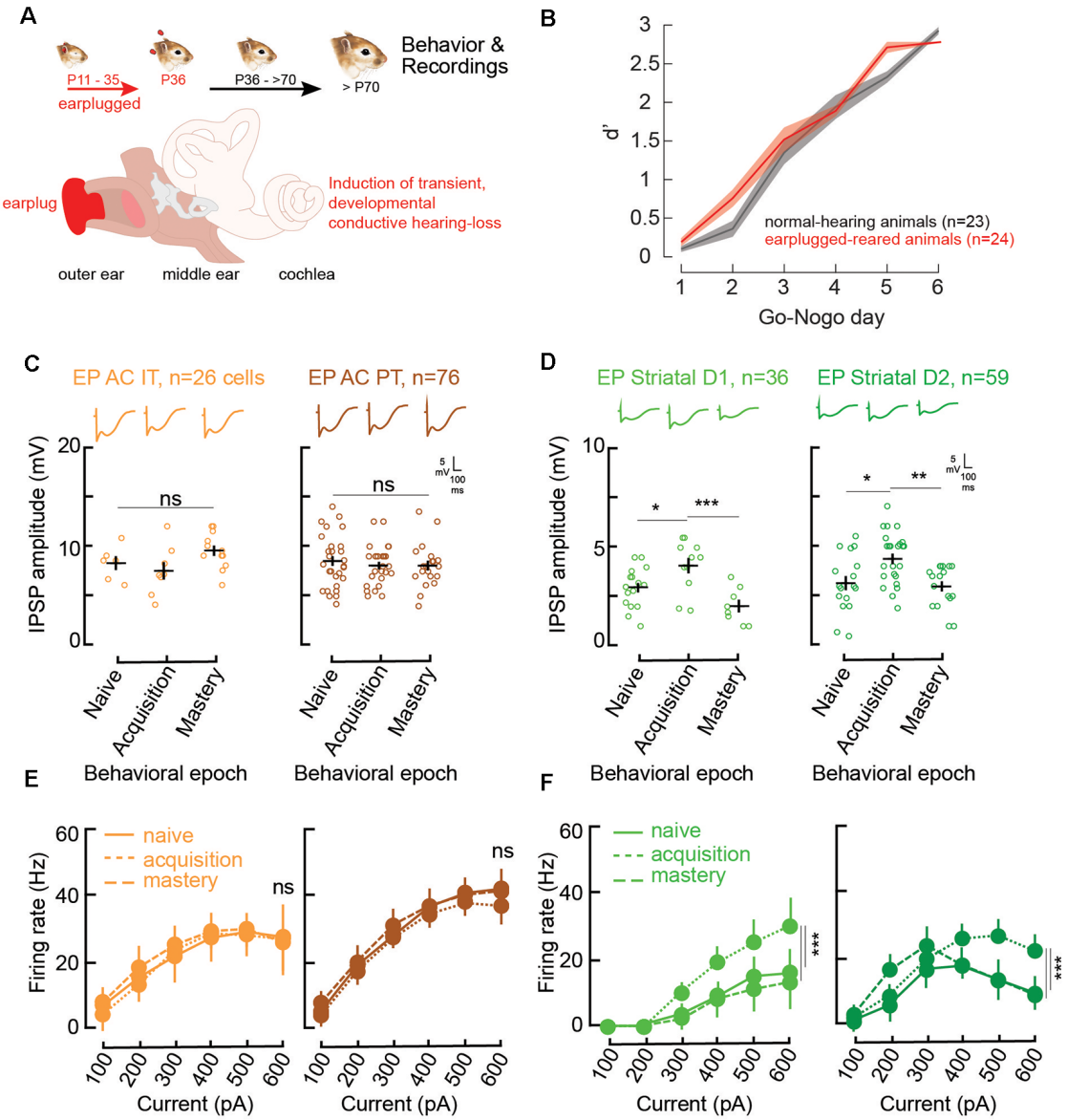

FIGURE 3 | Impaired corticostriatal circuit supports learning through increases in striatal inhibitory strengths and firing rates. **(A)** Illustration of the procedure for the induction of developmental auditory deprivation in gerbils. Animals were earplugged (EP) from P11 to P35. Behavioral testing and recordings began only from P70. **(B)** Mean (±SEM) d′ measures across Go-Nogo days for the control population (gray, $n = 23$) and the EP animals (red, $n = 24$). **(C)** Individual (open circles) and mean (±SEM, black lines) maximum evoked IPSP amplitudes of AC layer 5 IT and PT cells as a function of behavioral epochs for the EP animals. Representative traces are shown at the top. **(D)** Individual and mean (±SEM) IPSP amplitudes in striatal D1 and D2 cells as a function of behavioral epochs for the EP animals. **(E)** Input-output functions (firing rate patterns; mean ± SEM) for IT and PT cells as a function of behavioral epochs for the EP animals. **(F)** Input-output functions for striatal D1 and D2 cells as a function of behavioral epochs for the EP animals. Asterisks denote statistically significant differences at the following levels: $^{*}p < 0.05$, $^{**}p < 0.01$, $^{***}p < 0.001$, and ns = not significant.

decrease in striatal inhibition during learning in the control population (**Figure 2C**), we predicted that maintaining a high level of inhibition would impact the rate of task acquisition. With a series of additional *in vitro* experiments, we first tested the sensitivity of striatal cells to a GABAA-α2/3 subunit receptor agonist: TPA023 (50 μM), as GABAA-α1 containing receptors, are not as widely expressed in the striatum (Hörtnagl et al., 2013). As expected, during both the naïve and acquisition phases, significant increases in IPSP amplitudes were found after application of TPA023 to the bath (**Figure 5A**; $p = 0.001$ and $p = 0.004$, respectively). Those results suggest constant sensitivity to TPA023 during learning. Thus, we predicted that daily infusions of TPA023 would lead to a significant delay in learning.

Prior to behavioral training, we implanted bilateral cannulae in the auditory recipient regions of the dorsolateral striatum for a subset of animals ($n = 10$). The animals were allowed to recover

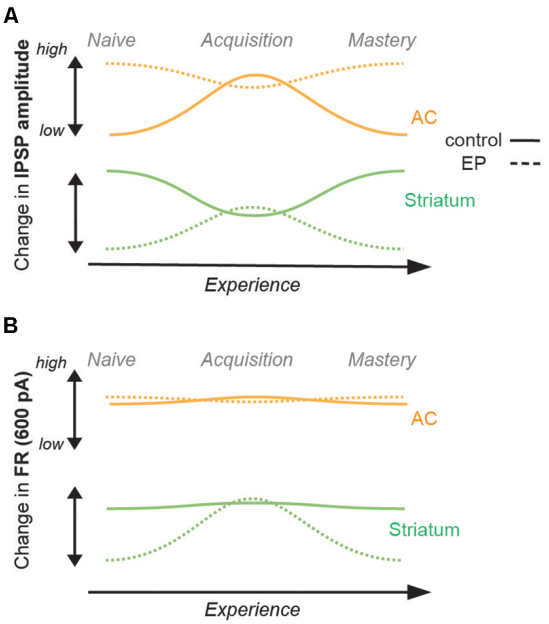

FIGURE 4 | Summary of changes in inhibition and firing rates with learning. **(A)** Changes in IPSP amplitudes with learning for the control population (straight line), and for the EP population (dashed line). AC (IT and PT) data are shown in orange, and striatal (D1 and D2) data are shown in green. While a significant increase was found in IPSP amplitude of AC cells (both IT and PT cells) in the control population, no significant change was found for the EP group. A significant decrease was found in the IPSP amplitude of striatal cells (both D1 and D2 cells) in the control population, but in contrast, a significant increase was found for the EP group. **(B)** Changes in FR (Hz, 600 pA) with learning. No change in FR of AC cells was found in the control population, or in the EP group. No change in FR of striatal cells was found for the control population, but in contrast, a significant increase was found for the EP group.

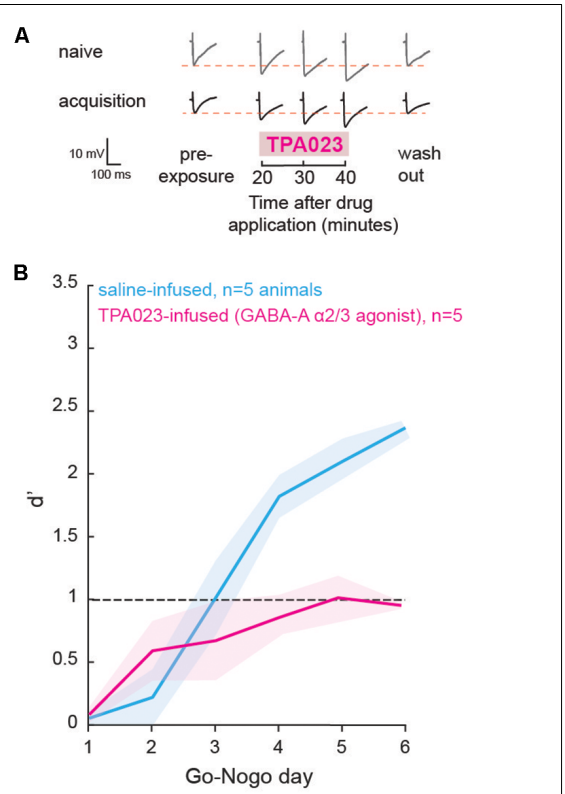

FIGURE 5 | Direct manipulation of inhibition affected learning. **(A)** Representative traces of maximum evoked IPSPs recorded from striatal cells of the control population during the naïve and acquisition phases, with the addition of a GABAA-α2/3 subunit receptor agonist (TPA023) to the bath. Pre- and post-exposure traces are shown for comparison. **(B)** Mean (±SEM) d′ measures of animals which received local infusions of TPA023 (pink) or saline (blue) bilaterally in the auditory striatum prior to each Go-Nogo session. Infusions of TPA023 caused a significant impact on learning as compared to saline infusions.

for a week and were then trained to perform a minimum of 80 Go trials correctly. Prior to each day of behavioral testing, a subset of animals (n = 5) received bilateral infusions of TPA023 (2 μl, 50 μM), and a second subset of animals (n = 5) received bilateral infusions of saline (0.9% NaCl, 2 μl). The performance d′ of both groups is shown in **Figure 5B** (TPA023-infused group in pink, and saline-infused group in blue). A mixed model ANOVA revealed significant group differences (ANOVA, $F_{(1,59)}$ = 12.25, p = 0.0009), with the TPA023-infused animals being significantly delayed as compared to the saline-infused groups. Together, these results showed that maintaining a high level of inhibition in the striatum, in other words, preventing the transient decrease in inhibition that accompanies learning (see **Figure 2**), was sufficient to prevent task acquisition in control animals.

DISCUSSION

In the current study, we first verified the role of the corticostriatal pathway in auditory learning. Through chemogenetic suppression of excitatory input from AC layer 5 to the auditory striatum, we showed that learning was significantly delayed when corticostriatal suppression was maintained across all testing days (**Figure 1C**, purple line). Precisely, when suppression occurred early during learning, there was a significant impact on learning (**Figure 1D**, pink) as compared to late suppression. While those results do not exclude the involvement of additional downstream cortical and non-cortical areas in auditory associative learning (e.g., thalamus, prefrontal cortex, and hippocampal regions: Pasupathy and Miller, 2005; Hart et al., 2018; Le Merre et al., 2018), our results are in line with previous studies using optogenetic manipulation of striatal cells (Znamenskiy and Zador, 2013; Xiong et al., 2015; Guo et al., 2018; Chen et al., 2019). Here, we also found a small improvement in behavioral d′ values when the corticostriatal pathway was suppressed, although d′ never rose beyond 1.0. This may suggest that other circuits, like the direct thalamic drive to the striatum, may also in part contribute to enhancing performances (Ponvert and Jaramillo, 2019). In addition, despite limiting the chemogenetic manipulations to layer 5 AC cells and selectively targeting the projections to the auditory striatum, input from other cortical layers (e.g., layer 2/3; Yamashita et al., 2018) may also have been suppressed.

While AC layer 5 IT and PT cells showed significant increases in inhibitory strengths during the acquisition phase, striatal D1 and D2 MSNs presented significant decreases in inhibitory strengths (**Figure 5**). A reduction of inhibitory synaptic gain has often been linked to associative learning. For instance, fear conditioning was found to be associated with the inhibition of parvalbumin-positive layer 2/3 interneurons in the AC (Letzkus et al., 2011; Sarro et al., 2015) and interneurons in the amygdala (Wolff et al., 2014). Similarly, reduced inhibitory strengths have also been associated with motor learning (Smyth et al., 2010; Baarbé et al., 2014; Coxon et al., 2014). Our findings for striatal D1 and D2 cells support the idea that a reduction of inhibition is a general mechanism involved in many forms of associative learning. In addition, our results suggest that co-activation of both the direct and indirect pathways may contribute to enhancing auditory discrimination performance. Conversely, the increase in inhibition in AC layer 5 IT and PT cells may potentially gate sensory information during task acquisition, in order to potentiate relevant cues and attenuate irrelevant sensory noise (Egger et al., 2020). Although we have attempted to classify D1 and D2 cells in the current study, there is a large overlap in the different physiological properties of those cells (Goodliffe et al., 2018). Since our results showed similar changes in both D1 and D2 cells, it is safe to consider that our classification did not impact the results. Although we did not directly test the interdependence of the cortical and striatal changes, the latter may potentially support LTP through the strengthening of different subsets of corticostriatal connections in order to elicit the Go response and the Nogo response.

We next assessed how the corticostriatal pathway supports learning in animals which had a transient period of developmental auditory deprivation. In line with Mowery et al. (2017), striatal dysfunctions were shown to persist long after the actual period of sensory deprivation. Indeed, inhibitory strengths and firing rates in striatal D1 and D2 cells were significantly lower as compared to the control population. While a transient reduction of inhibitory strengths of striatal cells was found during learning in the control group, in contrast for the EP striatal cells, augmented inhibition accompanied learning, and the firing rates of EP striatal cells approached control values during task acquisition (**Figure 3**, and **Supplementary Figure 4**). In addition, IPSP amplitudes of AC IT and PT cells of EP animals were higher than for control animals at the naïve stage, and learning was not accompanied by a change in IPSP amplitudes. This suggests that the increased inhibition seen for the control animals during learning, potentially for noise reduction purposes at the cortical level, was already present in the EP animals. Together, these results suggest that instead of reduced inhibition, a certain range of synaptic inhibition values, implying a certain balance of excitation and inhibition (Froemke, 2015), may be crucial for plasticity to occur. Such transient shifts in inhibitory synaptic strengths during learning in the control and EP animals may be required in order to achieve such an optimal state for plasticity.

The inhibitory and firing rate changes observed for the EP animals during learning could be further explained by phenotype-specific forms of cellular physiology compensation (**Supplementary Figure 5**). Changes in resting membrane potential, membrane resistance, and sensory adaptation allowed the direct and indirect pathway neurons to briefly achieve control level firing rates during task acquisition. D1 cells in the EP animals presented a brief increase in sensory adaptation ratio at all stimulation levels, and D2 cells presented increased intrinsic excitability through transiently more depolarized resting membrane potentials and a brief increase in membrane resistance. Such transient changes in intrinsic properties may enhance the probability of eLTP along the corticostriatal circuit and in downstream areas, that manifest behaviorally as an improvement in discrimination performances. Thus, through such phenotype-specific compensatory mechanisms, the acquisition of a Go-Nogo discrimination task in the EP animals was similar to control animals.

However, in more complex tasks (e.g., several Go and Nogo stimuli, closer modulation rates Go and Nogo stimuli) or poorer signal to noise conditions (e.g., in a noisy environment), EP animals may present significant learning deficits (e.g., perceptual learning deficits, see Caras and Sanes, 2015). In humans, transient hearing loss is associated with behavioral deficits that can outlast the period of elevated hearing thresholds (Pillsbury et al., 1991; Hall and Grose, 1994; Hogan et al., 1996; Hall et al., 1998; Hogan and Moore, 2003). Children presenting repeated episodes of ear infection (otitis media-related hearing loss) have been shown to have auditory processing and language impairments, even though audibility is normal at the time of testing (Hall et al., 1995; Whitton and Polley, 2011). Thus, the transient developmental sensory deprivation used here represents a good model to study changes in circuit dynamics both when the behavioral performance is impacted and in conditions of control-like behavioral performance.

Overall, the current study provides a better understanding of how the corticostriatal pathway supports auditory learning through transient inhibitory shifts in striatal D1 and D2 MSNs, governed at least in part by GABAA-α2/3 containing receptors (**Figure 5**). Those findings are of broad importance as the etiology of many neurological disorders is linked to abnormal synaptic set points of GABAA receptor-mediated inhibition (diminished GABAA in epilepsy: Treiman, 2001; autism: Chao et al., 2010; tinnitus: Richardson et al., 2012; fragile X syndrome: Braat and Kooy, 2015; increased GABAA in Down syndrome: de San Martin et al., 2018; Schulz et al., 2019; Huntington's Disease: Holley et al., 2019). In addition, chronic imbalance in cortical supragranular excitatory/inhibitory tone through diminished GABAA receptor-mediated inhibition is a common feature of developmental sensory deprivation (vision: Maffei et al., 2006; somatosensory: Jiao et al., 2006; auditory; Takesian et al., 2009; Mowery et al., 2014). Up or downregulation of GABAA-α1 containing receptors has previously been shown to govern mature forms of inhibitory synaptic transmission (Fritschy et al., 1994; Heinen et al., 2004; Bosman et al., 2005). Hence, restoration of GABAergic inhibition in cases of behavioral deficits could be a valuable target to investigate for potential therapy approaches (Verret et al., 2012; Schmid et al., 2016; Dargaei et al., 2018; Mowery et al., 2019).

DATA AVAILABILITY STATEMENT

The original contributions presented in the study are included in the article/**Supplementary Material**, further inquiries can be directed to the corresponding author.

ETHICS STATEMENT

The animal study was reviewed and approved by University Animal Welfare Committee at New York University.

AUTHOR CONTRIBUTIONS

NP and TM designed the experiments, performed the experiments, analyzed the data, and wrote the article.

FUNDING

This work was supported by National Institute on Deafness and Other Communication Disorders (NIDCD) R01 DC017163 (TM) and the Fyssen Foundation (NP).

ACKNOWLEDGMENTS

We would like to thank Dr. Justin Yao for contributing to **Supplementary Figure 1**.

SUPPLEMENTARY MATERIAL

The Supplementary Material for this article can be found online at: https://www.frontiersin.org/articles/10.3389/fncir.2021.670858/full#supplementary-material.

REFERENCES

Baarbé, J., Yielder, P., Daligadu, J., Behbahani, H., Haavik, H., and Murphy, B. (2014). A novel protocol to investigate motor training-induced plasticity and sensorimotor integration in the cerebellum and motor cortex. *J. Neurophysiol.* 111, 715–721. doi: 10.1152/jn.00661.2013

Balleine, B. W., and O'Doherty, J. P. (2010). Human and rodent homologies in action control: corticostriatal determinants of goal-directed and habitual action. *Neuropsychopharmacology* 35, 48–69. doi: 10.1038/npp.2009.131

Balleine, B. W., Delgado, M. R., and Hikosaka, O. (2007). The role of the dorsal striatum in reward and decision-making. *J. Neurosci.* 27, 8161–8165. doi: 10.1523/JNEUROSCI.1554-07.2007

Bilkey, D. K. (1996). Long-term potentiation in the *in vitro* perirhinal cortex displays associative properties. *Brain Res.* 733, 297–300. doi: 10.1016/0006-8993(96)00789-5

Bosman, L. W., Heinen, K., Spijker, S., and Brussaard, A. B. (2005). Mice lacking the major adult $GABA_A$ receptor subtype have normal number of synapses, but retain juvenile IPSC kinetics until adulthood. *J. Neurophysiol.* 94, 338–346. doi: 10.1152/jn.00084.2005

Braat, S., and Kooy, R. F. (2015). Insights into $GABA_A$ergic system deficits in fragile X syndrome lead to clinical trials. *Neuropsychopharmacology* 88, 48–54. doi: 10.1016/j.neuropharm.2014.06.028

Brucato, F. H., Levin, E. D., Mott, D. D., Lewis, D. V., Wilson, W. A., and Swartzelder, H. S. (1996). Hippocampal long-term potentiation and spatial learning in the rat: effects of $GABA_B$ receptor blockade. *Neuroscience* 74, 331–339. doi: 10.1016/0306-4522(96)00131-5

Budinger, E., Laszcz, A., Lison, H., Scheich, H., and Ohl, F. W. (2008). Non-sensory cortical and subcortical connections of the primary auditory cortex in Mongolian gerbils: bottom-up and top-down processing of neuronal information *via* field AI. *Brain Res.* 1220, 2–32. doi: 10.1016/j.brainres.2007.07.084

Calabresi, P., Picconi, B., Tozzi, A., and Di Filippo, M. (2007). Dopamine-mediated regulation of corticostriatal synaptic plasticity. *Trends Neurosci.* 30, 211–219. doi: 10.1016/j.tins.2007.03.001

Calabresi, P., Picconi, B., Tozzi, A., Ghiglieri, V., and Di Filippo, M. (2014). Direct and indirect pathways of basal ganglia: a critical reappraisal. *Nat. Neurosci.* 17, 1022–1030. doi: 10.1038/nn.3743

Caras, M. L., and Sanes, D. H. (2015). Sustained perceptual deficits from transient sensory deprivation. *J. Neurosci.* 35, 10831–10842. doi: 10.1523/JNEUROSCI.0837-15.2015

Cazorla, M., De Carvalho, F. D., Chohan, M. O., Shegda, M., Chuhma, N., Rayport, S., et al. (2014). Dopamine D2 receptors regulate the anatomical and functional balance of basal ganglia circuitry. *Neuron* 81, 153–164. doi: 10.1016/j.neuron.2013.10.041

Cepeda, C., André, V. M., Yamazaki, I., Wu, N., Kleiman-Weiner, M., and Levine, M. S. (2008). Differential electrophysiological properties of dopamine D1 and D2 receptor-containing striatal medium-sized spiny neurons. *Eur. J. Neurosci.* 27, 671–682. doi: 10.1111/j.1460-9568.2008.06038.x

Chao, H.-T., Chen, H., Samaco, R. C., Xue, M., Chahrour, M., Yoo, J., et al. (2010). Dysfunction in GABA signalling mediates autism-like stereotypies and Rett syndrome phenotypes. *Nature* 468, 263–269. doi: 10.1038/nature09582

Chen, L., Wang, X., Ge, S., and Xiong, Q. (2019). Medial geniculate body and primary auditory cortex differentially contribute to striatal sound representations. *Nat. Commun.* 10:418. doi: 10.1038/s41467-019-08350-7

Cho, K., Kemp, N., Noel, J., Aggleton, J. P., Brown, M. W., and Bashir, Z. I. (2000). A new form of long-term depression in the perirhinal cortex. *Nat. Neurosci.* 3, 150–156. doi: 10.1038/72093

Cox, J., and Witten, I. B. (2019). Striatal circuits for reward learning and decision-making. *Nat. Rev. Neurosci.* 20, 482–494. doi: 10.1038/s41583-019-0189-2

Coxon, J. P., Peat, N. M., and Byblow, W. D. (2014). Primary motor cortex disinhibition during motor skill learning. *J. Neurophysiol.* 112, 156–164. doi: 10.1152/jn.00893.2013

Cui, G., Jun, S. B., Jin, X., Pham, M. D., Vogel, S. S., Lovinger, D. M., et al. (2013). Concurrent activation of striatal direct and indirect pathways during action initiation. *Nature* 494, 238–242. doi: 10.1038/nature11846

Dargaei, Z., Liang, X., Serranilla, M., Santos, J., and Woodin, M. A. (2018). Alterations in hippocampal inhibitory synaptic transmission in the R6/2 mouse model of Huntington's disease. *Neuroscience* 404, 130–140. doi: 10.1016/j.neuroscience.2019.02.007

de San Martin, J. Z., Delabar, J. M., Bacci, A., and Potier, M. C. (2018). GABAergic over-inhibition, a promising hypothesis for cognitive deficits in Down syndrome. *Free Radical Biol. Med.* 114, 33–39. doi: 10.1016/j.freeradbiomed.2017.10.002

Dolan, R. J., and Dayan, P. (2013). Goals and habits in the brain. *Neuron* 80, 312–325. doi: 10.1016/j.neuron.2013.09.007

Egger, R., Narayanan, R. T., Guest, J. M., Bast, A., Udvary, D., Messore, L. F., et al. (2020). Cortical output is gated by horizontally projecting neurons in the deep layers. *Neuron* 105, 122–137. doi: 10.1016/j.neuron.2019.10.011

Freeze, B. S., Kravitz, A. V., Hammack, N., Berke, J. D., and Kreitzer, A. C. (2013). Control of basal ganglia output by direct and indirect pathway projection neurons. *J. Neurosci.* 33, 18531–18539. doi: 10.1523/JNEUROSCI.1278-13.2013

Fritschy, J. M., Paysan, J., Enna, A., and Mohler, H. (1994). Switch in the expression of rat $GABA_A$-receptor subtypes during postnatal development: an immunohistochemical study. *J. Neurosci.* 14, 5302–5324. doi: 10.1523/JNEUROSCI.14-09-05302.1994

Froemke, R. C. (2015). Plasticity of cortical excitatory-inhibitory balance. *Annu. Rev. Neurosci.* 38, 195–219. doi: 10.1146/annurev-neuro-071714-034002

Gertler, T. S., Chan, C. S., and Surmeier, D. J. (2008). Dichotomous anatomical properties of adult striatal medium spiny neurons. *J. Neurosci.* 28, 10814–10824. doi: 10.1523/JNEUROSCI.2660-08.2008

Goodliffe, J. W., Song, H., Rubakovic, A., Chang, W., Medalla, M., Weaver, C. M., et al. (2018). Differential changes to D1 and D2 medium spiny neurons in the 12-month-old Q175+/-mouse model of Huntington's disease. *PLoS One* 13:e0200626. doi: 10.1371/journal.pone.0200626

Green, D. M., and Swets, J. A. (1966). *Signal Detection Theory and Psychophysics Vol. 1*. New York, NY: Wiley.

Guo, L., Walker, W. I,, Ponvert, N. D., Penix, P. L., and Jaramillo, S. (2018). Stable representation of sounds in the posterior striatum during flexible auditory decisions. *Nat. Commun.* 9:1534. doi: 10.1038/s41467-018-03994-3

Guo, L., Weems, J. T., Walker, W. I., Levichev, A., and Jaramillo, S. (2019). Choice-selective neurons in the auditory cortex and in its striatal target encode reward expectation. *J. Neurosci.* 39, 3687–3697. doi: 10.1523/JNEUROSCI.2585-18.2019

Hackett, T. A. (2011). Information flow in the auditory cortical network. *Hear. Res.* 271, 133–146. doi: 10.1016/j.heares.2010.01.011

Hall, J. W., and Grose, J. H. (1994). The effect of otitis media with effusion on comodulation masking release in children. *J. Speech Hear. Res.* 37, 1441–1449. doi: 10.1044/jshr.3706.1441

Hall, J. III., Grose, J., Dev, M., Drake, A., and Pillsbury, H. C. (1998). The effect of otitis with effusion on complex masking tasks in children. *Arch. Otolaryngol. Head Neck Surg.* 124, 892–896. doi: 10.1001/archotol.124.8.892

Hall, J. W. III., Grose, J. H., and Pillsbury, H. C. (1995). Long-term effects of chronic otitis media on binaural hearing in children. *Arch. Otolaryngol. Head Neck Surg.* 121, 847–852. doi: 10.1001/archotol.1995.01890080017003

Hart, G., Bradfield, L. A., and Balleine, B. W. (2018). Prefrontal corticostriatal disconnection blocks the acquisition of goal-directed action. *J. Neurosci.* 38, 1311–1322. doi: 10.1523/JNEUROSCI.2850-17.2017

Hattox, A. M., and Nelson, S. B. (2007). Layer V neurons in mouse cortex projecting to different targets have distinct physiological properties. *J. Neurophysiol.* 98, 3330–3340. doi: 10.1152/jn.00397.2007

Heinen, K., Bosman, L. W. J., Spijker, S., Van Pelt, J., Smit, A. B., Voorn, P., et al. (2004). $GABA_A$ receptor maturation in relation to eye opening in the rat visual cortex. *Neuroscience* 124, 161–171. doi: 10.1016/j.neuroscience.2003.11.004

Hogan, S. C., Meyer, S. E., and Moore, D. R. (1996). Binaural unmasking returns to normal in teenagers who had otitis media in infancy. *Audiol. Neurootol.* 1, 104–111. doi: 10.1159/000259189

Hogan, S. C., and Moore, D. R. (2003). Impaired binaural hearing in children produced by a threshold level of middle ear disease. *J. Assoc. Res. Otolaryngol.* 4, 123–129. doi: 10.1007/s10162-002-3007-9

Holley, S. M., Galvan, L., Kamdjou, T., Dong, A., Levine, M. S., and Cepeda, C. (2019). Major contribution of somatostatin-expressing interneurons and cannabinoid receptors to increased GABA synaptic activity in the striatum of Huntington's disease mice. *Front. Synaptic Neurosci.* 11:14. doi: 10.3389/fnsyn.2019.00014

Hörtnagl, H., Tasan, R. O., Wieselthaler, A., Kirchmair, E., Sieghart, W., and Sperk, G. (2013). Patterns of mRNA and protein expression for 12 $GABA_A$ receptor subunits in the mouse brain. *Neuroscience* 236, 345–372. doi: 10.1016/j.neuroscience.2013.01.008

Humphries, M. D., Khamassi, M., and Gurney, K. (2012). Dopaminergic control of the exploration-exploitation trade-off *via* the basal ganglia. *Front. Neurosci.* 6:9. doi: 10.3389/fnins.2012.00009

Jiao, Y., Zhang, C., Yanagawa, Y., and Sun, Q. Q. (2006). Major effects of sensory experiences on the neocortical inhibitory circuits. *J. Neurosci.* 26, 8691–8701. doi: 10.1523/JNEUROSCI.2478-06.2006

Kawaguchi, Y. (1993). Physiological, morphological, and histochemical characterization of three classes of interneurons in rat neostriatum. *J. Neurosci.* 13, 4908–4923. doi: 10.1523/JNEUROSCI.13-11-04908.1993

Kotak, V. C., Mirallave, A., Mowery, T. M., and Sanes, D. H. (2017). GABAergic inhibition gates excitatory LTP in perirhinal cortex. *Hippocampus* 27, 1217–1223. doi: 10.1002/hipo.22799

Kreitzer, A. C., and Malenka, R. C. (2008). Striatal plasticity and basal ganglia circuit function. *Neuron* 60, 543–554. doi: 10.1016/j.neuron.2008.11.005

Kress, G. J., Yamawaki, N., Wokosin, D. L., Wickersham, I. R., Shepherd, G. M., and Surmeier, D. J. (2013). Convergent cortical innervation of striatal projection neurons. *Nat. Neurosci.* 16, 665–667. doi: 10.1038/nn.3397

Kupferschmidt, D. A., Juczewski, K., Cui, G., Johnson, K. A., and Lovinger, D. M. (2017). Parallel, but dissociable, processing in discrete corticostriatal inputs encodes skill learning. *Neuron* 96, 476–489. doi: 10.1016/j.neuron.2017.09.040

Le Merre, P., Esmaeili, V., Charrière, E., Galan, K., Salin, P. A., Petersen, C. C., et al. (2018). Reward-based learning drives rapid sensory signals in medial prefrontal cortex and dorsal hippocampus necessary for goal-directed behavior. *Neuron* 97, 83–91. doi: 10.1016/j.neuron.2017.11.031

Letzkus, J. J., Wolff, S. B., Meyer, E. M., Tovote, P., Courtin, J., Herry, C., et al. (2011). A disinhibitory microcircuit for associative fear learning in the auditory cortex. *Nature* 480, 331–335. doi: 10.1038/nature10674

Maffei, A., Nataraj, K., Nelson, S. B., and Turrigiano, G. G. (2006). Potentiation of cortical inhibition by visual deprivation. *Nature* 443, 81–84. doi: 10.1038/nature05079

McGeorge, A. J., and Faull, R. L. M. (1989). The organization of the projection from the cerebral cortex to the striatum in the rat. *Neuroscience* 29, 503–537. doi: 10.1016/0306-4522(89)90128-0

Mott, D. D., and Lewis, D. V. (1991). Facilitation of the induction of long-term potentiation by $GABA_B$ receptors. *Science* 252, 1718–1720. doi: 10.1126/science.1675489

Mowery, T. M., Caras, M. L., Hassan, S. I., Wang, D. J., Dimidschstein, J., Fishell, G., et al. (2019). Preserving inhibition during developmental hearing loss rescues auditory learning and perception. *J. Neurosci.* 39, 8347–8361. doi: 10.1523/JNEUROSCI.0749-19.2019

Mowery, T. M., Kotak, V. C., and Sanes, D. H. (2014). Transient hearing loss within a critical period causes persistent changes to cellular properties in adult auditory cortex. *Cereb. Cortex* 25, 2083–2094. doi: 10.1093/cercor/bhu013

Mowery, T. M., Penikis, K. B., Young, S. K., Ferrer, C. E., Kotak, V. C., and Sanes, D. H. (2017). The sensory striatum is permanently impaired by transient developmental deprivation. *Cell Rep.* 19, 2462–2468. doi: 10.1016/j.celrep.2017.05.083

Ormond, J., and Woodin, M. A. (2011). Disinhibition-mediated LTP in the hippocampus is synapse specific. *Front. Cell. Neurosci.* 5:17. doi: 10.3389/fncel.2011.00017

Pasupathy, A., and Miller, E. K. (2005). Different time courses of learning-related activity in the prefrontal cortex and striatum. *Nature* 433, 873–876. doi: 10.1038/nature03287

Perugini, A., Laing, M., Berretta, N., Aicardi, G., and Bashir, Z. I. (2012). Synaptic plasticity from amygdala to perirhinal cortex: a possible mechanism for emotional enhancement of visual recognition memory? *Eur. J. Neurosci.* 36, 2421–2427. doi: 10.1111/j.1460-9568.2012.08146.x

Pillsbury, H. C., Grose, J. H., and Hall, J. W. III. (1991). Otitis media with effusion in children: binaural hearing before and after corrective surgery. *Arch. Otolaryngol. Head Neck Surg.* 117, 718–723. doi: 10.1001/archotol.1991.01870190030008

Ponvert, N. D., and Jaramillo, S. (2019). Auditory thalamostriatal and corticostriatal pathways convey complementary information about sound features. *J. Neurosci.* 39, 271–280. doi: 10.1523/JNEUROSCI.1188-18.2018

Radtke-Schuller, S., Schuller, G., Angenstein, F., Grosser, O. S., Goldschmidt, J., and Budinger, E. (2016). Brain atlas of the Mongolian gerbil (Meriones unguiculatus) in CT/MRI-aided stereotaxic coordinates. *Brain Struct. Funct.* 221, 1–272. doi: 10.1007/s00429-016-1259-0

Reig, R., and Silberberg, G. (2014). Multisensory integration in the mouse striatum. *Neuron* 83, 1200–1212. doi: 10.1016/j.neuron.2014.07.033

Reiner, A., Hart, N. M., Lei, W., and Deng, Y. (2010). Corticostriatal projection neurons-dichotomous types and dichotomous functions. *Front. Neuroanat.* 4:142. doi: 10.3389/fnana.2010.00142

Richardson, B. D., Brozoski, T. J., Ling, L. L., and Caspary, D. M. (2012). Targeting inhibitory neurotransmission in tinnitus. *Brain Res.* 1485, 77–87. doi: 10.1016/j.brainres.2012.02.014

Rock, C., Zurita, H., Wilson, C., and Junior Apicella, A. (2016). An inhibitory corticostriatal pathway. *eLife* 5:e15890. doi: 10.7554/eLife.15890

Sarro, E. C., von Trapp, G., Mowery, T. M., Kotak, V. C., and Sanes, D. H. (2015). Cortical synaptic inhibition declines during auditory learning. *J. Neurosci.* 35, 6318–6325. doi: 10.1523/JNEUROSCI.4051-14.2015

Schmid, L. C., Mittag, M., Poll, S., Steffen, J., Wagner, J., Geis, H. R., et al. (2016). Dysfunction of somatostatin-positive interneurons associated with memory deficits in an Alzheimer's disease model. *Neuron* 92, 114–125. doi: 10.1016/j.neuron.2016.08.034

Schulz, J. M., Knoflach, F., Hernandez, M. C., and Bischofberger, J. (2019). Enhanced dendritic inhibition and impaired NMDAR activation

in a mouse model of Down syndrome. *J. Neurosci.* 39, 5210–5221. doi: 10.1523/JNEUROSCI.2723-18.2019

Shepherd, G. M. (2013). Corticostriatal connectivity and its role in disease. *Nat. Rev. Neurosci.* 14, 278–291. doi: 10.1038/nrn3469

Sippy, T., Lapray, D., Crochet, S., and Petersen, C. C. (2015). Cell-type-specific sensorimotor processing in striatal projection neurons during goal-directed behavior. *Neuron* 88, 298–305. doi: 10.1016/j.neuron.2015.08.039

Smyth, C., Summers, J. J., and Garry, M. I. (2010). Differences in motor learning success are associated with differences in M1 excitability. *Hum. Mov. Sci.* 29, 618–630. doi: 10.1016/j.humov.2010.02.006

Steward, O., Tomasulo, R., and Levy, W. B. (1990). Blockade of inhibition in a pathway with dual excitatory and inhibitory action unmasks a capability for LTP that is otherwise not expressed. *Brain Res.* 516, 292–300. doi: 10.1016/0006-8993(90)90930-a

Takesian, A. E., Kotak, V. C., and Sanes, D. H. (2009). Developmental hearing loss disrupts synaptic inhibition: implications for auditory processing. *Future Neurol.* 4, 331–349doi: 10.2217/FNL.09.5

Thorn, C. A., Atallah, H., Howe, M., and Graybiel, A. M. (2010). Differential dynamics of activity changes in dorsolateral and dorsomedial striatal loops during learning. *Neuron* 66, 781–795. doi: 10.1016/j.neuron.2010.04.036

Treiman, D. M. (2001). GABAergic mechanisms in epilepsy. *Epilepsia* 42, 8–12. doi: 10.1046/j.1528-1157.2001.042suppl.3008.x

Verret, L., Mann, E. O., Hang, G. B., Barth, A. M., Cobos, I., Ho, K., et al. (2012). Inhibitory interneuron deficit links altered network activity and cognitive dysfunction in Alzheimer model. *Cell* 149, 708–721. doi: 10.1016/j.cell.2012.02.046

Voorn, P., Vanderschuren, L. J., Groenewegen, H. J., Robbins, T. W., and Pennartz, C. M. (2004). Putting a spin on the dorsal-ventral divide of the striatum. *Trends Neurosci.* 27, 468–474. doi: 10.1016/j.tins.2004.06.006

Whitton, J. P., and Polley, D. B. (2011). Evaluating the perceptual and pathophysiological consequences of auditory deprivation in early postnatal life: a comparison of basic and clinical studies. *J. Assoc. Res. Otolaryngol.* 12, 535–547. doi: 10.1007/s10162-011-0271-6

Wickens, J. R., Horvitz, J. C., Costa, R. M., and Killcross, S. (2007). Dopaminergic mechanisms in actions and habits. *J. Neurosci.* 27, 8181–8183. doi: 10.1523/JNEUROSCI.1671-07.2007

Wickens, J. R., Reynolds, J. N., and Hyland, B. I. (2003). Neural mechanisms of reward-related motor learning. *Curr. Opin. Neurobiol.* 13, 685–690. doi: 10.1016/j.conb.2003.10.013

Wigström, H., and Gustafsson, B. (1986). Postsynaptic control of hippocampal long-term potentiation. *J. Physiol.* 81, 228–236.

Wolff, S. B., Gründemann, J., Tovote, P., Krabbe, S., Jacobson, G. A., Müller, C., et al. (2014). Amygdala interneuron subtypes control fear learning through disinhibition. *Nature* 509, 453–458. doi: 10.1038/nature13258

Xiong, Q., Znamenskiy, P., and Zador, A. M. (2015). Selective corticostriatal plasticity during acquisition of an auditory discrimination task. *Nature* 521, 348–351. doi: 10.1038/nature14225

Yamashita, T., Vavladeli, A., Pala, A., Galan, K., Crochet, S., Petersen, S. S., et al. (2018). Diverse long-range axonal projections of excitatory layer 2/3 neurons in mouse barrel cortex. *Front. Neuroanat.* 12:33. doi: 10.3389/fnana.2018.00033

Yartsev, M. M., Hanks, T. D., Yoon, A. M., and Brody, C. D. (2018). Causal contribution and dynamical encoding in the striatum during evidence accumulation. *eLife* 7:e34929. doi: 10.7554/eLife.34929

Ziakopoulos, Z., Brown, M. W., and Bashir, Z. I. (2000). $GABA_B$ receptors mediate frequency-dependent depression of excitatory potentials in rat perirhinal cortex *in vitro*. *Eur. J. Neurosci.* 12, 803–809. doi: 10.1046/j.1460-9568.2000.00965.x

Znamenskiy, P., and Zador, A. M. (2013). Corticostriatal neurons in auditory cortex drive decisions during auditory discrimination. *Nature* 497, 482–485. doi: 10.1038/nature12077

Conflict of Interest: The authors declare that the research was conducted in the absence of any commercial or financial relationships that could be construed as a potential conflict of interest.

frontiers in Neural Circuits

MINI REVIEW
published: 14 June 2021
doi: 10.3389/fncir.2021.688234

Oxytocinergic Feedback Circuitries: An Anatomical Basis for Neuromodulation of Social Behaviors

Arthur Lefevre[1], *Diego Benusiglio*[2,3], *Yan Tang*[4], *Quirin Krabichler*[1], *Alexandre Charlet*[5]* *and Valery Grinevich*[1]*

[1]*Department of Neuropeptide Research in Psychiatry, Central Institute of Mental Health, Medical Faculty Mannheim, University of Heidelberg, Mannheim, Germany,* [2]*European Molecular Biology Laboratory (EMBL), Epigenetics and Neurobiology Unit, Monterotondo, Italy,* [3]*Neuroscience and Behaviour Laboratory, Istituto Italiano di Tecnologia, Rome, Italy,* [4]*Department of Biomedical Sciences, Faculty of Biology and Medicine, University of Lausanne, Lausanne, Switzerland,* [5]*Centre National de la Recherche Scientifique (CNRS) and University of Strasbourg, Institute of Cellular and Integrative Neurosciences, Strasbourg, France*

Oxytocin (OT) is a neuropeptide produced by hypothalamic neurons and is known to modulate social behavior among other functions. Several experiments have shown that OT modulates neuronal activity in many brain areas, including sensory cortices. OT neurons thus project axons to various cortical and subcortical structures and activate neuronal subpopulations to increase the signal-to-noise ratio, and in turn, increases the saliency of social stimuli. Less is known about the origin of inputs to OT neurons, but recent studies show that cells projecting to OT neurons are often located in regions where the OT receptor (OTR) is expressed. Thus, we propose the existence of reciprocal connectivity between OT neurons and extrahypothalamic OTR neurons to tune OT neuron activity depending on the behavioral context. Furthermore, the latest studies have shown that OTR-expressing neurons located in social brain regions also project to other social brain regions containing OTR-expressing neurons. We hypothesize that OTR-expressing neurons across the brain constitute a common network coordinated by OT.

Keywords: oxytocin, oxytocin receptor (OTR), social brain, anatomy, loops

OPEN ACCESS

Edited by:
Max F. K. Happel,
Medical School Berlin, Germany

Reviewed by:
Markus Fendt,
University Hospital Magdeburg, Germany
Femke T. A. Buisman-Pijlman,
The University of Melbourne, Australia

***Correspondence:**
Alexandre Charlet
acharlet@unistra.fr
Valery Grinevich
valery.grinevich@zi-mannheim.de

Received: *30 March 2021*
Accepted: *18 May 2021*
Published: *14 June 2021*

Citation:
Lefevre A, Benusiglio D, Tang Y, Krabichler Q, Charlet A and Grinevich V (2021) Oxytocinergic Feedback Circuitries: An Anatomical Basis for Neuromodulation of Social Behaviors. Front. Neural Circuits 15:688234. doi: 10.3389/fncir.2021.688234

INTRODUCTION

Oxytocin (OT) is a neuropeptide mainly synthesized in the paraventricular (PVN), supraoptic (SON), and accessory nuclei of mammalian hypothalamus and is present, with some minor molecular variations, in all vertebrates (Knobloch and Grinevich, 2014; Banerjee et al., 2016). This peptide has two general ways of action: first, *via* projections to the posterior pituitary, it is secreted into the bloodstream as a hormone controlling various physiological processes, such as parturition, lactation, energetic metabolism, cardiovascular function, bone homeostasis, and muscle maintenance (Neumann et al., 1993; Gutkowska and Jankowski, 2012; Chaves et al., 2013; Kasahara et al., 2013; Elabd et al., 2014; Poisbeau et al., 2017; Sun et al., 2019). Secondly, OT acts in the brain as a non-canonical neurotransmitter or neuromodulator, regulating a number of behaviors ranging from pain to social behaviors (Macdonald and Feifel, 2014; Bowen and Neumann, 2017; Grinevich and Stoop, 2018; Lawson et al., 2019).

In this mini-review, we will primarily focus on brain OTergic circuits, which modulate social behavior. The current leading hypothesis to explain OT effects on social behavior is that the neuropeptide selectively increases the saliency of socially relevant stimuli in areas enriched with OTR-expressing neurons (Shamay-Tsoory and Abu-Akel, 2015; Marlin and Froemke, 2016). This hypothesis is mainly based on results obtained in studies of the auditory and olfactory centers, where OT modulation acts on the excitation/inhibition balance of sensory circuits to increase the signal to noise ratio in favor of social stimuli and by this mechanism filter out less relevant stimuli (Marlin et al., 2015; Oettl et al., 2016; Linster and Kelsch, 2019). Although it is becoming clearer how OT may affect sensory systems, the mechanisms underlying targeted axonal release of OT in the socially relevant brain regions remain elusive. While an extensive series of tracing experiments were performed in the 1970s and 1980s (Sawchenko and Swanson, 1983), only a few recent studies have described the inputs and outputs of OT neurons with modern neuroanatomical techniques (Grinevich and Stoop, 2018; Son et al., 2020; Tang et al., 2020; Zhang et al., 2020). Thus, here we will first review outputs of OT neurons and their effects with an emphasis on cortical sensory regions. We will then synthesize recent reports on inputs to OT neurons, suggesting the existence of functional feedback loops between OT neurons and OTR-containing regions. Finally, we will propose a hypothesis that brain regions containing OTR form interconnected networks to regulate various forms of complex social behaviors.

BRAIN-WIDE OT MODULATION

In addition to the well-described somatodendritic release of OT, which takes place within the hypothalamic nuclei, the PVN and SON, specifically during lactation (Landgraf and Neumann, 2004; Ludwig and Leng, 2006; Tobin et al., 2014), OT neurons project distant axons throughout most of the forebrain and parts of the brain stem (Knobloch et al., 2012; Zhang et al., 2020), releasing a small number of large dense-core vesicles containing OT within a target region in non-synaptic fashion (Chini et al., 2017). The distribution of OT axonal terminals largely overlaps with OTR in target brain areas (Tribollet et al., 1988, 1991; Campbell et al., 2009; Grinevich et al., 2016; Mitre et al., 2016).

In various subcortical regions innervated by OT axons, the neuropeptide release is known to attenuate anxiety, fear, and physiological stress responses. Specifically, OT modulation of neural circuits in the central amygdala reduces contextual fear response (Knobloch et al., 2012; Hasan et al., 2019) and anxiety (Wahis et al., 2021), and in the lateral septum (LS) prevents social fear during lactation (Menon et al., 2018) as well as decreases aggression of female virgins (Oliveira et al., 2020). OT axons also reach the paraventricular nucleus of the thalamus (PVT) promoting maternal behavior (Knobloch et al., 2012; Cilz et al., 2018; Watarai et al., 2020). Furthermore, the OT system interacts with the serotonergic system by projecting to the raphe nucleus, promoting socially rewarding behaviors (Dölen et al., 2013). Up to date, the global OT projections through the entire brain have been mapped (Knobloch et al., 2012; Son et al., 2020), but the outputs of individual OT neurons or their subpopulations remain to be explored. So far, subpopulations of OT neurons in rodents have been shown to selectively target only a few distinct extrahypothalamic regions (Menon et al., 2018; Ferretti et al., 2019; Hasan et al., 2019), but do not uniformly send axonal collaterals to all OTR-expressing regions. A recent study mapping individual OT neuron projections by Levkowitz's group in fish confirmed these results (Wircer et al., 2017). Thus, it is likely that the OT system is composed of anatomically and functionally distinct clusters (Althammer and Grinevich, 2017), which specifically modulate OT-sensitive brain regions, controlling distinct forms of behaviors (Menon et al., 2018; Oliveira et al., 2020). Elucidating the functional organization of these different ensembles of OT neurons in mammals including humans will be an important challenge for future research.

LONG-RANGE OXYTOCIN MODULATION OF SENSORY CORTICAL CIRCUITS

In the cortex, the projections from OT neurons reach several sensory cortical areas, such as primary auditory, olfactory, and somatosensory cortices, where OT regulates the processing of sensory stimuli *via* enhancement of social cues' saliency (Marlin and Froemke, 2016; Mitre et al., 2016). This principle is exemplified by the study of Oettl et al. who showed that endogenous release of OT in the anterior olfactory nucleus (AON) of the olfactory cortex increases its excitatory drive and activates its top-down projections to granule cells in the olfactory bulb, enhancing the signal-to-noise ratio of social odor responses. In addition, the authors showed that optogenetically evoked release of OT from axons residing in the AON stimulates olfactory exploration and social recognition, while ablation of OTR in this cortex resulted in a "social amnesia" (Oettl et al., 2016).

Another notable example is the role of OT signaling in the primary auditory cortex (A1) that enables the initiation of pup retrieval, a specific maternal care behavior in female mice (Noirot, 1972). Mouse pups isolated from the nest emit ultrasonic distress calls that experienced mothers (called "dams") recognize and use to find and retrieve them to the nest. Conversely, virgin inexperienced females do not retrieve pups, but they start retrieving pups after being co-housed with dam and pups (Ehret et al., 1987). Interestingly, female mice that learned to retrieve pups show a higher neural response in the auditory cortex to pup distress calls than naive ones (Liu et al., 2006). Froemke's group reported that OT is crucial to drive the cortical plasticity occurring in the auditory cortex of mice which initiated pup retrieval behavior (Marlin et al., 2015; Schiavo et al., 2020). The recruitment of OTR neurons in the left auditory cortex increases the signal-to-noise ratio of pup calls responses of principal neurons, enabling efficient pup retrieval by their mothers as well as experienced virgins trained by lactating dams. However, the question whether OT influences plasticity related to other auditory learning tasks needs further investigation.

OT- and experience-induced cortical plasticity are not exclusive to auditory processing. Rather, this seems to be a generalized principle occurring during critical physiological

transitions—such as motherhood (Brecht et al., 2018; Valtcheva and Froemke, 2018). Intriguingly, the area representing the nipples and areolae in the somatosensory barrel cortex (S1) is largely expanded (a two-fold increase) in lactating rats, and this is induced by somatosensory stimulations in the form of suckling, artificial suction, or nipple rubbing (Rosselet et al., 2006). Interestingly, the S1 barrel field receives OT projections from the PVN (Grinevich et al., 2016) and expresses OTR (Newmaster et al., 2020). Thus, it is tempting to propose that OT may facilitate nursing-induced cortical plasticity because the neuropeptide concentration in S1 is gradually increased after prolonged sensory stimulation of the nipples (Zheng et al., 2014). Similarly, sensory deprivation in mice *via* whisker trimming or dark rearing after birth leads to reduced synaptic transmission in somatosensory and visual cortices, respectively, as well as to abolished OT synthesis, release, and overall OT neuron activity (Zheng et al., 2014), supporting the involvement of OT in the condition-dependent cortical plastic changes.

DO OT NEURONS RECEIVE FEEDBACK PROJECTIONS FROM THEIR TARGETS?

Although OT projections have been extensively studied in various brain regions, little is known on which sensory modalities trigger the activation of these neurons. The pioneering works performed around the end of the last century employing conventional antero- and retrograde tracers showed a number of extrahypothalamic regions projecting to the PVN and SON without discrimination of cell types within these nuclei (Sawchenko and Swanson, 1983; Iovino et al., 2016) followed by verification of the synapses onto OT neurons by electrophysiology (Hatton and Yang, 1989; Leng et al., 1999) or electron microscopy (Oldfield et al., 1985; Cservenák et al., 2016).

Recent advances in viral vector-based technology have allowed us to more precisely trace the origin of synaptic inputs to a genetically defined cell population (Wickersham et al., 2007). Using cell-type-specific OT promoter inserted into viral vectors in rats, we mapped neurons that synapse onto OT neurons in the PVN (Tang et al., 2020) and we found that 22 extrahypothalamic regions terminate on OT neurons. Among the previously known inputs (Sawchenko and Swanson, 1983) we identified new regions projecting to OT neurons, such as the infralimbic and insular cortices (**Figure 1**).

Similar results were recently obtained in mice (Son et al., 2020), although a number of input structures were distinct from those identified in rats. The most important discrepancy in mice is the absence of input to OT neurons from cortical areas, such as the prelimbic and infralimbic, cingulate, orbital, and insular cortices as was shown in rats (Tang et al., 2020). This may reflect a joint evolution of increasingly complex social behaviors and their neuronal underpinnings in rats compared to mice. We also found

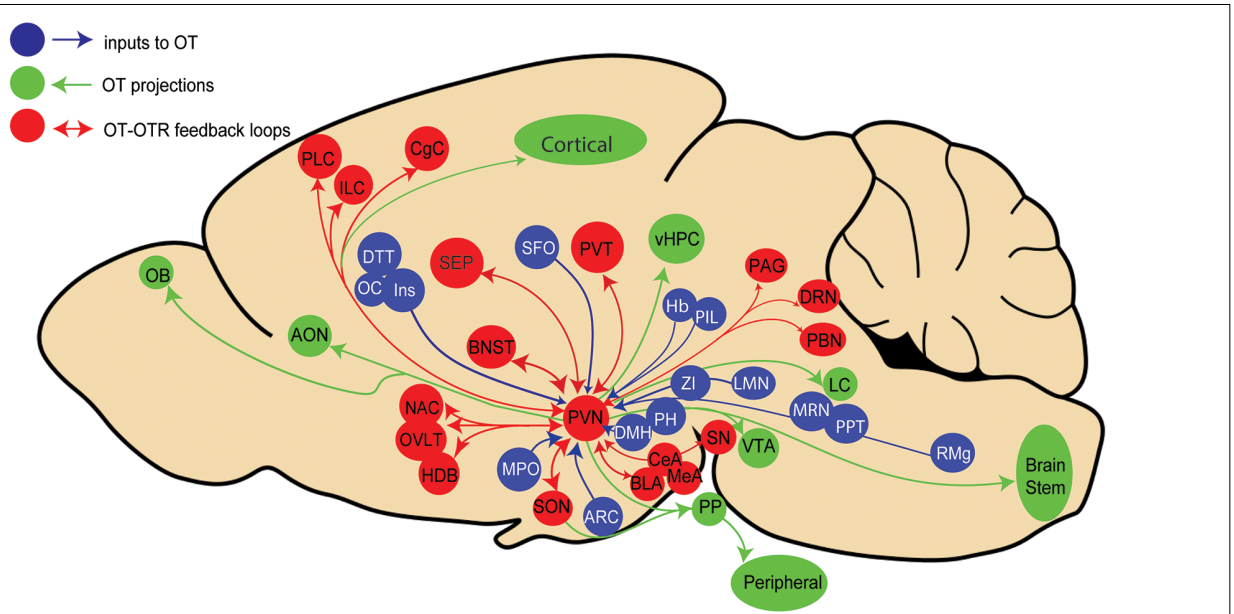

FIGURE 1 | Schema representing known paraventricular (PVN) oxytocin (OT) neurons inputs (blue), outputs (green), and areas providing both inputs to and receiving projections from PVN OT neurons in rats. Brain areas legend: AON, Accessory olfactory nucleus; Amygdala: Amy (central, basolateral and medial amygdala: CeA, BLA, MeA), ARC, Arcuate hypothalamic nucleus; BNST, Bed nucleus of stria terminalis; CgC, Cingulate cortex; Cl, Claustrum; DRN, Dorsal raphe nucleus; DTT, Dorsal tenia tecta; DMH, Dorsomedial hypothalamic area; Hb, Habenular nucleus; HDB, Horizontal limb of diagonal band nucleus; ILC, Infralimbic cortex; Ins, Insular cortex; LH, Lateral hypothalamic area; LMN, Lateral lemniscus nucleus; SEP, Lateral septal nucleus; LC, Locus Coeruleus; MMB, Mammillary body; MPO, Medial preoptic area; MRN, Median raphe nucleus; NAC, Nucleus accumbens; OB, Olfactory bulb; OC, Orbital cortex; PBN, Parabrachial nucleus; PVT, Paraventricular thalamus; PPT, Pedunculopontine tegmental nucleus; PAG, Periaqueductal gray area; PH, Posterior hypothalamic nucleus; PIL, Posterior intralaminar thalamus; PLC, Prelimbic cortex; PP, Posterior Pituitary; RMg, Raphe magnus nucleus; SFO, Subfornical organ; SN, Substancia nigra; OVLT, Vascular organ of lamina terminalis: vHPC, ventral hippocampus; VTA, Ventral tegme ZI, Zona incerta.

a large number of input cells in the subfornical organ, a known source of innervation to OT neurons (Anderson et al., 2001), that was not reported by Son et al. (2020), probably because this structure was not taken into account during the analysis.

While in both rodent species primary sensory cortices do not project to OT neurons, secondary sensory areas, such as the posterior and auditory thalamic nuclei do (Dobolyi et al., 2018; Valtcheva et al., 2021). This suggests that sensory information in rodents is conveyed to the OT system *via* secondary pathways, which could explain the activation of OT neurons by diverse sensory channels involved in social communication such as tactile (Tang et al., 2020) and auditory stimuli (Valtcheva et al., 2021), fear (Hasan et al., 2019), pain (Eliava et al., 2016), and reproductive and parental behaviors (Scott et al., 2015). However, we still do not know whether OT neurons and/or their subpopulations can be categorized based on their specific inputs (as well as outputs; Hasan et al., 2019).

Nevertheless, these recent results unveil an aspect, which was not previously considered: most regions receiving inputs from OT neurons, and/or expressing OTR seems to project back to OT neurons, thus potentially forming reciprocal connections between OT neurons and their target neurons expressing OTRs (**Figure 1**). However, it is as yet unclear whether these feedback connections are emanating from OTR neurons or non-OTR neurons. Thus, the behavioral role of such feedback loops to OT neurons remains to be elucidated.

DO OTR NEURONS IN DISTANT BRAIN REGIONS COMMUNICATE TO EACH OTHER?

Although OTR neurons are present in the vast majority of forebrain regions, the anatomical and functional connectivity between them has only been explored by a few studies. While the dominating view is that OTR neurons generally represent GABAergic local interneurons (Marlin and Froemke, 2016), it is now known that principal glutamatergic neurons, as well as astrocytes, are also capable to express OTR (Mitre et al., 2016; Tan et al., 2019; Wahis et al., 2021).

Using OTR-Cre knock-in mice in combination with a virus expressing GFP in a Cre dependent manner, a first study showed that VTA OTR neurons project to the medial prefrontal cortex (mPFC), nucleus accumbens (NAcc), amygdala (Amy), and lateral habenula (LHb; Peris et al., 2016). On the same line, another study, using a similar strategy revealed that OTR neurons in the mPFC project to the bed nucleus of stria terminalis (BNST), the NAcc, and Amy (Tan et al., 2019). Employing a different approach, Dölen and colleagues injected the retrograde monotranssynaptic rabies virus expressing tdTomato in the NAcc of OTR-Venus mice and found that NAcc (itself containing OTR cells) received direct inputs from OTR cells in some distant areas such as accessory olfactory nuclei (AON), mPFC, Amy, paraventricular thalamic nucleus (PVT), CA1, dorsal raphe nucleus (DRN), and ventral tegmental area (VTA; Dölen et al., 2013). Finally, similar findings have been obtained in novel OTR-Cre knock-in prairie voles that were recently generated by CRISPR/Cas9 technology (Horie et al., 2020). The authors showed that the prairie vole's NAcc receives direct inputs from OTR neurons of various areas, such as the AON, mPFC, Amy, cingulate cortex, PVT, and insula. Together, these findings suggest that the existence of long-range projecting OTR neurons is not exceptional, but rather a common feature of the brain OT system.

When summarizing all known connections between areas containing OTR neurons (as we have endeavored to do in **Figure 2**), it is striking that most of them are located in regions that are part of the "social brain," a network of areas regulating social behavior (Olsson et al., 2020). It is important to note that

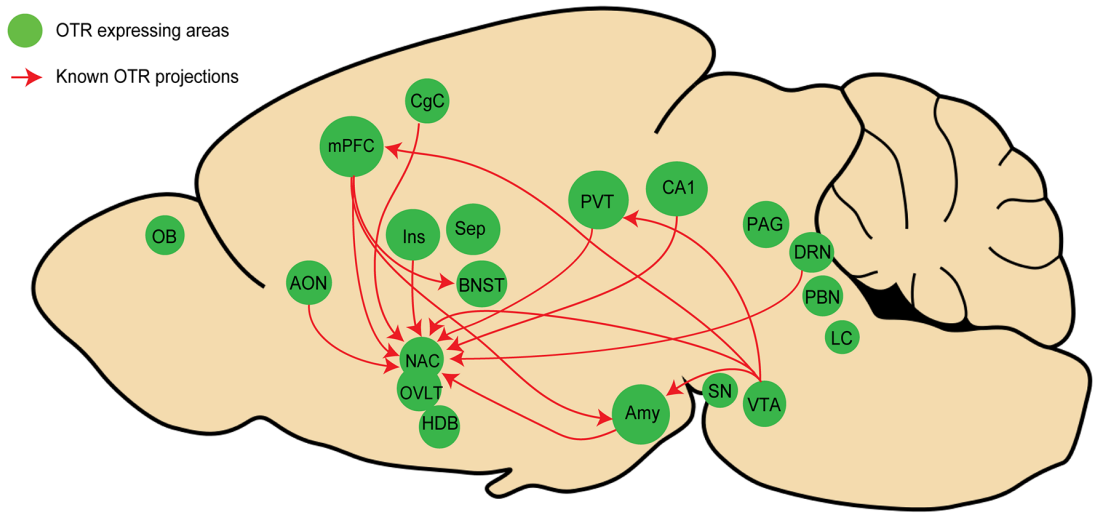

FIGURE 2 | Schema representing the known inter areas OT receptor (OTR) network in rodents. Regions in green contain OTR neurons, red arrows represent OTR projections in other regions containing OTR neurons. Note that only four studies (see text) have analyzed OTR projections, mostly focusing on the NAcc, indicating that numerous OTR connections have not been yet discovered. See **Figure 1** legends for abbreviations.

these networks are not necessarily involving OTR neurons at the postsynaptic level, meaning that as far as we know, OTR neurons projecting to a distant area could contact other OTR or non-OTR neurons. Although the role of a potential "OTR network" remains to be determined, we hypothesize that such a network is important for the regulation of social behaviors. Experimental evidence indicates that the stimulation of fibers originating from OTR neurons in the mPFC and terminating in the basolateral amygdala (BLA) disrupts social recognition in mice (Tan et al., 2019). Thus, OTR to OTR neurons could represent an anatomical substrate essential for synchronization of activity in this network, allowing OT to produce a coherent (e.g., "whole brain") response. This hypothesis should be addressed together with other key questions regarding the functional organization of the OT system, such as whether OT is released selectively or simultaneously in all these brain areas (i); to what degree OT-sensitive circuitries connect to each other, at least in the "social brain" (ii); and how activation of subpopulations of OT neurons upon distinct sensory modalities is transmitted to various OTR expressing brain regions (iii).

Several recent technological developments render possible the exploration of these questions. For instance, using pseudotype rabies infecting cells in a cre dependent manner combined with transgenic OTR-Cre animals could bring evidence that OTR neurons in one region are innervated by OTR neurons from another region. Another useful tool is the generation of non-toxic pseudotype rabies (Ciabatti et al., 2017; Chatterjee et al., 2018) that will allow functional interrogation of defined inputs to OT neurons. Finally, a new type of sensor (Wang et al., 2018) can be used to track OT concentration in multiple areas of the brain, allowing one to investigate question (i).

CONCLUSIONS/PERSPECTIVES

In this review, we proposed two novel features of OT signaling in the brain. First, we showed that OT neurons received reciprocal input from the OT-sensitive structures they are innervating. Although the functional significance of such potential feedback projections is not clear, it is tempting to postulate that OTR neurons of distant brain regions dynamically tune "positive" vs. "negative" balance of OT neurons to initiate, accelerate, or slow down behavioral responses. Secondly, we hypothesized that OTR neurons in spatially distant brain regions are communicating with each other to further control social behaviors elicited by an initial OT release. An important note is that all the studies reviewed here have been performed in rodents, and thus whether the proposed circuits might also exist in other mammals is unknown. Finally, we would like to point out that OT is the most studied neuropeptide at the moment, but that the mechanisms proposed here can be expanded towards other less renown neuropeptides, which are also important neuromodulators of social behaviors (Lefevre et al., 2018).

AUTHOR CONTRIBUTIONS

All authors discussed and elaborated the ideas, wrote the first draft and corrected it until the final version was obtained. All authors contributed to the article and approved the submitted version.

FUNDING

This work was supported by Fyssen foundation, a PROCOP grant, and SFB1158 Consortium seed grant for young scientists (to AL); Deutsche Forschungsgemeinschaft (DFG, German Research Foundation) Walter Benjamin Position—Projektnummer 459051339 (to QK); the IASP Early Career Research grant 2012, FP7 Career Integration grant 334455, Initiative of Excellence (IDEX) Attractiveness grant 2013, IDEX Interdisciplinary grant 2015, University of Strasbourg Institute for Advanced Study (USIAS) fellowship 2014–15, Foundation Fyssen research grant 2015, NARSAD Young Investigator Grant 24821 and ANR JCJC grant (to AC); DFG-RSF grant GR 3619/15-1, DFG grant GR 3619/10-1, SFB Consortium 1158-2, DFG grant GR 3619/13-1, and DFG-SNSF grant GR 3619/8-1 (to VG).

REFERENCES

Althammer, F., and Grinevich, V. (2017). Diversity of oxytocin neurons: beyond magno- and parvocellular cell types? *J. Neuroendocrinol.* 30:e12549. doi: 10.1111/jne.12549

Anderson, J. W., Smith, P. M., and Ferguson, A. V. (2001). Subfornical organ neurons projecting to paraventricular nucleus: whole-cell properties. *Brain Res.* 921, 78–85. doi: 10.1016/s0006-8993(01)03093-1

Banerjee, P., Joy, K. P., and Chaube, R. (2016). Structural and functional diversity of nonapeptide hormones from an evolutionary perspective: a review. *Gen. Comp. Endocrinol.* 15, 241–243. doi: 10.1016/j.ygcen.2016.04.025

Bowen, M. T., and Neumann, I. D. (2017). Rebalancing the addicted brain: oxytocin interference with the neural substrates of addiction. *Trends Neurosci.* 40, 691–708. doi: 10.1016/j.tins.2017.10.003

Brecht, M., Lenschow, C., and Rao, R. P. (2018). Socio-sexual processing in cortical circuits. *Curr. Opin. Neurobiol.* 52, 1–9. doi: 10.1016/j.conb.2018.04.003

Campbell, P., Ophir, A. G., and Phelps, S. M. (2009). Central vasopressin and oxytocin receptor distributions in two species of singing mice. *J. Comp Neurol.* 516, 321–333. doi: 10.1002/cne.22116

Chatterjee, S., Sullivan, H. A., MacLennan, B. J., Xu, R., Hou, Y., Lavin, T. K., et al. (2018). Nontoxic, double-deletion-mutant rabies viral vectors for retrograde targeting of projection neurons. *Nat. Neurosci.* 21, 638–646. doi: 10.1038/s41593-018-0091-7

Chaves, V. E., Tilelli, C. Q., Brito, N. A., and Brito, M. N. (2013). Role of oxytocin in energy metabolism. *Peptides* 45, 9–14. doi: 10.1016/j.peptides.2013.04.010

Chini, B., Verhage, M., and Grinevich, V. (2017). The action radius of oxytocin release in the mammalian CNS: from single vesicles to behavior. *Trends Pharmacol. Sci.* 38, 982–991. doi: 10.1016/j.tips.2017.08.005

Ciabatti, E., González-Rueda, A., Mariotti, L., Morgese, F., and Tripodi, M. (2017). Life-long genetic and functional access to neural circuits using self-inactivating rabies virus. *Cell* 170, 382–392.e14.doi: 10.1016/j.cell.2017.06.014

Cilz, N. I., Cymerblit-Sabba, A., and Young, W. S. (2018). Oxytocin and vasopressin in the rodent hippocampus. *Genes Brain Behav.* 18:e12535. doi: 10.1111/gbb.12535

Cservenák, M., Keller, D., Kis, V., Fazekas, E. A., Öllös, H., Lékó, A., et al. (2016). A thalamo-hypothalamic pathway that activates oxytocin neurons in social contexts in female rats. *Endocrinology* 158, 335–348. doi: 10.1210/en.2016-1645

Dobolyi, A., Cservenák, M., and Young, L. J. (2018). Thalamic integration of social stimuli regulating parental behavior and the oxytocin system. *Front. Neuroendocrinol.* 51, 102–115. doi: 10.1016/j.yfrne.2018.05.002

Dölen, G., Darvishzadeh, A., Huang, K. W., and Malenka, R. C. (2013). Social reward requires coordinated activity of nucleus accumbens oxytocin and serotonin. *Nature* 501, 179–184. doi: 10.1038/nature12518

Ehret, G., Koch, M., Haack, B., and Markl, H. (1987). Sex and parental experience determine the onset of an instinctive behavior in mice. *Naturwissenschaften* 74:47. doi: 10.1007/BF00367047

Elabd, C., Cousin, W., Upadhyayula, P., Chen, R. Y., Chooljian, M. S., Li, J., et al. (2014). Oxytocin is an age-specific circulating hormone that is necessary for muscle maintenance and regeneration. *Nat. Commun.* 5:4082. doi: 10.1038/ncomms5082

Eliava, M., Melchior, M., Knobloch-Bollmann, H. S., Wahis, J., da Silva Gouveia, M., Tang, Y., et al. (2016). A new population of parvocellular oxytocin neurons controlling magnocellular neuron activity and inflammatory pain processing. *Neuron* 89, 1291–1304. doi: 10.1016/j.neuron.2016.01.041

Ferretti, V., Maltese, F., Contarini, G., Nigro, M., Bonavia, A., Huang, H., et al. (2019). Oxytocin signaling in the central amygdala modulates emotion discrimination in mice. *Curr. Biol.* 29, 1938–1953. doi: 10.1016/j.cub.2019.04.070

Grinevich, V., and Stoop, R. (2018). Interplay between oxytocin and sensory systems in the orchestration of socio-emotional behaviors. *Neuron* 99, 887–904. doi: 10.1016/j.neuron.2018.07.016

Grinevich, V., Knobloch-Bollmann, H. S., Eliava, M., Busnelli, M., and Chini, B. (2016). Assembling the puzzle: pathways of oxytocin signaling in the brain. *Biol. Psychiatry* 79, 155–164. doi: 10.1016/j.biopsych.2015.04.013

Gutkowska, J., and Jankowski, M. (2012). Oxytocin Revisited: Its Role in Cardiovascular Regulation. *J. Neuroendocrinol.* 24, 599–608. doi: 10.1111/j.1365-2826.2011.02235.x

Hasan, M. T., Althammer, F., Silva da Gouveia, M., Goyon, S., Eliava, M., Lefevre, A., et al. (2019). A fear memory engram and its plasticity in the hypothalamic oxytocin system. *Neuron* 103, 133–146. doi: 10.1016/j.neuron.2019.04.029

Hatton, G. I., and Yang, Q. Z. (1989). Supraoptic nucleus afferents from the main olfactory bulb--II. Intracellularly recorded responses to lateral olfactory tract stimulation in rat brain slices. *Neuroscience* 31, 289–297. doi: 10.1016/0306-4522(89)90374-6

Horie, K., Inoue, K., Nishimori, K., and Young, L. J. (2020). Investigation of oxtr-expressing neurons projecting to nucleus accumbens using oxtr-ires-cre knock-in prairie voles (*Microtus ochrogaster*). *Neuroscience* 448, 312–324. doi: 10.1016/j.neuroscience.2020.08.023

Iovino, M., Giagulli, V. A., Licchelli, B., Iovino, E., Guastamacchia, E., and Triggiani, V. (2016). Synaptic inputs of neural afferent pathways to vasopressin- and oxytocin-secreting neurons of supraoptic and paraventricular hypothalamic nuclei. *Endocr. Metab. Immune Disord. Drug Targets* 16, 276–287. doi: 10.2174/1871530317666170104124229

Kasahara, Y., Sato, K., Takayanagi, Y., Mizukami, H., Ozawa, K., Hidema, S., et al. (2013). Oxytocin receptor in the hypothalamus is sufficient to rescue normal thermoregulatory function in male oxytocin receptor knockout mice. *Endocrinology* 154, 4305–4315. doi: 10.1210/en.2012-2206

Knobloch, H. S., and Grinevich, V. (2014). Evolution of Oxytocin Pathways in the Brain of Vertebrates. *Front. Behav. Neurosci.* 8:31. doi: 10.3389/fnbeh.2014.00031

Knobloch, H. S., Charlet, A., Hoffmann, L. C., Eliava, M., Khrulev, S., Cetin, A. H., et al. (2012). Evoked axonal oxytocin release in the central amygdala attenuates fear response. *Neuron* 73, 553–566. doi: 10.1016/j.neuron.2011.11.030

Lawson, E. A., Olszewski, P. K., Weller, A., and Blevins, J. E. (2019). The role of oxytocin in regulation of appetitive behavior, body weight and glucose homeostasis. *J. Neuroendocrinol.* 32:e12805. doi: 10.1111/jne.12805

Landgraf, R., and Neumann, I. D. (2004). Vasopressin and oxytocin release within the brain: a dynamic concept of multiple and variable modes of neuropeptide communication. *Front. Neuroendocrinol.* 25, 150–176. doi: 10.1016/j.yfrne.2004.05.001

Lefevre, A., Hurlemann, R., and Grinevich, V. (2018). Imaging neuropeptide effects on human brain function. *Cell Tissue Res.* 375, 379–386. doi: 10.1007/s00441-018-2899-6

Leng, G., Brown, C. H., and Russell, J. A. (1999). Physiological pathways regulating the activity of magnocellular neurosecretory cells. *Prog. Neurobiol.* 57, 625–655. doi: 10.1016/s0301-0082(98)00072-0

Linster, C., and Kelsch, W. (2019). A computational model of oxytocin modulation of olfactory recognition memory. *eNeuro* 6:ENEURO.0201–19.2019. doi: 10.1523/ENEURO.0201-19.2019

Liu, R. C., Linden, J. F., and Schreiner, C. E. (2006). Improved cortical entrainment to infant communication calls in mothers compared with virgin mice. *Eur. J. Neurosci.* 23, 3087–3097. doi: 10.1111/j.1460-9568.2006.04840.x

Ludwig, M., and Leng, G. (2006). Dendritic peptide release and peptide-dependent behaviours. *Nat. Rev. Neurosci.* 7, 126–136. doi: 10.1038/nrn1845

Macdonald, K., and Feifel, D. (2014). Oxytocin's role in anxiety: a critical appraisal. *Brain Res.* 1580, 22–56. doi: 10.1016/j.brainres.2014.01.025

Marlin, B. J., and Froemke, R. C. (2016). Oxytocin modulation of neural circuits for social behavior. *Dev. Neurobiol.* 77, 169–189. doi: 10.1002/dneu.22452

Marlin, B. J., Mitre, M., D'amour, J. A., Chao, M. V., and Froemke, R. C. (2015). Oxytocin enables maternal behaviour by balancing cortical inhibition. *Nature* 520, 499–504. doi: 10.1038/nature14402

Menon, R., Grund, T., Zoicas, I., Althammer, F., Fiedler, D., Biermeier, V., et al. (2018). Oxytocin signaling in the lateral septum prevents social fear during lactation. *Curr. Biol.* 28, 1066–1078. doi: 10.1016/j.cub.2018.02.044

Mitre, M., Marlin, B. J., Schiavo, J. K., Morina, E., Norden, S. E., Hackett, T. A., et al. (2016). A distributed network for social cognition enriched for oxytocin receptors. *J. Neurosci.* 36, 2517–2535. doi: 10.1523/JNEUROSCI.2409-15.2016

Neumann, I., Russell, J. A., and Landgraf, R. (1993). Oxytocin and vasopressin release within the supraoptic and paraventricular nuclei of pregnant, parturient and lactating rats: a microdialysis study. *Neuroscience* 53, 65–75. doi: 10.1016/0306-4522(93)90285-n

Newmaster, K. T., Nolan, Z. T., Chon, U., Vanselow, D. J., Weit, A. R., Tabbaa, M., et al. (2020). Quantitative cellular-resolution map of the oxytocin receptor in postnatally developing mouse brains. *Nat. Commun.* 11:1885. doi: 10.1038/s41467-020-15659-1

Noirot, E. (1972). Ultrasounds and maternal behavior in small rodents. *Dev. Psychobiol.* 5, 371–387. doi: 10.1002/dev.420050410

Oettl, L.-L., Ravi, N., Schneider, M., Scheller, M. F., Schneider, P., Mitre, M., et al. (2016). Oxytocin enhances social recognition by modulating cortical control of early olfactory processing. *Neuron* 90, 609–621. doi: 10.1016/j.neuron.2016.03.033

Oldfield, B. J., Hou-Yu, A., and Silverman, A. J. (1985). A combined electron microscopic HRP and immunocytochemical study of the limbic projections to rat hypothalamic nuclei containing vasopressin and oxytocin neurons. *J. Comp. Neurol.* 231, 221–231. doi: 10.1002/cne.902310209

Oliveira, V. E., de, M., Lukas, M., Wolf, H. N., Durante, E., Lorenz, A., et al. (2020). Concerted but segregated actions of oxytocin and vasopressin within the ventral and dorsal lateral septum determine female aggression. *bioRxiv* [Preprint]. doi: 10.1101/2020.07.28.224873

Olsson, A., Knapska, E., and Lindström, B. (2020). The neural and computational systems of social learning. *Nat. Rev. Neurosci.* 21, 197–212. doi: 10.1038/s41583-020-0276-4

Peris, J., MacFadyen, K., Smith, J. A., de Kloet, A. D., Wang, L., and Krause, E. G. (2016). Oxytocin receptors are expressed on dopamine and glutamate neurons in the mouse ventral tegmental area that project to nucleus accumbens and other mesolimbic targets. *J. Comp. Neurol.* 525, 1094–1108. doi: 10.1002/cne.24116

Poisbeau, P., Grinevich, V., and Charlet, A. (2017). Oxytocin signaling in pain: cellular, circuit, system and behavioral levels. *Curr. Top Behav. Neurosci.* 35, 193–211. doi: 10.1007/7854_2017_14

Rosselet, C., Zennou-Azogui, Y., and Xerri, C. (2006). Nursing-induced somatosensory cortex plasticity: temporally decoupled changes in neuronal receptive field properties are accompanied by modifications in activity-dependent protein expression. *J. Neurosci.* 26, 10667–10676. doi: 10.1523/JNEUROSCI.3253-06.2006

Sawchenko, P. E., and Swanson, L. W. (1983). The organization and biochemical specificity of afferent projections to the paraventricular and

supraoptic nuclei. *Prog. Brain Res.* 60, 19–29. doi: 10.1016/S0079-6123(08)64371-X

Schiavo, J. K., Valtcheva, S., Bair-Marshall, C. J., Song, S. C., Martin, K. A., and Froemke, R. C. (2020). Innate and plastic mechanisms for maternal behaviour in auditory cortex. *Nature* 587, 426–431. doi: 10.1038/s41586-020-2807-6

Scott, N., Prigge, M., Yizhar, O., and Kimchi, T. (2015). A sexually dimorphic hypothalamic circuit controls maternal care and oxytocin secretion. *Nature* 525, 519–522. doi: 10.1038/nature15378

Shamay-Tsoory, S. G., and Abu-Akel, A. (2015). The social salience hypothesis of oxytocin. *Biol. Psychiatry* 79, 194–202. doi: 10.1016/j.biopsych.2015.07.020

Son, S., Manjila, S. B., Newmaster, K. T., Wu, Y., Vanselow, D. J., Ciarletta, M., et al. (2020). Wiring diagram of the oxytocin system in the mouse brain. *bioRxiv* [Preprint]. doi: 10.1101/2020.10.01.320978

Sun, L., Lizneva, D., Ji, Y., Colaianni, G., Hadelia, E., Gumerova, A., et al. (2019). Oxytocin regulates body composition. *Proc. Natl. Acad. Sci. USA* 116, 26808–26815. doi: 10.1073/pnas.1913611116

Tan, Y., Singhal, S. M., Harden, S. W., Cahill, K. M., Nguyen, D.-T. M., Colon-Perez, L. M., et al. (2019). Oxytocin receptors are expressed by glutamatergic prefrontal cortical neurons that selectively modulate social recognition. *J. Neurosci.* 39, 3249–3263. doi: 10.1523/JNEUROSCI.2944-18.2019

Tang, Y., Benusiglio, D., Lefevre, A., Hilfiger, L., Althammer, F., Bludau, A., et al. (2020). Social touch promotes interfemale communication *via* activation of parvocellular oxytocin neurons. *Nat. Neurosci.* 23, 1125–1137. doi: 10.1038/s41593-020-0674-y

Tobin, V. A., Arechaga, G., Brunton, P. J., Russell, J. A., Leng, G., Ludwig, M., et al. (2014). Oxytocinase in the female rat hypothalamus: a novel mechanism controlling oxytocin neurones during lactation. *J. Neuroendocrinol.* 26, 205–216. doi: 10.1111/jne.12141

Tribollet, E., Barberis, C., Jard, S., Dubois-Dauphin, M., and Dreifuss, J. J. (1988). Localization and pharmacological characterization of high affinity binding sites for vasopressin and oxytocin in the rat brain by light microscopic autoradiography. *Brain Res.* 442, 105–118. doi: 10.1016/0006-8993(88)91437-0

Tribollet, E., Goumaz, M., Raggenbass, M., and Dreifuss, J. J. (1991). Appearance and transient expression of vasopressin and oxytocin receptors in the rat brain. *J. Recept. Res.* 11, 333–346. doi: 10.3109/10799899109066412

Valtcheva, S., and Froemke, R. C. (2018). Neuromodulation of maternal circuits by oxytocin. *Cell Tissue Res.* 375, 57–68. doi: 10.1007/s00441-018-2883-1

Valtcheva, S., Issa, H. A., Martin, K. A., Jung, K., Kwon, H.-B., and Froemke, R. C. (2021). Neural circuitry for maternal oxytocin release induced by infant cries. *bioRxiv* [Preprint]. doi: 10.1101/2021.03.25.436883

Wahis, J., Baudon, A., Althammer, F., Kerspern, D., Goyon, S., Hagiwara, D., et al. (2021). Astrocytes mediate the effect of oxytocin in the central amygdala on neuronal activity and affective states in rodents. *Nat. Neurosci.* 24, 529–541. doi: 10.1038/s41593-021-00800-0

Wang, H., Jing, M., and Li, Y. (2018). Lighting up the brain: genetically encoded fluorescent sensors for imaging neurotransmitters and neuromodulators. *Curr. Opin. Neurobiol.* 50, 171–178. doi: 10.1016/j.conb.2018.03.010

Watarai, A., Tsutaki, S., Nishimori, K., Okuyama, T., Mogi, K., and Kikusui, T. (2020). The blockade of oxytocin receptors in the paraventricular thalamus reduces maternal crouching behavior over pups in lactating mice. *Neurosci. Lett.* 720:134761. doi: 10.1016/j.neulet.2020.134761

Wickersham, I. R., Lyon, D. C., Barnard, R. J. O., Mori, T., Finke, S., Conzelmann, K.-K., et al. (2007). Monosynaptic restriction of transsynaptic tracing from single, genetically targeted neurons. *Neuron* 53, 639–647. doi: 10.1016/j.neuron.2007.01.033

Wircer, E., Blechman, J., Borodovsky, N., Tsoory, M., Nunes, A. R., Oliveira, R. F., et al. (2017). Homeodomain protein Otp affects developmental neuropeptide switching in oxytocin neurons associated with a long-term effect on social behavior. *eLife* 6:e22170. doi: 10.7554/eLife.22170

Zhang, B., Qiu, L., Xiao, W., Ni, H., Chen, L., Wang, F., et al. (2020). Reconstruction of the hypothalamo-neurohypophysial system and functional dissection of magnocellular oxytocin neurons in the brain. *Neuron* 109, 331–346. doi: 10.1016/j.neuron.2020.10.032

Zheng, J.-J., Li, S.-J., Zhang, X.-D., Miao, W.-Y., Zhang, D., Yao, H., et al. (2014). Oxytocin mediates early experience-dependent cross-modal plasticity in the sensory cortices. *Nat. Neurosci.* 17, 391–399. doi: 10.1038/nn.3634

Conflict of Interest: The authors declare that the research was conducted in the absence of any commercial or financial relationships that could be construed as a potential conflict of interest.

frontiers in Neural Circuits

ORIGINAL RESEARCH
published: 12 July 2021
doi: 10.3389/fncir.2021.659280

Laser-Induced Apoptosis of Corticothalamic Neurons in Layer VI of Auditory Cortex Impact on Cortical Frequency Processing

Katja Saldeitis[1,2,3], Marcus Jeschke[1,2,3], Eike Budinger[1,4], Frank W. Ohl[1,3,5] and Max F. K. Happel[1,4,6]**

[1] Department of Systems Physiology of Learning, Leibniz Institute for Neurobiology, Magdeburg, Germany, [2] Auditory Neuroscience and Optogenetics Group, Cognitive Hearing in Primates Lab, German Primate Center, Göttingen, Germany, [3] Institute for Auditory Neuroscience, University Medical Center Goettingen, Göttingen, Germany, [4] Center for Behavioral Brain Sciences, Magdeburg, Germany, [5] Institute of Biology (IBIO), University Magdeburg, Magdeburg, Germany, [6] Medical School Berlin, Berlin, Germany

Corticofugal projections outnumber subcortical input projections by far. However, the specific role for signal processing of corticofugal feedback is still less well understood in comparisonto the feedforward projection. Here, we lesioned corticothalamic (CT) neurons in layers V and/or VI of the auditory cortex of Mongolian gerbils by laser-induced photolysis to investigate their contribution to cortical activation patterns. We have used laminar current-source density (CSD) recordings of tone-evoked responses and could show that, particularly, lesion of CT neurons in layer VI affected cortical frequency processing. Specifically, we found a decreased gain of best-frequency input in thalamocortical (TC)-recipient input layers that correlated with the relative lesion of layer VI neurons, but not layer V neurons. Using cortical silencing with the $GABA_a$-agonist muscimol and layer-specific intracortical microstimulation (ICMS), we found that direct activation of infragranular layers recruited a local recurrent cortico-thalamo-cortical loop of synaptic input. This recurrent feedback was also only interrupted when lesioning layer VI neurons, but not cells in layer V. Our study thereby shows distinct roles of these two types of CT neurons suggesting a particular impact of CT feedback from layer VI to affect the local feedforward frequency processing in auditory cortex.

Keywords: auditory cortex, corticothalamic, laser-induced ablation, Mongolian gerbil (*Meriones unguiculatus*), current-source density, intracortical microstimulation

OPEN ACCESS

Edited by:
Patrick O. Kanold, Johns Hopkins University, United States

Reviewed by:
Daniel Llano, University of Illinois at Urbana-Champaign, United States
Paul B. Manis, University of North Carolina at Chapel Hill, United States

****Correspondence:***
Katja Saldeitis
KSaldeitis@dpz.eu
Max F. K. Happel
mhappel@lin-magdeburg.de

Received: *27 January 2021*
Accepted: *14 June 2021*
Published: *12 July 2021*

Citation:
Saldeitis K, Jeschke M, Budinger E, Ohl FW and Happel MFK (2021) Laser-Induced Apoptosis of Corticothalamic Neurons in Layer VI of Auditory Cortex Impact on Cortical Frequency Processing. Front. Neural Circuits 15:659280. doi: 10.3389/fncir.2021.659280

INTRODUCTION

Being positioned at the nexus between the ascending subcortical and descending higher-cortical auditory pathway, the auditory cortex (ACx) is central for auditory processing and behavior (Scheich et al., 2007; Schreiner and Winer, 2007; Budinger et al., 2008; Sharpee et al., 2011; King et al., 2018). A prominent hypothesis is that sensory-related population activity in ACx is generated and dynamically adjusted through recurrent feedback processing with its thalamic relays via gating mechanisms (Suga, 1977; Zhang et al., 1997; Destexhe, 2000; Yu et al., 2004; Crandall et al., 2015; Guo et al., 2017). Corticothalamic (CT) feedback signals from ACx shape the receptive field and filtering properties of neurons in the auditory thalamus, the medial geniculate body (MGB;

Suga and Ma, 2003; Zhang et al., 1997; Bäuerle et al., 2011; Anderson and Malmierca, 2013; Malmierca et al., 2015), and control the gain of thalamocortical (TC) transmission (Deschênes and Hu, 1990; He, 1997; Yu et al., 2004; Happel et al., 2014; Williamson and Polley, 2019). Such gain control via CT circuits was also shown for the visual (Olsen et al., 2012; Kirchgessner et al., 2020) and somatosensory system (Temereanca and Simons, 2004; Mease et al., 2014; Crandall et al., 2015).

CT neurons have been implicated in many cognitive functions, such as the regulation of attentional processes (Bollimunta et al., 2011), the perception of complex sounds (Homma et al., 2017), and dopamine-dependent auditory detection and discrimination learning (Happel et al., 2014; Guo et al., 2017; Deliano et al., 2018). CT feedback arising from cortical layers VI and V have distinct intra- and subcortical projection patterns to lemniscal and non-lemniscal thalamic nuclei (Hazama et al., 2004; Rouiller and Durif, 2004; Llano and Sherman, 2009). Recently, Williamson and Polley (2019) have suggested that the broader corticofugal projection neurons in layer V broadcast sensory inputs to distributed downstream targets, while CT neurons in layer VI regulate specifically TC response gain and selectivity. Layer VI neurons thereby exert strong feedforward amplification at the level of local columnar circuits adaptively during different behavioral states (Augustinaite and Kuhn, 2020; Clayton et al., 2020).

In a previous study, ferrets whose layer VI CT neurons of the ACx had been selectively lesioned by means of a chromophore-targeted laser photolysis showed impaired perceptual grouping of harmonics—one of the key cues in the perception of complex sounds (Homma et al., 2017).

Here, we applied this method in the Mongolian gerbil (*Meriones unguiculatus*) to investigate the contributions of CT neurons to acoustically and electrically evoked population activity patterns of primary ACx (field AI) as revealed by current-source density (CSD) analysis (Happel et al., 2010). Targeting of CT neuronal somata was achieved by injecting laser-activatable cytolytic chromophores attached to retrograde beads (Macklis, 1993; Bajo et al., 2010) into the MGB.

While the canonical spatiotemporal CSD pattern across cortical laminae evoked by acoustic stimulation (AcS) was generally preserved, photolytic apoptosis of specifically layer VI neurons led to frequency-selective changes with respect to strength and timing of columnar current flow. We found a reduced contrast between responses evoked by the best frequency (BF) and frequencies 2 octaves away of the BF (non-BF) in the main thalamorecipient layer IV (early granular sink, S1) and reduced BF-evoked input in layers Vb/VI (early infragranular sink, iS1). In contrast, current flow in layers I/II was increased (late supragranular sink, S2).

Infragranular intracortical microstimulation (ICMS) in ACx evoked local-field responses (Deliano et al., 2009) and translaminar CSD patterns (Happel et al., 2014) similar to acoustic stimulation. Here, we could demonstrate that intact CT feedback from layer VI is crucial for this electrically evoked columnar population pattern: Selective apoptosis of CT neurons in layer VI diminished this direct ICMS-evoked columnar activation significantly. This finding confirms our hypothesis that infragranular microstimulation activates a fast-acting recurrent CT loop via the ventral part of the MBG (MGv; Happel et al., 2014).

Our study thereby shows that particularly layer VI CT neurons affect the columnar frequency processing in ACx through a frequency-specific gain in TC-recipient layers.

MATERIALS AND METHODS

Experimental Animals

Experiments were performed on 21 adult male ketamine-xylazine anesthetized Mongolian gerbils (age: 4–6 months, body weight: 65–85 g). All experiments were conducted in accordance with the international NIH Guidelines for Animals in Research and with ethical standards for the care and use of animals in research defined by the German Law for the protection of experimental animals. Experiments were approved by an ethics committee of the state Saxony-Anhalt, Germany.

Experimental Design

An outline of the experimental procedure is depicted in **Figure 1**. The photolytic apoptosis of chromophore-targeted neuronal populations has been performed before in different species including mice, rats, and ferrets (Macklis, 1993; Bajo et al., 2010; Homma et al., 2017). In this study, animals received stereotactic unilateral injections of the photolytic tracer into the MGB (**Figures 1B,C**). After retrograde transport to the ACx and fluorescent labeling of CT projection neurons (**Figure 1C**; see also **Figure 2A**), the ipsilateral ACx was illuminated with laser light (670 nm, 10 days after injection), which induces a photolytic apoptosis of CT projection neurons by the release of reactive oxygen species. Following completion of the apoptotic process, electrophysiological cortical population activity was recorded (**Figure 1D**). Afterward, neuronal cell loss can be made visible by immunohistochemical markers such as NeuN, SMI-32 neurofilament, and caspase 3 (**Figure 2B** and **Supplementary Figure 1**).

Preparation of the Photolytic Tracer (Chlorin e6-Conjugated Retrobeads)

A 1 mM solution of Chlorin e6(-monoethylenediamineamide) (Phyto-chlorin, Frontier Scientific, United States, CAS# 19660-77-6, MW 596.68) was made up with 3 ml of 0.01 M PB (pH 7.4) and was activated with 5 mg N-Cyclohexyl-N'-(2-morpholinoethyl) carbodi-imide metho-p-toluenesulfonate (Sigma-Aldrich, Switzerland, CAS# 2491-17-0) for 30 min at 4°C on a rocker table (70 rpm). 50 µl Red Retrobeads IX (Lumafluor, United States, excitation: 530 nm, emission: 590 nm) were diluted in 300 µl PB and added to the solution. Chlorin e6 was then attached to the latex surface of the fluorescent microbeads by gentle agitation on a rocker table at 4°C. The reaction was stopped after 60 min with 335 µl 0.1 M glycine buffer (pH 8.0) and this mixture was pelleted by a series of high-speed centrifugations (Optima MAX Ultracentrifuge, Beckman Coulter, United States, 60 min each, 140,000 g, 45,000 rpm; MLA-80

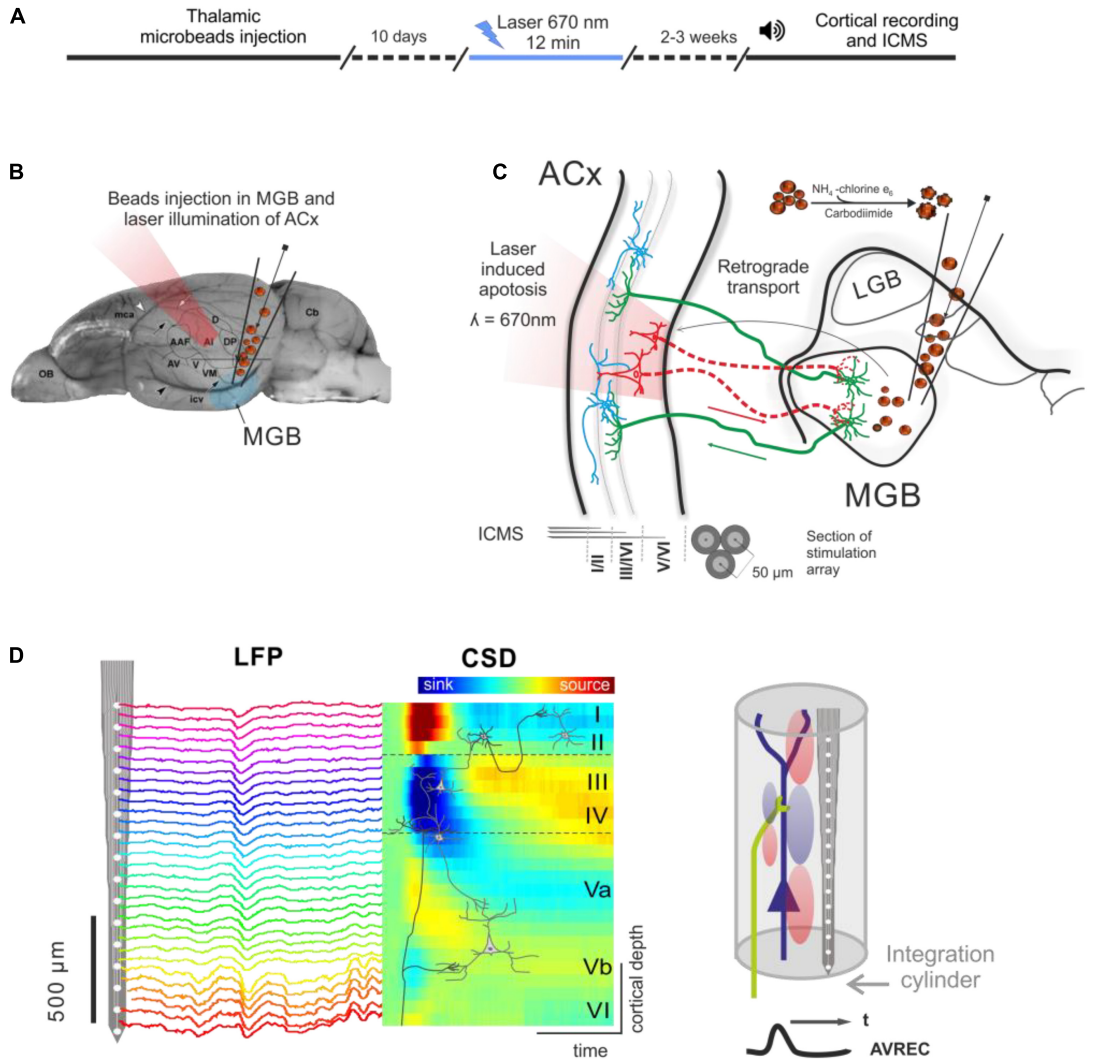

FIGURE 1 | Experimental design and photolytic apoptosis technique. **(A)** Timeline of the experiments from thalamic microbeads injection, laser illumination of ACx (10 days later), and cortical recordings (2–3 weeks later). **(B)** Unilateral injection of conjugated red retrobeads with chlorin e6 into the MGB is followed by transcranial illumination of the ACx 10 days later. **(C)** Retrograde transport to the CT projection neurons and laser illumination induces a photolytic apoptosis of CT feedback by the release of reactive oxygen species. Electrodes used for intracortical microstimulation (ICMS) were placed in supragranular, granular and infragranular layers of the auditory cortex. **(D)** Laminar recordings of the local field potential (LFP) across all cortical layers in the ACx are transformed into the current source density (CSD) distribution in order to map the spatiotemporal profile of synaptic transmission. Current sinks are thereby interpreted as locations of excitatory synaptic input (*right*). Roman numbers indicate cortical layers, as in all following figures. Dashed lines indicate boundaries between supragranular, granular and infragranular layers.

rotor, Beckman Coulter; 10 ml Centrifuge Tubes, Beckman) until the supernatant was fully clear (about 4 times). Following each round, the supernatant was removed and the pellet resuspended in 3 ml PB. The final pellet was resuspended in 50 µl PB and stored at 4°C. Conjugated beads were injected within 14 days (Macklis, 1993).

Tracer Injection Into the MGB

Immediately before use, the tube containing tracer solution was put into an ultrasound bath (Sonorex Super 10P, Bandelin, Germany, 15 min) to prevent clotting. Glass pipettes (outer diameter 1.2 mm, inner diameter 0.68 mm, WPI, United States; tip diameter broken to 20 µm) were filled backward using a 28 gauge MicroFil needle (WPI, United States). For the stereotaxic pressure injections, general initial anesthesia was induced intraperitoneally with a combination of 45% ketamine (10 mg/100 g body weight, Ratiopharm GmbH, Germany) and 5% xylazine (0.5 mg/100 g body weight; Rompun, 2%, Bayer, Germany) prepared in isotonic sodium chloride solution (50%). The level of anesthesia was controlled by monitoring the hindlimb withdrawal reflex and respiratory rate and maintenance doses were given as needed (˜0.06 ml/h). Body temperature was kept at 37°C using a heating blanket. The cranial skin was disinfected, locally anesthetized, and incised. A small hole was drilled unilaterally with a dental drill into the skull according to the stereotaxic coordinates of the MGB established previously

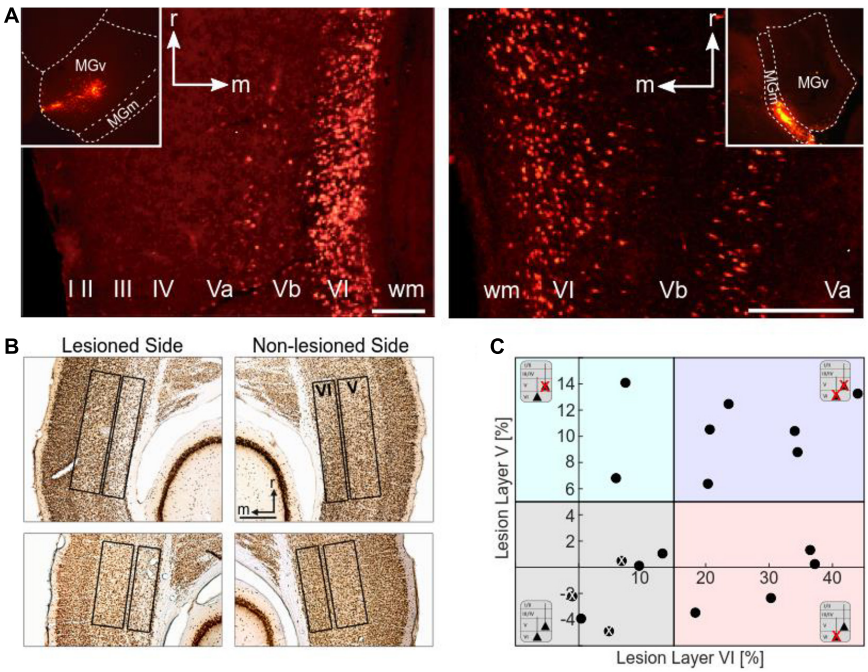

FIGURE 2 | Histological analysis. **(A)** Retrograde labeling of CT neurons. Images by fluorescence microscopy show examples of injection sites into the MGv (left inset) and MGm (right inset) of the MGB, and the corresponding retrograde labeling in layers VI and V of the ACx (field AI). MGv receives cortical input mainly from layer VI, but also from layer V. Cortical neurons from layers VI and V project to MGm. Scale bars: 200 μm (A left), 100 μm (A right). **(B)** Histological analysis of neuronal loss of the animals used for CSD analysis. Top: NeuN-stained section showing neuronal apoptosis in layer VI of the ipsilateral, i.e., illuminated cortical side of AI (case G12). Cellular density is much lower than in the contralateral non-lesioned side. Bottom: NeuN-stained section showing neuronal apoptosis in layers V and VI of the illuminated cortical hemisphere in another case (G13). Lesions in layer V were not as strong and not as clearly visible as layer VI lesions. Scale bar: 500 μm. **(C)** Scatter plot representing the percentage neuronal loss (positive values) compared to the contralateral side in layers V and VI of the individual animals (negative values result from statistical variance around mean). There is no correlation between lesion strengths in layers V and VI ($r = 0.394$, $p = 0.106$). The different background colors represent the ranges of the four lesion groups to which the cases were assigned according to their lesion strengths in layers V and VI. Animals injected with saline instead of the tracer are labeled with a white x.

(Saldeitis et al., 2014; Radtke-Schuller et al., 2016; 3.9–4.0 mm caudal and 2.85–2.9 mm lateral from Bregma) and conjugated microbeads (40 nl) were injected over a period of 2 min. The injection was performed with the help of a fine glass micropipette (outer diameter 1.2 mm, inner diameter 0.68 mm, WPI, United States), which was pulled (Sutter Instruments, United States), broken (tip diameter: 20 μm), and then mounted on an oil hydraulic nanoliter delivery system (WPI). The micropipette was advanced vertically into the brain. The depth of the tip, measured from the cortical surface, was 4.1–4.5 mm. Following the injections, the cranial opening was closed with bone wax (Ethicon, Germany), the surgical site was treated with an anti-inflammatory ointment (Volon A, Dermapharm GmbH, Germany), and the skin over the cranial opening was closed with a tissue adhesive (Histoacryl, Braun, Germany).

Laser Illumination of AI

Ten days following the injection, photolytic apoptosis of retrogradely labeled cortical neurons was induced by ipsilateral exposure of AI to laser light. Under anesthesia with ketamine (10 mg/100 g body weight) and xylazine (0.5 mg/100 g body weight) the skin and the temporal muscle overlaying the ACx were deflected laterally. The exposed AI, which can be identified by its vasculature landmarks (e.g., Thomas et al., 1993; Sugimoto et al., 1997) was illuminated transcranially with a 670-nm wavelength near-infrared light from a tunable 300 mW laser diode (Flatbeam-Laser 670, Schäfter + Kirchhoff, Germany). The laser light was adjusted with beam-shaping optics to create a 1.35-mm spot focused at the level of layer V/VI (1–1.5 mm deep) and the laser intensity was tuned to 50 mW (surface energy doses of ˜1,250 J/cm^2, exposure area approx. 2.86 mm^2) and maintained for 10–12 min (5–6 min at two cortical sites). Following illumination, the skin was closed using surgical thread and tissue adhesive (Histoacryl, Braun, Germany), and the animal was allowed to recover.

Surgery and Electrophysiological Recordings

Surgical and experimental procedures have been described in detail previously (Happel et al., 2014; Saldeitis et al., 2014; Brunk et al., 2019).

After 2–3 weeks post-laser exposure, gerbils were anesthetized and monitored as described above. The ipsilateral ACx was exposed by craniotomy (≈3 × 4 mm) of the temporal bone. Recordings were performed in an acoustically and electrically shielded recording chamber. Laminar profiles of local field

potentials (LFP) were measured using linear 32-channel-shaft electrodes (NeuroNexus, 50 μm inter-channel spacing, 413 μm^2 site area; type A1x32-5mm-50-413) inserted perpendicular to the cortical surface. Neuronal potentials were pre-amplified (500x), band-pass filtered between 0.7 and 170 Hz (3 dB cut-off frequency), digitized at 2 kHz (Multichannel Acquisition Processor, Plexon Inc.) and averaged over 40–80 stimulus repetitions. The location of the field AI in primary ACx was identified by vasculature landmarks and physiological parameters (Ohl et al., 2000, 2001; Brunk et al., 2019; Deane et al., 2020).

Auditory Stimulation and Estimation of Cortical Tuning

We presented pseudo-randomized series of pure tones (duration: 100 ms with 5 ms sinusoidal rising and falling ramps; inter-stimulus interval: 600 ms; digitally synthesized using Matlab and converted to analog signals by a data acquisition National Instruments card; PCI-6711) spanning eight octaves from 250 Hz to 32 kHz and using different sound pressure levels (34–74 dB SPL). Sound pressure intensities were calibrated prior to the experiments by means of a reference signal (0 dB attenuation corresponds to 94 dB SPL). Stimuli were delivered via a programmable attenuator (g.PAH, Guger Technologies; Austria), a wide-range audio amplifier (Thomas Tech Amp75) and a loudspeaker (Tannoy arena satellite KI-8710-32) positioned at 1 m distance in front of the animal's head. The response threshold was determined as the lowest intensity eliciting a significant response at any frequency 3SD over baseline.

Layer-Specific Intracortical Microstimulation

Intracortical microstimulation of biphasic (current-balanced), monopolar, cathodic-first rectangular single pulses were applied (phase duration: 100 μs, inter phase interval 50 μs, ISI: 500 ms, repetitions: 50) in three different cortical depths corresponding to supragranular, granular, and infragranular layers (SGstim, Gstim, IGstim). Stimulation arrays consisted of three attached Teflon-insulated stainless steel wires (Ø with isolation 50 μm; California Fine Wire) implanted at cortical depths of 100, 600, and 1,200 μm, respectively (see **Figure 1C**). The array was inserted proximal (300–400 μm ventrally, i.e., into the proposed same isofrequency contour) to the recording electrodes. Stimulation amplitudes were varied from 40 to 160 μA. Electrical stimuli were generated with a PC and a programmable electrostimulation device (STG2008, Multichannel Systems, Germany). The shape of the stimuli was generated using Matlab and sent to the stimulus generator.

Pharmacological Silencing of Cortical Activity

After recording of acoustically and electrically evoked CSD patterns of pharmacologically untreated animals, the $GABA_A$-agonist muscimol (7.5–8.4 mM, 20–30 μl, Tocris, United States; dissolved in 0.9% sodium-chloride) was applied onto the cortical surface for pharmacological blocking of intracortical transmission (Edeline et al., 2002). Axonal conductance should not be influenced; electrical stimulation of the cortex should therefore be able to excite for example CT projection fibers. Inputs with their neuronal generators outside of the pharmacologically inhibited region, like TC projections, should also still be excitable. The volume and concentration of muscimol used in this study has been shown to be an appropriate dosage for effective cortical silencing in gerbil ACx (Happel et al., 2010; Happel and Ohl, 2017). During diffusion of muscimol, acoustic stimuli (pure tones at 40 dB attenuation) were presented to monitor which layers have been silenced so far. After complete diffusion of muscimol across all cortical layers (takes approximately 0.5–1 h; see also Happel et al., 2010) the same set of acoustic and electrical stimuli was repeated.

Current Source Density Analysis

One-dimensional CSD profiles were calculated from the second spatial derivative of the LFP (Mitzdorf, 1985; Schroeder et al., 1998):

$$\sim CSD \approx \frac{\delta^2\theta\,(z)}{\delta z^2} = \frac{\theta\,(z + n\triangle z) - 2\theta\,(z) + \theta(z - n\triangle z)}{(n\triangle z)^2}$$

where θ is the field potential, z the spatial coordinate perpendicular to the cortical laminae, Δz the spatial sampling interval (50 μm), and n the differentiation grid. LFP profiles were smoothed with a weighted average (Hamming window) of 9 channels (corresponding to a spatial filter kernel of 450 μm; linear extrapolation of 4 channels at boundaries; see Happel et al., 2010). Main sink components were found to represent the architecture of primary sensory input from medial geniculate body (MGB). The sink that is associated with the main projections from the ventral division of the MGB (MGv) onto pyramidal neurons in cortical layers III/IV is referred to as S1. Collaterals of these TC projections also target infragranular layer Vb/VI (Winer et al., 2005; Constantinople and Bruno, 2013; Saldeitis et al., 2014; Schaefer et al., 2015), which result in the so-called early infragranular sink (iS1). Later CSD components include the supragranular sink S2 (layers I/II), and the infragranular sink S3 (layer Va).

In order to compare responses evoked by different stimuli (acoustic, electrical) and during treatments (pre/post muscimol) conditions, channels assigned to a corresponding cortical layer were kept constant. The location of electrically evoked S1 was derived from the location of the acoustically evoked granular sink. To facilitate comparison of activation between animals and/or conditions, we decided to always use the same time window for analysis of a given CSD sink, in which the respective sink could occur according to its definition (AcS: S1: 10–50 ms, iS1: 10–40 ms, S2: 40–300 ms, S3: 40–300 ms; ICMS: S1: 6–20 ms, iS1: 6–20 ms). We have chosen 10 and 6 ms as lower boundaries for AcS and ICMS, due to minimal onset latencies and length of stimulation artifacts, respectively.

For each animal and stimulus condition, we determined the tone-evoked mean integrals [INT; in ($mV/mm^{2*}ms$)] calculated for all identified acoustically evoked sinks at 54 dB SPL by averaging across the corresponding CSD channels for the above given time windows. Importantly, we only considered negative

(i.e., sink), but not positive (i.e., source) components of the INT to prevent distortions related to individually different sink durations. We further analyzed onset latencies (OL) of all acoustically evoked sink components, i.e., the time point, at which the response threshold was first exceeded for at least 5 ms. We determined a best frequency (BF) as the frequency of the stimulus set that elicited the highest amplitude/integral of the initial granular sink S1. The sharpness of frequency tuning was explored by calculating the change of the response two octaves away from the BF (non-BF) relative to the BF-evoked response in percent.

$$\Delta Resp.\ nonBF\ [\%] = \frac{Resp.\ nonBF - Resp.\ BF}{Resp.\ BF} * 100$$

For latency analysis, the differences between the respective onset latencies were analyzed. Since the late extragranular sinks (S2, S3) depend on initial activation, their values were related to the S1 measures.

We also transformed the CSD by rectifying and averaging waveforms of each channel (n) comprising the laminar CSD profile (AVREC).

$$AVREC = \frac{\sum_{i=1}^{n} |CSD_i|\,(t)}{n}$$

While information on the direction and laminar location of transmembrane current flow is lost by rectification, the AVREC waveform provides a useful measure of the temporal pattern of the overall strength of transmembrane current flow (Schroeder et al., 1998).

To compare the overall activation strength between animals, AVREC integrals within time windows from 10 to 50 ms (acoustic stimulation) and from 6 to 50 ms (ICMS) were calculated.

For comparison of different lesion groups (non/weakly lesioned, layer VI lesioned, layer VI plus layer V lesioned, see **Figure 2C**), to which the individual cases were allocated according to the histological results (see below), CSD profiles of animals belonging to the same group were spatially aligned with respect to the granular sink S1 and then averaged (Szymanski et al., 2009). Similarly, AVREC curves obtained from acoustic and electrical stimulation were averaged and plotted including standard error.

Immunohistochemistry

Following the electro-physiological experiments, the gerbils were perfused transcardially with 20 ml of 0.1 M PBS (pH 7.4) followed by 4% PFA (200 ml). Brains were postfixated in 4% PFA overnight, cryoprotected in 30% sucrose dissolved in PBS, frozen and cut into 50 μm thick horizontal slices. Every first out of three sections was mounted on slides and coverslipped using Immu-Mount (Thermo Scientific, Germany) to analyze the injection site and retrograde transport of beads under a fluorescence microscope. In addition, every second out of three sections was stained to visualize neuronal nuclei (NeuN) to verify the efficacy of the laser treatment indicated by reduction of cell number in layers V and VI. To this aim, sections were incubated in a solution containing a monoclonal mouse antibody to NeuN (1:1,000, Chemicon Europe), 0.1–0.3% Triton, and 1% BSA for 2 days. The brains of three pilot animals, which served to validate the photolytic apoptosis method, were in addition processed for the neurofilament protein SMI-32 (monoclonal mouse IgG, 1:5,000) and Caspase 3 (polyclonal rabbit IgG, 1:2,000), a key mediator of apoptosis. To ensure specificity of the later secondary antibody, control probes without primary antibodies were also made. After blocking against unspecific binding sites, appropriate secondary biotinylated antibodies were used (anti-host IgG 1:200, Vector Labs). The reaction product was visualized by incubating the sections in the ABC-solution (Vectastain Elite ABC Kit, Vector Labs) and using 3,3'-diaminobenzidine (0.4 mM of DAB, Sigma-Aldrich) as chromogen in the presence of 0.015% H_2O_2. After rinsing with TRIS-HCl (1x) and PBS (2x), the sections were mounted on gelatine-coated slides. The sections were dehydrated in isopropanol (2 min) and Roticlear (ROTH, Germany, 3 × 5 min) and then coverslipped using Merckoglass (Merck, Germany).

Histological Analysis

Light and fluorescence microscopic analyses and photography (to verify injection sites and determine lesion efficacy) were carried out using a microscope (Zeiss Axioskop 2, Germany), fitted with the appropriate filters for fluorescence and a digital camera (Leica DFC 500, Germany).

Calculations of neuronal cell loss in order to evaluate possible effects of neuronal lesions on cortical activation were made using ImageJ[1]. To this aim, color photographs of NeuN-stained sections were converted to 16 bit images (gray scale), and then to binary (black/white) images by choosing a threshold that removes as much background as possible without removing cells. The same threshold was applied for all sections of a given animal. Layers V and VI, which are well discernible in NeuN stained tissues, were outlined in six sections on average per hemisphere surrounding the electrodes on the lesioned side and, for comparison, at similar dorsoventral levels of the contraleral AI.

Then, as a measure of cell density, the percentage areas occupied by black particles (i.e., NeuN stained nuclei) within these laminar contours were determined, which served to calculate the percentage neuronal loss in both infragranular layers of the illuminated side relative to the contralateral side for each animal.

Statistical Analysis

To reveal possible gradual effects of CT lesions (see **Figures 4**, **6**), we performed simple linear correlation analysis between the measured values and lesion strength in either layer V or VI (two-sided, significance level: 0.05). To account for both layer V and VI effects simultaneously, we fitted a linear mixed effects model by means of the Matlabs fitlme function [Maximum likelihood estimation; t-statistics (for testing the null hypothesis that the coefficient is equal to zero)] using residual degrees of freedom with layer V and layer VI lesions as fixed, and subject as random factors. The predictor variables were treated as either continuous (exact individual cell losses) or categorical (grouped;

[1]http://imagej.nih.gov/ij/

i.e., considered as either lesioned or non-lesioned according to lesion strength thresholds). We thereby fitted pre- and post-muscimol data as dependent variable (Dep.Var) separately (see **Supplementary Tables 1, 2**).

$$Dep.Var \sim \ Les\ V + Les\ VI + (1|Subject)$$

To test for potential statistical interaction between layers, a model including an interaction term (LesV*LesVI) was also constructed. As all but one comparison were found to be insignificant, we opted for the simpler model without an interaction term resulting in increased statistical power. For graphical purposes, animal groups were pooled (animals with vs. animals without layer VI lesions, independent of lesion strength in layer V and vice versa), where applicable.

The effect of pharmacological cortical silencing and its possible interaction with CT cell loss was analyzed using a different mixed effects model:

$$Dep.Var \sim \ Les\ V * Treatment + LesVI * Treatment + (1|Subject)$$

where Dep.Var contains both pre and post muscimol measurements (see **Supplementary Table 3**).

RESULTS

After photolytic lesioning of auditory CT projection neurons in Mongolian gerbils we performed *in vivo* multichannel recordings of LFP and laminar CSD distributions from primary ACx (field AI) to investigate the impact of the lesions on auditory cortical processing at the circuit level using acoustic and electrical stimulation. This was done before and after cortical silencing with muscimol to dissociate the TC from polysynaptic intracortical inputs.

Method Validation

The areal and laminar specificity of the retrograde transport and photolytic apoptosis was evaluated by complementary microscopic inspection of fluorescent (i.e., location of retrobeads) and NeuN- and SMI32-stained brain sections (**Supplementary Figures 1A,B, 2**) of three pilot animals. Casp3-stain was used to confirm the completion of the apoptotic process at the selected time after laser illumination (**Supplementary Figure 1C**). Responsiveness of thalamic neurons near the injection site of the photolytic tracer was also checked in these animals (for details, see **Supplementary Figure 3**). The CSD profiles found in the six animals of our study without or with fairly weak CT cell loss ("non-lesioned" group), which were likewise exposed to the laser treatment, closely matched with those from untreated animals based on previous data (Happel et al., 2010; Happel and Ohl, 2017; Deane et al., 2020). We use this group of animals to demonstrate that the laser illumination did not unspecifically interfere with cortical physiology.

Laminar Origin of the Auditory CT Connections in Mongolian Gerbils

Retrogradely labeled CT neurons were located in layers VI and V. The number of fluorescent beads in layer VI of primary field AI of the ACx was particularly high after injections into MGv (**Figure 2A**, left). Labeling or apoptosis in layer V of AI and the anterior auditory field AAF was stronger if terminals in the dorsal (MGd) or medial division of the MGB (MGm) had incorporated the tracer (**Figure 2A**, right). In the posterior fields, prominent labeling in layer V was found after tracer deposits into any of the MGB divisions. Due to the wide intracellular distribution of the beads, many cells could be identified as pyramidal neurons by their characteristic shape including their basal and apical dendrites. The topography of projections from AI to MGv was tonotopic but not with the same anatomical precision compared to the TC projections (Saldeitis et al., 2014). This led to considerable labeling across the ACx even with confined thalamic injections.

Histological Quantification of Laser-Induced Neuronal Loss

To assess potential relationships between lesion strengths of CT connections and their possible physiological consequences we verified the thalamic injection sites (see **Table 1**) and quantified neuronal cell loss in the infragranular layers of AI. Images of brain slices stained for NeuN were used to determine the lesion efficacy, the contralateral side serving as reference. Moderate to strong neuronal loss, as frequently present in layer VI, was clearly visible (**Figure 2B**), whereas the rather weak lesions in layer V (**Figure 2B**, bottom) were less obvious. Neuronal cell loss ranged up to ∼15% in layer V, and up to ∼40% in layer VI, which corresponds to ∼80% CT neurons of layer VI (Kelly and Wong, 1981; Prieto and Winer, 1999). Based on individual lesion efficacy (i.e., percent cell loss compared to the contralateral side), we assigned animals to different lesion groups; non- or weakly lesioned (non-Les), layer V lesioned (LesV), layer VI lesioned (LesVI), layer V plus layer VI lesioned (LesV+VI) (**Figure 2C**). The thresholds (5% loss for lesion in layer V, 15% loss for lesion in layer VI) were chosen based on the range of the side differences in the saline animals (up to 4.9% for layer V, and 6.8% for layer VI), the absolute range of lesion (14% vs. 44%) as well as on the effects of lesion on cortical physiology, although for most parameters, a gradual lesion effect was found. Main findings were not affected by shifting the threshold (e.g., of layer VI lesions to 10% (**Supplementary Table 2B**) or 20% (**Supplementary Table 2C**). The lesion strengths in layer V and VI did not correlate with each other (**Figure 3C**), reflecting the target-specific anatomy of CT connections and allowing separate statistical analyses. Further, including layer interaction terms in our statistical analysis (see "Materials and Methods") did not result in significant alterations of main conclusions.

Acoustically Evoked Columnar Processing

In both animals with and without CT lesion, acoustic stimulation with pure tones evoked a canonical cross-laminar activation

TABLE 1 | Experimental animals used for CSD analysis[a].

Case	Hemi-sphere	Injection site	Cortical BF	Comments
G01	Right	Histologically undetectable	32 kHz	Control: injected with saline solution
G02	Left	Histologically undetectable	1 kHz	Control: injected with saline solution
G03	Left	Histologically undetectable	1 kHz	Control: injected with saline solution
G04	Left	Caudomedial MGv	4 kHz	Very small injection
G05	Left	Caudal MGv	1 kHz	
G06	Left	(Rostro)ventrolateral MGv	1 kHz	Labeling very ventral, i.e., out of laser focus
G07	Left	MGd	∼1 kHz	Small injection; Incomplete muscimol effect; BF could not be reliably defined; ICMS amplitudes: −40, −100, −120 μA
G08	Left	MGd	2 kHz	No non-BF data available for the post-silencing condition
G09	Right	Rostromedial MGB (RP)	2 kHz	
G10	Left	(Rostro)central MGv	8 kHz	
G11	Right	Rostral MGm and MGv	1 kHz	
G12	Left	Caudal MGv	1 kHz	
G13	Left	MGv, partly MGd	1 kHz	No muscimol applied; ICMS amplitude: −120 μA Large injection, lateral part of MGB necrotic
G14	Left	Central MGv	0.5 kHz	
G15	Left	Medial MGv, MGm and MGd-DD	0.5 kHz	
G16	Left	Lateral MGv	1 kHz	
G17	Left	MGB	1 kHz	Large injection, caudal part of MGB necrotic
G18	Left	Cental MGv	16–32 kHz	

[a]*For each case, the injected and illuminated hemisphere, intrathalamic location of the injection site, and the BF encountered at cortical recording site are depicted, and, where required, comments. Background colors indicate the respective group assignments defined by the lesion strengths, namely non-Les, LesV, LesVI, LesV+VI (see also* ***Figure 2C****). Control animals were injected into MGB with saline instead of the tracer solution.*

pattern as already seen across species in prior studies (Metherate et al., 2005; Szymanski et al., 2009; Bollimunta et al., 2011; Schaefer et al., 2015; Brunk et al., 2019; **Figure 3A**, top; **Figure 4A** and **Supplementary Figure 4**). Specifically, a prominent granular sink with short latency (referred to as S1) was followed by several sinks in supra- (S2) and infragranular (S3) layers. In agreement with earlier work (Schaefer et al., 2015; Brunk et al., 2019), an early sink in deep infragranular layers (Vb/VI) could also be observed, which we refer to as iS1. In addition to the layer-specific input, we analyzed the overall columnar response by the averaged rectified CSD (AVREC) and generally observed comparable waveforms across all animal groups (**Figure 3B**). The time course of the AVREC waveform is characterized by a prominent early peak, which corresponds to the early thalamocortically driven input response, while later components of the AVREC curve in the non-silenced cortex (**Figure 3B**, black curves) resemble subsequent intracortical synaptic activity (cf. Deane et al., 2020). Accordingly, pharmacological blocking of intracortical activity by topical application of muscimol largely abolished the later sinks and sources (**Figure 3A**, bottom) as well as later components of the AVREC curve (**Figure 3B**, gray curves). As expected due to blocking of recurrent excitatory activity, muscimol led also to a significant reduction of AVREC and S1 integrals (mean reduction of 80.3% relative to the pre-value; see also **Supplementary Table 3**, Dep.Vars: AcS AVR BF INT, AcS S1 BF INT). This effect was independent of lesion strength ($r = -0.184$, $p = 0.496$ for lesion in layer VI; $r = -0.399$, $p = 0.126$ for layer V).

Although group-averaged CSD profiles showed generally a similar cross-laminar activation pattern, we found a trend toward a reduction of the BF-evoked prominent granular sink S1 integral with layer VI CT lesions before cortical silencing (**Figure 4B**, left). At non-BF as well as after cortical silencing, we did not find any relationship between lesion and activation strength. Relating non-BF activations to the associated integrals at BF, however, revealed a larger difference (percentage change) between non-BF and BF in non-lesioned compared to layer VI lesioned animals in the pharmacologically untreated cortex (**Figure 4B**, right panel; **Supplementary Tables 1, 2A**, Dep.Var: AcS_pre S1 rel_nBF INT), which suggests an impact on the TC gain of BF-evoked responses.

We also assessed the onset latency (OL) of the granular input in layer IV and found shorter OL for non-BF stimulation in layer VI lesioned animals, but no changes of the BF-evoked OL (**Figure 4C** left panel, **Supplementary Tables 1, 2A**, Dep.Vars: AcS_pre S1 nBF OL, AcS_pre S1 BF OL). When comparing OL differences of BF- and non-BF-evoked responses, we found significant differences before, but not after cortical silencing (**Figure 4C**, right panel; pre: Pearson's $r = -0.658$, $p = 0.004$, post: $r = 0.206$, $p = 0.520$; **Supplementary Tables 1, 2A**, Dep.Var: AcS_pre S1 rel_nBF OL).

In addition, specifically the loss of layer VI CT neurons led to a significantly weaker short-latency infragranular sink iS1 at BF, but not at non-BF (**Figure 4D**, left panel; **Supplementary Table 2A**, Dep.Vars: AcS_pre iS1 BF INT, AcS_pre iS1 nBF INT). A linear correlation of the iS1 integral and the relative cell loss in layer VI was significant before cortical silencing (**Figure 4D**, right panel, Pearson's $r = 0.59$, $p = 0.013$; see also **Supplementary Table 1**, Dep.Var: AcS_pre iS1 BF INT), and a trend in the same direction

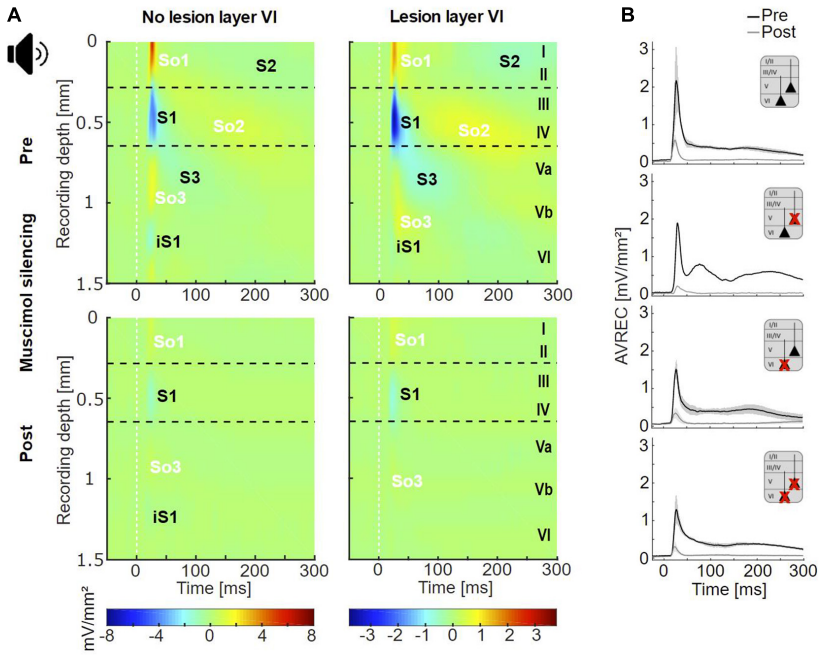

FIGURE 3 | Cortical responses evoked by acoustic stimulation. **(A)** Averaged acoustically evoked CSD profiles at BF (54 dB SPL), before (top), and after (bottom) cortical silencing with muscimol. The grand mean of cases without lesions in layer VI (lesion groups non-Les and LesV, $n = 7$) and that of cases with layer VI lesions [groups LesVI and LesV+VI, $n = 10$ (pre), 9 (post)] had comparable general activation patterns of current sinks (S1, S2, S3, iS1) and sources (So1, So2, So3), shown in blue and yellow/red, respectively. Animals without layer VI lesions displayed a stronger early infragranular sink (iS1). **(B)** Averaged AVREC traces at BF before (black) and after (gray) cortical silencing showing means (solid lines) and SEM (shaded areas) of the four lesion groups. Curves were similar across all groups. $n_{non-Les} = 6$, $n_{LesV} = 1$, $n_{LesVI} = 4$; $n_{LesV+VI} = 6$ (pre), 5 (post).

was observed after application of muscimol. The extent of layer V cell loss did not correlate with changes in the iS1 integral.

To differentiate the aforementioned effects on initial thalamocortically relayed activity from subsequent intracortical synaptic circuit processing, we analyzed the relative strengths (relative change compared to granular sink S1) of the extragranular sinks S2 and S3. At BF, the relative supragranular sink activity was stronger in layer VI lesioned animals (**Supplementary Table 2A**, Dep.Var: AcS_pre S2 rel_BF INT) than in cases without layer VI lesion. S2 activation increased linearly with cell loss in layer VI (**Figure 4E**, Person's $r = 0.671$, $p = 0.004$). The strength of the late infragranular sink S3 did not depend on lesion efficacy (**Figure 4F** and **Supplementary Tables 1, 2A**, Dep.Var: AcS_pre S3 rel_BF INT).

Electrically Evoked Columnar Processing

In non-lesioned animals, infragranular ICMS (IGstim) led to the strongest activation pattern compared to other stimulation depths (**Supplementary Figure 5A**). IGstim evoked a cross-laminar activation pattern similar to that seen after acoustic stimulation, i.e., a strong granular sink (S1), followed by sinks in supragranular (S2) and infragranular (S3) layers, as well as the early deep infragranular sink (iS1) (**Figure 5A**, top). After lesion in layer VI, electrically evoked cortical activation was generally weaker (**Supplementary Figure 5**). Conspicuously, S1 appeared strongly reduced in animals that included neuronal cell loss in layer VI (**Figure 5A**, top).

Following application of muscimol (**Figure 5A**, bottom), IGstim still evoked prominent sinks in the main lemniscal thalamic input layers in non-lesioned animals. In animals with lesions in layer VI (groups LesVI, LesV+VI), S1 was absent or very weak, but supra- and infragranular sinks were still present. Animals with lesions in layer V (LesV, LesV+VI) showed a comparable but slightly prolonged spatiotemporal CSD pattern compared to non-lesioned animals.

As expected based on the qualitative assessment, statistical analysis revealed that the strength of S1 evoked by infragranular ICMS decreased with increasing photolysis in layer VI, but not layer V, both before and after application of muscimol (**Figure 6Ab**; LesVI pre: Pearson's $r = 0.689$, $p = 0.0015$; LesVI post: $r = 0.696$, $p = 0.0019$, see also **Supplementary Tables 1, 2A**, Dep.Var: ICMS S1 IG INT). Thereby, S1 was generally smaller after cortical silencing (**Figure 6A** and **Supplementary Table 3**, Dep.Var: ICMS S1 IG INT).

Also the averaged AVREC curves suggest that before cortical silencing, the strongest activation is produced in non/weakly lesioned animals (**Figure 5B**, black curves). This is statistically supported by a significant correlation between integrals of the AVREC and lesion strength of layer VI (**Figure 6Bb**, right panel, Pearson's $r = -0.78$, $p = 1.37{*}10^{-4}$; **Supplementary Table 1**, Dep.Var: ICMS AVR IG INT) and a significantly different mean of AVREC integrals (**Figure 6Ba** and **Table 3**).

After cortical silencing (**Figure 5B**, gray curves), IGstim produced a short activation in non/weakly lesioned animals.

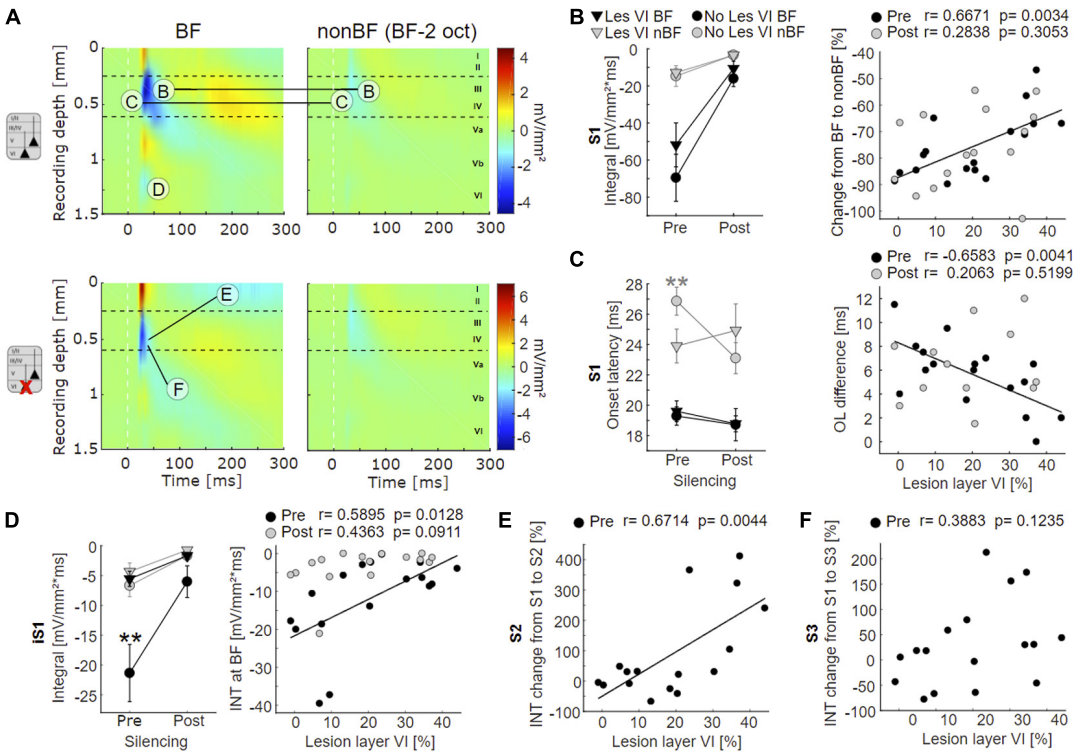

FIGURE 4 | Effects of layer VI lesions on acoustically evoked cortical activity. **(A)** On the left, exemplary CSD profiles of a non-lesioned (case G04) and a layer VI lesioned (case G10) animal are represented, both at BF and at non-BF (2 octaves below BF). The letters refer to specific parameters and spatial locations used for the quantitative analyses shown in 4B-F. **(B)** Left: Means ± SEM of S1 integrals (INT), before and after application of muscimol at BF (black) and non-BF (gray), comparing animals without lesions in layer VI (circle) and those with lesions in layer VI (triangle). There is a trend toward stronger activation at BF in non-lesioned animals. Right: Relationships between lesion strength in layer VI and percentual change of non-BF INT, before (black circles) and after (gray circles) cortical silencing. In the pharmacologically untreated cortex, the reduction of activation strength becomes gradually smaller (less negative) with lesion strength. **(C)** Left: Means ± SEM of S1 onset latencies (OL). Non-lesioned animals have longer latencies at non-BF than layer VI lesioned animals before, but not after cortical silencing. Right: Negative correlation between latency differences ($OL_{non-BF} - OL_{BF}$) and lesion strength in layer VI (pre-muscimol). **(D)** Left: Means ± SEM of early infragranular sink (iS1) integrals. Layer VI lesioned animals have weaker sinks at BF than animals without lesions in layer VI. Right: Significant linear correlation between lesion and activation strength before muscimol treatment. **(E)** Linear correlation between relative S2 strength and lesion in layer VI. S2 is relatively stronger in layer VI lesioned animals. **(F)** No significant correlation between relative S3 strength and lesion in layer VI. Asterisk in **(C,D)** display significant group differences according to linear mixed effects model with grouped data (**Supplementary Table 2A**). $^{*}p < 0.05$, $^{**}p < 0.01$.

Curves of animals that included lesions in layer V, however, in accordance with the before described CSD pattern, showed a more sustained, slowly decaying activation that had similar amplitudes than the curves of these animals before silencing. Mean plots (**Figure 6Ba** and **Supplementary Table 2A**, Dep.Var: ICMS AVR IG INT) and correlation analyses (**Figure 6Bb**, left panel, Pearson's $r = 0.624$, $p = 0.0075$; **Supplementary Figure 5B** and **Supplementary Table 1**, Dep.Var: ICMS AVR IG INT) between lesion strength in layer V and the INTs of AVREC underpin the observation, that after cortical silencing animals with layer V lesions displayed higher activation than those without (**Supplementary Table 3**, Dep.Var: ICMS AVR IG INT).

DISCUSSION

In this study, we have focused on the corticofugal output system, originating in the infragranular cortical layers and influencing subcortical targets thereby affecting sensory, motor and cognitive functions (Williamson and Polley, 2019; Clayton et al., 2020; Prasad et al., 2020). We lesioned CT projection neurons in the primary ACx of anesthetized Mongolian gerbils, while leaving all other components of the TC and intracortical feedforward circuitry intact. Whereas lesion of CT neurons in layer V had no or only moderate effects on tone or ICMS-evoked cortical processing, lesion of CT neurons in layer VI led to layer-specific changes of the tone-evoked spatiotemporal cortical activity profile with a reduced input gain for preferred frequency input. By direct ICMS of corticoefferent output circuits in deeper layers, we furthermore revealed circuit-specific effects of lesioning layer VI CT neurons. Electrically evoked columnar responses in the intact ACx mimicked the spatiotemporal cascade of synaptic activity during auditory processing. Lesion of layer VI neurons led to a profound reduction of electrically evoked overall translaminar activity, confirming the hypothesis of recurrent extracortical feedback originating from the corticothalamic circuitry after cortical stimulation (Happel et al., 2014). Our study thereby suggests an

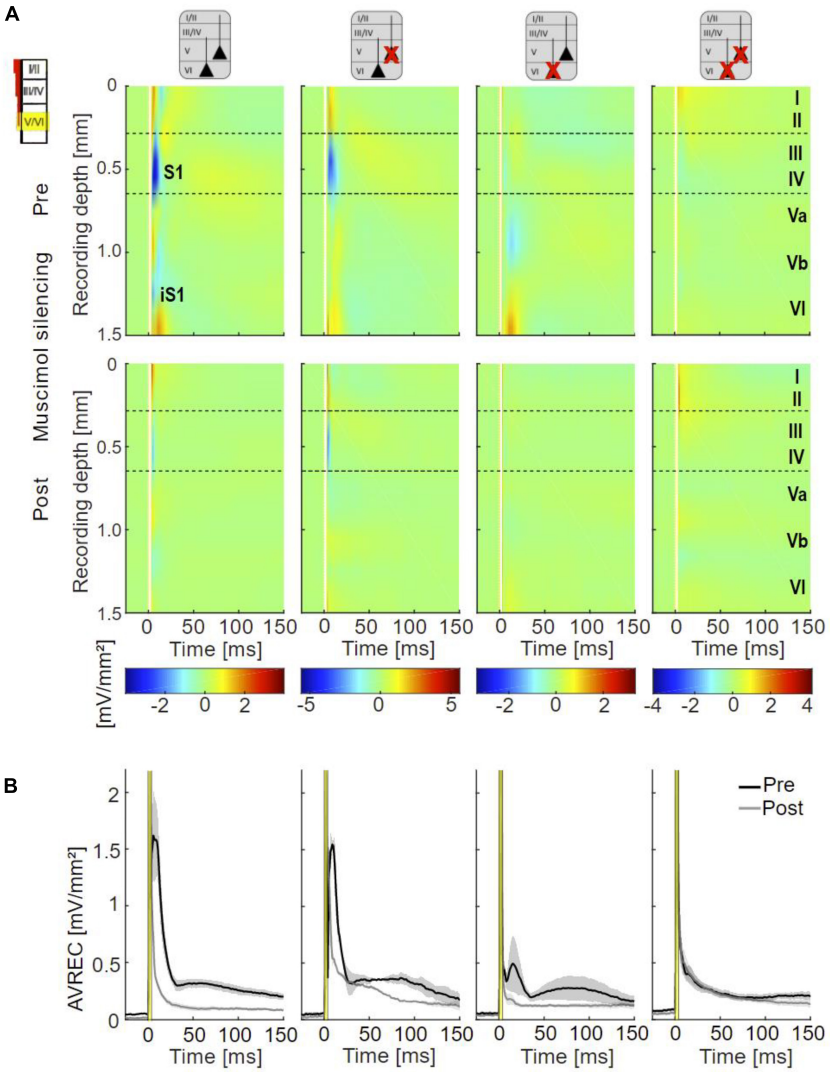

FIGURE 5 | Cortical responses evoked by infragranular ICMS. **(A)** Averaged CSD profiles of all four groups (non-Les, LesV, LesVI, LesV+VI) evoked by infragranular ICMS (160 μA, stimulus artifact masked by white line), before (top) and after (bottom) application of muscimol. In the untreated condition, non (or weakly) lesioned animals show a cross-laminar activation pattern similar to that evoked by acoustic stimulation. In animals with considerable loss of layer VI neurons, S1 is much smaller than in non-lesioned animals and other rather weak sinks are observed in extragranular layers. After cortical silencing with muscimol, animals without lesions in layer VI display the two initial sinks (S1, iS1) also seen upon acoustic stimulation in the silenced cortex. In contrast, both groups with layer VI lesions lack or have only a very small S1. In the LesVI group, only weak activation remained present, while in animals with exclusive (LesV) or additional (LesV+VI) loss of layer V neurons, a stronger and longer lasting pattern of sinks and sources was observed. $n_{non-Les}$ = 6, n_{Les5} = 2; n_{LesVI} = 4; $n_{LesV+VI}$ = 6 (pre), 5 (post). **(B)** Grand-averaged AVREC curves evoked by layer-specific infragranular ICMS in the untreated (black) and silenced (gray) condition, showing means (solid lines) and SEM (shaded areas) of the different lesion groups. The first short peak represents the stimulus artifact (labeled by a yellow box). Before cortical silencing, strongest activation is seen in non-lesioned animals. After application of muscimol a more sustained activation was seen in animals that involved lesions in layer V, while curves of animals having no or pure layer VI lesions declined rapidly to very low values.

important role of particularly the CT feedback neurons in layer VI in orchestrating the feedforward translaminar information flow in auditory cortex via recurrent CT feedback.

Lesion Specificity of Corticothalamic Neurons

Lesion specificity was determined based on the location of retrograde fluorescent labeling of neuronal somata or by laser-induced cell loss (NeuN-stained slices) in relation to the thalamic injection site. While labeling was particularly high in layers VI after injections into MGv, labeling of layer V neurons in auditory cortical fields AI and AAF was stronger after terminals in MGd or MGm had incorporated the beads. We targeted mainly the lemniscal thalamus with our injections, where layer VI CT neurons are likely to constitute a larger portion of the total target cells compared to layer V CT neurons (Williamson and Polley, 2019). In accordance, cell loss in layer VI was up to

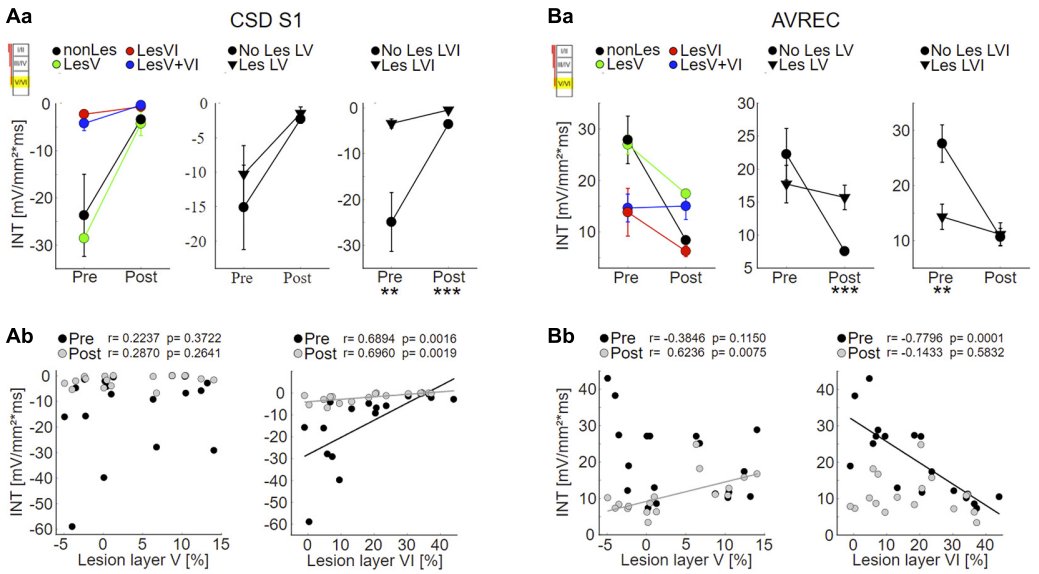

FIGURE 6 | Effects of layer VI and layer V CT lesions on electrically evoked cortical activity (infragranular ICMS). **(A)** Effects on sink S1. **(Aa)** S1 means+SEM of all four groups (left), of layer V lesioned (groups LesV and LesV+VI) vs. non-layer V lesioned animals (middle), and of layer VI (groups LesVI and LesV+VI) vs. non-layer VI lesioned animals (right). **(Ab)** Individual S1 INT plotted against lesion strengths in layer V (left) or VI (right), before (black) and after (gray) application of muscimol. Animals with loss of layer VI CT neurons had weaker (less negative) granular sinks, both before and after cortical silencing. **(B)** Effects on AVRECs. **(Ba)** AVREC group means and **(Bb)** scatterplots as described for (A). Before silencing, strongest activation was evoked in animals without cell loss in layer VI. After application of muscimol, highest activity was seen in animals having lesions in layer V. Significant group comparisons **(Aa,Ba)** using a linear mixed effects model (**Supplementary Table 2A**) are labeled by asterisks (*$p < 0.05$, **$p < 0.01$, ***$p < 0.001$).

40% and in layer V max. 15%. Based on the available literature, the observed reduced cell density in layer VI corresponds to a reduction of approx. 80% of CT neurons of layer VI (Kelly and Wong, 1981; Prieto and Winer, 1999; Homma et al., 2017). The distinct lesion patterns are in accordance with previous reports linking layer VI CT neurons more to the lemniscal auditory pathway, while layer V corticofugal neurons project less specifically to non-lemniscal and other subcortical target areas (Alitto and Usrey, 2003; Briggs and Usrey, 2007; Usrey and Sherman, 2019; Williamson and Polley, 2019). It has been suggested that layer V corticofugal neurons broadcast sensory information to distributed non-lemniscal targets, while layer VI CT neurons with their more lemniscal interconnectivity are ideal regulators of the local TC gain control (Llano and Sherman, 2009; Olsen et al., 2012; Guo et al., 2017; Williamson and Polley, 2019).

Corticothalamic Gain Control of Layer-Specific Subcortical Input

Deeper layer CT neurons are glutamate-releasing pyramidal neurons (Bortone et al., 2014) and have strong local intracortical connections spanning all cortical layers (Guo et al., 2017; Baker et al., 2018). In order to observe their impact on the overall columnar response characteristics, we used laminar multichannel CSD recordings across all cortical laminae giving rise to layer-specific synaptic population activity. We have used physiological stimulation of the primary ACx via its primarily lemniscal input system, and direct artificial stimulation of the cortical network by layer-specific ICMS bypassing the bottom-up pathway. Selective elimination of CT neurons in layer VI, but not layer V led to reduced initial tone-evoked synaptic activity in cortical layer Vb/VI quantified by a reduced current flow of the thalamocortically relayed sink iS1 (Szymanski et al., 2009; Brunk et al., 2019; Deane et al., 2020). Also, we observed less specific frequency processing in terms of the relative input strength and onset latency of sink S1. We further found increased subsequent intracortical activity in supragranular layers (sink S2) correlating with the lesion efficacy in layer VI. In contrast, synaptic current flow in upper layer Va (sink S3) was not affected by lesioning cells in layer VI. Lesion of layer V CT neurons did not affect the columnar current flow in a significant manner. This data suggests that layer VI CT neurons play a pivotal role for a local gain control of TC inputs and their integration with broader spectral inputs relayed via upper layers at a given cortical patch (Larkum, 2013; Brunk et al., 2019; Zempeltzi et al., 2020). We observed these effects after a physical lesion of CT layer VI neurons, which, as circuit manipulations in general, may lead to short-term and compensatory circuit adaptations (Otchy et al., 2015). However, recent work has revealed a particular function of layer VI CT neurons in frequency integration in agreement with our findings (Guo et al., 2017). We further used direct ICMS in order to perform a detailed circuit analysis of potential contributions of recurrent cortico-subcortical loops to the observed network effects. In non-lesioned animals, infragranular ICMS evoked feedforward synaptic activity patterns with translaminar information flow in agreement with previous reports (Lison et al., 2013; Happel et al., 2014). Effective lesioning of layer VI neurons strongly

reduced the translaminar activation cascade, which was not observed when lesioning layer V cells. In a previous study, we have hypothesized that recurrent CT feedback recruited by infragranular layer stimulation routes back to granular input layers of the ACx (Happel et al., 2014) most likely via the MGv (Saldeitis et al., 2014). This granular feedback signal thereby may trigger granular synaptic recurrent excitation regulating TC gain control and hence initiate translaminar activity patterns (Liu et al., 2007; Deane et al., 2020). In agreement, lesion strength of layer VI neurons was negatively correlated with synaptic input in granular layers III/IV quantified by the integral of the dominant current sink S1 before cortical silencing, and further with an impaired translaminar activation cascade. The residual granular activation after cortical silencing was likewise diminished in animals with a layer VI lesion (cf. Happel et al., 2014). Henceforth, our data corroborate the hypothesis that layer VI CT neurons are the cellular substrate for this recurrent and excitatory loop and are an essential circuit element for ICMS-generated columnar activity patterns. Whether our finding is alternatively due to the eliminated intracortical collaterals of these layer VI neurons (Oviedo et al., 2010; Kratz and Manis, 2015), or a mixture of diminished intracortical and cortico-thalamo-cortical activation, cannot be resolved with our experimental design and would need further investigation. In a similar way, the less prominent effects on ICMS-evoked responses after lesioning layer V neurons may also arise via different possible changes of the circuit processing.

Our study investigated effects of CT lesion in anesthetized gerbils. It therefore remains open, how CT feedback from layers V and VI would affect auditory perception and behavior. It was shown before, that particularly layer VI CT neurons are involved in auditory detection and discrimination behavior (Guo et al., 2017).

Perspectives in Corticofugal Pathway Research

Corticothalamic feedback originating from layer VI neurons acts more locally, while the system originating in layer V acts more globally. Layer V neurons project to various downstream target regions including other cortices or subcortical regions, such as the striatum. They have been linked to sensorimotor integration, sensory-guided movement control (Znamenskiy and Zador, 2013; Guo et al., 2017), attentive functions (Yu et al., 2004) and might also receive inhibition from corollary discharges (Schneider et al., 2014). Lesioning of these neurons may have appeared as the prolonged electrically evoked activity after cortical silencing, because their apoptosis probably affected both lemniscally (LesV only) and non-lemniscally (LesV+VI) driven TC input (see **Figure 5**). We hypothesize that a release from inhibition of otherwise sustained firing neurons in subcortical nuclei such as the inferior colliculus (Smith, 1992; Sivaramakrishnan and Oliver, 2001), which may normally be mediated by layer V CT neurons sending axon collaterals to the IC (Asokan et al., 2018), plays a role for the prolonged cortical activation. Before cortical silencing, this activity may remain hidden due to intracortical inhibitory mechanisms. However, more animals with CT lesions restricted to layer V are required to ultimately confirm and interpret this effect.

Dopaminergic synapses have been preferentially found in infragranular layers of ACx (Schicknick et al., 2008). Further studies need to reveal how dopaminergic neuromodulation may affect the different corticofugal cell types, as it has been shown that deeper layers specifically integrate sensory and reward-related signals in the sensory cortex in the potential service of action-outcome integration and adaptive coding of expectancy (Mylius et al., 2014; Happel, 2016; Brunk et al., 2019).

DATA AVAILABILITY STATEMENT

The raw data supporting the conclusions of this article will be made available by the authors, without undue reservation.

ETHICS STATEMENT

All experiments were conducted in accordance with the international NIH Guidelines for Animals in Research and with ethical standards for the care and use of animals in research defined by the German Law for the protection of experimental animals. Experiments were approved by an ethics committee of the state Saxony-Anhalt, Germany.

AUTHOR CONTRIBUTIONS

KS carried out the experiments and data analysis. MH and MJ supervised the experiments and data analysis. MH and KS wrote the first draft of the manuscript. All authors finalized the manuscript and designed the experiments.

FUNDING

The work was supported by grants from the Deutsche Forschungsgemeinschaft DFG (SFB779 and SFB1436; Project-ID 425899996, TP A06 and C02).

SUPPLEMENTARY MATERIAL

The Supplementary Material for this article can be found online at: https://www.frontiersin.org/articles/10.3389/fncir.2021.659280/full#supplementary-material

REFERENCES

Alitto, H. J., and Usrey, W. M. (2003). Corticothalamic feedback and sensory processing. *Curr. Opin. Neurobiol.* 13, 440–445. doi: 10.1016/S0959-4388(03)00096-5

Anderson, L. A., and Malmierca, M. S. (2013). The effect of auditory cortex deactivation on stimulus-specific adaptation in the inferior colliculus of the rat. *Eur. J. Neurosci.* 37, 52–62. doi: 10.1111/ejn.12018

Asokan, M. M., Williamson, R. S., Hancock, K. E., and Polley, D. B. (2018). Sensory overamplification in layer 5 auditory corticofugal projection neurons following cochlear nerve synaptic damage. *Nat. Commun.* 9:2468. doi: 10.1038/s41467-018-04852-y

Augustinaite, S., and Kuhn, B. (2020). Complementary Ca2+ activity of sensory activated and suppressed layer 6 corticothalamic neurons reflects behavioral state. *Curr. Biol.* 30, 3945–3960.e5. doi: 10.1016/j.cub.2020.07.069

Bajo, V. M., Nodal, F. R., Moore, D. R., and King, A. J. (2010). The descending corticocollicular pathway mediates learning-induced auditory plasticity. *Nat. Neurosci.* 13, 253–260. doi: 10.1038/nn.2466

Baker, A., Kalmbach, B., Morishima, M., Kim, J., Juavinett, A., Li, N., et al. (2018). Specialized subpopulations of deep-layer pyramidal neurons in the neocortex: Bridging cellular properties to functional consequences. *J. Neurosci.* 38, 5441–5455. doi: 10.1523/JNEUROSCI.0150-18.2018

Bäuerle, P., von der Behrens, W., Kössl, M., and Gaese, B. H. (2011). Stimulus-specific adaptation in the gerbil primary auditory thalamus is the result of a fast frequency-specific habituation and is regulated by the corticofugal system. *J. Neurosci.* 31, 9708–9722. doi: 10.1523/JNEUROSCI.5814-10.2011

Bollimunta, A., Mo, J., Schroeder, C. E., and Ding, M. (2011). Neuronal mechanisms and attentional modulation of corticothalamic alpha oscillations. *J. Neurosci.* 31, 4935–4943. doi: 10.1523/JNEUROSCI.5580-10.2011

Bortone, D. S., Olsen, S. R., and Scanziani, M. (2014). Translaminar inhibitory cells recruited by layer 6 corticothalamic neurons suppress visual cortex. *Neuron* 82, 474–485. doi: 10.1016/j.neuron.2014.02.021

Briggs, F., and Usrey, W. M. (2007). A fast, reciprocal pathway between the lateral geniculate nucleus and visual cortex in the macaque monkey. *J. Neurosci.* 27, 5431–5436. doi: 10.1523/JNEUROSCI.1035-07.2007

Brunk, M. G. K., Deane, K. E., Kisse, M., Deliano, M., Vieweg, S., Ohl, F. W., et al. (2019). Optogenetic stimulation of the VTA modulates a frequency-specific gain of thalamocortical inputs in infragranular layers of the auditory cortex. *Sci. Rep.* 9:20385.

Budinger, E., Laszcz, A., Lison, H., Scheich, H., and Ohl, F. W. (2008). Non-sensory cortical and subcortical connections of the primary auditory cortex in Mongolian gerbils: Bottom-up and top-down processing of neuronal information via field AI. *Brain Res.* 1220, 2–32.

Clayton, K. K., Williamson, R. S., Hancock, K. E., Tasaka, G. I., Mizrahi, A., Hackett, T. A., et al. (2020). Auditory corticothalamic neurons are recruited by motor preparatory inputs. *Curr. Biol.* 31, 310–321.e5. doi: 10.1016/j.cub.2020.10.027

Constantinople, C. M., and Bruno, R. M. (2013). Deep cortical layers are activated directly by thalamus. *Science* 340, 1591–1594. doi: 10.1126/science.1236425

Crandall, S. R., Cruikshank, S. J., and Connors, B. W. (2015). A Corticothalamic switch: controlling the thalamus with dynamic synapses. *Neuron* 86, 768–782. doi: 10.1016/j.neuron.2015.03.040

Deane, K. E., Brunk, M. G. K., Curran, A. W., Zempeltzi, M. M., Ma, J., Lin, X., et al. (2020). Ketamine anesthesia induces gain enhancement via recurrent excitation in granular input layers of the auditory cortex. *J. Physiol.* 598, 2741–2755. doi: 10.1113/jp279705

Deliano, M., Brunk, M. G. K., El-Tabbal, M., Zempeltzi, M. M., Happel, M. F. K., and Ohl, F. W. (2018). Dopaminergic neuromodulation of high gamma stimulus phase-locking in gerbil primary auditory cortex mediated by D1/D5-receptors. *Eur. J. Neurosci.* 51, 1315–1327. doi: 10.1111/ejn.13898

Deliano, M., Scheich, H., and Ohl, F. W. (2009). Auditory cortical activity after intracortical microstimulation and its role for sensory processing and learning. *J. Neurosci.* 29, 15898–15909. doi: 10.1523/JNEUROSCI.1949-09.2009

Deschênes, M., and Hu, B. (1990). Membrane resistance increase induced in thalamic neurons by stimulation of brainstem cholinergic afferents. *Brain Res.* 513, 339–342. doi: 10.1016/0006-8993(90)90478-T

Destexhe, A. (2000). Modelling corticothalamic feedback and the gating of the thalamus by the cerebral cortex. *J. Physiol. Paris* 94, 391–410. doi: 10.1016/S0928-4257(00)01093-7

Edeline, J.-M., Hars, B., Hennevin, E., and Cotillon, N. (2002). Muscimol diffusion after intracerebral microinjections: a reevaluation based on electrophysiological and autoradiographic quantifications. *Neurobiol. Learn. Mem.* 78, 100–124. doi: 10.1006/nlme.2001.4035

Guo, W., Clause, A. R., Barth-Maron, A., and Polley, D. B. (2017). A Corticothalamic circuit for dynamic switching between feature detection and discrimination. *Neuron* 95, 180–194.e5. doi: 10.1016/j.neuron.2017.05.019

Happel, M. F. K. (2016). Dopaminergic impact on local and global cortical circuit processing during learning. *Behav. Brain Res.* 299, 32–41. doi: 10.1016/j.bbr.2015.11.016

Happel, M. F. K., Deliano, M., Handschuh, J., and Ohl, F. W. (2014). Dopamine-modulated recurrent corticoefferent feedback in primary sensory cortex promotes detection of behaviorally relevant stimuli. *J. Neurosci.* 34, 1234–1247. doi: 10.1523/JNEUROSCI.1990-13.2014

Happel, M. F. K., Jeschke, M., and Ohl, F. W. (2010). Spectral integration in primary auditory cortex attributable to temporally precise convergence of thalamocortical and intracortical input. *J. Neurosci.* 30, 11114–11127. doi: 10.1523/JNEUROSCI.0689-10.2010

Happel, M. F. K., and Ohl, F. W. (2017). Compensating level-dependent frequency representation in auditory cortex by synaptic integration of corticocortical input. *PLoS One* 12:e0169461. doi: 10.1371/journal.pone.0169461

Hazama, M., Kimura, A., Donishi, T., Sakoda, T., and Tamai, Y. (2004). Topography of corticothalamic projections from the auditory cortex of the rat. *Neuroscience* 124, 655–667. doi: 10.1016/j.neuroscience.2003.12.027

He, J. (1997). Modulatory effects of regional cortical activation on the onset responses of the cat medial geniculate neurons. *J. Neurophysiol.* 77, 896–908.

Homma, N., Happel, M. F. K., Nodal, F. R., Ohl, F. W., King, A. J., and Bajo, V. M. (2017). A role for auditory corticothalamic feedback in the perception of complex sounds. *J. Neurosci.* 37, 6149–6161.

Kelly, J. P., and Wong, D. (1981). Laminar connections of the cat's auditory cortex. *Brain Res.* 212, 1–15. doi: 10.1016/0006-8993(81)90027-5

King, A. J., Teki, S., and Willmore, B. D. B. (2018). Recent advances in understanding the auditory cortex. *F1000Research* 7:1555. doi: 10.12688/f1000research.15580.1

Kirchgessner, M. A., Franklin, A. D., and Callaway, E. M. (2020). Context-dependent and dynamic functional influence of corticothalamic pathways to first- And higher-order visual thalamus. *Proc. Natl. Acad. Sci. U.S.A.* 117, 13066–13077. doi: 10.1073/pnas.2002080117

Kratz, M. B., and Manis, P. B. (2015). Spatial organization of excitatory synaptic inputs to layer 4 neurons in mouse primary auditory cortex. *Front. Neural Circuits* 9:17. doi: 10.3389/fncir.2015.00017

Larkum, M. (2013). A cellular mechanism for cortical associations: an organizing principle for the cerebral cortex. *Trends Neurosci.* 36, 141–151. doi: 10.1016/j.tins.2012.11.006

Lison, H., Happel, M. F. K., Schneider, F., Baldauf, K., Kerbstat, S., Seelbinder, B., et al. (2013). Disrupted cross-laminar cortical processing in β amyloid pathology precedes cell death. *Neurobiol. Dis.* 63C, 62–73.

Liu, B., Wu, G. K., Arbuckle, R., Tao, H. W., and Zhang, L. I. (2007). Defining cortical frequency tuning with recurrent excitatory circuitry. *Nat. Neurosci.* 10, 1594–1600. doi: 10.1038/nn2012

Llano, D. A., and Sherman, S. M. (2009). Differences in intrinsic properties and local network connectivity of identified layer 5 and layer 6 adult mouse auditory corticothalamic neurons support a dual corticothalamic projection hypothesis. *Cereb. Cortex* 19, 2810–2826. doi: 10.1093/cercor/bhp050

Macklis, J. D. (1993). Transplanted neocortical neurons migrate selectively into regions of neuronal degeneration produced by chromophore-targeted laser photolysis. *J. Neurosci.* 13, 3848–3863.

Malmierca, M. S., Anderson, L. A., and Antunes, F. M. (2015). The cortical modulation of stimulus-specific adaptation in the auditory midbrain and thalamus: a potential neuronal correlate for predictive coding. *Front. Syst. Neurosci.* 9:19. doi: 10.3389/fnsys.2015.00019

Mease, R. A., Krieger, P., and Groh, A. (2014). Cortical control of adaptation and sensory relay mode in the thalamus. *Proc. Natl. Acad. Sci. U.S.A.* 111, 6798–6803. doi: 10.1073/pnas.1318665111

Metherate, R., Kaur, S., Kawai, H., Lazar, R., Liang, K., and Rose, H. J. (2005). Spectral integration in auditory cortex: mechanisms and modulation. *Hear. Res.* 206, 146–158. doi: 10.1016/j.heares.2005.01.014

Mitzdorf, U. (1985). Current source-density method and application in cat cerebral cortex: investigation of evoked potentials and EEG phenomena. *Physiol. Rev.* 65, 37–100.

Mylius, J., Happel, M. F. K., Gorkin, A. G., Huang, Y., Scheich, H., and Brosch, M. (2014). Fast transmission from the dopaminergic ventral midbrain to the sensory cortex of awake primates. *Brain Struct. Funct.* 220, 3273–3294. doi: 10.1007/s00429-014-0855-0

Ohl, F. W., Scheich, H., and Freeman, W. J. (2000). Topographic analysis of epidural pure-tone-evoked potentials in gerbil auditory cortex. *J. Neurophysiol.* 83, 3123–3132.

Ohl, F. W., Scheich, H., and Freeman, W. J. (2001). Change in pattern of ongoing cortical activity with auditory category learning. *Nature* 412, 733–736. doi: 10.1038/35089076

Olsen, S. R., Bortone, D. S., Adesnik, H., and Scanziani, M. (2012). Gain control by layer six in cortical circuits of vision. *Nature* 483, 47–52. doi: 10.1038/nature10835

Otchy, T. M., Wolff, S. B. E., Rhee, J. Y., Pehlevan, C., Kawai, R., Kempf, A., et al. (2015). Acute off-target effects of neural circuit manipulations. *Nature* 528, 358–363. doi: 10.1038/nature16442

Oviedo, H. V., Bureau, I., Svoboda, K., and Zador, A. M. (2010). The functional asymmetry of auditory cortex is reflected in the organization of local cortical circuits. *Nat. Neurosci.* 13, 1413–1420. doi: 10.1038/nn.2659

Prasad, J. A., Carroll, B. J., and Sherman, S. M. (2020). Layer 5 Corticofugal Projections from diverse cortical areas: variations on a pattern of thalamic and extrathalamic targets. *J. Neurosci.* 40, 5785–5796. doi: 10.1523/JNEUROSCI.0529-20.2020

Prieto, J. J., and Winer, J. A. (1999). Layer VI in cat primary auditory cortex: golgi study and sublaminar origins of projection neurons. *J. Comp. Neurol.* 404, 332–358. doi: 10.1002/(SICI)1096-9861(19990215)404:3<332::AID-CNE5<3.0.CO;2-R

Radtke-Schuller, S., Schuller, G., Angenstein, F., Grosser, O. S., Goldschmidt, J., and Budinger, E. (2016). Brain atlas of the Mongolian gerbil (*Meriones unguiculatus*) in CT/MRI-aided stereotaxic coordinates. *Brain Struct. Funct.* 221, 1–272. doi: 10.1007/s00429-016-1259-0

Rouiller, E. M., and Durif, C. (2004). The dual pattern of corticothalamic projection of the primary auditory cortex in macaque monkey. *Neurosci. Lett.* 358, 49–52. doi: 10.1016/j.neulet.2004.01.008

Saldeitis, K., Happel, M. F. K., Ohl, F. W., Scheich, H., and Budinger, E. (2014). Anatomy of the auditory thalamocortical system in the mongolian gerbil: nuclear origins and cortical field-, layer-, and frequency-specificities. *J. Comp. Neurol.* 522, 2397–2430. doi: 10.1002/cne.23540

Schaefer, M. K. K., Hechavarría, J. C. C., and Kössl, M. (2015). Quantification of mid and late evoked sinks in laminar current source density profiles of columns in the primary auditory cortex. *Front. Neural Circuits* 9:52. doi: 10.3389/fncir.2015.00052

Scheich, H., Brechmann, A., Brosch, M., Budinger, E., and Ohl, F. W. (2007). The cognitive auditory cortex: task-specificity of stimulus representations. *Hear. Res.* 229, 213–224. doi: 10.1016/j.heares.2007.01.025

Schicknick, H., Schott, B. H., Budinger, E., Smalla, K.-H., Riedel, A., Seidenbecher, C. I., et al. (2008). Dopaminergic modulation of auditory cortex-dependent memory consolidation through mTOR. *Cereb. Cortex* 18, 2646–2658. doi: 10.1093/cercor/bhn026

Schneider, D. M., Nelson, A., and Mooney, R. (2014). A synaptic and circuit basis for corollary discharge in the auditory cortex. *Nature* 513, 189–194. doi: 10.1038/nature13724

Schreiner, C. E., and Winer, J. A. (2007). Auditory cortex mapmaking: principles, projections, and plasticity. *Neuron* 56, 356–365. doi: 10.1016/j.neuron.2007.10.013

Schroeder, C. E., Mehta, A. D., and Givre, S. J. (1998). A spatiotemporal profile of visual system activation revealed by current source density analysis in the awake macaque. *Cereb. Cortex* 8, 575–592. doi: 10.1093/cercor/8.7.575

Sharpee, T. O., Atencio, C. A., and Schreiner, C. E. (2011). Hierarchical representations in the auditory cortex. *Curr. Opin. Neurobiol.* 21, 761–767. doi: 10.1016/j.conb.2011.05.027

Sivaramakrishnan, S., and Oliver, D. L. (2001). Distinct K currents result in physiologically distinct cell types in the inferior colliculus of the rat. *J. Neurosci.* 21, 2861–2877. doi: 10.1523/jneurosci.21-08-02861.2001

Smith, P. H. (1992). Anatomy and physiology of multipolar cells in the rat inferior collicular cortex using the in vitro brain slice technique. *J. Neurosci.* 12, 3700–3715. doi: 10.1523/jneurosci.12-09-03700.1992

Suga, N. (1977). Amplitude spectrum representation in the Doppler-shifted-CF processing area of the auditory cortex of the mustache bat. *Science* 196, 64–67.

Suga, N., and Ma, X. (2003). Multiparametric corticofugal modulation and plasticity in the auditory system. *Nat. Rev. Neurosci.* 4, 783–794. doi: 10.1038/nrn1222

Sugimoto, S., Sakurada, M., Horikawa, J., and Taniguchi, I. (1997). The columnar and layer-specific response properties of neurons in the primary auditory cortex of Mongolian gerbils. *Hear Res.* 112, 175–185. doi: 10.1016/S0378-5955(97)00119-6

Szymanski, F. D., Garcia-Lazaro, J. A., and Schnupp, J. W. H. (2009). Current source density profiles of stimulus-specific adaptation in rat auditory cortex. *J. Neurophysiol.* 102, 1483–1490. doi: 10.1152/jn.00240.2009

Temereanca, S., and Simons, D. J. (2004). Functional topography of corticothalamic feedback enhances thalamic spatial response tuning in the somatosensory whisker/barrel system. *Neuron* 41, 639–651. doi: 10.1016/S0896-6273(04)00046-7

Thomas, H., Tillein, J., Heil, P., and Scheich, H. (1993). Functional organization of auditory cortex in the mongolian gerbil (Meriones unguiculatus). I. Electrophysiological mapping of frequency representation and distinction of fields. *Eur. J. Neurosci.* 5, 882–897. doi: 10.1111/j.1460-9568.1993.tb00940.x

Usrey, W. M., and Sherman, S. M. (2019). Corticofugal circuits: communication lines from the cortex to the rest of the brain. *J. Comp. Neurol.* 527, 640–650. doi: 10.1002/cne.24423

Williamson, R. S., and Polley, D. B. (2019). Parallel pathways for sound processing and functional connectivity among layer 5 and 6 auditory corticofugal neurons. *Elife* 8:e42974. doi: 10.7554/eLife.42974

Winer, J. A., Miller, L. M., Lee, C. C., and Schreiner, C. E. (2005). Auditory thalamocortical transformation: structure and function. *Trends Neurosci.* 28, 255–263. doi: 10.1016/j.tins.2005.03.009

Yu, Y. Q., Xiong, Y., Chan, Y. S., and He, J. (2004). Corticofugal gating of auditory information in the thalamus: an in vivo intracellular recording study. *J. Neurosci.* 24, 3060–3069. doi: 10.1523/JNEUROSCI.4897-03.2004

Zempeltzi, M. M., Kisse, M., Brunk, M. G. K., Glemser, C., Aksit, S., Deane, E., et al. (2020). Task rule and choice are reflected by layer-specific processing in rodent auditory cortical microcircuits. *Comm. Biol.* 3:345. doi: 10.1038/s42003-020-1073-3

Zhang, Y., Suga, N., and Yan, J. (1997). Corticofugal modulation of frequency processing in bat auditory system. *Nature.* 387, 900–903. doi: 10.1038/43180

Znamenskiy, P., and Zador, A. M. (2013). Corticostriatal neurons in auditory cortex drive decisions during auditory discrimination. *Nature* 497, 482–485. doi: 10.1038/nature12077

Conflict of Interest: The authors declare that the research was conducted in the absence of any commercial or financial relationships that could be construed as a potential conflict of interest.

frontiers in Neural Circuits

REVIEW
published: 19 August 2021
doi: 10.3389/fncir.2021.721186

Corticothalamic Pathways in Auditory Processing: Recent Advances and Insights From Other Sensory Systems

Flora M. Antunes[1,2]* *and Manuel S. Malmierca*[1,2,3]*

[1] Cognitive and Auditory Neuroscience Laboratory (CANELAB), Institute of Neuroscience of Castilla y León (INCYL), University of Salamanca, Salamanca, Spain, [2] Institute for Biomedical Research of Salamanca, University of Salamanca, Salamanca, Spain, [3] Department of Cell Biology and Pathology, School of Medicine, University of Salamanca, Salamanca, Spain

The corticothalamic (CT) pathways emanate from either Layer 5 (L5) or 6 (L6) of the neocortex and largely outnumber the ascending, thalamocortical pathways. The CT pathways provide the anatomical foundations for an intricate, bidirectional communication between thalamus and cortex. They act as dynamic circuits of information transfer with the ability to modulate or even drive the response properties of target neurons at each synaptic node of the circuit. L6 CT feedback pathways enable the cortex to shape the nature of its driving inputs, by directly modulating the sensory message arriving at the thalamus. L5 CT pathways can drive the postsynaptic neurons and initiate a transthalamic corticocortical circuit by which cortical areas communicate with each other. For this reason, L5 CT pathways place the thalamus at the heart of information transfer through the cortical hierarchy. Recent evidence goes even further to suggest that the thalamus via CT pathways regulates functional connectivity within and across cortical regions, and might be engaged in cognition, behavior, and perceptual inference. As descending pathways that enable reciprocal and context-dependent communication between thalamus and cortex, we venture that CT projections are particularly interesting in the context of hierarchical perceptual inference formulations such as those contemplated in predictive processing schemes, which so far heavily rely on cortical implementations. We discuss recent proposals suggesting that the thalamus, and particularly higher order thalamus via transthalamic pathways, could coordinate and contextualize hierarchical inference in cortical hierarchies. We will explore these ideas with a focus on the auditory system.

Keywords: corticothalamic circuits, hierarchical inference, feedback loops, reticular thalamic nucleus, transthalamic pathways

OPEN ACCESS

Edited by:
Julio C. Hechavarría, Goethe University Frankfurt, Germany

Reviewed by:
Eike Budinger, Leibniz Institute for Neurobiology (LG), Germany
Tania Rinaldi Barkat, University of Basel, Switzerland

***Correspondence:**
Flora M. Antunes
floraa@usal.es
Manuel S. Malmierca
msm@usal.es

Received: *06 June 2021*
Accepted: *28 July 2021*
Published: *19 August 2021*

Citation:
Antunes FM and Malmierca MS (2021) Corticothalamic Pathways in Auditory Processing: Recent Advances and Insights From Other Sensory Systems. Front. Neural Circuits 15:721186. doi: 10.3389/fncir.2021.721186

INTRODUCTION

A massive set of glutamatergic corticothalamic projections arising from the pyramidal cells in Layers 5 (L5) or 6 (L6) of the cortex outnumber the ascending, thalamocortical projections and inextricably link the cortex to the thalamus (Kelly and Wong, 1981; Sherman and Guillery, 1998; Winer et al., 2001; Harris et al., 2019). These CT projections are not homogeneous but differ anatomically and functionally paving the way to different modes of interaction between thalamus and cortex in both ways. The small but numerous terminals

of upper L6 (L6a) CT axons, together with their collaterals to the thalamic reticular nucleus (Ojima, 1994; Rouiller and Welker, 2000; Hazama et al., 2004), send a reciprocal feedback to the thalamus and are known to modulate the sensory message arriving at the thalamus in a myriad of ways (Yu et al., 2004; Zhang and Yan, 2008; Guo et al., 2017; Homma et al., 2017). In contrast, the giant terminals carried by L5 axons (Bajo et al., 1995; Bartlett et al., 2000) can drive their own messages to thalamic neurons *via* non-reciprocal projections, and then feedforward these messages to a different, hierarchically higher cortical area, forming a transthalamic corticocortical circuit (Llano and Sherman, 2008; Theyel et al., 2010; Mo and Sherman, 2019). Very recent studies suggest that some CT neurons emanating from deep layer 6 (L6b) have distinct anatomical and physiological properties from neurons emanating from both L6a and L5 and could represent a third CT circuit (Hoerder-Suabedissen et al., 2018; Ansorge et al., 2020; Buchan, 2020; Zolnik et al., 2020).

Altogether, these different CT circuits enrich and diversify the opportunities for bidirectional communication between thalamus and cortex. At the thalamic node, CT circuits actively transform and/or gate the transmission of sensory information en route to the cortex (Yu et al., 2004; Antunes and Malmierca, 2011; Mease et al., 2014; Cai et al., 2016; Guo et al., 2017; Homma et al., 2017; Ibrahim et al., 2021) but also regulate functional connectivity within and across cortical areas (Saalmann et al., 2012; Sherman, 2016; Zhou et al., 2016; Schmitt et al., 2017; Jaramillo et al., 2019). CT circuits expand the computational capabilities of the thalamus, reflecting its active role in sensory processing and beyond (Nakajima and Halassa, 2017; Rikhye et al., 2018). It is now widely accepted that the thalamus and CT pathways are engaged in high level computations previously thought to be exclusively cortical, such as language (Bartlett, 2013; Llano, 2013; Crosson, 2019; Mihai et al., 2019), learning and memory (Wolff and Vann, 2019), attention (Zhou et al., 2016; Schmitt et al., 2017), behavioral flexibility (Nakayama et al., 2018), and perceptual decision making (Halassa and Sherman, 2019). Recent evidence suggests that CT pathways may play a role in sensory attenuation of self-generated stimuli (Hua et al., 2020; Clayton et al., 2021) and perceptual inference (Bastos et al., 2012; Kanai et al., 2015; Auksztulewicz and Friston, 2016; Rikhye et al., 2018; Asilador and Llano, 2020).

In the following, we first review the circuitry, physiology, and function of CT projections (section L5 and L6 Corticothalamic Projections Provide Different Inputs to Thalamic Neurons). Then, we will discuss the participation of L5 CT projections in transthalamic pathways (section L5 Corticothalamic Projections Initiate Transthalamic Corticocortical Pathways). Finally, we propose that the thalamus and the CT pathways participate in the coordination and contextualization of hierarchical inference in cortical hierarchies (section Role of Corticothalamic Pathways in the Implementation of Predictive Processing Frameworks) (Mumford, 1991; Kanai et al., 2015; Rikhye et al., 2018).

L5 AND L6 CORTICOTHALAMIC PROJECTIONS PROVIDE DIFFERENT INPUTS TO THALAMIC NEURONS

In this review, we will adopt the conceptualization proposed by Sherman and Guillery (1998) in which glutamatergic pathways can be divided into *drivers* and *modulators*. Drivers are the main conduits of information and strongly activate the postsynaptic neuron, whereas modulators serve to modify the processing of information carried by driver inputs without changing the basic nature (such as the receptive field shape) of the message to be relayed. In this context, L5 CT projection provides driver input to thalamic neurons, similarly to the ascending, feedforward inputs whereas L6 cortical feedback modulates thalamic relay neurons, performing similar operations as the classical neuromodulators do (e.g., acetylcholine, noradrenaline, serotonin; Usrey and Sherman, 2019). Thalamic nuclei that receive subcortical driver inputs are referred to as first *order* and represent the first sensory input to cortex, whereas nuclei that receive driver influence from cortical L5 are referred to as *higher order* and represent part of a corticothalamocortical, or transthalamic, pathway that conveys information from one cortical area to another (Sherman, 2016). In the auditory thalamus, they correspond to the ventral (MGV) and dorsal (MGD) subdivisions of the MGB, respectively (Ojima, 1994; Llano and Sherman, 2008; Lee and Murray Sherman, 2010). According to this model, first *order* nuclei (e.g., MGV) receive a reciprocal feedback input from L6 but no input from L5, whereas *higher order* nuclei (e.g., MGD and MGM) receive two distinct cortical inputs: one from L6 that is a reciprocal feedback, and another from L5 that is non-reciprocal (**Figure 1G**; Llano and Sherman, 2008; Usrey and Sherman, 2019). In this review, we consider as feedforward connections all bottom-up connections with driver properties, and feedback connections all top-down connections with modulatory properties. According to this classification, and from a cortical perspective, we consider L6 reciprocal connections as top-down feedback connections whereas L5 non-reciprocal connections as bottom-up feedforward connections within transthalamic pathways.

Recent studies that selectively targeted and manipulated distinct neuronal subtypes in L6 suggest that the previous classification might be incomplete, because not all L6 CT neurons send a reciprocal feedback to thalamus or provide modulator-like input. A subpopulation of neurons in L6b seems to be involved in a CT circuit that differs anatomically and physiologically from both L5 and L6a, the canonical L6 feedback circuit, and likely represent a third type of CT circuit (**Figure 1**; Hoerder-Suabedissen et al., 2018; Ansorge et al., 2020; Buchan, 2020; Zolnik et al., 2020), as we will explain in section L6b non-reciprocal Corticothalamic Projections.

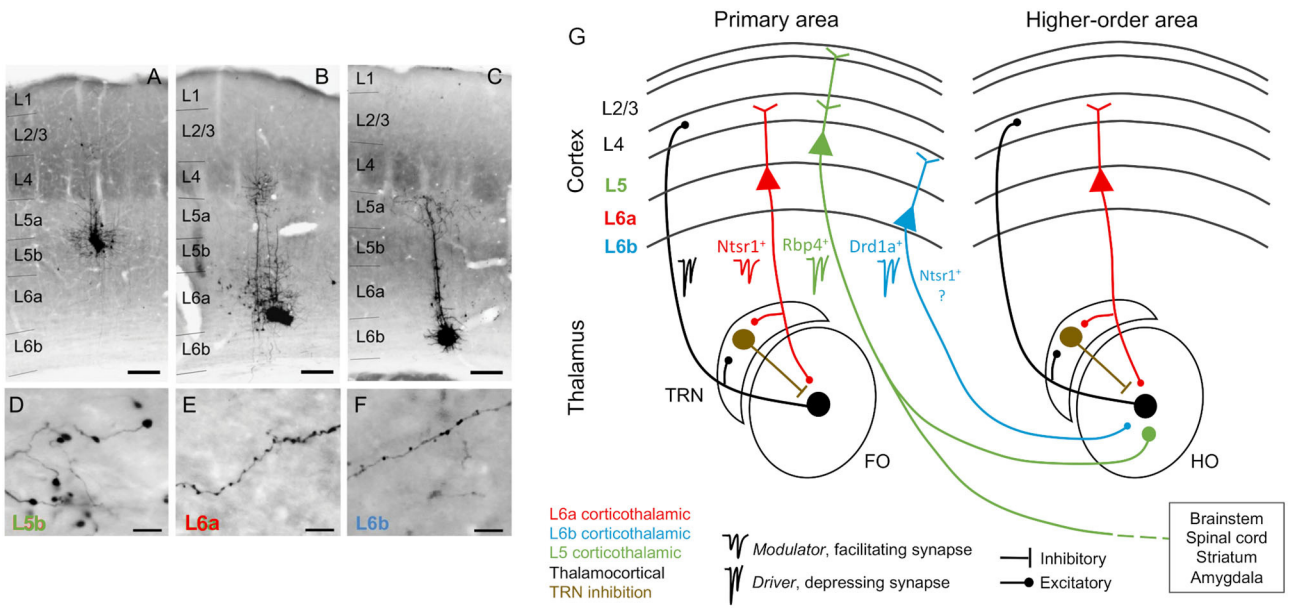

FIGURE 1 | Corticothalamic neurons and circuits. **(A–C)** Photomicrographs showing BDA microdeposits in L5b, L6a, and L6b neurons of primary somatosensory barrel field **(D–F)**, and their respective axonal arborizations in (higher order) posterior thalamic nucleus. Cortical pyramidal neurons differ in the morphology of their axonal varicosities. Scale bars: A–C = 150 μm, D–F = 10 μm. **(G)** Schematic and simplified view of corticothalamic and thalamocortical circuits, based on information from several sensory systems (auditory, visual, and somatosensory). Red, L6a CT projections, *modulator* (Ntsr1$^+$): feedback projections that send collaterals to the TRN, a GABAergic nucleus that provides inhibition to the thalamus (brown). Black, thalamocortical, feedforward projections that form reciprocal loops with L6a feedback projections. Green, L5 CT projections, *driver* (Rbp4$^+$): project non-reciprocally to a hierarchically higher order thalamic nucleus and form part of transthalamic corticocortical pathways; they are collaterals from long-range axons that project to other subcortical centers (e.g., brainstem, spinal cord, striatum, and amygdala). Blue, L6b CT projections, *driver* (Drd1a$^+$): project non-reciprocally to a hierarchically higher order thalamic nucleus; it is unknown if Drd1a+ and Ntsr1+ neurons in L6b are overlapping or distinct neuronal populations. As insets, examples of specific markers from Cre mouse lines that can be used to selectively target neurons of each CT circuit [Ntsr1-Cre, Drd1a-Cre, and Rbp4-Cre mice, for L6a (red), L6b (blue), and L5 (green) CT neurons]. FO, first order thalamic nuclei; HO, higher order thalamic nuclei; TRN, thalamic reticular nucleus; L2/3, cortical layers 2 and 3; L4, cortical layer 4; L5, cortical layer 5; L6a, cortical layer 6a; L6b, cortical layer 6b; Photomicrographs **(A–F)** after Hoerder-Suabedissen et al. (2018).

L6a Corticothalamic Feedback Forms a Corticothalamic Loop

Feedback signals to thalamus from cortex arise from pyramidal neurons in the upper layer 6 (L6a; Bourassa and Deschênes, 1995; Thomson, 2010; Malmierca, 2015). These feedback neurons can be genetically targeted using expression of the type 1 neurotensin receptor (Ntsr1- Cre transgenic mice; Olsen et al., 2012; Bortone et al., 2014; Guo et al., 2017). L6a CT neurons specifically target the region of sensory thalamus from which they receive direct input, and their dendrites and ascending collaterals target L4, the major thalamorecipient layer, thus preserving thalamocortical-corticothalamic reciprocal connectivity (**Figure 1**). This forms a thalamocortical loop, by which thalamus and cortex concurrently stimulate (and are stimulated by) each other (Bajo et al., 1995; Zhang and Deschênes, 1997; But see Kim et al., 2014, who report that L6 CT neurons strongly innervate, and excite, pyramidal neurons in layer 5). For example, L6 from primary auditory cortex (A1) projects to tonotopically comparable laminae of the same subdivision from which it received its main thalamocortical input, the MGV (Winer et al., 2001; Hazama et al., 2004; Llano and Sherman, 2008). The L6 A1-MGV projections constitutes one of the largest feedback pathways in the auditory system (Rouiller and Welker, 1991; Ojima, 1994; Prieto and Winer, 1999; Kimura et al., 2005). Similar reciprocal connectivity occurs between the MGD and secondary auditory cortex (A2). L6 feedback axons are composed of thin fibers having small but numerous glutamatergic boutons that synapse on distal dendrites and evoke facilitating EPSPs *via* ionotropic and metabotropic receptors (**Figure 1**; Ojima, 1994; Bajo et al., 1995; Winer et al., 2001; Bartlett and Smith, 2002), leading to their characterization as modulators (Sherman and Guillery, 1998).

The Corticothalamic Loop Engages the GABAergic Thalamic Reticular Nucleus

In their way to thalamus, L6 axons send collaterals to the TRN. The TRN is a thin shell of GABAergic neurons surrounding the thalamus that projects to the same thalamic nucleus (but not exclusively) as the L6 fibers passing through it (**Figure 1**; Crabtree, 1998; Pinault, 2004; Kimura et al., 2005). When the TRN is activated by L6 collaterals, it provides feedforward inhibition to the MGB. For this reason, the passage of L6 collaterals by the TRN determines to great extent the modulatory effect exerted by L6 excitatory terminals on MGB neurons (Guillery, 1995; Deschênes et al., 1998; Kimura et al., 2012). The excitatory or inhibitory sign of L6 CT modulation will depend on a delicate balance between a prevalent effect exerted on

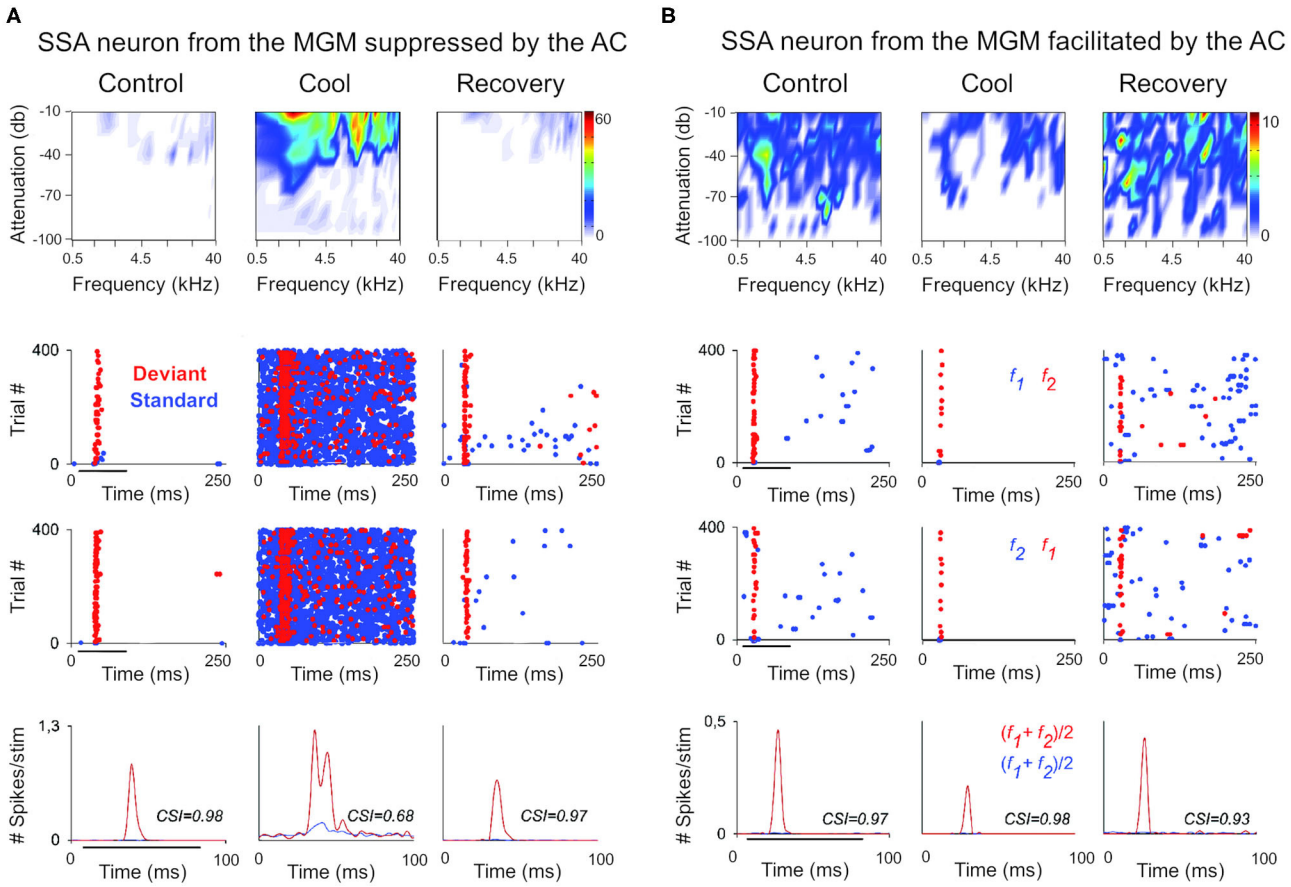

FIGURE 2 | The cortex exerts suppressive and facilitating influences in neurons of the auditory thalamus. Examples of single-unit responses to auditory stimulation in the MGB of the anesthetized rat before, during, and after AC deactivation by cooling. **(A)** A neuron localized to the MGM that receives suppressive influences from the AC. The frequency response areas (first row), and the responses of the neuron to the oddball paradigm (second-fourth rows), in the control, cool and recovery conditions. The oddball paradigm was used to elicit SSA in these neurons. Briefly, the oddball paradigm consisted of a sequence of a repetitive stimulus (standard; 90% probability) that was infrequently interrupted by a different stimulus (deviant; 10% probability. The standard (blue) and the deviant (red) stimulus were pure tones selected from within the frequency response area of the neuron. Two blocks of 400 trials each (middle panels) were presented in which the standard and deviant frequencies were reversed (second panel, first block: f1/f2 as standard/deviant; third panel, second block: f2/f1 as standard/deviant). Dot rasters show individual spikes to the deviant and standard (red and blue dots, respectively), in the three conditions for the two stimulus presentation blocks (stacked along the y-axis; repetition rate 4 Hz; stimulus duration: 75 ms, black horizontal lines under the plots). PSTHs (last row) show the number of spikes/stimulus (bin duration: 3 ms) averaged over the two blocks [(f1+f2)/2; blue line is standard, red line is deviant]. The CSI calculated for each condition is noted as an inset on the PSTHs. The CSI quantifies the amount of SSA and is calculated as CSI = [d(f1)+d(f2)-s(f1)-s(f2)]/[d(f1)+d(f2)+s(f1)+s(f2)], where d(fi) and s(fi) are responses (# spikes/stimulus) to frequency fi when deviant or standard, respectively ($0 \leq CSI \leq 1$). Higher CSI values, higher SSA. **(B)** Responses of another neuron localized to the MGM that receives facilitatory influences from the AC, presented as in **(A)**. AC, auditory cortex; MGB, medial geniculate body; MGM, medial subdivision of the medial geniculate body; SSA, stimulus specific adaptation; CSI, common SSA index; f1, frequency 1; f2, frequency 2. Adapted from Antunes and Malmierca (2011).

TRN-mediated disynaptic inhibition or direct, monosynaptic CT excitation (Crandall et al., 2015; Li and Ebner, 2016; Guo et al., 2017). For example, low frequency thalamocortical oscillations that occur during slow-wave sleep depend on rhythmic inhibition of thalamocortical neurons. This rhythmic inhibition is likely caused by a stronger CT effect on disynaptic inhibition that overcomes monosynaptic excitation (Golshani et al., 2001; Steriade, 2001).

The intricate and delicate corticothalamic interactions together with the fact that the TRN is a very small nucleus closely adjacent to the thalamus, both lying deep in the brain, makes the study of the relative contribution of disynaptic inhibition and direct excitation in CT modulation difficult to disentangle. A study using brain slices that preserved L6 CT circuitry has shown a dynamic excitatory-inhibitory balance shift in thalamic excitability that depended on the rate and time-course of L6 CT activation (Crandall et al., 2015). Thalamic excitability was mainly suppressed during low frequency CT activity, whereas it shifted to facilitation following higher frequency CT activity. The shifting to facilitation was the result of facilitation of monosynaptic CT-evoked EPSCs (as expected, because L6 feedback projection is facilitatory), together with a reduction of CT-triggered disynaptic IPSCs (*via* TRN). This reduction was due to short-term synaptic depression of the

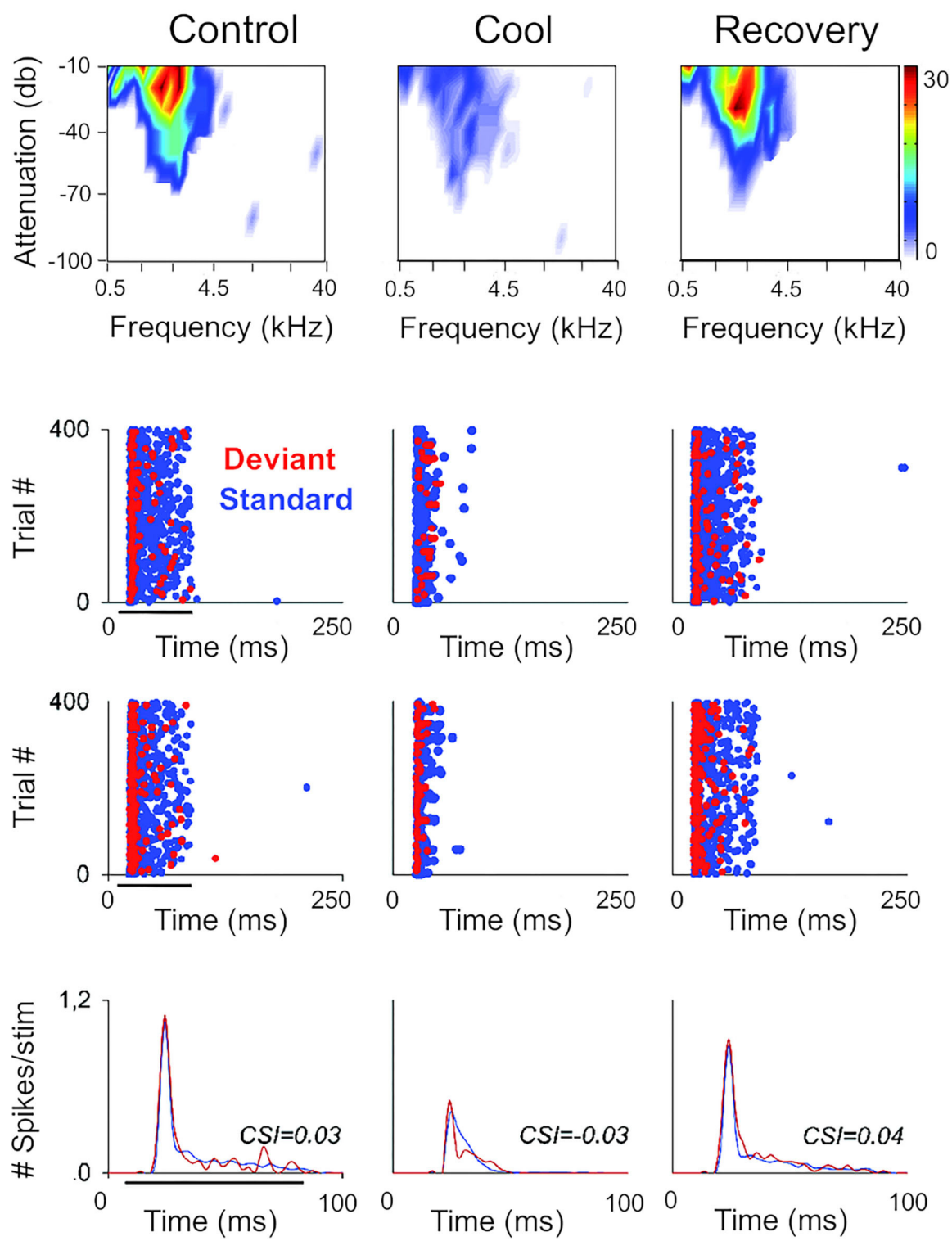

FIGURE 3 | Non-SSA neurons primarily receive facilitatory influences from the AC. Example of a neuron recorded from the MGV that was facilitated by the AC, presented as in **Figure 2**. The neuron responds consistently to both the standard and the deviant over the trials, i.e., it does not show SSA as confirmed by the low CSI value (~0). The CSI value was not significantly changed by AC deactivation. AC, auditory cortex; MGV, ventral subdivision of the medial geniculate body; CSI, common SSA index. Adapted from Antunes and Malmierca (2011).

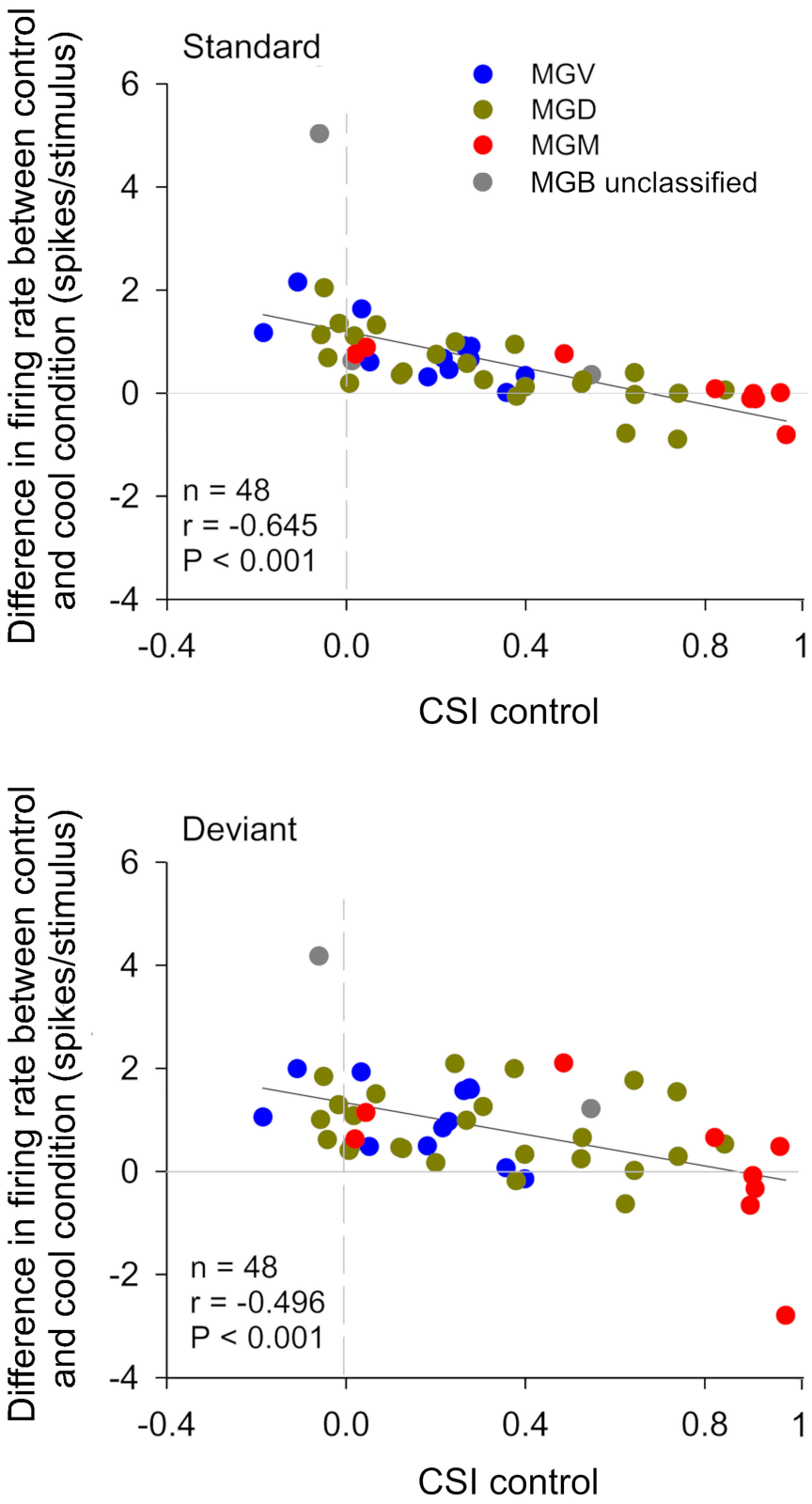

FIGURE 4 | The gain exerted by the cortex in auditory thalamic neurons depends on their ability to signal a deviance from previous stimulation context. Scatterplots of the CSI (control condition) vs. the difference in firing rate between the control and cool conditions (spikes/stimulus difference) in response to the standard (upper panel) *(Continued)*

FIGURE 4 | and deviant stimulus (lower panel), for each neuron. Blue, green, and red dots represent the neurons that were localized to the ventral ($n = 12$), dorsal ($n = 24$), and medial ($n = 9$) subdivisions of the MGB, respectively ($n = 45$, neurons that were localized to one of the three MGB subdivision). Gray dots represent MGB neurons that were not localized to a specific MGB subdivisions ($n = 3$). In both plots, positive values (above the horizontal line at the origin) indicate a reduction in firing rate with cortical deactivation (neurons receive facilitatory cortical influences), whereas negative values (bellow the horizontal line) indicate an increment in firing rate with cortical deactivation (neurons receive suppressive influences from the cortex). The difference in firing rate was inversely correlated with CSI for both standard and deviant stimuli. The slopes of the standard and deviant regression lines are not significantly different from each other [ANCOVA: main effect of stimuli, $F_{(1,92)} = 1.89$, $p = 0.172$; main effect of CSI, $F_{(1,92)} = 43.27$, $p = 0$; interaction, $F_{(1,92)} = 0.23$, $p = 0.634$; $n = 48$], indicating that the correlation coefficients between standard and deviant are not different. The AC differentially affects the discharge rate of neurons depending on their SSA level. Neurons without SSA are mainly facilitated, whereas some neurons with high SSA are suppressed by the cortex. AC, auditory cortex; MGB, medial geniculate body; MGV, ventral subdivision of the MGB; MGD, dorsal subdivision of the MGB; MGM, medial subdivision of the MGB; SSA, stimulus specific adaptation; CSI, common SSA index; Adapted from Antunes and Malmierca (2011).

TRN-thalamus synapse, with a minimal contribution from the intrinsically mediated reductions in TRN spiking (the intrinsic burst properties of TRN neurons cannot follow high frequencies; Crandall et al., 2015). A recent study in the auditory system investigated the mechanisms underlying the gating of all-or-none population responses in the auditory cortex *via* L6 CT-TRN feedback (Ibrahim et al., 2021). They present an alternative mechanism by which the gating of cortical activity mediated by L6 CT-TRN feedback is dependent on the ability of the TRN to desynchronize thalamocortical neurons rather than diminishing thalamic activity (Ibrahim et al., 2021). They suggest that thalamic synchronization by the TRN can be a mechanism to recruit neuronal populations for sensory representations (Ibrahim et al., 2021).

In summary, the TRN node empowers the CT circuits with the ability to flexibly change functional connectivity by acting as a regulator that can favor or oppose the relay of sensory information to the cortex as required by ongoing behavioral demands (Kimura et al., 2012; Li and Ebner, 2016; Guo et al., 2017), for example, during sleep (Steriade and Deschenes, 1984; Golshani et al., 2001; Barthó et al., 2014), sensorimotor processing (Marlinski et al., 2012) or attention (Crick, 1984; McAlonan et al., 2008; Wells et al., 2016).

Thalamic Modulation by CT Feedback Is Difficult to Disambiguate From Classical Studies

Classical studies in the intact brain used techniques to silence (Ryugo and Weinberger, 1976; Orman and Humphrey, 1981) or stimulate (Watanabe et al., 1966; Aitkin and Dunlop, 1969) entire cortical regions without discriminating between cortical layers or accounting for the effects that this non-specific manipulation could have on subthalamic regions that may themselves provide inputs to the thalamus. Largely because of these limitations, the general view of corticothalamic interactions from classical studies is one of very large variability, with divergent effects. These effects are often difficult to interpret in terms of perception and behavior.

In the auditory system, cortical inactivation (Villa and Abeles, 1990; Villa et al., 1991; Zhang et al., 1997; Palmer et al., 2007) and/or stimulation (He, 2003; Xiong et al., 2004; Yu et al., 2004; Zhang and Yan, 2008; Ojima and Rouiller, 2011) experiments have demonstrated that the AC can modulate the MGB either by facilitation or by suppression, resulting in changes in receptive field properties and firing patterns. Indeed, a previous study corroborates these findings by showing that the basic properties of MGB neurons (e.g., spontaneous activity, discharge rates, latencies) were altered during cortical silencing by cooling (**Figures 2**, **3**; Antunes and Malmierca, 2011). However, stimulus-specific adaptation (SSA), the property that we were investigating in this study was not altered during cortical silencing (**Figure 2**). SSA measures the neuronal adaptation to repeated sounds (standards) that does not generalize to rare sounds (deviants; Ulanovsky et al., 2003). In fact, responses to deviant sounds are enhanced following the repetition, and consequent adaptation, of the standard sound (Parras et al., 2017). For this reason, these neurons are believed to be context-sensitive: they signal a deviance from the previous context (repetition of a stimulus). It was shown that SSA is implemented at the MGB level largely independently of cortical activity (**Figure 2**; Antunes and Malmierca, 2011). Contrast adaptation, a type of adaptation that is also dependent on stimulus statistics, has also been demonstrated to occur in auditory thalamus independently of cortical activity (Lohse et al., 2020). Regarding SSA, the auditory cortex modulates the discharge rate of MGB neurons affecting similarly the responses to the standard and the deviant stimuli, probably by providing a gain-control mechanism (because the amount of SSA is quantified by a ratio of driving rates, it is largely unaffected by cortical silencing; **Figures 2**, **3**). But perhaps the most interesting finding of Antunes and Malmierca (2011) study was the fact that the gain exerted on MGB neurons depended on the level of SSA that they exhibited: high SSA was related to weaker cortical gain (**Figure 4**). Because this relationship is not dependent on the subdivision to which the MGB neurons belong, this finding provided strong evidence for a clear rule that relates cortical modulation to a neuronal property (Antunes and Malmierca, 2011). We will speculate about the possible mechanism underlying this SSA-dependent CT modulation of MGB neurons on section Role of CT Pathways in Coordinating and Contextualizing Inference in Cortical Hierarchies. Altogether, our results are consistent with the idea that the CT feedback scales the sensitivity of MGB neurons to its driving inputs by controlling their gain (Villa and Abeles, 1990; Villa et al., 1991; He, 2003; Mease et al., 2014). Such gain control might improve coding of low salience stimuli (Cai et al., 2016), promote detection or discrimination of behaviorally relevant stimuli (Happel et al., 2014; Guo et al., 2017; Homma et al., 2017), mediate sound-specific plastic changes in thalamic neurons (Zhang and Yan, 2008; Nelson et al., 2015), and underly auditory attention (He, 2003).

Selective Manipulation of L6 CT Pathways Disentangles Their Roles in Auditory Perception and Behavior

Recent studies using a combination of layer or cell-type specific selective manipulation, electrophysiology and behavior testing have just started to unravel the roles of CT pathways in behavior and perception (Guo et al., 2017; Nakayama et al., 2018; Clayton et al., 2021; Ibrahim et al., 2021; Lohse et al., 2021). For example, Homma et al. (2017) used chromophore-targeted laser photolysis to selectively eliminate the input from layer VI to the MGV. In their study, the authors provided behavioral evidence that L6 CT—MGV feedback pathway contributes to the perception of complex sounds, by showing that this pathway is needed for the normal ability of ferrets to detect a mistuned harmonic within a complex sound. Since normal hearing uses deviations from harmonicity to segregate concurrent sounds, L6 CT feedback may play a role in auditory scene analysis (Homma et al., 2017). In humans, task-dependent modulation of the MGV (but not the other MGB subdivisions) facilitates speech recognition performance (fMRI study; Mihai et al., 2019). Such modulation might be provided by L6 CT feedback, as Mihai et al. (2019) suggested, although this hypothesis needs further confirmation. Happel et al. (2014) demonstrated that dopaminergic modulation regulates a corticothalamocortical positive-feedback circuit in A1 that boosts horizontal intracortical processing (long range corticocortical networks) and enhances the detection of behaviorally relevant stimuli.

L6 CT neurons not only send a feedback to the thalamus but also have dense intracortical connections with both excitatory and inhibitory neurons throughout the cortical column (Zhang and Deschênes, 1997; Winer et al., 2001; Llano and Sherman, 2008; Williamson and Polley, 2019). This means that activation of L6 CT neurons could modulate both thalamocortical transmission and intracortical processing (Olsen et al., 2012; Bortone et al., 2014; Guo et al., 2017), producing mixed excitatory and inhibitory effects on both thalamic and cortical neurons (Temereanca and Simons, 2004; Mease et al., 2014; Denman and Contreras, 2015). A recent study in the auditory system demonstrated that spontaneous and sound-evoked activity of A1 in awake mice was enhanced during optogenetic activation of L6 CT neurons [Ntsr1+; Guo et al. (2017)]. Interestingly, this study went further to investigate whether activity in A1 and thalamus in the awake animal could also depend on timing between L6 CT activation and sensory stimulation, similarly to what occurs in barrel cortex slices (the sign of CT modulation depends on frequency and timing of CT activation; Crandall et al., 2015). This is indeed the case in the auditory system of the awake animal (Guo et al., 2017): at short delays following offset of L6 CT activation, tone-evoked responses in A1 were suppressed but more precisely tuned, whereas at long delays, responses were enhanced but less precisely tuned (**Figure 5**, compare middle to right panels). Noteworthily, this bidirectional modulation serves as a behavioral switch, favoring either tone discrimination or detection (**Figure 5**). The ability to discriminate between similar stimuli is favored in the short delay period following L6 CT activation, whereas the ability to detect faint sounds is favored in the long delay period.

Intense firing of L6 CT neurons activates a subpopulation of fast spiking (FS) cortical interneurons (Olsen et al., 2012; Bortone et al., 2014). Activation of FS interneurons increases the power and resets the phase of low-frequency oscillations, a mechanism identified by Guo et al. (2017) that might explain the differences found (**Figure 5**). In brief, cortical suppression and improved sound discrimination following offset of L6 CT activation arise from induction of the early, low excitability phase of an intracortical delta-theta rhythm. This rhythm is reset in the short delay period by the FS resetters (**Figure 5**). In contrast, cortical enhancement and improved tone detection in the long delay period arise primarily from an intra-thalamic shift in excitatory-inhibitory balance between MGV and TRN, where disynaptic inhibition is scaled down over time, similarly to that described by Crandall et al. (2015).

As Linden (2017) noted, the question remains as to whether the low-frequency phase reset mechanism unraveled by Guo et al. (2017) has a role during active listening. During active listening, entrainment of low-frequency oscillations to the attended auditory stream is believed to enhance neuronal responses and perception (Zion Golumbic et al., 2013; Obleser and Kayser, 2019). This entrainment ensures that local neurons are in the high excitability phase of the oscillations when relevant inputs arrive, so they can be forwarded up the hierarchy. In contrast, sensory inputs from the non-attended stream will arrive at the low excitability phase of the oscillations, and will be suppressed (Schroeder and Lakatos, 2009; Zion Golumbic et al., 2013). Recently, it was shown that L6 CT neurons can be activated by motor-related input prior to anticipated sounds during active sensing (Clayton et al., 2021), which might contribute to sensory attenuation of self-generated sounds as demonstrated in humans (Hua et al., 2020).

In summary, the prominent feedback projections from cortical L6 to thalamus have intrigued auditory scientists since many decades, as displayed by the numerous studies dedicated to investigating their role in thalamic function. However, as we have reviewed above, L6 CT projections cannot be studied with classical techniques that are blind to the complexity of the circuits to which they belong. In recent years, the interest in meticulously studying these circuits and their roles in auditory processing and behavior has increased tremendously. This was largely propelled by the advent of new techniques that now enable the selective manipulation of L6a projections in the awake behaving animal. These studies have just started to unveil the powerful roles L6a feedback circuits have in auditory perception and behavior.

L6b Non-reciprocal Corticothalamic Projections

Some CT neurons emanate from deep layer 6 (L6b) and have long been known to primarily innervate higher order thalamic nuclei (**Figure 1**; visual and auditory system; Bourassa and Deschênes, 1995; Llano and Sherman, 2008). However, the connectivity as well as behavioral and functional roles of L6b CT neurons are largely unknown. Like most L6a CT neurons, some CT neurons

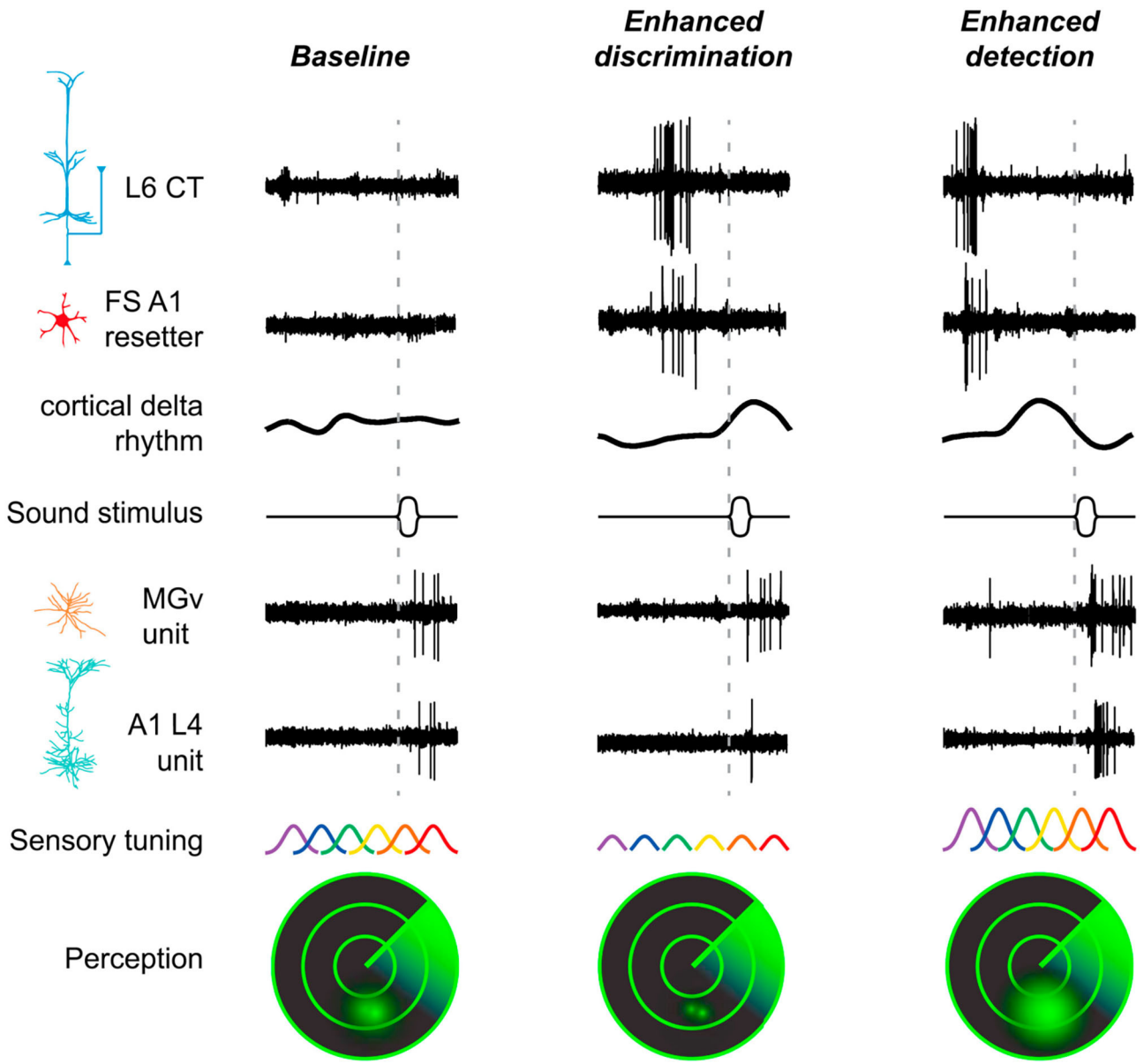

FIGURE 5 | L6 CT neurons are involved in the behavioral switch between sound detection and discrimination. This scheme summarizes the findings by Guo et al. (2017) who demonstrate the participation of L6 CT neurons (Ntsr1+), via both their intracortical and corticothalamic connections to perceptual modes of enhanced detection or discrimination. Left column, in a baseline condition with low activity in L6 CT neurons and fast-spiking interneurons (FS resetters), the sound-evoked activity in MGV and L4 cortical neurons is moderate. FS resetters are activated following intense firing of L6 CT neurons. Activity of FS resetters increases the power and resets the phase of low frequency rhythms. Middle column, at a short delay period following intense activity of L6 CT and FS resetter neurons, the delta-theta rhythm is at a positive, low excitability phase, and sound-evoked activity is suppressed in A1 but not in the MGV, which favors tone discrimination at the expense of sound sensitivity (the reduced excitability of cortical neurons sharpens frequency tuning). Right column, at longer delays following L6 CT activity, the phase of the cortical rhythm has rotated to a negative, high excitability phase, and sound-evoked activity is enhanced both in A1 and MGV. The enhanced excitability of cortical neurons is expected to increase the overlap in sensory tuning between neighboring tuning regions, which favors tone detection at the expense of reduced tone discrimination. A1, primary auditory cortex; CT, corticothalamic; L6, cortical layer 6; L4, cortical layer 4; MGV, ventral subdivision of the medial geniculate body; FS, fast-spiking interneurons. Reproduced, with permission, from Guo et al. (2017).

in L6b also express Ntsr1 (visual and somatosensory system; Olsen et al., 2012; Chevée et al., 2018). For this reason, using Ntsr1-Cre mice to manipulate L6 CT neurons, possibly engages the circuits of layers 6a and 6b. However, Ntsr1 neurons seem to have different projection patterns depending on their laminar position within L6 (visual and somatosensory system, Kim et al., 2014; Chevée et al., 2018; Frandolig et al., 2019). Ntsr1 neurons in layer 6a are thought to project exclusively reciprocally (e.g., from AI to MGV), and their apical dendrites to innervate cortical L4 to form a corticothalamic loop (see section L6a Corticothalamic

Feedback Forms a Corticothalamic Loop). In contrast, Ntsr1 neurons in L6b can branch to project to first- and higher-order thalamic nuclei, although preferentially to higher order nuclei (e.g., from AI to MGD; Llano and Sherman, 2008), and their dendrites are believed to innervate cortical L5 (somatosensory system; Chevée et al., 2018; Frandolig et al., 2019), a cortical output layer where some long-range axons with collaterals to higher order thalamic nuclei emanate, as we will discuss bellow (section L5 Corticothalamic Projections).

The fact that using Ntsr1-Cre mice to manipulate Ntsr1 neurons engages neurons from both sublayers 6a and 6b makes it difficult to disambiguate their distinct roles and connectivity. Recently, it has become possible to selectively target a subpopulation of neurons in L6b using expression of the type 1a dopamine receptor (Drd1a; Drd1a-Cre transgenic mouse; somatosensory system; Zolnik et al., 2020). It is still unknown if Drd1a neurons are a subpopulation of Ntsr1 neurons or belong to distinct population. Ongoing research in motor, somatosensory and visual cortex targeting Drd1a neurons is unraveling key connectivity and functional differences between layers 6a and 6b projections, indicating that they are engaged in different circuits (**Figure 1**). These studies confirmed that L6b CT neurons strongly innervate L5 of the cortex and preferentially target higher order thalamic nuclei (somatosensory system; Zhang and Deschênes, 1997; Ansorge et al., 2020; Zolnik et al., 2020) but form few side branches or synapses in first order thalamic nuclei (e.g., the MGV of the auditory thalamus; **Figure 6D**; Hoerder-Suabedissen et al., 2018). Perhaps the most surprising findings were that L6b Drd1a neurons receive their main input from long range intracortical neurons (e.g., from motor, auditory, and visual regions) with little or no contribution from thalamic input (Zolnik et al., 2020), and do not have side branches or synapses in TRN (Hoerder-Suabedissen et al., 2018), as opposed to L6a neurons (**Figure 1**). Functionally, Drd1 neurons seem to carry a driver-like signature, like L5 CT neurons, because their synapses are depressing (somatosensory system; Ansorge et al., 2020; Buchan, 2020), although L6b axon terminals are significantly smaller and simpler than the majority from L5 axons [somatosensory system, posterior thalamic nucleus; **Figure 1**, compare photomicrographs in plots D and F; Hoerder-Suabedissen et al. (2018)].

Altogether, these findings suggest that L6b is positioned outside the canonical corticothalamocortical loop (**Figure 1**). Their connectivity to cortical L5 and higher order thalamic nuclei, regions that are associated with cognitive functions, suggests that Drd1a neurons have a role in cognition. One possibility is that these neurons participate in transthalamic connections with higher order cortical areas, similarly to L5 CT neurons. Because neurons in L6b and higher order thalamic nuclei are responsive to the wake-promoting neuropeptide orexin, it has been suggested that L6b CT neurons might be recruited in an arousal dependent manner (Hoerder-Suabedissen et al., 2018; Zolnik et al., 2020). Future studies using awake, behaving animals are needed to unveil the roles L6b neurons might have in brain state control and cognition.

L5 Corticothalamic Projections

CT projections from cortical layer 5 are collateral projections issued from long-range axons that project to other subcortical regions in the brainstem and/or the spinal cord (**Figure 1**; auditory, motor, somatosensory and visual systems; Kelly and Wong, 1981; Deschênes et al., 1994; Prasad et al., 2020). In the auditory system, L5 collaterals produce few but thick axons with large glutamatergic terminals that synapse on proximal dendrites of higher order thalamic nuclei *via* ionotropic but not metabotropic receptors and do not innervate the TRN (Rouiller and Welker, 1991; Ojima, 1994; Bajo et al., 1995; Winer et al., 1999; Hazama et al., 2004; Rovó et al., 2012). However, global mappings of L5 terminals across multiple thalamic and extrathalamic sites revealed that there is a considerable variation in size of L5 terminals, ranging from small to giant terminals (entire macaque thalamus; Rovó et al., 2012), varying with cortical area of origin and target (afferents originating from somatosensory, visual, motor, and prefrontal cortex; Prasad et al., 2020). It is still unknown if small and large L5 terminals have different physiological properties and if this variation occurs in the auditory system.

L5 terminals evoke large and fast EPSCs that can trigger action potentials in the thalamic postsynaptic neurons (somatosensory system; Reichova and Sherman, 2004; Groh et al., 2008), leading to their classification as drivers (Sherman and Guillery, 1998). L5 giant synapses are not always in a driver transmission mode, because they undergo frequency-dependent short-term synaptic depression (due to their high initial Pr) by which activity is reduced during repeated presynaptic firing (e.g., spontaneous activity; lateral posterior nucleus: Li et al., 2003; posterior medial nucleus: Groh et al., 2008). In other words, due to synaptic depression, driver synapses are expected to act as low-pass filters that are most effective at transmitting impulses at the onset of presynaptic activity (Abbott and Regehr, 2004). This form of synaptic plasticity could allow switching the gating mode of L5 CT giant synapses from a dominant driver (following periods of silence) to a coincidence detector (when L5B depressed neurons fire synchronously, for example after a sensory stimulus; Groh et al., 2008). This has been demonstrated for L5B synapses onto neurons of the posterior medial nucleus (POm), a higher order thalamic nucleus of the whisker somatosensory system (Groh et al., 2008).

In vivo studies from the whisker system of the anesthetized mouse support the driving role of L5 corticothalamic projections (Diamond et al., 1992; Groh et al., 2014), by showing a robust transfer of spikes from a few active L5B cortical inputs to the POm (Mease et al., 2016). Interestingly, CT gain at these synapses is not constant, but it is controlled by global cortical up and down states (Mease et al., 2016). CT gain is maximal at the beginning phase of the up state but then declines during the up state due to frequency-dependent adaptation (possibly due to synaptic depression), resulting in periodic high- vs low-gain oscillations (Mease et al., 2016). Because higher order somatosensory thalamus projects to various cortical areas, single or synchronized spikes of a few L5B neurons can be amplified *in vivo* at the CT driver synapse and broadcast *via* thalamus

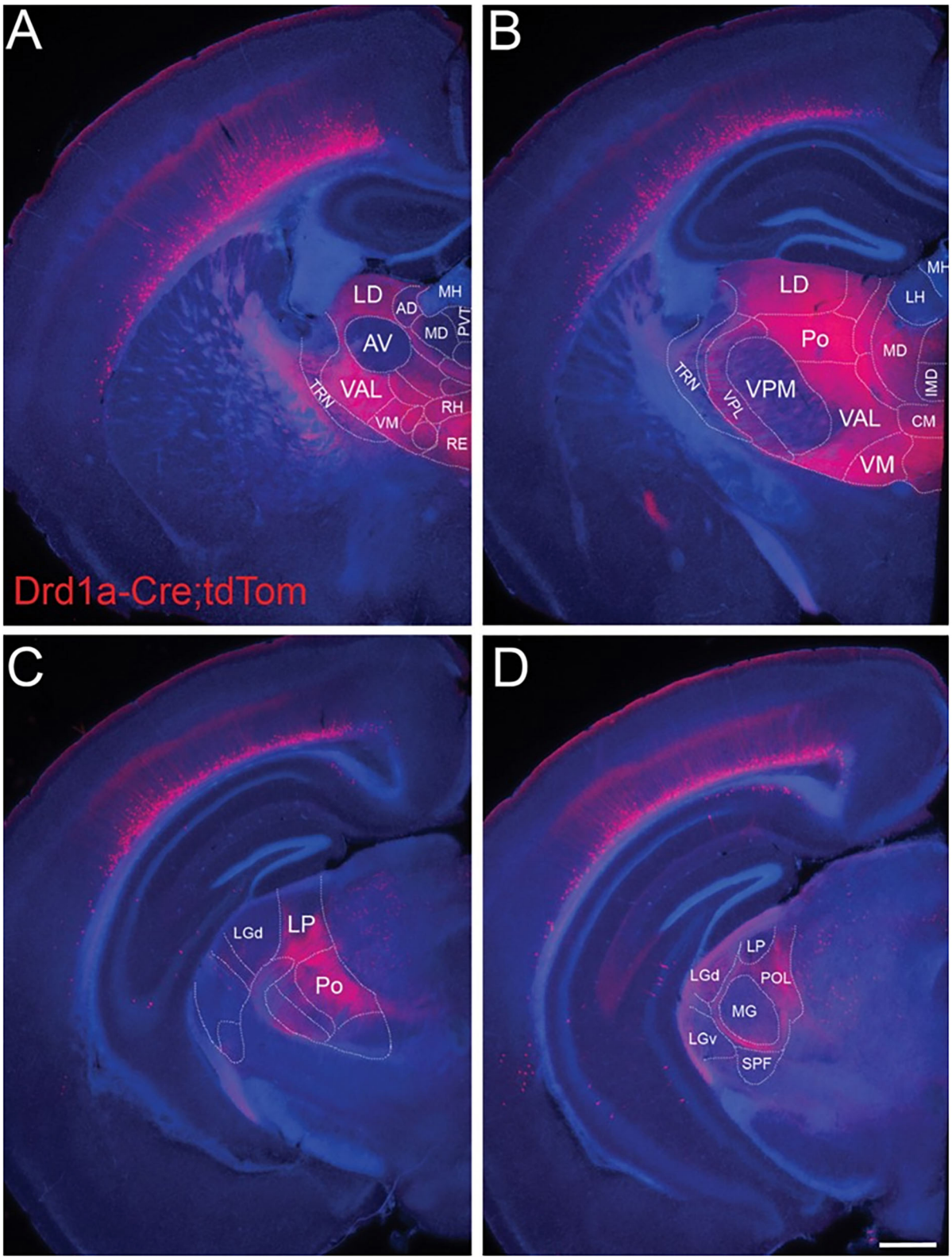

FIGURE 6 | L6b neurons project to higher order and avoid first order thalamic nuclei. Drd1a-Cre expression in fibers arising from neurons in L6b of the entire cortical mantle in adult mice (P35) visualized by tdTomato labeling (Drd1a-Cre::tdTom+ fibers). Projections from L6b avoid first order auditory and non-auditory thalamic nuclei

(Continued)

FIGURE 6 | such as **(A)** the anteroventral nucleus, **(B)** the ventral-posterior medial nucleus, **(C)** the lateral geniculate nucleus anteriorly, and **(D)** the MGV in the auditory thalamus. In contrast, they innervate heavily higher order thalamic nuclei such as the lateral dorsal nucleus, the posterior nucleus, the ventral medial nucleus, and the ventral anterior lateral complex. Fibers pass through TRN without apparent branching. Scale bar Scale bar = 500 μm. AD, anterodorsal nucleus; AV, anteroventral nucleus; CM, central medial nucleus; IMD, intermediodorsal nucleus; LD, lateral dorsal nucleus; LH, lateral habenula; LGd, dorsal lateral geniculate nucleus; LGv, ventral lateral geniculate nucleus; LP, lateral posterior nucleus; MD, mediodorsal nucleus; MG, medial geniculate nucleus; MH, medial habenula; Po, posterior nucleus; POL, posterior limiting nucleus; PVT, paraventricular nucleus; RE, nucleus reuniens; RH, rhomboid nucleus; SPF, subparafascicular nucleus; TRN, thalamic reticular nucleus; VAL, ventral anterior lateral complex; VM, ventral medial nucleus; VPL, ventral-posterior lateral nucleus; VPM, ventral-posterior medial nucleus. Reproduced from Hoerder-Suabedissen et al. (2018).

simultaneously to motor, primary, and secondary sensory cortical regions (Deschênes et al., 1998; Theyel et al., 2010), to enhance and prolong cortical responses (Mease et al., 2016).

Anatomical and Physiological Evidence for L5 Driver Terminals in the Auditory System

In the auditory system, electrophysiology studies focusing on synaptic transmission of L5 terminals-MGD synapses are largely missing (but see Williamson and Polley, 2019, who recorded extracellularly L5 CT neurons in auditory cortex). This contrasts with the abundance of anatomical studies that undoubtedly show the driver-like properties of L5 terminals synapsing on neurons in MGD (Bajo et al., 1995; Rouiller and Welker, 2000; Llano and Sherman, 2008). Overall, L5 axons resemble in their structure and synaptic contacts the ascending, driving inputs that carry sensory messages to the thalamus (Sherman and Guillery, 1998). As Bajo et al. (1995) noted, the giant L5 corticothalamic boutons are reminiscent of the large auditory nerve endings, the so-called endbulbs of Held, that innervate cells in the ventral cochlear nucleus (Ramón y Cajal, 1904), as well as the calyces of Held in the medial nucleus of the trapezoid body (Held, 1891). These auditory nerve endings are known to provide highly secure synapses, with large and fast EPSCs that show strong activity-dependent synaptic depression due to their large probability of vesicle release (Pr; Schneggenburger et al., 1999; Antunes et al., 2020), similarly to L5 driver synapses. Given their anatomical similarities to the driver terminals in the visual and somatosensory systems, it is tempting to speculate that L5 projection should evoke large, depressing EPSCs mediated by ionotropic receptors without the contribution of metabotropic receptors (Li et al., 2003; Reichova and Sherman, 2004; Lee and Sherman, 2011). Furthermore, the burst-firing mode of L5 CT neurons in auditory cortex enables the transmission of a highly secure signal well-suited for a driver synapse (Llano and Sherman, 2009). Consistent with this, a few neurons (4 out of 24) recorded *in vivo* from the MGD of anesthetized rats had their sound-evoked responses eliminated during reversible cortical deactivation, suggesting that these responses were inherited from L5 driver axons (Antunes and Malmierca, 2011). However, this study deactivated the entire auditory cortex making it impossible to disentangle the effects of L5 or L6 on the observed thalamic responses. *In vivo* and *in vitro* studies manipulating specific layers and regions of the auditory cortex are needed to confirm that L5 terminals effectively behave as drivers of auditory thalamic activity, following the rule of the other sensory systems studied so far.

L5 CORTICOTHALAMIC PROJECTIONS INITIATE TRANSTHALAMIC CORTICOCORTICAL PATHWAYS

The message conveyed by L5 to the thalamus is then feedforwarded to the cortex to form a non-reciprocal corticothalamocortical circuit by which activity in a lower order cortical area is distributed, *via* the thalamus, to a higher order cortical area (visual, somatosensory and motor system; Kato, 1990; Theyel et al., 2010; Sherman, 2016; Mo and Sherman, 2019). Llano and Sherman (2008) provided anatomical evidence that L5 CT projections emanating from A1 are endowed with the properties necessary to initiate such a transthalamic circuit. L5 of A1 projects non-reciprocally to the MGD *via* driver-like terminals (Rouiller and Welker, 1991; Ojima, 1994; Bartlett et al., 2000), and then route this information to A2 (Llano and Sherman, 2008). Theyel et al. (2010) showed that these transthalamic pathways can effectively transfer information between somatosensory cortical areas. They used flavoprotein autofluorescence *in vitro* to demonstrate that stimulation of L5B, but not L6, in primary somatosensory cortex drove robust activity in higher-order somatosensory cortex, *via* corticothalamocortical pathway activation (Theyel et al., 2010). Information transfer between primary and secondary areas continued even after permanent disruption of the direct corticocortical afferents connecting them and was only interrupted by chemically induced thalamic inhibition (Theyel et al., 2010).

Transthalamic Pathways Can Connect Functionally Distinct Cortical Areas

The existence of transthalamic pathways paralleling the direct, hierarchical corticocortical pathways, is not restricted to communication circuits between primary and secondary auditory, visual, and somatosensory areas, but can be a more general principle bridging functionally distinct cortical areas, similar to what occurs in most higher order nuclei that receive connections from and project to multiple cortical areas (Mo and Sherman, 2019; Zajzon and Morales-Gregorio, 2019; Lohse et al., 2021). Optogenetic stimulation of a small local cluster of L5 primary visual cortical neurons in the *in vivo* mouse brain is sufficient to initiate and propagate corticothalamic Ca2+ waves as a global neuronal wave of activity *via* long-range corticothalamic integration (Stroh et al., 2013).

In the auditory system, Lohse et al. (2021) unraveled a multisensory circuit by which activation of primary somatosensory cortex by whisker stimulation suppresses

responses to auditory stimuli in A1, which is implemented by a crossmodal circuit connecting somatosensory cortex, *via* auditory midbrain, to A1-projecting MGB neurons (corticocolliculo-thalamocortical circuit; **Figure 7**). This study demonstrates a clear role for the auditory thalamus, midbrain and descending connections in bridging cortical areas that belong to different sensory systems, as an alternative to direct corticocortical pathways (Lohse et al., 2021). It is unknown, however, if L5 is involved in the corticocolliculo-thalamocortical circuit. However, a direct projection from L5 in somatosensory cortex to the MGM exists and has been shown to facilitate responses to auditory stimuli in the MGM (Lohse et al., 2021), a nucleus that projects to other cortical areas (**Figure 7**; for a review see Bartlett, 2013).

Strong evidence that L5 transthalamic pathways can bridge distant and functionally distinct cortical areas comes from a study by Mo and Sherman (2019). They demonstrated that a transthalamic circuits exists between the primary somatosensory cortex and the primary motor cortex through the POm. This sensorimotor circuit is initiated in L5 primary somatosensory cortex and shows driver properties at both the corticothalamic and thalamocortical synapses. The demonstration that the primary motor cortex is involved in a transthalamic non-reciprocal circuit just like the sensory cortices, challenged previous ideas that higher order cortices would diverge from this model, with connections instead organized in reciprocal loops (Svoboda and Li, 2018; Collins and Anastasiades, 2019). Work by Guo et al. (2018) reveals that in fact this distinct organization in higher-order motor regions exists, where neurons in the ventromedial thalamus receive L5 and L6 inputs from the same high order cortical region, the anterolateral motor cortex, forming two parallel reciprocal loops. However, the study by Mo and Sherman (2019) shows us that these reciprocal cortical loops are not the only way by which higher order cortices (at least the primary motor cortex) interact with thalamic nuclei *via* L5 pyramidal neurons. The interesting discussion initiated by Collins and Anastasiades (2019) is far from being over. Most likely, the complexity of corticothalamocortical circuits will continue to surprise us as more studies come to light.

Evidence for Convergence of Cortical and Subcortical Driver Inputs in Higher Order Thalamic Neurons

A largely unresolved and very interesting question is whether thalamic processing in higher order thalamus involves significant integration of information from convergent driver inputs. While it is generally assumed that integration occurs at cortical level rather than at the thalamus (Sherman, 2017), very interesting evidence exists that L5 and subcortical driver inputs converge and interact onto single neurons in higher order somatosensory thalamus (POm; Groh et al., 2008, 2014). Such convergence occurs when both cortical and thalamic driver inputs are active, leading to non-linear responses driven by the coincidence of these inputs within a well-defined time window, similarly to a "AND-gate" response (in an AND-gate the output equals the binary product of the inputs, meaning that a cell can only transfer the combination of the two inputs; Groh et al., 2014; Ahissar and Oram, 2015). This evidence proposes an alternative model by which thalamic neurons act as integrators of the sensory and cortical information they receive, and it is this integrated activity that they transfer back to the cortical network (Groh et al., 2014; Ahissar and Oram, 2015). Anatomical evidence suggests that the convergence of cortical and subcortical driver afferents is not widespread through the thalamus but is restricted to well-defined thalamic territories at the boundaries of first- and higher-order territories (e.g., border regions of the ventrolateral nucleus with the lateral pulvinar; Rovó et al., 2012).

The model proposed by Groh et al. (2014) entails a powerful control of ascending sensory information at the level of the thalamus by cortical L5: a strong instructive cortical signal summates with sensory information. Thus, a sensory stimulus can be fundamentally changed in the thalamus by L5 descending cortical signals and thus be perceived differently by the cortex (Groh et al., 2014). In this scenario, the role of the transthalamic pathway at the thalamic junction gains another dimension, by incorporating information from the ascending, sensory pathway before feedforwarding information to a higher order cortical region. Hypothetically, this could be a strategy for enhancing behaviorally relevant environmental features. It might be interesting in the context of model-based inferences, such as those implicated in predictive processing framework (Rao and Ballard, 1999; Friston, 2005). These theoretical frameworks rely on comparisons between prior information—in the form of prediction- and incoming sensory information (Friston, 2005; Bastos et al., 2012). In this context, the convergence of L5 CT signals with sensory information in higher order thalamic neurons (Groh et al., 2014), would enable these neurons to extract possible relationships and/or discrepancies between cortical and peripheral information (as contemplated in predictive processing frameworks; Friston, 2005; Kanai et al., 2015; discussed in section Role of Corticothalamic Pathways in the Implementation of Predictive Processing Frameworks).

The Transthalamic Pathway Is Not Just a Relay of Information Between Cortical Regions

The view of transthalamic pathways (and the thalamus) as higher order circuits that relay information between cortical regions is now recognized to be incomplete. Multiple lines of evidence suggest that the thalamus operates as a master regulator of functional cortical connectivity within and between cortical areas *via* transthalamic pathways (Nakajima and Halassa, 2017; and perhaps concurrently with feedback pathways, Jaramillo et al., 2019). By such regulatory power, the thalamus can modulate attention (Saalmann et al., 2012; Zhou et al., 2016; Schmitt et al., 2017), impact language processing (Crosson, 2019), participate in working memory and encode confidence during decision making (Komura et al., 2013; Jaramillo et al., 2019). Considering that the thalamus receives abundant projections from subcortical, cortical and neuromodulator regions, thalamic circuits seem to be uniquely suited to provide contextual modulation to cortical computations associated with cognition (Rikhye et al.,

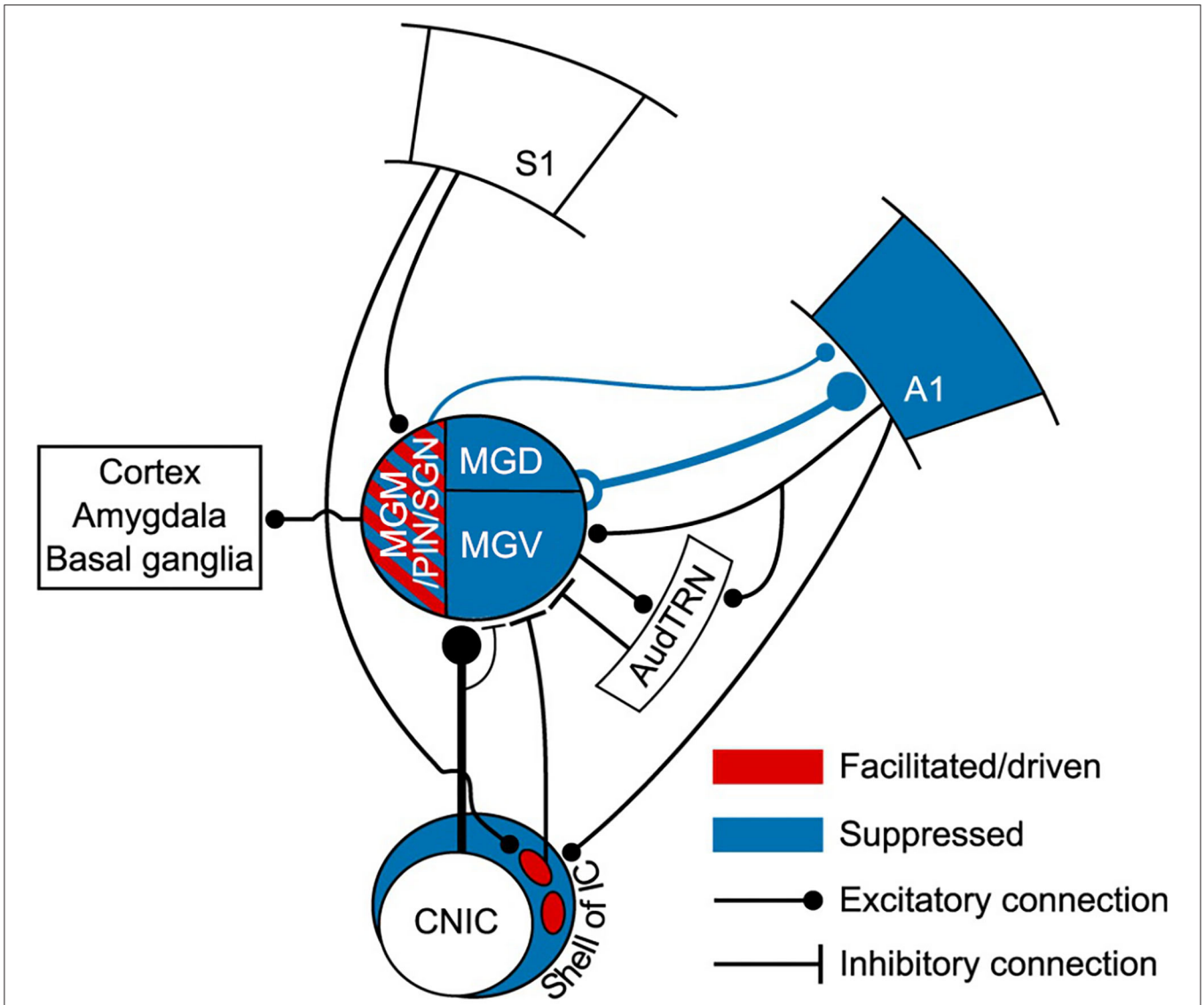

FIGURE 7 | Auditory thalamus and midbrain bridging primary somatosensory cortex (S1) to primary auditory cortex (A1). This scheme summarizes the findings of Lohse et al. (2021) study. This study elegantly undisclosed the multisensory circuits by which the primary somatosensory cortex controls activity in the thalamocortical system in mice. In blue, regions of the auditory system (midbrain, thalamus and A1) that were suppressed to auditory stimulation (tones) by concurrent whisker stimulation (whisker deflection). Suppression occurred via a descending connection from S1 to neurons in the lateral shell of the inferior colliculus that project to the MGB. This resulted in a suppression of thalamocortical neurons and suppression of auditory activity in A1. Altogether, this forms a corticocolliculo-thalamocortical multisensory circuit by which somatosensory information exerts a dominance over auditory processing in A1. In red, some neurons in the medial sector of the auditory thalamus, including the MGM, had their auditory responses enhanced or driven with whisker stimulation. A direct connection arising in L5 of S1 to the medial sector of the MGB could mediate this enhancement. Because the MGM projects to cortical areas, including A1, this could form a transthalamic circuit bridging S1 to AC. However, this hypothesis needs further confirmation. A1, primary auditory cortex; AudTRN, auditory sector of the thalamic reticular nucleus; CNIC, central nucleus of the inferior colliculus; MGM/PIN/SGN, medial subdivision of the MGB/posterior intralaminar nucleus/suprageniculate nucleus; MGD, dorsal subdivision of the MGB; MGV, ventral subdivision of the MGB; S1, primary somatosensory cortex. Adapted from Lohse et al. (2021).

2018; Wolff and Vann, 2019). Using computational modeling, Jaramillo et al. (2019) aggregates these ideas that altogether sustain that higher order thalamus *via* corticothalamic pathways participates in major cognitive functions and is implicated in psychiatric disorders. Furthermore, they show that transthalamic and feedback pathways (concurrently) participate in frequency-dependent inter-areal interactions that modify the relative hierarchical positions of cortical areas (Saalmann et al., 2012; Zhou et al., 2016; Jaramillo et al., 2019).

The extent to which signal transmission in the cortex is routed *via* transthalamic pathways is unknown (Sherman, 2016). The studies that we have reviewed above support the notion that higher order thalamus can use task-dependent contextual information to shape cortical responses (Kanai et al., 2015;

Jaramillo et al., 2019). Because of the computational capabilities of the thalamo-cortical circuit, Jaramillo et al. (2019) suggests that thalamic nuclei predominantly modulate cortical computations. It is possible that circuits dedicated to encoding contextual information cohabit with circuits relaying information (or other computations) in the same thalamic nucleus. The utilization of these circuits according to behavioral demands can underlie attention, working memory and decision-making (Rikhye et al., 2018).

Evidence for Top-Down Transthalamic Pathways

An interesting possibility is that the transthalamic pathways described above, which convey information up the cortical hierarchy *via* driver connections, are accompanied by transthalamic pathways that convey modulatory information down the cortical hierarchy (Sherman, 2017). From a cortical perspective, the first could be considered as bottom-up (feedforward, driver) pathways, whereas the second could be considered as top-down (feedback, modulatory) pathways. Making a parallelism with the corticothalamic loop, where feedforward thalamocortical connections are accompanied by feedback CT connections (L6a feedback) to form a corticothalamic loop, the feedforward transthalamic connections could (hypothetically) be accompanied by feedback transthalamic connections to form a transthalamic corticocortical loop. However, there is still no direct evidence that such transthalamic top-down, modulatory pathways exist. Evidence exists that higher order thalamic nuclei provide modulator inputs to first order, primary cortical areas in visual (Purushothaman et al., 2012; Roth et al., 2016), somatosensory (Viaene et al., 2011) and auditory systems (Pardi et al., 2020). Because modulation is provided by a higher order thalamic nucleus to a lower order cortical area, these circuits can be viewed as descending, top-down circuits. Using a combination of optogenetics, whole-cell recordings, behavior, and computational modeling, Pardi et al. (2020) identified an auditory top-down circuit that conveys information about the experience-dependent behavioral relevance of sounds from higher order auditory thalamus (all nuclei surrounding the MGV) to layer 1 in primary auditory cortex (anatomical evidence for this pathway in classical studies: Lorente de No, 1938; Malmierca et al., 2002). Interestingly, synaptic transmission in A1 is in turn modulated by local inhibition acting on GABAB receptors at the presynaptic thalamic terminal. Because higher order thalamic neurons that specifically project to A1 receive inputs from a diversity of higher order cortical areas (e.g., secondary auditory and association cortices), the top-down circuit identified by Pardi et al. (2020) might well be part of a transthalamic feedback circuit that conveys internally generated top-down signals. At the thalamic node, these top-down signals have the chance to be integrated and compared with sensory information conveyed by subcortical inputs to A1-projecting thalamic neurons (e.g., superior colliculus and external cortex of the inferior colliculus; Malmierca et al., 2002; Cai et al., 2019; Pardi et al., 2020).

Such transthalamic feedback pathways would provide modulatory or non-linear context-sensitive effects consistent with the tenets of predictive coding (Friston, 2005; Bastos et al., 2012). In this context, the fact that synaptic transmission of higher order MGB-A1 neurons synapses can be modulated by local inhibition in L1 as Pardi et al. (2020) demonstrated, is particularly interesting because it provides the computational flexibility that feedback connections require to convey predictions in a context-sensitive manner (Bastos et al., 2012; discussed in section Role of Corticothalamic Pathways in the Implementation of Predictive Processing Frameworks).

ROLE OF CORTICOTHALAMIC PATHWAYS IN THE IMPLEMENTATION OF PREDICTIVE PROCESSING FRAMEWORKS

Predictive coding frameworks envisage the brain as a predictive machine that is highly constrained by prior experiences, where signals from the external world shape but do not drive perception. Perception is viewed as an entirely inferential process in which higher brain areas use generative models to make predictions about the outside world and inform lower brain areas of these predictions (Rao and Ballard, 1999; Friston, 2005; Keller and Mrsic-Flogel, 2018). These ideas invert the conventional view of perception as a mostly bottom-up process (Sherrington, 1906), and highlight the importance of top-down, backward pathways that convey predictions to shape sensory-driven activity in lower brain areas (Helmholtz and von, 1867; Craik, 1943).

The canonical computations of predictive processing rely on the circuitry of the cortical column and connections between cortical areas, in which inference is implemented *via* message passing along the cortical hierarchy. However, as we have reviewed in the above sections, the cortex is inextricably linked to the thalamus. Any theoretical framework that ignores the strong link between cortex and thalamus will likely be incomplete (Mumford, 1991; Auksztulewicz and Friston, 2015; Kanai et al., 2015; Rikhye et al., 2018; Carbajal and Malmierca, 2020). In this section, after a brief explanation of how predictive processing is implemented (section Predictive Processing Is Implemented via Hierarchical Perceptual Inference), we will review evidence proposing that the thalamus and the CT pathways are in a key position to dynamically coordinate and contextualize hierarchical inference in cortical hierarchies (section Role of CT Pathways in Coordinating and Contextualizing Inference in Cortical Hierarchies).

Predictive Processing Is Implemented *via* Hierarchical Perceptual Inference

Higher levels generate the predictions about the pattern of sensory input they should be receiving from the level below across multiple and highly interdependent levels of processing (Bastos et al., 2012; **Figure 8)**. These predictions are the best guesses or Bayesian optimal estimates based simultaneously on both sensory data and prior experience (or beliefs) (Friston, 2005; Bastos et al., 2012). Predictions are sent down the processing hierarchy (*via* feedback, modulatory connections),

suppressing congruent incoming sensory signals by "explaining away" whatever differences, or prediction errors, they can by inferring likely causes for the discrepancies (Friston, 2005; Bastos et al., 2012). Only the unexplained components of sensory information pass to higher levels as prediction errors, conveyed by feedforward, driving connections (Friston, 2005; Bastos et al., 2012). This process requires two types of neurons: the neurons encoding the prediction (prediction neurons, associated with activity of pyramidal neurons in deep cortical layers), and the neurons comparing the prediction with the actual bottom-up input (prediction error neurons, associated with activity of pyramidal neurons in superficial cortical layers; Friston, 2005; Bastos et al., 2012; **Figure 8**). Prediction errors are progressively explained away as they climb each level of the hierarchy, while internal models at higher levels become more global and stable. In other words, the brain continuously exploits these error signals to revise and update its predictive models (new posterior beliefs) in an iterative process to produce better predictions (i.e., minimize prediction errors) with every new piece of reliable sensory evidence (Friston, 2005; Bastos et al., 2012). In this process, the different error signals are not treated equally but their relative influence is adjusted according to their precision. Error precision is estimated as the inverse variance of the prediction error and informs the brain about the relative reliability of that error (Feldman and Friston, 2010; Kanai et al., 2015). High precision errors have greater postsynaptic gain and increased influence, whereas prediction errors with very low precision may be unable to drive postsynaptic responses and lack influence (Feldman and Friston, 2010; Kanai et al., 2015).

Role of CT Pathways in Coordinating and Contextualizing Inference in Cortical Hierarchies

Predictive processing requires a dual role for backward (top-down) connections (Kanai et al., 2015; Auksztulewicz and Friston, 2016). First, it requires backward connections to exert strong inhibitory influences on their targets—the prediction error neurons on lower hierarchical areas—to suppress or counter their feedforward (bottom-up) driving inputs (Bastos et al., 2012; Auksztulewicz and Friston, 2016; **Figure 8**). However, because predictive processing requires backward connections to influence neurons in lower areas in a context-sensitive manner, it also needs non-linear (modulatory) inputs to these postsynaptic neurons (Bastos et al., 2012; Auksztulewicz and Friston, 2016). Both roles are fulfilled by L6a CT projections. L6a projections can provide excitatory, modulatory influences on thalamic relay neurons but can also effectively suppress these neurons *via* TRN-mediated inhibition (section L6a Corticothalamic Feedback Forms a Corticothalamic Loop). Since pyramidal cells in deep cortical layers are thought to convey predictions by top-down connections (Bastos et al., 2012; Kanai et al., 2015), it is reasonable to suggest that L6a projections can convey predictions to thalamic neurons (Auksztulewicz and Friston, 2015; Shipp, 2016), as we will discuss in the next section (L6a CT Projection Can Bidirectionally Switch the Excitability of Thalamic Neurons According to Contextual Information and/or Behavioral Demands). This hypothesis is particularly interesting because L6a forms part of corticothalamic loops that embody important functional architecture attributes for predictive coding (Adams et al., 2013): (1) a hierarchical organization with (2) reciprocal connections that are (3) functionally asymmetrical (thalamocortical driver vs. CT modulator). In contrast, L5 rather represents a bottom-up connection because it conveys information from a lower to a higher order region. This is consistent with the fact that L5 has a driving, feedforward nature (Sherman and Guillery, 1998; Llano and Sherman, 2008). For this reason, it is very unlikely that L5 conveys predictions to higher order thalamic nuclei (predictions are conveyed by top-down connections; Friston, 2005). Instead, L5 CT projections can be involved in prediction error related computations (Kanai et al., 2015), as we will discuss in the last section of this review (3.2.2).

L6a CT Projection Can Bidirectionally Switch the Excitability of Thalamic Neurons According to Contextual Information and/or Behavioral Demands

L6a CT projection carries the potential to either suppress or facilitate thalamic activity, through the dynamic interaction with GABAergic neurons in the TRN (Pinault, 2004; Crandall et al., 2015). This L6-TRN interaction powerfully controls the thalamus in an activity-dependent manner: low frequency CT activity primarily suppresses thalamic excitability, whereas higher frequency activity shifts CT influence from suppression to enhancement (Crandall et al., 2015; see section 1.1 for synaptic mechanisms). The suppression exerted by low frequency CT activity is compatible with the implementation of predictive coding where feedback predictions are linked to low frequency oscillations that exert a suppressive effect on prediction error units of the level below (Bastos et al., 2012). However, brief periods of sustained activity in L6 can generate a local cortical gamma rhythm that, *via* CT neurons, can quickly shift the cortical effect on thalamic excitability from suppression to enhancement (Crandall et al., 2015).

L6a CT Pathway Could Modulate the Gain of Thalamic Error Units According to Their Precision

The ability of L6 projection to bidirectionally switch the excitability of thalamic neurons would make these neurons tunable according to contextual information and/or behavioral demands (**Figure 5**; Crandall et al., 2015; Guo et al., 2017). For example, suppression of responses to predictable stimuli can coexist with (top-down) attentional enhancement of signal processing (Wyart et al., 2012). Attention has been suggested to optimize precision expectations during hierarchical inference by increasing the gain of neurons encoding prediction errors (Feldman and Friston, 2010; Auksztulewicz and Friston, 2015; Smout et al., 2019), which can override the suppressive influence of top-down expectation (Kok et al., 2012). Similarly, the hippocampus may facilitate both a prediction signal and memory, respectively, by inhibiting neocortical prediction errors or increasing their gain, a mechanism probably dependent on the precision ascribed to prediction error units (Barron et al., 2020).

An enhancement of prediction error can also be useful to facilitate perception to challenging conditions (Auksztulewicz

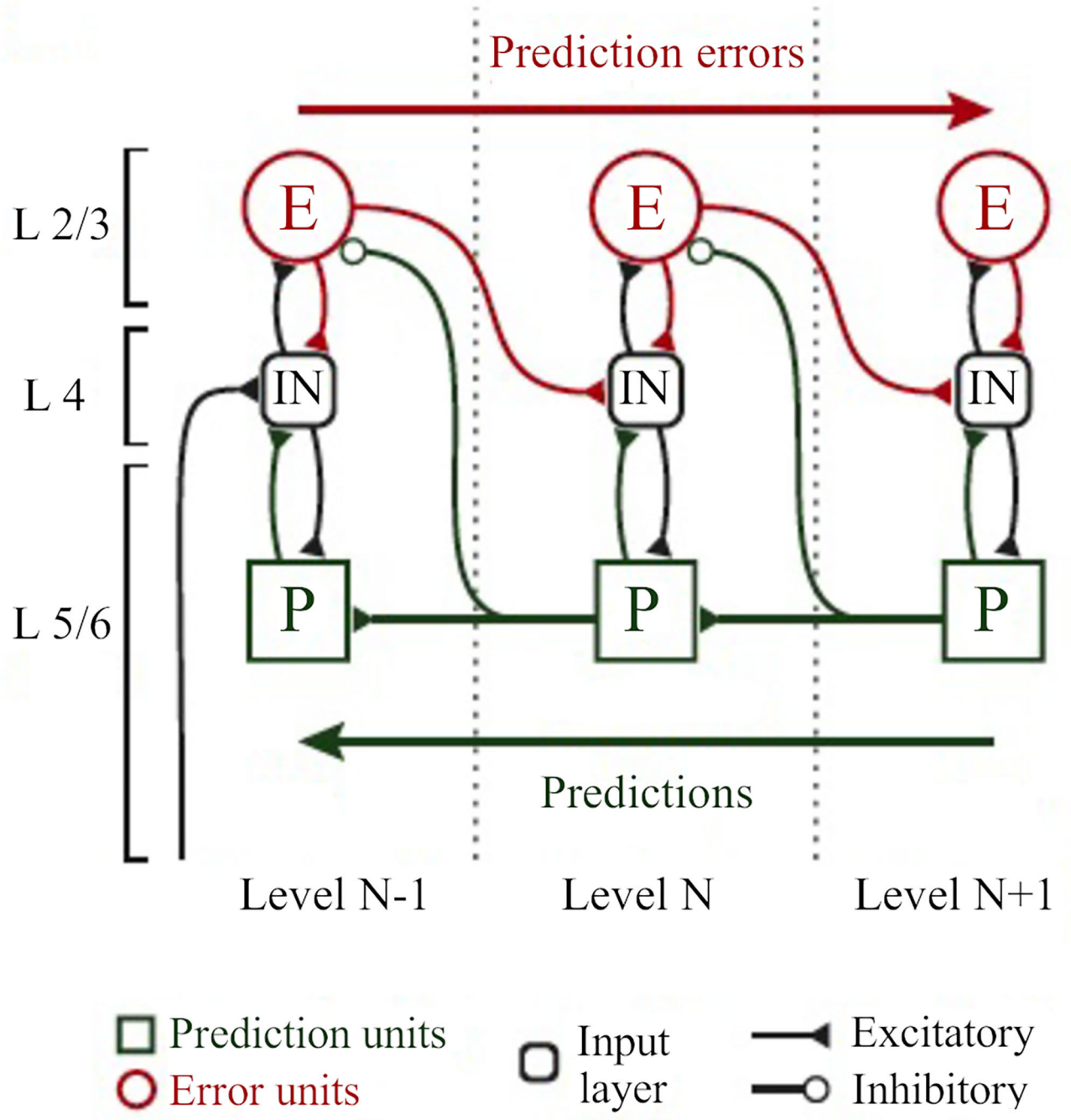

FIGURE 8 | The classical implementation of predictive coding relies on the cortical hierarchy. A simplified hierarchical model based on the classical implementation of predictive coding (Bastos et al., 2012). Vertical dashed lines delimit hierarchically arranged cortical columns (left to right: bottom up). Prediction errors climb up the cortical hierarchy through the feedforward, bottom-up connections, whereas predictions are sent backwards (top-down) to suppress prediction error units of the levels below, via inhibitory connections. Superficial layers (L2/3) above the subcortical input layer (L4) carry prediction errors, whereas deep cortical layers (L5/6) carry predictions. Adapted, with permission, from Heilbron and Chait (2018) and Carbajal and Malmierca (2020).

and Friston, 2016), such as to improve detection of low salience visual (Hup et al., 1998) and auditory stimuli (Parras et al., 2017), but also to detect a salient acoustic event in the natural soundscape while performing a competing attentional task (Huang and Elhilali, 2020) or a novel event while listening passively or actively to multiple concurrent acoustic sources

(Sohoglu and Chait, 2016). Accordingly, behavioral detection of low salience sounds is improved by the enhancement of tone-evoked cortical responses (Guo et al., 2017). This cortical enhancement is driven by CT influences and arises from an intrathalamic shift in excitatory-inhibitory balance between the auditory thalamus and the TRN (responses are increased in the MGV and reduced in the TRN; **Figure 5**; Guo et al., 2017). An enhanced thalamic response driven by CT influences can also be a mechanism to compensate for impaired, age-related ascending auditory signals (Cai et al., 2016). Under this scenario, L6 CT projections would have the potential to perform two complementary tasks needed for predictive processing: (1) the ability to convey predictions of perceptual content (first order predictions) that will suppress thalamic neurons encoding prediction errors (*via* TRN inhibition); and (2) the ability to convey predictions of precision (second order predictions) that carry context information in the form of salience or precision ascribed to these prediction errors in order to change their gain (excitatory modulatory effect; higher precision, higher excitation). Whether L6 can perform these tasks is still unknown, but the remarkable ability of L6 to switch the excitatory-inhibitory balance of thalamic neurons (Crandall et al., 2015; Guo et al., 2017) suggests that L6 can provide gain control over thalamic neurons compatible with precision weighting (Kanai et al., 2015).

Suppression and Enhancement Coexist in Auditory Thalamic Neurons That Signal a Deviance From Previous Stimulus Context

In higher order auditory thalamus (medial and dorsal subdivisions), suppression of repeated sounds coexists with enhancement to rare, surprising sounds in single neurons, the so-called stimulus-specific adaptation (SSA; **Figure 2**; Ulanovsky et al., 2003) or neuronal mismatch (Parras et al., 2017). This property is not restricted to the thalamus but is distributed hierarchically from as early as the auditory midbrain to the auditory cortex and prefrontal cortex (some classical studies: AC, Ulanovsky et al., 2003; inferior colliculus, Pérez-González et al., 2005; TRN, Yu et al., 2009; MGB, Antunes et al., 2010; prefrontal cortex, Casado-Román et al., 2020). Classically, SSA is elicited using an oddball paradigm, where two tones that differ in their probability of appearance in a sequence are played (a repeated sound interrupted randomly by a deviant sound; **Figure 2**). As we progress along the auditory hierarchy, responses to the repeated sound are suppressed, but responses to the deviant are enhanced. Responses to the deviant are maximal in prefrontal cortex (Casado-Román et al., 2020). Because their enhanced responses to surprising sounds cannot be explained solely by bottom-up mechanisms of neural fatigue, these neurons are believed to signal expectancy deviance that can be regarded as a prediction error signal (Parras et al., 2017; Malmierca et al., 2019; Hamm et al., 2021). This enhancement would be the result of modulatory mechanisms exerted by higher order cortical areas (e.g., prefrontal cortex; Hamm et al., 2021) and/or neuromodulatory gain mechanisms compatible with precision-weighting (e.g., dopaminergic neuromodulation; Valdés-Baizabal et al., 2020). For example, in awake rats, this enhancement is stronger when the intensity of stimulation is low. A gain mechanism to facilitate perceptual saliency could underlie this enhancement (Parras et al., 2017; Carbajal and Malmierca, 2018). Although SSA in the MGB is not inherited from the auditory cortex (**Figure 2**; Antunes and Malmierca, 2011), it is still unknown if this error enhancement is generated by cortical influences, because Antunes and Malmierca (2011) did not use the control sequences used to discern between repetition suppression and error enhancement (for details, see Parras et al., 2017; Casado-Román et al., 2020).

The Gain Exerted by the Auditory Cortex on Thalamic Neurons Depends on Their Context-Sensitivity

Although SSA is not inherited from the AC, the AC modulates the excitability of thalamic neurons in a gain-like mechanism that depends on their level of SSA (**Figures 2–4**; section L6a Corticothalamic Feedback Forms a Corticothalamic Loop; Antunes and Malmierca, 2011). By mainly suppressing high SSA neurons and facilitating non-SSA neurons, the cortex, *via* CT pathways, seems to discriminate between neurons that encode prediction errors (context sensitive, high SSA), and those that perform other type of computations (non-SSA; Antunes and Malmierca, 2011; **Figure 4**). The suppression of SSA neurons is consistent with an overall inhibitory effect of backward projections (conveying predictions) on prediction error units of the level below (Bastos et al., 2012; **Figure 2A**). In this case, a precise prediction (repetition of the standard tone) is sent backwards to suppress or "explain away" the sensory prediction error (Auksztulewicz and Friston, 2016). However, some of these prediction error units (high SSA) in the thalamus are facilitated by the cortex (**Figure 2B**; Antunes and Malmierca, 2011). Hypothetically, this facilitation could be the result of precision-weighting gain mechanisms imposed by CT pathways, probably elicited by the unexpected appearance of a deviant sound (Hamm et al., 2021). However, in our opinion, the discussion of whether SSA neurons are prediction error units in terms of predictive coding is highly speculative. If SSA neurons are indeed error units, they should be accompanied by activity of neurons encoding expectancy in upper hierarchical levels (see Fiser et al., 2016, for an elegant protocol and experiment of this kind). We do not yet have such evidence for SSA (but see Hamm et al., 2021). It remains an open question if the effects observed using the oddball paradigm in single units are a consequence of perceptual expectations.

L5 and the Pulvinar at the Crossroads of Contextual Information

The Pulvinar is the multisensory higher order thalamic nucleus per excellence. Because it receives inputs from a diversity of cortical and subcortical areas (e.g., superior colliculus), the pulvinar is uniquely positioned to provide sensory and contextual information to cortical computations (Roth et al., 2016; Jaramillo et al., 2019; Chou et al., 2020). For example, the rodent homolog of the pulvinar (lateral posterior nucleus), conveys diverse contextual information to primary visual cortex neurons that informs these neurons about changes in external motion not predicted by the animal's own actions (Ishiko and

Huberman, 2016; Roth et al., 2016). In the auditory system, the lateral posterior nucleus, driven by input from the superior colliculus, provides contextual and cross-modality modulation of A1 responses to enhance the salience of acoustic information (Chou et al., 2020). Specifically, it contributes to the maintenance and enhancement of A1 processing, respectively, in the presence of background noise and threatening visual looming stimuli.

The mouse pulvinar can strongly influence the activity of extrastriate cortical neurons, and particularly of those that project to the striatum and amygdala (Zhou et al., 2018). Because the pulvinar also projects to the striatum and amygdala, Zhou et al. (2018) proposed that the pulvinar can function as a hub linking the visual cortex with subcortical regions involved in coordinating body movement and sensory information (Roth et al., 2016). The fact that the pulvinar exerts strong influences on extrastriate cortical areas challenges the conventional hierarchical view of visual cortical processing in which information transfer to extrastriate areas occurs primarily *via* corticocortical connections (van Essen, 2005; Zhou et al., 2018). However, the rodent pulvinar is not a homogeneous nucleus but has distinct subregions (Nakamura et al., 2015; Foik et al., 2020; Scholl et al., 2021). Based on connectivity and functional properties, Bennett et al. (2019) distinguished three subregions in the mouse pulvinar. The posterior-dorsal subregion is driven by the superior colliculus and responds to looming stimuli and small moving objects, whereas the anterior-ventral region is driven by visual cortex and responds to large stimuli and full-filled motion (Bennett et al., 2019). Their study further suggests that a medial subregion might be involved in transthalamic pathways connecting frontal and associational cortex to visual cortices (Bennett et al., 2019).

The pulvinar provides contextual and cross-modality information to A1 (Chou et al., 2020). However, it certainly processes contextual auditory information in a different way than visual information. Perhaps the analog structure of the visual pulvinar in the auditory system could be the MGM, the principal multisensory subdivision of the auditory thalamus (for a review see Bartlett, 2013). The MGM is intensively connected with auditory and non-auditory cortical areas (e.g., somatosensory cortex; Lohse et al., 2021), other sensory areas (e.g., visual, somatosensory and vestibular), and, like the pulvinar, projects to the amygdala and striatum (for a review see Bartlett, 2013).

Kanai et al. (2015) proposed a model were neurons in higher order multisensory thalamic nucleus such as the pulvinar would encode expected precision (**Figure 9**). This model predicts two different types of streams of information between thalamus and cortex: the first-order streams convey predictions and prediction errors between first order thalamic nucleus and primary cortical areas, *via* L6 CT feedback connections; and the second order streams convey precision-related information between (lower and higher order) cortical areas and higher order thalamic nuclei (**Figure 9**). This model includes neurons in deep pyramidal cells of (lower and higher order) cortical areas encoding the amplitude of prediction error (squared) that inform, *via* L5 projections, posterior expectations about precision in the cells of the pulvinar (Kanai et al., 2015; **Figure 9**). Here, it is assumed that these neurons in the pulvinar send a reciprocal feedback to modulate the gain of superficial pyramidal cells in the cortex. This in accordance with Bennett et al. (2019) study in the rodent pulvinar that suggests that L5 participates in reciprocal cortico-pulvinar feedback loops. This model implies that L5 itself forms part of corticothalamic loops that would coordinate precise (direct) corticocortical message passing among different cortical areas (Kanai et al., 2015; **Figure 9**). Under this scenario, inference about the first order content of perception is attributed to direct corticocortical message passing, whereas parallel transthalamic connections contextualize (second order) corticocortical processing *via* precision-weighted gain control of ascending prediction errors (Kanai et al., 2015).

CONCLUSIONS AND FUTURE DIRECTIONS

The diversity and abundance of CT circuits that tightly link the cortex to the thalamus underscores the functional importance of these circuits to brain function. In recent years, the use of genetic tools to selectively manipulate layer or cell-type specific neuronal populations combined with electrophysiology in the awake animal opened the possibility to directly test the role of CT pathways in behavior (e.g., L6a CT circuit; Guo et al., 2017; Clayton et al., 2021). Importantly, the use of these genetic tools is unraveling a much more complex and diverse CT circuitry than previously evaluated through classical anatomical and physiological studies. The recent discovery that neurons in L6b participate in a CT circuit that differs from both L6a and L5 circuits (Ansorge et al., 2020; Zolnik et al., 2020), just reflects how sparse our knowledge still is about corticothalamic interactions. In the auditory system, specifically, basic physiological studies are lacking regarding L6b and L5 CT circuits. However, new exciting evidence is unraveling the importance of L6a CT feedback in auditory behavior (e.g., perception of complex sounds; Homma et al., 2017).

In this review we have paid particular attention to the transthalamic circuits mediated by L5 CT neurons. The disclosure of their roles, although still incipient, largely contributed to pull apart the old, corticocentric ideas that the thalamus is a passive relay center receiving instructions from the cortex. The existence of transthalamic corticocortical routes challenges the prevailing view that cortical areas communicate with each other exclusively by means of direct, hierarchical corticocortical connections (Felleman and van Essen, 1991; Sherman and Guillery, 2011). Are transthalamic pathways just redundant circuits that convey the same information between cortical areas as the direct corticocortical connections? The radically different anatomical architecture of these routes makes this hypothesis highly unlikely (Usrey and Sherman, 2019). Taking as an example the connection between primary somatosensory cortex and primary motor cortex, the cells of origin of the direct and transthalamic corticocortical routes represent separate populations (Mo and Sherman, 2019). Furthermore, higher order thalamic nuclei (e.g., the pulvinar) not only receive driver inputs from L5 of a lower order cortical area but integrate inputs from a diversity of cortical and

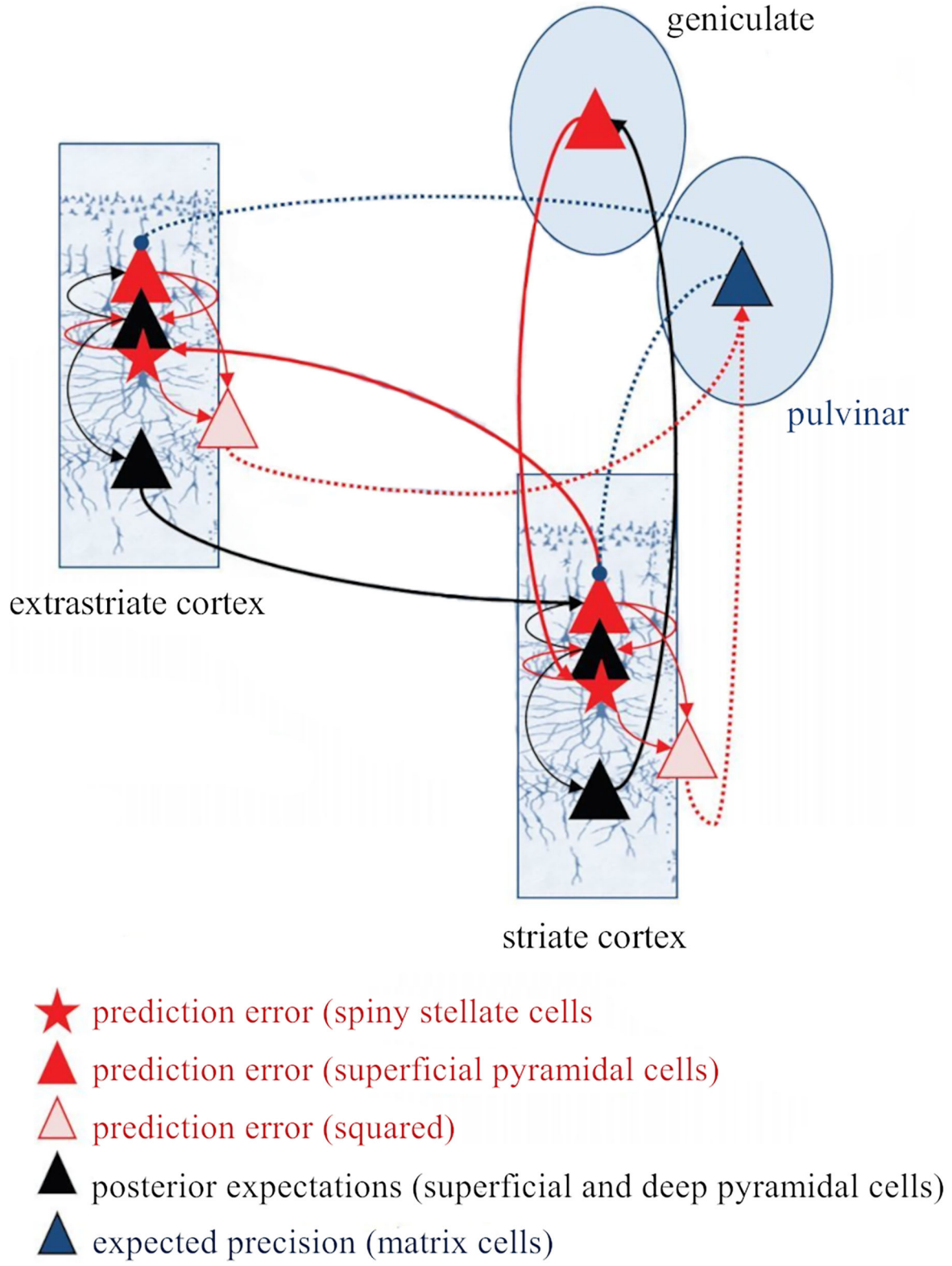

FIGURE 9 | The thalamus and the corticothalamic pathways as key players in the implementation of predictive coding. This scheme, proposed by Kanai et al. (2015) expands the classical implementation of predictive coding [Bastos et al. (2012), Shipp (2016)] as **Figure 7** shows, because it incorporates the thalamus and the

(Continued)

FIGURE 9 | corticothalamic pathways (both L6a and L5 CT projections) as key players in its implementation. A very interesting aspect of this model is the inclusion of deep pyramidal cells (presumably L5 CT cells) that convey the squared prediction error (second-order forward connections) to enable the pulvinar (matrix cells) to estimate precision. These cells in the pulvinar send back projections to modulate the gain of superficial pyramidal cells in the cortex. Red, forward connections; Black, backward connections; Full lines, first order streams; Dashed lines, second order (precision-related) streams. CT, corticothalamic; L5, cortical layer 5; L6a, cortical layer 6a. Adapted from Kanai et al. (2015).

subcortical areas (e.g., superior colliculus), offering the possibility of combining sensory signals with the context in which they arise (Roth et al., 2016; Blot et al., 2020; Chou et al., 2020). It is possible that the direct and transthalamic corticocortical routes dynamically interact, and that the recurrent activity resultant from this interaction would allow for the shaping of neural activity necessary for high-level cognitive processes (e.g., language processing; Crosson, 2019).

A remarkable difference between transthalamic and direct corticocortical routes lies on their extrinsic connection targets. Direct projections involve axons without subcortically directed branches (Bourassa and Deschênes, 1995), whereas L5 axons of the transthalamic pathway branch extensively to target extra-thalamic structures in the brainstem and spinal cord as well as higher order thalamic regions and the amygdala (Deschênes et al., 1994; Usrey and Sherman, 2019; Williamson and Polley, 2019). Therefore, the message passing along the cortical hierarchy *via* transthalamic pathways is broadcasted to other subcortical centers (Williamson and Polley, 2019). Many of these centers are motor in nature (e.g., tectum, striatum), suggesting that L5 far-ranging CT axons (including those in primary sensory areas) may be involved in sensorimotor behavior (Prasad et al., 2020).

As descending pathways that enable reciprocal and context-dependent communication between thalamus and cortex, we venture that CT projections are particularly interesting in the context of hierarchical perceptual inference formulations such as those contemplated in predictive processing schemes (Friston, 2005), which so far heavily rely on cortical implementations. However, the thalamus, and particularly higher order thalamus, is in a key position to coordinate and contextualize hierarchical inference in cortical hierarchies (Kanai et al., 2015). An expanded, upgraded version of predictive coding that includes the role of corticothalamic interactions or even (recursive) coupling with other subcortical structures (Auksztulewicz and Friston, 2015; Kanai et al., 2015; Barron et al., 2020), will certainly broaden its explanatory power.

AUTHOR CONTRIBUTIONS

FMA and MSM: conceptualization and planning. FMA: writing—original draft and review and editing. MSM: review and editing. Both authors contributed to the article and approved the submitted version.

FUNDING

This work was supported by the Spanish *Agencia Estatal de Investigación* [(AEI), PID2019-104570RB-I00] and Junta de Castilla y León, (SA252P20) to MSM. FMA held a postdoctoral fellowship from the University of Salamanca (*Contratos Postdoctorales, USAL, Programa II*).

REFERENCES

Abbott, L. F., and Regehr, W. G. (2004). Synaptic computation. *Nature* 431, 796–803. doi: 10.1038/nature03010

Adams, R. A., Shipp, S., and Friston, K. J. (2013). Predictions not commands: active inference in the motor system. *Brain Struct. Funct.* 218, 611–643. doi: 10.1007/s00429-012-0475-5

Ahissar, E., and Oram, T. (2015). Thalamic relay or cortico-thalamic processing? Old question, new answers. *Cereb. Cortex* 25, 845–848. doi: 10.1093/cercor/bht296

Aitkin, L. M., and Dunlop, C. W. (1969). Inhibition in the medial geniculate body of the cat. *Experi. Brain Res.* 7, 68–83. doi: 10.1007/BF00236108

Ansorge, J., Humanes-Valera, D., Pauzin, F. P., Schwarz, M. K., and Krieger, P. (2020). Cortical layer 6 control of sensory responses in higher-order thalamus. *J. Physiol.* 598, 3973–4001. doi: 10.1113/JP279915

Antunes, F. M., and Malmierca, M. S. (2011). Effect of auditory cortex deactivation on stimulus-specific adaptation in the medial geniculate body. *J. Neurosci.* 31, 17306–17316. doi: 10.1523/JNEUROSCI.1915-11.2011

Antunes, F. M., Nelken, I., Covey, E., and Malmierca, M. S. (2010). Stimulus-specific adaptation in the auditory thalamus of the anesthetized rat. *PLoS ONE* 5:14071. doi: 10.1371/journal.pone.0014071

Antunes, F. M., Rubio, M. E., and Kandler, K. (2020). Role of GluA3 AMPA receptor subunits in the presynaptic and postsynaptic maturation of synaptic transmission and plasticity of endbulb-bushy cell synapses in the cochlear nucleus. *J. Neurosci.* 40, 2471–2484. doi: 10.1523/JNEUROSCI.2573-19.2020

Asilador, A. R., and Llano, D. A. (2020). Top-down inference in the auditory system: Potential roles for corticofugal projections. *Front. Neural Circuits* 14:615259. doi: 10.3389/fncir.2020.615259

Auksztulewicz, R., and Friston, K. (2015). Attentional Enhancement of Auditory Mismatch Responses: a DCM/MEG Study. *Cerebral Cortex* 25, 4273–4283. doi: 10.1093/cercor/bhu323

Auksztulewicz, R., and Friston, K. (2016). Repetition suppression and its contextual determinants in predictive coding. *Cortex* 80, 125–140. doi: 10.1016/j.cortex.2015.11.024

Bajo, V. M., Rouiller, E. M., Welker, E., Clarke, S., Villa, A. E. P., Ribaupierre, Y., et al. (1995). Morphology and spatial distribution of corticothalamic terminals originating from the cat auditory cortex. *Hear. Res.* 83, 161–174. doi: 10.1016/0378-5955(94)00199-Z

Barron, H. C., Auksztulewicz, R., and Friston, K. (2020). Prediction and memory: A predictive coding account. *Prog. Neurobiol.* 192:101821. doi: 10.1016/j.pneurobio.2020.101821

Barthó, P., Slézia, A., Mátyás, F., Faradzs-Zade, L., Ulbert, I., Harris, K. D., et al. (2014). Ongoing network state controls the length of sleep spindles via inhibitory activity. *Neuron* 82, 1367–1379. doi: 10.1016/j.neuron.2014.04.046

Bartlett, E. L. (2013). The organization and physiology of the auditory thalamus and its role in processing acoustic features important for speech perception. *Brain Lang.* 126, 29–48. doi: 10.1016/j.bandl.2013.03.003

Bartlett, E. L., and Smith, P. H. (2002). Effects of paired-pulse and repetitive stimulation on neurons in the rat medial geniculate body. *Neuroscience* 113, 957–974. doi: 10.1016/s0306-4522(02)00240-3

Bartlett, E. L., Stark, J. M., Guillery, R. W., and Smith, P. H. (2000). Comparison of the fine structure of cortical and collicular terminals in the rat medial geniculate body. *Neuroscience* 100, 811–828. doi: 10.1016/S0306-4522(00)00340-7

Bastos, A. M., Usrey, W. M., Adams, R. A., Mangun, G. R., Fries, P., and Friston, K. J. (2012). Canonical microcircuits for predictive coding. *Neuron* 76, 695–711. doi: 10.1016/j.neuron.2012.10.038

Bennett, C., Gale, S. D., Garrett, M. E., Newton, M. L., Callaway, E. M., Murphy, G. J., et al. (2019). Higher-order thalamic circuits channel parallel streams of visual information in mice. *Neuron* 102, 477–492.e5. doi: 10.1016/j.neuron.2019.02.010

Blot, A., Roth, M., Gasler, I., Javadzadeh, M., Imhof, F., and Hofer, S. (2020). Visual intracortical and transthalamic pathways carry distinct information to cortical areas. *Neuron* 109:1996–2008.e6. doi: 10.1101/2020.07.06.189902

Bortone, D. S., Olsen, S. R., and Scanziani, M. (2014). Translaminar inhibitory cells recruited by layer 6 corticothalamic neurons suppress visual cortex. *Neuron* 82, 474–485. doi: 10.1016/j.neuron.2014.02.021

Bourassa, J., and Deschênes, M. (1995). Corticothalamic projections from the primary visual cortex in rats: a single fiber study using biocytin as an anterograde tracer. *Neuroscience* 66, 253–263. doi: 10.1016/0306-4522(95)00009-8

Buchan, M. J. (2020). A subpopulation of L6b neurons provides driver-like input to the posteromedial thalamus. *J. Physiol.* 598, 5313–5315. doi: 10.1113/JP280472

Cai, D., Yue, Y., Su, X., Liu, M., Wang, Y., You, L., et al. (2019). Distinct anatomical connectivity patterns differentiate subdivisions of the nonlemniscal auditory thalamus in mice. *Cereb. Cortex* 29, 2437–2454. doi: 10.1093/cercor/bhy115

Cai, R., Richardson, B. D., and Caspary, D. M. (2016). Responses to predictable versus random temporally complex stimuli from single units in auditory thalamus: impact of aging and anesthesia. *J. Neurosci.* 36, 10696LP−10706. doi: 10.1523/JNEUROSCI.1454-16.2016

Carbajal, G. V., and Malmierca, M. S. (2018). The neuronal basis of predictive coding along the auditory pathway: from the subcortical roots to cortical deviance detection. *Trends Hear.* 22:2331216518784822. doi: 10.1177/2331216518784822

Carbajal, G. V., and Malmierca, M. S. (2020). "Novelty processing in the auditory system: detection, adaptation or expectation?" in *The Senses: A Comprehensive Reference*, ed S. E. Fritzsch (Oxford: Elsevier). doi: 10.1016/B978-0-12-809324-5.24154-0

Casado-Román, L., Carbajal, G. V, Pérez-González, D., and Malmierca, M. S. (2020). Prediction error signaling explains neuronal mismatch responses in the medial prefrontal cortex. *PLoS Biol.* 18:e3001019. doi: 10.1371/journal.pbio.3001019

Chevée, M., Robertson, J. D. J., Cannon, G. H., Brown, S. P., and Goff, L. A. (2018). Variation in activity state, axonal projection, and position define the transcriptional identity of individual neocortical projection neurons. *Cell Rep.* 22, 441–455. doi: 10.1016/j.celrep.2017.12.046

Chou, X.-L., Fang, Q., Yan, L., Zhong, W., Peng, B., Li, H., et al. (2020). Contextual and cross-modality modulation of auditory cortical processing through pulvinar mediated suppression. *Elife* 9:e54157. doi: 10.7554/eLife.54157

Clayton, K. K., Williamson, R. S., Hancock, K. E., Tasaka, G.-I., Mizrahi, A., Hackett, T. A., et al. (2021). Auditory corticothalamic neurons are recruited by motor preparatory inputs. *Curr. Biol.* 31, 310–321.e5. doi: 10.1016/j.cub.2020.10.027

Collins, D. P., and Anastasiades, P. G. (2019). Cellular specificity of cortico-thalamic loops for motor planning. *J. Neurosci.* 39, 2577–2580. doi: 10.1523/JNEUROSCI.2964-18.2019

Crabtree, J. W. (1998). Organization in the auditory sector of the cat's thalamic reticular nucleus. *J. Comp. Neurol.* 390, 167–182.

Craik, K. J. W. (1943). *The Nature of Explanation*. Cambridge: Cambridge University Press.

Crandall, S. R., Cruikshank, S. J., and Connors, B. W. (2015). A corticothalamic switch: controlling the thalamus with dynamic synapses. *Neuron* 86, 768–782. doi: 10.1016/j.neuron.2015.03.040

Crick, F. (1984). Function of the thalamic reticular complex: the searchlight hypothesis. *Proc. Natl. Acad. Sci. U.S.A.* 81, 4586–4590. doi: 10.1073/pnas.81.14.4586

Crosson, B. (2019). The role of cortico-thalamo-cortical circuits in language: recurrent circuits revisited. *Neuropsychol. Rev.* 113, 2646–2652. doi: 10.1007/s11065-019-09421-8

Denman, D. J., and Contreras, D. (2015). Complex effects on *in vivo* visual responses by specific projections from mouse cortical layer 6 to dorsal lateral geniculate nucleus. *J. Neurosci.* 35, 9265–9280. doi: 10.1523/JNEUROSCI.0027-15.2015

Deschênes, M., Bourassa, J., and Pinault, D. (1994). Corticothalamic projections from layer V cells in rat are collaterals of long-range corticofugal axons. *Brain Res.* 664, 215–219. doi: 10.1016/0006-8993(94)91974-7

Deschênes, M., Veinante, P., and Zhang, Z.-W. (1998). The organization of corticothalamic projections: reciprocity versus parity. *Brain Res. Rev.* 28, 286–308. doi: 10.1016/S0165-0173(98)00017-4

Diamond, M. E., Armstrong-James, M., Budway, M. J., and Ebner, F. F. (1992). Somatic sensory responses in the rostral sector of the posterior group (POm) and in the ventral posterior medial nucleus (VPM) of the rat thalamus: Dependence on the barrel field cortex. *J. Compar. Neurol.* 319, 66–84. doi: 10.1002/cne.903190108

Feldman, H., and Friston, K. (2010). Attention, uncertainty, and free-energy. *Front. Hum. Neurosci.* 4:215. doi: 10.3389/fnhum.2010.00215

Felleman, D. J., and van Essen, D. C. (1991). Distributed hierarchical processing in the primate cerebral cortex. *Cereb. Cortex* 1, 1–47. doi: 10.1093/cercor/1.1.1

Fiser, A., Mahringer, D., Oyibo, H. K., Petersen, A., v, Leinweber, M., and Keller, G. B. (2016). Experience-dependent spatial expectations in mouse visual cortex. *Nat. Neurosci.* 19, 1658–1664. doi: 10.1038/nn.4385

Foik, A. T., Scholl, L. R., Lean, G. A., and Lyon, D. C. (2020). Visual response characteristics in lateral and medial subdivisions of the rat pulvinar. *Neuroscience* 441, 117–130. doi: 10.1016/j.neuroscience.2020.06.030

Frandolig, J. E., Matney, C. J., Lee, K., Kim, J., Chevée, M., Kim, S.-J., et al. (2019). The synaptic organization of layer 6 circuits reveals inhibition as a major output of a neocortical sublamina. *Cell Rep.* 28, 3131–3143.e5. doi: 10.1016/j.celrep.2019.08.048

Friston, K. (2005). A theory of cortical responses. *Philo. Transact. R. Soc. B: Biol. Sci.* 360, 815–836. doi: 10.1098/rstb.2005.1622

Golshani, P., Liu, X.-B., and Jones, E. G. (2001). Differences in quantal amplitude reflect GLuR4-subunit number at corticothalamic synapses on two populations of thalamic neurons. *Proc. Natl. Acad. Sci. U.S.A.* 98, 4172–4177. doi: 10.1073/pnas.061013698

Groh, A., Bokor, H., Mease, R. A., Plattner, V. M., Hangya, B., Stroh, A., et al. (2014). Convergence of cortical and sensory driver inputs on single thalamocortical cells. *Cereb. Cortex* 24, 3167–3179. doi: 10.1093/cercor/bht173

Groh, A., de Kock, C. P. J., Wimmer, V. C., Sakmann, B., and Kuner, T. (2008). Driver or coincidence detector: modal switch of a corticothalamic giant synapse controlled by spontaneous activity and short-term depression. *J. Neurosci.* 28, 9652–9663. doi: 10.1523/JNEUROSCI.1554-08.2008

Guillery, R. W. (1995). Anatomical evidence concerning the role of the thalamus in corticocortical communication: a brief review. *J. Anatomy* 187, 583–592.

Guo, K., Yamawaki, N., Svoboda, K., and Shepherd, G. M. G. (2018). Anterolateral motor cortex connects with a medial subdivision of ventromedial thalamus through cell type-specific circuits, forming an excitatory thalamo-cortico-thalamic loop via layer 1 apical tuft dendrites of layer 5B pyramidal tract type neurons. *J. Neurosci.* 38, 8787–8797. doi: 10.1523/JNEUROSCI.1333-18.2018

Guo, W., Clause, A. R., Barth-Maron, A., and Polley, D. B. (2017). A corticothalamic circuit for dynamic switching between feature detection and discrimination. *Neuron* 95, 180–194.e5. doi: 10.1016/j.neuron.2017.05.019

Halassa, M. M., and Sherman, S. M. (2019). Thalamocortical circuit motifs: a general framework. *Neuron* 103, 762–770. doi: 10.1016/j.neuron.2019.06.005

Hamm, J. P., Shymkiv, Y., Han, S., Yang, W., and Yuste, R. (2021). Cortical ensembles selective for context. *Proc. Natl. Acad. Sci. U.S.A.* 118:79118. doi: 10.1073/pnas.2026179118

Happel, M. F. K., Deliano, M., Handschuh, J., and Ohl, F. W. (2014). Dopamine-modulated recurrent corticoefferent feedback in primary sensory cortex promotes detection of behaviorally relevant stimuli. *J. Neurosci.* 34, 1234LP−1247. doi: 10.1523/JNEUROSCI.1990-13.2014

Harris, J. A., Mihalas, S., Hirokawa, K. E., Whitesell, J. D., Choi, H., Bernard, A., et al. (2019). Hierarchical organization of cortical and thalamic connectivity. *Nature* 575, 195–202. doi: 10.1038/s41586-019-1716-z

Hazama, M., Kimura, A., Donishi, T., Sakoda, T., and Tamai, Y. (2004). Topography of corticothalamic projections from the auditory cortex of the rat. *Neuroscience* 124, 655–667. doi: 10.1016/j.neuroscience.2003.12.027

He, J. (2003). Corticofugal modulation of the auditory thalamus. *Experi. Brain Res.* 153, 579–590. doi: 10.1007/s00221-003-1680-5

Heilbron, M., and Chait, M. (2018). Great expectations: is there evidence for predictive coding in auditory cortex? *Neuroscience* 389, 54–73. doi: 10.1016/j.neuroscience.2017.07.061

Held, H. (1891). Die centralen Bahnen des Nervus acusticus bei der Katze. Archiv für Anatomie und Physiologie. *Anatomische Abteilung* 15, 271–290.

Helmholtz, H., von (1867). *Handbuch der physiologischen Optik*. Leipzig: Voss.

Hoerder-Suabedissen, A., Hayashi, S., Upton, L., Nolan, Z., Casas-Torremocha, D., Grant, E., et al. (2018). Subset of cortical layer 6b neurons selectively innervates higher order thalamic nuclei in mice. *Cereb. Cortex* 28, 1882–1897. doi: 10.1093/cercor/bhy036

Homma, N. Y., Happel, M. F. K., Nodal, F. R., Ohl, F. W., King, A. J., and Bajo, V. M. (2017). A role for auditory corticothalamic feedback in the perception of complex sounds. *J. Neurosci.* 37, 6149LP—6161. doi: 10.1523/JNEUROSCI.0397-17.2017

Hua, L., Recasens, M., Grent-'T-Jong, T., Adams, R. A., Gross, J., and Uhlhaas, P. J. (2020). Investigating cortico-subcortical circuits during auditory sensory attenuation: A combined magnetoencephalographic and dynamic causal modeling study. *Hum. Brain Mapp.* 41, 4419–4430. doi: 10.1002/hbm.25134

Huang, N., and Elhilali, M. (2020). Push-pull competition between bottom-up and top-down auditory attention to natural soundscapes. *eLife* 9:52984. doi: 10.7554/eLife.52984

Hup,é, J. M., James, A. C., Payne, B. R., Lomber, S. G., Girard, P., and Bullier, J. (1998). Cortical feedback improves discrimination between figure and background by V1, V2 and V3 neurons. *Nature* 394, 784–787. doi: 10.1038/29537

Ibrahim, B. A., Murphy, C. A., Yudintsev, G., Shinagawa, Y., Banks, M. I., and Llano, D. A. (2021). Corticothalamic gating of population auditory thalamocortical transmission in mouse. *Elife* 10:56645. doi: 10.7554/eLife.56645

Ishiko, N., and Huberman, A. D. (2016). Life goes by: a visual circuit signals perceptual-motor mismatch. *Nat. Neurosci.* 19, 177–179. doi: 10.1038/nn.4233

Jaramillo, J., Wang, X., and Mejias, J. (2019). Engagement of pulvino-cortical feedforward and feedback pathways in cognitive computations. *Neuron* 101:23. doi: 10.1016/j.neuron.2018.11.023

Kanai, R., Komura, Y., Shipp, S., and Friston, K. (2015). Cerebral hierarchies: Predictive processing, precision and the pulvinar. *Philo. Transact. R. Soc. B: Biol. Sci.* 370:169. doi: 10.1098/rstb.2014.0169

Kato, N. (1990). Cortico-thalamo-cortical projection between visual cortices. *Brain Res.* 509, 150–152. doi: 10.1016/0006-8993(90)90323-4

Keller, G. B., and Mrsic-Flogel, T. D. (2018). Predictive processing: a canonical cortical computation. *Neuron* 100, 424–435. doi: 10.1016/j.neuron.2018.10.003

Kelly, J. P., and Wong, D. (1981). Laminar connections of the cat's auditory cortex. *Brain Res.* 212, 1–15. doi: 10.1016/0006-8993(81)90027-5

Kim, J., Matney, C. J., Blankenship, A., Hestrin, S., and Brown, S. P. (2014). Layer 6 corticothalamic neurons activate a cortical output layer, layer 5a. *J. Neurosci.* 34, 9656–9664. doi: 10.1523/JNEUROSCI.1325-14.2014

Kimura, A., Donishi, T., Okamoto, K., and Tamai, Y. (2005). Topography of projections from the primary and non-primary auditory cortical areas to the medial geniculate body and thalamic reticular nucleus in the rat. *Neuroscience* 135, 1325–1342. doi: 10.1016/j.neuroscience.2005.06.089

Kimura, A., Yokoi, I., Imbe, H., Donishi, T., and Kaneoke, Y. (2012). Auditory thalamic reticular nucleus of the rat: anatomical nodes for modulation of auditory and cross-modal sensory processing in the loop connectivity between the cortex and thalamus. *J. Comp. Neurol.* 520, 1457–1480. doi: 10.1002/cne.22805

Kok, P., Rahnev, D., Jehee, J. F. M., Lau, H. C., and de Lange, F. P. (2012). Attention reverses the effect of prediction in silencing sensory signals. *Cereb. Cortex* 22, 2197–2206. doi: 10.1093/cercor/bhr310

Komura, Y., Nikkuni, A., Hirashima, N., Uetake, T., and Miyamoto, A. (2013). Responses of pulvinar neurons reflect a subject's confidence in visual categorization. *Nat. Neurosci.* 16, 749–755. doi: 10.1038/nn.3393

Lee, C. C., and Murray Sherman, S. (2010). Drivers and modulators in the central auditory pathways. *Front. Neurosci.* 4:2010. doi: 10.3389/neuro.01.014.2010

Lee, C. C., and Sherman, S. M. (2011). On the classification of pathways in the auditory midbrain, thalamus, and cortex. *Hear. Res.* 276, 79–87. doi: 10.1016/j.heares.2010.12.012

Li, J., Guido, W., and Bickford, M. E. (2003). Two distinct types of corticothalamic EPSPs and their contribution to short-term synaptic plasticity. *J. Neurophysiol.* 90, 3429–3440. doi: 10.1152/jn.00456.2003

Li, L., and Ebner, F. F. (2016). Cortex dynamically modulates responses of thalamic relay neurons through prolonged circuit-level disinhibition in rat thalamus *in vivo*. *J. Neurophysiol.* 116, 2368–2382. doi: 10.1152/jn.00424.2016

Llano, D. A. (2013). Functional imaging of the thalamus in language. *Brain Lang.* 126, 62–72. doi: 10.1016/j.bandl.2012.06.004

Llano, D. A., and Sherman, S. M. (2008). Evidence for nonreciprocal organization of the mouse auditory thalamocortical-corticothalamic projection systems. *J. Comp. Neurol.* 507, 1209–1227. doi: 10.1002/cne.21602

Llano, D. A., and Sherman, S. M. (2009). Differences in intrinsic properties and local network connectivity of identified layer 5 and layer 6 adult mouse auditory corticothalamic neurons support a dual corticothalamic projection hypothesis. *Cereb. Cortex* 19, 2810–2826. doi: 10.1093/cercor/bhp050

Lohse, M., Bajo, V. M., King, A. J., and Willmore, B. D. B. (2020). Neural circuits underlying auditory contrast gain control and their perceptual implications. *Nat. Commun.* 11, 1–13. doi: 10.1038/s41467-019-14163-5

Lohse, M., Dahmen, J. C., Bajo, V. M., and King, A. J. (2021). Subcortical circuits mediate communication between primary sensory cortical areas in mice. *Nat. Commun.* 12:3916. doi: 10.1038/s41467-021-24200-x

Lorente de No, R. (1938). "Cerebral cortex: architecture, intracortical connections, motor projections," in *Physiology of the Nervous System*, ed J. Fulton (Oxford: Oxford University Press).

Malmierca, M. S. (2015). "Chapter 29 - auditory system," in ed F. E. Paxinos (San Diego, CA: Academic Press). doi: 10.1016/B978-0-12-374245-2.00029-2

Malmierca, M. S., Carbajal, G., v., and Escera, C. (2019). "Deviance detection and encoding acoustic regularity in the auditory midbrain," in *The Oxford Handbook of the Auditory Brainstem*, ed K. Kandler (Oxford: Oxford University Press). doi: 10.1093/oxfordhb/9780190849061.013.19

Malmierca, M. S., Merchán, M. A., Henkel, C. K., and Oliver, D. L. (2002). Direct projections from cochlear nuclear complex to auditory thalamus in the rat. *J. Neurosci.* 22, 10891–10897. doi: 10.1523/JNEUROSCI.22-24-10891.2002

Marlinski, V., Sirota, M. G., and Beloozerova, I. N. (2012). Differential gating of thalamocortical signals by reticular nucleus of thalamus during locomotion. *J. Neurosci.* 32, 15823–15836. doi: 10.1523/JNEUROSCI.0782-12.2012

McAlonan, K., Cavanaugh, J., and Wurtz, R. H. (2008). Guarding the gateway to cortex with attention in visual thalamus. *Nature* 456, 391–394. doi: 10.1038/nature07382

Mease, R. A., Krieger, P., and Groh, A. (2014). Cortical control of adaptation and sensory relay mode in the thalamus. *Proc. Natl. Acad. Sci. U.S.A.* 111, 6798LP—6803. doi: 10.1073/pnas.1318665111

Mease, R. A., Sumser, A., Sakmann, B., and Groh, A. (2016). Corticothalamic spike transfer via the L5B-POm pathway *in vivo*. *Cereb. Cortex* 26, 3461–3475. doi: 10.1093/cercor/bhw123

Mihai, P. G., Moerel, M., de Martino, F., Trampel, R., Kiebel, S., and von Kriegstein, K. (2019). Modulation of tonotopic ventral medial geniculate body is behaviorally relevant for speech recognition. *eLife* 8:44837. doi: 10.7554/eLife.44837

Mo, C., and Sherman, S. M. (2019). A sensorimotor pathway via higher-order thalamus. *J. Neurosci.* 39, 692–704. doi: 10.1523/JNEUROSCI.1467-18.2018

Mumford, D. (1991). On the computational architecture of the neocortex. *Biol. Cybern.* 65, 135–145. doi: 10.1007/BF00202389

Nakajima, M., and Halassa, M. M. (2017). Thalamic control of functional cortical connectivity. *Curr. Opin. Neurobiol.* 44, 127–131. doi: 10.1016/j.conb.2017.04.001

Nakamura, H., Hioki, H., Furuta, T., and Kaneko, T. (2015). Different cortical projections from three subdivisions of the rat lateral posterior thalamic nucleus: a single-neuron tracing study with viral vectors. *Eur. J. Neurosci.* 41, 1294–1310. doi: 10.1111/ejn.12882

Nakayama, H., Ibañez-Tallon, I., and Heintz, N. (2018). Cell-type-specific contributions of medial prefrontal neurons to flexible behaviors. *J. Neurosci.* 38, 4490LP—4504. doi: 10.1523/JNEUROSCI.3537-17.2018

Nelson, S. L., Kong, L., Liu, X., and Yan, J. (2015). Auditory cortex directs the input-specific remodeling of thalamus. *Hear. Res.* 328, 1–7. doi: 10.1016/j.heares.2015.06.016

Obleser, J., and Kayser, C. (2019). Neural entrainment and attentional selection in the listening brain. *Trends Cogn. Sci.* 23, 913–926. doi: 10.1016/j.tics.2019.08.004

Ojima, H. (1994). Terminal morphology and distribution of corticothalamic fibers originating from layers 5 and 6 of cat primary auditory cortex. *Cereb. Cortex.* 4, 646–663. doi: 10.1093/cercor/4.6.646

Ojima, H., and Rouiller, E. M. (2011). "Auditory cortical projections to the medial geniculate body BT - the auditory cortex," in eds J. A. Winer and C. E. Schreiner (Boston, MA: Springer US). doi: 10.1007/978-1-4419-0074-6_8

Olsen, S. R., Bortone, D. S., Adesnik, H., and Scanziani, M. (2012). Gain control by layer six in cortical circuits of vision. *Nature* 483, 47–52. doi: 10.1038/nature10835

Orman, S. S., and Humphrey, G. L. (1981). Effects of changes in cortical arousal and of auditory cortex cooling on neuronal activity in the medial geniculate body. *Experi. Brain Res.* 42, 475–482. doi: 10.1007/BF00237512

Palmer, A. R., Hall, D. A., Sumner, C., Barrett, D. J. K., Jones, S., Nakamoto, K., et al. (2007). Some investigations into non-passive listening. *Hear. Res.* 229, 148–157. doi: 10.1016/j.heares.2006.12.007

Pardi, M. B., Vogenstahl, J., Dalmay, T., Spanò, T., Pu, D.-L., Naumann, L. B., et al. (2020). A thalamocortical top-down circuit for associative memory. *Science* 370, 844–848. doi: 10.1126/science.abc2399

Parras, G. G., Nieto-Diego, J., Carbajal, G. V., Valdés-Baizabal, C., Escera, C., and Malmierca, M. S. (2017). Neurons along the auditory pathway exhibit a hierarchical organization of prediction error. *Nat. Commun.* 8:2148. doi: 10.1038/s41467-017-02038-6

Pérez-González, D., Malmierca, M. S., and Covey, E. (2005). Novelty detector neurons in the mammalian auditory midbrain. *Eur. J. Neurosci.* 22, 2879–2885. doi: 10.1111/j.1460-9568.2005.04472.x

Pinault, D. (2004). The thalamic reticular nucleus: structure, function and concept. *Brain Res. Rev.* 46, 1–31. doi: 10.1016/j.brainresrev.2004.04.008

Prasad, J. A., Carroll, B. J., and Sherman, S. M. (2020). Layer 5 Corticofugal Projections from diverse cortical areas: variations on a pattern of thalamic and extrathalamic targets. *J. Neurosci.* 40, 5785–5796. doi: 10.1523/JNEUROSCI.0529-20.2020

Prieto, J. J., and Winer, J. A. (1999). Layer VI in cat primary auditory cortex: Golgi study and sublaminar origins of projection neurons. *J. Comp. Neurol.* 404, 332–358. doi: 10.1002/(sici)1096-9861(19990215)404:3<332::aid-cne5>3.0.co;2-r

Purushothaman, G., Marion, R., Li, K., and Casagrande, V. A. (2012). Gating and control of primary visual cortex by pulvinar. *Nat. Neurosci.* 15, 905–912. doi: 10.1038/nn.3106

Ramón y Cajal, S. (1904). Textura del Sistema Nervioso del Hombre y de los Vertebrados, tomo II, primera parte. Imprenta y Libreria de Nicolas Moya, Madrid, reprinted by Graficas Vidal Leuka. *Alicante* 1992, 399–402.

Rao, R. P., and Ballard, D. H. (1999). Predictive coding in the visual cortex: a functional interpretation of some extra-classical receptive-field effects. *Nat. Neurosci.* 2, 79–87. doi: 10.1038/4580

Reichova, I., and Sherman, S. M. (2004). Somatosensory corticothalamic projections: distinguishing drivers from modulators. *J. Neurophysiol.* 92, 2185–2197. doi: 10.1152/jn.00322.2004

Rikhye, R. V., Wimmer, R. D., and Halassa, M. M. (2018). Toward an integrative theory of thalamic function. *Annu. Rev. Neurosci.* 41, 163–183. doi: 10.1146/annurev-neuro-080317-062144

Roth, M. M., Dahmen, J. C., Muir, D. R., Imhof, F., Martini, F. J., and Hofer, S. B. (2016). Thalamic nuclei convey diverse contextual information to layer 1 of visual cortex. *Nat. Neurosci.* 19, 299–307. doi: 10.1038/nn.4197

Rouiller, E. M., and Welker, E. (1991). Morphology of corticothalamic terminals arising from the auditory cortex of the rat: A Phaseolus vulgaris-leucoagglutinin (PHA-L) tracing study. *Hear. Res.* 56, 179–190. doi: 10.1016/0378-5955(91)90168-9

Rouiller, E. M., and Welker, E. (2000). A comparative analysis of the morphology of corticothalamic projections in mammals. *Brain Res. Bull.* 53, 727–741. doi: 10.1016/S0361-9230(00)00364-6

Rovó, Z., Ulbert, I., and Acsády, L. (2012). Drivers of the primate thalamus. *J. Neurosci.* 32, 17894–17908. doi: 10.1523/JNEUROSCI.2815-12.2012

Ryugo, D. K., and Weinberger, N. M. (1976). Corticofugal modulation of the medial geniculate body. *Exp. Neurol.* 51, 377–391. doi: 10.1016/0014-4886(76)90262-4

Saalmann, Y. B., Pinsk, M. A., Wang, L., Li, X., and Kastner, S. (2012). The pulvinar regulates information transmission between cortical areas based on attention demands. *Science* 337, 753–756. doi: 10.1126/science.1223082

Schmitt, L. I., Wimmer, R. D., Nakajima, M., Happ, M., Mofakham, S., and Halassa, M. M. (2017). Thalamic amplification of cortical connectivity sustains attentional control. *Nature* 545, 219–223. doi: 10.1038/nature22073

Schneggenburger, R., Meyer, A. C., and Neher, E. (1999). Released fraction and total size of a pool of immediately available transmitter quanta at a calyx synapse. *Neuron* 23, 399–409. doi: 10.1016/S0896-6273(00)80789-8

Scholl, L. R., Foik, A. T., and Lyon, D. C. (2021). Projections between visual cortex and pulvinar in the rat. *J. Comp. Neurol.* 529, 129–140. doi: 10.1002/cne.24937

Schroeder, C. E., and Lakatos, P. (2009). Low-frequency neuronal oscillations as instruments of sensory selection. *Trends Neurosci.* 32, 9–18. doi: 10.1016/j.tins.2008.09.012

Sherman, S. M. (2016). Thalamus plays a central role in ongoing cortical functioning. *Nat. Neurosci.* 19, 533–541. doi: 10.1038/nn.4269

Sherman, S. M. (2017). Functioning of circuits connecting thalamus and cortex. *Compr. Physiol.* 7, 713–739. doi: 10.1002/cphy.c160032

Sherman, S. M., and Guillery, R. W. (1998). On the actions that one nerve cell can have on another: Distinguishing "drivers" from "modulators." *Proc. Natl. Acad. Sci. U.S.A.* 95, 7121–7126. doi: 10.1073/pnas.95.12.7121

Sherman, S. M., and Guillery, R. W. (2011). Distinct functions for direct and transthalamic corticocortical connections. *J. Neurophysiol.* 106, 1068–1077. doi: 10.1152/jn.00429.2011

Sherrington, C. S. (1906). *The Integrative Action of the Nervous System*. Yale University Press.

Shipp, S. (2016). Neural elements for predictive coding. *Front. Psychol.* 7:1792. doi: 10.3389/fpsyg.2016.01792

Smout, C. A., Tang, M. F., Garrido, M. I., and Mattingley, J. B. (2019). Attention promotes the neural encoding of prediction errors. *PLoS Biol.* 17:e2006812. doi: 10.1371/journal.pbio.2006812

Sohoglu, E., and Chait, M. (2016). Detecting and representing predictable structure during auditory scene analysis. *eLife* 5:19113. doi: 10.7554/eLife.19113

Steriade, M. (2001). The GABAergic reticular nucleus: A preferential target of corticothalamic projections. *Proc. Natl. Acad. Sci. U.S.A.* 98, 3625–3627. doi: 10.1073/pnas.071051998

Steriade, M., and Deschenes, M. (1984). The thalamus as a neuronal oscillator. *Brain Res.* 320, 1–63. doi: 10.1016/0165-0173(84)90017-1

Stroh, A., Adelsberger, H., Groh, A., Rühlmann, C., Fischer, S., Schierloh, A., et al. (2013). Making waves: initiation and propagation of corticothalamic Ca2+ waves *in vivo*. *Neuron* 77, 1136–1150. doi: 10.1016/j.neuron.2013.01.031

Svoboda, K., and Li, N. (2018). Neural mechanisms of movement planning: motor cortex and beyond. *Curr. Opin. Neurobiol.* 49, 33–41. doi: 10.1016/j.conb.2017.10.023

Temereanca, S., and Simons, D. J. (2004). Functional topography of corticothalamic feedback enhances thalamic spatial response tuning in the somatosensory whisker/barrel system. *Neuron* 41, 639–651. doi: 10.1016/s0896-6273(04)00046-7

Theyel, B. B., Llano, D. A., and Sherman, S. M. (2010). The corticothalamocortical circuit drives higher-order cortex in the mouse. *Nat. Neurosci.* 13, 84–88. doi: 10.1038/nn.2449

Thomson, A. (2010). Neocortical layer 6, a review. *Front. Neuroanat.* 4:13. doi: 10.3389/fnana.2010.00013

Ulanovsky, N., Las, L., and Nelken, I. (2003). Processing of low-probability sounds by cortical neurons. *Nat. Neurosci.* 6, 391–398. doi: 10.1038/nn1032

Usrey, W., and Sherman, S. (2019). Corticofugal circuits: Communication lines from the cortex to the rest of the brain. *J. Compar. Neurol.* 527:24423. doi: 10.1002/cne.24423

Valdés-Baizabal, C., Carbajal, G. V., Pérez-González, D., and Malmierca, M. S. (2020). Dopamine modulates subcortical responses to surprising sounds. *PLoS Biol.* 18:e3000744. doi: 10.1371/journal.pbio.3000744

van Essen, D. C. B. T.-P. (2005). "Corticocortical and thalamocortical information flow in the primate visual system," in *Cortical Function: A View From the Thalamus*, eds V. A. Casagrande, R. W. Guillery, and S. M. Sherman (Amsterdam; Oxford: Elsevier). doi: 10.1016/S0079-6123(05)49013-5

Viaene, A. N., Petrof, I., and Sherman, S. M. (2011). Properties of the thalamic projection from the posterior medial nucleus to primary and secondary

somatosensory cortices in the mouse. *Proc. Natl. Acad. Sci. U.S.A.* 108, 18156–18161. doi: 10.1073/pnas.1114828108

Villa, A. E. P., and Abeles, M. (1990). Evidence for spatiotemporal firing patterns within the auditory thalamus of the cat. *Brain Res.* 509, 325–327. doi: 10.1016/0006-8993(90)90558-S

Villa, A. E. P., Rouiller, E. M., Simm, G. M., Zurita, P., de Ribaupierre, Y., and de Ribaupierre, F. (1991). Corticofugal modulation of the information processing in the auditory thalamus of the cat. *Experi. Brain Res.* 86, 506–517. doi: 10.1007/BF00230524

Watanabe, T., Yanagisawa, K., Kanzaki, J., and Katsuki, Y. (1966). Cortical efferent flow influencing unit responses of medial geniculate body to sound stimulation. *Experi. Brain Res.* 2, 302–317. doi: 10.1007/BF00234776

Wells, M. F., Wimmer, R. D., Schmitt, L. I., Feng, G., and Halassa, M. M. (2016). Thalamic reticular impairment underlies attention deficit in Ptchd1(Y/-) mice. *Nature* 532, 58–63. doi: 10.1038/nature17427

Williamson, R., and Polley, D. (2019). Parallel pathways for sound processing and functional connectivity among layer 5 and 6 auditory corticofugal neurons. *eLife* 8:42974. doi: 10.7554/eLife.42974

Winer, J. A., Diehl, J. J., and Larue, D. T. (2001). Projections of auditory cortex to the medial geniculate body of the cat. *J. Comp. Neurol.* 430, 27–55. doi: 10.1002/1096-9861(20010129)430:1<27::AID-CNE1013>3.0.CO;2-8

Winer, J. A., Larue, D. T., and Huang, C. L. (1999). Two systems of giant axon terminals in the cat medial geniculate body: convergence of cortical and GABAergic inputs. *J. Compar. Neurol.* 413, 181–197. doi: 10.1002/(SICI)1096-9861(19991018)413:2<181::AID-CNE1>3.0.CO;2-7

Wolff, M., and Vann, S. (2019). The cognitive thalamus as a gateway to mental representations. *J. Neurosci.* 39, 3–14. doi: 10.1523/JNEUROSCI.0479-18.2018

Wyart, V., Nobre, A. C., and Summerfield, C. (2012). Dissociable prior influences of signal probability and relevance on visual contrast sensitivity. *Proc. Natl. Acad. Sci. U.S.A.* 109, 3593–3598. doi: 10.1073/pnas.1120118109

Xiong, Y., Yu, Y.-Q., Chan, Y.-S., and He, J. (2004). Effects of cortical stimulation on auditory-responsive thalamic neurones in anaesthetized guinea pigs. *J. Physiol.* 560, 207–217. doi: 10.1113/jphysiol.2004.067686

Yu, X.-J., Xu, X.-X., He, S., and He, J. (2009). Change detection by thalamic reticular neurons. *Nat. Neurosci.* 12, 1165–1170. doi: 10.1038/nn.2373

Yu, Y.-Q., Xiong, Y., Chan, Y.-S., and He, J. (2004). Corticofugal gating of auditory information in the thalamus: an *in vivo* intracellular recording study. *J. Neurosci.* 24, 3060–3069. doi: 10.1523/JNEUROSCI.4897-03.2004

Zajzon, B., and Morales-Gregorio, A. (2019). Trans-thalamic pathways: strong candidates for supporting communication between functionally distinct cortical areas. *J. Neurosci.* 39, 7034–7036. doi: 10.1523/JNEUROSCI.0656-19.2019

Zhang, Y., Suga, N., and Yan, J. (1997). Corticofugal modulation of frequency processing in bat auditory system. *Nature* 387, 900–903. doi: 10.1038/43180

Zhang, Y., and Yan, J. (2008). Corticothalamic feedback for sound-specific plasticity of auditory thalamic neurons elicited by tones paired with basal forebrain stimulation. *Cereb. Cortex* 18, 1521–1528. doi: 10.1093/cercor/bhm188

Zhang, Z.-W., and Deschênes, M. (1997). Intracortical axonal projections of lamina VI cells of the primary somatosensory cortex in the rat: a single-cell labeling study. *J. Neurosci.* 17, 6365–6379. doi: 10.1523/JNEUROSCI.17-16-06365.1997

Zhou, H., Schafer, R. J., and Desimone, R. (2016). Pulvinar-Cortex Interactions in Vision and Attention. *Neuron* 89, 209–220. doi: 10.1016/j.neuron.2015.11.034

Zhou, N., Masterson, S. P., Damron, J. K., Guido, W., and Bickford, M. E. (2018). The mouse pulvinar nucleus links the lateral extrastriate cortex, striatum, and amygdala. *J. Neurosci.* 38, 347–362. doi: 10.1523/JNEUROSCI.1279-17.2017

Zion Golumbic, E. M., Ding, N., Bickel, S., Lakatos, P., Schevon, C. A., McKhann, G. M., et al. (2013). Mechanisms underlying selective neuronal tracking of attended speech at a "cocktail party." *Neuron* 77, 980–991. doi: 10.1016/j.neuron.2012.12.037

Zolnik, T. A., Ledderose, J., Toumazou, M., Trimbuch, T., Oram, T., Rosenmund, C., et al. (2020). Layer 6b is driven by intracortical long-range projection neurons. *Cell Rep.* 30, 3492–3505.e5. doi: 10.1016/j.celrep.2020.02.044

Conflict of Interest: The authors declare that the research was conducted in the absence of any commercial or financial relationships that could be construed as a potential conflict of interest.

Publisher's Note: All claims expressed in this article are solely those of the authors and do not necessarily represent those of their affiliated organizations, or those of the publisher, the editors and the reviewers. Any product that may be evaluated in this article, or claim that may be made by its manufacturer, is not guaranteed or endorsed by the publisher.

frontiers in Neural Circuits

REVIEW
published: 09 September 2021
doi: 10.3389/fncir.2021.730211

Corticothalamic Pathways From Layer 5: Emerging Roles in Computation and Pathology

Rebecca A. Mease and Antonio J. Gonzalez*

Institute of Physiology and Pathophysiology, Medical Biophysics, Heidelberg University, Heidelberg, Germany

Large portions of the thalamus receive strong driving input from cortical layer 5 (L5) neurons but the role of this important pathway in cortical and thalamic computations is not well understood. L5-recipient "higher-order" thalamic regions participate in cortico-thalamo-cortical (CTC) circuits that are increasingly recognized to be (1) anatomically and functionally distinct from better-studied "first-order" CTC networks, and (2) integral to cortical activity related to learning and perception. Additionally, studies are beginning to elucidate the clinical relevance of these networks, as dysfunction across these pathways have been implicated in several pathological states. In this review, we highlight recent advances in understanding L5 CTC networks across sensory modalities and brain regions, particularly studies leveraging cell-type-specific tools that allow precise experimental access to L5 CTC circuits. We aim to provide a focused and accessible summary of the anatomical, physiological, and computational properties of L5-originating CTC networks, and outline their underappreciated contribution in pathology. We particularly seek to connect single-neuron and synaptic properties to network (dys)function and emerging theories of cortical computation, and highlight information processing in L5 CTC networks as a promising focus for computational studies.

Keywords: pyramidal neurons, corticothalamic, higher-order thalamus, bursting, thalamus, layer 5, neural coding, pathology

OPEN ACCESS

Edited by:
Max F. K. Happel,
MSB Medical School Berlin, Germany

Reviewed by:
Ralf D. Wimmer,
Massachusetts Institute of Technology, United States
Mathieu Wolff,
Centre National de la Recherche Scientifique (CNRS), France

****Correspondence:***
Rebecca A. Mease
rebecca.mease@physiologie.uni-heidelberg.de

Received: *24 June 2021*
Accepted: *10 August 2021*
Published: *09 September 2021*

Citation:
Mease RA and Gonzalez AJ (2021) Corticothalamic Pathways From Layer 5: Emerging Roles in Computation and Pathology. Front. Neural Circuits 15:730211. doi: 10.3389/fncir.2021.730211

INTRODUCTION

The thalamus is a bilateral structure of the diencephalon that serves integral roles in a significant range of neurophysiological functions including sensory information relay, learning and memory, motor control, and regulation of sleep and wakefulness (Herrero et al., 2002; Yuan et al., 2016). Positioned above the midbrain, the thalamus displays widespread connectivity with the cerebral cortex, as well as subcortical and temporal structures (e.g., mammillary bodies, fornix,

Abbreviations: AHP, afterhyperpolarization; AD, Alzheimer's disease; ACC, anterior cingulate cortex; APT, anterior pretectal nucleus; CT, corticothalamic; CTC, cortico-thalamo-cortical; MGBd, dorsal aspect of medial geniculate body; EPSP, excitatory postsynaptic potential; EPSC, excitatory postsynaptic current; FO, first-order; HO, higher-order; I_H, hyperpolarization-activated cation current; LP, lateral posterior nucleus; L5, layer-V; L6, layer-VI; MD, mediodorsal nucleus; PV, parvalbumin; POm, posterior medial nucleus; PO, posterior nucleus; PPC, posterior parietal cortex; PFC, prefrontal cortex; A1, primary auditory cortex; M1, primary motor cortex; S1, primary somatosensory cortex; V1, primary visual cortex; PuV, pulvinar nucleus; A2, secondary auditory cortex; S2, secondary somatosensory cortex; SOM, somatostatin; SNI, spared nerve injury; SZ, schizophrenia; TT, thick-tufted; I_T, transient low-threshold calcium current; VIP, vasoactive intestinal peptide; ZI, zona incerta.

and hippocampus), acting as a central hub for functional brain networks (Hwang et al., 2017). The thalamus is traditionally fractionated into functional nuclei, each of which participates in feedback and/or feedforward communication with unique cortical areas (Morel et al., 1997; Yuan et al., 2016; Halassa and Kastner, 2017).

The thalamus is massively innervated by deep corticofugal cells in layer 5 (L5) and layer 6 (L6) (**Figure 1**). While these dense projections have been documented since the early 20th century (Cajal, 1906), in-depth study of the pathways and their functional impact on the thalamus has only recently become experimentally accessible (Guy and Staiger, 2017). Indeed, technological advances in high-yield electrophysiology as well as cell-type-specific optogenetics and anatomical tracing have elucidated interactions between specific cortical layers and thalamic nuclei (Luo et al., 2018). In particular, such approaches have refined our understanding of "higher-order" (HO) thalamic nuclei – those regions of the thalamus that are strongly innervated by cortical L5 pyramidal neurons (Sherman, 2007; **Figure 1A**). However, this understanding still lags that of "first-order" (FO) thalamic nuclei (**Figure 1B**), which do not receive L5 input and have proven more tractable with typical sensory physiological experiments.

A recent study provides beginning evidence that L5-HO thalamus connectivity may represent a "default" scheme: while each sensory modality (e.g., somatosensation, vision, and audition) retains a distinct FO and HO nucleus, FO and HO nuclei are each genetically homologous across modalities. Intriguingly, the transcriptional identity of FO nuclei depends on the presence of peripheral input, as neonatal ablation of these inputs leads to FO nuclei transitioning to a HO transcriptional program and descending cortical input that is typically HO-directed (Frangeul et al., 2016). In addition, recent studies have highlighted the importance of L5-originating CTC networks in diverse functions, such as permitting selective thalamic-driven modulation, dynamic cortical coupling, sending motor instructions, and informing higher cortical areas about which motor instructions have been issued, as well as roles in learning and plasticity in cortical networks (Sherman and Guillery, 2011; Gambino et al., 2014; Audette et al., 2019; Usrey and Sherman, 2019). However, a synthesized view of HO CTC computation is still elusive, given the diverse nonlinear single-neuron and synaptic properties of these networks, and complex connectivity with other subcortical regions.

In this focused review, we discuss foundational and recent studies of L5-originating HO CTC networks across cortical regions. In particular, we emphasize findings distinguishing HO CTC networks from better-studied FO regions of thalamus that serve as bottom-up relays to the cortex. Many excellent existing reviews summarize the recent rapid progress in understanding anatomical and functional properties of CTC networks (e.g., Usrey and Sherman, 2019; Shepherd and Yamawaki, 2021), particularly contrasting FO and HO CTC connectivity. For context, we review this material but focus mainly on studies relevant to understanding computation within HO CTC networks as well as the emerging importance of these networks in learning and pathology.

Our aim is to present a unified yet comprehensible overview of these increasingly appreciated circuits that is accessible to experimental and computational neuroscientists from outside the thalamocortical field. The schematic in **Figure 1** outlines the networks of interest and **Figure 2** illustrates available information on synaptic inputs to HO thalamus. Key literature is organized according to modality and methodology (**Table 1**) and relevance to pathology (**Table 2**). This review is structured as follows:

1. L5-HO thalamus definitions and network connectivity schemes.
2. HO thalamic nuclei across modalities.
3. Inhibitory control of HO thalamus.
4. Synaptic properties of L5-HO thalamus projections.
5. HO thalamus intrinsic properties and single-cell information processing.
6. HO encoding of L5 cortical information.
7. HO thalamocortical innervation of cortex and roles in sensory processing and cognition.
8. Clinical relevance of L5-originating CTC networks.

Throughout, we attempt to highlight missing experimental data and theoretical perspectives.

L5 TO HIGHER-ORDER THALAMUS: CORTICOTHALAMIC CONNECTIVITY FROM THE PYRAMIDAL TRACT

Pyramidal neurons in L5 of the cortex serve as the major exit point by which cortical signals are directed to subcortical circuits. Aside from L6 corticothalamic (CT) neurons, only L5 neurons are reported to make synapses outside of the neocortex; in contrast to the L6A CT pathway which is restricted largely to thalamus, L5 neurons project to several subcortical targets, including thalamus, superior colliculus, pons, brainstem, and spinal cord. Despite its complexity and computational power, these L5- and L6-originating outputs represent the only means by which the cortex can influence subcortical processes and thereby influence behavior (Sherman and Guillery, 2013; Usrey and Sherman, 2019; Prasad et al., 2020; Sherman and Usrey, 2021). Indeed, innervation by L5 driving inputs is the criterion for the influential and useful "higher-order" terminology introduced by Sherman and colleagues. Presently, several L5-originating CTC networks have been identified across sensory modalities including somatosensation, audition, and vision (Sherman, 2016; **Table 1**).

Recently, the development of novel transgenic mouse lines has granted refined experimental access to cell-type- and layer-specific observations (Gong et al., 2007; Gerfen et al., 2013; Harris et al., 2014, 2018; Daigle et al., 2018). In conjunction, advancements in optogenetics and electrophysiology have

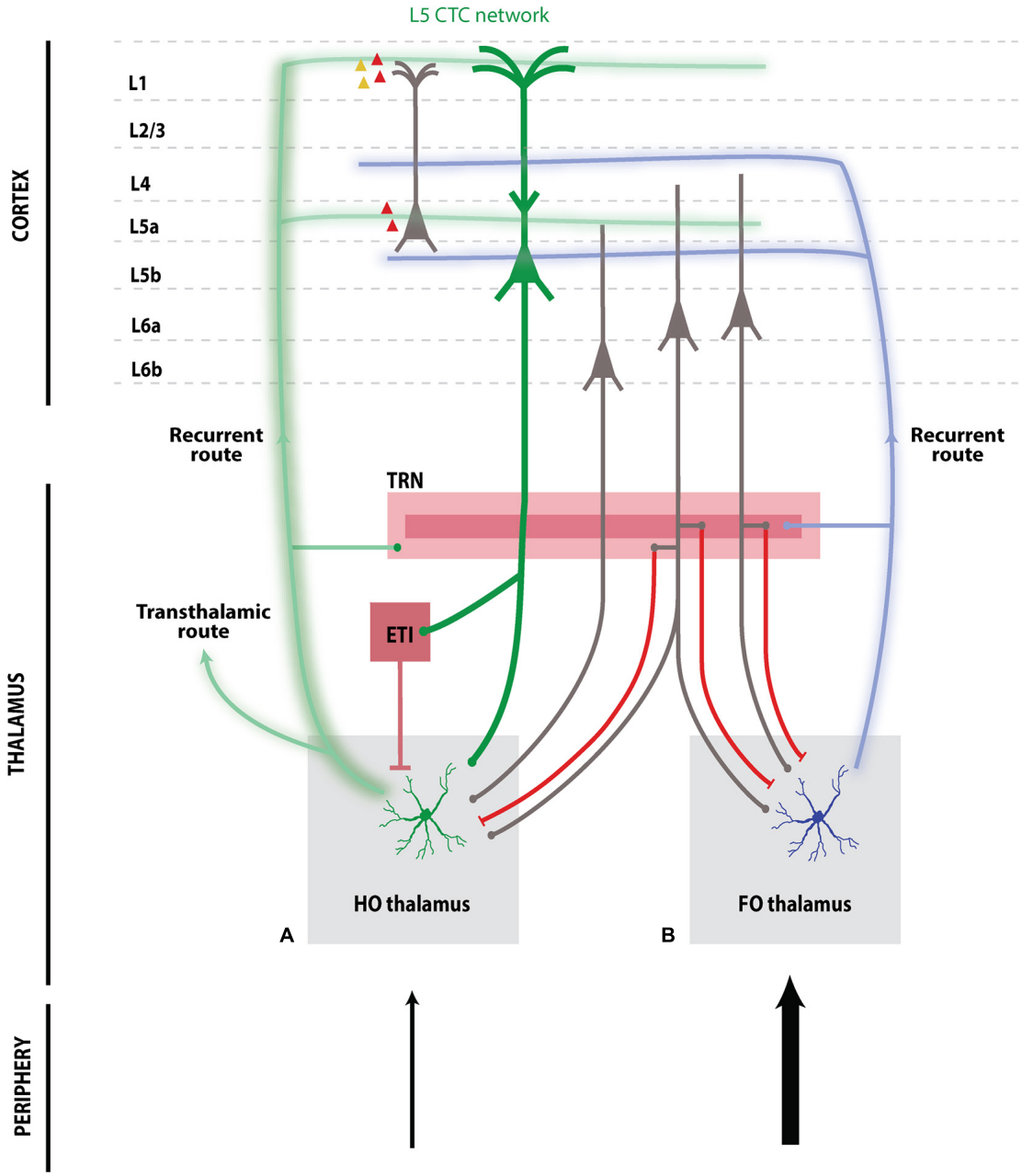

FIGURE 1 | Schematic of higher-order **(A)** and first-order **(B)** cortico-thalamo-cortical networks. L5 thick-tufted pyramidal cells in L5B send projections to HO thalamic nuclei and to additional subcortical targets including extrathalamic inhibitory (ETI) sources, e.g., the ZI and APT, which exert strong inhibition on HO nuclei. HO thalamus **(A)** sends TC projections across transthalamic routes to other cortical regions, or forms a recurrent route back to the same cortical region targeting L5A and upper layers. HO TC projections target excitatory pyramidal cells, as well as PV (red) and 5HT3-positive inhibitory (yellow) interneurons, although there are modality-specific variations (e.g., associative thalamus). In contrast, FO thalamus **(B)** sends recurrent TC projections to cortical layers L5B and L4. L6 corticothalamic cell subpopulations display distinct connectivity with thalamic nuclei: Upper L6A cells specifically target FO thalamus, while lower L6A cells target both FO and HO thalamus; both populations send collaterals to inhibitory TRN. L6B cells specifically target HO thalamus but do not send collaterals to TRN. Both HO and FO nuclei engage intrathalamic inhibitory feedback loops via excitatory projections to TRN. Outer "shell" TRN sends inhibitory projections to HO thalamus while inner "core" TRN sends inhibitory projections to FO thalamus.

enabled targeted monitoring and manipulation of neuronal circuits, and dissection of physiological and functional circuit properties. These powerful approaches have begun to disentangle the properties of L5-HO thalamus pathways from L6-thalamus pathways, for example, through the use of *Rbp4, Npr3,* and *thy-1* mouse lines (Groh et al., 2013; Daigle et al., 2018; Guo et al., 2020; Prasad et al., 2020; Kirchgessner et al., 2021), establishing key characteristics of L5 projections to the thalamus. Most

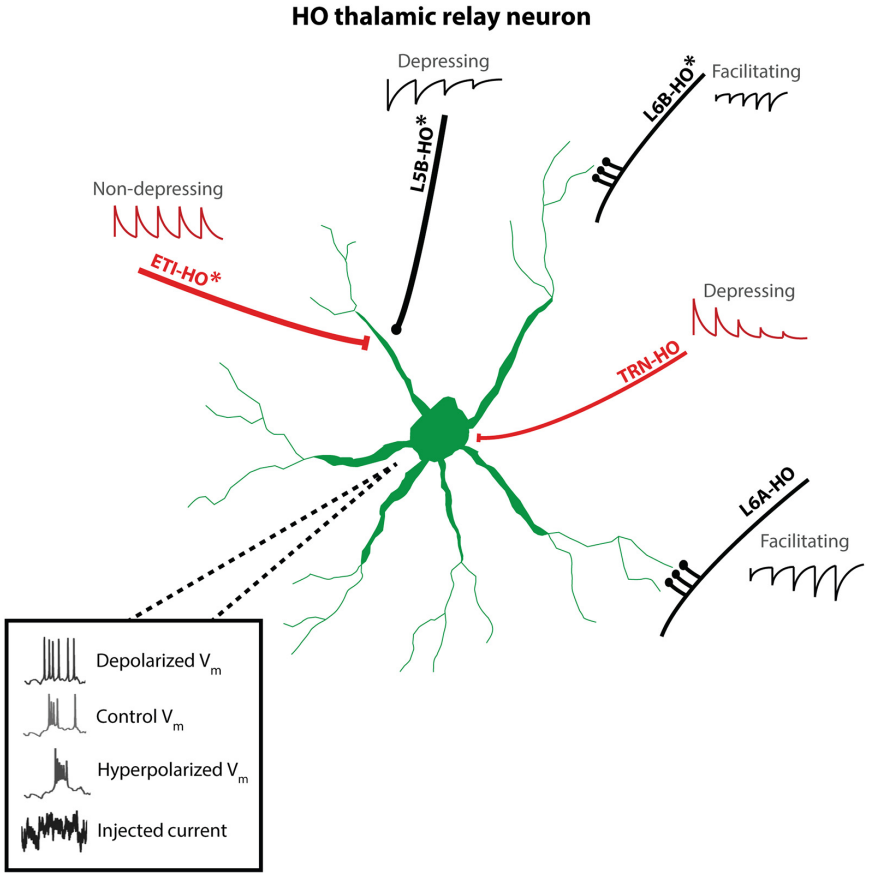

FIGURE 2 | Cartoon of synaptic inputs to HO thalamic relay neurons and intrinsic excitability patterns. Asterisks (*) indicate inputs which target HO thalamus and are not present in FO nuclei. L5tt neurons provide strong, depressing "driving" excitatory input to proximal dendrites via large synapses, while L6A CT *en passant* synapses provide relatively weaker, facilitating, modulatory excitatory input to distal dendrites. L6B provides *en passant* excitatory inputs (synaptic dynamics not yet reported). Inhibitory TRN inputs show strong depression. In contrast, powerful inhibitory ETI synapses are located in close proximity to L5tt excitatory inputs and show little depression. Not shown: additional area-specific sources of driver input reported in "convergence" zones of HO thalamus and feedforward inhibitory loops L5tt-ETI-thalamus and L6A-TRN-thalamus. Inset voltage traces: HO thalamic neurons show characteristic voltage-dependent bursting: depolarization inactivates bursting mechanisms and promotes tonic spiking.

importantly, L5 inputs to HO nuclei are sparse and display characteristic "driver" properties, in contrast to L6 projections, which target both HO and FO thalamic nuclei and provide modulatory input (Sherman and Guillery, 2002; Reichova and Sherman, 2004; Sherman, 2016).

Higher-order thalamic nuclei are specifically targeted by L5 "thick-tufted" (L5tt) pyramidal tract neurons in L5B (Harris and Shepherd, 2015; **Figure 1A**, green). As recipients of information from all cortical layers, L5tt neurons are well-suited for integrating cortical signals–particularly characteristic are the elaborately branched apical dendrites that cover nearly a column in width. Notably, L5tt neurons show minimal axonal branching within the cortex, suggesting a main role is to distribute information subcortically and coordinate behavior (Ramaswamy and Markram, 2015). In line with this predicted function, many anatomical studies demonstrate that L5tt neurons send branching collaterals to subcortical targets including the HO thalamus, brainstem, and spinal cord–even at the level of single L5 neurons innervating more than one subcortical region (Veinante et al., 2000; Sherman, 2016; Guo et al., 2017; Rockland, 2019; Prasad et al., 2020). However, there is also evidence that L5tt subpopulations with distinct intrinsic properties innervate specific subcortical targets (Hattox and Nelson, 2007; Rojas-Piloni et al., 2017). This point raises the intriguing possibility that L5tt populations may have excitability and synaptic properties matched to their innervation targets. L5tt axonal branching is a matter of ongoing study and appears to be species-specific (Smith et al., 2014; Rockland, 2019). Reports also depend on specific experimental methodology, with axonal reconstructions reporting more branching versus retrograde tracing. High-throughput reconstruction efforts will be key to sharpening our understanding of L5tt innervation of subcortical targets in the near future.

Transthalamic and Recurrent Pathways

From the perspective of the HO thalamus, L5tt projections provide a strong but sparse drive to individual neurons (discussed in the next section). Where does this information go after being

TABLE 1 | Key literature describing anatomical and/or physiological properties of CTC networks across sensory modalities and an example non-sensory modality.

	Somatosensation	Vision	Audition	Cognitive/non-sensory
Origin of L5tt CT projections	S1	V1	A1	PFC
HO thalamic nucleus	POm	LP/pulvinar	MGBd	MD
Reported cortical targets	S1, S2, M1	All visual cortical areas	All auditory cortical areas	PFC
CT anatomy (L5 to HO thalamus)	Hoogland et al., 1991; Bourassa et al., 1995; Veinante et al., 2000; Groh et al., 2008, 2013; Theyel et al., 2010; Guo et al., 2017, 2020; Sumser et al., 2017; Mo and Sherman, 2019; Prasad et al., 2020; Sampathkumar et al., 2021	Bourassa and Deschenes, 1995; Li et al., 2003c; Masterson et al., 2009; Stitt et al., 2018; Bennett et al., 2019; Prasad et al., 2020; Blot et al., 2021	Ojima, 1994; Bartlett et al., 2000; Rouiller and Welker, 2000; Llano and Sherman, 2008, 2009; Williamson and Polley, 2019; Pardi et al., 2020	Xiao et al., 2009; Collins et al., 2018; Prasad et al., 2020; Anastasiades et al., 2021
L5-HO synaptic/intrinsic physiology	Reichova and Sherman, 2004; Landisman and Connors, 2007; Groh et al., 2008; Theyel et al., 2010; Seol and Kuner, 2015; Mease et al., 2017; Guo et al., 2020; Desai and Varela, 2021	Li et al., 2003a,b; de Souza et al., 2019; Desai and Varela, 2021	Desai and Varela, 2021	Collins et al., 2018; Anastasiades et al., 2021
TC anatomy	Koralek et al., 1988; Lu and Lin, 1993; Bureau et al., 2006; Groh et al., 2010; Meyer et al., 2010a; Theyel et al., 2010; Wimmer et al., 2010; Viaene et al., 2011; Audette et al., 2017; Casas-Torremocha et al., 2019; Sermet et al., 2019; El-Boustani et al., 2020; Rodriguez-Moreno et al., 2020	Saalmann et al., 2012; Stitt et al., 2018; Bennett et al., 2019	Pardi et al., 2020	Delevich et al., 2015; Collins et al., 2018; Mukherjee et al., 2020; Anastasiades et al., 2021
TC physiology	Bureau et al., 2006; Lee and Sherman, 2008; Petreanu et al., 2009; Theyel et al., 2010; Audette et al., 2017; Casas-Torremocha et al., 2019; Mo and Sherman, 2019; Sermet et al., 2019; El-Boustani et al., 2020; Guo et al., 2020	Purushothaman et al., 2012; Stitt et al., 2018	Lee and Sherman, 2008; Pardi et al., 2020	Delevich et al., 2015; Collins et al., 2018; Anastasiades et al., 2021
L5 CTC function *in vivo*	Groh et al., 2013; Gambino et al., 2014; Mease et al., 2016a,b,c; Rojas-Piloni et al., 2017; Audette et al., 2019; Williams and Holtmaat, 2019; Zhang and Bruno, 2019; LaTerra et al., 2020; Suzuki and Larkum, 2020; Takahashi et al., 2020; Pagès et al., 2021	Bender, 1983; Purushothaman et al., 2012; Saalmann et al., 2012; Stitt et al., 2018; Yu et al., 2018; Bennett et al., 2019; de Souza et al., 2019; Blot et al., 2021; Kirchgessner et al., 2021	Asokan et al., 2018; Williamson and Polley, 2019; Pardi et al., 2020	Parnaudeau et al., 2013; Schmitt et al., 2017; Rikhye et al., 2018; Mukherjee et al., 2020

Recent studies using cell-type-specific approaches are emphasized.

further processed in HO thalamus? (Sherman and Guillery, 2011) suggested a significant revision to our understanding of thalamocortical processing with the "transthalamic" hypothesis, specifically that cortical L5tt neurons in one source region send information to a secondary cortical recipient region via HO thalamus. Recent anatomical and functional data suggest that transthalamic pathways paralleling "direct" cortico-cortical pathways could be a common feature of the thalamocortical system and that these pathways carry distinct rather than redundant information (Sherman, 2016; Bennett et al., 2019; Mo and Sherman, 2019; Blot et al., 2021). However, there is recent evidence that certain HO circuits can also be involved in recurrent "closed-loop" networks, in which the same cortical region providing L5tt input to HO thalamus is itself reciprocally

TABLE 2 | Summary of key literature findings on the relevance of higher-order CTC pathway components across pathological states including pain, tinnitus, and neuropsychiatric disorders.

Relevant pathology	Authors	Findings
Chronic pain	Cichon et al. (2017)	• Chronic pain (SNI model) elicits hyperactivity in L5 cells in S1; correlates with degree of mechanical allodynia • Reduction in PV and SOM interneurons; increase in VIP interneurons • DREADD-based activation of SOM interneurons prevented development of mechanical allodynia; activation of PV interneurons not effective
	Masri et al. (2009)	• Animal model of central pain syndrome • Spinal cord lesions elicited higher spontaneous firing rates and responsiveness to innocuous/noxious stimulus in the PO • Lower spontaneous firing rate in ZI, causing PO disinhibition
	Whitt et al. (2013)	• Spinal cord lesions elicited higher spontaneous firing rate and magnitude/duration of responses to noxious stimuli in the MD
	Meda et al. (2019)	• Optogenetic activation of MD-ACC pathway in SNI and chemotherapy-induced neuropathy mice models produced a conditioned place-aversion • Same effect observed following direct inhibition of L5 ACC-MD projection
	Saadé et al. (2007)	• Inactivation/lesions of MD nucleus reduced thermal and mechanical hyperalgesia in neuropathic pain model
Tinnitus/noise-induced damage	Asokan et al. (2018)	• Noise-induced damage to cochlear afferents elicits hyperactivity of L5 projection cells in the auditory cortex for several weeks • May drive hyperexcitability and strengthened coupling in tinnitus-associated brain networks
Neuropsychiatric disorders	Kim et al. (2011)	• Hypoxic-like damage in PFC enhanced MD/PFC theta-frequency coherence and burst frequency of MD neurons • T-type calcium channel knockdown decreased theta-frequency coherence and attenuated associated symptoms (e.g., frontal lobe seizures

innervated by HO thalamus (Wimmer et al., 2010; Guo et al., 2020). This reciprocal connectivity motif is seen in FO CTC networks, where L6A modulatory CT projections originate from the same cortical region innervated by FO TC projections. However, the transthalamic and recurrent network motifs are not mutually exclusive and may subserve different functions. As we highlight below, based on region-specific descending CT and ascending HO TC connectivity patterns, different combinations of recurrent and transthalamic communication are possible. An important focus for future studies is to understand the distinct signals transmitted by transthalamic and recurrent pathways, and to uncover the computational scheme integrating these information channels with cortico-cortical signals.

Currently, it is understood that HO nuclei, which represent a majority of the thalamus by volume, participate in the generation of activity in distinct cortico-thalamo-cortical (CTC) networks (Guillery, 1995; Sherman and Guillery, 2011; Sherman, 2016). Additionally, these CTC networks serve to integrate a diverse range of cortical and subcortical signals (Groh et al., 2013; Bickford, 2015). While a full assessment of this literature is beyond the scope of this review, we note that these "convergence zones" have been reported across modalities (Groh et al., 2013; Bickford, 2015). For example, projections from the primary visual cortex in the HO lateral posterior (LP) nucleus overlap with terminals originating in the superior colliculus (Li et al., 2003c; Masterson et al., 2009). Elsewhere, Bosch-Bouju et al. (2013) introduce the concept of a "super-integrator," where motor regions of the thalamus integrate information from the cortex with information from the basal ganglia and cerebellum. Additional convergence zones have been identified by exploiting the differential distribution of type 1 and type 2 vesicular glutamate transporters, which are specific to cortical and subcortical inputs, respectively (Rovó et al., 2012; Bickford, 2015). Recent anatomical evidence points to a role for HO thalamus in integrating information from different cortical regions (Prasad et al., 2020), even at the level of single cells (Sampathkumar et al., 2021).

HIGHER-ORDER NUCLEI ACROSS MODALITIES

In this focused review, we center our discussion on HO nuclei (**Table 1**) involved in primary sensory modalities (somatosensation, audition, and vision), as well as on HO nuclei that have been implicated in pathology (e.g., pain and cognitive dysfunction). A very recent anatomical survey of L5tt-subcortical projections has identified additional HO thalamic regions (Prasad et al., 2020); the functional properties of these projections remain to be characterized.

In the somatosensory system, the medial subdivision of the posterior nucleus (POm) receives L5tt input from the primary

somatosensory cortex (S1), and thereafter recurrently targets S1 (Audette et al., 2017; Guo et al., 2020) and relays information trans-thalamically to the secondary somatosensory cortex (S2) (Theyel et al., 2010) and the primary motor cortex (M1) (Mo and Sherman, 2019). As **Table 1** reflects, the somatosensory HO CTC circuit has provided a wealth of recent anatomical and functional data on cell-type-specific interactions and the *in vivo* impact of HO thalamus on cortical function.

In the visual system, the pulvinar nucleus (PuV) [or the homologous LP nucleus in rodents] is the L5tt-receiving HO nucleus, and is connected to all visual cortices (Bender, 1983; Saalmann et al., 2012; Bennett et al., 2019; de Souza et al., 2019). While pulvinar has been largely studied in primates, recent cell-type-specific and optogenetic studies have made increasing use of mouse models (**Table 1**). Regions within the LP that are reciprocally connected to the cortex are dominated by small terminals, while those that lack reciprocal connectivity are dominated by large terminals (Van Horn and Sherman, 2004). LP projections to higher visual areas have been shown to integrate descending information from L5tt cells in V1 with that from several cortical and subcortical areas, and the information conveyed to higher-order visual areas differs from that conveyed by cortico-cortical projections from V1. For example, while intracortical V1 projections convey information to the anteriolateral higher visual area about visual motion, the transthalamic route to this region (i.e., through the LP nucleus) integrates information about visual motion and the animals' movement (Purushothaman et al., 2012; Stitt et al., 2018; Blot et al., 2021).

In the auditory system, the dorsal aspect of the medial geniculate nucleus (MGBd) receives L5tt input from the primary auditory cortex (A1), and relays to higher-order auditory regions (e.g., A2) (Lee and Sherman, 2011; Lee, 2015; Sherman, 2017). Cortical projections to the inferior colliculus (IC) have axon collaterals in the MGBd, although the degree and functional relevance of this branching is unclear (Asokan et al., 2018; Williamson and Polley, 2019). Notably, detailed physiological characterizations of the L5-MGBd-cortical pathways are lacking (**Table 1**).

While these sensory HO nuclei have received significant attention, there also exist "associative" L5tt-receiving HO nuclei that participate in non-sensory modalities. Here we emphasize rodent studies in the mediodorsal (MD) nucleus (**Table 1**), which contributes to learning, memory, and decision-making processes. MD's influence on cognitive abilities results from interactions with L5tt-projecting frontal areas such as the prefrontal cortex (PFC) (Mitchell, 2015; Bolkan et al., 2017; Schmitt et al., 2017; Alcaraz et al., 2018; Pergola et al., 2018; Rikhye et al., 2018). Indeed, 20% of PFC projections (mainly from dorsal and medial areas) to MD stem from L5 (Xiao et al., 2009). It has been found that PFC output neurons in fact branch to both MD and the functionally diverse ventromedial (VM) nucleus, which may enable synchronized thalamic spiking across nuclei (Collins et al., 2018). In addition, the MD nucleus is implicated in mediating affective and emotional aspects of pain (Whitt et al., 2013; Mitchell, 2015).

INHIBITION OF HIGHER-ORDER THALAMUS

A small but growing body of work demonstrates that HO thalamus is subject to inhibitory effects that either differ or are entirely distinct from those seen in FO circuits. Here we summarize the main points of distinction, and refer readers to Halassa and Acsady (2016) for a more comprehensive treatment of inhibitory control of thalamus.

Intrathalamic Inhibition of HO Thalamus

A central regulator of thalamic function is feedback inhibition via thalamic reticular nucleus (TRN), a thin layer of GABAergic neurons partially encapsulating the relay nuclei which project to cortex (Pinault, 2004). As well as TC afferents to cortex, thalamic relay neurons also send thalamoreticular projections to TRN which in turn provide feedback inhibition to relay neurons (**Figure 1**); the temporal scale of this inhibition is sensitive to spiking patterns (**Figure 2**), with high-frequency bursts triggering long-lasting IPSCs due to GABA "spillover" to extrasynaptic receptors, while tonic spiking patterns trigger shorter IPSCs (Halassa and Acsady, 2016). A recent pair of milestone studies in the somatosensory thalamus reveal that properties of HO and FO intrathalamic inhibitory circuitry differ significantly: HO nucleus POm excites and is inhibited by a discrete shell population of TRN neurons; furthermore, the synaptic dynamics of POm-TRN connections as well as the intrinsic properties of POm-connected TRN neurons are functionally distinct from those in VP-TRN circuits (Li et al., 2020; Martinez-Garcia et al., 2020). Thus, it may be that the dynamics of intrathalamic inhibition are matched to the distinct signal processing requirements of HO and FO circuits carrying L5tt and sensory information, respectively.

Given its role in gating thalamocortical transmission as well as its positional and physiological properties, the TRN has been implicated in the regulation of attention in the "searchlight hypothesis" (Crick, 1984; Crabtree, 2018). Regions in the TRN show increased activity in response to attentional stimuli, and the specific region in which this response is found is modality-dependent (McAlonan et al., 2000, 2006). Moreover, limbic TRN projections correlate with arousal states, while sensory TRN projections are suppressed by attentional states (Halassa et al., 2014). Work by Halassa et al. (2011) demonstrates TRN-dependent control of thalamocortical firing mode and state regulation, where selective drive of TRN causes a switch from tonic to burst firing and generates state-dependent neocortical spindles (Halassa et al., 2011).

Likewise, there is evidence for an attentional role of HO thalamus. For example, the MD is activated in humans during tasks requiring a rule-dependent shift in attentional allocation (i.e., set-shifting), such as the Wisconsin card-sorting task (Monchi et al., 2001; Halassa and Kastner, 2017). Human and monkey studies also point to a role of the pulvinar in visual attention. Pulvinar lesions in patients result in impairments in filtering distracting information, while pulvinar inactivation in monkey impairs spatial attention (Danziger et al., 2004; Snow et al., 2009; Wilke et al., 2010; Halassa and Kastner, 2017). In

addition, Yu et al. (2008) describe the pulvinar's role in sustained attention, employing the five-choice serial reaction time task to show that half of recorded units in this nucleus were attention-modulated (Yu et al., 2018). However, TRN control of HO thalamus in the context of attention and arousal has yet to be systematically investigated.

L6 CT Inputs to HO Thalamus

Thalamic reticular nucleus inhibition is also influenced by topographically organized CT projections from L6A which innervate both relay neurons and neurons in TRN (Lam and Sherman, 2010; **Figure 1**). Thus, these CT inputs simultaneously provide direct excitatory input to relay neurons and exert additional top-down control on inhibition via TRN, providing a cortical signal for task or attention-specific modulation of the thalamus. Overall, the net functional impact of L6A CT signals on thalamic relay neurons is determined by an excitation-inhibition balancing act of rate-dependent synaptic depression and facilitation (Crandall et al., 2015); this dynamic balance is seen *in vivo* in both HO and FO nuclei (Kirchgessner et al., 2020). It should be noted that HO and FO nuclei are targeted by partially disjoint populations of neurons in L6A (Thomson, 2010; Whilden et al., 2021; **Figure 1**), perhaps in keeping with the distinct reticular inhibitory circuits discussed above. Finally, aside from the L6A CT pathways, recent studies have identified a HO-thalamus specific pathway from layer 6B (**Figure 1**) which does not send collaterals to TRN and appears to exert strong excitatory influences on relay neurons (Hoerder-Suabedissen et al., 2018; Ansorge et al., 2020), although detailed physiological measures of these inputs are currently lacking. Notably, L6B neurons are orexin-sensitive (Bayer et al., 2004), suggesting that the cortex may provide HO thalamus with descending excitation based on wakefulness.

Extrathalamic Inhibition

Another key differentiator of HO thalamic circuits is the presence of additional subcortical inhibition from sources of "extrathalamic inhibition" (ETI) (**Figures 1**, **2**), such as the zona incerta (ZI) and the anterior pretectal nucleus (APT) [reviewed in Halassa and Acsady (2016)]. Anatomical and experimental studies have suggested that these ETI sources exert a significantly more powerful inhibitory effect on the thalamus than do intrathalamic inhibition sources (Barthó et al., 2002; Lavallée et al., 2005; Park et al., 2018). In contrast to the TRN, which targets all thalamic nuclei, ETI inputs display greater target selectivity, a property that is evolutionarily highly conserved (Halassa and Acsady, 2016). Across sensory modalities, studies have demonstrated that HO, but not FO nuclei, receive ETI input, and this appears to serve as the inhibitory counterpart of L5tt excitatory inputs. This topographical restriction means that these ETI projections do not interact with ascending sensory relays, nor do they directly impact FO thalamus activity. Overall, ET inhibition of HO nuclei is notably strong, rapid, and precise, rendering it capable of influencing the timing of individual spikes in target cells (Halassa and Acsady, 2016). Further spatial selectivity has been established within subregions of the ZI. For example, Lavallée et al. (2005) found that the posterior (PO) HO nucleus receives inhibitory input from the ventral division of the ZI, which is in fact the same ZI subregion that receives input from the APT (Giber et al., 2008; Murray et al., 2010). Further underscoring the importance of ETI nuclei in sculpting HO thalamus processing of L5tt inputs, ZI and APT are also strongly driven by L5tt collaterals (**Figure 1**)–thus, HO nuclei are embedded in an additional feedforward inhibitory loop similar in motif to the L6A-TRN loop, but specific to HO nuclei and with different synaptic properties (Barthó et al., 2002, 2007; Halassa and Acsady, 2016).

PROPERTIES OF PT CORTICOTHALAMIC SYNAPSES

L5tt-HO thalamus projections form sparse, large glutamatergic synapses electronically close to the soma of target thalamic relay neurons (**Figure 2**), typically on thick proximal dendrites near branch points (Hoogland et al., 1991; Bourassa et al., 1995; Deschênes et al., 1998; Rouiller and Welker, 2000). Terminals vary widely in size (2–10+μm), notably these distributions include a heavy tail of "giant" synapses reported in somatosensory, visual, and auditory HO nuclei (Llano and Sherman, 2008; Hoerder-Suabedissen et al., 2018; Prasad et al., 2020). "Giant" boutons are glomerular structures containing multiple synapses (Hoerder-Suabedissen et al., 2018) and development of these structures appears to be use-dependent (Hayashi et al., 2021). A recent anatomical comparison of L5tt-HO thalamus terminals (Prasad et al., 2020) reports some pathway-specific variation in size: V1 to pulvinar/LP, and PFC to MD terminals are somewhat smaller than S1 L5tt-POm benchmark "giant" synapses, but still larger than L6A-thalamus terminals.

These "driver" synapses have high release probability and high postsynaptic density of AMPA and NMDA receptors (Hoogland et al., 1991; Li et al., 2003b; Reichova and Sherman, 2004; Groh et al., 2008). While sparse–for example, single L5tt fibers form an average of only three boutons onto single POm neurons–single fiber activation can nevertheless trigger extremely large (∼3 nA in rat, ∼ 800 pA in mouse) excitatory postsynaptic currents (EPSCs), which drive large, unitary EPSPs (>10 mV) (Li et al., 2003b; Groh et al., 2008; Seol and Kuner, 2015). Aside from sheer synaptic strength, the EPSCs have exceptionally fast (<1 ms/2 ms rise/decay in rat) kinetics due to the presence of the GluA4 AMPA subunit (Seol and Kuner, 2015). While strong, L5tt-HO thalamus synapses are characterized by rapid and pronounced frequency-dependent depression due to presynaptic depletion of releasable vesicles (Reichova and Sherman, 2004; Groh et al., 2008; Seol and Kuner, 2015; **Figure 2**). At the L5tt-POm synapse, frequencies greater than ∼2 Hz induce depression, with paired-pulse ratios of 0.5 at 20 Hz, with similar values reported for L5tt-LP (Li et al., 2003b) and L5tt-MD and L5tt-VM (Collins et al., 2018), although comparable physiological data for the auditory system is lacking. In sum, despite some modality-specific anatomical variations which require further functional characterization (Prasad et al., 2020), L5tt-HO synapses appear to have relatively conserved

properties supporting powerful, temporally precise, adaptive information transmission.

HIGHER-ORDER THALAMUS SINGLE NEURON COMPUTATION

Strong synaptic drive by L5 prompts the question of how HO neurons encode descending cortical information. In the context of neural coding, corticothalamic information transfer has been widely studied as L6A's modulatory influence on FO neurons' encoding of sensory drivers, in combination with aligned feedforward inhibition from TRN (e.g., Contreras et al., 1996; Wolfart et al., 2005; Béhuret et al., 2013). In HO nuclei, the situation is different: L5tt driver synapses provide a mechanism by which L5tt neurons' precise spike times reach HO thalamus with minimal temporal distortion as large, fast EPSCs; via synaptic depression, EPSC amplitude will reflect L5's preceding spiking history. To generate thalamic spikes, these cortically generated EPSCs must be integrated with other driver inputs (if present, e.g., Groh et al., 2013; Bickford, 2015; Blot et al., 2021), and finally transformed to spikes by intrinsic membrane properties.

Bursting

Intrinsic thalamic contributions to a corticothalamic code from L5tt to HO thalamus are expected to be considerable, given the nonlinear bursting properties of thalamic neurons (Llinás and Jahnsen, 1982) and increased appreciation for bursting as a significant mode of information processing (Zeldenrust et al., 2018b). In brief, across modalities, HO neurons display the well-known burst-tonic excitability switch characteristic of thalamic relay neurons (**Figure 2**). Burst spiking–high-frequency sodium APs superimposed on a transient calcium plateau or "low-threshold spike"–arises from the interplay of slow voltage-dependent currents, namely I_T, carried by the Cav3 subfamily of calcium channels, with some contribution from I_H, the hyperpolarization-activated cation current (Jahnsen and Llinas, 1984; Destexhe et al., 1993; Sherman, 2001). In particular, the phenomenon of bursting in thalamic neurons is well-studied, but a limitation to understanding HO bursting is that most detailed biophysical measurements come from FO neurons, typically from the visual system.

Several reports indicate that bursting properties differ between HO and FO nuclei: (Ramcharan et al., 2005) report more bursting in primate HO MD and HO pulvinar; cortico-recipient LP in rat shows enhanced bursting (Li et al., 2003a) and likewise, in tree shrew pulvinar (Wei et al., 2011), increased bursting was associated with increased expression of Cav3.2 and SK2, an afterhyperpolarization-generating K+ channel which can support repetitive firing. The somatosensory system appears to be an exception, as (Landisman and Connors, 2007) found that HO POm spikes at lower frequencies relative to FO VPM, both within bursts and during tonic spiking, associated with a higher voltage threshold for AP initiation in HO POm. A recent comparison across sensory modalities (Desai and Varela, 2021) provides a mechanistic framework for understanding some of these differences based on electrophysiology and simulations. Rebound burst size (number of APs) in HO nuclei was comparable across sensory modalities. However, differences between FO and HO bursting were modality specific and in agreement with data previously reported for single modalities: in visual and auditory thalamus, FO nuclei were less bursty than HO nuclei, while in somatosensory thalamus, the FO nucleus was more bursty than HO. This spectrum of bursting properties could be reproduced by changing the voltage-dependence and maximal conductance of I_T. Taken together, these studies suggest functionally relevant differences in fast and slow intrinsic excitability mechanisms in HO and FO thalamic neurons.

Indeed, a recent comprehensive report of the thalamus transcriptome (Phillips et al., 2019) found that HO and FO nuclei show distinct transcriptomic profiles based on expression of genes tightly linked to neuronal identity (ion channels, receptors), in line with distinct intrinsic excitability of HO neurons. These points underscore the need for additional basic functional data from HO neurons, particularly voltage-clamp studies of biophysical properties necessary for computational studies, and at minimum, caution in using FO models as stand-ins for HO neurons in simulations.

Intrinsic Transformation of L5tt-HO EPSCs

We emphasize that careful consideration of bursting mechanisms is key to understanding how HO thalamus performs computations on descending cortical signals, as these mechanisms are responsible for nonlinear transformation of L5tt-evoked EPSCs to EPSPs. In the simple case of synaptic input after a period of inactivity, e.g., the beginning of a cortical Up state–large undepressed EPSCs will be further enhanced by activation of I_T; functionally, this means that a single L5tt spike can evoke bursts of spikes in a post-synaptic HO neuron (supralinear corticothalamic spike transfer) (Groh et al., 2008; Seol and Kuner, 2015). In the more complicated case of higher input rates, synaptic depression will decrease EPSC size and preceding depolarization will simultaneously inactivate I_T, supporting a more linear EPSC→ EPSP transformation. Here, integration of coincident inputs from different L5tt neurons can be required to drive output spikes (Groh et al., 2008). Although L5tt neurons' drive of HO neurons at the single-neuron level has been most studied in the somatosensory system, the parallel effect of synaptic depression paired with inactivation of bursting is also apparent in data from other modalities (Li et al., 2003b; Collins et al., 2018).

The information processing role of bursts is an active area of study, and our understanding of thalamic burst coding continues to be refined. Recent studies (Elijah et al., 2015; Mease et al., 2017; Zeldenrust et al., 2018a; Park et al., 2019) make it clear that various properties of thalamic bursts (number of spikes, timing of spikes, burst onset, etc.) can convey information about presynaptic inputs, so it may be that the distinct bursting properties of HO thalamus subserve a particular functional role. In HO POm, we found that intrinsic bursting and high spiking threshold of POm neurons provides a mechanism

for "multiplexed coding" of low- and high-frequency (∼5 Hz and >100 Hz) information, and that high-frequency encoding channel showed information-preserving adaptation (Mease et al., 2017). Furthermore, the exact bandwidth of the "slow" encoding channel was tuned by depolarization. This finding suggests that POm spike trains could carry information both in burst size and precise spike timing within bursts. However, the implications of this intrinsic code in combination with strong L5tt-HO synaptic depression have yet to be assessed. While it is not clear if these findings can be generalized to other nuclei, the observation that HO bursts seem to show less variation across modalities (Desai and Varela, 2021) suggests that further investigation of a common HO thalamic computational scheme for encoding L5tt inputs may provide new insights beyond those gleaned from studies focusing on computation in FO thalamus.

Neuromodulation

A final unexplored factor in HO thalamic encoding of L5tt inputs is neuromodulation. As membrane potential is a critical mediator of bursting properties, any modulatory input altering baseline depolarization or hyperpolarization would be expected to exert strong control over HO thalamic encoding. While neuromodulation specific to HO thalamus has not been widely studied, evidence suggests that it may dynamically regulate HO CTC network activity. For example, Stitt et al. (2018) suggest that activity in the HO thalamus may be state-dependent and influenced by ongoing levels of arousal. Elsewhere, it was found that the brainstem cholinergic system preferentially suppresses spontaneous activity in the POm-targeting region of ZI, thereby enhancing whisker responses in the POm (Masri et al., 2006; Trageser et al., 2006). Furthermore, Varela and Sherman found neuromodulation may exert differential effects on FO and HO neurons: while all FO and most HO neurons are depolarized by muscarinic and serotonergic activation, a significant fraction (15–20%) of HO neurons are hyperpolarized (Varela and Sherman, 2007, 2009). Taken in combination with attentional control of TRN and arousal-dependent activation of L6B discussed in the previous section, these studies tentatively point to an unexplored state-dependence of HO thalamus's processing of L5tt drive. Future studies of this topic are warranted, particularly incorporating insight from recent molecular profiling work (Phillips et al., 2019) which may provide specific candidate mechanisms for state-dependent control.

HIGHER-ORDER THALAMIC ENCODING OF L5TT CORTICAL INFORMATION

A wealth of evidence demonstrates that HO thalamus spike output is strongly affected or even contingent upon L5tt output, in line with the driver characteristics of this pathway. Manipulations of S1 cortex (Diamond et al., 1992) showed that spiking in HO POm but not FO VPM depend on S1 input; more specific optogenetic drive of L5 *in vivo* is sufficient to drive large driver EPSPs and bursts in POm, and VGAT optogenetic inhibition of S1 eliminates POm spiking (Groh et al., 2013; Mease et al., 2016c). Similarly, portions of HO LP (Bennett et al., 2019; Kirchgessner et al., 2021) are driven by L5tt inputs from V1. This situation is supported by findings that receptive fields in HO thalamus *in vivo* are typically broad and less specific for primary sensory drive (Moore et al., 2015; Urbain et al., 2015; Mease et al., 2016b; Williamson and Polley, 2019), suggesting that HO nuclei receive most sensory information after it has been processed by L5. Given the relatively low convergence of L5tt neurons onto HO neurons (Sumser et al., 2017; Rockland, 2019), single HO neurons may integrate the spiking of small cortical ensembles; indeed, in anesthetized mice, there is some evidence that HO thalamus may be driven to spike by just 1–3 active L5tt neurons *in vivo* (Mease et al., 2016c). Thus, the question becomes: what particular patterns of L5tt activation could be encoded by HO thalamus?

A critical piece of information necessary for understanding what L5tt signals HO neurons transmit back to the cortex is exactly what L5tt neurons encode and what the "raw" cortical input arriving in HO looks like via single fibers and convergent inputs from groups of L5tt neurons. L5tt neurons have been the focus of intense experimental and theoretical research interest over decades (Larkum, 2013; Ramaswamy and Markram, 2015; Sakmann, 2017), but despite this arguably focused attention, the exact signals propagated through L5tt pathways are not yet fully understood, despite being one of the most active neurons during behavior (de Kock et al., 2007; O'Connor et al., 2010; Senzai et al., 2019). The emerging picture is that L5tt spiking on both single-neuron and population levels carries complex information, with L5tt neurons typically showing broad sensory tuning (de Kock et al., 2007; Williamson and Polley, 2019) in line with their integration of multilaminar information in basal and apical dendrites, which is presumably inherited by HO thalamic targets. Extensive discussion of L5's coding across modalities is beyond our scope; here we attempt to orient two key characteristics of L5tt output–bursting and ensemble synchrony–to what is known about further subcortical processing in HO thalamus.

L5tt Bursting

The active, nonlinear dendritic properties of L5tt neurons [reviewed in Larkum (2013); Ramaswamy and Markram (2015)] provide a single-neuron substrate for the integration of "top-down" and "bottom-up" information streams arriving at different lamina. Excitation of either basal or apical dendrites leads to sparse spiking, but near-coincident excitation of both regions triggers a burst of high-frequency (>100 Hz) APs which depends on a backpropagating AP in the soma triggering a calcium plateau in the apical tuft (Larkum et al., 1999; Larkum, 2013). In this framework, bursts indicate a temporal alignment of internal representation and novel external information. Such high-frequency bursts are characteristic of L5tt neurons in the primary somatosensory (Larkum et al., 1999; de Kock and Sakmann, 2008), visual (Shai et al., 2015), and auditory (Llano and Sherman, 2009; Williamson and Polley, 2019) cortices, and are associated with perception (Takahashi et al., 2016, 2020) and exploratory whisker touch (de Kock et al., 2021). While bursting appears to be an important nonlinear computational property of L5tt neurons, it remains to be determined if these spiking patterns are relevant for postsynaptic targets such as HO thalamus, i.e.,

are these high-frequency patterns faithfully transferred across the L5tt-HO thalamus synapse?

L5tt Synchrony and Ensemble Activity

Particular patterns of L5tt synchronization often involve inhibitory feedback interactions with interneurons, reviewed in Naka and Adesnik (2016). In particular, L5tt neurons excite both Martinotti cells (a subset of somatostatin-positive interneurons) which inhibit L5tt apical tufts, and PV neurons, which provide perisomatic inhibition to L5tt neurons. Inhibition from Martinotti neurons seems particularly tuned to L5tt bursting, as Martinotti neurons are preferentially recruited by high-frequency inputs from L5tt due to synaptic facilitation. This "frequency-dependent disynaptic inhibition" is a mechanism linking L5tt bursting to population synchrony, as bursting in a handful of L5tt neurons preferentially inhibits and synchronizes neighboring L5tt neurons (Silberberg and Markram, 2007; Hilscher et al., 2017).

Synchronous activity in particular frequency bands is an important mechanism by which cortical circuits transfer information (Buzsáki and Draguhn, 2004) and recent work has begun to relate understanding of cortical rhythms to specific neuronal cell types. For example, Adesnik and Scanziani (2010), Otsuka and Kawaguchi (2021) report that stimulation of L2/3 pyramidal neurons evokes beta/gamma band activity in L5tt neurons. Corticothalamic synchrony has been explored extensively from the perspective of CTL6 inputs to thalamus (e.g., Contreras et al., 1996; Bal et al., 2000; Béhuret et al., 2013), but how L5 synchrony might propagate to the HO thalamus is only beginning to be studied. For example (Stitt et al., 2018) find that alpha and theta band coherence is prominent in deep-layer PPC and pulvinar interactions; while this study did not specifically isolate layer 5, the involvement of HO nuclei suggest that L5tt input could participate in driving these corticothalamic oscillations. In sum, L5 synchronous population oscillations over a wide range (alpha, beta, theta, and gamma) of frequencies suggest that L5tt-HO thalamus synapses will have synchronized activation at diverse temporal scales that will engage different degrees of synaptic depression.

Recent efforts have begun to explore how pyramidal single-cell properties and population activity in the cortex are linked to implement network-level information coding strategies. The recently proposed Burst Ensemble (Naud and Sprekeler, 2018) theory suggests that ensemble event rate in L5tt (spike or burst count/time) reflects somatic input, burst probability reflects apical input, and burst rate reflects coincident somatic and apical input, while a simple spike rate code cannot disambiguate these combinations of inputs. Lipshutz et al. (2020) explored how simple model networks of pyramidal neurons can implement canonical correlation analysis, finding the features in apical and basal inputs which have maximal correlation; in this framework bursts indicate maximal alignment between the two input sources. Lankarany et al. (2019) demonstrate synchrony-division multiplexing: S1 neurons receiving common input can use the rate of asynchronous spiking to encode the intensity of low-contrast stimulus features while using the timing of synchronous spikes to encode the occurrence of high-contrast features. These studies highlight the importance of simultaneously considering cortical bursts and synchronous spikes as putatively informative signals for postsynaptic targets such as HO thalamus.

In sum, L5tt spike trains appear to carry information in spike count and timing and population synchrony; it is not well understood to what degree these information streams are disentangled and further transformed in HO thalamus. Groh et al. (2008) show that stimulating L5tt-POm synapses with *in vivo* L5tt spiking patterns resulted in single L5tt spikes driving POm spiking or bursting after long periods of silence in contrast to subthreshold EPSPs evoked at higher presynaptic L5tt rates sufficient to induce depression. Similarly, Collins et al. (2018) report that PFC L5tt EPSCs depress and only drive spiking in HO MD at the onset of 10 Hz stimulation. However, Groh et al. (2008) found that coincident activation of separate L5tt inputs served to overcome synaptic depression, and suggested a role for HO thalamus in detecting synchronous firing of L5tt neurons. Within the HO thalamus multiplexing framework (Mease et al., 2017), such coincident L5tt upstream activity could be encoded by the timing and spike count of POm bursts. Such coincidence detection may also work similarly in the case of integration of cortical and subcortical drivers, as in anesthetized animals, POm output reflects the latency between L5 activation and whisker stimulation (Groh et al., 2013).

Abundant evidence highlights L5tt bursts as somewhat privileged spiking patterns, both in terms of selective encoding of inputs and intracortical impact. From the point of view of HO thalamus, bursts would be translated into temporally discrete EPSCs of decreasing size. We hypothesized that the intrinsic properties of POm neurons may allow these EPSCs to influence spike timing within HO bursts, a situation which would preserve much of the temporal information with L5tt bursts (Mease et al., 2017), but this possibility remains to be tested particularly in awake animals during which HO thalamus bursting is less pronounced. An alternative hypothesis is that subsequent spikes in L5tt bursts evoke EPSCs too small to drive spiking in HO thalamus, or require coincident bursts from multiple presynaptic L5tt neurons to drive HO spiking. Combining cell-type-specific approaches with depth-resolved high-yield recordings in cortex (e.g., Senzai et al., 2019) and HO thalamus (e.g., Kirchgessner et al., 2020) will likely provide data to test these hypotheses.

HIGHER-ORDER THALAMOCORTICAL PROJECTIONS TO CORTEX

How do signals computed by HO thalamus functionally impact the cortex? As we have reviewed above, although the exact features in L5tt spiking encoded by HO neurons and sent back to cortex remain to be determined, several recent studies have begun to clarify the function of HO TC inputs within the cortical microcircuit. These insights have built upon foundational anatomy studies demonstrating that HO TC projections follow the "matrix" pattern of TC innervation in that projections are not somatotopically precise and tend to be wide-ranging across cortical areas [reviewed in Harris and Shepherd (2015)]. In this section, we differentiate HO and FO TC pathways and

highlight recent advances in understanding cell-type-specific HO TC innervation. We close with a discussion of recent evidence for the functional importance of HO TC inputs in higher-level CTC computations.

The function of HO CTC circuits cannot be viewed in isolation from other components of the cortical microcircuit–we refer to Shepherd and Yamawaki (2021) for a comprehensive review of CTC wiring, functional connectivity, and integration with feed-forward cortico-cortico circuits. Moreover, we also restrict our scope to differentiating HO and FO TC pathways in reciprocally connected circuits (e.g., S1→ POm→ S1). Readers are referred to other sources for discussion of HO properties for identified transthalamic sensory pathways S1-POm-S2 (Theyel et al., 2010; Viaene et al., 2011); there is evidence that TC inputs may have different laminar targets and synaptic properties in transthalamic circuits (e.g., Casas-Torremocha et al., 2019; Rodriguez-Moreno et al., 2020).

In S1, layer-specific HO TC inputs tend to interdigitate with and complement FO TC inputs (**Figure 1**), with dense HO projections to L5A and L1 (Koralek et al., 1988; Lu and Lin, 1993; Bureau et al., 2006; Meyer et al., 2010b; Wimmer et al., 2010), These distinct innervation patterns predict that HO thalamus provides synaptic input to particular cortical neuronal targets with dendrites in these lamina; the degree of expected TC innervation is often predicted as a function of depth as the TC projection density multiplied by the dendritic reconstruction's summed cross-section. Optogenetic-aided circuit-mapping methods, (e.g., Bureau et al., 2006; Audette et al., 2017; Sermet et al., 2019) have provided the means to assess these anatomical predictions on a functional level, albeit largely *in vitro* in brain slices, and it has become clear that HO TC inputs provide input both excitatory and inhibitory neurons distinct from that provided by FO TC inputs.

Cell-Type-Specific Innervation

Excitatory Neurons

HO TC inputs provide direct excitation to both L2/3 and L5 pyramidal neurons (**Figure 1** green), although different degrees of cell-type-specific excitation are seen across cortical regions. In S1, HO POm fibers evoke EPSPs in excitatory neurons across all cortical layers (Audette et al., 2017; Sermet et al., 2019), with the largest responses in L5A pyramidal neurons (Bureau et al., 2006; Audette et al., 2017; Sermet et al., 2019), which is sufficient to evoke robust spiking (Audette et al., 2017). Audette et al. (2017) also report significant but smaller input to L2/3 pyramidal neurons *in vitro*. While earlier reports found little direct HO input to L5tt neurons (Petreanu et al., 2009), small but significant inputs were reported by Audette et al. (2017); Sermet et al. (2019). A main point is that POm only provides weak inputs to L4, the main cortical recipient layer of FO TC inputs (Audette et al., 2017; **Figure 1** blue). Similarly, in the auditory system, projections from HO MGd to A1 L1 equally excite pyramidal neurons in L2/3 and L5 (Pardi et al., 2020). In HO nuclei targeted by PFC, the situation is different (Collins et al., 2018): excitatory inputs to L2/3 pyramidal neurons by HO MD are more than ∼3x greater than those to L5A neurons, while inputs from HO VM to both layers are comparably strong, suggesting that MD preferentially activates superficial neurons in L2/3. The relevance of L3 MD-PFC is further evidenced by the finding that the MD also drives disynaptic inhibition in L3 of medial PFC through excitation of PV interneurons, tightening the time window during which PFC pyramidal neurons can fire (Delevich et al., 2015).

Optogenetic manipulations of HO TC inputs *in vivo* have provided some evidence for how these inputs impact different cortical cell types in the intact brain. Gambino et al. (2014) find that HO POm evokes long-lasting NMDA-dependent plateaus in L2/3 pyramidal neurons, while (Mease et al., 2016a) show that HO POm projections provide long-lasting depolarizations in L5 neurons and enhance sensory responses *in vivo*, and this effect is even stronger under awake conditions (Zhang and Bruno, 2019). The recently proposed embedded ensemble encoding (Antic et al., 2018) theory suggests that ensembles of neurons experiencing a synchronized somatic depolarization are in a transient "prepared state" to respond with precise spike timing to additional inputs. Given this evidence for HO TC induction of sustained depolarizations, HO thalamus could play a role in coordinating such transient ensembles of "prepared" neurons and sensitizing the cortex to additional synaptic inputs. One experimental difficulty in assessing HO TC's impact *in vivo* that mass optogenetic excitation and inhibition does not lend itself to physiological stimulation patterns and it is likely that more naturalistic interventions will reveal nuances of the effect of HO TC projections–for example, the use of step-opsins by Mukherjee et al. (2020) to show that enhancement of MD thalamus led to inhibition dominating activity in PFC.

Interneurons

HO-thalamus innervation of specific interneuron types in cortex (**Figure 1**) appears to be key to understanding the functional impact of HO TC inputs, with several recent studies taking advantage of molecular markers for different interneuron populations. In particular, in S1, POm HO TC inputs provide strong excitation to PV interneurons in L5a and L2/3 but little direct input to SOM interneurons (Audette et al., 2017; Sermet et al., 2019; Williams and Holtmaat, 2019). Thus HO TC provides disynaptic inhibition via PV to L5a pyramidal neurons, as well as direct excitation (Audette et al., 2017). A future direction will be to understand how PV interneurons encode naturalistic HO inputs *in vivo*, as PV neurons are particularly excitable, with low membrane time constants and high repetitive firing ability. Intriguingly Cruikshank et al. (2007) showed that, due to these single-cell properties, fast-spiking (presumed PV) interneurons are intensively driven by FO TC inputs. More recently, Jouhanneau et al. (2018) found that precise PV spiking can be evoked by unitary cortico-cortical EPSPs. Although HO TC to PV neuron encoding remains to be assessed, the strong synaptic drive in combination with high post-synaptic temporal precision suggests PV neurons may be able to follow high-frequency information in HO spike trains.

Interneurons in L1 are increasingly appreciated as targets of HO TC inputs, although direct comparison across studies is somewhat challenging due to variations in exact methodology and specificity of classification. A small group of studies has

begun to clarify the importance of differential HO TC innervation of 5HT3 neurons in layer 1, which include VIP and NDNF populations (Schuman et al., 2021), particularly suggesting roles in disinhibition of deeper layers. In S1, 5HT3 interneurons receive direct HO POm input which evokes spiking *in vitro* (Audette et al., 2017). Notably, while somatostatin-positive (SOM) interneurons receive little direct HO TC input (Audette et al., 2017; Sermet et al., 2019; Williams and Holtmaat, 2019) find that PO excitation of VIP interneurons disynaptically inhibits SOM neurons. Similarly, Anastasiades et al. (2021) show that in PFC, HO MD projections directly target VIP neurons in L1, which then inhibit SOM neurons. These studies point to HO TC disinhibition of the pyramidal targets of SOM neurons, with possible implications for network synchronization, i.e., via Martinotti neurons' interactions with L5tt discussed in the previous section. Finally, results from two different cortical regions demonstrate a role for neurogliaform/NDNF interneurons' interaction with HO TC inputs in controlling pyramidal neuron excitability. Pardi et al. (2020) find that neurogliaform interneurons provide presynaptic inhibition of the HO MGd terminals involved in learning and triggering long-lasting NMDA potentials. Anastasiades et al. (2021) show that L1 NDNF interneurons in PFC are innervated by HO VM and inhibit SOM interneurons, but also act to block VM's direct excitation of L5tt neurons' apical tufts.

HO Thalamus in Sensory Processing and Cognition

Cell-type-specific circuit interventions have revealed roles for HO thalamus in conveying signals important for learning, perception, and behavioral salience. Recent *in vivo* studies in behaving animals are also providing insight into the qualitative content of these HO thalamus signals, supporting roles for HO TC in promoting awake cortical behavior patterns associated with learning, cognitive flexibility, perception, and even consciousness.

In S1, studies by Holtmaat and colleagues provide a strong line of evidence for HO POm in generating long-term potentiation of intracortical synapses onto L2/3 pyramidal neurons via NMDA-dependent plateau potentials which depend on VIP-mediated disinhibition (Gambino et al., 2014; Williams and Holtmaat, 2019); these plateau potentials also provide a mechanism for cortical map plasticity (Pagès et al., 2021). In a multi-whisker sensory association task, Audette et al. (2019) found that training sequentially induces plasticity at HO POm TC synapses onto L5 and L2 pyramidal neurons, thereby increasing POm-driven spiking without changes in cortical single-cell properties. In an auditory associative learning task, Pardi et al. (2020) also demonstrated learning-related HO TC plasticity, finding that HO TC input to A1 transmits memory-related information which reflects task-specific relevance of sensory stimuli. El-Boustani et al. (2020) find that HO thalamus inputs show goal-directed modulation in mice trained in a whisker discrimination task; similarly (LaTerra et al., 2020) find that HO POm axons in S1 signal correct performance during goal-directed behavior and that inhibition of POm impedes task performance.

In the context of cognition, it is suggested that a generic role for the thalamus may be to coordinate and maintain cortical representations relevant for particular cognitive tasks (Halassa and Kastner, 2017; Nakajima and Halassa, 2017). For example, in an auditory-visual cue-switching attentional task, Schmitt et al. (2017) find that HO MD maintains PFC ensemble representations of task rules by control of functional connectivity. In the same behavioral paradigm, Rikhye et al. (2018) found that interactions between the PFC and HO MD provide a mechanism for cognitive flexibility to switch cortical representations, with MD thalamus encoding behavioral context. Although the specific contributions of L5 inputs to such cognitive tasks remain to be assessed, recent evidence suggests that L5-CTC loops may be key to conscious perception. For example, Suzuki and Larkum (2020) show that HO POm TC input enables L5tt dendro-somatic coupling necessary for awake activity patterns and robust somatic spiking, and that general anesthesia blocks this coupling. Although not specific to L5, Redinbaugh et al. (2020) find that in primates, activity in central lateral (CL) HO thalamus and deep-layer cortical neurons correlate with consciousness level; indeed, gamma stimulation in CL could rouse monkeys from anesthesia. These studies point to diverse but unexplored functions for HO nuclei in higher-level cognitive computations in the cortex.

We emphasize here that a core component of disentangling HO thalamus's role in critical cortical function is quantification of how patterns of L5tt spiking are selected and transmitted back to the cortex. Finally, understanding the impact of specific patterns of HO neuron activity in cortex will require combining emerging knowledge of cell-type-specific TC synaptic dynamics with the state-dependent, nonlinear dendritic integration properties of cortical neurons, along with detailed microcircuit connectivity patterns.

THE CLINICAL RELEVANCE OF L5tt-HO CTC NETWORKS

The Pathological Role of L5-Originating CTC Networks in Pain

While further work is required to assess the underlying mechanisms and functionality of L5-originating CTC networks, recent studies have emphasized their potential clinical relevance (see **Table 2**). Among these, an increasing number of studies highlight the importance of these CTC networks in processing nociceptive information in both acute and chronic pain states. For example, spared nerve injury (SNI) in rodents- a model of neuropathic pain–results in a three-fold increase in Ca^{2+} activity in the somata of L5 pyramidal neurons in S1, as well as an increase in dendritic spine Ca^{2+} activity (Cichon et al., 2017). However, this study did not assess the impact of enhanced cortical activity on HO thalamic nuclei. Indeed, the development of chronic pain is associated with several maladaptive alterations in S1 and other cortical regions (e.g., hyperexcitability, somatotopic reorganization), but there remains a need to characterize how these alterations specifically influence CTC networks, especially given that these cortical alterations typically correlate with the

degree of mechanical allodynia (i.e., a painful sensation resulting from typically innocuous mechanical stimuli) (Tan and Kuner, 2021). The relevance of these cortical alterations, and their potential impact on HO nuclei and CTC networks, is further exemplified by the fact that targeting S1 alterations beneficially alters pain trajectories (Flor et al., 2001; Moseley and Flor, 2012; Cichon et al., 2017). Hyperactive states in L5 neurons have also been observed in other cortical areas under inflammatory states–for instance, a study employing a peripheral inflammatory mouse model found transient hyperactivity in L5 pyramidal neurons in the frontal/motor cortex (Odoj et al., 2021). However, this study did not observe L5 hyperactivity in S1, so it is unclear whether the frontal/motor cortex alterations are pain-relevant.

Cichon et al. (2017) further investigated the role of inhibitory circuits in the development of S1 alterations, specifically, the source of L5 hyperactivity in chronic pain. It was shown that 1 month following SNI induction, somatostatin (SOM) interneuron activity, which regulates somatic and dendritic pyramidal cell activity, was reduced by half. Likewise, PV interneuron activity was reduced. In part, these findings were the result of a 90% increase in vasoactive intestinal peptide (VIP)-expressing interneuron activity in SNI animals, which directly inhibit SOM and PV interneurons. The SOM contribution to L5 pyramidal cell hyperactivity was confirmed through selective SOM cell activation, which decreased L5 dendritic and somatic Ca^{2+} activity and prevented the development of mechanical allodynia (Cichon et al., 2017). However, activation of PV interneurons did not alter mechanical thresholds for pain, perhaps because these cells predominantly synapse perisomatically, or because they provide only brief inhibition of somata (Cichon et al., 2017). Given the specific interaction of HO TC inputs with PV and VIP interneurons covered in the previous section and the plasticity of these connections (Audette et al., 2017, 2019; Williams and Holtmaat, 2019), it may be productive to further assess how HO TC inputs contribute to maladaptive cortical plasticity related to chronic pain.

It may be that L5 alterations in part contribute to changes observed in HO nuclei during chronic pain. For example, the PO nucleus, which is involved in pain processing, displays higher spontaneous firing rates and greater responses to both noxious and innocuous peripheral stimuli in a chronic pain state (Perl and Whitlock, 1961; Whitlock and Perl, 1961; Casey, 1966; Mao et al., 1993; Masri et al., 2009; Park et al., 2018). Another relevant HO nucleus is the MD, which mediates affective aspects of pain and is similarly hyperactive in chronic pain states. However, as with the PO, it is not understood if these changes in part stem from CTC alterations at the level of the cortex (Rinaldi et al., 1991; Wang et al., 2007; Whitt et al., 2013; Mitchell, 2015). Reinforcing its role in affective components of pain, optogenetic activation of MD inputs in the anterior cingulate cortex (ACC) elicits a conditioned place-aversion in the SNI model and chemotherapy-induced neuropathy, but intriguingly, direct inhibition of L5tt ACC projection neurons to the MD nucleus also produces this effect (Meda et al., 2019). In addition, inactivation and lesioning of the MD nucleus both resulted in a reduction in thermal and mechanical hyperalgesia in a rodent model of neuropathic pain (Saadé et al., 2007). Overall, while further effort is required to assess the overall role of CTC networks in pain, evidence suggests that both HO-projecting L5tt cells and HO thalamic nuclei are altered in pain states, and that targeting these alterations may serve to benefit pain trajectories.

The Pathological Role of CTC Networks in Auditory Disorders

In the auditory system, comparable to the findings in chronic pain, Asokan et al. (2018) observed a hyperactive state of L5 projection cells in the auditory cortex following noise-induced damage to cochlear afferents, and this effect was sustained for several weeks (Asokan et al., 2018). Specifically, this L5 potentiation–which represents a form of compensatory plasticity–was observed in projections to the IC, but the same study also found axon collaterals to the HO MGBd nucleus (Asokan et al., 2018). Alterations in inhibitory networks are also implicated in this L5 pathology–for instance, PV interneuron-mediated intracortical inhibition is significantly reduced for at least 45 days following cochlear synaptopathy (Resnik and Polley, 2017). Increased sensory gain is a characteristic finding across noise-induced hearing-loss pathologies (e.g., tinnitus), and it is proposed that L5 projection neurons are responsible for driving hyperexcitability and strong coupling across tinnitus-associated brain networks (Asokan et al., 2018). As with the pain example discussed above, the impact of such pathological L5 activity on auditory HO nuclei remains to be assessed.

The Pathological Role of CTC Networks in Cognitive/Behavioral Dysfunction

In addition to the apparent involvement of CTC networks in sensory modalities, recent work has alluded to their relevance to pathologies characterized by cognitive and behavioral dysfunction, such as schizophrenia (SZ) and Alzheimer's disease (AD). Studies have demonstrated the involvement of the MD in these dysfunctions, and there is human, rodent and primate evidence that they can be elicited by damaging this thalamic nucleus (Mitchell et al., 2007, 2014; Mitchell and Gaffan, 2008; Mitchell, 2015; Perry et al., 2021). For instance, monkeys with damage in the MD display impairments in complex associated learning tasks (Mitchell et al., 2007). MD damage-associated impairment has been postulated to result from disruption of the influence of the MD nucleus on the PFC, since the MD nucleus and PFC are reciprocally connected within specific subdivisions (e.g., the pars parvicellularis of the MD is reciprocally connected to the dorsolateral PFC), but this view is contested (Mitchell, 2015; Collins et al., 2018). Specifically, the MD has been shown to activate cortico-cortical projections in layers 2 and 3 in the PFC (Collins et al., 2018). Further work on thalamic innervation of associative brain structures has shown that enhanced excitability in the MD elicits suppression of PFC excitatory neurons (Mukherjee et al., 2020).

Moreover, it was found that hypoxic-like damage to the PFC results in enhanced theta-frequency coherence between the MD and the PFC, as well as an increase in the frequency of bursting in MD neurons, while subsequent knockdown of T-type calcium channels (Cav3.1) in the MD nucleus decreased

theta-frequency coherence and attenuated associated symptoms (e.g., frontal lobe seizures and locomotor hyperactivity). The authors propose that the observed neurological and behavioral abnormalities result from impaired thalamocortical feedback between the PFC and the MD, driven by the activation of thalamic T-type calcium channels (Kim et al., 2011). Moreover, abnormalities have been reported in HO nuclei in SZ patients, including reductions in the volume and activity of the MD nucleus and the PuV. This may disrupt transthalamic networks and account for schizophrenia-associated cognitive impairments (Sherman, 2017). In fact, Parnaudeau et al. (2013) show that pharmacogenetic inhibition of the MD nucleus disrupts MD-PFC synchrony in the beta range, causing cognitive impairment with relevance to SZ. Similarly, there is evidence that CT dysfunction contributes to cognitive and behavioral impairments observed in AD (Jagirdar and Chin, 2019).

In addition to these findings, it is increasingly understood that dendritic integration in pyramidal neurons, which plays essential roles in sensory processing and cognition, is disrupted in a range of neurodevelopmental disorders (Nelson and Bender, 2021). For example, autism spectrum disorder is associated with genetic changes that elicit functional, morphological, and organizational alterations in L5, but it is not understood if and how these cortical changes affect the rest of the CTC network (Nelson and Bender, 2021).

DISCUSSION

The thalamocortical field has clearly moved on from the historical view of the thalamus as simply a passive provider of input to the cortex, although this view is still surprisingly entrenched in general neuroscience literature. As comprehensively framed by Sherman and Guillery (2006); Sherman (2016), any adequate theory of cortical function must include active, dynamic, and iterative information processing by the thalamus. With unique L5tt input and output connectivity patterns in combination with distinct synaptic and intrinsic properties, HO thalamic nuclei are well-suited to support top-down information transformation and exchange critical for novelty detection and prediction (Keller and Mrsic-Flogel, 2018) or propagation of learning-related signals (Chéreau et al., 2021).

Here, we have sought to present a broad overview of L5tt corticothalamic information transfer to HO thalamus and back to the cortex. Rather than attempting comprehensive coverage, we have highlighted mechanistic properties and functional findings underscoring the point that insights from FO nuclei may not transfer well to HO nuclei as points of orientation for neuroscientists new to the vast, complex thalamocortical literature. Although we have attempted to balance findings across sensory modalities and HO regions where data are present, many recent illuminating studies were done only in single regions–for example, many of the very recent cell-type-specific functional insights about HO TC inputs are from the somatosensory system. Lastly, in focusing largely on studies using cell-type-specific and/or experimental methods tractable in rodents, by necessity most of the presented information comes from experiments in mouse and rat models.

A key point is that in comparison to the relatively rich theoretical framework focused on cortical function, further subcortical processing of L5tt signals has been comparatively neglected. Cortico-centric models have yet to be fully integrated with the transthalamic communication model (Sherman and Guillery, 2011)–we emphasize that a central missing piece is how exactly L5tt signals are processed and encoded in HO thalamus. Whatever the modality-specific information L5tt spike trains send to HO thalamus, these signals will be further transformed by a heady blend of strong synaptic depression, the nonlinear input/output properties of single HO thalamic neurons tuned by dynamic L6A and TRN-driven excitation and inhibition, and finally, integration with other subcortical drivers and strong extrathalamic sources of inhibition.

Cast in this light, it is not particularly surprising that the question of what HO thalamus encodes is currently unanswered–but solving this puzzle appears increasingly central to understanding cortical network function underpinning cognition and perception. We have emphasized the viewpoint that it may be more productive to consider HO thalamus's encoding of driving cortical signals from L5tt, rather than any particular parameterization of raw sensory stimuli. Given the evidence for HO integration of L5tt inputs with non-cortical drivers and various neuromodulatory signals, this viewpoint is clearly an oversimplification–but possibly still a useful beginning step in linking L5tt drive of HO thalamus to general theories of cortical computation. More specifically, we hypothesize that HO thalamus may be able to simultaneously detect and transmit distinct patterns of L5tt synchrony and high-frequency spiking, and that these signals may have cell-type-specific functions in the cortex depending on HO TC postsynaptic targets. In the future, these ideas could be tested by combining high-yield electrophysiology approaches, cell-type-specific interventions, and recent advances quantifying selective information transfer between brain regions, such as the "communication subspace" scheme described by Semedo et al. (2019).

Although the synaptic and intrinsic mechanistic pieces appear to exist for an adaptive information-dense corticothalamic code from L5 to HO thalamus, there are still significant experimental and theoretical efforts to be made. Computational modeling would expedite understanding of how HO thalamus encodes cortical L5 spike trains, but based on our survey of ModelDB (Hines et al., 2004), very few models of HO thalamic neurons have been published (Golomb et al., 2006; Desai and Varela, 2021) and certainly none with the level of biophysical detail as recent modeling efforts focused on FO neurons (e.g., Connelly et al., 2016; Iavarone et al., 2019). Such efforts could boost further assessment of the relationship between bursting in L5 and HO thalamus, as it is clear that bursts can play privileged roles in both transmitting information and engaging plasticity mechanisms (Larkum, 2013; Crunelli et al., 2018; Zeldenrust et al., 2018b; Payeur et al., 2021). In the future, it will be important to expand

existing network models of thalamocortical interactions which are mainly but not always (see Golomb et al., 2006) based on FO data to include HO and FO distinctions in driving input, intrathalamic inhibition, and intrinsic properties which we have attempted to summarize here.

Finally, studies have begun to shed light on the clinical relevance of HO-thalamus CTC pathways, as a range of disruptions along these pathways, especially in HO nuclei, have been implicated in pathologies including chronic pain, SZ, and AD. However, present studies have largely concentrated efforts on characterizing either cortical or HO thalamic dysfunction in pathological contexts, but do not consider the interregional relationships. As such, further efforts are merited to transfer recent fundamental insights from sensory processing and cognition to pathology in L5tt-HO thalamus circuits, in particular studies that assess CTC pathways in their entirety. In the future, improving our understanding of these pathways in both pathological and non-pathological settings may serve to facilitate the identification of novel therapeutic targets and inform clinical strategies.

AUTHOR CONTRIBUTIONS

RM: conception, planning, and funding acquisition. RM and AG: research, writing, and editing. Both authors contributed to the article and approved the submitted version.

FUNDING

This work was funded by the Brigitte-Schlieben-Lange-Program, Baden-Württemberg (RM), Deutsche Forschungsgemeinschaft Collaborative Research Center 1158 (RM and AG), and Chica and Heinz Schaller Foundation (RM).

ACKNOWLEDGMENTS

The authors thank Alexander Groh for comments on early versions of this manuscript and the reviewers for their constructive suggestions for improvement.

REFERENCES

Adesnik, H., and Scanziani, M. (2010). Lateral competition for cortical space by layer-specific horizontal circuits. *Nature* 464, 1155–1160. doi: 10.1038/nature08935

Alcaraz, F., Fresno, V., Marchand, A. R., Kremer, E. J., Coutureau, E., and Wolff, M. (2018). Thalamocortical and corticothalamic pathways differentially contribute to goal-directed behaviors in the rat. *Elife* 7:e32517.

Anastasiades, P. G., Collins, D. P., and Carter, A. G. (2021). Mediodorsal and ventromedial thalamus engage distinct L1 circuits in the prefrontal cortex. *Neuron* 109, 314–330.e4.

Ansorge, J., Humanes-Valera, D., Pauzin, F. P., Schwarz, M. K., and Krieger, P. (2020). Cortical layer 6 control of sensory responses in higher-order thalamus. *J. Physiol.* 598, 3973–4001. doi: 10.1113/JP279915

Antic, S. D., Hines, M., and Lytton, W. W. (2018). Embedded ensemble encoding hypothesis: the role of the "Prepared" cell. *J. Neurosci. Res.* 96, 1543–1559. doi: 10.1002/jnr.24240

Asokan, M. M., Williamson, R. S., Hancock, K. E., and Polley, D. B. (2018). Sensory overamplification in layer 5 auditory corticofugal projection neurons following cochlear nerve synaptic damage. *Nat. Commun.* 9:2468.

Audette, N. J., Bernhard, S. M., Ray, A., Stewart, L. T., and Barth, A. L. (2019). Rapid plasticity of higher-order thalamocortical inputs during sensory learning. *Neuron* 103, 277–291.e4. doi: 10.1016/j.neuron.2019.04.037

Audette, N. J., Urban-Ciecko, J., Matsushita, M., and Barth, A. L. (2017). POm thalamocortical input drives layer-specific microcircuits in somatosensory cortex. *Cereb. Cortex* 28, 1312–1328. doi: 10.1093/cercor/bhx044

Bal, T., Debay, D., and Destexhe, A. (2000). Cortical feedback controls the frequency and synchrony of oscillations in the visual thalamus. *J. Neurosci.* 20, 7478–7488. doi: 10.1523/jneurosci.20-19-07478.2000

Barthó, P., Freund, T. F., and Acsády, L. (2002). Selective GABAergic innervation of thalamic nuclei from zona incerta. *Eur. J. Neurosci.* 16, 999–1014. doi: 10.1046/j.1460-9568.2002.02157.x

Barthó, P., Slézia, A., Varga, V., Bokor, H., Pinault, D., Buzsáki, G., et al. (2007). Cortical control of zona incerta. *J. Neurosci.* 27, 1670–1681. doi: 10.1523/jneurosci.3768-06.2007

Bartlett, E. L., Stark, J. M., Guillery, R. W., and Smith, P. H. (2000). Comparison of the fine structure of cortical and collicular terminals in the rat medial geniculate body. *Neuroscience* 100, 811–828. doi: 10.1016/s0306-4522(00)00340-7

Bayer, L., Serafin, M., Eggermann, E., Saint-Mleux, B., Machard, D., Jones, B. E., et al. (2004). Exclusive postsynaptic action of hypocretin-orexin on sublayer 6b cortical neurons. *J. Neurosci.* 24, 6760–6764. doi: 10.1523/jneurosci.1783-04.2004

Béhuret, S., Deleuze, C., Gomez, L., Frégnac, Y., and Bal, T. (2013). Cortically-controlled population stochastic facilitation as a plausible substrate for guiding sensory transfer across the thalamic gateway. *PLoS Comput. Biol.* 9:e1003401. doi: 10.1371/journal.pcbi.1003401

Bender, D. B. (1983). Visual activation of neurons in the primate pulvinar depends on cortex but not colliculus. *Brain Res.* 279, 258–261. doi: 10.1016/0006-8993(83)90188-9

Bennett, C., Gale, S. D., Garrett, M. E., Newton, M. L., Callaway, E. M., Murphy, G. J., et al. (2019). Higher-order thalamic circuits channel parallel streams of visual information in mice. *Neuron* 102, 477–492.e5.

Bickford, M. E. (2015). Thalamic circuit diversity: modulation of the driver/modulator framework. *Front. Neural Circuits* 9:86. doi: 10.3389/fncir.2015.00086

Blot, A., Roth, M. M., Gasler, I., Javadzadeh, M., Imhof, F., and Hofer, S. B. (2021). Visual intracortical and transthalamic pathways carry distinct information to cortical areas. *Neuron* 109, 1996–2008.e6. doi: 10.1016/j.neuron.2021.04.017

Bolkan, S. S., Stujenske, J. M., Parnaudeau, S., Spellman, T. J., Rauffenbart, C., Abbas, A. I., et al. (2017). Thalamic projections sustain prefrontal activity during working memory maintenance. *Nat. Neurosci.* 20, 987–996. doi: 10.1038/nn.4568

Bosch-Bouju, C., Hyland, B. I., and Parr-Brownlie, L. C. (2013). Motor thalamus integration of cortical, cerebellar and basal ganglia information: implications for normal and parkinsonian conditions. *Front. Comput. Neurosci.* 7:163. doi: 10.3389/fncom.2013.00163

Bourassa, J., and Deschenes, M. (1995). Corticothalamic projections from the primary visual cortex in rats: a single fiber study using biocytin as an anterograde tracer. *Neuroscience* 66, 253–263. doi: 10.1016/0306-4522(95)00009-8

Bourassa, J., Pinault, D., and Deschênes, M. (1995). Corticothalamic projections from the cortical barrel field to the somatosensory thalamus in rats: a single-fibre study using biocytin as an anterograde tracer. *Eur. J. Neurosci.* 7, 19–30. doi: 10.1111/j.1460-9568.1995.tb01016.x

Bureau, I., von Saint Paul, F., and Svoboda, K. (2006). Interdigitated paralemniscal and lemniscal pathways in the mouse barrel cortex. *PLoS Biol.* 4:e382. doi: 10.1371/journal.pbio.0040382

Buzsáki, G., and Draguhn, A. (2004). Neuronal oscillations in cortical networks. *Science* 304, 1926–1929. doi: 10.1126/science.1099745

Cajal, S. R. Y. (1906). *Santiago Ramón y Cajal – Nobel Lecture*. Available online at: https://www.nobelprize.org/uploads/2018/06/cajal-lecture.pdf (accessed December 31, 2017).

Casas-Torremocha, D., Porrero, C., Rodriguez-Moreno, J., García-Amado, M., Lübke, J. H. R., Núñez, Á, et al. (2019). Posterior thalamic nucleus axon terminals have different structure and functional impact in the motor and somatosensory vibrissal cortices. *Brain Struct. Funct* 224, 1627–1645. doi: 10.1007/s00429-019-01862-4

Casey, K. L. (1966). Unit analysis of nociceptive mechanisms in the thalamus of the awake squirrel monkey. *J. Neurophysiol.* 29, 727–750. doi: 10.1152/jn.1966.29.4.727

Chéreau, R., Williams, L. E., Bawa, T., and Holtmaat, A. (2021). Circuit mechanisms for cortical plasticity and learning. Semin. *Cell Dev. Biol.* S1084-9521(21)00199-3. doi: 10.1016/j.semcdb.2021.07.012

Cichon, J., Blanck, T. J. J., Gan, W.-B., and Yang, G. (2017). Activation of cortical somatostatin interneurons prevents the development of neuropathic pain. *Nat. Neurosci.* 20, 1122–1132. doi: 10.1038/nn.4595

Collins, D. P., Anastasiades, P. G., Marlin, J. J., and Carter, A. G. (2018). Reciprocal circuits linking the prefrontal cortex with dorsal and ventral thalamic nuclei. *Neuron* 98, 366–379.e4.

Connelly, W. M., Crunelli, V., and Errington, A. C. (2016). Passive synaptic normalization and input synchrony-dependent amplification of cortical feedback in thalamocortical neuron dendrites. *J. Neurosci.* 36, 3735–3754. doi: 10.1523/jneurosci.3836-15.2016

Contreras, D., Destexhe, A., Sejnowski, T. J., and Steriade, M. (1996). Control of spatiotemporal coherence of a thalamic oscillation by corticothalamic feedback. *Science* 274, 771–774. doi: 10.1126/science.274.5288.771

Crabtree, J. W. (2018). Functional diversity of thalamic reticular subnetworks. *Front. Syst. Neurosci.* 12:41. doi: 10.3389/fnsys.2018.00041

Crandall, S. R., Cruikshank, S. J., and Connors, B. W. (2015). A corticothalamic switch: controlling the thalamus with dynamic synapses. *Neuron* 86, 768–782. doi: 10.1016/j.neuron.2015.03.040

Crick, F. (1984). Function of the thalamic reticular complex: the searchlight hypothesis. *Proc. Natl. Acad. Sci. U.S.A.* 81, 4586–4590. doi: 10.1073/pnas.81.14.4586

Cruikshank, S. J., Lewis, T. J., and Connors, B. W. (2007). Synaptic basis for intense thalamocortical activation of feedforward inhibitory cells in neocortex. *Nat. Neurosci.* 10, 462–468. doi: 10.1038/nn1861

Crunelli, V., Lõrincz, M. L., Connelly, W. M., David, F., Hughes, S. W., Lambert, R. C., et al. (2018). Dual function of thalamic low-vigilance state oscillations: rhythm-regulation and plasticity. *Nat. Rev. Neurosci.* 19, 107–118. doi: 10.1038/nrn.2017.151

Daigle, T. L., Madisen, L., Hage, T. A., Valley, M. T., Knoblich, U., Larsen, R. S., et al. (2018). A suite of transgenic driver and reporter mouse lines with enhanced brain-cell-type targeting and functionality. *Cell* 174, 465--480.e22.

Danziger, S., Ward, R., Owen, V., and Rafal, R. (2004). Contributions of the human pulvinar to linking vision and action. *Cogn. Affect. Behav. Neurosci.* 4, 89–99. doi: 10.3758/cabn.4.1.89

de Kock, C. P. J., Pie, J., Pieneman, A. W., Mease, R. A., Bast, A., Guest, J. M., et al. (2021). High-frequency burst spiking in layer 5 thick-tufted pyramids of rat primary somatosensory cortex encodes exploratory touch. *Commun. Biol.* 4, 1–14.

de Kock, C. P., and Sakmann, B. (2008). High frequency action potential bursts (> or= 100 Hz) in L2/3 and L5B thick tufted neurons in anaesthetized and awake rat primary somatosensory cortex. *J. Physiol.* 586, 3353–3364. doi: 10.1113/jphysiol.2008.155580

de Kock, C. P., Bruno, R. M., Spors, H., and Sakmann, B. (2007). Layer- and cell-type-specific suprathreshold stimulus representation in rat primary somatosensory cortex. *J. Physiol.* 581, 139–154. doi: 10.1113/jphysiol.2006.124321

de Souza, B. O. F., Cortes, N., and Casanova, C. (2019). Pulvinar modulates contrast responses in the visual cortex as a function of cortical hierarchy. *Cereb. Cortex* 30, 1068–1086. doi: 10.1093/cercor/bhz149

Delevich, K., Tucciarone, J., Huang, Z. J., and Li, B. (2015). The mediodorsal thalamus drives feedforward inhibition in the anterior cingulate cortex via parvalbumin interneurons. *J. Neurosci.* 35, 5743–5753. doi: 10.1523/jneurosci.4565-14.2015

Desai, N. V., and Varela, C. (2021). Distinct burst properties contribute to the functional diversity of thalamic nuclei. *J. Comp. Neurol* doi: 10.1002/cne.25141

Deschênes, M., Veinante, P., and Zhang, Z. W. (1998). The organization of corticothalamic projections: reciprocity versus parity. *Brain Res. Brain Res. Rev.* 28, 286–308. doi: 10.1016/s0165-0173(98)00017-4

Destexhe, A., Babloyantz, A., and Sejnowski, T. J. (1993). Ionic mechanisms for intrinsic slow oscillations in thalamic relay neurons. *Biophys. J.* 65, 1538–1552. doi: 10.1016/s0006-3495(93)81190-1

Diamond, M. E., Armstrong-James, M., Budway, M. J., and Ebner, F. F. (1992). Somatic sensory responses in the rostral sector of the posterior group (POm) and in the ventral posterior medial nucleus (VPM) of the rat thalamus: dependence on the barrel field cortex. *J. Comp. Neurol.* 319, 66–84. doi: 10.1002/cne.903190108

El-Boustani, S., Sermet, B. S., Foustoukos, G., Oram, T. B., Yizhar, O., and Petersen, C. C. H. (2020). Anatomically and functionally distinct thalamocortical inputs to primary and secondary mouse whisker somatosensory cortices. *Nat. Commun.* 11, 3342.

Elijah, D. H., Samengo, I., and Montemurro, M. A. (2015). Thalamic neuron models encode stimulus information by burst-size modulation. *Front. Comput. Neurosci.* 9:113. doi: 10.3389/fncom.2015.00113

Flor, H., Denke, C., Schaefer, M., and Grüsser, S. (2001). Effect of sensory discrimination training on cortical reorganisation and phantom limb pain. *Lancet* 357, 1763–1764. doi: 10.1016/s0140-6736(00)04890-x

Frangeul, L., Pouchelon, G., Telley, L., Lefort, S., Luscher, C., and Jabaudon, D. (2016). A cross-modal genetic framework for the development and plasticity of sensory pathways. *Nature* 538, 96–98. doi: 10.1038/nature19770

Gambino, F., Pagès, S., Kehayas, V., Baptista, D., Tatti, R., Carleton, A., et al. (2014). Sensory-evoked LTP driven by dendritic plateau potentials in vivo. *Nature* 515, 116–119. doi: 10.1038/nature13664

Gerfen, C. R., Paletzki, R., and Heintz, N. (2013). GENSAT BAC cre-recombinase driver lines to study the functional organization of cerebral cortical and basal ganglia circuits. *Neuron* 80, 1368–1383. doi: 10.1016/j.neuron.2013.10.016

Giber, K., Slézia, A., Bokor, H., Bodor, A. L., Ludányi, A., Katona, I., et al. (2008). Heterogeneous output pathways link the anterior pretectal nucleus with the zona incerta and the thalamus in rat. *J. Comp. Neurol.* 506, 122–140. doi: 10.1002/cne.21545

Golomb, D., Ahissar, E., and Kleinfeld, D. (2006). Coding of stimulus frequency by latency in thalamic networks through the interplay of GABAB-mediated feedback and stimulus shape. *J. Neurophysiol.* 95, 1735–1750. doi: 10.1152/jn.00734.2005

Gong, S., Doughty, M., Harbaugh, C. R., Cummins, A., Hatten, M. E., Heintz, N., et al. (2007). Targeting cre recombinase to specific neuron populations with bacterial artificial chromosome constructs. *J. Neurosci.* 27, 9817–9823. doi: 10.1523/jneurosci.2707-07.2007

Groh, A., Bokor, H., Mease, R. A., Plattner, V. M., Hangya, B., Stroh, A., et al. (2013). Convergence of cortical and sensory driver inputs on single thalamocortical cells. *Cereb. Cortex* 24, 3167–3179. doi: 10.1093/cercor/bht173

Groh, A., de Kock, C. P. J., Wimmer, V. C., Sakmann, B., and Kuner, T. (2008). Driver or coincidence detector: modal switch of a corticothalamic giant synapse controlled by spontaneous activity and short-term depression. *J. Neurosci.* 28, 9652–9663. doi: 10.1523/jneurosci.1554-08.2008

Groh, A., Meyer, H. S., Schmidt, E. F., Heintz, N., Sakmann, B., and Krieger, P. (2010). Cell-type specific properties of pyramidal neurons in neocortex underlying a layout that is modifiable depending on the cortical area. *Cereb. Cortex* 20, 826–836. doi: 10.1093/cercor/bhp152

Guillery, R. W. (1995). Anatomical evidence concerning the role of the thalamus in corticocortical communication: a brief review. *J. Anat.* 187 (Pt 3), 583–592.

Guo, C., Peng, J., Zhang, Y., Li, A., Li, Y., Yuan, J., et al. (2017). Single-axon level morphological analysis of corticofugal projection neurons in mouse barrel field. *Sci. Rep.* 7:2846.

Guo, K., Yamawaki, N., Barrett, J. M., Tapies, M., and Shepherd, G. M. G. (2020). Cortico-thalamo-cortical circuits of mouse forelimb S1 are organized primarily as recurrent loops. *J. Neurosci.* 40, 2849–2858. doi: 10.1523/jneurosci.2277-19.2020

Guy, J., and Staiger, J. F. (2017). The functioning of a cortex without layers. *Front. Neuroanat.* 11:54. doi: 10.3389/fnana.2017.00054

Halassa, M. M., and Acsady, L. (2016). Thalamic inhibition: diverse sources, diverse scales. *Trends Neurosci.* 39, 680–693. doi: 10.1016/j.tins.2016.08.001

Halassa, M. M., and Kastner, S. (2017). Thalamic functions in distributed cognitive control. *Nat. Neurosci.* 20, 1669–1679. doi: 10.1038/s41593-017-0020-1

Halassa, M. M., Chen, Z., Wimmer, R. D., Brunetti, P. M., Zhao, S., Zikopoulos, B., et al. (2014). State-dependent architecture of thalamic reticular subnetworks. *Cell* 158, 808–821. doi: 10.1016/j.cell.2014.06.025

Halassa, M. M., Siegle, J. H., Ritt, J. T., Ting, J. T., Feng, G., and Moore, C. I. (2011). Selective optical drive of thalamic reticular nucleus generates thalamic bursts and cortical spindles. *Nat. Neurosci.* 14, 1118–1120. doi: 10.1038/nn.2880

Harris, J. A., Hirokawa, K. E., Sorensen, S. A., Gu, H., Mills, M., Ng, L. L., et al. (2014). Anatomical characterization of Cre driver mice for neural circuit mapping and manipulation. *Front. Neural Circuits* 8:76. doi: 10.3389/fncir.2014.00076

Harris, J. A., Mihalas, S., Hirokawa, K. E., Whitesell, J. D., Knox, J. E., Bernard, A., et al. (2018). The organization of intracortical connections by layer and cell class in the mouse brain. *bioRxiv* [Preprint] doi: 10.1101/292961 bioRxiv: 292961,

Harris, K. D., and Shepherd, G. M. (2015). The neocortical circuit: themes and variations. *Nat. Neurosci.* 18, 170–181. doi: 10.1038/nn.3917

Hattox, A. M., and Nelson, S. B. (2007). Layer V neurons in mouse cortex projecting to different targets have distinct physiological properties. *J. Neurophysiol.* 98, 3330–3340. doi: 10.1152/jn.00397.2007

Hayashi, S., Hoerder-Suabedissen, A., Kiyokage, E., Maclachlan, C., Toida, K., Knott, G., et al. (2021). Maturation of complex synaptic connections of layer 5 cortical axons in the posterior thalamic nucleus requires SNAP25. *Cereb. Cortex* 31, 2625–2638. doi: 10.1093/cercor/bhaa379

Herrero, M., Barcia, C., and Navarro, J. M. (2002). Functional anatomy of thalamus and basal ganglia. *Childs. Nerv. Syst.* 18, 386–404. doi: 10.1007/s00381-002-0604-1

Hilscher, M. M., Leão, R. N., Edwards, S. J., Leão, K. E., and Kullander, K. (2017). Chrna2-martinotti cells synchronize layer 5 type a pyramidal cells via rebound excitation. *PLoS Biol.* 15:e2001392. doi: 10.1371/journal.pbio.2001392

Hines, M. L., Morse, T., Migliore, M., Carnevale, N. T., and Shepherd, G. M. (2004). ModelDB: a database to support computational neuroscience. *J. Comput. Neurosci.* 17, 7–11. doi: 10.1023/b:jcns.0000023869.22017.2e

Hoerder-Suabedissen, A., Hayashi, S., Upton, L., Nolan, Z., Casas-Torremocha, D., Grant, E., et al. (2018). Subset of cortical layer 6b neurons selectively innervates higher order thalamic nuclei in mice. *Cereb. Cortex* 28, 1882–1897. doi: 10.1093/cercor/bhy036

Hoogland, P. V., Wouterlood, F. G., Welker, E., and Van der Loos, H. (1991). Ultrastructure of giant and small thalamic terminals of cortical origin: a study of the projections from the barrel cortex in mice using Phaseolus vulgaris leucoagglutinin (PHA-L). *Exp. Brain Res.* 87, 159–172. doi: 10.1007/bf00228517

Hwang, K., Bertolero, M. A., Liu, W. B., and D'Esposito, M. (2017). The human thalamus is an integrative hub for functional brain networks. *J. Neurosci.* 37, 5594–5607. doi: 10.1523/jneurosci.0067-17.2017

Iavarone, E., Yi, J., Shi, Y., Zandt, B.-J., O'Reilly, C., Van Geit, W., et al. (2019). Experimentally-constrained biophysical models of tonic and burst firing modes in thalamocortical neurons. *PLoS Comput. Biol.* 15:e1006753. doi: 10.1371/journal.pcbi.1006753

Jagirdar, R., and Chin, J. (2019). Corticothalamic network dysfunction and Alzheimer's disease. *Brain Res.* 1702, 38–45. doi: 10.1016/j.brainres.2017.09.014

Jahnsen, H., and Llinas, R. (1984). Ionic basis for the electro-responsiveness and oscillatory properties of guinea-pig thalamic neurones in vitro. *J. Physiol.* 349, 227–247. doi: 10.1113/jphysiol.1984.sp015154

Jouhanneau, J.-S., Kremkow, J., and Poulet, J. F. A. (2018). Single synaptic inputs drive high-precision action potentials in parvalbumin expressing GABA-ergic cortical neurons in vivo. *Nat. Commun.* 9, 1540.

Keller, G. B., and Mrsic-Flogel, T. D. (2018). Predictive processing: a canonical cortical computation. *Neuron* 100, 424–435. doi: 10.1016/j.neuron.2018.10.003

Kim, J., Woo, J., Park, Y.-G., Chae, S., Jo, S., Choi, J. W., et al. (2011). Thalamic T-type Ca2+ channels mediate frontal lobe dysfunctions caused by a hypoxia-like damage in the prefrontal cortex. *J. Neurosci.* 31, 4063–4073. doi: 10.1523/jneurosci.4493-10.2011

Kirchgessner, M. A., Franklin, A. D., and Callaway, E. M. (2020). Context-dependent and dynamic functional influence of corticothalamic pathways to first- and higher-order visual thalamus. *Proc. Natl. Acad. Sci. U. S. A.* 117, 13066–13077. doi: 10.1073/pnas.2002080117

Kirchgessner, M. A., Franklin, A. D., and Callaway, E. M. (2021). Distinct "driving" versus "modulatory" influences of different visual corticothalamic pathways. *bioRxiv* [Preprint] doi: 10.1101/2021.03.30.437715 bioRxiv: 2021.03.30.437715.

Koralek, K. A., Jensen, K. F., and Killackey, H. P. (1988). Evidence for two complementary patterns of thalamic input to the rat somatosensory cortex. *Brain Res.* 463, 346–351. doi: 10.1016/0006-8993(88)90408-8

Lam, Y.-W., and Sherman, S. M. (2010). Functional organization of the somatosensory cortical layer 6 feedback to the thalamus. *Cereb. Cortex* 20, 13–24. doi: 10.1093/cercor/bhp077

Landisman, C. E., and Connors, B. W. (2007). VPM and PoM nuclei of the rat somatosensory thalamus: intrinsic neuronal properties and corticothalamic feedback. *Cereb. Cortex* 17, 2853–2865. doi: 10.1093/cercor/bhm025

Lankarany, M., Al-Basha, D., Ratté, S., and Prescott, S. A. (2019). Differentially synchronized spiking enables multiplexed neural coding. *Proc. Natl. Acad. Sci. U. S. A.* 116, 201812171. doi: 10.1073/pnas.1812171116

Larkum, M. (2013). A cellular mechanism for cortical associations: an organizing principle for the cerebral cortex. *Trends Neurosci.* 36, 141–151. doi: 10.1016/j.tins.2012.11.006

Larkum, M. E., Zhu, J. J., and Sakmann, B. (1999). A new cellular mechanism for coupling inputs arriving at different cortical layers. *Nature* 398, 338–341. doi: 10.1038/18686

LaTerra, D., Petryszyn, S., Rosier, M., and Palmer, L. M. (2020). Higher order thalamus encodes correct goal-directed action. *bioRxiv* [Preprint]. 2020.07.05.188821. doi: 10.1101/2020.07.05.188821

Lavallée, P., Urbain, N., Dufresne, C., Bokor, H., Acsády, L., and Deschênes, M. (2005). Feedforward inhibitory control of sensory information in higher-order thalamic nuclei. *J. Neurosci.* 25, 7489–7498. doi: 10.1523/JNEUROSCI.2301-05.2005

Lee, C. C. (2015). Exploring functions for the non-lemniscal auditory thalamus. *Front. Neural Circuits* 9:69. doi: 10.3389/fncir.2015.00069

Lee, C. C., and Sherman, S. M. (2008). Synaptic properties of thalamic and intracortical inputs to layer 4 of the first- and higher-order cortical areas in the auditory and somatosensory systems. *J. Neurophysiol.* 100, 317–326. doi: 10.1152/jn.90391.2008

Lee, C. C., and Sherman, S. M. (2011). On the classification of pathways in the auditory midbrain, thalamus, and cortex. *Hear. Res.* 276, 79–87. doi: 10.1016/j.heares.2010.12.012

Li, J., Bickford, M. E., and Guido, W. (2003a). Distinct firing properties of higher order thalamic relay neurons. *J. Neurophysiol.* 90, 291–299. doi: 10.1152/jn.01163.2002

Li, J., Guido, W., and Bickford, M. E. (2003b). Two distinct types of corticothalamic EPSPs and their contribution to short-term synaptic plasticity. *J. Neurophysiol.* 90, 3429–3440. doi: 10.1152/jn.00456.2003

Li, J., Wang, S., and Bickford, M. E. (2003c). Comparison of the ultrastructure of cortical and retinal terminals in the rat dorsal lateral geniculate and lateral posterior nuclei. *J. Comp. Neurol.* 460, 394–409. doi: 10.1002/cne.10646

Li, Y., Lopez-Huerta, V. G., Adiconis, X., Levandowski, K., Choi, S., Simmons, S. K., et al. (2020). Distinct subnetworks of the thalamic reticular nucleus. *Nature.* 583, 819–824. doi: 10.1038/s41586-020-2504-5

Lipshutz, D., Bahroun, Y., Golkar, S., Sengupta, A. M., and Chklovskii, D. B. (2020). *A biologically plausible neural network for multi-channel Canonical Correlation Analysis. arXiv [q-bio.NC]*. Available online at: http://arxiv.org/abs/2010.00525 (accessed March 26, 2021).

Llano, D. A., and Sherman, S. M. (2008). Evidence for nonreciprocal organization of the mouse auditory thalamocortical-corticothalamic projection systems. *J. Comp. Neurol.* 507, 1209–1227. doi: 10.1002/cne.21602

Llano, D. A., and Sherman, S. M. (2009). Differences in intrinsic properties and local network connectivity of identified layer 5 and layer 6 adult mouse auditory corticothalamic neurons support a dual corticothalamic projection hypothesis. *Cereb. Cortex* 19, 2810–2826. doi: 10.1093/cercor/bhp050

Llinás, R., and Jahnsen, H. (1982). Electrophysiology of mammalian thalamic neurones in vitro. *Nature* 297, 406–408. doi: 10.1038/297406a0

Lu, S. M., and Lin, R. C. (1993). Thalamic afferents of the rat barrel cortex: a light- and electron-microscopic study using *Phaseolus vulgaris* leucoagglutinin

as an anterograde tracer. *Somatosens. Mot. Res.* 10, 1–16. doi: 10.3109/08990229309028819

Luo, L., Callaway, E. M., and Svoboda, K. (2018). Genetic dissection of neural circuits: a decade of progress. *Neuron* 98, 256–281. doi: 10.1016/j.neuron.2018.03.040

Mao, J., Mayer, D. J., and Price, D. D. (1993). Patterns of increased brain activity indicative of pain in a rat model of peripheral mononeuropathy. *J. Neurosci.* 13, 2689–2702. doi: 10.1523/jneurosci.13-06-02689.1993

Martinez-Garcia, R. I., Voelcker, B., Zaltsman, J. B., Patrick, S. L., Stevens, T. R., Connors, B. W., et al. (2020). Two dynamically distinct circuits drive inhibition in the sensory thalamus. *Nature* 583, 813–818. doi: 10.1038/s41586-020-2512-5

Masri, R., Quiton, R. L., Lucas, J. M., Murray, P. D., Thompson, S. M., and Keller, A. (2009). Zona incerta: a role in central pain. *J. Neurophysiol.* 102, 181–191. doi: 10.1152/jn.00152.2009

Masri, R., Trageser, J. C., Bezdudnaya, T., Li, Y., and Keller, A. (2006). Cholinergic regulation of the posterior medial thalamic nucleus. *J. Neurophysiol.* 96, 2265–2273. doi: 10.1152/jn.00476.2006

Masterson, S. P., Li, J., and Bickford, M. E. (2009). Synaptic organization of the tectorecipient zone of the rat lateral posterior nucleus. *J. Comp. Neurol.* 515, 647–663. doi: 10.1002/cne.22077

McAlonan, K., Brown, V. J., and Bowman, E. M. (2000). Thalamic reticular nucleus activation reflects attentional gating during classical conditioning. *J. Neurosci.* 20, 8897–8901. doi: 10.1523/jneurosci.20-23-08897.2000

McAlonan, K., Cavanaugh, J., and Wurtz, R. H. (2006). Attentional modulation of thalamic reticular neurons. *J. Neurosci.* 26, 4444–4450. doi: 10.1523/jneurosci.5602-05.2006

Mease, R. A., Kuner, T., Fairhall, A. L., and Groh, A. (2017). Multiplexed spike coding and adaptation in the thalamus. *Cell Rep.* 19, 1130–1140. doi: 10.1016/j.celrep.2017.04.050

Mease, R. A., Metz, M., and Groh, A. (2016a). Cortical sensory responses are enhanced by the higher-order thalamus. *Cell Rep.* 14, 208–215. doi: 10.1016/j.celrep.2015.12.026

Mease, R. A., Sumser, A., Sakmann, B., and Groh, A. (2016b). Cortical dependence of whisker responses in posterior medial thalamus in vivo. *Cereb. Cortex* 26, 3534–3543. doi: 10.1093/cercor/bhw144

Mease, R. A., Sumser, A., Sakmann, B., and Groh, A. (2016c). Corticothalamic spike transfer via the L5B-POm pathway in vivo. *Cereb. Cortex* 26, 3461–3475. doi: 10.1093/cercor/bhw123

Meda, K. S., Patel, T., Braz, J. M., Malik, R., Turner, M. L., Seifikar, H., et al. (2019). Microcircuit mechanisms through which mediodorsal thalamic input to anterior cingulate cortex exacerbates pain-related aversion. *Neuron* 102, 944–959.e3.

Meyer, H. S., Wimmer, V. C., Hemberger, M., Bruno, R. M., de Kock, C. P. J., Frick, A., et al. (2010a). Cell type-specific thalamic innervation in a column of rat vibrissal cortex. *Cereb. Cortex* 20, 2287–2303. doi: 10.1093/cercor/bhq069

Meyer, H. S., Wimmer, V. C., Oberlaender, M., de Kock, C. P. J., Sakmann, B., and Helmstaedter, M. (2010b). Number and laminar distribution of neurons in a thalamocortical projection column of rat vibrissal cortex. *Cereb. Cortex* 20, 2277–2286. doi: 10.1093/cercor/bhq067

Mitchell, A. S. (2015). The mediodorsal thalamus as a higher order thalamic relay nucleus important for learning and decision-making. *Neurosci. Biobehav. Rev.* 54, 76–88. doi: 10.1016/j.neubiorev.2015.03.001

Mitchell, A. S., and Gaffan, D. (2008). The magnocellular mediodorsal thalamus is necessary for memory acquisition. *But Not Retrieval. J. Neurosci.* 28, 258–263. doi: 10.1523/jneurosci.4922-07.2008

Mitchell, A. S., Baxter, M. G., and Gaffan, D. (2007). Dissociable performance on scene learning and strategy implementation after lesions to magnocellular mediodorsal thalamic nucleus. *J. Neurosci.* 27, 11888–11895. doi: 10.1523/jneurosci.1835-07.2007

Mitchell, A. S., Murray Sherman, S., Sommer, M. A., Mair, R. G., Vertes, R. P., and Chudasama, Y. (2014). Advances in understanding mechanisms of thalamic relays in cognition and behavior. *J. Neurosci.* 34, 15340–15346. doi: 10.1523/jneurosci.3289-14.2014

Mo, C., and Sherman, S. (2019). A sensorimotor pathway via higher-order thalamus. *J. Neurosci.* 39, 692–704. doi: 10.1523/jneurosci.1467-18.2018

Monchi, O., Petrides, M., Petre, V., Worsley, K., and Dagher, A. (2001). Wisconsin Card Sorting revisited: distinct neural circuits participating in different stages of the task identified by event-related functional magnetic resonance imaging. *J. Neurosci.* 21, 7733–7741. doi: 10.1523/jneurosci.21-19-07733.2001

Moore, J. D., Mercer Lindsay, N., Deschênes, M., and Kleinfeld, D. (2015). Vibrissa self-motion and touch are reliably encoded along the same somatosensory pathway from brainstem through thalamus. *PLoS Biol.* 13:e1002253. doi: 10.1371/journal.pbio.1002253

Morel, A., Magnin, M., and Jeanmonod, D. (1997). Multiarchitectonic and stereotactic atlas of the human thalamus. *J. Comp. Neurol.* 387, 588–630. doi: 10.1002/(sici)1096-9861(19971103)387:4<588::aid-cne8>3.0.co;2-z

Moseley, G. L., and Flor, H. (2012). Targeting cortical representations in the treatment of chronic pain: a review. *Neurorehabil. Neural Repair.* 26, 646–652. doi: 10.1177/1545968311433209

Mukherjee, A., Bajwa, N., Lam, N. H., Porrero, C., Clasca, F., and Halassa, M. M. (2020). Variation of connectivity across exemplar sensory and associative thalamocortical loops in the mouse. *Elife* 9:e62554.

Murray, P. D., Masri, R., and Keller, A. (2010). Abnormal anterior pretectal nucleus activity contributes to central pain syndrome. *J. Neurophysiol.* 103, 3044–3053. doi: 10.1152/jn.01070.2009

Naka, A., and Adesnik, H. (2016). Inhibitory circuits in cortical layer 5. *Front. Neural Circuits* 10:35. doi: 10.3389/fncir.2016.00035

Nakajima, M., and Halassa, M. M. (2017). Thalamic control of functional cortical connectivity. *Curr. Opin. Neurobiol.* 44, 127–131. doi: 10.1016/j.conb.2017.04.001

Naud, R., and Sprekeler, H. (2018). Sparse bursts optimize information transmission in a multiplexed neural code. *Proc. Natl. Acad. Sci. U.S.A.* 115, E6329–E6338. doi: 10.1073/pnas.1720995115

Nelson, A. D., and Bender, K. J. (2021). Dendritic integration dysfunction in neurodevelopmental disorders. *Dev. Neurosci.* 43, 1–21. doi: 10.1159/000516657

O'Connor, D. H., Peron, S. P., Huber, D., and Svoboda, K. (2010). Neural activity in barrel cortex underlying vibrissa-based object localization in mice. *Neuron* 67, 1048–1061. doi: 10.1016/j.neuron.2010.08.026

Odoj, K., Brawek, B., Asavapanumas, N., Mojtahedi, N., Heneka, M. T., and Garaschuk, O. (2021). In vivo mechanisms of cortical network dysfunction induced by systemic inflammation. *Brain Behav. Immun.* 96, 113–126. doi: 10.1016/j.bbi.2021.05.021

Ojima, H. (1994). Terminal morphology and distribution of corticothalamic fibers originating from layers 5 and 6 of cat primary auditory cortex. *Cereb. Cortex* 4, 646–663. doi: 10.1093/cercor/4.6.646

Otsuka, T., and Kawaguchi, Y. (2021). Pyramidal cell subtype-dependent cortical oscillatory activity regulates motor learning. *Commun. Biol.* 4:495.

Pagès, S., Chenouard, N., Chéreau, R., Kouskoff, V., Gambino, F., and Holtmaat, A. (2021). An increase in dendritic plateau potentials is associated with experience-dependent cortical map reorganization. *Proc. Natl. Acad. Sci. U.S.A.* 118, e2024920118. doi: 10.1073/pnas.2024920118

Pardi, M. B., Vogenstahl, J., Dalmay, T., Spanò, T., Pu, D.-L., Naumann, L. B., et al. (2020). A thalamocortical top-down circuit for associative memory. *Science* 370, 844–848. doi: 10.1126/science.abc2399

Park, A., Uddin, O., Li, Y., Masri, R., and Keller, A. (2018). Pain after spinal cord injury is associated with abnormal presynaptic inhibition in the posterior nucleus of the thalamus. *J. Pain* 19, 727.e1–727.e15.

Park, S., Sohn, J.-W., Cho, J., and Huh, Y. (2019). A computational modeling reveals that strength of inhibitory input, E/I balance, and distance of excitatory input modulate thalamocortical bursting properties. *Exp. Neurobiol.* 28:568. doi: 10.5607/en.2019.28.5.568

Parnaudeau, S., O'Neill, P.-K., Bolkan, S. S., Ward, R. D., Abbas, A. I., Roth, B. L., et al. (2013). Inhibition of mediodorsal thalamus disrupts thalamofrontal connectivity and cognition. *Neuron* 77, 1151–1162. doi: 10.1016/j.neuron.2013.01.038

Payeur, A., Guerguiev, J., Zenke, F., Richards, B. A., and Naud, R. (2021). Burst-dependent synaptic plasticity can coordinate learning in hierarchical circuits. *Nat. Neurosci.* 24, 1010–1019. doi: 10.1038/s41593-021-00857-x

Pergola, G., Danet, L., Pitel, A.-L., Carlesimo, G. A., Segobin, S., Pariente, J., et al. (2018). The regulatory role of the human mediodorsal thalamus. *Trends Cogn. Sci.* 22, 1011–1025.

Perl, E. R., and Whitlock, D. G. (1961). Somatic stimuli exciting spinothalamic projections to thalamic neurons in cat and monkey. *Exp. Neurol.* 3, 256–296. doi: 10.1016/0014-4886(61)90016-4

Perry, B. A. L., Lomi, E., and Mitchell, A. S. (2021). Thalamocortical interactions in cognition and disease: the mediodorsal and anterior thalamic nuclei. *Neurosci. Biobehav. Rev.* (in press). doi: 10.1016/j.neubiorev.2021.05.032

Petreanu, L., Mao, T., Sternson, S. M., and Svoboda, K. (2009). The subcellular organization of neocortical excitatory connections. *Nature* 457, 1142–1145. doi: 10.1038/nature07709

Phillips, J. W., Schulmann, A., Hara, E., Winnubst, J., Liu, C., Valakh, V., et al. (2019). A repeated molecular architecture across thalamic pathways. *Nat. Neurosci.* 22, 1925–1935. doi: 10.1038/s41593-019-0483-3

Pinault, D. (2004). The thalamic reticular nucleus: structure, function and concept. *Brain Res. Brain Res. Rev.* 46, 1–31. doi: 10.1016/j.brainresrev.2004.04.008

Prasad, J. A., Carroll, B. J., and Sherman, S. M. (2020). Layer 5 corticofugal projections from diverse cortical areas: variations on a pattern of thalamic and extra-thalamic targets. *J. Neurosci.* 40, 5785–5796. doi: 10.1523/JNEUROSCI.0529-20.2020

Purushothaman, G., Marion, R., Li, K., and Casagrande, V. A. (2012). Gating and control of primary visual cortex by pulvinar. *Nat. Neurosci.* 15, 905–912. doi: 10.1038/nn.3106

Ramaswamy, S., and Markram, H. (2015). Anatomy and physiology of the thick-tufted layer 5 pyramidal neuron. *Front. Cell. Neurosci.* 9:233. doi: 10.3389/fncel.2015.00233

Ramcharan, E. J., Gnadt, J. W., and Sherman, S. M. (2005). Higher-order thalamic relays burst more than first-order relays. *Proc. Natl. Acad. Sci. U. S. A.* 102, 12236–12241. doi: 10.1073/pnas.0502843102

Redinbaugh, M. J., Phillips, J. M., Kambi, N. A., Mohanta, S., Andryk, S., Dooley, G. L., et al. (2020). Thalamus modulates consciousness via layer-specific control of cortex. *Neuron* 106, 66–75.e12.

Reichova, I., and Sherman, S. M. (2004). Somatosensory corticothalamic projections: distinguishing drivers from modulators. *J. Neurophysiol.* 92, 2185–2197. doi: 10.1152/jn.00322.2004

Resnik, J., and Polley, D. B. (2017). Fast-spiking GABA circuit dynamics in the auditory cortex predict recovery of sensory processing following peripheral nerve damage. *Elife* 6:e21452. doi: 10.7554/eLife.21452

Rikhye, R. V., Gilra, A., and Halassa, M. M. (2018). Thalamic regulation of switching between cortical representations enables cognitive flexibility. *Nat. Neurosci.* 21, 1753–1763. doi: 10.1038/s41593-018-0269-z

Rinaldi, P. C., Young, R. F., Albe-Fessard, D., and Chodakiewitz, J. (1991). Spontaneous neuronal hyperactivity in the medial and intralaminar thalamic nuclei of patients with deafferentation pain. *J. Neurosurg.* 74, 415–421. doi: 10.3171/jns.1991.74.3.0415

Rockland, K. S. (2019). Corticothalamic axon morphologies and network architecture. *Eur. J. Neurosci.* 49, 969–977. doi: 10.1111/ejn.13910

Rodriguez-Moreno, J., Porrero, C., Rollenhagen, A., Rubio-Teves, M., Casas-Torremocha, D., Alonso-Nanclares, L., et al. (2020). Area-specific synapse structure in branched posterior nucleus axons reveals a new level of complexity in thalamocortical networks. *J. Neurosci.* 40, 2663–2679. doi: 10.1523/jneurosci.2886-19.2020

Rojas-Piloni, G., Guest, J. M., Egger, R., Johnson, A. S., Sakmann, B., and Oberlaender, M. (2017). Relationships between structure, in vivo function and long-range axonal target of cortical pyramidal tract neurons. *Nat. Commun.* 8:870.

Rouiller, E. M., and Welker, E. (2000). A comparative analysis of the morphology of corticothalamic projections in mammals. *Brain Res. Bull.* 53, 727–741. doi: 10.1016/s0361-9230(00)00364-6

Rovó, Z., Ulbert, I., and Acsády, L. (2012). Drivers of the primate thalamus. *J. Neurosci.* 32, 17894–17908. doi: 10.1523/jneurosci.2815-12.2012

Saadé, N. E., Al Amin, H., Abdel Baki, S., Chalouhi, S., Jabbur, S. J., and Atweh, S. F. (2007). Reversible attenuation of neuropathic-like manifestations in rats by lesions or local blocks of the intralaminar or the medial thalamic nuclei. *Exp. Neurol.* 204, 205–219. doi: 10.1016/j.expneurol.2006.10.009

Saalmann, Y. B., Pinsk, M. A., Wang, L., Li, X., and Kastner, S. (2012). The pulvinar regulates information transmission between cortical areas based on attention demands. *Science* 337, 753–756. doi: 10.1126/science.1223082

Sakmann, B. (2017). From single cells and single columns to cortical networks: dendritic excitability, coincidence detection and synaptic transmission in brain slices and brains. *Exp. Physiol.* 102, 489–521.

Sampathkumar, V., Miller-Hansen, A., Sherman, S. M., and Kasthuri, N. (2021). Integration of signals from different cortical areas in higher order thalamic neurons. *Proc. Natl. Acad. Sci. U. S. A* 118:e2104137118. doi: 10.1073/pnas.2104137118

Schmitt, L. I., Wimmer, R. D., Nakajima, M., Happ, M., Mofakham, S., and Halassa, M. M. (2017). Thalamic amplification of cortical connectivity sustains attentional control. *Nature* 545, 219–223. doi: 10.1038/nature22073

Schuman, B., Dellal, S., Prönneke, A., Machold, R., and Rudy, B. (2021). Neocortical layer 1: an elegant solution to top-down and bottom-up integration. *Annu. Rev. Neurosci.* 44, 221–252. doi: 10.1146/annurev-neuro-100520-012117

Semedo, J. D., Zandvakili, A., Machens, C. K., Yu, B. M., and Kohn, A. (2019). Cortical areas interact through a communication subspace. *Neuron* 102, 249–259.e4.

Senzai, Y., Fernandez-Ruiz, A., and Buzsáki, G. (2019). Layer-specific physiological features and interlaminar interactions in the primary visual cortex of the mouse. *Neuron* 101, 500–513.e5.

Seol, M., and Kuner, T. (2015). Ionotropic glutamate receptor GluA4 and T-type calcium channel Cav 3.1 subunits control key aspects of synaptic transmission at the mouse L5B-POm giant synapse. *Eur. J. Neurosci.* 42, 3033–3044. doi: 10.1111/ejn.13084

Sermet, B. S., Truschow, P., Feyerabend, M., Mayrhofer, J. M., Oram, T. B., Yizhar, O., et al. (2019). Pathway-, layer- and cell-type-specific thalamic input to mouse barrel cortex. *Elife* 8:e52665.

Shai, A. S., Anastassiou, C. A., Larkum, M. E., and Koch, C. (2015). Physiology of layer 5 pyramidal neurons in mouse primary visual cortex: coincidence detection through bursting. *PLoS Comput. Biol.* 11:e1004090. doi: 10.1371/journal.pcbi.1004090

Shepherd, G. M. G., and Yamawaki, N. (2021). Untangling the cortico-thalamo-cortical loop: cellular pieces of a knotty circuit puzzle. *Nat. Rev. Neurosci.* 22, 389–406. doi: 10.1038/s41583-021-00459-3

Sherman, S. M. (2001). Tonic and burst firing: dual modes of thalamocortical relay. *Trends Neurosci.* 24, 122–126. doi: 10.1016/s0166-2236(00)01714-8

Sherman, S. M. (2007). The thalamus is more than just a relay. *Curr. Opin. Neurobiol.* 17, 417–422. doi: 10.1016/j.conb.2007.07.003

Sherman, S. M. (2016). Thalamus plays a central role in ongoing cortical functioning. *Nat. Neurosci.* 19, 533–541. doi: 10.1038/nn.4269

Sherman, S. M. (2017). Functioning of circuits connecting thalamus and cortex. *Compr. Physiol.* 7, 713–739. doi: 10.1002/cphy.c160032

Sherman, S. M., and Guillery, R. W. (2002). The role of the thalamus in the flow of information to the cortex. *Philos. Trans. R. Soc. Lond. B Biol. Sci.* 357, 1695–1708. doi: 10.1098/rstb.2002.1161

Sherman, S. M., and Guillery, R. W. (2006). *Exploring The Thalamus And Its Role In Cortical Function*. Cambridge, MA: MIT Press.

Sherman, S. M., and Guillery, R. W. (2011). Distinct functions for direct and transthalamic corticocortical connections. *J. Neurophysiol.* 106, 1068–1077. doi: 10.1152/jn.00429.2011

Sherman, S. M., and Usrey, W. M. (2021). Cortical control of behavior and attention from an evolutionary perspective. *Neuron* S0896-6273(21)00462-1. doi: 10.1016/j.neuron.2021.06.021

Sherman, S., and Guillery, R. W. (2013). *Functional Connections of Cortical Areas: A New View from the Thalamus*. Cambridge, MA: MIT Press.

Silberberg, G., and Markram, H. (2007). Disynaptic inhibition between neocortical pyramidal cells mediated by martinotti cells. *Neuron* 53, 735–746. doi: 10.1016/j.neuron.2007.02.012

Smith, Y., Wichmann, T., and DeLong, M. R. (2014). Corticostriatal and mesocortical dopamine systems: do species differences matter? *Nat. Rev. Neurosci.* 15:63. doi: 10.1038/nrn3469-c1

Snow, J. C., Allen, H. A., Rafal, R. D., and Humphreys, G. W. (2009). Impaired attentional selection following lesions to human pulvinar: Evidence for homology between human and monkey. *Proc. Natl. Acad. Sci. U.S.A.* 106, 4054–4059. doi: 10.1073/pnas.0810086106

Stitt, I., Zhou, Z. C., Radtke-Schuller, S., and Fröhlich, F. (2018). Arousal dependent modulation of thalamo-cortical functional interaction. *Nat. Commun.* 9, 1–13.

Sumser, A., Mease, R. A., Sakmann, B., and Groh, A. (2017). Organization and somatotopy of corticothalamic projections from L5B in mouse barrel cortex. *Proc. Natl. Acad. Sci. U.S.A.* 114, 8853–8858. doi: 10.1073/pnas.1704302114

Suzuki, M., and Larkum, M. E. (2020). General anesthesia decouples cortical pyramidal neurons. *Cell* 180, 666–676.e13.

Takahashi, N., Ebner, C., Sigl-Glöckner, J., Moberg, S., Nierwetberg, S., and Larkum, M. E. (2020). Active dendritic currents gate descending cortical outputs in perception. *Nat. Neurosci.* 23, 1277–1285. doi: 10.1038/s41593-020-0677-8

Takahashi, N., Oertner, T. G., Hegemann, P., and Larkum, M. E. (2016). Active cortical dendrites modulate perception. *Science* 354, 1587–1590. doi: 10.1126/science.aah6066

Tan, L. L., and Kuner, R. (2021). Neocortical circuits in pain and pain relief. *Nat. Rev. Neurosci* 22, 458–471. doi: 10.1038/s41583-021-00468-2

Theyel, B. B., Llano, D. A., and Sherman, S. M. (2010). The corticothalamocortical circuit drives higher-order cortex in the mouse. *Nat. Neurosci.* 13, 84–88. doi: 10.1038/nn.2449

Thomson, A. M. (2010). Neocortical layer 6, a review. *Front. Neuroanat.* 4:13. doi: 10.3389/fnana.2010.00013

Trageser, J. C., Burke, K. A., Masri, R., Li, Y., Sellers, L., and Keller, A. (2006). State-dependent gating of sensory inputs by zona incerta. *J. Neurophysiol.* 96, 1456–1463. doi: 10.1152/jn.00423.2006

Urbain, N., Salin, P. A., Libourel, P. A., Comte, J. C., Gentet, L. J., and Petersen, C. C. (2015). Whisking-related changes in neuronal firing and membrane potential dynamics in the somatosensory thalamus of awake mice. *Cell Rep.* 13, 647–656. doi: 10.1016/j.celrep.2015.09.029

Usrey, W. M., and Sherman, S. M. (2019). Corticofugal circuits: communication lines from the cortex to the rest of the brain. *J. Comp. Neurol.* 527, 640–650. doi: 10.1002/cne.24423

Van Horn, S. C., and Sherman, S. M. (2004). Differences in projection patterns between large and small corticothalamic terminals. *J. Comp. Neurol.* 475, 406–415. doi: 10.1002/cne.20187

Varela, C., and Sherman, S. M. (2007). Differences in response to muscarinic activation between first and higher order thalamic relays. *J. Neurophysiol.* 98, 3538–3547. doi: 10.1152/jn.00578.2007

Varela, C., and Sherman, S. M. (2009). Differences in response to serotonergic activation between first and higher order thalamic nuclei. *Cereb. Cortex* 19, 1776–1786. doi: 10.1093/cercor/bhn208

Veinante, P., Lavallée, P., and Deschênes, M. (2000). Corticothalamic projections from layer 5 of the vibrissal barrel cortex in the rat. *J. Comp. Neurol.* 424, 197–204. doi: 10.1002/1096-9861(20000821)424:2<197::aid-cne1>3.0.co;2-6

Viaene, A. N., Petrof, I., and Murray Sherman, S. (2011). Properties of the thalamic projection from the posterior medial nucleus to primary and secondary somatosensory cortices in the mouse. *Proc. Natl. Acad. Sci. U.S.A.* 108, 18156–18161. doi: 10.1073/pnas.1114828108

Wang, J.-Y., Chang, J.-Y., Woodward, D. J., Baccalá, L. A., Han, J.-S., and Luo, F. (2007). Corticofugal influences on thalamic neurons during nociceptive transmission in awake rats. *Synapse* 61, 335–342. doi: 10.1002/syn.20375

Wei, H., Bonjean, M., Petry, H. M., Sejnowski, T. J., and Bickford, M. E. (2011). Thalamic burst firing propensity: a comparison of the dorsal lateral geniculate and pulvinar nuclei in the tree shrew. *J. Neurosci.* 31, 17287–17299. doi: 10.1523/jneurosci.6431-10.2011

Whilden, C. M., Chevée, M., An, S. Y., and Brown, S. P. (2021). The synaptic inputs and thalamic projections of two classes of layer 6 corticothalamic neurons in primary somatosensory cortex of the mouse. *J. Comp. Neurol.* doi: 10.1002/cne.25163

Whitlock, D. G., and Perl, E. R. (1961). Thalamic projections of spinothalamic pathways in monkey. *Exp. Neurol.* 3, 240–255. doi: 10.1016/0014-4886(61)90015-2

Whitt, J. L., Masri, R., Pulimood, N. S., and Keller, A. (2013). Pathological activity in mediodorsal thalamus of rats with spinal cord injury pain. *J. Neurosci.* 33, 3915–3926. doi: 10.1523/jneurosci.2639-12.2013

Wilke, M., Turchi, J., Smith, K., Mishkin, M., and Leopold, D. A. (2010). Pulvinar inactivation disrupts selection of movement plans. *J. Neurosci.* 30, 8650–8659. doi: 10.1523/jneurosci.0953-10.2010

Williams, L. E., and Holtmaat, A. (2019). Higher-order thalamocortical inputs gate synaptic long-term potentiation via disinhibition. *Neuron* 101, 91–102.e4.

Williamson, R. S., and Polley, D. B. (2019). Parallel pathways for sound processing and functional connectivity among layer 5 and 6 auditory corticofugal neurons. *Elife* 8:e42974. doi: 10.7554/eLife.42974

Wimmer, V. C., Bruno, R. M., de Kock, C. P. J., Kuner, T., and Sakmann, B. (2010). Dimensions of a projection column and architecture of VPM and POm axons in rat vibrissal cortex. *Cereb. Cortex* 20, 2265–2276. doi: 10.1093/cercor/bhq068

Wolfart, J., Debay, D., Le Masson, G., Destexhe, A., and Bal, T. (2005). Synaptic background activity controls spike transfer from thalamus to cortex. *Nat. Neurosci.* 8, 1760–1767. doi: 10.1038/nn1591

Xiao, D., Zikopoulos, B., and Barbas, H. (2009). Laminar and modular organization of prefrontal projections to multiple thalamic nuclei. *Neuroscience* 161, 1067–1081. doi: 10.1016/j.neuroscience.2009.04.034

Yu, C., Li, Y., Stitt, I. M., Zhou, Z. C., Sellers, K. K., and Frohlich, F. (2018). Theta oscillations organize spiking activity in higher-order visual thalamus during sustained attention. *eNeuro* 5:ENEURO.0384-17.2018. doi: 10.1523/ENEURO.0384-17.2018

Yu, J., Anderson, C. T., Kiritani, T., Sheets, P. L., Wokosin, D. L., Wood, L., et al. (2008). Local-circuit phenotypes of layer 5 neurons in motor-frontal cortex of YFP-H mice. *Front. Neural Circuits* 2:6. doi: 10.3389/neuro.04.006.2008

Yuan, R., Di, X., Taylor, P. A., Gohel, S., Tsai, Y.-H., and Biswal, B. B. (2016). Functional topography of the thalamocortical system in human. *Brain Struct. Funct.* 221, 1971–1984. doi: 10.1007/s00429-015-1018-7

Zeldenrust, F., Chameau, P., and Wadman, W. J. (2018a). Spike and burst coding in thalamocortical relay cells. *PLoS Comput. Biol.* 14:e1005960. doi: Spike and burst coding in thalamocortical relay

Zeldenrust, F., Wadman, W. J., and Englitz, B. (2018b). Neural Coding With Bursts-Current State and Future Perspectives. *Front. Comput. Neurosci.* 12:48. doi: 10.3389/fncom.2018.00048

Zhang, W., and Bruno, R. M. (2019). High-order thalamic inputs to primary somatosensory cortex are stronger and longer lasting than cortical inputs. *Elife* 8:e44158.

Conflict of Interest: The authors declare that the research was conducted in the absence of any commercial or financial relationships that could be construed as a potential conflict of interest.

Publisher's Note: All claims expressed in this article are solely those of the authors and do not necessarily represent those of their affiliated organizations, or those of the publisher, the editors and the reviewers. Any product that may be evaluated in this article, or claim that may be made by its manufacturer, is not guaranteed or endorsed by the publisher.

frontiers in Neural Circuits

ORIGINAL RESEARCH
published: 25 October 2021
doi: 10.3389/fncir.2021.752804

Higher-Order Thalamic Encoding of Somatosensory Patterns and Bilateral Events

Carlos Castejon[1], Jesus Martin-Cortecero[1,2] and Angel Nuñez[1]*

[1] Department of Anatomy, Histology and Neuroscience, Autónoma de Madrid University, Madrid, Spain, [2] Institute of Physiology and Pathophysiology, Medical Biophysics, Heidelberg University, Heidelberg, Germany

The function of the higher-order sensory thalamus remains unclear. Here, the posterior medial (POm) nucleus of the thalamus was examined by *in vivo* extracellular recordings in anesthetized rats across a variety of contralateral, ipsilateral, and bilateral whisker sensory patterns. We found that POm was highly sensitive to multiwhisker stimuli involving diverse spatiotemporal interactions. Accurate increases in POm activity were produced during the overlapping time between spatial signals reflecting changes in the spatiotemporal structure of sensory patterns. In addition, our results showed for first time that POm was also able to respond to tactile stimulation of ipsilateral whiskers. This finding challenges the notion that the somatosensory thalamus only computes unilateral stimuli. We found that POm also integrates signals from both whisker pads and described how this integration is generated. Our results showed that ipsilateral activity reached one POm indirectly from the other POm and demonstrated a transmission of sensory activity between both nuclei through a functional POm-POm loop formed by thalamocortical, interhemispheric, and corticothalamic projections. The implication of different cortical areas was investigated revealing that S1 plays a central role in this POm-POm loop. Accordingly, the subcortical and cortical inputs allow POm but not the ventral posteromedial thalamic nucleus (VPM) to have sensory information from both sides of the body. This finding is in agreement with the higher-order nature of POm and can be considered to functionally differentiate and classify these thalamic nuclei. A possible functional role of these higher-order thalamic patterns of integrated activity in brain function is discussed.

Keywords: thalamocortical (TC), corticothalamic circuit, whisker, POm, bilateral, sensory patterns, thalamus

OPEN ACCESS

Edited by:
Julio C. Hechavarría, Goethe University Frankfurt, Germany

Reviewed by:
Ehud Ahissar, Weizmann Institute of Science, Israel
Juan Aguilar, National Paraplegic Hospital, Spain

****Correspondence:***
Carlos Castejon
castejon.neuro@gmail.com

Received: *03 August 2021*
Accepted: *30 September 2021*
Published: *25 October 2021*

Citation:
Castejon C, Martin-Cortecero J and Nuñez A (2021) Higher-Order Thalamic Encoding of Somatosensory Patterns and Bilateral Events. Front. Neural Circuits 15:752804. doi: 10.3389/fncir.2021.752804

INTRODUCTION

Traditionally, sensory systems have mostly been studied using simple and discrete stimuli. However, in natural conditions, sensory events usually have complex and dynamical spatiotemporal structures and normally multiple sensory signals occur simultaneously with different onsets, offsets, and overlappings, challenging the computational capacities of sensory systems. However, it is still

unclear how these systems generate a representation of these dynamics. Moreover, how sensory systems extract relevant patterns from the raw sensory flow is poorly understood. Here, we propose the hypothesis that higher-order sensory thalamus could have a fundamental role in that function.

The rodent whisker system has an extraordinary ability to extract patterns and regularities from the environment and provides a perfect model in which to test our proposal. Rodents have an array of whiskers on each side of the face and during tactile exploration, multiple whiskers are stimulated simultaneously. Accordingly, the activation of individual whiskers strongly overlaps. These multiple contacts with the whiskers generate different patterns of sensory information. How the somatosensory system transforms these merged raw sensory signals into reliable neural representations and extracts information from that apparent noise is incompletely understood.

In these animals, tactile information from whiskers is processed by parallel ascending pathways toward the cortex (Chiaia et al., 1991; Diamond et al., 1992; Sherman and Guillery, 1998; Ahissar et al., 2000; Veinante et al., 2000a; Ohno et al., 2012; Clascá et al., 2016). The ventral posteromedial thalamic nucleus (VPM) and the posteromedial thalamic nucleus (POm) are implicated in these pathways. Although the function of VPM has been broadly studied, less is known about the function of POm. In contrast to VPM, POm neurons are characterized by large multiwhisker receptive fields (Chiaia et al., 1991; Diamond et al., 1992; Castejon et al., 2016). The functional implication of this characteristic of POm remains unclear.

In addition, also in contrast to VPM, POm projects to primary and higher-order cortical areas (Theyel et al., 2010; Ohno et al., 2012; Clascá et al., 2016; Casas-Torremocha et al., 2019; Zhang and Bruno, 2019; El-Boustani et al., 2020) and receives cortical driver input from layer 5 of these areas (Veinante et al., 2000b; Theyel et al., 2010; Groh et al., 2014; Mease et al., 2016). Accordingly, POm is well positioned to encode higher-order information of sensory, motor and associative nature. However, the content of POm representations and the nature of the messages that POm transfers to and receives from the cortex remain unclear.

Importantly, sensory events are usually characterized by bilateral sensory patterns. Therefore, the integration of tactile information from the two sides of the body seems to be fundamental in the coding of sensory patterns in bilateral perceptual function. Although, somatosensory cortical implication in the processing of bilateral stimuli has been much more studied (Armstrong-James and George, 1988; Shuler et al., 2001; Debowska et al., 2011), the role of the thalamus in these tactile bilateral interactions remains unknown.

The following experiments were thought to study the implication of POm in the encoding of these phenomena. Our results show for first time that POm is also able to respond to tactile stimulation of ipsilateral whiskers. We found that POm constantly integrates bilateral sensory information and that ipsilateral activity reaches POm *via* corticofugal projections mostly from S1. This in agreement with previous findings showing the convergence of ascending driver inputs from the periphery and descending driver inputs from L5 of S1 in POm (Groh et al., 2014; Castejon et al., 2016). In our study, we took advantage of the fact that ipsilateral sensory stimulation produced the activation of these corticothalamic fibers to investigate the functional interaction of these two streams in the codification of bilateral events. Our observations reveal a different implication of VPM and POm in bilateral perception. This finding is in agreement with the higher-order nature of POm and can be considered to functionally classify these thalamic nuclei.

MATERIALS AND METHODS

Ethical Approval

All experimental procedures involving animals were carried out under protocols approved by the ethics committee of the Autónoma de Madrid University and the competent Spanish Government agency (PROEX175/16), in accordance with the European Community Council Directive 2010/63/UE.

Animal Procedures and Electrophysiology

Experiments were performed on adult Sprague Dawley rats (220–300 g) of both sexes (40 males and 56 females). Animals were anesthetized (urethane, 1.3–1.5 g/kg i.p.) and placed in a Kopf stereotaxic frame. Local anesthetic (Lidocaine 1%) was applied to all skin incisions. The skull was exposed and openings were made to allow electrode penetrations to different neuronal stations in the trigeminal complex, thalamus and cortex.

Our recordings were performed several hours after the application of urethane (typically after 5–6 h). During the first hours after the application of urethane power spectra were dominated by 1–2 Hz (deeply anesthetized state). However, after 5–6 h, the level of anesthesia decreased and power spectra shifted indicating a lightly anesthetized state (**Figure 1E**; Friedberg et al., 1999). Our recordings were performed in this lightly anesthetized state. Supplementary doses of urethane were applied in those cases in which the level of anesthesia excessively decreased allowing the appearance of whisker movements. The body temperature was monitored and maintained at 37°C with a heating pad.

Extracellular recordings were performed using single microelectrodes in the Principal (PrV; Posterior from bregma 9–10; Lateral from midline 3–3.5, Depth 8.5–9.5; in mm) and Interpolar trigeminal nuclei (SpVi; P 11.5–14; L 2.5–3.5, D 8.5–9.5) of the trigeminal complex, in the posteromedial thalamic nucleus (POm; P 2.5–4.5, L 2–2.5, D 5–6.5), in the ventral posteromedial thalamic nucleus (VPM; P 2.8–4.6, L 2–3.5, D 5.5–7), and in the vibrissal region of the primary somatosensory cortex (S1; AP 0.5–4, L 5–7). Laminar recordings in supra- (D 150–550 μm), granular (D 650–850 μm), and infragranular (D $>$ 950 μm) layers of S1 were also performed. Unanalyzed gaps were left between layers to compensate for differences in cortical thickness across this area and as a safeguard against potential errors in laminar localization. Tungsten microelectrodes (2–5 MΩ) were driven using an electronically controlled microdrive system (David Kopf).

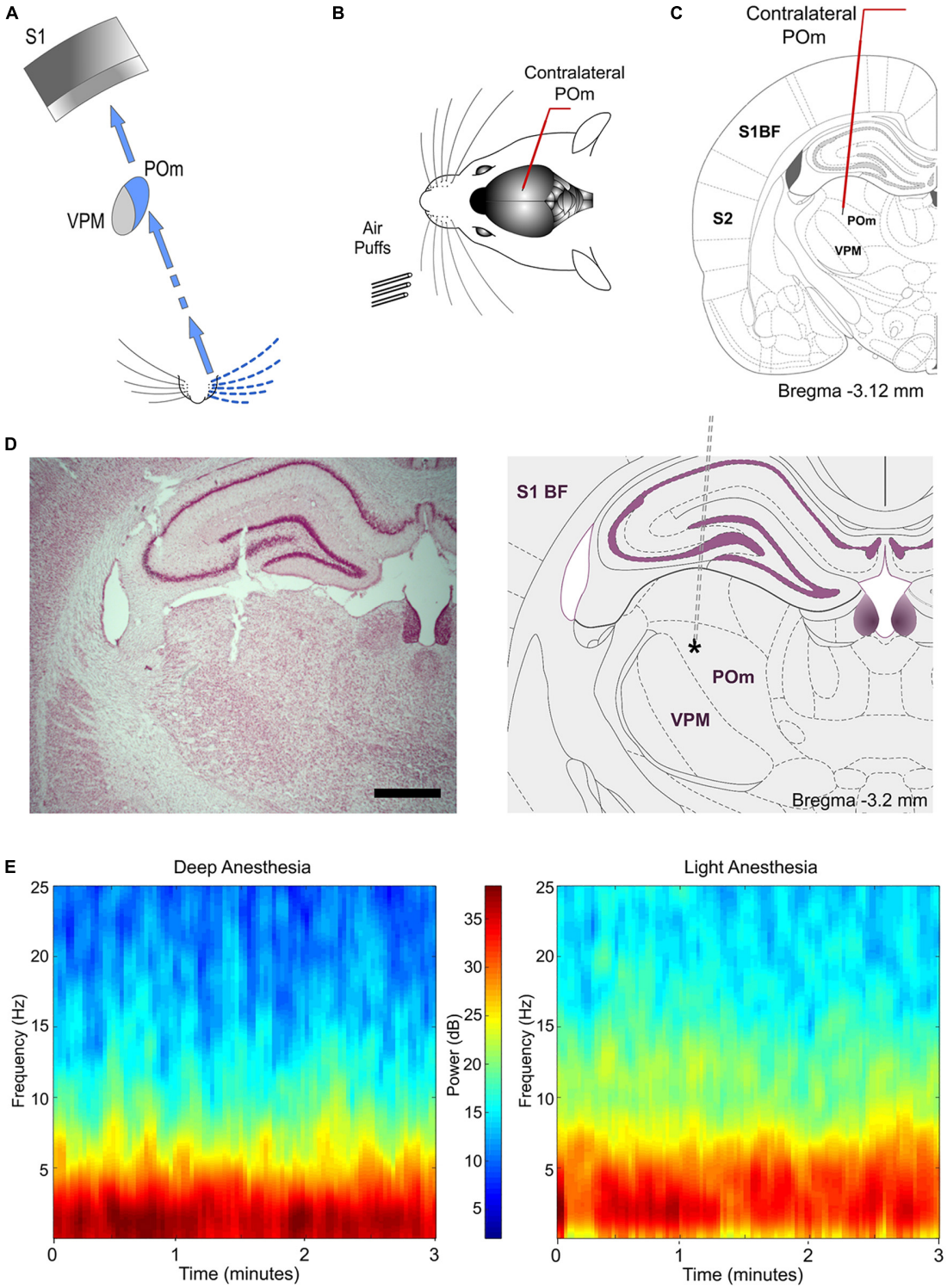

FIGURE 1 | Experimental paradigm. **(A)** Illustration of the paralemniscal pathway. **(B)** Schematic drawing displaying the sensory stimulation *via* patterns of multiwhisker deflections. Recordings were made in the contralateral POm **(C)**. Coronal section illustrating a recording electrode inserted into POm. Bregma anteroposterior level is indicated. **(D)** The left panel shows a representative Nissl stained coronal section displaying the location of the recording site in the dorsolateral part of POm and the track left by the electrode. An atlas schematic reconstruction of this recording site within POm is shown in the right panel (Paxinos and Watson, 2007). Tip position is indicated by an asterisk. Scale bar, 1 mm. S1 BF, primary somatosensory cortex barrel field. S2, secondary somatosensory cortex. **(E)** POm LFP spectrograms of both deeply and lightly anesthetized states. Power spectra dominated by 1–2 Hz were only observed during deep anesthesia (Friedberg et al., 1999). Our recordings were mostly performed in the lightly anesthetized state.

Sensory Stimulation and Patterns Generation

Sensory stimulation was characterized by spatiotemporal patterns of multiwhisker deflections simulating possible real stimuli or sequences of stimuli. Details of the multiwhisker stimulation patterns are described in **Figures 2A**, **3A**, **4A**, **5A,B**. Anesthetized rats were used to facilitate their application. Using a pneumatic pressure pump (Picospritzer) that delivers air pulses through polyethylene tubes (1 mm inner diameter; 1–2 kg/cm^2), sensory patterns were generated using controlled multiwhisker deflections performed by overlapping air puffs of different durations (20–2000 ms) applied to different whiskers in one or both sides of the face and avoiding skin stimulation. Accordingly, many whiskers were activated simultaneously producing different spatiotemporal overlapping dynamics. The air-puffers were precisely placed and the whiskers were trimmed to a length of 10–30 mm to allow precise overlapping stimulations. To simulate natural stimuli, overlappings produced by the activation of whiskers in different directions were also included. A variant order was adopted for delivering the stimulation patterns to avoid possible temporal dependency. We applied 20–70 trials per pattern at low frequency (0.3–0.5 Hz). Receptive field sizes were determined by deflecting individual vibrissae with a hand-held probe and monitoring the audio conversion of the amplified activity signal.

Inactivation and Lesion of Thalamic Nuclei and Cortical Areas

We inactivated the cortex with local infusions of lidocaine (1%) or muscimol (1 mg/ml). To evaluate the proper level of cortical inactivation, the basal activity and sensory responses to whisker stimulation were continuously checked in the inactivated cortical area. Infusions were repeated every 15 min until cortical activity recorded in deep layers was silenced, on average 25 min after the first application. Pharmacological deactivation of POm was performed by injecting 100–200 nL of muscimol (1 mg/ml) in this thalamic nucleus. The drug was slowly delivered through a cannula connected to a Hamilton syringe (1 μl) over a one-minute period.

Lesions of different cortical areas were also performed in our experiments. To assure the precision of cortical lesions, the skull was exposed and openings were precisely restricted to the corresponding cortical area according to stereotaxic coordinates [S1, described above; secondary somatosensory cortex (S2), P 0–3.7; L 5.5–7.5; primary motor cortex (M1), A 0.5–2.5, L 0.2–3]. Lesions were made by cutting and aspirating the cortical tissue and included superficial and deep layers of these areas.

Histology

After the last recording session, animals were deeply anesthetized with sodium-pentobarbital (50 mg/kg i.p.) and then perfused transcardially with saline followed by formaldehyde solution (4%). After perfusion, brains were removed and post-fixed. Serial 50 μm-thick coronal sections were cut on a freezing microtome (Leica, Germany). These sections were then prepared for Nissl staining histochemistry for verification of electrodes tracks, delimitation of cortical lesions and discrimination of thalamic nuclei. Positions of the electrode tips and extensions of cortical lesions were histologically verified by comparing these coronal brain sections with reference planes of the rat brain stereotaxic atlas (Paxinos and Watson, 2007).

Data Acquisition and Analysis

Data were recorded from PrV, SpVi, VPM, POm, and S1. The raw signal of the *in vivo* extracellular recordings was filtered (0.3–300 Hz for local field potentials and 0.3–5 kHz for units), amplified (DAM80 preamplifier, WPI) and digitalized (Power 1401 data acquisition unit, CED, United Kingdom). We applied a semi-automatic spike sorting technique (template-matching) provided by the Spike2 software (CED). Threshold crossing events were used to compute templates of spike waveforms which were subsequently used to assign individual spikes. To control for single unit separation, we applied principal component analysis (PCA) of the detected waveforms. Single units had to show cluster separation after plotting their first three principal components. Furthermore, we plotted inter-spike interval (ISI) distributions of the units, which was allowed to be only above 1 ms. Multi-units were collected by amplitude sorting. Local field potentials were obtained and a short-time Fourier transform was computed using MATLAB to construct a color-coded spectrogram.

To quantify the spontaneous activity, the number of spikes occurring in the 100 ms preceding the stimulus was counted. We defined response magnitude as the total number of spikes per stimulus occurring between response onset and offset from the peristimulus time histogram (PSTH, bin width 1 ms unless noted otherwise). Response onset was defined as the first of three consecutive bins displaying significant activity (more than three standard deviations above the mean spontaneous activity) after stimulus and response offset as the last bin of the last three consecutive bins displaying significant activity. Response duration was defined as the time elapsed from the onset to offset responses. In all figures, raster plots represent each spike as a dot and each line corresponds to one trial. Spikes were aligned on stimulus presentation (Time 0 ms). The temporal interval between the trigger command and whisker deflection following air puff was calculated (quantified in ∼9 ms; tube placed at ∼10 mm from the whiskers) and used as the reference onset time for whisker deflection following the air puff trigger command. This delay was corrected during analysis.

All data are expressed as the mean ± standard error of the mean (SEM). Error bars in the figures correspond to SEM. For normally distributed data (Shapiro-Wilk normality test), statistical analyses were conducted using a Student's *t*-test. Non-normally distributed data were evaluated using a Wilcoxon matched-pairs test. Multiple comparisons were evaluated using a One-way ANOVA test. *Z*-scores were computed relative to the activity across all bins in the PSTH from −100 to 400 ms respect to stimulus onset. These computations and plots were done in

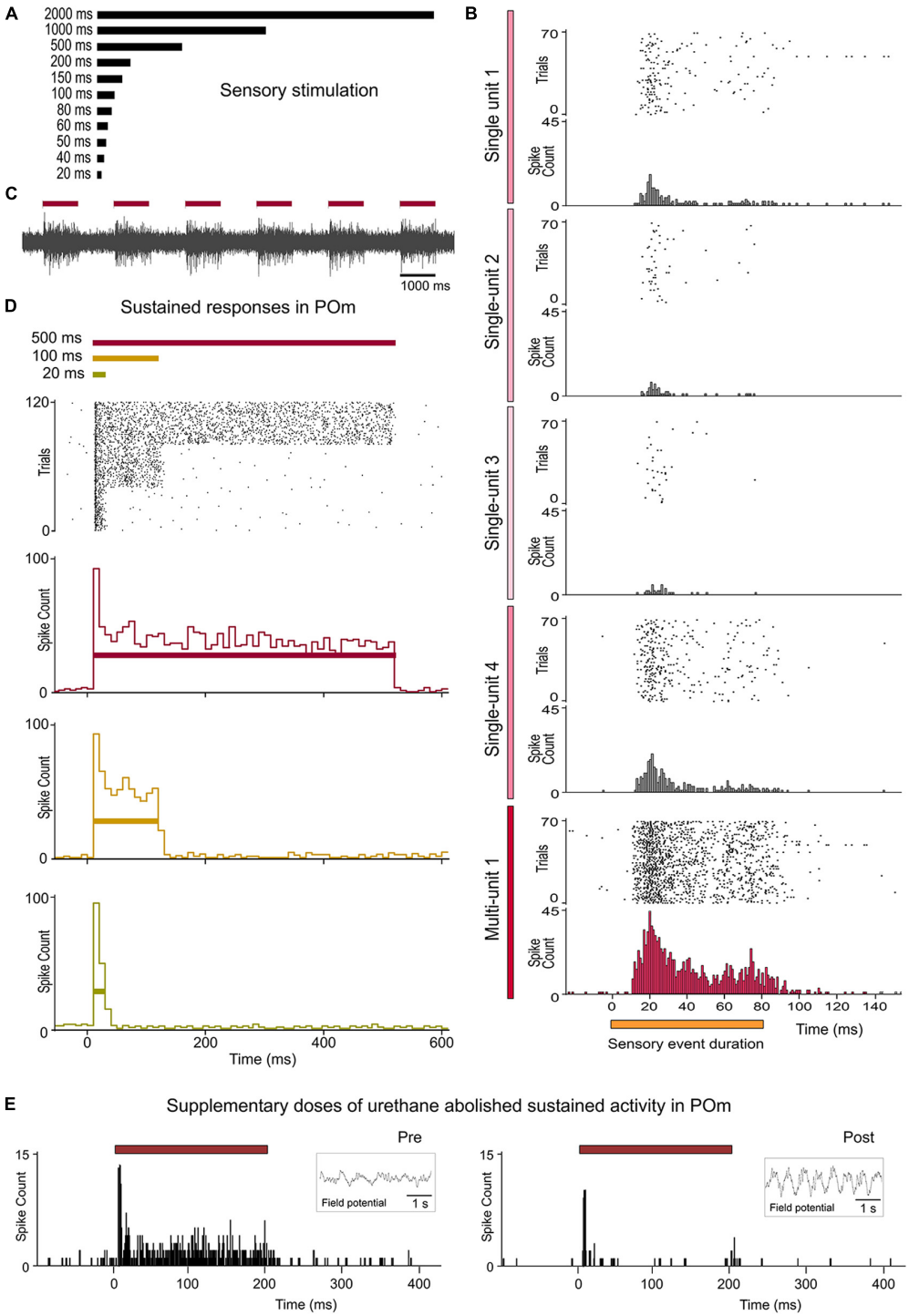

FIGURE 2 | Sustained activity in POm. **(A)** Air-puffs used for sensory stimulation varied in duration from 20 ms to 2 s. **(B)** The encoding of the duration of sensory events by POm was studied at single-unit and multi-unit level. Raster plots and PSTHs showing one multi-unit and four single-unit POm responses extracted from the same recording and evoked by a sensory pattern of 80 ms duration. Note that the robustness of this form of encoding by POm sustained activity is obtained from population response formed by the superposition of spikes from individual neurons. The gradual color intensity of vertical lines represents a simulated contribution of each single-unit in this example to the encoding of stimulus duration. **(C)** Example recording in POm showing evoked sustained activity lasting the duration of the stimulus. **(D)** POm responds throughout the entire duration of the stimuli. Raster plot and PSTHs (bin width 10 ms) showing sustained multi-unit POm responses evoked by different stimulus duration (40 trials shown for each stimulus). Note that the duration of the stimulus did not alter the onset latency of responses. **(E)** POm sustained responses were highly affected by the level of anesthesia. They were only observed during the lightly anesthetized state. Supplementary doses of urethane abolished sustained activity in POm. Field potential activity recorded in each condition is shown in the insets. Horizontal color lines indicate the duration of the stimulus. Time 0 indicates the onset of the stimulus.

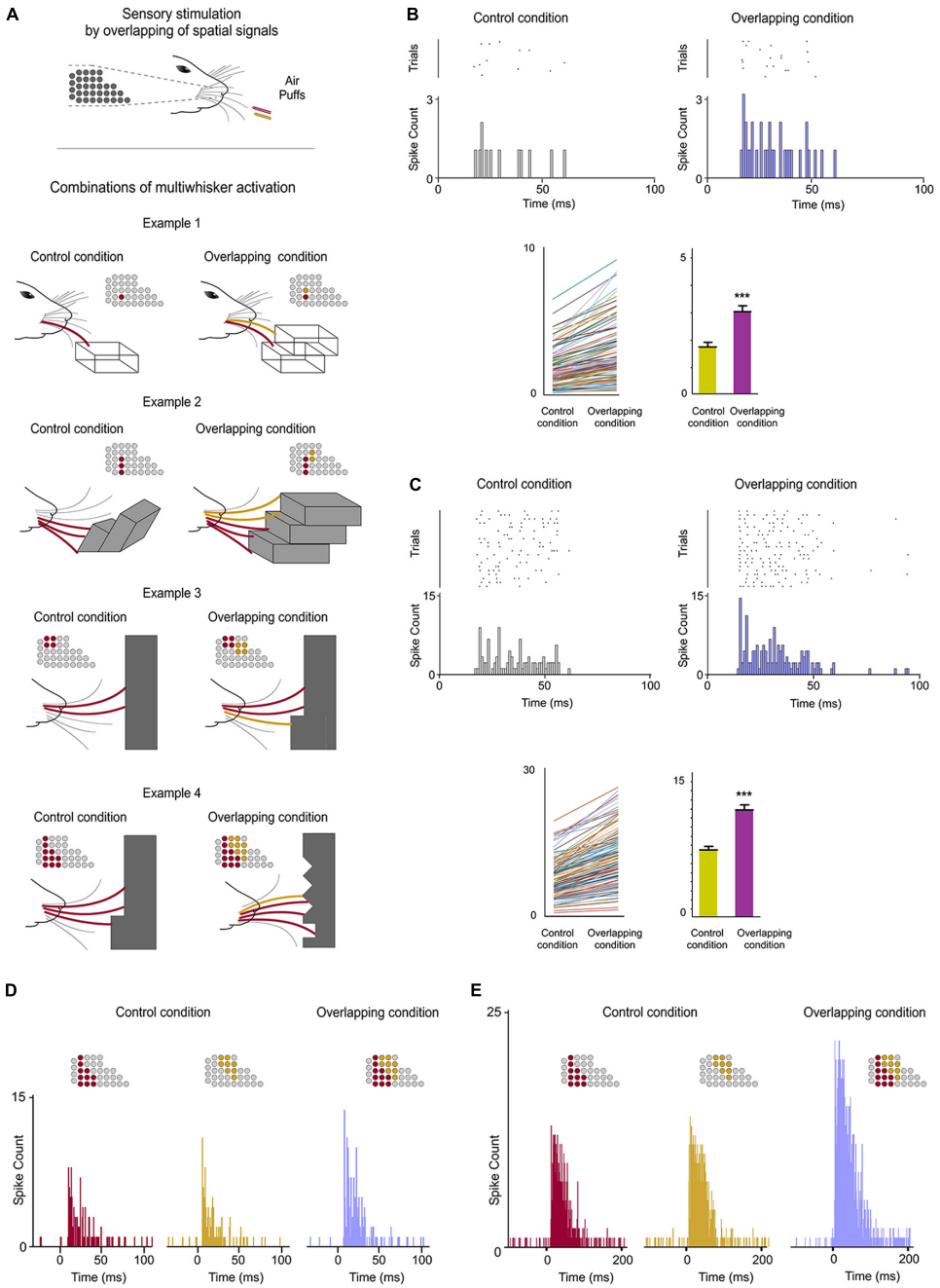

FIGURE 3 | POm integration of spatial signals. **(A)** Sensory stimulation was produced by the application of individual (Control Condition) or simultaneous air puffs (Overlapping Condition) activating different whiskers and producing diverse combinations of multiwhisker activation. The number of whiskers stimulated by each air puff was varied to generate different combinations. They were repeated multiple times (range 20–70 repeats) and POm responses to them were studied and quantified by comparison between Control and Overlapping conditions. Four examples of these combinations are shown. The whiskers stimulated are depicted in different colors in the schematic representations of the whisker pads. Simulated objects and surfaces are only shown to illustrate similar real overlappings. **(B)** POm response magnitude increased when whiskers were activated simultaneously as can be appreciated in the peri-stimulus time raster plots and histograms of a representative POm single-unit response for 20 trials evoked by the example 2 in panel **(A)**. Data comparing the spike rate in Control and Overlapping conditions of single-units (n = 102, depicted in different colors) across stimulation combinations and the total mean response magnitude in both conditions are also shown. The mean firing rate of all single-units was significantly increased in the Overlapiing condition (72%; $p < 0.001$; Wilcoxon matched-pairs test). **(C)** Same as in panel **(B)**, but for multi-unit activity. Raster plots and PSTHs of a demonstrative POm multi-unit response for 40 trials evoked by the example 3 in panel **(A)**. The spike rate in Control and Overlapping conditions of multi-units (n = 136, depicted in different colors) across stimulation combinations and the total mean response magnitude in both conditions are shown. The mean firing rate of all multi-units was significantly increased in the Overlapiing condition (56%; $p < 0.001$; Wilcoxon matched-pairs test). **(D)** PSTHs of POm single-unit responses evoked by the example 4 in panel **(A)** (40 trials). To visualize the facilitative integration of overlapping spatial signals, individual evoked responses in the Control Condition are displayed separately. **(E)** Same as in panel **(D)**, but for multi-unit activity.

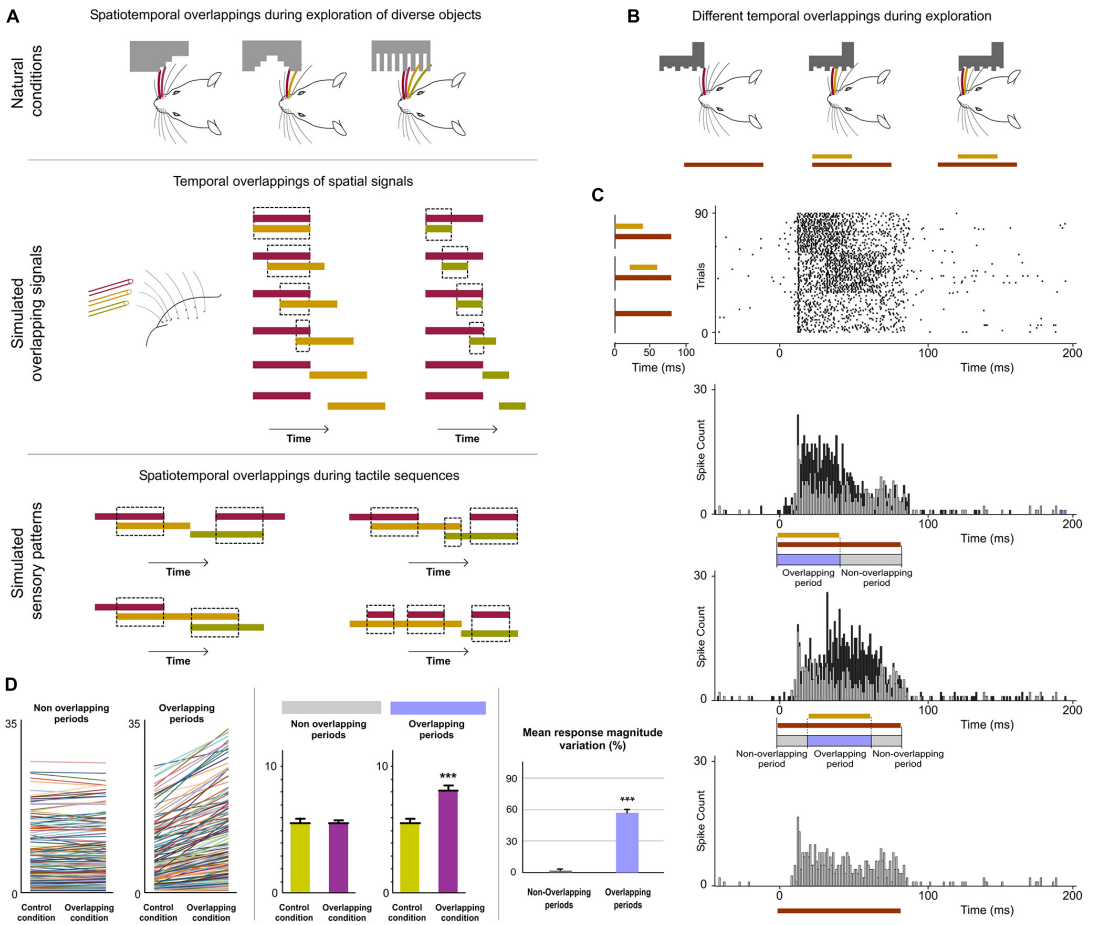

FIGURE 4 | POm integration of spatiotemporal overlapping dynamics. **(A)** Sensory patterns can be simulated by the simultaneous activation of different whiskers and by varying the number of whiskers stimulated, their combination and the order and duration of air pulses to produce different spatiotemporal overlappings. A variety of spatiotemporal patterns were designed to simulate possible real stimuli or sequences of stimuli using controlled multiwhisker deflections performed by overlapping air puffs of different durations applied to different whiskers including neighboring whiskers or whiskers farther apart across the whisker pad. The duration of air puffs and the temporal overlapping between them were varied to generate different combinations (protocols). The number of whiskers stimulated by each air puff was varied to generate different sensory patterns using the same protocol. Some examples are shown. Air puffs are represented by color lines. Their length reflects the duration of the signal. Temporal overlappings between sensory signals are highlighted. **(B)** Schematic illustration of a simulated tactile sequence reflecting the generation of different temporal overlappings. **(C)** Raster plots and PSTHs of representative POm responses evoked by temporal overlappings illustrated in the tactile sequence in panel **(B)** are shown. The appearance of a new signal during the presence of an existing signal was integrated by POm. This was reflected in precise increases in POm activity. These increases in sustained responses were only produced during the overlapping time between them (Overlapping period) but not during the non-overlapping time (Non-overlapping period of response). The duration of the Overlapping and Non-overlapping periods is indicated. Note that the increases in POm activity during overlapping periods were sustained along the temporal overlapping. **(D)** Plots comparing the spike rate of all recorded multi-units (n = 155, depicted in different colors) during the Overlapping and Non-overlapping response periods in Control and Overlapping conditions across sensory patterns. The mean firing rate was increased in the Overlapping periods ($p < 0.001$; Wilcoxon matched-pairs test) but not in the Non-overlapping periods where the mean magnitude of responses did not change ($p = 0.43$; Wilcoxon matched-pairs test). Response magnitude variation (%) between Control and Overlapping conditions in Non-Overlapping and Overlapping periods ($p < 0.001$, Wilcoxon matched-pairs test) is also shown. $^{***}P < 0.001$.

MATLAB. Statistical significance was considered at $^{*}P < 0.05$, $^{**}P < 0.01$, $^{***}P < 0.001$.

RESULTS

Sustained Activity in POm

Whisker-evoked responses in POm were examined by *in vivo* extracellular recordings from rats in a lightly anesthetized state using stimuli with different durations within the range used by these animals during their natural explorations (**Figures 1**, **2**). While studying multi-unit activity, we found that this nucleus was able to generate sustained responses even to long-duration stimuli. This capacity was consistent across all animals (n = 12). The duration of the stimulus did not alter the mean onset latency of responses (11.12 ± 0.60 ms, ranged from 7 to 16 ms, n = 119 multi-units, p = 0.52, One-way ANOVA; **Figure 2D**). To study how this multi-unit activity replicated the response profile of individual POm neurons, we also characterized this phenomenon studying POm single-units (n = 91). We found

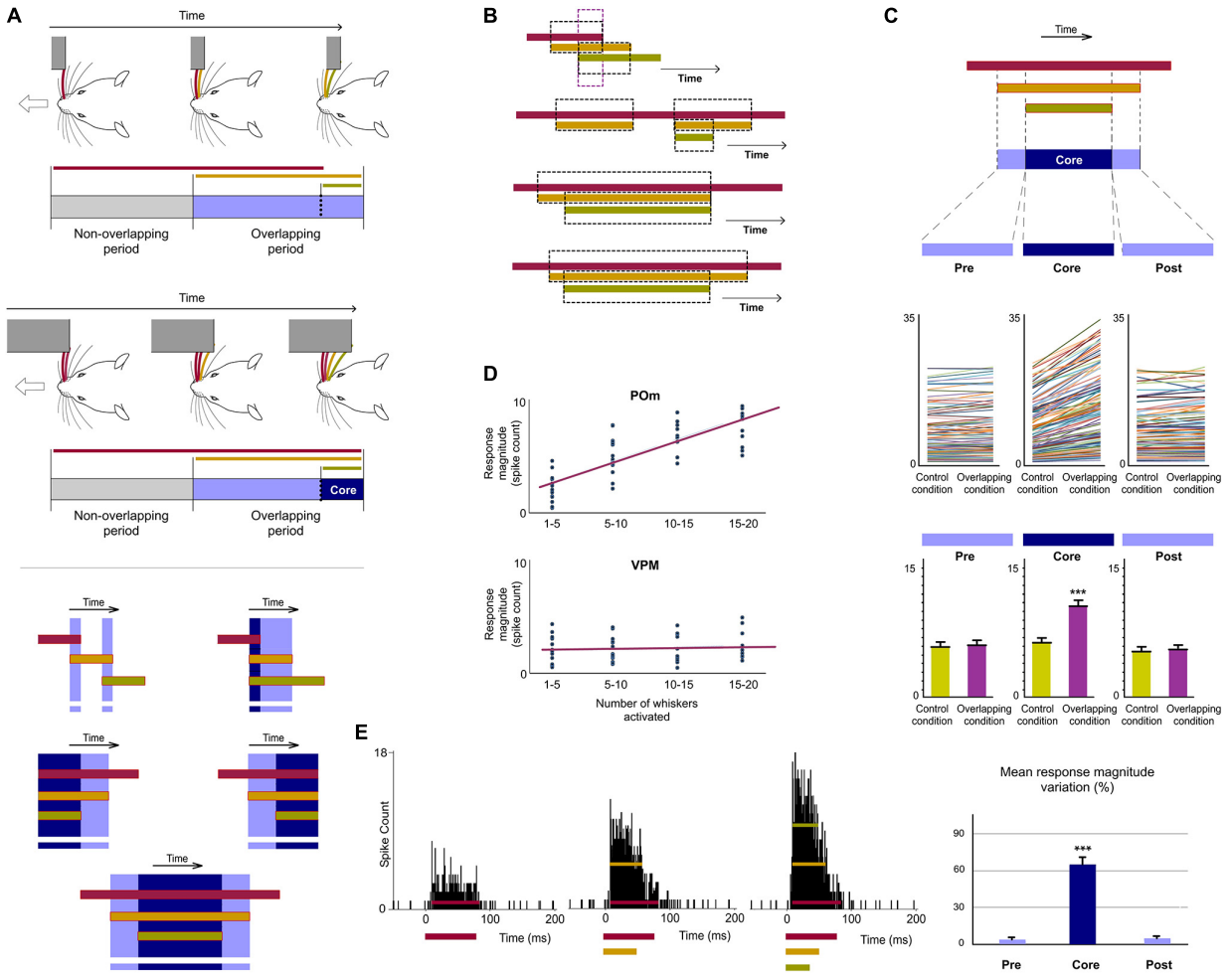

FIGURE 5 | POm is highly sensitive to the dynamical spatiotemporal structure of sensory patterns and to the variability of their parts. **(A)** Multiple and constantly changing overlappings occur dynamically during contacts with objects and surfaces during active exploration. Accordingly, the number of whiskers implicated is constantly changing. As can be appreciated in these schematic illustrations of two simulated tactile sequences, their Overlapping periods are different. Defined by the number of whiskers simultaneously activated, "simple" overlappings (in light blue) and more "complex" overlappings (in dark blue) were used to understand how POm codifies this variability (bottom panel). The parts of the Overlapping periods with the mayor number of whiskers were selected and defined as "Core" parts. **(B)** Spatiotemporal patterns produced by the simultaneous application of a third air puff activating additional whiskers. Different spatiotemporal overlappings were generated by varying the onset and duration of the third air puff and the number of extra whiskers stimulated by this air puff. **(C)** POm responses during Overlapping periods were divided in three subperiods (Pre, Core, and Post). They were compared before (Control condition) and after the application of the third air puff (Overlapping condition). Data comparing the spike rate of all recorded multi-units (n = 101, depicted in different colors) in these conditions during Pre, Core, and Post subperiods across sensory patterns and the total mean response magnitude in both conditions in these subperiods are described. The mean firing rate was increased in the Core subperiod ($p < 0.001$; Wilcoxon matched-pairs test) but not in the Pre ($p = 0.63$; Wilcoxon matched-pairs test) and Post ($p = 0.74$; Wilcoxon matched-pairs test) subperiods. **(D)** Correlation between POm response magnitude and the number of whiskers simultaneously overlapped. Data from VPM are also shown for comparison. POm: Pearson correlation coefficient, $r = 0.79$, $p < 0.001$, $n = 51$ multi-units in 10 rats; VPM: $r = 0.19$, $p < 0.001$, $n = 45$ multi-units in 8 rats. The number of whiskers simultaneously activated is computed by POm. Note the profound functional difference between these nuclei. **(E)** PSTHs for a representative example showing that POm response magnitude in Overlapping periods gradually increased as more whiskers were temporally overlapped. Note that the temporal structure of these different sensory events is reflected in their corresponding POm responses. ***$P < 0.001$.

that POm neurons responded tending to generate sustained responses. This indicated that the population response formed by the combination of spikes from these neurons allowed for the encoding of stimuli duration by POm sustained activity (**Figure 2B**). Thus, we mainly used POm multi-unit responses for further analyses.

Since POm receives strong sensory projections from the trigeminal complex (Chiaia et al., 1991; Veinante et al., 2000a; El-Boustani et al., 2020), whisker-evoked responses were also investigated in the principal (Pr5; n = 47 multi-units) and in the interpolar (SpVi, n = 52 multi-units) trigeminal nuclei (11 rats). Sustained responses were only found in SpVi. The mean onset latency of these sustained responses was 8.31 ± 0.57 ms (ranged from 5 to 11 ms).

These results show that POm has the capacity to sustain its activity to encode and represent tactile input duration with high

accuracy (Castejon et al., 2016). Given that tactile inputs are usually longer than the duration of multiple whisk cycles, this capacity could be used to codify sensory patterns and sequences of stimuli. The following experiments were designed to study the implication of POm in the encoding of these phenomena.

POm Spatial Integration of Multiwhisker Stimulation

During whisking rats integrate signals from many whiskers to obtain accurate tactile information from their environment. Our next experiments were designed to map how sensory information, produced when multiple whiskers are activated simultaneously during a tactile event, is encoded in the activity of POm. First, we characterized the response properties of POm to simple spatial overlapping stimuli precisely delivering simultaneous air-puffs to different whiskers at different locations across the whisker pad. Consistent with published data (Diamond et al., 1992; Ahissar et al., 2000), we found large multiwhisker receptive fields (mean receptive field size: 10.9 ± 3.1 whiskers; n = 42 units). We observed that POm responses exhibited increases in firing rate when different whiskers were activated simultaneously. To investigate this POm capacity in detail, we studied the integration of signals by POm across a variety of reproducible spatial overlapping combinations (**Figure 3A**). Across them, we found that POm multi-unit responses showed increases in response magnitude during overlappings of spatial signals (quantified in **Figure 3C**). This was produced by a facilitative integration of overlapping signals (**Figures 3D,E**). The spatial integration was also observed between remote whiskers. The mean onset latency and duration of POm responses to different signals were not changed by their overlapping (**Figure 3C**). We also investigated these effects studying POm single-units (quantified in **Figure 3B**). These findings were consistent across all animals (n = 15). Importantly, the robustness of this capacity of encoding seemed to be obtained from population response (**Figure 3C**). Accordingly, we used POm multi-unit responses for further analyses of POm integration.

POm Encoding of Spatiotemporal Overlapping Dynamics

Next, since tactile events typically have spatiotemporal structures that change dynamically in time, we studied how spatial integration (spatial dimension) occurs throughout the duration of the sensory pattern (temporal dimension) in 18 rats (**Figure 4**). Interestingly, when overlappings of spatial signals were produced by delivering simultaneous air-puffs with different durations or with the same duration but applied at different times (**Figure 4A** middle panel), increases in sustained responses were only observed during the overlapping time between them (data showing the quantification of this effect are described in **Figure 4D**). The spatial integration of multiwhisker activation was only produced during the temporal overlapping. Importantly, the increases of POm activity were sustained along the temporal overlappings (**Figure 4C**). Therefore, the time shared by overlapping signals is also encoded by POm activity.

Then, we studied these effects using sensory patterns formed by diverse temporal overlappings (**Figure 4A** bottom panel). We designed these patterns to simulate possible real stimuli or sequences of stimuli similar to those occurring in natural circumstances, such as sequential activation of multiple whiskers with partial temporal overlapping between them, simultaneous and delayed activation of different whiskers with different durations producing sequences with diverse spatiotemporal overlappings and precise sequences of long sustained activation of several neighboring whiskers overlapped with repetitive brief stimulations of remote whiskers. Across patterns, precise changes in POm sustained activity consistent with the spatiotemporal structure of the patterns were observed. Accurate increases in POm sustained activity were produced during the overlapping time between spatial signals reflecting changes in the spatiotemporal structure of sensory patterns.

Additionally, since in natural conditions the spatiotemporal structure of sensory patterns changes dynamically, the number of whiskers simultaneously implicated is not homogeneous along their duration. As can be appreciated in **Figure 5A**, dissimilar overlappings of spatial signals can produce sensory patterns formed by different parts with diverse complexities. To investigate the capacity of POm to represent these parts and to obtain a better quantification of this form of encoding, more sensory patterns were generated by overlapping additional spatial signals and by varying their onset and duration (**Figure 5B**). We selected the part with the mayor number of whiskers ("Core") in the overlapping period of each pattern and divided the POm response into three subperiods: Pre, Core and Post. Precise POm activity changes were found during these different times of POm response reflecting the diversity between parts along the patterns. Across them, POm activity was significantly increased in the Core subperiod compared to Pre and Post subperiods (described and quantified in **Figure 5C**). This demonstrated that when additional signals were temporally overlapped, POm codified this by increasing its activity only during the temporal presence of these signals. We found that POm response magnitude in all overlapping periods gradually increased as more inputs were temporally overlapped in the patterns (**Figures 5D,E**). Together, these results showed that the dynamical spatiotemporal structure of sensory patterns and the different variety of their parts was accurately reflected in precise POm activity fluctuations. Importantly, we observed that POm generated very similar patterns of integrated activity when different whiskers were activated by the same stimulation protocol. This finding is in agreement with the less accurate somatotopy of the nucleus and suggests that the function of POm integration is not the combined representation of specific whiskers but the encoding and extraction of generic sensory patterns from the entire vibrissal array.

No Sustained Activity in VPM. Stimuli Overlapping Did Not Alter Whisker Responses in VPM

To complement the analyses described above, whisker-evoked responses in VPM were examined using stimuli with different

durations (**Figure 6**). Consistent with published data (Diamond et al., 1992), VPM responses showed high spatial resolution (mean receptive field size: 2.3 ± 0.7 whiskers; $n = 44$). In contrast to POm responses and in agreement with previous findings (Castejon et al., 2016), VPM responses did not show sustained response patterns. Therefore, response modes differed drastically between these nuclei. POm was persistently activated during whisker stimulation, whereas VPM was only transiently activated at the onset of stimuli (**Figure 7A**). Long stimuli evoked an onset response at the beginning of the stimulus and, occasionally, an offset response at the end but we did not find sustained responses during stimulus presence in VPM.

Since VPM responses were transient lasting tens of milliseconds, they seem to be excessively short for integrating over multiple whisks or longer sensory events. This suggests that the temporal integration in VPM is comparatively weak. To corroborate this, we characterized VPM responses delivering the same spatiotemporal patterns of multiwhisker activation used to characterized POm responses. Consistently across animals ($n = 15$), we did not find a significant change of VPM responses by multiwhisker stimuli application (**Figures 7B,C**, see also **Figure 5D**). This is in agreement with previous findings showing that VPM response to simultaneous multiwhisker activation is very similar to individual whisker activation alone (Aguilar and Castro-Alamancos, 2005).

Together, our results show that VPM responses are different from those of POm and suggest significant functional differences between POm and VPM thalamic nuclei in the processing of sensory patterns.

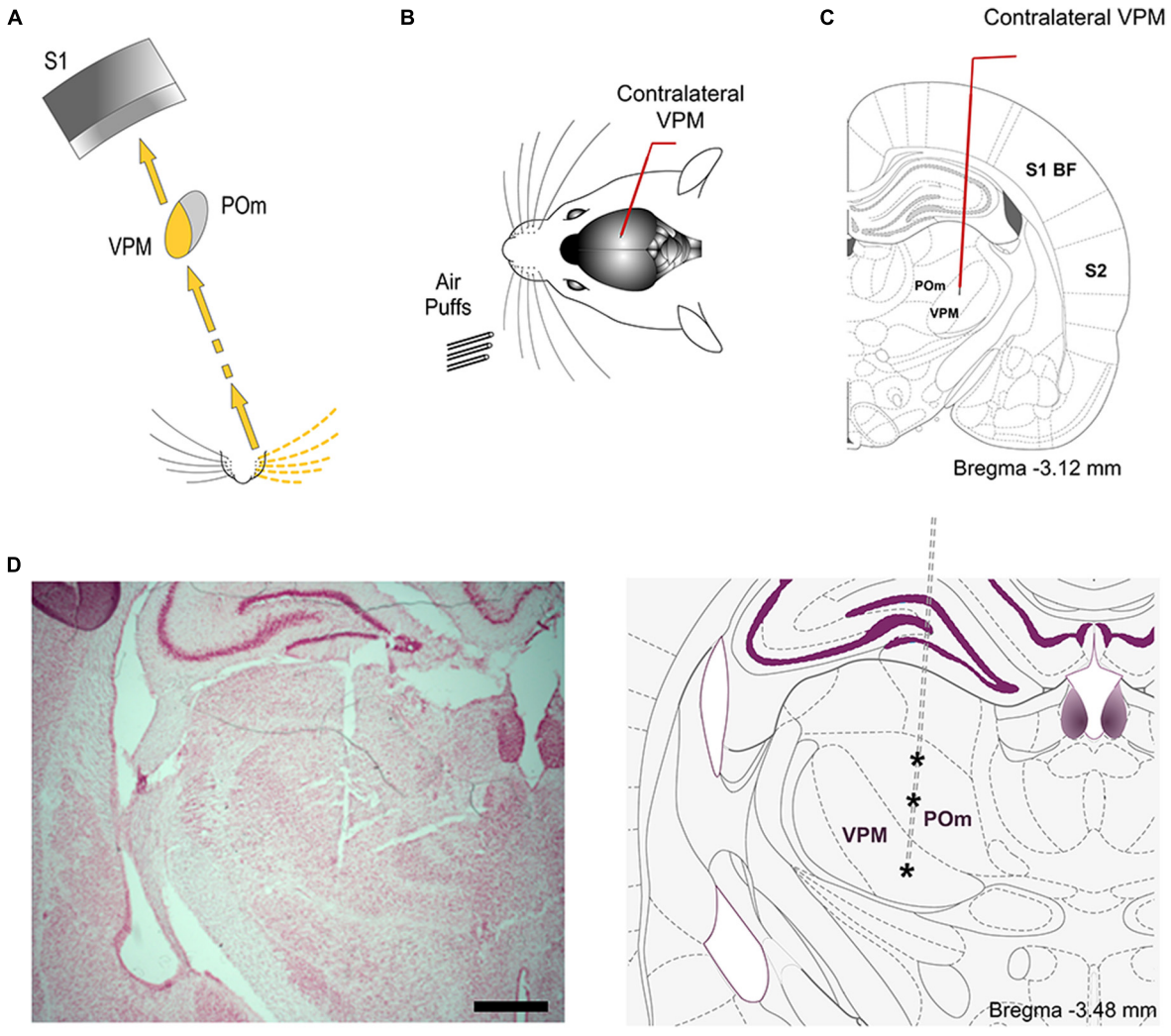

FIGURE 6 | VPM. **(A)** Schematic illustration of the lemniscal pathway. **(B)** Schematic drawing displaying the sensory stimulation *via* patterns of multiwhisker deflections. Recordings were made in the contralateral VPM nucleus. **(C)** Coronal section illustrating a recording electrode inserted into the VPM. **(D)** The left panel shows a representative Nissl stained coronal section displaying the location of the sequence of recording sites (indicated by asterisks in the other panel) in POm and VPM and the track left by the electrode. An atlas schematic reconstruction of this coronal section is shown in the right panel (Paxinos and Watson, 2007). Scale bar, 1 mm.

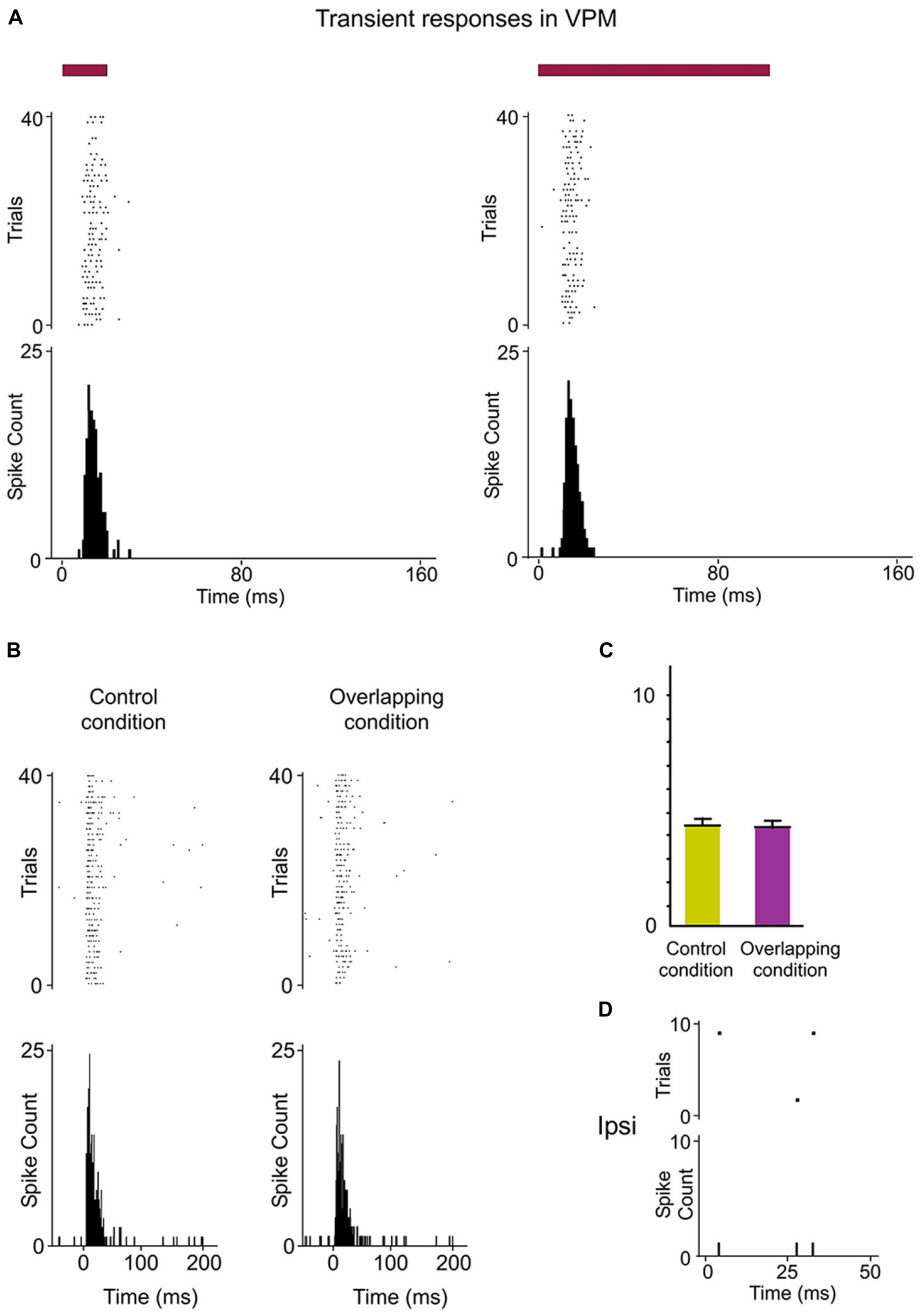

FIGURE 7 | Response modes differed drastically between VPM and POm. **(A)** VPM responses were not sustained along stimulus presence. They were transient responses just to the onset of stimuli. Raster plots and PSTHs showing multi-unit VPM transient responses evoked by the same stimulus with different durations (20 and 100 ms). Note that VPM responses do not allow the discrimination between them. Red color lines indicate the duration of the stimulus. **(B)** Raster plots and PSTHs showing that VPM response to simultaneous multiwhisker activation (Overlapping condition) is very similar to individual whisker activation alone (Control condition). **(C)** The mean response magnitude across multi-units (n = 96) recorded in VPM did not change by the overlapping of spatial signals (−2%, p = 0.17, Wilcoxon matched-pairs test). The mean onset latency of VPM responses was 8.32 ± 0.31 ms (ranged from 6 to 11 ms). **(D)** VPM did not respond to ipsilateral stimuli.

POm Responses to Ipsilateral Whisker Stimulation

Since during tactile exploration whiskers are usually stimulated bilaterally, it is then possible that POm could be implicated in the integration of bilateral signals. To test this hypothesis, we recorded POm responses to contralateral and ipsilateral stimuli during the lightly anesthetized state. Strikingly, we found that POm was also able to respond to tactile stimulation of ipsilateral

whiskers (**Figure 8**). Our experiments showed multiwhisker ipsilateral receptive fields (mean receptive field size: 9.3 ± 2.7 whiskers; n = 42) and demonstrated that POm is not only characterized by broad contralateral receptive fields but also by broad ipsilateral ones. Across recorded multi-units (n = 90), the ipsilateral responses were weaker in magnitude than contralateral responses (**Figures 8C–E**) and longer in latency (mean response onset latency: 22.31 ± 1.28 ms versus 11.36 ± 0.82 ms). The difference between ipsi- and contralateral response onset latencies (∼10 ms, **Figure 8F**) suggests that ipsilateral sensory information is mediated by a different pathway. In agreement with this, we did not find evoked responses to contralateral whisker stimulation in the Pr5 and SpVi trigeminal nuclei (11 rats; **Figure 8G**), therefore POm responses to ipsilateral whisker stimulation were not driven by ascending peripheral activity conveyed directly *via* the trigeminal complex.

Next, using air-puffs that varied in duration, we found that POm has also the capacity to sustain its activity to encode and represent tactile input duration of ipsilateral stimuli. Although the ipsilateral response was weaker in magnitude, the capacity to codify the duration of the stimulus remained robust (**Figures 8E,H**). The duration of the ipsilateral stimuli did not alter the mean onset latency of responses (One-way ANOVA, p = 0.79). These findings were consistent across all animals (n = 10).

POm Integration of Overlapping Ipsilateral Signals

Next, we investigated the implication of POm in the encoding of ipsilateral stimuli or patterns of stimuli. Accordingly, we studied POm responses to ipsilateral multiwhisker stimulation protocols producing different sensory patterns of spatiotemporal overlappings. Across these patterns, the firing rate was significantly increased in the Overlapping periods (**Figure 9**). These increases were also sustained along the temporal overlappings (**Figure 9D**). However, in the Non-overlapping periods, the magnitude of responses did not change. Again, we found precise changes in POm activity consistent with the spatiotemporal structure of the ipsilateral patterns (**Figure 9D**). These findings were consistent across all animals (n = 11).

We also characterized VPM thalamic responses delivering the same spatiotemporal patterns of ipsilateral multiwhisker activation in 7 rats. In contrast to POm, VPM did not respond to ipsilateral stimuli or to ipsilateral overlapping protocols (**Figure 7D**). Since the integration of tactile information from the two sides of the body is fundamental in bilateral perception, our results suggest a different implication of these thalamic nuclei in this function.

Transmission of Integrated Sensory Activity Between Both POm Nuclei

Our findings raised the question of by which route(s) is the ipsilateral information relayed to POm. The delay (10 ms) that we observed for ipsilateral information suggested an indirect transfer of ipsilateral information between hemispheres from the other POm. To test this possibility, unilateral overlapping sensory patterns were applied while extracellular recordings were performed in both POm nuclei simultaneously in 6 rats (**Figure 10**). We found that responses evoked by these patterns were similar in both nuclei. In agreement with data described above, they showed different onset latencies (**Figure 10B**) suggesting that evoked activity first arrives at the contralateral POm and is then transferred to the ipsilateral POm in the other hemisphere. This would indicate that both POm nuclei are indirectly connected forming a POm–POm loop.

Importantly, precise changes in POm activity caused by the integration of overlapping stimuli reflecting the spatiotemporal structure of the sensory pattern were precisely conserved (**Figure 10B**). Therefore, these patterns of integrated information encoded by one POm were transmitted through the loop to the other POm preserving their integrated structure (**Figure 10C**).

To confirm that ipsilateral activity reaches one POm from the other POm, we pharmacologically deactivated one of them by muscimol (1 mg/ml) injection (**Figure 10E**). We found that evoked responses in the second POm to ipsilateral stimulation were abolished in the majority of cases (4 out of 6 rats; **Figure 10F**). However, they were almost abolished but not completely eliminated in 2 cases (−91%, $p < 0.001$). The residual activity in these cases may be attributed to an incomplete deactivation of the opposite POm.

Together, these findings demonstrated a transmission of integrated sensory activity between both POm nuclei.

POm Integration of Bilateral Events

Finally, since bilateral events occur concurrently producing different overlappings, the next question to investigate was whether POm would be able to codify these bilateral dynamics. It would require the precise integration of contralateral and ipsilateral sensory inputs. To investigate the implication of POm in these intricate computations, we applied spatiotemporal overlapping patterns of bilateral multiwhisker stimulation simulating possible real bilateral sensory events. We measured the responses of the nucleus to the overlapping patterns and found that POm precisely integrates tactile events from both sides (**Figure 11**). We found that precise changes in the spatiotemporal structure of bilateral events evoked different patterns of POm integrated activity. Across sensory patterns, the firing rate was increased in the Overlapping periods (quantified in **Figure 11**) but not during the non-overlapping time. This indicated that the time shared by overlapping ipsi- and contralateral stimuli was encoded by POm activity. These increases in firing rate were sustained along the Overlapping periods (**Figure 11C**). Similar effects were found stimulating identical (mirror) or different whiskers (non-mirror whiskers) on both sides. This is in agreement with the less accurate somatotopy of the nucleus and again indicates that the function of POm integration is not the combined representation of specific whiskers but the generic encoding of sensory patterns integrated from both whisker pads. Moreover, during Overlapping periods, facilitation of responses was found as more ipsilateral, contralateral or bilateral temporal overlapping

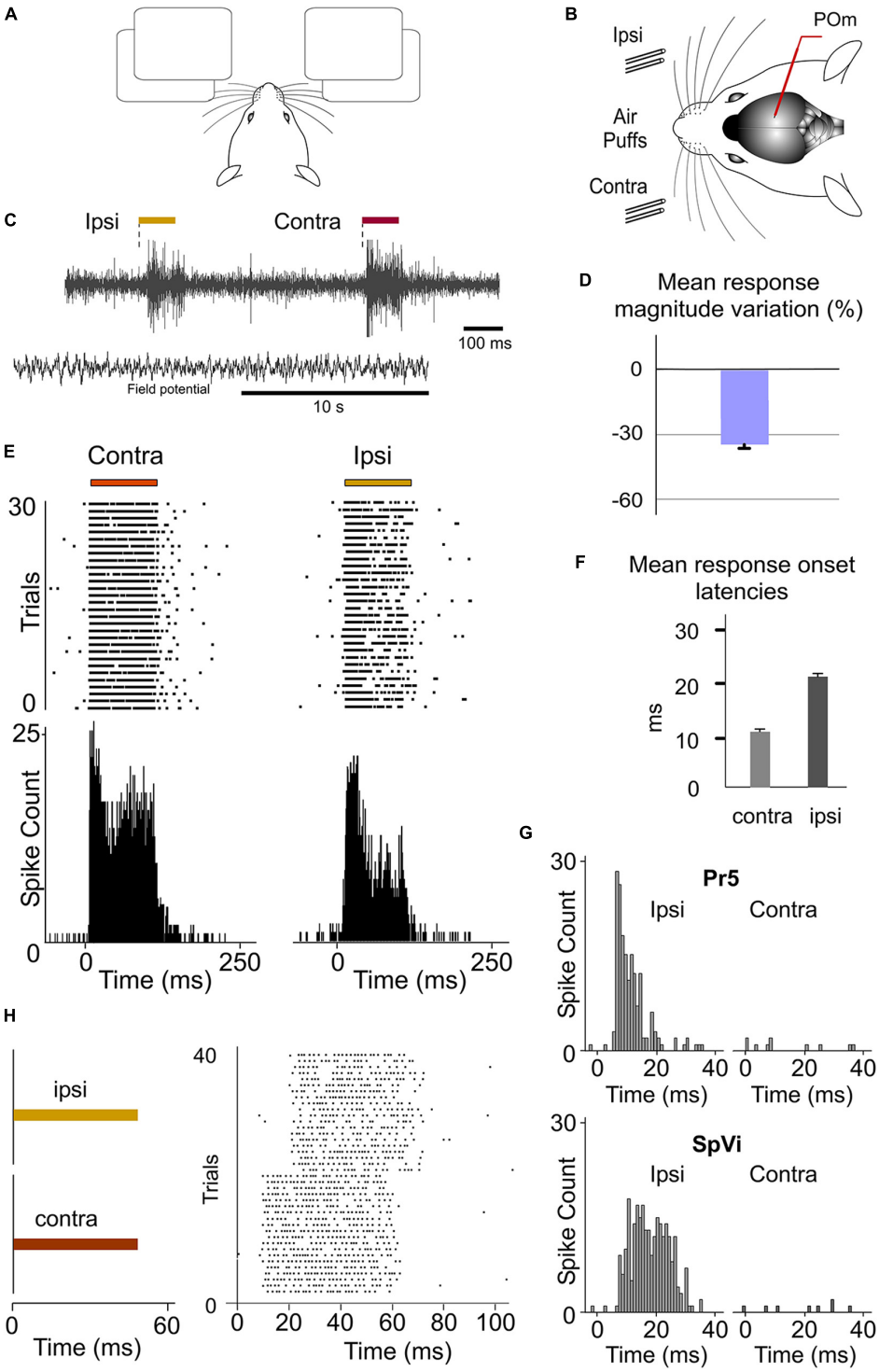

FIGURE 8 | POm responses to tactile stimulation of ipsilateral whiskers. **(A)** Simulated illustration representing the use of bilateral information. **(B)** Schematic drawing displaying the sensory stimulation *via* patterns of contra-, ipsi-, or bilateral multiwhisker deflections. Recordings were made in POm. **(C)** Evoked activity produced by ipsi- and contralateral stimuli from the same recording in POm during the lightly anesthetized state. Field potential activity recorded in this state is also shown. **(D)** Mean ipsilateral response magnitude was significantly less than contralateral one ($p < 0.001$, Wilcoxon matched-pairs test, $n = 90$ multi-units). **(E)** Raster plots and PSTHs showing sustained POm responses evoked by contra- and ipsilateral multiwhisker stimulation. **(F)** Mean onset latencies of contra- and ipsilateral responses ($n = 90$ multi-units). The onset latency of ipsilateral responses ranged from 18 to 35 ms. **(G)** Evoked responses to contralateral whisker stimulation were not found in the Pr5 and SpVi trigeminal nuclei. Sustained responses to ipsilateral stimulation were only found in SpVi. **(H)** POm responses also lasted the duration of the ipsilateral stimulus.

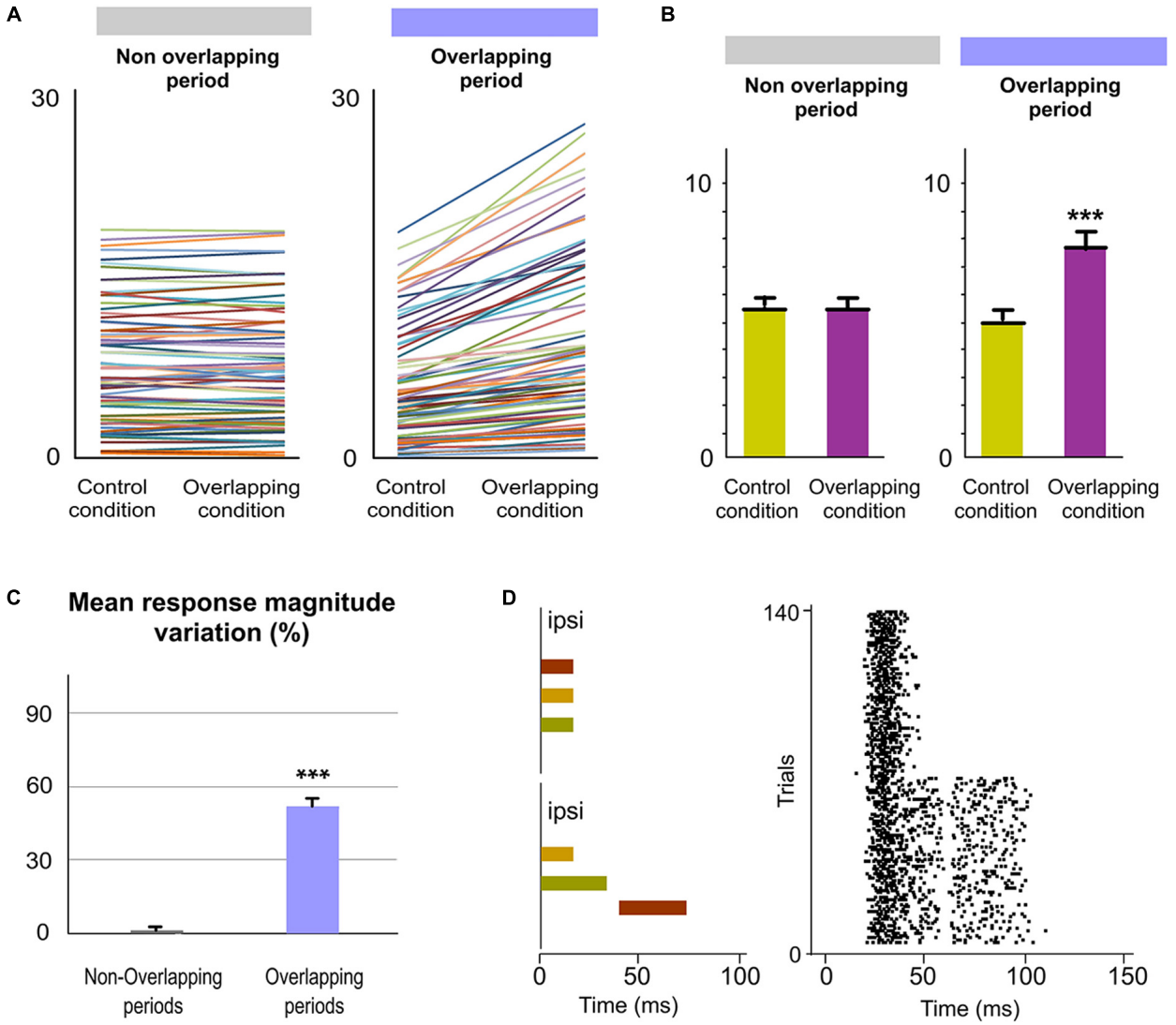

FIGURE 9 | POm integration of ipsilateral overlapping events. **(A)** Data showing the quantification of the facilitative integration during overlappings of ipsilaterally evoked signals. Plots comparing the spike rate of all recorded multi-units (n = 80, depicted in different colors) during the Overlapping and Non-overlapping response periods in Control and Overlapping conditions across sensory patterns. **(B)** The mean firing rate was significantly increased in the Overlapping periods ($p < 0.001$; Wilcoxon matched-pairs test) but not in the Non-overlapping periods where the mean magnitude of responses did not change ($p = 0.97$; Wilcoxon matched-pairs test). **(C)** Mean response magnitude variation (%) between Control and Overlapping conditions in Non-Overlapping and Overlapping periods ($p < 0.001$, Wilcoxon matched-pairs test). **(D)** Raster plots of representative POm responses to two different overlapping protocols of multiwhisker ipsilateral stimulation. An increase in POm response magnitude can be appreciated as more inputs were temporally overlapped in these protocols. Note that the general temporal structure of the sensory pattern, the temporal position of its components (depicted in different colors) and their corresponding overlappings are reflected in the structure of POm response. ***$P < 0.001$.

inputs were added showing that the variability of the bilateral spatiotemporal overlappings was replicated in POm activity variations. These findings were consistently found across animals (n = 17).

Crucially, we found that the temporal interval between bilateral stimuli is critical to bilateral integration of sensory information. The delay (∼10 ms) that we observed for ipsilateral information determines the interaction between bilateral stimuli (**Figure 11D**). This is in agreement with previous findings showing that the activation of corticofugal projections from L5 in S1 by optogenetic stimulation increases ascending sensory responses within a well-defined time window (Groh et al., 2014).

POm Nuclei Are Indirectly Connected Through the Cortex

Our results prompted us to examine the route(s) by which sensory information is transferred from one POm to the other. Cortical responses to ipsilateral whisker stimulation have been described in the somatosensory cortex (Shuler et al., 2001;

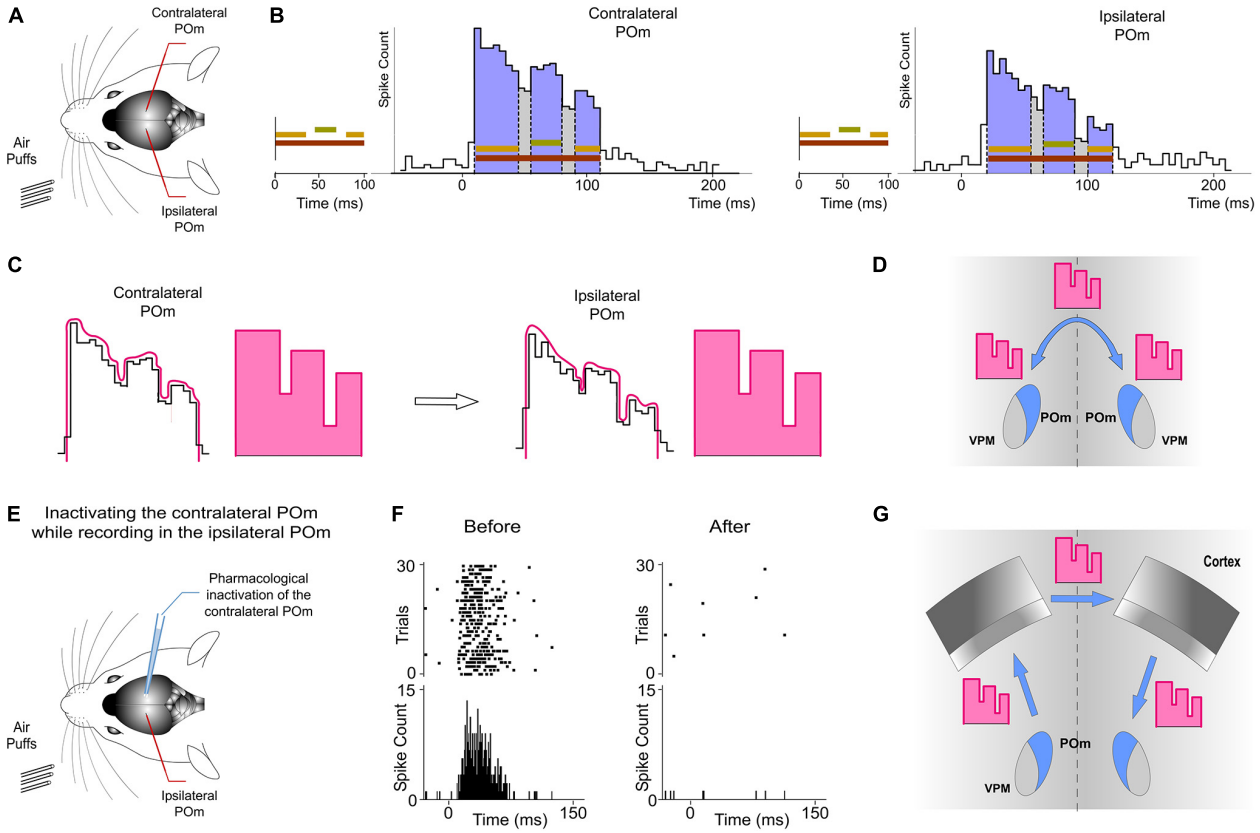

FIGURE 10 | Ipsilateral sensory information is received by one POm from the other POm. This activity was transmitted preserving its integrated structure across the POm-POm loop. **(A)** Unilateral overlapping sensory patterns were applied while extracellular recordings were performed in both POm nuclei simultaneously. **(B)** POm responses evoked by these patterns showed different onset latencies but similar integrated structure in the contra- and ipsilateral POm nuclei. As can be appreciated in these representative PSTHs (bin width 5 ms) of POm responses, precise changes in POm activity caused by the integration of overlapping signals were similar in the contra- and ipsilateral POm nuclei. Note that the onset latency was longer in the ipsilateral POm. **(C)** PSTHs in B show that precise changes (fluctuations represented by lines in pink) in POm sustained activity caused by the integration of overlapping stimuli were precisely conserved. Therefore, these "structured patterns" of integrated information encoded by POm (represented by schematic patterns in pink) were interhemispherically transmitted to the other POm preserving their integrated structure **(D)**. **(E)** POm responses to ipsilateral stimulation were studied before and after pharmacological deactivation by muscimol (1 mg/ml) injection in the opposite POm. **(F)** POm responses to ipsilateral stimulation were abolished when the opposite POm was pharmacologically deactivated. **(G)** The latencies suggest that the POm-POm loop could be formed by a thalamocortical-callosal-corticothalamic route.

Debowska et al., 2011). Therefore, ipsilateral activity seems to arrive at the contralateral POm by crossing the corpus callosum and descending from the cortex. Since POm receives strong innervation from corticofugal projection neurons in S1 (Veinante et al., 2000b), it is then possible that ipsilateral sensory stimulation could produce the activation of these descending corticofugal projections. This could have important implications on the integration of cortical inputs by POm and suggests that ipsilateral stimulation can be used to study the nature and content of the messages traveling through these corticofugal projections. To confirm that ipsilateral activity reaches POm *via* corticothalamic axons and to investigate whether these thalamic capacities are generated or mediated by cortical influence, we studied POm response properties before and after pharmacological deactivation of S1 (of the same hemisphere) by lidocaine (1%) or muscimol (1 mg/ml) application. As a control, we simultaneously recorded neuronal activity in the injected area. The electrodes were placed in the infragranular layer and the inactivation was confirmed by the absence of spontaneous and evoked activity. We found that POm responses to ipsilateral stimulation were almost abolished when S1 was inactivated (−89%, $p < 0.001$, paired t-test, $n = 8$ rats; **Figure 12B**). However, since the attempt to pharmacologically inactivate S1 can produce its partial deactivation and also can affect surrounding cortical areas, we confirmed our result by cortical lesion. The lesion was restricted to S1 and included superficial and deep layers of this area. This approach showed similar results. POm responses to ipsilateral stimulation were almost eliminated (−92%, $p < 0.001$, paired t-test, $n = 6$ rats).

POm also receives cortical projections from M1 and S2 (Alloway et al., 2008; Liao et al., 2010). However, we did not find a significant reduction of ipsilateral responses when only M1 and S2 were lesioned (−7%, $p = 0.32$, paired t-test, $n = 4$ rats). Together, these findings are in agreement with previous studies showing that cortical "driver" input (Sherman and Guillery,

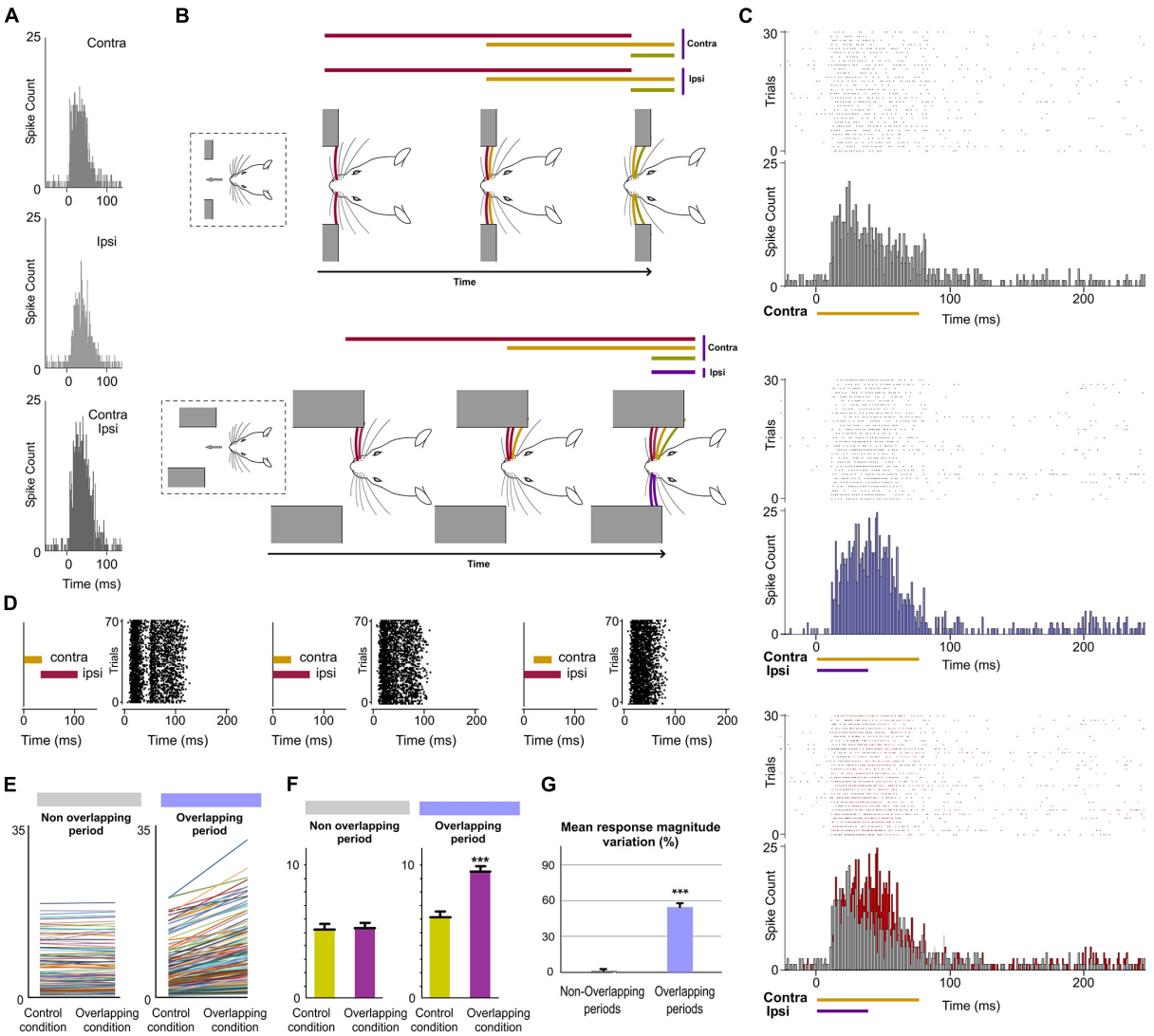

FIGURE 11 | POm integration of bilateral events. **(A)** PSTHs of POm responses evoked by contra-, ipsi- and bilateral whisker stimulations (stimulus duration 40 ms; 30 trials shown for each stimulus). To visualize the facilitative integration of bilateral signals, contra- and ipsilateral evoked responses are displayed separately. **(B)** As can be appreciated in these two simulated tactile sequences, many whiskers on both sides are sequentially deflected simultaneously. In our experiments, bilateral sensory patterns were generated by the application of contralateral and ipsilateral stimuli activating different subsets of whiskers on both sides of the face at mirror (matched whiskers on each side) and non-mirror positions. **(C)** Raster plots and PSTHs showing demonstrative POm responses evoked by contralaterally (top) and bilaterally (middle) evoked overlapping stimulation using stimuli with different durations. Note that the time shared by these bilateral overlapping inputs is encoded by a precise increase in POm activity. This increment is depicted in red in the bottom panel. **(D)** The time interval between contralateral and ipsilateral stimuli was varied to produce different overlappings and to study their integration. Raster plots of POm responses to different bilateral overlapping stimulation protocols are shown. As can be appreciated in the left panel, no integration was observed when the contra- and ipsilateral stimuli were not temporally overlapped. **(E)** Data showing the quantification of the facilitative integration during overlappings of contralaterally and ipsilaterally evoked signals. Plots comparing the spike rate of all recorded multi-units (n = 187, depicted in different colors) during the Overlapping and Non-overlapping response periods in Control and Overlapping conditions across bilateral sensory patterns. **(F)** The mean firing rate was significantly increased in the Overlapping periods ($p < 0.001$; Wilcoxon matched-pairs test) but not in the Non-overlapping periods where the mean magnitude of responses did not change ($p = 0.41$; Wilcoxon matched-pairs test). **(G)** Mean response magnitude variation (%) between control and overlapping conditions in Non-Overlapping and Overlapping periods ($p < 0.001$, Wilcoxon matched-pairs test). ***$P < 0.001$.

1998) to POm originates almost exclusively from S1 (Veinante et al., 2000b).

When a wider cortical extension was lesioned including S1, M1, and S2, POm responses to ipsilateral stimulation was completely abolished in the majority of cases (4 out of 6 rats). However, we still found very small responses to ipsilateral stimulation in 2 cases (−94%, $p < 0.001$). Importantly, we found robust contralateral whisker-evoked responses in POm even when the cortex of the same hemisphere was inactivated. Cortical inactivation slightly affected the magnitude of POm responses to contralateral whiskers. We only found a minimal reduction of spikes (−8%; paired t-test, p = 0.06,

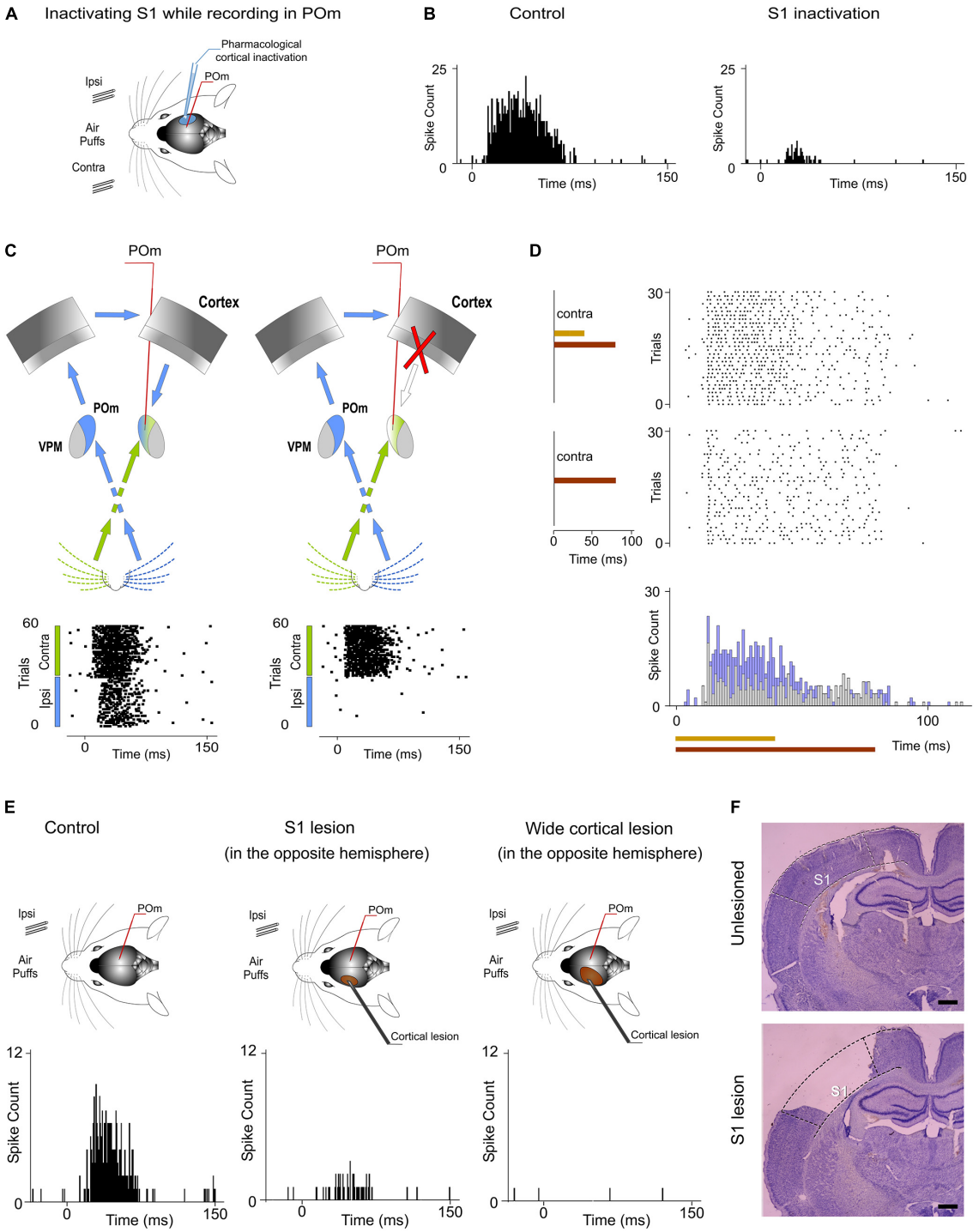

FIGURE 12 | Ipsilateral and contralateral POm nuclei are indirectly connected through the cortex. **(A)** POm responses were recorded before and after S1 inactivation (*n* = 23 multi-units). **(B)** POm responses to ipsilateral whisker stimulation were almost abolished when S1 was inactivated or lesioned. PSTHs of representative POm responses before and after S1 inactivation. **(C)** Schematic illustration representing the transmission of contralateral and ipsilateral information to POm. As can be appreciated in the corresponding raster plots, POm response to ipsilateral whisker stimulation was eliminated when the POm-POm loop was interrupted by cortical removal. Note that POm response to contralateral stimulation was still present in this condition. **(D)** Cortical removal did not affect the capacity of POm to sustain its activity to codify stimuli duration and its capacity to integrate overlapping stimuli as can be appreciated in these POm responses recorded during this condition. **(E)** Representative POm responses in control, S1 lesion (in the opposite hemisphere) and wide cortical lesion (in the opposite hemisphere) conditions. An almost complete reduction but not a total elimination of ipsilateral responses was produced by the S1 lesion. POm responses to ipsilateral stimulation were completely eliminated only when a wider cortical extension was lesioned. **(F)** Example histology showing the removal of S1 from a lesioned animal. An unlesioned example is also shown for comparison. Scale bars, 1 mm.

n = 6 rats; **Figure 12C**) indicating that contralateral whisker-evoked responses were fundamentally driven by ascending activity. Furthermore, using air-puffs that varied in duration to stimulate contralateral whiskers, we found that cortical inactivation did not affect the capacity of POm to sustain its activity to codify stimuli duration (**Figure 12D**). We also measured POm responses to contralateral overlapping sensory patterns in this condition and found that cortical inactivation did not affect the capacity of POm to integrate overlapping stimuli (**Figure 12D**). On the basis of these results, we conclude that POm does not inherit these capacities from cortical influence.

Together, these results demonstrated that POm nuclei are indirectly connected through the cortex by showing that ipsilateral activity reaches POm *via* descending parallel corticofugal projections mainly from S1 of the same hemisphere. But, by which route(s) is the ipsilateral information relayed to S1? Since projections from POm to the cortex in the other hemisphere have not been described and since it is known that corticocortical transmission between hemispheres *via* callosal projections is the main route for ipsilateral sensory inputs (Shuler et al., 2001; Petreanu et al., 2007), it seemed that the POm-POm loop could be formed by a thalamocortical-callosal-corticothalamic route. To test this, we studied POm responses to ipsilateral stimulation before and after deactivation of S1 in the other hemisphere by lidocaine (1%) or muscimol (1 mg/ml) application. We found an almost complete reduction but not a total elimination of ipsilateral responses (−86%, $p < 0.001$, paired t-test, n = 6 rats). This was confirmed by S1 lesion ($p < 0.001$, paired t-test, n = 5 rats; **Figure 12E**). Again, when a wider cortical extension was lesioned including S1, M1, and S2, POm responses to ipsilateral stimulation were completely abolished in the majority of cases (4 out of 5 rats). We still found residual responses to ipsilateral stimulation in one case. It could be possible that the remaining activity in this case could be attributable to other cortical areas projecting to POm or to subcortical interhemispheric pathways such as the collicular commissure. These possibilities remain to be tested.

Finally, to investigate the implication of cortical layers in the processing and transmission of sustained activity between the thalamus and the cortex in the POm-POm loop, evoked responses across recorded multi-units in supra, granular and infragranular layers of S1 were examined using contralateral stimuli with different durations in 19 rats. Examination of the laminar profile of evoked activity across layers showed profound differences between them. We only found sustained responses lasting the duration of the stimulus in the infragranular layer (**Figure 13**). Similar to VPM responses, supra- and granular responses were only transiently activated at the onset of stimuli (**Figure 13D**). Long stimuli usually evoked an onset response at the beginning of the stimulus and an offset response at the end but we did not find sustained responses during stimulus presence in these layers. Moreover, we found that only the infragranular layer showed evoked responses to ipsilateral stimulation (**Figure 13D**). These results demonstrated different laminar implication in the processing of sustained activity and its transmission between hemispheres.

DISCUSSION

Functional Significance of POm Capacities: POm Activity Fluctuations to Codify Patterns

Our findings show that POm capacities to sustain and integrate activity allow the representation of tactile events. Varying the spatiotemporal structure of sensory inputs, we found that POm is highly sensitive to sensory patterns in which the activation of individual whiskers strongly overlaps. Accurate increases in POm activity were produced during the overlapping time between spatial signals reflecting changes in the spatiotemporal structure of sensory patterns. Precise fluctuations of POm integrated activity seem to generate representations of these dynamics. This was produced by a facilitative integration of simultaneous signals. What could be the function of these precise thalamic activity fluctuations? Since rodents and other mammals have the ability to detect patterns embedded in a continuous stream of sensory activity, they may provide a mechanism for detecting spatiotemporal landmarks in the continuous flow of incoming sensory signals. They could be used to precisely decode sequence boundaries allowing for extraction of regularities and patterns from the flow of raw sensory information. Moreover, these fluctuations can also serve as relevant cues in sensorimotor adjustment, pattern recognition, perceptual discrimination and decision-making. From a functional perspective, active whisking and palpation movements can intentionally optimize the number, frequency and variation of overlappings to maximize the extraction of information (i.e., regularities) from objects, surfaces and textures during their exploration. Accordingly, adapting the active generation of precise overlappings of specific subsets of whiskers and their frequency would allow these animals to obtain the optimal resolution necessary to solve different perceptual or tasks requirements. In addition, VPM may provide the exact somatotopy to identify the specific whiskers activated in each fluctuation (see below). During active whisking, this may occur in every whisk cycle.

Across protocols, we found that varying the spatiotemporal structure of the sensory input produced different patterns of POm integrated activity. We observed that POm generates very similar patterns of activity (fluctuations) when different whiskers were activated by the same stimulation protocol. This finding is in agreement with the less accurate somatotopy of this nucleus and suggests that the function of POm integration is not the combined representation of specific whiskers but the encoding of generic sensory spatiotemporal patterns from the array of whiskers. Accordingly, our findings suggest that POm is a general encoder of tactile patterns. It is then possible that an important

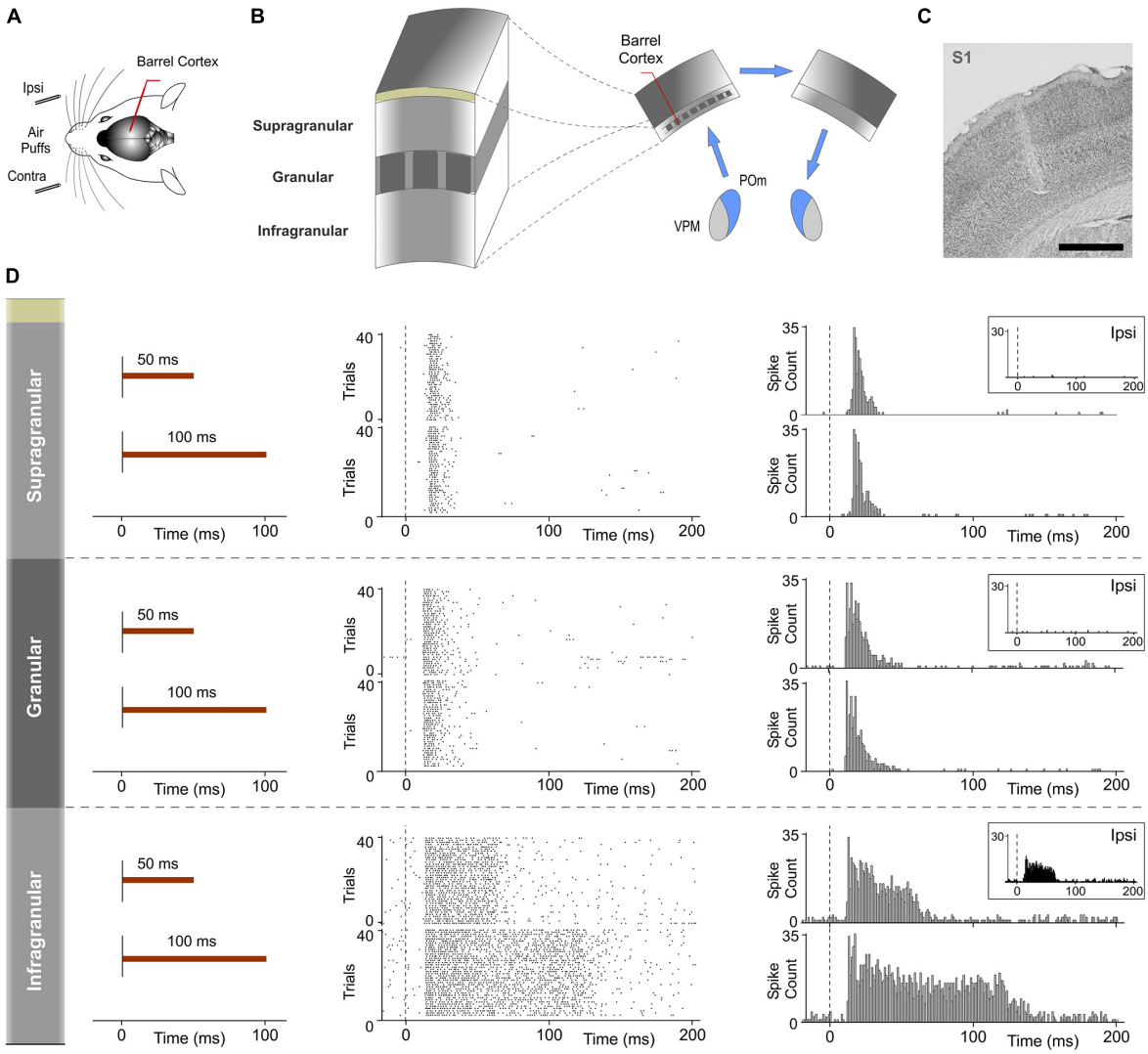

FIGURE 13 | Response modes differed between cortical layers in S1. Sustained responses along the stimulus presence were found in the infragranular layer but not in granular and supragranular layers. **(A)** Recordings were made in the barrel cortex in S1 using ipsi- and contralateral stimuli with different durations. **(B)** Evoked responses in supra-, granular, and infragranular layers of the barrel cortex were examined to study the laminar implication in the processing of sustained activity and its transmission across the POm-POm loop. **(C)** Histological section displaying the location of the sequence of recording sites across cortical layers in S1 and the track left by the electrode. Scale bar, 1 mm. **(D)** Raster plots and PSTHs showing representative responses in supragranular, granular, and infragranular layers evoked by contralateral stimuli with different durations. The mean onset latencies of these responses were 15.42 ± 0.22 ms (ranged from 12 to 25 ms, n = 117), 11.81 ± 0.21 ms (ranged from 8 to 15 ms, n = 88), and 12.67 ± 0.34 ms (ranged from 8 to 16 ms, n = 102), respectively. Note that evoked responses in granular and supragranular layers were transient just to the onset of stimuli and that they do not allow the discrimination between different durations of the same stimulus. Responses to ipsilateral stimuli were only found in the infragranular layer (insets). The mean onset latency of these responses was 17.82 ± 0.55 ms (ranged from 16 to 28 ms, n = 36).

function of higher-order thalamic nuclei could be the encoding of patterns. This needs to be confirmed in other sensory modalities.

POm Mediates Bilateral Sensory Processing

Our results show that ipsilateral activity reaches one POm indirectly from the other POm (**Figure 10**). Moreover, these findings demonstrate a transmission of sensory activity between both nuclei through a functional POm-POm loop formed by thalamocortical, interhemispheric, and corticothalamic projections. We confirmed this interhemispheric pathway by inactivating different areas of the cortex in both hemispheres (**Figure 12**) and demonstrating that ipsilateral activity reaches POm mainly *via* S1 but not exclusively (**Figures 14A–C**). This suggests that POm nuclei are indirectly connected forming a complex network of parallel thalamocortical, interhemispheric, and corticothalamic projections. In agreement with this finding, it is anatomically well described that S1, MI, and S2

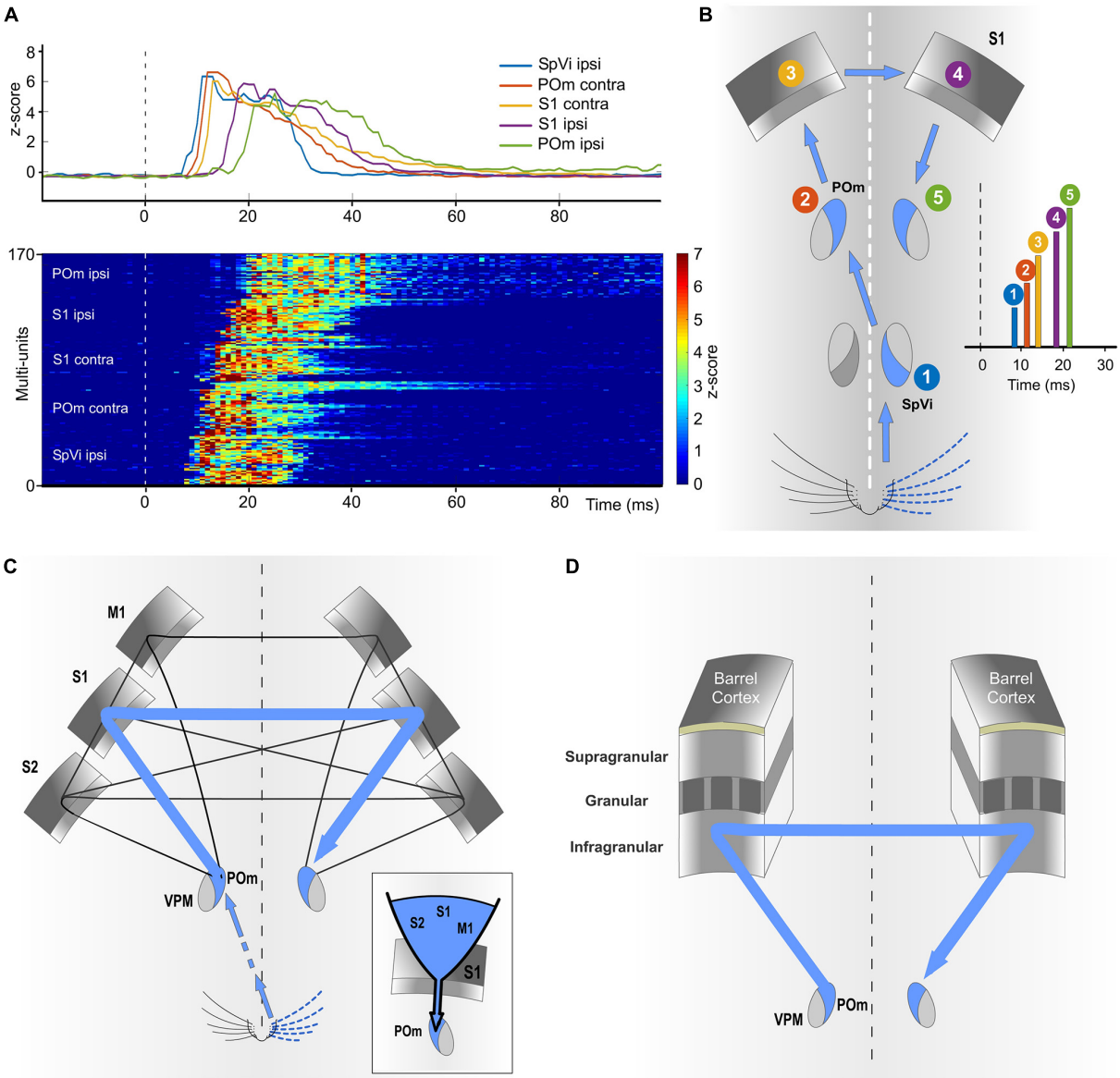

FIGURE 14 | The POm-POm loop is formed by a functional network of parallel thalamocortical, interhemispheric, and corticothalamic projections. **(A)** Demonstrative responses to whisker stimulation in *z*-score across multi-units sequentially displayed along the POm-POm loop. The average responses are shown above. **(B)** Illustration recapitulating the mean onset latencies across the different brain structures implicated in the POm-POm loop. **(C)** Although different cortical areas are implicated, our results revealed that S1 plays a central role in this functional loop. The inset illustrates the idea that S1 may act as a funnel collecting activity from different areas and sending this information *via* corticothalamic projections to POm of the same hemisphere. This complex interhemispheric loop allows bilateral integration in the thalamus and is implicated in the bidirectional transmission of sustained activity between the higher-order thalamus and the cortex. **(D)** Our results indicate that the transmission of sustained activity across the POm-POm loop is supported by the infragranular layer. This loop could be also present in other sensory modalities.

receive thalamocortical projections from POm (Ohno et al., 2012; El-Boustani et al., 2020), that they are, respectively, interhemispherically connected (Carvell and Simons, 1987; Kinnischtzke et al., 2014) and that they have corticothalamic projections to POm (Alloway et al., 2008; Liao et al., 2010). Moreover, POm is a strong driver of activity in S1, S2, and M1 (Theyel et al., 2010; Gambino et al., 2014; Casas-Torremocha et al., 2019; Zhang and Bruno, 2019; Gharaei et al., 2020) and bilateral sensory responses in S2 have also been described (Debowska et al., 2011).

The implication of different cortical areas was investigated revealing that S1 plays a central role in the POm-POm loop. Since S1 receives intra- and interhemispheric projections from these cortical areas (Carvell and Simons, 1987; Kinnischtzke et al., 2014), it is possible that S1 could collect activity from them (mostly from the other S1) and funnel this information *via*

corticothalamic projections from layer 5 to POm (**Figure 14A**). This novel idea is in agreement with our results and with previous studies showing that cortical "driver" input (Sherman and Guillery, 1998) from layer 5 to POm originates almost exclusively from S1 (Veinante et al., 2000b). Moreover, it is known that motor and S2 cortical regions elicited strong direct input to L6b and L5 in S1 (Mao et al., 2011; Zolnik et al., 2020). This cortical architecture in which one specific area (S1 in the somatosensory system) acts as a functional funnel may be a common characteristic of the cerebral cortex and could be probably present in other sensory modalities.

Importantly, we found that cortical inactivation abolished POm responses to ipsilateral whiskers. However, cortical inactivation or lesion only minimally reduced POm responses to contralateral whiskers. This demonstrates that contralateral responses are mainly driven by input from subcortical sources whereas ipsilateral responses are driven by input from the cortex. This cortical input allows POm to obtain sensory information also from the ipsilateral part of the body. However, we found that VPM did not respond to ipsilateral stimuli. Unlike POm, VPM does not receive cortical input from L5 or L6b corticofugal projections of S1 (Hoerder-Suabedissen et al., 2018). Accordingly, the subcortical and cortical inputs allow POm to have sensory information from both sides of the body. This finding is central to functionally define and classify these thalamic nuclei.

Interhemispheric Transmission of Integrated Activity Between Thalamic Nuclei

As far as we know, no studies had been performed to define the transfer of sustained activity through the thalamocortical-callosal-corticothalamic loops. These pathways have usually been studied separately. We investigated the nature and content of the activity carried by these projections and found that precise fluctuations in sustained activity caused by the integration of overlapping stimuli were precisely conserved (**Figure 10**). On the basis of this finding, we propose that these "structured patterns" of integrated information encoded by POm and transmitted through the loop preserving their integrated structure could have important functional implications in the representation of sensory information. They could be used as functional "templates" for different brain processes.

Since POm neurons have "multispecific" thalamocortical axons (Clascá et al., 2016) innervating several cortical areas including S1, S2, and M1 with different laminar profiles, our results suggest that these patterns of integrated activity generated by POm can be sent in parallel to different cortical targets. Therefore, the same message can be used by these areas and layers for different functions (i.e., perceptual, attentional, and motor). Moreover, since POm also projects to different brain structures including the amygdala, basal ganglia, insular, or ectorhinal cortex (Ohno et al., 2012; Smith et al., 2012), our results suggest that the same "templates" generated by POm can be used by these targets for diverse functions such as perceptual discrimination, familiarity, behavioral relevance, motivational meaning, or decision-making.

Different Laminar Implication in the Processing and Transmission of Sustained Activity

The laminar analysis revealed that sensory-evoked responses in S1 had different temporal structures across layers (**Figure 13**). We only found sustained responses lasting the duration of the stimulus in the infragranular layer. However, not all responses in the infragranular layer were sustained. This in agreement with the complexity of this layer formed by different sublayers. Sustained responses were mostly observed in the superficial part of the infragranular layer corresponding to layer 5. In addition, similar to VPM responses, supra- and granular responses were only transiently activated at the onset of the contralateral stimuli but we did not find sustained responses along the stimulus presence. This is in agreement with previous findings that show higher sensory-evoked firing rates in L5 neurons (de Kock et al., 2007; Castejon et al., 2016) and sparse firing to sensory stimulation in supragranular layers of vibrissal cortex in S1 (de Kock et al., 2007; Petersen and Crochet, 2013; Clancy et al., 2015; Peron et al., 2015). Moreover, consistent with other studies (Shuler et al., 2001; Manns et al., 2004), responses to ipsilateral stimuli were only found in the infragranular layer (**Figure 13**). Together, these results indicate that the transmission of sustained activity across the POm-POm loop is supported by the infragranular layer (**Figure 14D**). This loop could be also present in other sensory modalities and animals (for example, a possible pulvinar-pulvinar loop in primates).

POm Responses to Ipsilateral Stimulation, POm Sustained Activity and Its Interhemispheric Transmission Are Highly Sensitive to Anesthesia

During wakefulness or under light anesthesia, POm activity is significantly higher than during the deeply anesthetized state (Masri et al., 2008; Sobolewski et al., 2015; Zhang and Bruno, 2019). This suggests that normal POm functioning can be affected in this condition. Our findings are in agreement with this idea. In our experiments, we did not find POm responses to ipsilateral stimulation during the deeply anesthetized state (first hours after the application of urethane, 1.3–1.5 g/kg i.p.). These responses were only found during the lightly anesthetized state (**Figure 1E**). Moreover, supplementary doses of urethane abolished POm responses to ipsilateral whisker stimulation. These observations indicate that the transmission of sensory activity between hemispheres across the POm-POm loop could be highly sensitive to anesthesia. In agreement with this, it has been previously shown that increasing the level of anesthesia produces the elimination of evoked responses in S1 to ipsilateral stimulation (Armstrong-James and George, 1988; Shuler et al., 2001). This fact could explain why POm responses to ipsilateral stimulation had not been reported before. Together, this evidence indicates that high levels of anesthesia impair the real dynamics of POm functioning.

Different but Complementary Functional Roles of VPM and POm. The Hypothesis of Complementary Components

As described above, two main parallel ascending pathways convey input from the whiskers to barrel cortex (Diamond et al., 1992; Veinante et al., 2000a). This anatomical segregation suggests a different functional role of these pathways and their corresponding thalamic nuclei in somatosensory processing. Our results showed that sensory stimulation protocols with similar spatiotemporal structures produced similar patterns of POm activity fluctuations even when different whiskers were activated by the same protocol. This suggests that accurate somatotopy is not a functional characteristic of this nucleus. Accordingly, we propose that to optimize the extraction of information from the sensory flow, the paralemniscal system must be complemented with an additional system providing precise somatotopy. This can be the functional role of the lemniscal pathway, phylogenetically more recent and characterized by a precise somatotopy (Diamond et al., 1992). Previous studies have shown that in this pathway the response properties of VPM neurons are very similar to those of PrV neurons (Chiaia et al., 1991). Our results, described here, are in agreement with this proposal showing important but functionally complementary differences between POm and VPM. This functional proposal which we have called the hypothesis of "Complementary Components" can explain why tactile information from whiskers is processed by parallel ascending pathways toward the cortex. This parallel architecture is also present in the majority of sensory systems in the brain and is conserved across animals. Accordingly, we propose that sensory systems have evolved to optimize the extraction of information from the environment and that the appearance of "complementary" pathways (as the somatosensory lemniscal pathway) during evolution was essential in that functional optimization.

In addition, our results demonstrate distinct laminar processing of the same stimulus by the cortex. They show that the content, type and nature of the messages that these layers receive, process and transfer are different. Therefore, different "Components" are also associated with distinct laminar profiles. They may play different but complementary functional roles. This could account for the different profiles of activity found in cortical layers (**Figure 13D**).

We propose that "Complementary Components" could be a basic principle of brain functioning. The nature (structured versus discrete), type (sustained versus transient), and content (integrated versus segregated) of neural activity processed and transmitted by different brain structures may determine their functional implication and must be differentiated.

DATA AVAILABILITY STATEMENT

The raw data supporting the conclusions of this article will be made available by the authors, without undue reservation.

ETHICS STATEMENT

The animal study was reviewed and approved by Ethics Committee of the Autónoma de Madrid University and the Competent Spanish Government Agency (PROEX175/16), in accordance with the European Community Council Directive 2010/63/UE.

AUTHOR CONTRIBUTIONS

CC conceived the hypotheses, designed and conducted the experiments, analyzed the results, and wrote and edited the manuscript. JM-C conducted the experiments, analyzed the results, and reviewed the manuscript. AN designed and conducted the experiments, analyzed the results, and reviewed and edited the manuscript. All authors contributed to the article and approved the submitted version.

FUNDING

This work was supported by a Grant from Spain's Ministerio de Economia y Competitividad (SAF2016-76462 AEI/FEDER and PID2019-107809RB-I00).

REFERENCES

Aguilar, J. R., and Castro-Alamancos, M. A. (2005). Spatiotemporal Gating of Sensory Inputs in Thalamus during Quiescent and Activated States. *J. Neurosci.* 25, 10990–11002. doi: 10.1523/JNEUROSCI.3229-05.2005

Ahissar, E., Sosnik, R., and Haidarliu, S. (2000). Transformation from temporal to rate coding in a somatosensory thalamocortical pathway. *Nature* 406, 302–306. doi: 10.1038/35018568

Alloway, K. D., Olson, M. L., and Smith, J. B. (2008). Contralateral corticothalamic projections from MI whisker cortex: potential route for modulating hemispheric interactions. *J. Comp. Neurol.* 510, 100–116. doi: 10.1002/cne.21782

Armstrong-James, M., and George, M. J. (1988). Bilateral receptive fields of cells in rat Sm1 cortex. *Exp. Brain Res.* 70, 155–165.

Carvell, G. E., and Simons, D. J. (1987). Thalamic and corticocortical connections of the second somatic sensory area of the mouse. *J. Comp. Neurol.* 265, 409–427. doi: 10.1002/cne.902650309

Casas-Torremocha, D., Porrero, C., Rodriguez-Moreno, J., García-Amado, M., Lübke, J. H. R., Núñez, Á, et al. (2019). Posterior thalamic nucleus axon terminals have different structure and functional impact in the motor and somatosensory vibrissal cortices. *Brain Struct. Funct.* 224, 1627–1645. doi: 10.1007/s00429-019-01862-4

Castejon, C., Barros-Zulaica, N., and Nuñez, A. (2016). Control of Somatosensory Cortical Processing by Thalamic Posterior Medial Nucleus: a New Role of Thalamus in Cortical Function. *PLoS One* 11:e0148169. doi: 10.1371/journal.pone.0148169

Chiaia, N. L., Rhoades, R. W., Bennett-Clarke, C. A., Fish, S. E., and Killackey, H. P. (1991). Thalamic processing of vibrissal information in the rat. I. Afferent input to the medial ventral posterior and posterior nuclei. *J. Comp. Neurol.* 314, 201–216. doi: 10.1002/cne.903140202

Clancy, K. B., Schnepel, P., Rao, A. T., and Feldman, D. E. (2015). Structure of a single whisker representation in layer 2 of mouse somatosensory cortex. *J. Neurosci.* 35, 3946–3958. doi: 10.1523/JNEUROSCI.3887-14.2015

Clascá, F., Porrero, C., Galazo, M. J., Rubio-Garrido, P., and Evangelio, M. (2016). "Anatomy and development of multi-specific thalamocortical axons: implications for cortical dynamics and evolution," in *Axons And Brain Architecture*, ed. K. S. Rockland (Amsterdam: Elsevier), 69–92. doi: 10.1016/B978-0-12-801393-9.00004-9

de Kock, C. P. J., Bruno, R. M., Spors, H., and Sakmann, B. (2007). Layer- and cell-type-specific suprathreshold stimulus representation in rat primary somatosensory cortex. *J. Physiol.* 581, 139–154. doi: 10.1113/jphysiol.2006.124321

Debowska, W., Liguz-Lecznar, M., and Kossut, M. (2011). Bilateral Plasticity of Vibrissae SII Representation Induced by Classical Conditioning in Mice. *J. Neurosci.* 31, 5447–5453. doi: 10.1523/JNEUROSCI.5989-10.2011

Diamond, M. E., Armstrong-James, M., Budway, M. J., and Ebner, F. F. (1992). Somatic sensory responses in the rostral sector of the posterior group (POm) and in the ventral posterior medial nucleus (VPM) of the rat thalamus: dependence on the barrel field cortex. *J. Comp. Neurol.* 319, 66–84. doi: 10.1002/cne.903190108

El-Boustani, S., Sermet, B. S., Foustoukos, G., Oram, T. B., Yizhar, O., and Petersen, C. C. H. (2020). Anatomically and functionally distinct thalamocortical inputs to primary and secondary mouse whisker somatosensory cortices. *Nat. Commun.* 11:3342. doi: 10.1038/s41467-020-17087-7

Friedberg, M. H., Lee, S. M., and Ebner, F. F. (1999). Modulation of receptive field properties of thalamic somatosensory neurons by depth of anesthesia. *J. Neurophysiol.* 81, 2243–2252. doi: 10.1152/jn.1999.81.5.2243

Gambino, F., Pagès, S., Kehayas, V., Baptista, D., Tatti, R., Carleton, A., et al. (2014). Sensory-evoked LTP driven by dendritic plateau potentials in vivo. *Nature* 515, 116–119. doi: 10.1038/nature13664

Gharaei, S., Honnuraiah, S., Arabzadeh, E., and Stuart, G. J. (2020). Superior colliculus modulates cortical coding of somatosensory information. *Nat. Commun.* 11:1693. doi: 10.1038/s41467-020-15443-1

Groh, A., Bokor, H., Mease, R. A., Plattner, V. M., Hangya, B., Stroh, A., et al. (2014). Convergence of cortical and sensory driver inputs on single thalamocortical cells. *Cereb. Cortex* 24, 3167–3179. doi: 10.1093/cercor/bht173

Hoerder-Suabedissen, A., Hayashi, S., Upton, L., Nolan, Z., Casas-Torremocha, D., Grant, E., et al. (2018). Subset of cortical layer 6b neurons selectively innervates higher order thalamic nuclei in mice. *Cereb. Cortex* 28, 1882–1897. doi: 10.1093/cercor/bhy036

Kinnischtzke, A. K., Simons, D. J., and Fanselow, E. E. (2014). Motor cortex broadly engages excitatory and inhibitory neurons in somatosensory barrel cortex. *Cereb. Cortex* 24, 2237–2248. doi: 10.1093/cercor/bht085

Liao, C. C., Chen, R. F., Lai, W. S., Lin, R. C. S., and Yen, C. T. (2010). Distribution of large terminal inputs from the primary and secondary somatosensory cortices to the dorsal thalamus in the rodent. *J. Comp. Neurol.* 518, 2592–2611. doi: 10.1002/cne.22354

Manns, I., Sakmann, B., and Brecht, M. (2004). Sub- and suprathreshold receptive field properties of pyramidal neurones in layers 5A and 5B of rat somatosensory barrel cortex. *J. Physiol.* 556, 601–622. doi: 10.1113/jphysiol.2003.053132

Mao, T., Kusefoglu, D., Hooks, B. M., Huber, D., Petreanu, L., and Svoboda, K. (2011). Long-range neuronal circuits underlying the interaction between sensory and motor cortex. *Neuron* 72, 111–123. doi: 10.1016/j.neuron.2011.07.029

Masri, R., Bezdudnaya, T., Trageser, J. C., and Keller, A. (2008). Encoding of stimulus frequency and sensor motion in the posterior medial thalamic nucleus. *J. Neurophysiol.* 100, 681–689. doi: 10.1152/jn.01322.2007

Mease, R. A., Sumser, A., Sakmann, B., and Groh, A. (2016). Cortical dependence of whisker responses in posterior medial thalamus in vivo. *Cereb. Cortex* 26, 3534–3543. doi: 10.1093/cercor/bhw144

Ohno, S., Kuramoto, E., Furuta, T., Hioki, H., Tanaka, Y. R., Fujiyama, F., et al. (2012). A morphological analysis of thalamocortical axon fibers of rat posterior thalamic nuclei: a single neuron tracing study with viral vectors. *Cereb. Cortex* 22, 2840–2857. doi: 10.1093/cercor/bhr356

Paxinos, G., and Watson, C. (2007). *The Rat Brain in Stereotaxic Coordinates*. San Diego: Academic Press. doi: <doi>

Peron, S. P., Freeman, J., Iyer, V., Guo, C., and Svoboda, K. (2015). A cellular resolution map of barrel cortex activity during tactile behavior. *Neuron* 86, 783–799. doi: 10.1016/j.neuron.2015.03.027

Petersen, C. C. H., and Crochet, S. (2013). Synaptic computation and sensory processing in neocortical layer 2/3. *Neuron* 78, 28–48. doi: 10.1016/j.neuron.2013.03.020

Petreanu, L., Huber, D., Sobczyk, A., and Svoboda, K. (2007). Channelrhodopsin-2-assisted circuit mapping of long-range callosal projections. *Nat. Neurosci.* 10, 663–668. doi: 10.1038/nn1891

Sherman, S. M., and Guillery, R. W. (1998). On the actions that one nerve cell can have on another: distinguishing "drivers" from "modulators". *Proc. Natl. Acad. Sci. U. S. A.* 95, 7121–7126. doi: 10.1073/pnas.95.12.7121

Shuler, M. G., Krupa, D. J., and Nicolelis, M. A. L. (2001). Bilateral Integration of Whisker Information in the Primary Somatosensory Cortex of Rats. *J. Neurosci.* 21, 5251–5261. doi: 10.1523/JNEUROSCI.21-14-05251.2001

Smith, J. B., Mowery, T. M., and Alloway, K. D. (2012). Thalamic POm projections to the dorsolateral striatum of rats: potential pathway for mediating stimulusresponse associations for sensorimotor habits. *J. Neurophysiol.* 108, 160–174. doi: 10.1152/jn.00142.2012

Sobolewski, A., Kublik, E., Swiejkowski, D. A., Kamiński, J., and Wróbel, A. (2015). Alertness opens the effective flow of sensory information through rat thalamic posterior nucleus. *Eur. J. Neurosci.* 41, 1321–1331. doi: 10.1111/ejn.12901

Theyel, B. B., Llano, D. A., and Sherman, S. M. (2010). The corticothalamocortical circuit drives higher-order cortex in the mouse. *Nat. Neurosci.* 13, 84–88. doi: 10.1038/nn.2449

Veinante, P., Jacquin, M. F., and Deschênes, M. (2000a). Thalamic projections from the whisker-sensitive regions of the spinal trigeminal complex in the rat. *J. Comp. Neurol.* 420, 233–243. doi: 10.1002/(SICI)1096-9861(20000501)420:2<233::AID-CNE6>3.0.CO;2-T

Veinante, P., Lavallée, P., and Deschênes, M. (2000b). Corticothalamic projections from layer 5 of the vibrissal barrel cortex in the rat. *J. Comp. Neurol.* 424, 197–204. doi: 10.1002/1096-9861(20000821)424:2<197::AID-CNE1>3.0.CO;2-6

Zhang, W., and Bruno, R. M. (2019). High-order thalamic inputs to primary somatosensory cortex are stronger and longer lasting than cortical inputs. *Elife* 8:e44158. doi: 10.7554/eLife.44158.018

Zolnik, T. A., Ledderose, J., Toumazou, M., Trimbuch, T., Oram, T., Rosenmund, C., et al. (2020). Layer 6b Is Driven by Intracortical Long-Range Projection Neurons. *Cell Rep.* 30, 3492–3505.e5. doi: 10.1016/j.celrep.2020.02.044

Conflict of Interest: The authors declare that the research was conducted in the absence of any commercial or financial relationships that could be construed as a potential conflict of interest.

frontiers in Neural Circuits

BRIEF RESEARCH REPORT
published: 07 December 2021
doi: 10.3389/fncir.2021.710925

Crossed Connections From Insular Cortex to the Contralateral Thalamus

*Tolulope Adeyelu, Tanya Gandhi and Charles C. Lee**

Department of Comparative Biomedical Sciences, Louisiana State University, School of Veterinary Medicine, Baton Rouge, LA, United States

Sensory information in all modalities, except olfaction, is processed at the level of the thalamus before subsequent transmission to the cerebral cortex. This incoming sensory stream is refined and modulated in the thalamus by numerous descending corticothalamic projections originating in layer 6 that ultimately alter the sensitivity and selectivity for sensory features. In general, these sensory thalamo-cortico-thalamic loops are considered strictly unilateral, i.e., no contralateral crosstalk between cortex and thalamus. However, in contrast to this canonical view, we characterize here a prominent contralateral corticothalamic projection originating in the insular cortex, utilizing both retrograde tracing and cre-lox mediated viral anterograde tracing strategies with the Ntsr1-Cre transgenic mouse line. From our studies, we find that the insular contralateral corticothalamic projection originates from a separate population of layer 6 neurons than the ipsilateral corticothalamic projection. Furthermore, the contralateral projection targets a topographically distinct subregion of the thalamus than the ipsilateral projection. These findings suggest a unique bilateral mechanism for the top-down refinement of ascending sensory information.

Keywords: thalamus, insular cortex (IC), corticothalamic circuitry, VPMpc, contralateral connections, chemosensation, nociception, interoception

OPEN ACCESS

Edited by:
Max F. K. Happel,
Medical School Berlin, Germany

Reviewed by:
Bernd Kuhn,
Okinawa Institute of Science and Technology Graduate University, Japan
Alexander Groh,
Heidelberg University, Germany

****Correspondence:***
Charles C. Lee
cclee@lsu.edu

Received: *17 May 2021*
Accepted: *10 November 2021*
Published: *07 December 2021*

Citation:
Adeyelu T, Gandhi T and Lee CC (2021) Crossed Connections From Insular Cortex to the Contralateral Thalamus. Front. Neural Circuits 15:710925. doi: 10.3389/fncir.2021.710925

INTRODUCTION

The canonical picture of sensory information processing depicts a serial flow of information ascending from the periphery, eventually reaching the thalamus and then the cerebral cortex (Felleman and Van Essen, 1991; Rouiller et al., 1991; Bullier and Nowak, 1995; Carrasco and Lomber, 2009). The thalamus is also the target of numerous descending projections originating from cortical layer 6 that refine and modulate this incoming sensory stream (Reichova and Sherman, 2004; Briggs and Usrey, 2009; Thomson, 2010; Lee et al., 2012; Olsen et al., 2012; Augustinaite et al., 2014). In addition, a separate corticothalamic pathway originating from layer 5 has been implicated in the feedforward processing of information to higher thalamic nuclei, which in turn project to higher cortical areas (Sherman and Guillery, 2002; Reichova and Sherman, 2004; Lee and Sherman, 2008; Llano and Sherman, 2008; Lee, 2015). These interactions between thalamic nuclei and cortical areas are generally viewed as being restricted unilaterally, with interhemispheric communication not considered as occurring between cortex and thalamus (Jones, 1981, 2001; Ghosh et al., 1990; Grant et al., 2012; Brandt and Dietrich, 2019). Interestingly though, this hemispheric segregation of thalamus from cortex is not globally true, with several bilaterally crossed connections identified between midline thalamic nuclei and cortical areas (Reep and Winans, 1982; Molinari et al., 1985; Preuss and Goldman-Rakic, 1987; Dermon and Barbas, 1994;

Carretta et al., 1996; Négyessy and Bentivoglio, 1998; Alloway et al., 2008). These crossed connections have been mainly implicated in higher-order cognitive processes, such as memory, but some may be involved in the processing of sensory information (Reep and Winans, 1982; Preuss and Goldman-Rakic, 1987; Dermon and Barbas, 1994; Carretta et al., 1996; Négyessy and Bentivoglio, 1998).

The insular cortex is a key site for the processing of sensory information from several modalities (nociception, chemosensation, interception, etc.) and is the target of multiple convergent inputs, including ipsi- and contra-lateral cortical, limbic, neuromodulatory, as well as ascending thalamic inputs from the parvicellular part of the ventral posteromedial nucleus (VPMpc; Kosar et al., 1986b; Cechetto and Saper, 1987; Ogawa et al., 1992; Shi and Cassell, 1998; Nakashima et al., 2000; Schier and Spector, 2019; Gehrlach et al., 2020). This convergence likely results in the complex spatial coding that integrates information across the insular cortical surface (Kosar et al., 1986a; Ogawa et al., 1992; Chen et al., 2011; Nieuwenhuys, 2012; Gogolla et al., 2014; Peng et al., 2015; Fletcher et al., 2017; Gehrlach et al., 2020). Like other cortical areas, layer 6 insular cortical neurons target the ipsilateral thalamus (Shi and Cassell, 1998; Nakashima et al., 2000; Holtz et al., 2015; Schier and Spector, 2019), but intriguingly may also send projections to the contralateral thalamus (Reep and Winans, 1982; Oh et al., 2014).

These potential crossed insular corticothalamic projections from layer 6 have received little attention in prior studies (Shi and Cassell, 1998; Nakashima et al., 2000; Holtz et al., 2015); as such, key questions remain regarding their organization. Among these, do distinct neuronal sources in the cortex target the ipsilateral and contralateral thalamus? And do bilateral corticothalamic projections converge on the same thalamic targets? To address these questions, we employed both retrograde and anterograde tracing approaches to examine these crossed corticothalamic projections in a mouse model system. We employed the Ntsr1-Cre transgenic mouse strain, which expresses Cre-recombinase in a subset of layer 6 cortical neurons that project to the thalamus (Lee et al., 2012; Olsen et al., 2012; Mease et al., 2014; Sundberg et al., 2018; Williamson and Polley, 2019; Augustinaite and Kuhn, 2020a,b; Clayton et al., 2021). Overall, we find a novel crossed corticothalamic projection originating from the insular cortex, whose organization is discussed below.

METHODS

Animals and Surgery

Adult mice were used to examine the organization of the insular corticothalamic projections. The following procedures were approved by the Institutional Animal Care and Use Committee (IACUC) of the Louisiana State University School of Veterinary Medicine. Wild-type C57BL/6J mice (n = 5; strain: 000664; Jackson Labs, Bar Harbor, ME, United States) were used for retrograde tracer injections. Ntsr1 Cre-transgenic mice [Tg(Ntsr1-cre)GN220Gsat; MMRRC, U.C. Davis, Davis, CA, United States] were used to examine the anterograde projections of layer 6 corticothalamic neurons (n = 6) and to colocalize retrogradely labeled corticothalamic neurons with Cre-recombinase expressing neurons (n = 3). For surgeries, mice were first anesthetized with an injection of a ketamine/xylazine cocktail (at 30 mg/kg), until fully sedated as assessed by toe-pinch withdrawal reflex. The head of the animals were shaved, then secured in a stereotaxic apparatus. The scalp was cleaned with alcohol and betadine, an incision made across the midline, and a craniotomy performed above the injection sites. Following the injections described below, the site was sutured, and a generic triple antibiotic ointment applied. Animals were recovered and monitored daily for any signs of distress following surgery until sacrifice.

Tracer Injections

To examine the anterograde terminations of layer 6 corticothalamic neurons, we utilized dual injections of "floxed" viruses (800 nl at 200 nl/min) in the insular cortex of Ntsr1-Cre transgenic mice. Viral injections to express either EYFP or mCherry in layer 6 corticothalamic axons [AAV5-CaMKIIa-hChR2(H134R)-EYFP or AAV5-CaMKIIa-eNpHR3.0-mCherry; UNC Vector Core, Chapel Hill, NC, United States] were stereotaxically targeted with a Hamilton Neuros syringe (Hamilton Company, Reno, NV, United States) bilaterally to either the left or right insular cortices, respectively (relative to bregma: AP + 1.54 mm; ML ± 2.7 mm; V −3.5 mm). The animals were euthanized after 21 days to allow for adequate expression of the virally encoded fluorophores. Next, to examine the origins of insular cortical projections to the thalamus, we employed a dual retrograde tracing strategy. Injections (500 nl at 200 nl/min) of fluorogold (Fluorochrome, Denver, CO, United States) and fluororuby (ThermoFisher, Waltham, MA, United States) were stereotaxically targeted using a Hamilton Neuros syringe (Hamilton Company) to the left or right VPMpc, respectively [relative to bregma: anterior–posterior (AP) −2.06 mm; lateral (ML) ± 0.5 mm; ventral (V) −4 mm]. Animals were then allowed to recover for 7 days prior to sacrifice to allow for transport. Finally, to assess colocalization of retrogradely labeled neurons with AAV-transfected, Cre-recombinase positive neurons, we combined both retrograde fluorogold (Fluorochrome) injection in the thalamus and AAV5-CaMKIIa-eNpHR3.0-mCherry (UNC Chapel Hill) in the cortex on the same side of the brain, using the same injection parameters detailed above. These animals were allowed to recover for 21 days to allow for the transport of both retrograde tracer and the expression of the virally encoded fluorophore.

Histological Analysis

Mice were sacrificed by first anesthetizing with isoflurane inhalation, then transcardially perfusing with 4% paraformaldehyde (PFA) in 10 mM phosphate buffered saline (PBS). The brains were extracted and post-fixed in 4% PFA in 10 mM PBS overnight, followed by transferring to a solution of 30% sucrose/4% PFA in 10 mM PBS for cryoprotection for 3 days. Brains were then blocked in the coronal plane and sectioned at 50 μm thickness with a cryostat

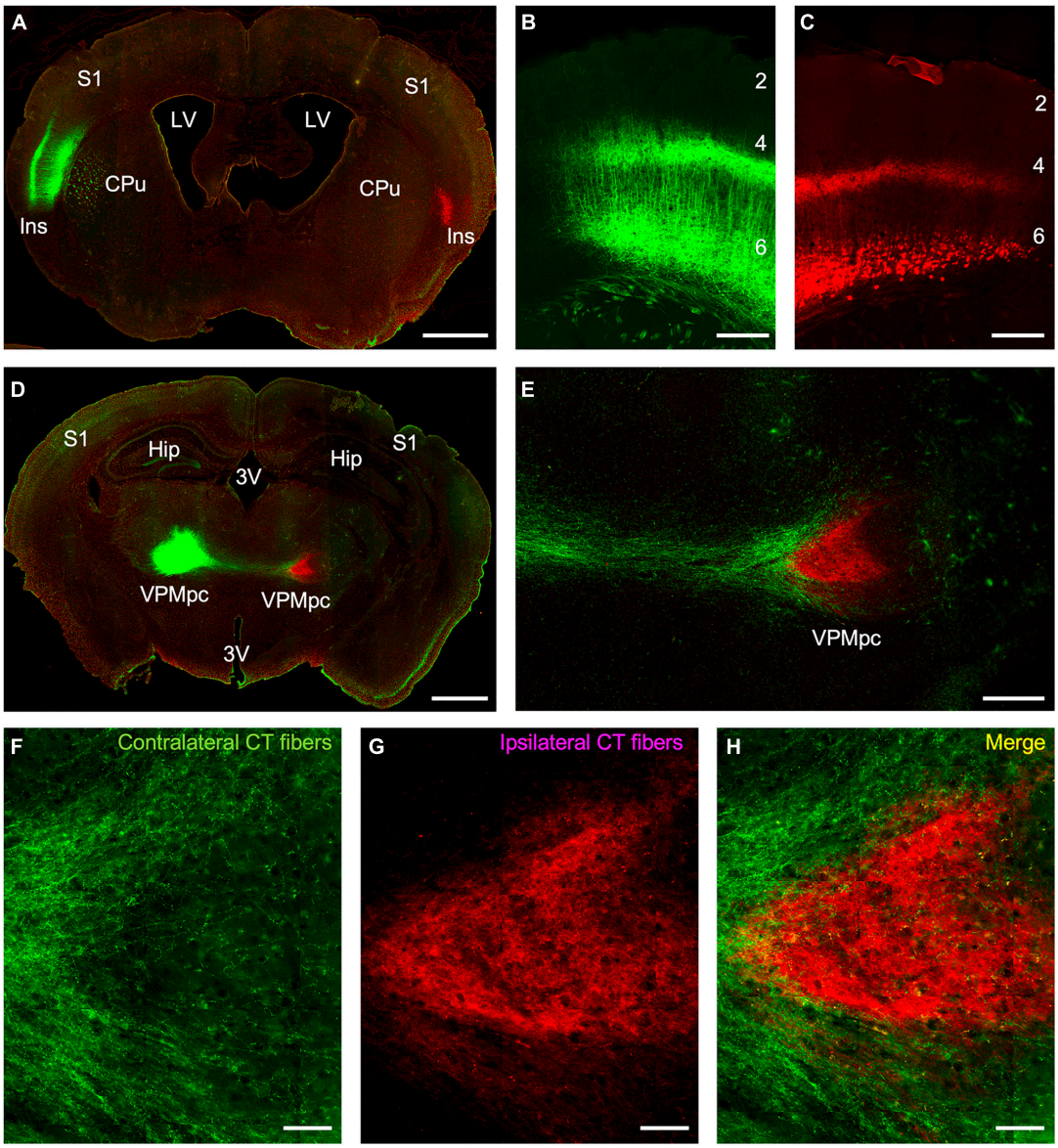

FIGURE 1 | Anterograde tracing of insular corticothalamic projections originating from layer 6 neurons in Ntsr1 Cre-recombinase expressing transgenic mice. **(A)** Injections of "floxed" AAV vectors expressing either EYFP (green) or mCherry (red) were stereotactically targeted to the left and right insular cortices, respectively. **(B,C)** Expression of virally encoded fluorescent proteins labeled the predicted population of layer 6 corticothalamic pyramidal neurons and their dendritic and axonal processes. **(D)** Anterograde fibers from both injections formed dense terminals in the respective ipsilateral thalamus, but also sent fibers to the contralateral thalamus. **(E)** Contralateral fibers (green fibers in this instance) crossed the midline and terminated in a region surrounding the ipsilateral fiber terminations (red fibers in this instance). **(F–H)** Despite the gross separation of terminal fields, some of the ipsilateral and contralateral corticothalamic (CT) labeling formed puncta in closely apposed regions, suggesting possible convergence of bilateral CT inputs on the same thalamic neuron. Abbreviations: CPu: caudate putamen; Hip: hippocampus; Ins: insular cortex; LV: lateral ventricle; S1: primary somatosensory cortex; VPMpc: parvicellular part of the ventral posteromedial nucleus; 3V: third ventricle; #s: layers 1–6. Scale bars: **(A,D)**: 1 mm; **(B–C,E)**: 250 μm; **(F–H)**: 50 μm.

(Leica Biosystems, Wetzlar, Germany). A 1:4 series of sections was mounted on gelatinized slides, then coverslipped with anti-fade medium (Vector Labs, Burlingame, CA, United States). To assess colocalization of retrograde labeling with Ntsr1 Cre-recombinase positive neurons in the insular cortex, some sections were stained immunohistochemically with a mouse monoclonal primary antibody (1:1000) for Cre-Recombinase (MAB3120, Clone 2D8, Millipore Sigma, Burlington, MA, United States) and an Alexa488-goat-anti-mouse secondary antibody (1:1000) (A-11001, ThermoFisher Scientific, Waltham, MA, United States), using methods previously described (Sultana et al., 2021).

Sections were imaged using either a Nanozoomer slide scanner (Hamamatsu Photonics, Hamamatsu City, Shizuoka,

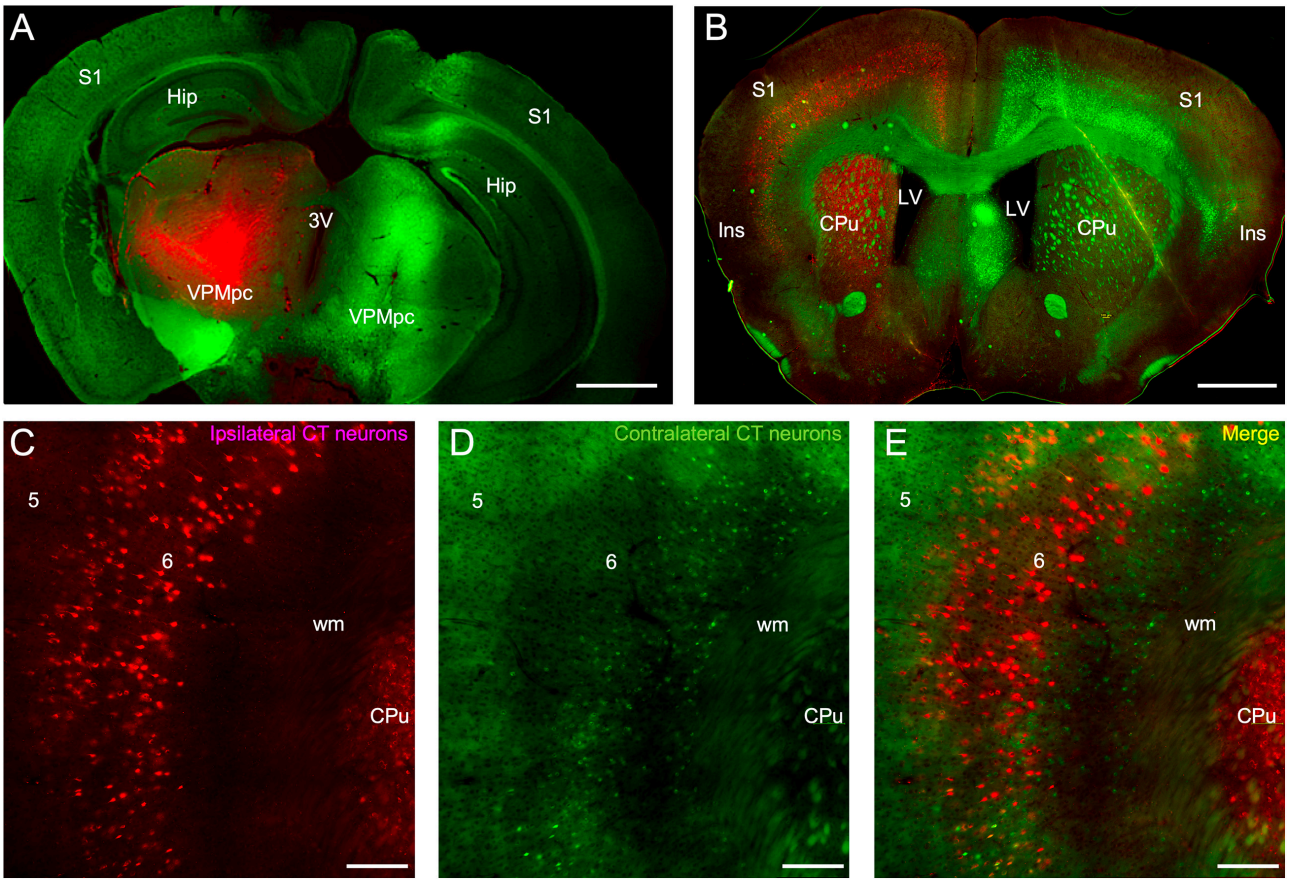

FIGURE 2 | Retrograde labeling of insular corticothalamic neurons. **(A)** Injections of either fluorogold (green) or fluororuby (red) were stereotactically targeted to the left and right VPMpc. Some injection site damage was observed, possibly due to injection speed. **(B)** Retrograde labeling was observed in the respective ipsilateral insular cortical area but was also evident in the contralateral insular cortex. Labeling was also found in other ipsilateral cortical areas, such as S1, indicative of some injection spread into adjacent thalamic nuclei, such as the ventral posterior nuclei (VP) and posteromedial nucleus (POm). **(C–E)** Both the retrogradely labeled ipsilateral CT neurons (red labeling in this instance) and the contralateral CT neurons (green neurons in this instance) originated from layer 6. Contralateral projecting neurons appeared smaller than ipsilateral projecting neurons, perhaps reflecting differences of labeling efficiency or morphological class. However, the contralateral CT neurons were interdigitated with the ipsilateral CT neurons and double-labeled neurons projecting to both thalami were rare, indicating that separate neuronal populations project to either the ipsilateral or contralateral thalami. Abbreviations are the same as in **Figure 1**. Scale bars: **(A,B)**: 1 mm; **(C–E)**: 200 μm.

Japan) or a Nikon-NiU florescence microscope (Nikon Instruments, Tokyo Japan). Nanozoomer captured images were first processed and analyzed using the NDP.view2 software (Hamamatsu Photonics). Nikon-NiU images were captured as Z-stacks, then converted into 2-D images through the extended depth of focus provided by the Nikon Element Advanced Research software (Nikon Instruments). Images were then further analyzed in ImageJ (NIH, Bethesda, MD, United States) to assess counts of retrogradely labeled neurons and fluorescence intensity (Collins, 2007; Grishagin, 2015; Schindelin et al., 2015). Areal and nuclear boundaries were gauged using cyto- and myeloarchitecture discerned from background staining and from gross section morphology compared to a standard atlas (Franklin and Paxinos, 2001). Quantitative data was compiled and analyzed in Excel (Microsoft Corporation, Redmond, WA, United States) and figures were composed in CorelDraw (Corel Corporation, Ottowa, ON, Canada).

RESULTS

To specify the origins and terminations of the insular corticothalamic projections, we employed a cell-type specific anterograde tracing approach utilizing Ntsr1 Cre-recombinase expressing transgenic mice. We assessed whether the genetically tagged layer 6 neurons in the insular cortex project to both the ipsilateral and contralateral thalamus and whether their terminations overlapped. Dual injections of "floxed" viral constructs expressing either EYFP or mCherry in layer 6 neurons of the left and right insular cortices, respectively, were made and the pattern of anterograde terminations assessed in the thalamus (**Figure 1**). Viral expression of both fluorophores fully labeled the predicted layer 6 pyramidal neurons and their processes in both insular cortical hemispheres (**Figures 1A–C**). Expression of fluorophores spanned a broad area (averaging ~3 mm^2) and likely encompassed several insular subregions (**Figures 1A–C**). Interestingly, we found that the Ntsr1-cre tagged layer 6 neurons

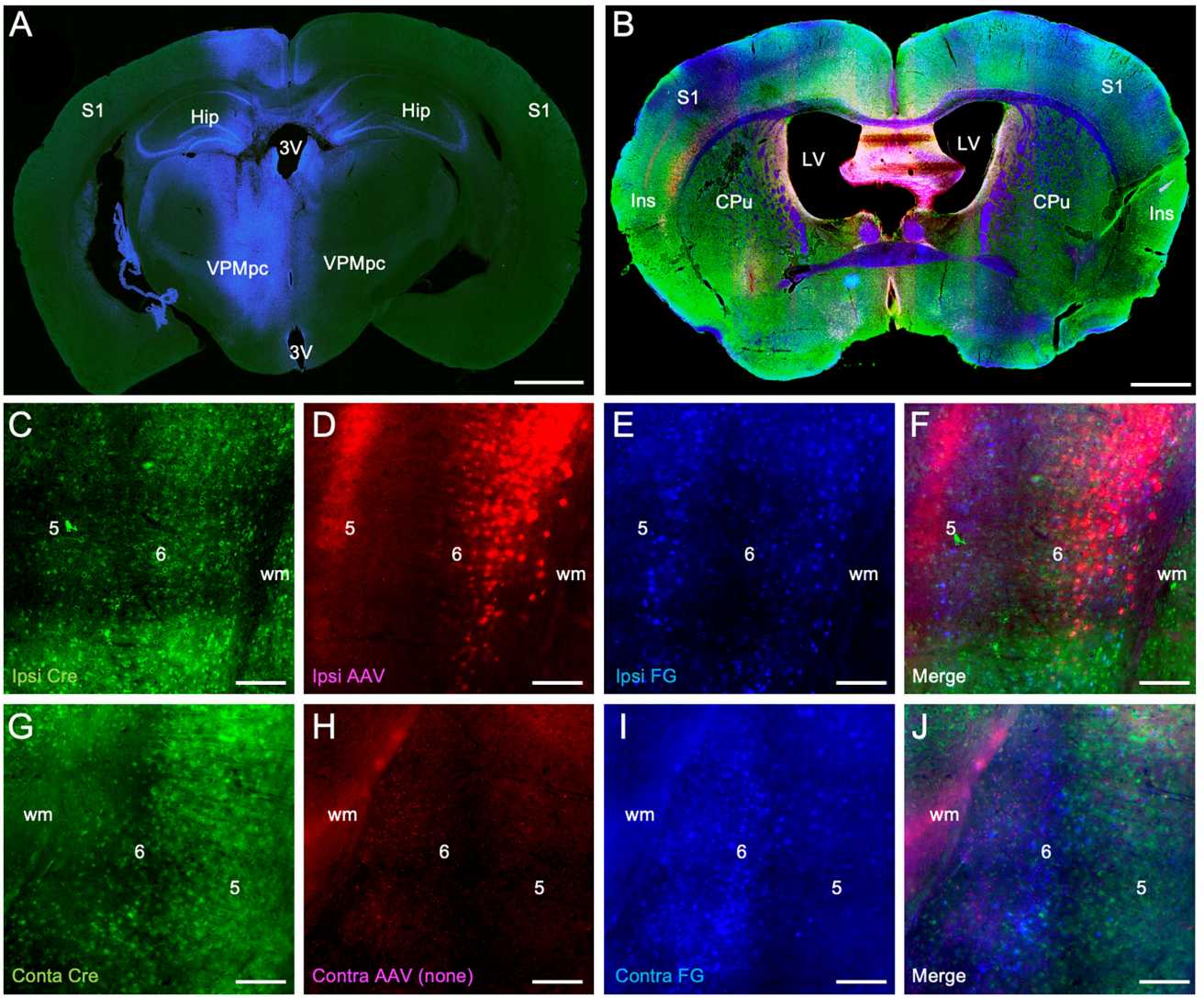

FIGURE 3 | Colocalization of retrograde corticothalamic labeling with Ntsr1-Cre-recombinase positive insular corticothalamic neurons. **(A)** Injections of fluorogold (blue) were stereotactically centered in the left VPMpc, as in **Figure 2**. **(B)** In the same animal, injection of an AAV vector expressing mCherry (red) was stereotactically targeted to the ipsilateral insular cortex, as in **Figure 1**. Retrogradely labeled sections were immunohistochemically stained for Cre-recombinase expression (green). **(C–F)** Retrogradely labeled corticothalamic neurons (blue) were again observed in layer 6 of the insular cortex. Many retrogradely labeled neurons (blue) were found to colocalize with both Cre-recombinase positive neurons (green) and with neurons expressing mCherry (red) following viral transfection. **(G–J)** Similarly, in the contralateral insular cortex, retrogradely labeled neurons (blue) were found to colocalize with Cre-recombinase positive neurons (green), although to a lesser extent than that observed in the ipsilateral insular cortex. Abbreviations are the same as in **Figure 1**. Scale bars: **(A,B)**: 1 mm; **(C–J)**: 100 μm.

project to both ipsilateral and contralateral thalami; but on a broad scale, the terminal fields were topographically segregated (**Figures 1D–H**). Notably, the ipsilateral insular corticothalamic projections terminated primarily in a "core" region of the presumed VPMpc (**Figures 1D–E,G**), while the contralateral projection terminated in "shell" regions on the dorsal and ventral aspects of the ipsilateral terminal field (**Figures 1D–F**). The "shell" terminal fields potentially included nuclei outside of the presumed VPMpc core, indicating an asymmetric nuclear organization of the contralateral corticothalamic projections (**Figures 1D–F**). The contralateral projection was also much less intense than the ipsilateral projection (22.7 ± 8.6% of the total fluorescence intensity from both thalami; averaged across all viral injections), concomitant with the relative contributions suggested by the retrograde results. On a finer scale though, these projections were not strictly segregated, with some labeled axons from each projection found overlapping and some puncta in proximity near void regions (presumed cell bodies), suggesting that bilateral projections may converge on individual thalamic neurons (**Figure 1H**).

The insular origins of corticothalamic projections were then assessed using a dual retrograde tracing approach. Fluorogold

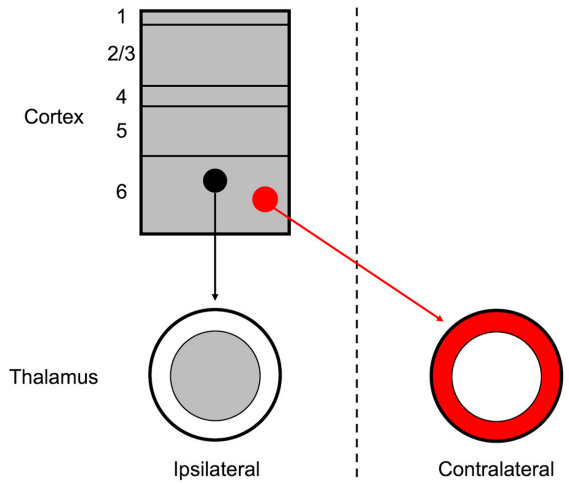

FIGURE 4 | Schematic organization of the layer 6 insular corticothalamic projections. The insular cortex is composed of both ipsilaterally projecting (black) and contralaterally projecting (red) corticothalamic (CT) neurons, which form separate, yet interdigitated, groups across layer 6. The ipsilateral CT projection terminates in a "core" region of the thalamus, the presumed VPMpc, while the contralateral CT projection terminates in a "shell" region surrounding the ipsilateral projection.

was injected into the thalamus of one hemisphere and fluororuby was injected into the other hemisphere (**Figure 2**). Relatively large thalamic injections were made to ensure near complete labeling of the cortical projection sources (**Figure 2A**). The pattern of retrograde labeling was then assessed in each cortical hemisphere (**Figure 2B**). Overall, bilateral corticothalamic projections originated from layer 6 in the insular cortex of both hemispheres, but varied in their relative contribution, with the ipsilateral projection neurons dominating and comprising 87.1 ± 6.9% of the total convergent projection from both insular cortices (**Figures 2B–E**). Retrogradely labeled neurons were found spanning a broad area in the insular cortex resulting from the large thalamic injections, and likely encompassing several functional thalamic regions (**Figures 2B–E**). In some cases, retrograde labeling was observed ipsilaterally in surrounding cortical areas, such as S1, and in cortical layer 5, indicative of tracer injection spread into other thalamic nuclei (**Figure 2B**). Topographically, the ipsilateral and contralateral projection neurons overlapped and originated from similar areal domains across the insular cortical surface (**Figures 2B–E**). However, double-labeled neurons were exceedingly rare (<1%), indicating that separate populations of layer 6 corticothalamic neurons target either the ipsilateral or contralateral thalamus, with no (or vanishingly few) branched axons connecting both (**Figure 2E**). Furthermore, the contralateral corticothalamic projection neurons appeared to originate from a lower sublaminar region than the ipsilateral projection (**Figures 2C–E**).

Finally, we assessed the extent to which the population of Ntsr1-Cre-recombinase expressing neurons overlapped with retrogradely labeled corticothalamic neurons. In these experiments, fluorogold was injected into the thalamus (blue labeling) and an AAV vector expressing mCherry (red labeling) injected into the insular cortex, both in the left hemisphere (**Figures 3A–B**). Sections were subsequently stained immunohistochemically for Cre-recombinase expressing neurons (green labeling **Figures 3B,C,G**). We found significant double-labeling of retrogradely labeled layer 6 corticothalamic neurons in the overlap zone of the ipsilateral insular cortex with Cre-recombinase expressing neurons identified immunohistochemically (blue/green: 83.6 ± 11.9%), virally (blue/red: 66.4 ± 16.7%), and with all combined (blue/red/green: 40.5 ± 13.3%). In the contralateral insular cortex, we also observed double-labeling of retrogradely labeled cells with immunohistochemically identified Cre-recombinase expressing neurons, albeit at a reduced level (blue/green: 29.3 ± 6.6%), which is consonant with the relatively reduced intensity of anterogradely labeled contralateral corticothalamic fibers (**Figure 1**) and the topographic separation of retrogradely labeled ipsilateral and contralateral corticothalamic neuronal cell bodies (**Figure 2**).

DISCUSSION

We examined the origins and terminations of bilateral insular corticothalamic projections using retrograde and cell-type specific anterograde tracing approaches (**Figures 1–3**). Methodologically, both approaches have their caveats. First, our anterograde tracer studies focused on identifying the projection patterns of a genetically specified neuronal population, i.e., the Ntsr1 Cre-recombinase tagged layer 6 corticothalamic neurons (Lee et al., 2012; Olsen et al., 2012; Mease et al., 2014; Sundberg et al., 2018; Williamson and Polley, 2019; Augustinaite and Kuhn, 2020a,b; Clayton et al., 2021). As expected, we found that this population of layer 6 neurons was a major source of the corticothalamic projection to the ipsilateral thalamus (∼80%), but comprised about a quarter of the contralateral projection (**Figure 3**). As such, there are likely other neuronal subtypes in the insular cortex that project to the ipsilateral and contralateral thalamus, which remain to be investigated (Reep and Winans, 1982; Holtz et al., 2015; Fletcher et al., 2017; Schier and Spector, 2019).

In addition, in our retrograde studies, we made relatively large thalamic injections to completely label the insular corticothalamic projections. The injection sites often encompassed not only the VPMpc, but surrounding nuclei as well (**Figure 2A**). As such, the retrogradely labeled insular cortical neurons may represent targets to other thalamic nuclei. From our injection site analyses and based on prior studies, such involvement is possible, since the other main target of insular corticothalamic projections, the mediodorsal nucleus (MD), may have been labeled following some injections. However, corticothalamic projections to these higher-order nuclei are distinguished by their origins in layer 5 and thus were readily distinguished from the feedback corticothalamic projections originating in layer 6. Nevertheless, the overall retrograde results might more precisely be considered as that of the bilateral insular connections to the thalamus, rather than to the VPMpc, *per se*. Future parcelation of these crossed

projections topographically and functionally will require more focal injections that specifically target the many insular cortical and related thalamic subregions (Kosar et al., 1986a; Ogawa et al., 1992; Chen et al., 2011; Nieuwenhuys, 2012; Gogolla et al., 2014; Peng et al., 2015; Fletcher et al., 2017; Gehrlach et al., 2020).

Although the thalamus and cortex are typically regarded as unilaterally linked, several exceptions to this "rule" have been noted, primarily among non-sensory and higher-order nuclei (Reep and Winans, 1982; Preuss and Goldman-Rakic, 1987; Dermon and Barbas, 1994; Carretta et al., 1996; Négyessy and Bentivoglio, 1998; Oh et al., 2014). Among these, the insular cortex is a potential source of corticothalamic projections to both the ipsilateral and contralateral thalamus (Reep and Winans, 1982; Oh et al., 2014). In the extensive investigation of mesoscale connectivity in the mouse by Oh et al. (2014), their dataset contains evidence of anterograde labeling of insular cortical projections to both the ipsilateral and contralateral thalami (the presumed VPMpc). In the present study, we have specifically demonstrated that these ipsilateral and contralateral corticothalamic projections originate from separate cortical populations in insular cortical layer 6, which target topographically distinct thalamic regions (**Figure 4**).

Overall, our findings suggest that layer 6 of the insular cortex is the source of parallel pathways to the ipsilateral and contralateral thalamus. The functional role of the contralateral corticothalamic connections (CCCs) remains to be defined, but in comparison, the layer 6 ipsilateral corticothalamic connections (ICCs) typically are regarded as modulatory pathways (Reichova and Sherman, 2004; Briggs and Usrey, 2009; Thomson, 2010; Lee et al., 2012; Olsen et al., 2012). On a synaptic physiological level, the layer 6 ICCs generally exhibit "modulator" properties, such as a graded-response, paired-pulse facilitation, and activation of both ionotropic and metabotropic glutamate receptors (Bartlett and Smith, 2002; Reichova and Sherman, 2004). Whether the insular layer 6 CCCs also exhibit such "modulator" properties, or alternatively "driver" properties more typical of layer 5 neurons, remains unresolved and could define the potential functional significance of these connections (Molinari et al., 1985; Négyessy and Bentivoglio, 1998; Sherman and Guillery, 2002; Reichova and Sherman, 2004; Alloway et al., 2008; Lee and Sherman, 2008; Llano and Sherman, 2008; Lee, 2015). Moreover, whether and how ICCs and CCCs functionally converge on single thalamic neurons could further denote the role of contralateral descending control of information processing in the thalamus.

The insular cortex is composed of distinct subregions that are implicated in a variety of functions, including integrating sensory information across multiple modalities, e.g., nociceptive, thermoceptive, gustatory, interoceptive, and others (Nieuwenhuys, 2012; Gogolla et al., 2014; Gehrlach et al., 2020). We speculate that the CCCs may engage gustatory and viscerocceptive neurons in the VPMpc (Holtz et al., 2015; Fletcher et al., 2017; Schier and Spector, 2019). Given the unique nature of chemosensory information processing, descending cortical control may not necessarily be predicted as restricted hemispherically, and similar crossed connections have been noted for the olfactory thalamus and cortex (Dermon and Barbas, 1994). Considering the nature of the receptor epithelium, lateralization of chemosensation has fewer obvious benefits, compared with other sensory modalities, i.e., vision, audition, and somatosensation (Sherman and Guillery, 2002; Alitto and Usrey, 2003; Briggs and Usrey, 2009). Indeed, integration of bilateral information at the level of the thalamus and cortex may be essential for fully processing incoming chemosensory information. However, the apparent lack of reciprocity of the CCCs, i.e., absent contralateral thalamocortical inputs, remains intriguing (Kosar et al., 1986a; Ogawa et al., 1992; Chen et al., 2011; Nieuwenhuys, 2012; Gogolla et al., 2014; Peng et al., 2015; Fletcher et al., 2017; Gehrlach et al., 2020). At present though, our findings do not resolve whether the observed CCCs are specific to chemosensory processing or more broadly related to other functions noted above. Consequently, future studies are needed to specifically define the role of these crossed corticothalamic projections in normal insular operations.

DATA AVAILABILITY STATEMENT

The raw data supporting the conclusions of this article will be made available by the authors, without undue reservation.

ETHICS STATEMENT

The animal study was reviewed and approved by the Institutional Animal Care and Use Committee of the Louisiana State University School of Veterinary Medicine.

AUTHOR CONTRIBUTIONS

CL: conceived of the study. TA and TG: conducted the experimental procedures. TA, TG, and CL: analyzed the data and drafted and revised the manuscript. All authors contributed to the article and approved the submitted version.

FUNDING

This work was supported by grants from the National Science Foundation (NSF) IOS1652432 and the National Institutes of Health R03NS109682, R03AG056956, and R03MH104851 to CL.

ACKNOWLEDGMENTS

We thank Sherry Ring for assistance with histological sectioning and Pete Mottram for microscopy assistance. We also thank David Burk and D'Andreas Williams at the LSU Pennington Biomedical Research Center, Cell Biology and Bioimaging Core. This work was supported by grants: NSF IOS1652432, R03NS109682, R03AG056956, R03MH104851, and P30GM118430-3. The Cell Biology and Bioimaging Core is supported in part by COBRE (P20 GM135002 & P20 GM103528) and NORC (NIH P30 DK072476) center grants from the National Institutes of Health.

REFERENCES

Alitto, H. J., and Usrey, W. M. (2003). Corticothalamic feedback and sensory processing. *Curr. Opin. Neurobiol.* 13, 440–445. doi: 10.1016/s0959-4388(03)00096-5

Alloway, K. D., Olson, M. L., and Smith, J. B. (2008). Contralateral corticothalamic projections from MI whisker cortex: potential route for modulating hemispheric interactions. *J. Comp. Neurol.* 510, 100–116. doi: 10.1002/cne.21782

Augustinaite, S., and Kuhn, B. (2020a). Chronic cranial window for imaging cortical activity in head-fixed mice. *Star Protoc.* 1:100194. doi: 10.1016/j.xpro.2020.100194

Augustinaite, S., and Kuhn, B. (2020b). Complementary Ca2+ activity of sensory activated and suppressed layer 6 corticothalamic neurons reflects behavioral state. *Curr. Biol.* 30, 3945–3960. doi: 10.1016/j.cub.2020.07.069

Augustinaite, S., Kuhn, B., Helm, P. J., and Heggelund, P. (2014). NMDA spike/plateau potentials in dendrites of thalamocortical neurons. *J. Neurosci.* 34, 10892–10905. doi: 10.1523/JNEUROSCI.1205-13.2014

Bartlett, E. L., and Smith, P. H. (2002). Effects of paired-pulse and repetitive stimulation on neurons in the rat medial geniculate body. *Neuroscience* 113, 957–974.

Brandt, T., and Dietrich, M. (2019). Thalamocortical network: a core structure for integrative multimodal vestibular functions. *Curr. Opin. Neurobiol.* 32, 154–164. doi: 10.1097/WCO.0000000000000638

Briggs, F., and Usrey, W. M. (2009). Emerging views of corticothalamic function. *Curr. Opin. Neurobiol.* 18, 403–407. doi: 10.1016/j.conb.2008.09.002

Bullier, J., and Nowak, J. G. (1995). Parallel versus serial processing: new vistas on the distributed organization of the visual system. *Curr. Opin. Neurosci.* 5, 497–503. doi: 10.1016/0959-4388(95)80011-5

Carrasco, A., and Lomber, S. G. (2009). Evidence for hierarchical processing in cat auditory cortex: nonreciprocal influence of primary auditory cortex on the posterior auditory field. *J. Neurosci.* 29, 14323–14333. doi: 10.1523/JNEUROSCI.2905-09.2009

Carretta, D., Sbriccoli, A., Santarelli, M., Pinto, F., Granato, A., and Minciacchi, D. (1996). Crossed thalamo-cortical and cortico-thalamic projections in adult mice. *Neurosci. Lett.* 204, 69–72. doi: 10.1016/0304-3940(96)12319-3

Cechetto, D. F., and Saper, C. B. (1987). Evidence for a viscerotopic sensory representation in the cortex and thalamus in the rat. *J. Comp. Neurol.* 262, 27–45. doi: 10.1002/cne.902620104

Chen, X., Gabitto, M., Peng, Y., Ryba, N. J., and Zuker, C. S. (2011). A gustotopic map of taste qualities in the mammalian brain. *Science* 333, 1262–1266. doi: 10.1126/science.1204076

Clayton, K. K., Williamson, R. S., Hancock, K. E., Tasaka, G. I., Mizrahi, A., Hackett, T. A., et al. (2021). Auditory corticothalamic neurons are recruited by motor preparatory inputs. *Curr. Biol.* 31, 310–321. doi: 10.1016/j.cub.2020.10.027

Collins, T. J. (2007). ImageJ for microscopy. *Biotechniques* 43, 25–30.

Dermon, C. R., and Barbas, H. (1994). Contralateral thalamic projections predominantly reach transitional cortices in the rhesus monkey. *J. Comp. Neurol.* 344, 508–531. doi: 10.1002/cne.903440403

Felleman, D. J., and Van Essen, D. C. (1991). Distributed hierarchical processing in the primate cerebral cortex. *Cereb. Cortex* 1, 1–47.

Fletcher, M. L., Ogg, C., Lu, L., Ogg, R. J., and Boughter, J. D. (2017). Overlapping representation of primary tastes in a defined region of the gustatory cortex. *J. Neurosci.* 37, 7595–7605. doi: 10.1523/JNEUROSCI.0649-17.2017

Franklin, K. B. J., and Paxinos, G. (2001). *The Mouse Brain in Stereotaxic Coordinates*, 2nd Edn. New York, NY: Academic Press.

Gehrlach, D. A., Weiand, C., Gaitanos, T. N., Cho, E., Klein, A. S., Hennrich, A. A., et al. (2020). A whole-brain connectivity map of mouse insular cortex. *Elife* 9:e55585.

Ghosh, A., Antonini, A., Mcconnell, S. K., and Shatz, C. J. (1990). Requirement for subplate neurons in the formation of thalamocortical connections. *Nature* 347, 179–181.

Gogolla, N., Takesian, A. E., Feng, G., Fagiolini, M., and Hensch, T. K. (2014). Sensory integration in mouse insular cortex reflects GABA circuit maturation. *Neuron* 83, 894–905. doi: 10.1016/j.neuron.2014.06.033

Grant, E., Hoerder-Suabedissen, A., and Molnár, Z. (2012). Development of the corticothalamic projections. *Front. Neurosci.* 6:53. doi: 10.3389/fnins.2012.00053

Grishagin, I. V. (2015). Automatic cell counting with ImageJ. *Anal. Biochem.* 473, 63–65.

Holtz, S. L., Fu, A., Loflin, W., Corson, J. A., and Erisir, A. (2015). Morphology and connectivity of parabrachial and cortical inputs to gustatory thalamus in rats. *J. Comp. Neurol.* 523, 139–161. doi: 10.1002/cne.23673

Jones, E. G. (1981). Functional subdivision and synaptic organization of the mammalian thalamus. *Int. Rev. Physiol.* 25, 173–245.

Jones, E. G. (2001). The thalamic matrix and thalamocortical synchrony. *Trends Neurosci.* 24, 595–601.

Kosar, E., Grill, H. J., and Norgren, R. (1986b). Gustatory cortex in the rat. II. Thalamocortical projections. *Brain Res.* 379, 342–352. doi: 10.1016/0006-8993(86)90788-2

Kosar, E., Grill, H. J., and Norgren, R. (1986a). Gustatory cortex in the rat. I. Physiological properties and cytoarchitecture. *Brain Res.* 379, 329–341. doi: 10.1016/0006-8993(86)90787-0

Lee, C. C. (2015). Exploring functions for the non-lemniscal auditory thalamus. *Front. Neural Circuits* 9:69. doi: 10.3389/fncir.2015.00069

Lee, C. C., Lam, Y. W., and Sherman, S. M. (2012). Intracortical convergence of layer 6 neurons. *Neuroreport* 23, 736–740. doi: 10.1097/wnr.0b013e328356c1aa

Lee, C. C., and Sherman, S. M. (2008). Synaptic properties of thalamic and intracortical intputs to layer 4 of the first- and higher-order cortical areas in the auditory and somatosensory systems. *J. Neurophysiol.* 100, 317–326. doi: 10.1152/jn.90391.2008

Llano, D. A., and Sherman, S. M. (2008). Evidence for non-reciprocal organization of the mouse auditory thalamocortical-corticothalamic projections systems. *J. Comp. Neurol.* 507, 1209–1227. doi: 10.1002/cne.21602

Mease, R. A., Krieger, P., and Groh, A. (2014). Cortical control of adaptation and sensory relay mode in the thalamus. *Proc. Natl. Acad. Sci. U.S.A.* 111, 6798–6803. doi: 10.1073/pnas.1318665111

Molinari, M., Minciacchi, D., Bentivoglio, M., and Macchi, G. (1985). Efferent fibers from the motor cortex terminate bilaterally in the thalamus of rats and cats. *Exp. Brain Res.* 57, 305–312. doi: 10.1007/BF00236536

Nakashima, M., Uemura, M., Yasui, K., Ozaki, H. S., Tabata, S., and Taen, A. (2000). An anterograde and retrograde tract- tracing study on the projections from the thalamic gustatory area in the rat: distribution of neurons projecting to the insular cortex and amygdaloid complex. *Neurosci. Res.* 36, 297–309. doi: 10.1016/s0168-0102(99)00129-7

Négyessy, L., and Bentivoglio, J. H. (1998). Contralateral cortical projection to the mediodorsal thalamic nucleus: origin and synaptic organization in the rat. *Neuroscience* 84, 741–753. doi: 10.1016/s0306-4522(97)00559-9

Nieuwenhuys, R. (2012). The insular cortex: a review. *Prog. Brain Res.* 195, 123–163.

Ogawa, H., Hasegawa, K., and Murayama, N. (1992). Difference in taste quality coding between two cortical taste areas, granular and dysgranular insular areas, in rats. *Exp. Brain Res.* 91, 415–424. doi: 10.1007/BF00227838

Oh, S. W., Harris, J. A., Ng, L., Winslow, B., Cain, N., Mihalas, S., et al. (2014). A mesoscale connectome of the mouse brain. *Nature* 508, 207–214.

Olsen, S. R., Bortone, D. S., Adesnik, H., and Scanziani, M. (2012). Gain control by layer six in cortical circuits of vision. *Nature* 483, 47–52. doi: 10.1038/nature10835

Peng, Y., Gillis-Smith, S., Jin, H., Trankener, D., Ryba, N. J., and Zuker, C. S. (2015). Sweet and bitter taste in the brain of awake behaving animals. *Nature* 527, 512–515. doi: 10.1038/nature15763

Preuss, T. M., and Goldman-Rakic, P. S. (1987). Crossed corticothalamic and thalamocortical connections of macaque prefrontal cortex. *J. Comp. Neurol.* 257, 269–281. doi: 10.1002/cne.902570211

Reep, R. L., and Winans, S. S. (1982). Efferent connections of dorsal and ventral agranular insular cortex in the hamster, *Mesocricetus auratus*. *Neuroscience* 7, 2609–2635. doi: 10.1016/0306-4522(82)90087-2

Reichova, I., and Sherman, S. M. (2004). Somatosensory corticothalamic projections: distinguishing drivers from modulators. *J. Neurophysiol.* 92, 2185–2197. doi: 10.1152/jn.00322.2004

Rouiller, E. M., Simm, G. M., Villa, A. E., De Ribaupierre, Y., and De Ribaupierre, F. (1991). Auditory corticocortical interconnections in the cat: evidence for parallel and hierarchical arrangement of the auditory cortical areas. *Exp. Brain Res.* 86, 483–505. doi: 10.1007/BF00230523

Schier, L. A., and Spector, A. C. (2019). The functional and neurobiological properties of bad taste. *Physiol. Rev.* 99, 605–613. doi: 10.1152/physrev.00044.2017

Schindelin, J., Rueden, C. T., Hiner, M. C., and Eliceiri, K. W. (2015). The ImageJ ecosystem: an open platform for biomedical image analysis. *Mol. Reprod. Dev.* 82, 518–529. doi: 10.1002/mrd.22489

Sherman, S. M., and Guillery, R. W. (2002). The role of the thalamus in the flow of information to the cortex. *Philos. Trans. R Soc. Lond. B Biol. Sci.* 357, 1695–1708.

Shi, C. J., and Cassell, M. D. (1998). Cortical, thalamic, and amygdaloid connections of the anterior and posterior insular cortices. *J. Comp. Neurol.* 399, 440–468.

Sultana, R., Brooks, C. B., Shrestha, A., Ogundele, O. M., and Lee, C. C. (2021). Perineuronal nets in the prefrontal cortex of a schizophrenia mouse model: assessment of neuroanatomical, electrophysiological, and behavioral contributions. *Int. J. Mol. Sci.* 22:11140. doi: 10.3390/ijms222011140

Sundberg, S. C., Lindström, S. H., Sanchez, G. M., and Granseth, B. (2018). Cre-expressing neurons in visual cortex of Ntsr1-Cre GN220 mice are corticothalamic and are depolarized by acetylcholine. *J. Comp. Neurol.* 526, 120–132. doi: 10.1002/cne.24323

Thomson, A. M. (2010). Neocortical layer 6, a review. *Front. Neuroanat.* 4:13. doi: 10.3389/fnana.2010.00013

Williamson, R. S., and Polley, D. B. (2019). Parallel pathways for sound processing and functional connectivity among layer 5 and 6 auditory corticofugal neurons. *Elife* 8:e42974. doi: 10.7554/eLife.42974

Conflict of Interest: The authors declare that the research was conducted in the absence of any commercial or financial relationships that could be construed as a potential conflict of interest.

Publisher's Note: All claims expressed in this article are solely those of the authors and do not necessarily represent those of their affiliated organizations, or those of the publisher, the editors and the reviewers. Any product that may be evaluated in this article, or claim that may be made by its manufacturer, is not guaranteed or endorsed by the publisher.

frontiers in Neural Circuits

ORIGINAL RESEARCH
published: 05 January 2022
doi: 10.3389/fncir.2021.786740

Effects of Cortical Cooling on Sound Processing in Auditory Cortex and Thalamus of Awake Marmosets

Marcus Jeschke[1,2,3]*, *Frank W. Ohl*[2,4,5] *and Xiaoqin Wang*[1]*

[1] *Laboratory of Auditory Neurophysiology, Department of Biomedical Engineering, Johns Hopkins University School of Medicine, Baltimore, MD, United States,* [2] *Department Systems Physiology of Learning, Leibniz Institute for Neurobiology, Magdeburg, Germany,* [3] *Auditory Neuroscience and Optogenetics Group, Cognitive Hearing in Primates Laboratory, German Primate Center-Leibniz Institute for Primate Research, Göttingen, Germany,* [4] *Institute of Biology, Otto-von-Guericke-University Magdeburg, Magdeburg, Germany,* [5] *Center for Behavioral Brain Sciences (CBBS), Magdeburg, Germany*

The auditory thalamus is the central nexus of bottom-up connections from the inferior colliculus and top-down connections from auditory cortical areas. While considerable efforts have been made to investigate feedforward processing of sounds in the auditory thalamus (medial geniculate body, MGB) of non-human primates, little is known about the role of corticofugal feedback in the MGB of awake non-human primates. Therefore, we developed a small, repositionable cooling probe to manipulate corticofugal feedback and studied neural responses in both auditory cortex and thalamus to sounds under conditions of normal and reduced cortical temperature. Cooling-induced increases in the width of extracellularly recorded spikes in auditory cortex were observed over the distance of several hundred micrometers away from the cooling probe. Cortical neurons displayed reduction in both spontaneous and stimulus driven firing rates with decreased cortical temperatures. In thalamus, cortical cooling led to increased spontaneous firing and either increased or decreased stimulus driven activity. Furthermore, response tuning to modulation frequencies of temporally modulated sounds and spatial tuning to sound source location could be altered (increased or decreased) by cortical cooling. Specifically, best modulation frequencies of individual MGB neurons could shift either toward higher or lower frequencies based on the vector strength or the firing rate. The tuning of MGB neurons for spatial location could both sharpen or widen. Elevation preference could shift toward higher or lower elevations and azimuth tuning could move toward ipsilateral or contralateral locations. Such bidirectional changes were observed in many parameters which suggests that the auditory thalamus acts as a filter that could be adjusted according to behaviorally driven signals from auditory cortex. Future work will have to delineate the circuit elements responsible for the observed effects.

Keywords: auditory cortex, auditory thalamus, cooling, corticofugal feedback, inactivation, spatial processing, temporal modulations

OPEN ACCESS

Edited by:
Julio C. Hechavarría, Goethe University Frankfurt, Germany

Reviewed by:
Victoria M. Bajo Lorenzana, University of Oxford, United Kingdom
Paul Hinckley Delano, University of Chile, Chile

***Correspondence:**
Marcus Jeschke
mjeschke@dpz.eu
Xiaoqin Wang
xiaoqin.wang@jhu.edu

Received: *30 September 2021*
Accepted: *10 December 2021*
Published: *05 January 2022*

Citation:
Jeschke M, Ohl FW and Wang X (2022) Effects of Cortical Cooling on Sound Processing in Auditory Cortex and Thalamus of Awake Marmosets. Front. Neural Circuits 15:786740. doi: 10.3389/fncir.2021.786740

INTRODUCTION

The thalamus is traditionally conceptualized as a gateway between upstream inputs from subcortical structures to cortical areas (Sherman and Guillery, 2006). In the auditory system the medial geniculate body receives inputs from the inferior colliculus and sends its output to various cortical areas in the primary and secondary auditory cortex (De La Mothe et al., 2006; de la Mothe et al., 2012; Cappe et al., 2009; Saldeitis et al., 2014), but it also receives numerous feedback connections (Rouiller and Durif, 2004; De La Mothe et al., 2006; de la Mothe et al., 2012) that outnumber feedforward connections by far (Deschênes et al., 1998). Together, the feedforward and feedback connections between cortex and thalamus form an intricate cortico-thalamo-cortical loop (Winer and Larue, 1987; Happel et al., 2014; Mukherjee et al., 2020) whose structure-function relationship is still poorly understood (Usrey and Sherman, 2019).

While corticothalamic projections are excitatory, cortical feedback has both excitatory and inhibitory effects on thalamic neurons through disynaptic connections *via* the thalamic reticular nucleus (Cruikshank et al., 2010; Crandall et al., 2015). Diverse functions have been proposed for corticothalamic feedback in the auditory system, including gating of thalamocortical transmission (Yu et al., 2004; Ibrahim et al., 2021), supporting thalamic plasticity during learning (He, 2003; Suga, 2020; Taylor et al., 2021), gain control of cortical input (Saldeitis et al., 2021) and switching dynamics of processing to favor detection or discrimination of stimuli (Guo et al., 2017). Thalamic sensory processing can also be influenced by altering activity further downstream e.g. via further corticofugal projections such as the corticocollicular pathway targeting mostly the non-lemniscal pathway (Winer, 2005; Yudintsev et al., 2021). Thus, more generally, it is apparent that thalamic sensory processing results from the dynamic interplay of feedforward and feedback pathways (Alitto and Usrey, 2003).

Relatively little is known about the role of corticofugal feedback in non-human primates and especially in the auditory system. Although highly successful in rodents, in primates very few studies employed optogenetics to study corticofugal influences up to date (Galvan et al., 2016; Suzuki et al., 2021). This scarcity of studies reflects the technical difficulties associated with implantation of relatively bulky light sources in the area of interest, the required strong light intensities to reach corticofugal output layers 5 and 6 (Yizhar et al., 2011; Dong et al., 2018) as well as the difficulty in translating optogenetic tools from rodents to primates (Jüttner et al., 2019). Another concern particularly relevant for long-term primate experiments is the potential influence on cell physiology due to the introduction and potential overexpression of a foreign protein (Miyashita et al., 2013). In contrast, local cooling is a simple and flexible approach to reversibly inactivate cortical areas and to investigate the role of feedback and feedforward connections of a structure under investigation (Girardin and Martin, 2009; Anderson and Malmierca, 2012; Cooke et al., 2012; Takei et al., 2021). To this end several different designs of cooling devices have been presented so far (Lomber et al., 1999; Cooke et al., 2012). Almost all of these were designed to be implanted and/or affect a larger brain structure or area as a whole. Accordingly, most designs were relatively large with an interface area between cooling device and brain tissue of more than 12 mm^2. Here, we have developed a small, repositionable cooling device which also allows for simultaneous recording of neural activity directly underneath the probe. The device consists of a small stainless steel foot ($\sim$2 mm^2 footprint) with stainless steel tubing wrapped around via which chilled methanol is pumped to lower the temperature of the device. We used this device in a chronic recording preparation in awake marmosets to study the effect of manipulating corticofugal feedback on cortical and thalamic neural responses to complex sounds that were varied temporally or spatially.

MATERIALS AND METHODS

The experiments were conducted at the Johns Hopkins University, Baltimore. All procedures were in accordance with the National Institutes of Health (U.S.) guidelines for the care and use of animals in research. The surgical and experimental techniques were approved by the institutional animal care and use committee of the Johns Hopkins University. Data reported in this article was collected from a total of 4 hemispheres in 3 adult, male common marmosets (*Callithrix jacchus*). **Table 1** provides an overview of the number of neurons recorded under the various experimental conditions. The general surgical approach to prepare common marmosets for neurophysiological recordings has been previously reported in detail elsewhere (Lu et al., 2001; Gao and Wang, 2020) and is only briefly described below.

Design and Manufacturing of the Repositionable Cooling Probe

The main foot of the cooling probe was machined from 316 stainless steel rods (McMaster-Carr) using standard milling and lathing techniques. **Figure 1** provides an overview of the cooling probe. The back of the foot was lathed to a final diameter of 1.5 mm at a length of $\sim$5–6 mm. The front part of the foot consisted of a plate with dimensions of 0.9 mm width, 2.5 mm length and 3.5 mm height. A small hole was drilled through the center of the foot using a tailstock drill chuck on a lathe and a 0.5 mm drill bit. This enabled recording neuronal activity directly underneath the probe during later experiments. Then, 23 gauge 316 stainless steel tubing (B004UNEY32, Small Parts Inc.) was first wound around a 1 mm stainless steel rod to support tight spiraling around the larger 1.5 mm diameter foot plate shaft and then soldered in place using acid flux and lead free solder. To prevent kinking of the stainless steel tubing while winding, a thinner metal wire was inserted into the stainless steel tube and removed afterwards.

Thermocouples were custom made from T type thermocouple wire (Omega TG-T-30) by soldering the ends of the copper and constantan wires under microscopic control. To achieve this, a small piece of lead free solder was placed on a glass petry dish and molten using a hot stream of air from a

TABLE 1 | Overview of single units recorded for the current study split between the various experimental conditions.

	Left	Right	Total
Total cooling dataset			
Hemispheres	2	2	4
Cortical units	17	21	38
Thalamic units	74	84	158
Analysis	**Condition**	**Number of units**	
Cortex cooling dataset			
Waveform distance effects	Baseline + cooled or cooled + recovery	33	
	Baseline/cooled/recovered	21	
Spontaneous and driven activity/distance effects	Baseline + cooled or cooled + recovery	34	
Analysis	**Condition**	**Number of units**	
Thalamus cooling dataset			
Spontaneous and driven activity/distance effects	Baseline + cooled	144	
Waveform distance effects	Baseline + cooled	142	
	Baseline/cooled/recovered	89	
Frequency tuning	Baseline + cooled	52	
Amplitude modulated sounds	Baseline + cooled	58	
Spatial processing	Baseline + cooled	48	

heat gun. The thermocouple wire ends were then dipped into the molten solder and the heat gun was turned off to allow the solder to harden leaving a small pellet at the ends of the thermocouple wires (∼0.5 mm diameter, see **Figure 1**). Thermocouples manufactured this way were calibrated at 2 fixed temperature points at 0 and 40°C in a water bath by comparing the measured temperature with a liquid in glass thermometer. These thermocouples were then positioned and glued at bottom of the steel foot and served to monitor the temperature manipulation as well as to ensure proper contact between the brain and the cooling probe.

Maintenance of Large Scale Craniotomies for Long Term Cooling and Recording

To record from marmoset auditory cortex, small craniotomies of ca. 1 mm diameter have commonly been used. From day to day these craniotomies are cleaned and usually closed after 1 to 2 weeks with dental acrylic to perform another craniotomy elsewhere. This approach keeps the dura mater relatively fresh and prevents excessive scarring. In contrast, in the current study craniotomies were substantially larger (1.2 × 3.5–4 mm; **Figure 2A**) and had to be kept open for several weeks to study cooling effects in the auditory thalamus. Consequently, growth of connective tissue was observed similar to findings during long term recordings in macaques (**Figure 2B**; see e.g., Spinks et al., 2003). Once a thin layer of connective tissue formed (after 2–3 weeks we estimated a thickness of ca. 200 μm), the craniotomy was thoroughly cleaned and excess tissue removed with hypodermic needles bent into small hooks (26G; **Figures 2C–E**). This procedure allowed to keep the craniotomy open for several weeks while maintaining a stable distance of the cooling probe placed atop the dura and the cortical elements to be cooled.

Cooling Procedure

Similar to published work (Lomber et al., 1999; Coomber et al., 2011; Wood et al., 2017; Peel et al., 2020) we opted for a methanol based cooling system were methanol was pumped with an adjustable flow rate (Fluidmetering.com, Q1CSC/QSY (MB) [pump head/pump drive, respectively]; maximum possible flow rate of 92 ml/min) through PTFE tubing (Diba Industries Inc., 008T16-050-20, 008T16-080-20, 008T32-150-10) and the cooling probe. The pump was located outside the recording chamber and placed on foam to reduce vibrations and to eliminate an influence of pumping noise during the experiments. The pump noise was below 45 dB SPL and not measurable inside the double walled recording chamber (attenuation > 47 dB for frequencies higher than 125 Hz; 22 dB SPL noise floor). A styrofoam box with a dry ice bath was used to cool down methanol and was kept on the recording chair ca. 50 cm away from the animals' head. Tubing from the dry ice bath to the cooling probe was insulated with PE foam foil to reduce ice buildup.

The cooling probe was positioned once per day at the beginning of a recording session with a manual stereotaxic micromanipulator (Narishige SM-11) under microscopic control (D.F. Vasconcellos). The probe was advanced until dimpling of the surrounding tissue was observed and then pulled back until dimpling ceased. Due to the small size of the craniotomy relative to the cooling probe it was not always possible to visually verify good contact of the foot plate and dura. In these cases, the cooling probe was advanced until the temperature reading of the thermocouple junction was stabilized above room temperature. Positioning the probe under visual guidance or thermal guidance resulted in similar temperatures recorded at the dura of around 36°C (Omega HH-25TC). During neurophysiological recordings the temperature was monitored

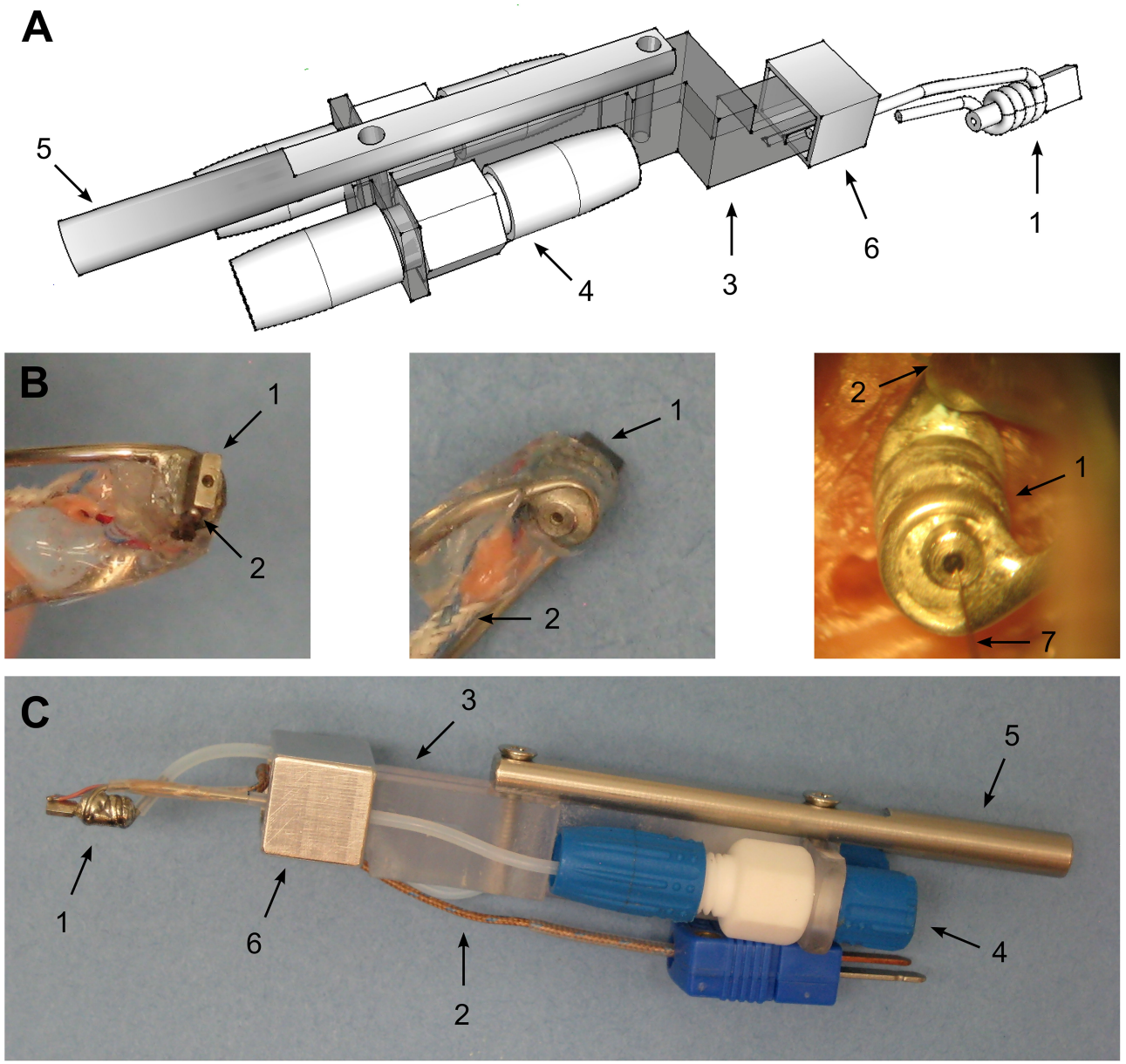

FIGURE 1 | Design of the cooling probe. **(A)** CAD drawing of the developed cooling probe and the holder for use with standard micromanipulators. 1—cooling probe itself consisting of a small stainless steel plate (footsize: 0.95 × 2.5 mm) around whose back a 21G stainless steel tubing was soldered to pump chilled methanol through. 3—plastic holder with an offset front piece to allow for close positioning of recording electrodes. 4—Omnifit® 2-way connector screwed onto the plastic holder to allow the connection of larger diameter cooling fluid supply tubing to smaller tubing leading to the probe itself. 5—Stainless steel adaptor to micromanipulator. Different micromanipulators can be used choosing the appropriate diameter. 6—aluminum clamp to screw the cooling probe onto the probe holder. **(B)** Photographs of the manufactured cooling probe. LEFT – bottom view. Shown is the stainless steel foot with a recording hole drilled to allow access for microelectrodes. This side is touching the dura during experiments. 2 – T-type thermocouple to measure the achieved temperature at the junction of the cooling probe and the dura. MIDDLE – 1 – top view. RIGHT – picture taken during an actual experiment. 7 – single tungsten electrode entering the brain *via* the hole drilled into the cooling probe to record neuronal activity underneath the cooling probe. **(C)** Photograph of the assembled cooling probe and holder. Numbering as in the panels before.

and logged to PC with a USB based thermocouple interface (Measurement Computing, USB-2001-TC). For cooling, the pump was set to a nominal flow rate of 10–12% of maximum flow rate. This flow rate led to a temperature of 1–3°C. Once the recorded temperature settled in this range, we recorded single neuron responses to auditory stimuli during a cooled phase. After cessation of cooling by stopping the pump, temperature quickly rose to body temperature and we defined a recovery phase to commence when temperature at the dura reached more than 30°C.

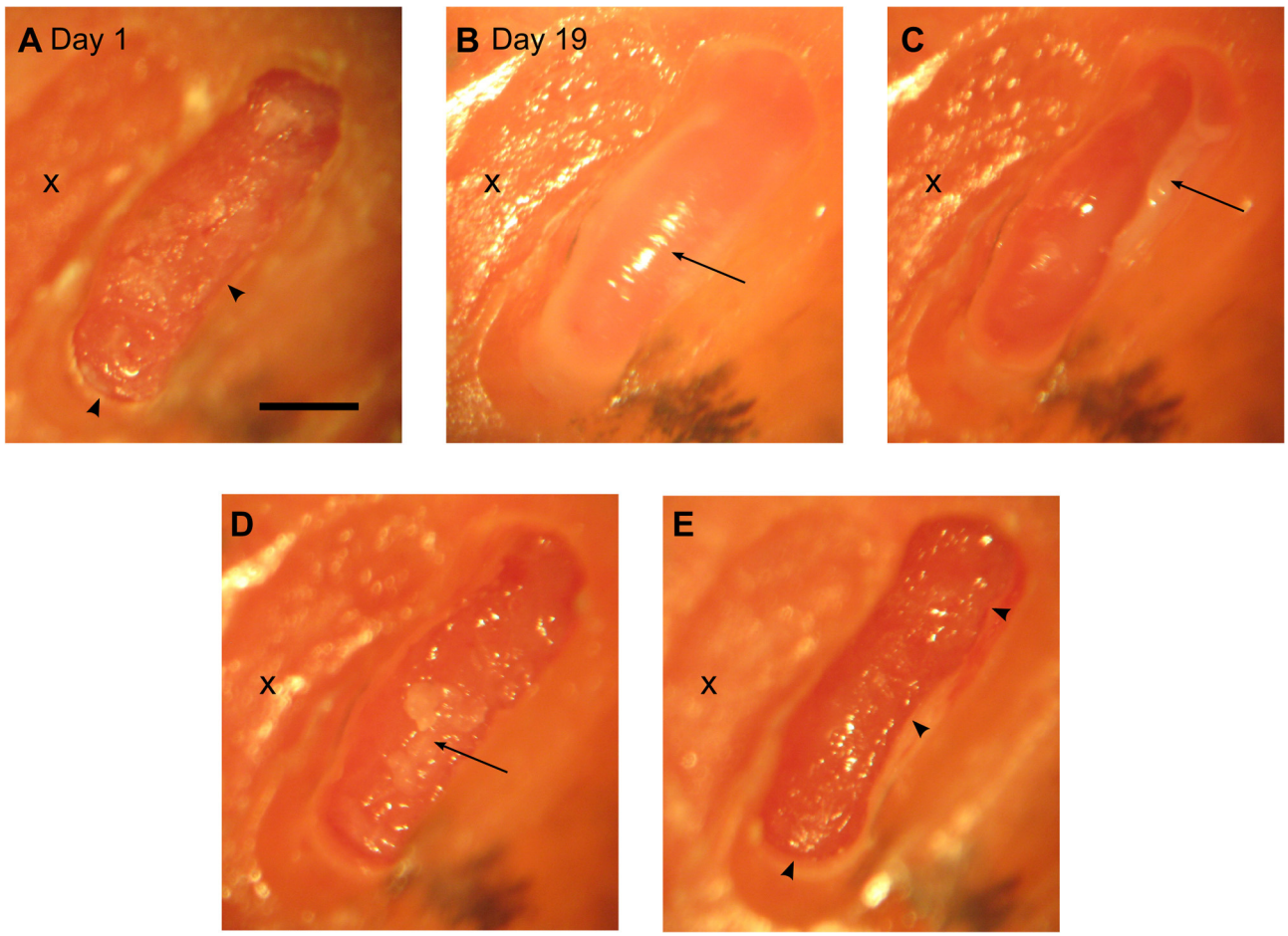

FIGURE 2 | Overview of a progression of a craniotomy to allow access for the cooling probe. **(A)** Day 1: x – old craniotomy. The arrows point to bone edges observed after drilling. Scale bar for all panels = 1 mm. Day 19: the following figures illustrate that it is possible to keep a relatively large craniotomy open for ca. 3 weeks while containing tissue growth. **(B)** – arrow pointing to a layer of tissue on top of the dura. **(C)** – arrow pointing to the tissue pulled aside. **(D)** – arrow pointing to a second layer of tissue about to be removed. **(E)** – final picture after cleaning the tissue again showing the bone edges found at day 1.

We tested the spread of the cooling manipulation across the cortical surface of awake animals. Toward this goal, we opened a 3 × 3 mm large craniotomy located approximately above area MT in the left hemisphere of one animal. A cooling probe was positioned at one edge of the craniotomy and a separate needle style micro-thermocouple was used to measure temperature at various distances to the cooling probe. Our data demonstrate that temperature changes can be observed even several millimeters away from the cooling probe (**Figure 3**). These findings are qualitatively in line with earlier reports (Coomber et al., 2011), describing a temperature drop to 20–24°C in a radius of 2.5 mm. As large craniotomies were required for further assessment, which would have precluded subsequent long-term evaluation of physiological changes, we did not study temperature gradients in more detail.

Recording Procedure

All experiments were performed in a double-walled soundproof booth (Industrial Acoustics, New York) lined with 3" acoustic foam (Sonex, Illbruck). Animals were tested in daily sessions lasting maximally 6 h but were typically 4.5 h long. We employed the same recording setup as described in Remington and Wang (2019). Briefly, a modified marmoset primate chair was mounted on a pole and acoustic stimulation was performed through one of 16 (covering the upper hemisphere) or 24 (covering a complete sphere) speakers (Fostex dome tweeters, FT28D) located at 1 m from the animal's head. The setup was calibrated to 95 dB SPL at 0 dB attenuation and had a relatively flat frequency response curve (± 3–7 dB) across the frequency range of the presented stimuli. During the experiments, animals were awake, seated in the primate chair and their heads fixed with implanted stainless steel head posts. Single tungsten electrodes (3–12 MΩ; A-M Systems) were employed to either record from the auditory thalamus or the core regions of the auditory cortex, both as described previously (Bendor and Wang, 2005; Bartlett and Wang, 2007). We focused on field AI which we identified by its caudal-to-rostral tonotopic gradient from high to low frequencies. Based on the coarse mapping of field AI the MGB

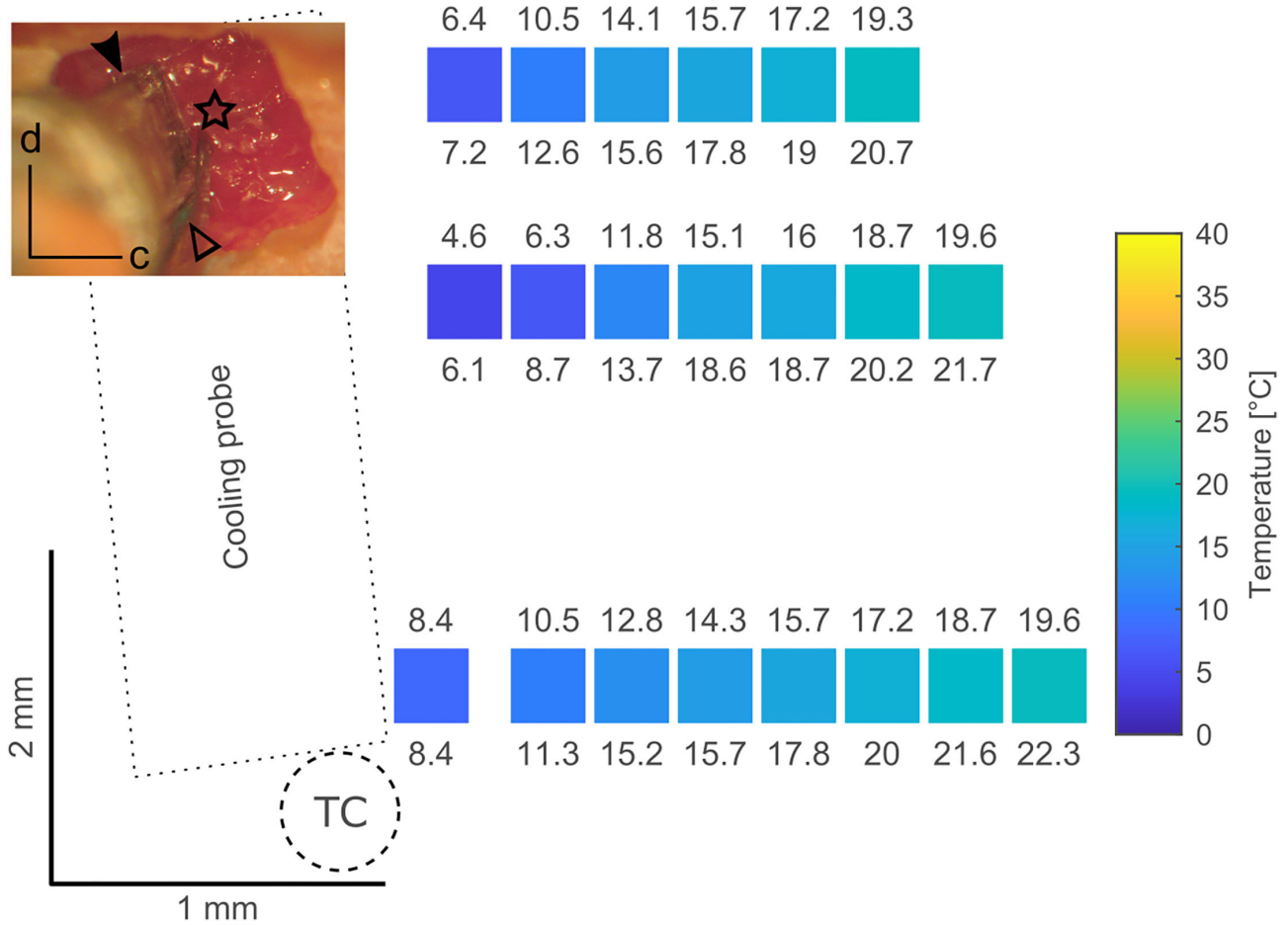

FIGURE 3 | Tests have been conducted using a 3 × 3 mm craniotomy located approximately above area MT in the left hemisphere (inset; d – dorsal, c - caudal). The top part of the craniotomy was overlying the lateral sulcus and thus it's blood vessel. The dimension of the cooling probe (filled arrowhead) in combination with the size of the craniotomy limits the area over which a surface map of temperatures at the dura during cooling can be obtained. In these tests a micromanipulator was used to position a separate microthermocouple (star, located at the thermocouple tip) at several spots over the dura. Coordinates obtained from the micromanipulator during positioning served as a coordinate system to plot the recorded temperatures. All temperatures have been measured after a steady state was achieved (> 10 min) as indicated by the thermocouple (open arrowhead) glued to the cooling probe. In the surface map created from the image in the inset, the position of the colored squares corresponds to the location of a microthermocouple measurement, the color of the squares to the mean temperature and the numbers above and below indicate the minimum and maximum temperature recorded, respectively. Cooling the probe to ca. 5–6°C (measured at the probe thermocouple, TC) results in a temperature of 20°C at a distance of ∼1.5 mm thus limiting the cooling effects to the vicinity of the cooling probe. These results are comparable to data presented by Lomber et al. (1999).

could be approached laterally to AI at an angle of generally 60° from the horizontal plane (Bartlett and Wang, 2007). Entering the brain this way allows to further identify the MGB after passing through a layer of visually responsive neurons (lateral geniculate nucleus). Although we did not attempt to reconstruct electrode tracts, this approach has been shown to lead to the majority of neurons being located in the ventral part of the MGB (Bartlett and Wang, 2011). A hydraulic microdrive (Trent-Wells) mounted on a second manual, stereotaxic micromanipulator (Narishige SM-11) allowed to remotely control the recording depth. In case we studied the effects of cooling cortex on cortical neurons directly underneath the recording probe, the recording electrode was first visually aligned with the axis of the cooling probe and positioned at the top of the cooling probe hole. Then, the electrode was advanced for the height of the cooling probe (measured with a vernier caliper) making sure that the electrode did not bend or make contact with the hole. This electrode position was then defined as 0 μm recording depth. In all other instances the recording depth 0 μm was defined as the position where the electrode made contact with the dura. Where relevant, lateral offsets from the cooling probe were measured from the center of the recording probe and read from the vernier scale of the micromanipulator resulting in an accuracy of 100 μm. For most recording sessions two craniotomies within one hemisphere were used: one for the cortical cooling probe and one for recordings from the ipsilateral auditory thalamus. For an overview of typically recorded data from a hemisphere the reader is referred to the **Figure 4**.

Under the conditions described here thalamic neurons which are not quickly lost within a few minutes can be held for roughly 45 min. Therefore, we restricted our stimulus sets to be finished within 15–20 min to allow for recording during baseline, cooling, cooled and at least rewarming conditions. Consequently, no attempt was made to characterize the tuning properties of recorded neurons in greater detail and data were only further analyzed if a neuron's response was recorded during baseline, cooled and rewarming phase. Due to the limited time of holding a respective neuron, after cessation of cooling we also did not attempt to recover the tuning properties of the recorded neurons but rather to verify that a unit was not lost during recording in case firing ceased completely during the cooled phase. A neuron was therefore included if we either recovered its response properties and/or could hold a neuron throughout the recording as identified by its waveform. In our hands all waveform related changes were observed to be either gradual allowing to confidently conclude that a single neuron was recorded throughout the procedure or abrupt in which case we did not consider the unit for further analysis. To assess the effects of cortical cooling on thalamic response properties we focused on two types of stimuli: in a subset of neurons we focused on processing of temporal modulations and hereto typically tested neurons with pure tones at various intensities to characterize both frequency (in steps of $1/8^{th}$ to $1/10^{th}$ of an octave) and intensity tuning (in steps of 10 dB). At the neurons best frequency (BF, defined as the pure tone frequency eliciting the highest spike rate during stimulus presentation) and 2 levels (one close to threshold and one ca. 30 dB above threshold) or best level [occasionally for non-monotonic neurons; (see Sadagopan and Wang, 2008)] amplitude modulated pure tones were presented spanning several octaves from 2 to 1,024 Hz modulation frequency (modulation depth = 1). Pure tones had a duration of 250 ms while amplitude modulated sounds were presented for at least 500 ms. In another subset of neurons, we studied processing of spatial location. Toward this aim, neurons were typically presented with 250 ms long broadband, frozen noise bursts with a flat frequency spectrum from 2 to 32 kHz at least 10 dB above threshold. The spatial location was systematically varied by changing speaker locations. At the neurons best speaker location (defined as the speaker that led to the highest average firing rate during stimulus presentation), we systematically varied the sound level of the noise burst in steps of 10 dB. All sounds had onset and offset cosine squared ramps lasting 5 ms. The repetition rate of stimuli was slower or equal to 1 Hz.

Data Analysis

Significantly driven recorded neurons were defined as having at least one stimulus which significantly elevated the firing rate (*t*-test by comparing the spontaneous firing rate with the firing rate during stimulus presentation plus 50 ms; i.e., stimulus related firing). Amplitude modulated sounds were employed to investigate modulation transfer functions (MTF) based on the vector strength revealing stimulus synchronized responses (Goldberg and Brown, 1969; Bartlett and Wang, 2007) or the stimulus related firing rate. To assess statistical significance of synchronized firing the Rayleigh statistic was used (> 13.8 corresponding to a $p < 0.001$). The vector strength based MTF was used to identify the best modulation frequency (BMF vector strength) defined as the modulation frequency leading to the highest significant vector strength and a significant response based on the firing rate. The highest frequency leading to a significant vector strength and significant response was taken as the synchronization boundary (Fcutoff vector strength). Similarly, firing rate based MTFs were analyzed to reveal the best modulation frequency (BMF rate) defined as the modulation frequency leading to the highest significant firing rate. The highest modulation frequency leading to a significant response was taken as the rate boundary (Fcutoff rate). A detailed description of the data analysis of spatial location processing in the auditory thalamus of awake common marmosets is prepared in a separate publication and followed procedures presented in an earlier publication (Remington and Wang, 2019). Briefly, based on the stimulus related firing rate, a spatial receptive field with higher resolution was created by projecting the responses at the various speaker locations onto an array of virtual locations placed on a $5 \times 5^{\circ}$ grid using a weighted sum of responses at all speaker locations. For graphical representation these responses to virtual locations expressed in a contralateral-to-ipsilateral axis were plotted as a heatmap using a Fournier projection. To express the width of spatial tuning the area of responses at virtual locations with firing rates of at least 50% of the midpoint between the maximum and minimum firing rate was taken and called tuning area (TA). The main tuning vector (centroid) of a given virtual spatial receptive field (essentially the center of mass of the spatial receptive field defined by the firing rate) was calculated with its respective elevation and azimuth. Wilcoxon's signed rank test was used to compare firing between baseline and cooled conditions. A modulation index (MI) was defined as $MI = \frac{rate_{baseline} - rate\_cooled}{rate_{baseline} + rate\_cooled}$ to assess the percentage of neurons with changed firing rates ($|MI| > 0.2$) between cooling ($rate_{cooled}$) and baseline conditions ($rate_{baseline}$). Pearson correlations were employed to test for a correspondence of changes in one parameter with respect to changes in another. Data were plotted as mean ± STD unless mentioned otherwise. An alpha value of <0.05 was considered to be statistically significant.

RESULTS

In the current study we developed a repositionable cooling probe with small footprint for local cooling and the opportunity for unit recording in close and more distant vicinity of the cooling site (**Figure 1**). The probe was placed at different locations overlying field AI of the core auditory cortex exposed by craniotomy (**Figure 2**) to study the effect of manipulating cortical feedback on thalamic processing in the auditory pathway. Experiments were conducted to assess the extent of cooling spread (**Figure 3**) in awake common marmosets seated in a primate chair. Initial experiments revealed that animals might be able to feel and react to a too rapid decrease in cortical temperature showing discomfort by actively starting to move. Accordingly, flowrate

was adjusted such that animals did not show overt reactions to the cooling itself. This precaution allowed for a time constant of ca. 2 min and a stable, steady state temperature of 1–3°C which was reached after 5 min (see **Figure 5**, a speed for which no overt reaction was observable). Over time we studied the effects of cooling of different parts of field AI by successively opening new craniotomies while closing old craniotomies with bone wax and dental acrylic (**Figure 2**). Recordings from single neurons in the auditory cortex were used to study the tonotopic organization of the cooled area in order to identify field AI as well as to study direct cooling effects on the physiology of individual cortical cells (**Figure 4**). In separate recording sessions, the effects of cortical cooling on the physiology of individual thalamic neurons was studied (**Figure 4**).

Effects of Cortical Cooling on Single-Unit Responses in the Auditory Cortex

Effects of cortical cooling in awake animals with our custom build probe was tested by investigating spiking properties recorded directly underneath the cooling probe (**Figure 5**) advancing a single tungsten electrode through the recording hole (see **Figure 1B**). Based on the available literature (Payne and Lomber, 1999; Malhotra et al., 2004; Nakamoto et al., 2008; Coomber et al., 2011; Wood et al., 2017), we expected single units in the auditory cortex to display a reduction in both, spontaneous and stimulus driven spiking activity upon cooling. For the neuron shown in **Figure 5A**, recorded at a depth of 1.36 mm underneath the cooling probe, this was indeed observed. The raw data filtered between 0.3 and 6 kHz (**Figure 5A** top panel) demonstrates the spontaneous activity of a well-isolated single unit waveform which got smaller in amplitude and sparser, indicating a reduction in firing rate. We quantified our observations by calculating the time between successive spikes (inter spike interval, ISI) and observed increases in ISI which depended on the cortical temperature (**Figure 5A** bottom left). The recorded spike waveform also became wider which we analyzed by calculating the full width at half height of the spike waveforms. This half maximum duration followed the change in temperature closely—almost looking like an inversion of the temperature profile (**Figure 5A** bottom right). Unlike the expectation stated above not all units in the auditory cortex exhibited decreased firing rates. In contrast, some neurons actually increased their spontaneous firing rate. The unit depicted in **Figure 5B** was recorded even closer to the cooling probe than the unit in **Figure 5A** and therefore will have encountered a lower temperature. Still, the ISI decreased substantially from 12.5 s at the beginning of cooling to 2.2 s when 5°C was reached after 5 min. During the same time the spike waveform gradually widened from a half maximum duration of 0.28 s to 0.43 s at 1.8°C. These exemplary data suggest that a consistent effect of local temperature reduction on single neuron physiology could be a widening of spike waveforms. To investigate this further, we pooled data from cortical recordings with cortical cooling and expressed the spike width at half height (WHH) as a function of distance from the cooling probe (**Figure 6A**). Together, the data demonstrate that the spike waveform of all investigated single units widened to various degrees during cooling (**Figure 6B**). Directly underneath the cooling probe only widening of spike waveforms was observed. Further, we observed negative correlations for all changes in measures of spike waveforms and the recording depth (Pearson correlation; WHH: Rho $= -0.37$, $p = 0.037$; time from peak-to-peak: Rho $= -0.3$, $p = 0.036$; center frequency: Rho $= 0.448$, $p = 0.01$). Next to the probe, waveforms generally did not widen as much. When plotted against the total distance to the cooling probe waveforms widened in a consistent manner with smaller distances leading to larger widening (Pearson correlation; WHH: Rho $= -0.33$, $p = 0.06$; time from peak to peak: Rho $= -0.366$; $p = 0.039$). These results are compatible with a temperature gradient achieved during cooling spreading from the cooling probe itself. Changes in spike waveforms were also reversible. All investigated spike measures including signal-to-noise ratio (SNR), the WHH, the time from peak to peak as well as the center frequency were indistinguishable during baseline and recovery conditions (**Figure 6C**), while cooling increased the WHH, the time from peak-to-peak and decreased the center frequency (repeated measures ANOVAs with factor cooling stage; WHH: $F_{(2,74)} = 33.8$, $p = 3.67\text{e-}11$; time from peak-to-peak: $F_{(2,74)} = 32.3$, $p = 8.11\text{e-}11$; center frequency: $F_{(2,74)} = 61.9$, $p = 2.85\text{e-}12$). The SNR changed very little during cooling suggesting, on average, a stable recording quality throughout the experiment (repeated measures ANOVA with factor cooling stage $F_{(2,74)} = 6.49$, $p = 0.00693$; no significant *post-hoc* test).

Effects of Cortical Cooling on Spontaneous and Stimulus Driven Activity in the Auditory Cortex

Next, we investigated how processing of sounds is changed locally due to cooling cortex. **Figure 7** illustrates two representative single units recorded concomitantly in a depth of 750 μm. Under baseline conditions, the unit in panel A displayed a non-monotonic response function to pure tones around 4.6 kHz at sound pressure levels from 10 to 20 dB SPL and also exhibited a phasic response to sinusoidal amplitude modulated tones (sAM) with modulation frequencies between 2 and 128 Hz, while the unit in panel B was not driven by these stimuli. In a cooled state the driven firing rate of the unit in panel A decreased and the response pattern was prolonged. In contrast, the unit in panel B now displayed an offset response to pure tones around 4 kHz and had a threshold for 4.6 kHz (the best frequency identified for the unit in A) around 10–20 dB SPL. Further, the unit now responded to amplitude modulated tones. These observations suggest that the effect of cortical cooling on local processing of sounds could be diverse. When analyzing the spike waveforms for both units (**Figures 7B,D**) a substantial widening was observed in each case. A potential alternative explanation to spike waveform changes than a local reduction in temperature would be relative movements of the recording electrode and the recorded neuron (Gold et al., 2006) which could be due to shrinkage or expansion of the cooled tissue. During the recovery phase after cooling was ceased we therefore deliberately moved

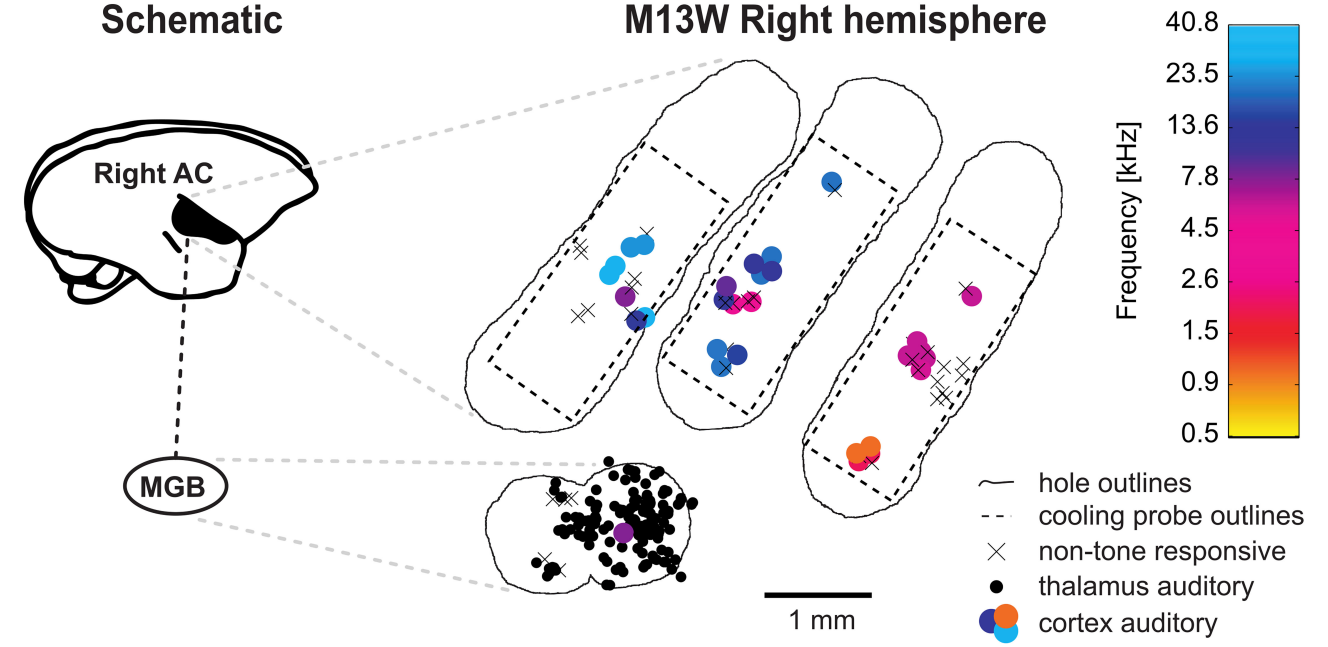

FIGURE 4 | Schematic representation of a typical experiment. Recording from the right hemisphere of animal M13 commonly involved multiple craniotomies (outlined by irregular lines) which were successively created. Usually, one craniotomy for access to the auditory cortex (AC) as well as cooling and a craniotomy for thalamic recordings were open simultaneously. The position of the cooling probe was kept fixed for each craniotomy but the probe was repositioned daily. Through single unit recordings in the auditory cortex field A1 in the core of the auditory cortex was identified by its caudal-to-rostral high-to-low tonotopic gradient. Tone responsive neurons were plotted as filled circles with color depicting their best frequency drawn from a heatmap. Access to the medial geniculate body (MGB) of the thalamus was achieved by offsetting recording holes ventrally at the high frequency region (around 32 kHz) of A1 and inserting recording electrodes at an angle of 60° from vertical. The recording holes for the MGB access are thus located at the lateral belt of the secondary auditory cortex and are, consequently less likely to be tone responsive in cortex.

the recording electrode. As expected, the amplitude of the spike waveform changed with varying electrode depth. While electrode movements resulted in instances where the spike waveform amplitudes were comparable between the baseline and the cooled state (unit in **Figure 7B** had a peak amplitude of 80–120 μV and in a depth of 675–750 μm during cooled state and baseline; **Figure 7D**: peak amplitude of 350–500 μV in the cooled state and in a depth of 660–675 μm during recovery), the WHH calculated was about 3 times longer in the cooled state (**Figure 7B**: 0.2 ms during baseline and ca. 0.6 ms in a cooled state; **Figure 7D**: 0.2 ms during baseline and ca. 0.6 ms in a cooled state) and never overlapped between both states. This suggests that changes in spike waveform are a direct consequence of cooling and are in line with earlier reports in anesthetized cats (Girardin and Martin, 2009).

Next, we separately analyzed spontaneous and stimulus driven firing rates across the sample of units studied. As suggested from the individual examples illustrated above, decreased, but also increased, spontaneous and driven firing rates were found due to cortical cooling. Overall, we observed a significant reduction of driven firing rates (Wilcoxon signed rank test, $Z = -3{,}103$, $p = 0.0019$, 44% of neurons decreased [with a modulation index (MI) > 0.2] while 18% increased their firing rate [MI < -0.2]; **Figure 8A** right) and a trend for reduced spontaneous firing rates (Wilcoxon signed rank test, $Z = -1{,}769$, $p = 0.0768$; 47% of neurons decreased [MI > 0.2] while 32% increased their firing rate [MI < -0.2]; **Figure 8A** left). Many units stopped responding to sound stimulation in the cooled state. For units with an increase in driven firing rates the increase was comparatively small. The lack of a clear reduction of spontaneous firing rates might be due to the overall low spontaneous firing rate of auditory cortical neurons. For units that were recorded directly underneath the cooling probe, we observed decreased spike rates that expanded to a depth of at least until 2.5 mm. When plotting the observed changes in driven firing rate against the distance of the recorded unit to the cooling probe (**Figure 8B**), no dependence of the change in firing rate between the baseline and cooled state and the distance was observed (Pearson correlation; recording depth: Rho $= 0.052$, $p = 0.77$; total distance: Rho $= 0.114$, $p = 0.52$). This finding held when the analysis was focused only on units directly underneath the cooling probe. Here, neither the change in spontaneous activity nor the change in driven firing rate displayed a correlation with recording depth (Pearson correlation: spontaneous activity: Rho $= 0.080615$; $p = 0.70167$; driven activity: Rho $= 0.29927$; $p = 0.14614$). Together, these data suggest that cortical cooling affects sound processing locally and exerts an influence which extends for several millimeters

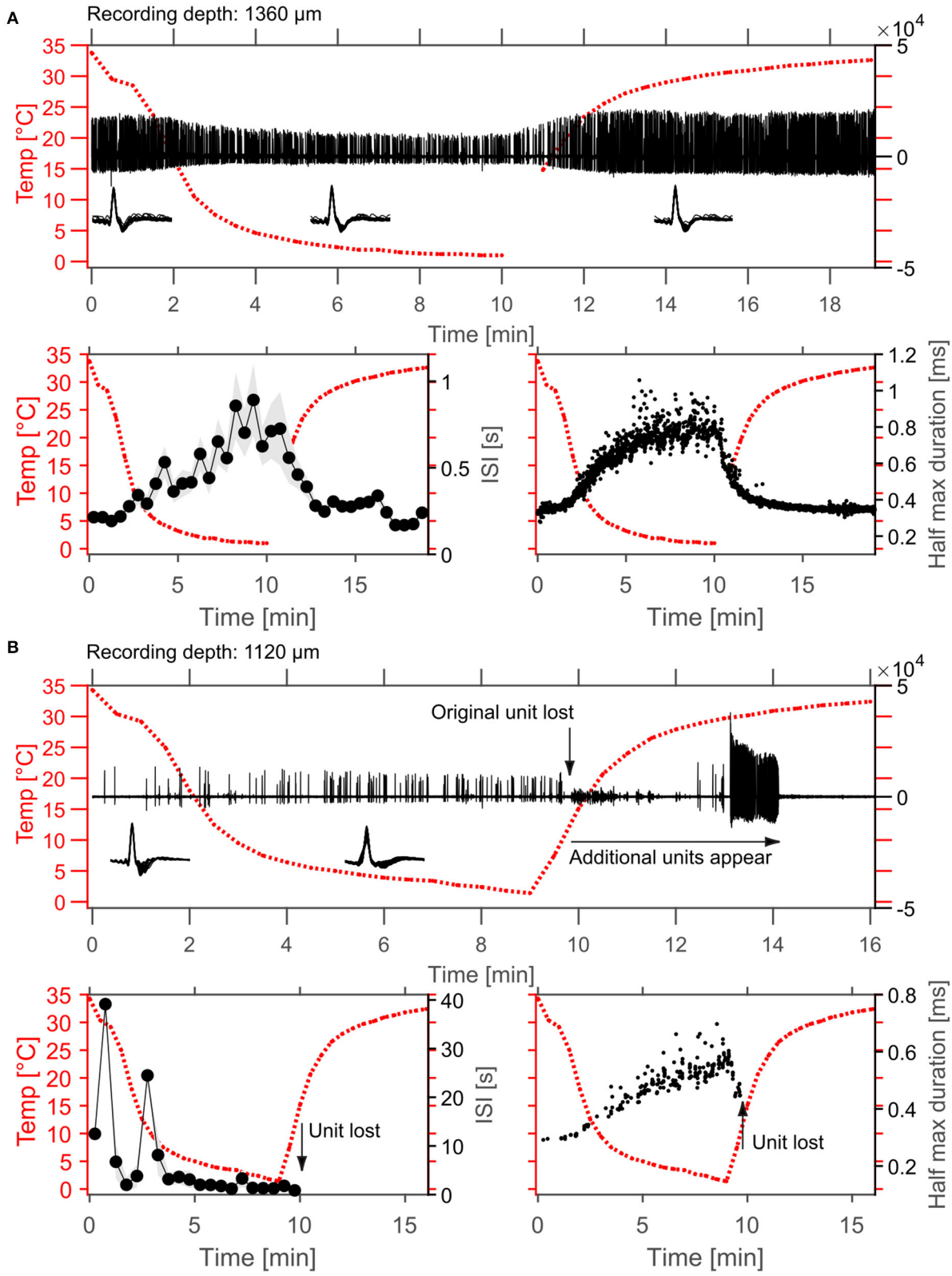

FIGURE 5 | Example effects of cortical cooling on single unit spiking behavior in cortex. **(A)** Spontaneous spiking activity recorded at a depth of 1,360 µm without sound stimulation. In the top panel the high-pass filtered signal is plotted as well as the cortical temperature measured at the dura adjacent to the cooling probe. The

(Continued)

FIGURE 5 | isolated single unit waveforms are plotted as insets and sorted according to the different temperatures achieved (before 10°C were reached during cooling, in cooled conditions and after 10°C were reached after cooling). During cooling the firing rate of the unit decreased which was demonstrated by calculation of the average interspike interval (ISI) within 30 s time windows (bottom left panel, plotted as mean ± STD). Interestingly, the recorded unit also changed its' waveform such that amplitude changes were observed during cooling and that the spike width was increased, resulting in an increase of the duration at the half maximum spike amplitude by roughly 2-fold (0.35–0.8 ms). Both, spontaneous firing rate as well as spike widening recovered to baseline levels after cessation of cooling. **(B)** While increases in spike rate during cooling were also observed even at smaller distances to the cooling probe, the waveform changes resulting in widened spike shapes during cooling were consistent (bottom right). Note that the unit depicted in **(B)** was lost during rewarming after ca. 9.5 min. Here, cooling was ceased after 9 min.

including the corticothalamic output layers 5 and 6 in marmoset field AI (**Figure 6A**).

Effects of Cortical Cooling on Spontaneous and Stimulus Driven Activity in the MGB

To address whether and how the manipulation of corticofugal feedback *via* cortical cooling affects the physiology of individual neurons in the auditory thalamus, we recorded single units in the MGB under baseline and cooled conditions. First, we explored how spontaneous and stimulus driven firing rates as well as basic frequency tuning were affected by cortical cooling (**Figure 9A**). For all 3 parameters, bidirectional changes were observed: both spontaneous as well as stimulus driven firing rates could decrease or increase during cooling, while a single unit's best frequency could increase or decrease. Twenty-five out of 52 units tested displayed the same best frequency during baseline and cooling, while for the remaining units the median change was −0.2 octaves (median absolute change = 0.5 octaves). Overall there was a significant relationship between the best frequencies recorded during baseline and cooling (Pearson correlation; Rho = 0.74, p = 1.9e-5). During cortical cooling, spontaneous firing rates were significantly increased (Wilcoxon signed rank test, n = 144, Z = 4.88, p = 1.06e-5; 13% of neurons decreased [with a modulation index (MI) > 0.2] while 36% increased their firing rate [MI < −0.2]). In contrast no significant change in stimulus driven firing rates was observed (Wilcoxon signed rank test, n = 144, Z = −0.47, p = 0.87; 28% of neurons decreased [with a modulation index (MI) > 0.2] while 22% increased their firing rate [MI < −0.2]). To address the possibility of direct cooling effects in thalamus, we plotted the changes of spontaneous and stimulus driven firing rates as a function of recording depth. Here, no relationship between depth and single unit firing rates was observed (Pearson correlation; spontaneous activity, Rho = −0.140, p = 0.088, stimulus driven, Rho = −0.057, p = 0.50, **Figure 9B**). Changes in shape of spike waveforms were small for thalamic neurons (**Figure 9C**) and were bidirectional, demonstrating both widening as well as narrowing of spike waveforms, and generally less than ± 0.1 ms (median change = 0.008 ms). Further, no relationship between waveform changes and recording depth was observed (Pearson correlation; Rho = −0.08, p = 0.37). To test whether these changes were due to cortical cooling or due to additional factors, we calculated a correlation between changes in spike waveforms contrasting cooled and baseline condition as well as changes during recovery and baseline. Any temperature related changes should be temporary and recover when cooling ceases especially if the temperature change is small given the distance to the cooling probe as in the case of MGB neurons. In contrast, changes in spike waveforms did not recover and consequently were highly correlated between the contrasted conditions (Pearson correlation, n = 89, Rho = 0.50, p = 6.2e-7). This observation is consistent with small electrode drift during the recording. Therefore, together, the data indicate that cortical cooling does not exert a direct influence on the physiology of neurons in the MGB.

Effects of Cortical Cooling on MGB Responses to Amplitude Modulated Sounds

During processing of amplitude modulations, responses in the inferior colliculus are generally synchronized to the sound and thus provide temporally modulated input to the thalamus. Thus, the timing of cortical feedback on thalamic single neurons might influence their processing of temporal modulations. Consequently, we studied how the processing of amplitude modulated sounds might be altered during cortical cooling. After establishing a neuron's best frequency (BF, **Figure 10A**) and rate-level response function at BF (**Figure 10B**), amplitude modulated pure tones centered at the BF were presented at 2 different sound levels: close to threshold (0–10 dB above) and 30–40 dB above threshold (**Figure 10C**). Both, before and during cooling the example neuron depicted in **Figure 10** had a BF of 4.7 kHz. However, upon cooling the BF threshold increased to 35 dB SPL from 25 dB SPL during baseline. Further, the response pattern to pure tones remained stable with a phasic increase in firing followed by a tonic suppression. In contrast, responses to AMs at the BF changed substantially. During baseline conditions, the neuron showed clear phase locking to the amplitude modulation up to 32 Hz. For AMs close to threshold the response regime also included non-synchronized responses to faster modulations while 30 dB above threshold only onset responses were observed. During cortical cooling, responses to 25 dB SPL AMs ceased as expected on the basis of the observed rate-level response functions. However, at 55 dB SPL responses to AMs were less synchronized and included a non-synchronized region from 128 Hz modulation frequency which was not observed during baseline. These exemplary data suggest that corticofugal feedback can have a profound effect on the processing of temporal modulations despite stable frequency tuning and response regimes. For quantitative analysis we calculated best modulation frequencies (BMF) and cutoff frequencies (Fcutoff) based on the vector strength (Goldberg and Brown, 1969; Bartlett and Wang, 2007) as a measure of the temporal reliability of responses and based on the firing

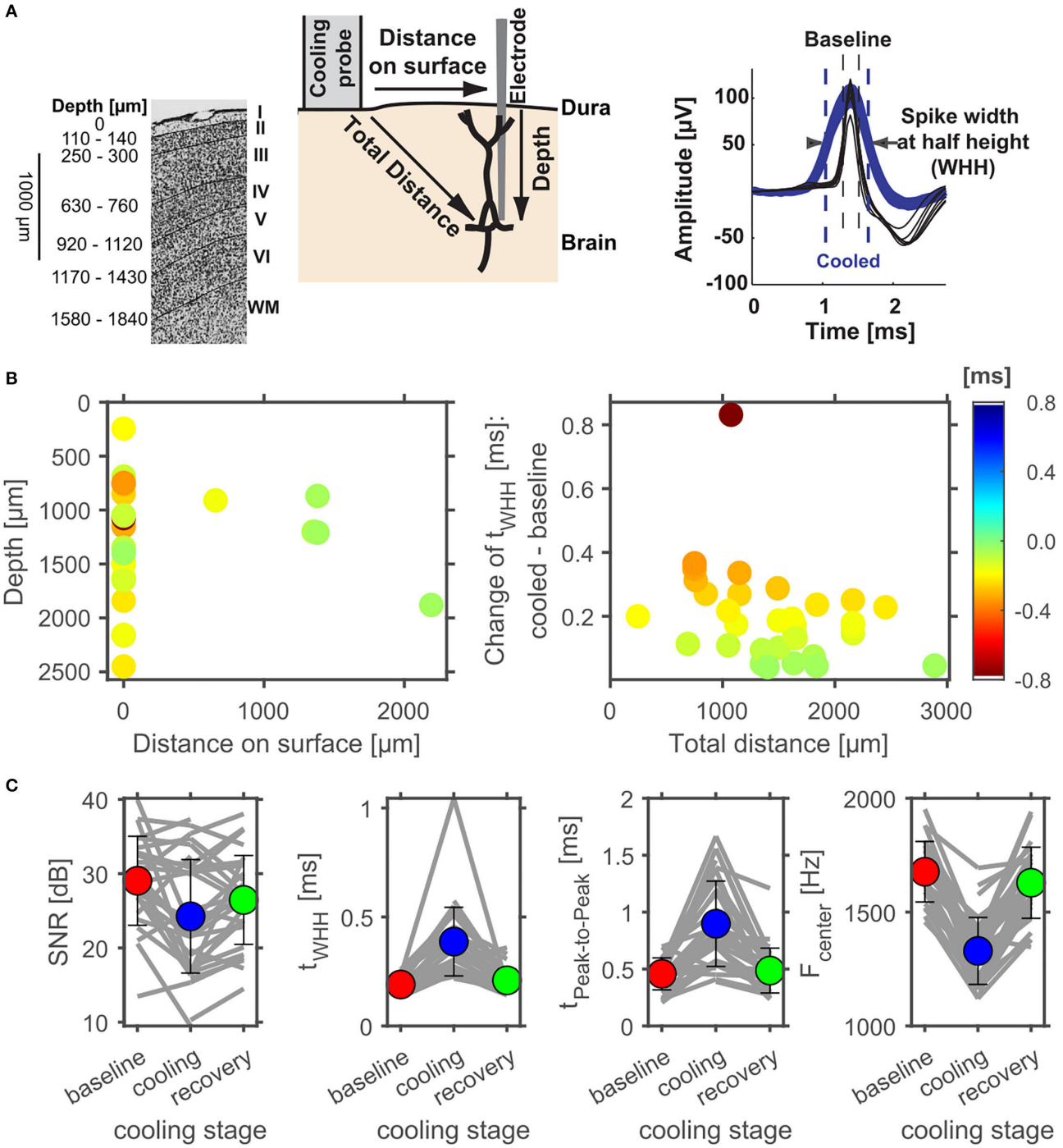

FIGURE 6 | Effect of cortical cooling on spike waveforms at various distances to the cooling probe. **(A)** Schematic representation of the cooling experiment with respect to cortical layers (modified from: Aitkin et al., 1986). Individual layers are identified on the right (WM, white matter) and the estimated average depth of layer transitions are plotted on the left. On the Nissl stain, layer boundaries are indicated by solid black lines. During experiments an electrode was inserted into the brain either through the small hole within the cooling probe itself (see **Figure 1B**) or at some distance to the cooling probe. Effects of cooling on spike waveforms could therefore be tested at various total distances to the cooling probe. To analyze potential effects of lowering cortical temperature the spike width at half height (WHH) was calculated and compared between different phases of a cooling experiment (right). **(B)** illustrates the change of WHH (color coded) of cortical neurons between the baseline and the cooled condition. Directly underneath the cooling probe only widening of spike waveforms were observed. Next to the probe, waveforms generally did not widen as much. When plotted against the total distance to the cooling probe waveforms widened in a consistent manner with smaller distances leading to larger widening. **(C)** Evaluation of the reversible nature of cooling effects on spike waveforms in cortex. The signal to noise ratio (SNR) did not change consistently due to cooling, while the spike width at half height (WHH) as well as the time between peaks increased during cooling and recovered to a large extent. Conversely, the center frequency of the power spectrum of the spike waveforms decreased during cooling and recovered upon cessation of cooling.

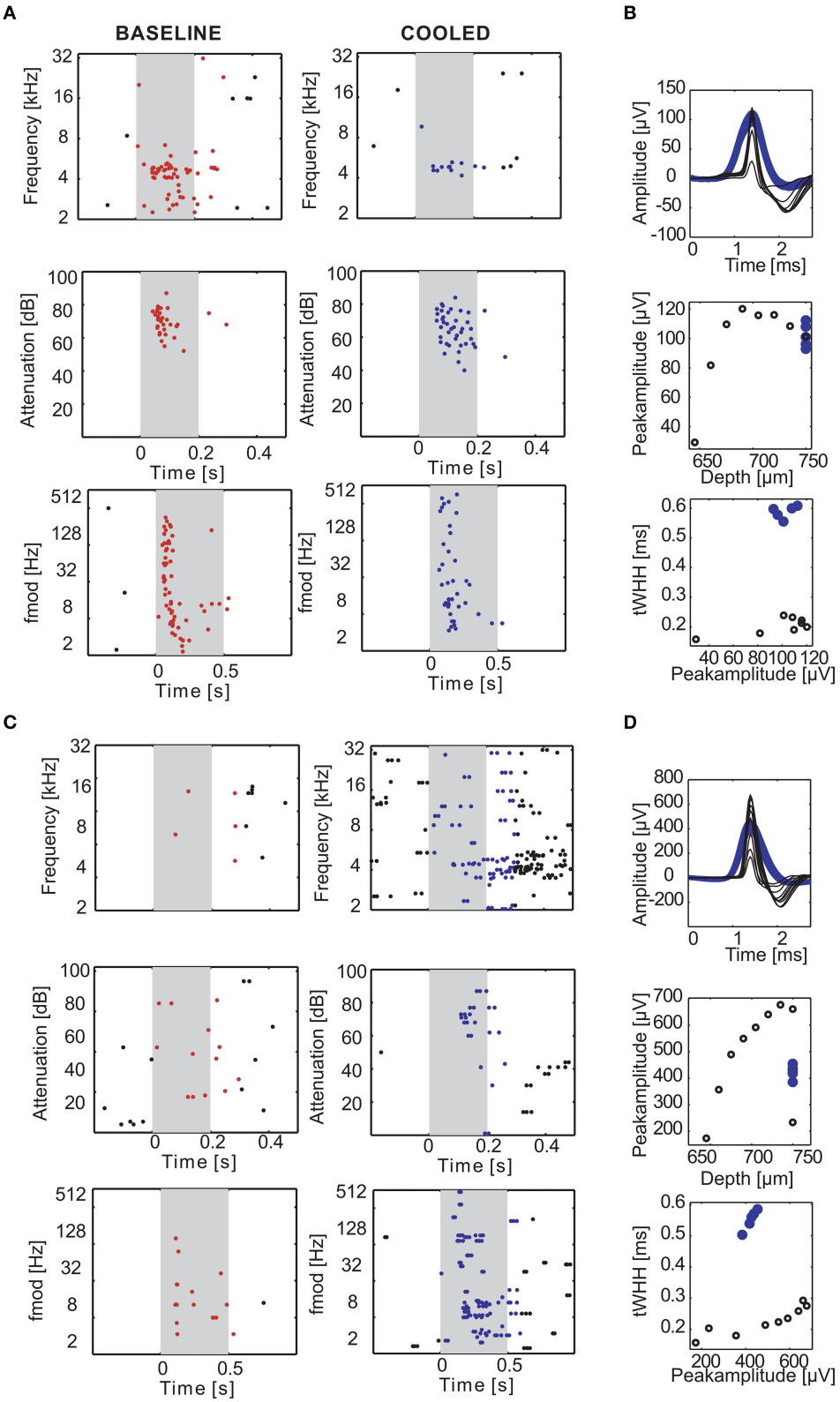

FIGURE 7 | Examples of cortical cooling effects on single units in the auditory cortex. During cortical cooling response properties of cortical neurons can change in diverse ways. The rasterplots in **(A,B)** illustrate an experiment in which 2 neurons were recorded simultaneously at the same electrode 750 µm directly

(Continued)

FIGURE 7 | underneath the cooling probe. The gray shaded area corresponds to the stimulus duration. Stimulus related firing was evaluated based on a time window which included the stimulus duration plus 50 ms. Spikes that contributed to this stimulus related firing were plotted in red during baseline and blue during cooling. While the single unit in **(A)** was driven by pure tones around 4.6 kHz (top) at 10–20 dB SPL (middle) and various amplitude modulation frequencies (bottom) the second single unit was not **(B)**. Cortical cooling led to reduced firing rates in **(A)** without changing the overall tuning properties of the neuron. In contrast, cooling increased firing rates in **(B)** and revealed frequency tuning to around 4 kHz. Note that, since the neuron in **(B)** was not driven during the baseline condition the stimulus sets were only tailored toward neuron A. Even though the effects of cortical cooling on tuning properties of the two neurons were different, the waveforms of both neurons widened **(C,D)**. Average waveforms for different stimulus sets during baseline condition were plotted in black and blue for cooled condition. The waveform changes cannot be explained by undeliberate movements of the electrode as purposeful movements resulted in different peak amplitudes without significant changes in spike width **(C,D)**.

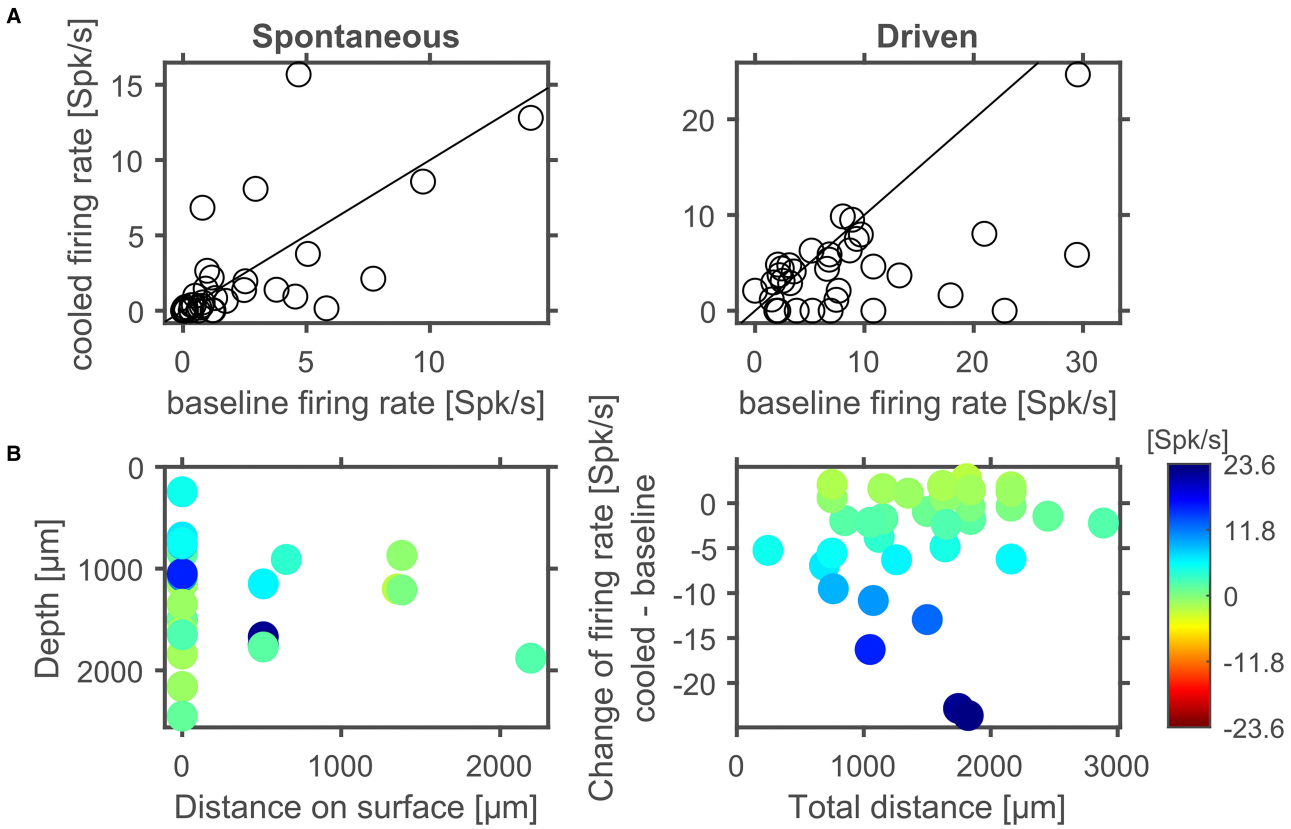

FIGURE 8 | In cortex spontaneous and driven firing rates were effected by cortical cooling. **(A)** Cortical cooling leads mostly to decreased, but also increased, spontaneous and driven firing rates in cortex. Across the ensemble of neurons tested the stimulus driven activity was significantly reduced while the change of spontaneous activity showed a trend for reduced firing rates. Changes in stimulus driven activity did not show a clear correlation with distance indicating that the effects of cortical cooling spread over several millimeters **(B)**.

rate (**Figure 11A**). Cortical cooling did not just lead to shifts in $BMF_{vector\ strength}$ toward lower modulation frequencies but also toward higher modulation frequencies. When BMF was calculated based on firing rate (BMF_{rate}) a similar pattern emerged in that bidirectional shifts toward higher and lower modulation frequencies were found. For both parameters, $BMF_{vector\ strength}$ and BMF_{rate}, overall no differences between baseline and cooled conditions were observed (Wilcoxon signed rank test, $BMF_{vector\ strength}$: $n = 59$, $Z = 0.0378$, $p = 0.969$, 31% of neurons with decreased and 32% with increased $BMF_{vector\ strength}$; BMF_{rate}: $n = 82$, $Z = -0.372$, $p = 0.71$, 30% of neurons with decreased and 26% with increased BMF_{rate}) but significant correlations between values observed during baseline and cooled conditions (Pearson correlation; $BMF_{vector\ strength}$: $n = 59$, Rho = 0.40, $p = 0.001$; BMF_{rate}: $n = 82$, Rho = 0.41, $p = 0.0001$). The highest frequencies at which synchronized or significant firing rates were observed ($Fcutoff_{vector\ strength}$ and $Fcutoff_{rate}$, respectively), were also compared between baseline and cooling. As for BMF, bidirectional changes toward lower but also higher modulation frequencies were observed while on average baseline and cooled conditions did not differ (Wilcoxon signed rank test, $Fcutoff_{vector\ strength}$: $n = 59$, $Z = 0.255$, $p = 0.80$, 27% of neurons with decreased and 25% with increased $Fcutoff_{vector\ strength}$; $Fcutoff_{rate}$: $n = 82$, $Z = -0.712$, $p = 0.48$, 26% of neurons with decreased and 21% with increased $Fcutoff_{vector\ strength}$). Here, also significant correlations between

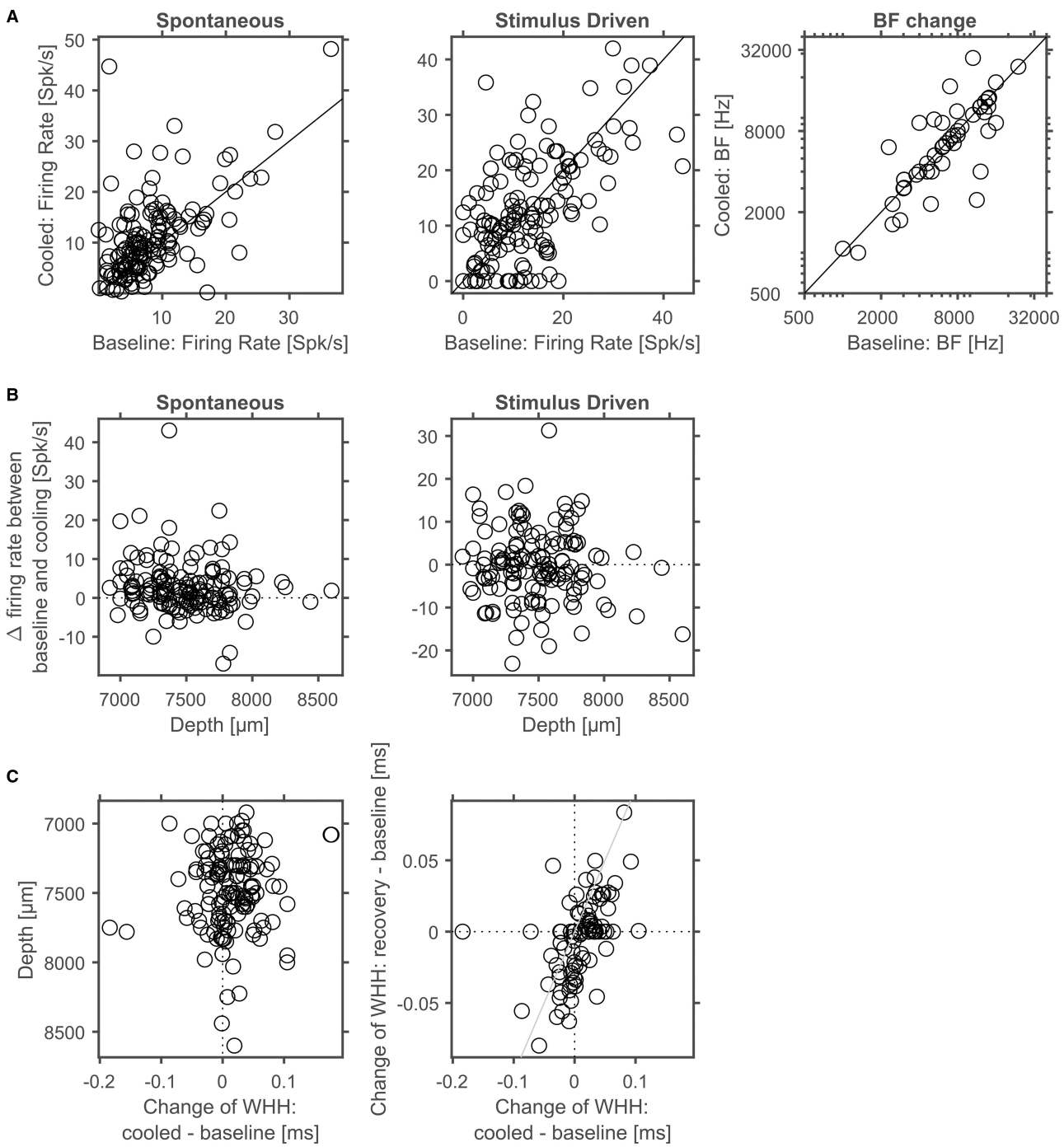

FIGURE 9 | Corticofugal feedback alters spontaneous and stimulus driven activity in thalamus. **(A)** Cortical cooling led to significant modulation of thalamic neurons as indicated by increased spontaneous activity. In contrast, stimulus evoked activity shifted in both directions. The BF of the majority of neurons did not change in response to cooling. **(B)** In thalamus no depth dependent changes of spontaneous or stimulus driven firing rates were observed. **(C)** Changes of spike waveforms in relation to changes observed at different cortical depths were small (< 0.1 ms). In addition, changes in WHH did not recover indicating that at larger distances from the probe observed waveform changes were not related to cooling.

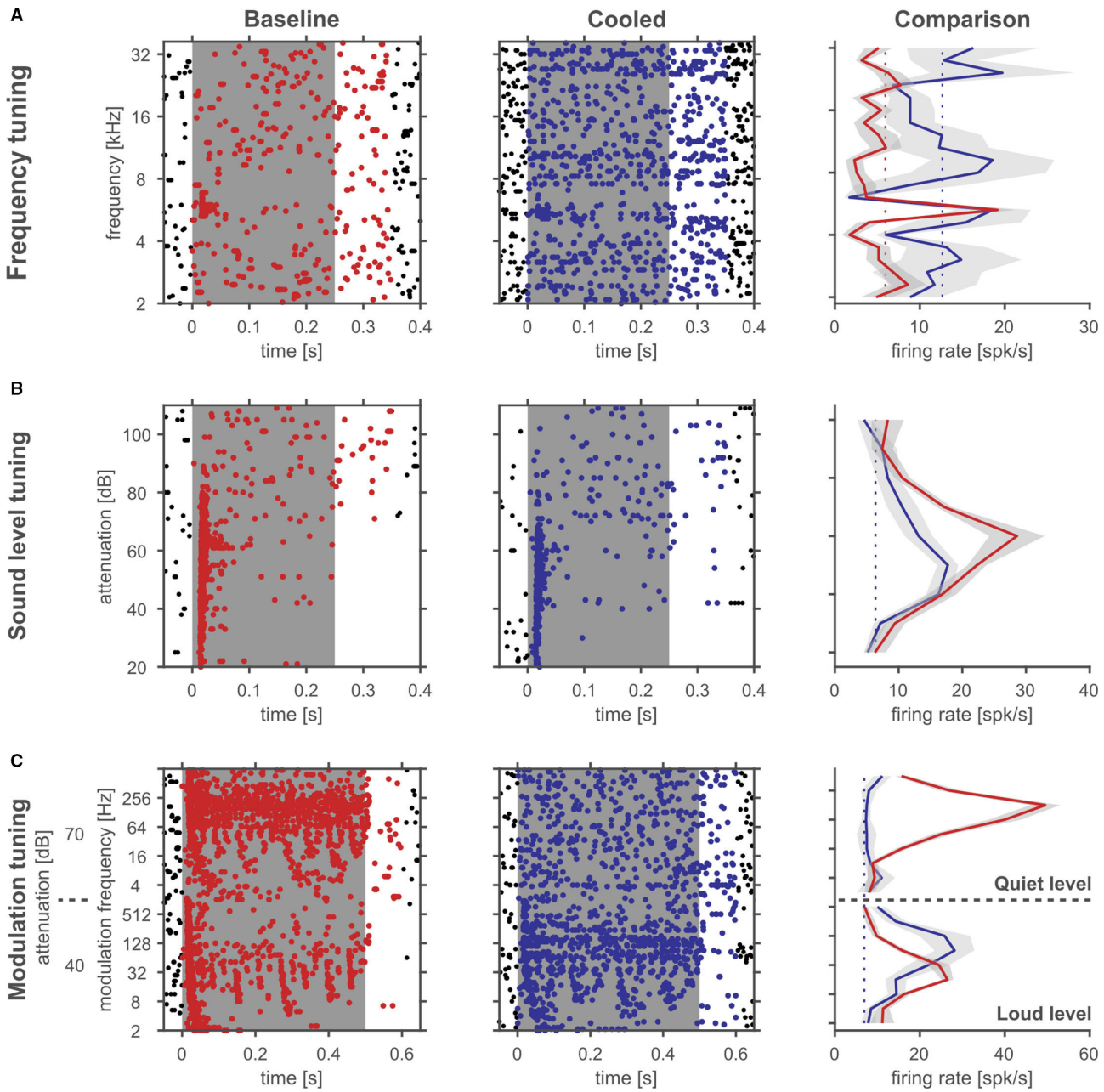

FIGURE 10 | Cortical cooling can lead to large changes in rate level functions and temporal response patterns despite stable frequency tuning. Rasterplots of an example single unit in the auditory thalamus at baseline (left panels) and cooling condition (right panels). The gray shaded area corresponds to the stimulus duration. Stimulus related firing was evaluated based on a time window which included the stimulus duration plus 50 ms. Spikes that contributed to this stimulus related firing were plotted in red during baseline and blue during cooling. For a quantitative comparison average stimulus related firing rates were plotted on the right (gray shadows correspond to the standard error of the mean, red and blue solid lines indicate firing rate during baseline and cooling, respectively, while dashed lines indicate the spontaneous firing rate). **(A)** Responses to pure tones of various frequencies at a fixed sound level were used to determine the neurons' frequency tuning and best frequency (4.7 kHz). **(B)** At the neurons' best frequency pure tones with different sound levels revealed response threshold and a non-monotonic sound level tuning with a best level of 35 dB SPL or 45 dB SPL and a threshold of 25 dB SPL or 35 dB SPL during baseline and in the cooled condition, respectively, and in response to amplitude modulated tones of systematically varied modulation frequency with the best frequency as the carrier frequency presented at threshold and 30 dB above **(C)** during baseline and cooled conditions.

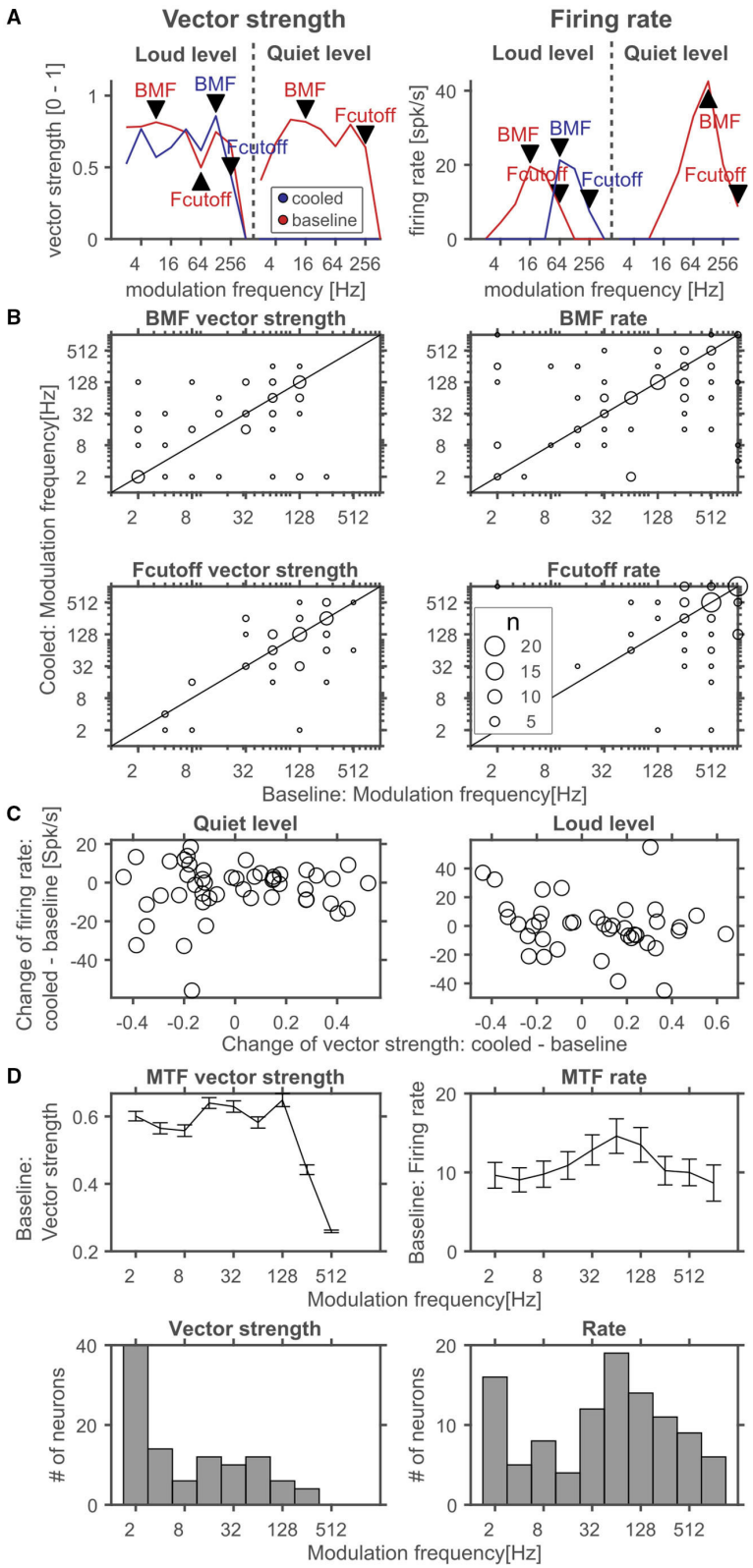

FIGURE 11 | Quantitative analysis of corticofugal influences on thalamic modulation tuning. **(A)** Schematic representation of analyzed parameters in comparison of cooled and baseline conditions. Modulation transfer functions (MTF) based on the vector strength (left panel) during baseline (red) and cooling (blue) were used to

(Continued)

FIGURE 11 | identify the best modulation frequency (BMF vector strength) defined as the modulation frequency leading to the highest significant vector strength and a significant response based on the firing rate. The highest frequency leading to a significant vector strength and significant response was taken as the synchronization boundary (Fcutoff vector strength). Similarly, MTFs based on the stimulus related firing rate (right panel) were analyzed to reveal the best modulation frequency (BMF rate) defined as the modulation frequency leading to the highest significant firing rate. The highest modulation frequency leading to a significant response was taken as the rate boundary (Fcutoff rate). Note, that the MTFs shown in **(A)** correspond to the exemplar unit illustrated in **Figure 10**. The best modulation frequencies and modulation frequency boundaries during baseline and cooling were identified by labeled arrowheads (red – baseline, blue – cooled). **(B)** Scatter plots of best modulation frequencies (BMF) as well as synchronization and rate boundaries (Fcutoff) contrasting cooling and baseline conditions. The sizes of the circles correspond to the number of observations (common legend in the lower right panel). BMFs and Fcutoffs of thalamic neurons were found to change toward lower or higher modulation frequencies with cortical cooling based on vector strength or firing rate. **(C)** Changes in vector strength could in principle be linked to changes in firing rate. However, neither close to the threshold of a neuron (quiet level) nor ca. 30 dB above (loud level) significant correlations were observed. **(D)** During baseline, average vector strength based MTFs calculated from the population of neurons were flat up to 128 Hz modulation and rolled off steeply at higher modulation frequencies (top left panel). Despite this, strongest changes in vector strength observed during cooling occurred at low modulation frequencies for a large number of neurons as indicated by the histogram of largest changes in vector strength as a function of modulation frequency (bottom left panel). Mean MTFs based on the firing rate (top right panel) exhibited a slight peak at 64 Hz modulation and rolled of softly toward slower and faster modulation frequencies. The histogram of neuron counts that had their largest change in firing rate between baseline and cooling also had a peak at 64 Hz modulation and rolled off toward lower and higher modulation frequencies (bottom right panel).

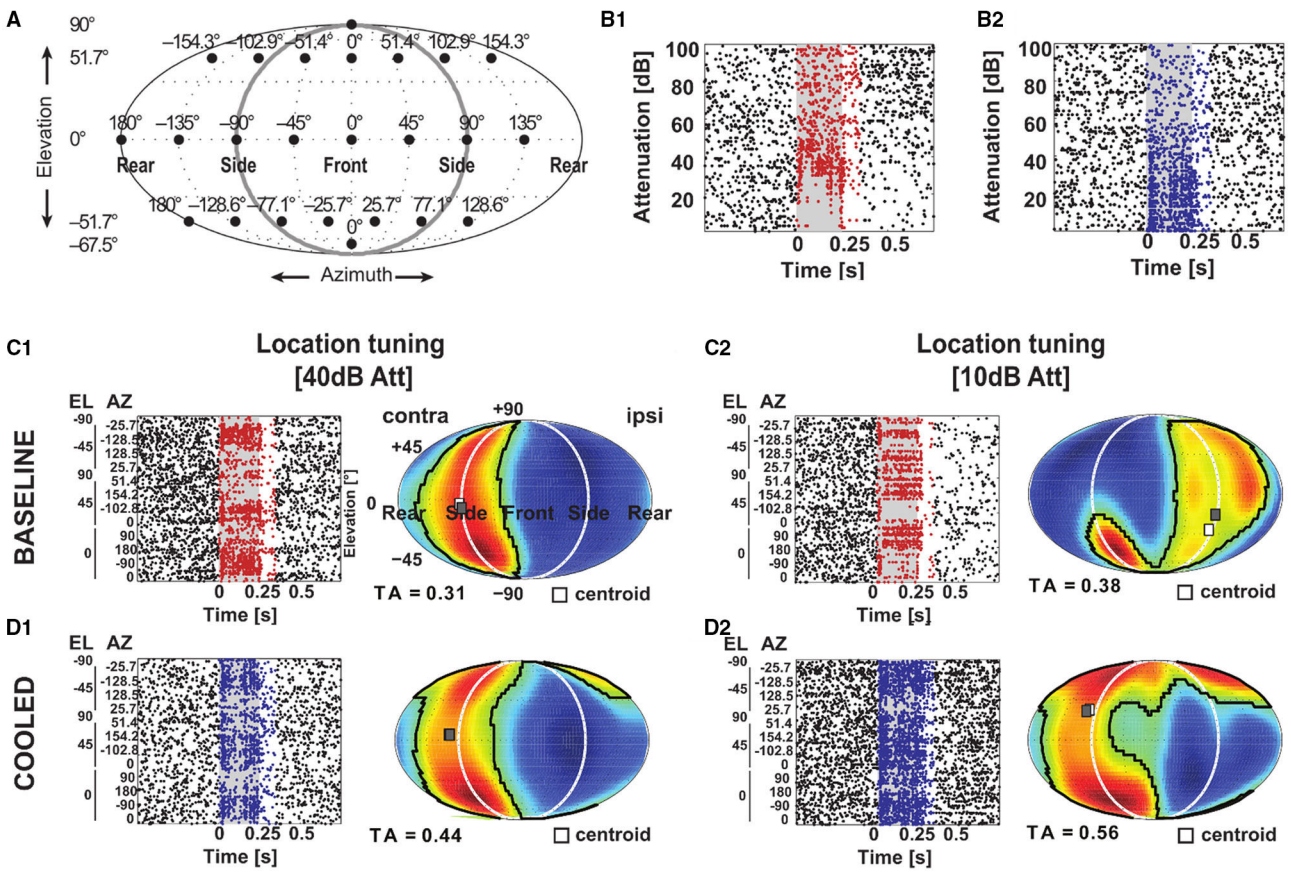

FIGURE 12 | Corticofugal feedback shapes tuning to spatial location in the MGB. **(A)** Schematic of speaker layout to investigate tuning to spatial location. A total of 24 speakers (filled black circles) were positioned at the azimuth and elevation indicated above the speaker and on the left, respectively. The setup was the same as in Remington and Wang (2019). For the rasterplots in **(B–D)** the gray shaded area corresponds to the stimulus duration. Stimulus related firing was evaluated based on a time window which included the stimulus duration plus 50 ms. Spikes that contributed to this stimulus related firing were plotted in red during baseline and blue during cooling. **(B)** Responses to different sound levels of an exemplar neuron under baseline **(B1)** and cooled **(B2)** conditions obtained from the best speaker location identified during baseline 10 dB above threshold. During cooling the sound level tuning turned from non-monotonic to monotonic. **(C,D)** Based on the stimulus related firing rate, a graphical representation of the spatial receptive field was created by projecting the responses at the various speaker locations onto an array of virtual locations using a weighted sum of responses at all speaker locations. These responses to virtual locations expressed in a contralateral-to-ipsilateral axis were plotted as a heatmap using a Fournier projection. Here, warm colors correspond to higher and cold colors to lower firing rates, respectively. The area of responses at least 50% of the mid-point between the maximum and minimum firing rate was taken as the tuning area (TA). The centroid (white square) describes the center of mass of the spatial receptive field defined by the firing rate. During baseline condition, the neuron illustrated in **(B)** mostly responded to speaker locations contralateral to the recorded hemisphere **(C1)** at 10 dB above threshold (see **B1**) but had an ipsilateral receptive field at 30 dB above threshold **(C2)**. **(D)** During cooling, the receptive field remained contralateral 10 dB above threshold **(D1)** but shifted toward the contralateral side 30 dB above threshold **(D2)**.

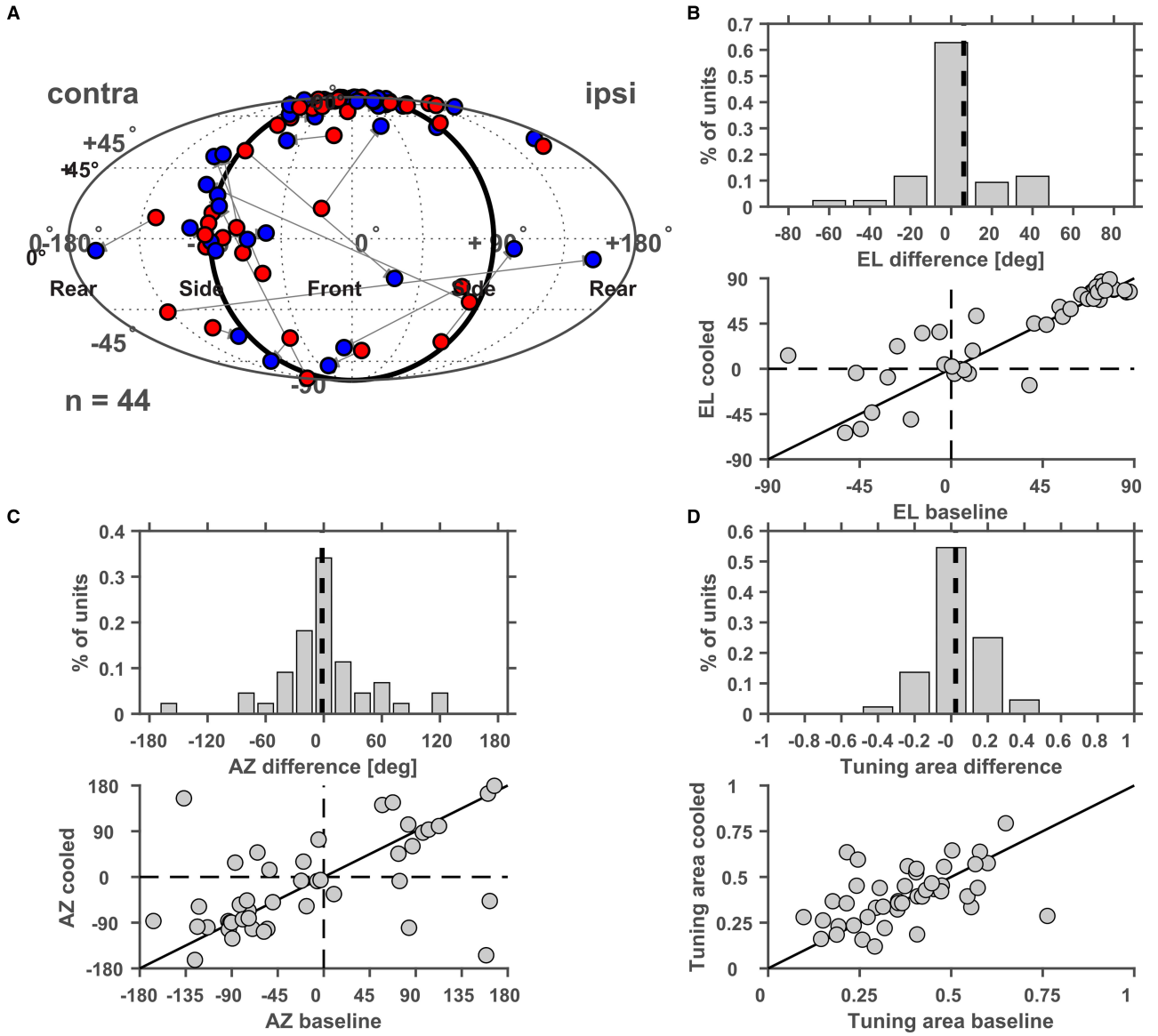

FIGURE 13 | (A) Changes of the centroid of the spatial receptive field of thalamic neurons during cortical cooling. The centroid determined under baseline conditions was plotted in red and the centroid under cooled conditions was plotted in blue. The centroids are characterized by their azimuth and elevation and cooling related changes of both parameters were analyzed separately and plotted either as a distribution of changes between cooled and baseline conditions or as a scatter plot of baseline and cooled values. For elevation a decrease or increase was indicated by negative and positive elevation difference values, respectively **(B)**, while azimuth shifts toward the contralateral or ipsilateral side were indicated by negative and positive values, respectively **(C)**. For both parameters the distribution of changes was centered on zero. No significant correlation between azimuth or elevation values recorded during baseline or cooling was observed. **(D)** Changes in the size of the spatial receptive fields as measured by the tuning area were plotted and were again represented either as a distribution (negative values indicate reduced receptive field size under cooled conditions) or as a scatter plot.

conditions were found (Pearson correlation; $Fcutoff_{vector\ strength}$: $n = 59$, Rho $= 0.52$, $p = 2.1e\text{-}5$; $Fcutoff_{rate}$: $n = 82$, Rho $= 0.457$, $p = 1.6e\text{-}5$). Changes in synchronization of responses to amplitude modulations as studied by the vector strength could in principle be due to concomitant changes in firing rate (Goldberg and Brown, 1969). Therefore, we tested whether changes in vector strength were related to changes in firing rate between baseline and cooling separated for AMs close to threshold and 30–40 dB above (**Figure 11C**). No significant correlation was observed. In addition, we studied at which modulation frequencies the largest changes in vector strength or firing rate occurred (**Figure 11D**). Under baseline conditions the averaged modulation transfer function (MTF) calculated for the vector strength was essentially flat until 128 Hz modulation. Despite this, the majority of neurons were found to change strongest at the lowest modulation frequency tested (2 Hz). In contrast, the MTF based on the

neurons, firing rates and the histogram of largest changes closely mimicked each other with a peak of the MTF and histogram at 64 Hz.

Tuning of MGB Neurons to Spatial Locations During Cortical Cooling

Furthermore, we studied cortical influences on processing of spatial location in the MGB. Toward this, neurons were tested with white noise bursts presented from speakers distributed on a sphere of 1 m diameter centered on the animals' head (**Figure 12A**). Under baseline condition the exemplar neuron in **Figure 12** responded in a phasic-tonic manner to noise bursts (**Figure 12B1**) and displayed contralateral (i.e., responded to sounds from locations opposite from the recorded hemisphere) tuning for spatial location close to threshold but ipsilateral (i.e., responded to sounds from locations at the same side as the recorded hemisphere) tuning at 30 dB above threshold (**Figure 12C1**). This ipsilateral shift at higher sound levels was accompanied by a suppression of tonic response components at previously driven locations (**Figure 12C2**). In line with this observation, the rate level response function at the best speaker location was found to be strongly non-monotonic (**Figure 12B1**). During cooling the pattern of tuning changed quite dramatically. While close to threshold contralateral tuning was still observed (**Figure 12D1**), the tuning for spatial location changed from ipsilateral to contralateral at 30 dB above threshold (**Figure 12D2**). In a cooled state some additional responses were also observed: the single unit now also responded to locations ipsilateral and above the median plane (45 degree elevation and 51.4 degree azimuth; **Figures 12D1,D2**). The rate level response also switched its behavior from non-monotonic to monotonic but exhibited a stable response threshold of 40 dB attenuation (**Figure 12B2**). As expected the cooling-induced unmasking of previously unseen responses resulted in the receptive field becoming larger (as indicated by the tuning area [TA], see Materials and Methods; from 0.31 and 0.38 TA at threshold and 30 dB above during baseline to 0.44 and 0.56 TA during cooling). For all single units investigated, the centroid (the geometric center of the receptive field calculated *via* the weighted mean of firing rates) of the spatial receptive field was calculated and compared between baseline and cooling conditions (**Figure 13A**). Although shifts of centroids were observed for a substantial number of units, these shifts were found in random directions (to higher and lower elevations, toward ipsilateral and contralateral azimuths) and did not display a bias toward a particular location, e.g., the contralateral pole. We also split the change in centroid location with respect to elevation (**Figure 13B**) and azimuth (**Figure 13C**). In both cases, the distribution of the difference in elevation or azimuth between baseline and cooling was centered on zero (elevation: mean change $= 6.1^{\circ}$ [upwards]; azimuth: mean change $= -1.6^{\circ}$ [contralateral]), indicating stable tuning for spatial location in the population (Wilcoxon signed rank test, elevation: $n = 44$, Z $= 1.494$, $p = 0.14$; azimuth: $n = 44$, Z $= 0.292$, $p = 0.77$) while individual neurons shifted their location preference. When plotting the azimuth or elevation preference for baseline and cooled conditions, significant correlations between both states were observed (Pearson correlation; elevation: $n = 44$, Rho $= 0.87$, $p =$ 1.5e-14; azimuth: $n = 44$, Rho $= 0.533$, $p = 0.0002$). The distribution of the change in size of the spatial receptive fields as calculated by TA was slightly skewed toward larger TA during cooled conditions (mean change $= 0.024$) also suggesting stable receptive field sizes in the population of neurons (Wilcoxon signed rank test, $n = 44$, $Z = 1.266$, $p = 0.21$). The TA observed during baseline and cooled conditions were significantly correlated (Pearson correlation; $n = 44$, Rho $= 0.50$, $p = 0.0006$).

DISCUSSION

To study the role of corticothalamic feedback on the processing of sounds in the medial geniculate body of awake, non-human primates we developed a small, freely repositionable cooling probe and compared responses to sounds under conditions of normal and reduced cortical temperature. In cortical neurons we observed cooling-induced increases in the width of the extracellularly recorded spike waveform over distances to the cooling probe of several hundred micrometers. Concomitantly, cortical neurons displayed reduced spontaneous as well as stimulus driven firing rates. At the thalamic level, cortical cooling led to increased spontaneous firing and both increased and decreased stimulus driven activity. Also, response tuning to modulation frequencies of amplitude-modulated tones and spatial tuning to sound source location could be altered in a bidirectional fashion by cortical cooling. Specifically, best modulation frequencies of individual MBG neurons could shift to either higher or lower frequencies based on vector strength or firing rate. Spatial tuning could sharpen or widen, elevation preference could shift toward higher or lower elevations and azimuth tuning could move toward ipsilateral or contralateral locations.

Cortical Cooling Effects

When a recorded neuron continued to fire during cortical cooling, changes in spike waveforms associated with an increased width at half height were the most obvious effect on the physiology of individual neurons. Similar effects have been reported *in vitro* (Volgushev et al., 2000a,b) and *in vivo* in the visual cortex of anesthetized cats (Girardin and Martin, 2009). Such widening of spike waveforms was observed at a distance of at least 2 mm underneath the cooling probe, demonstrating that the local temperature was lowered throughout all cortical layers in the auditory cortex (with an estimated thickness of 1.5–2 mm; Aitkin et al., 1986) including the corticofugal output layers 5 and 6 (Llano and Sherman, 2009). The correlation of changes in spike width with distance from the cooling probe allows to disentangle direct (i.e., temperature related) and indirect (i.e., due to changes in network activity) effects of cooling as suggested before (Girardin and Martin, 2009). Interestingly, even when large changes in spike width were observed neuronal activity was not always suppressed but could also be enhanced. While with our data it is not possible to relate those changes to a particular

mechanism, they can be explained by the differential effects of lowering temperature on membrane potential, spike threshold, transmitter release and synaptic transmission (Volgushev et al., 2000a,b, 2004). In these experiments complete cessation of neuronal firing was only observed upon lowering the local temperature to below 10°C. As demonstrated in our experiments and others this is not observed for distances from the cooling probe larger than 1 mm (Lomber et al., 1999; Coomber et al., 2011) even when the dura temperature is lowered to 1–5°C. Therefore, at least in unanesthetized animals, the effect of cooling even on relatively local network activity seems to be more diverse than previously suggested based on experiments in anesthetized preparations (Villa et al., 1991; Lomber et al., 1999; Volgushev et al., 2000b). On average, though, cortical cooling leads to a reduction of activity up to a distance of at least 2 mm. This suggests that the main effect of superficial cooling on corticofugal feedback originating from layers 5 and 6 is a reduction but not a cessation of feedback. This potentially limited reduction of corticothalamic feedback can nonetheless have strong network effects as shown by experiments with moderate cooling in the barrel cortex of rats (Burkhanova et al., 2020).

Effects of Cortical Feedback on Thalamic Processing of Temporally Modulated Sounds

The control of thalamocortical information flow *via* corticofugal feedback (Ibrahim et al., 2021; Saldeitis et al., 2021) can be expected to have strong influence on cortical responses despite small changes to thalamic population activity (Wang et al., 2010; Ibrahim et al., 2021). This can be explained by the convergence of synchronized, weak thalamocortical inputs (Bruno and Sakmann, 2006) in combination with desynchronized thalamic neurons (Wang et al., 2010; Ibrahim et al., 2021) or reduced stimulus locked firing due to switches of thalamic response mode (Whitmire et al., 2021) under altered corticothalamic and/or corticofugal feedback.

Corticofugal feedback arises from layers 5 and 6 with different projection patterns and synaptic strengths (Llano and Sherman, 2009). In the rodent, A1 to MGBv feedback is predominantly of the so-called modulator type (i.e. small synapses) (Bartlett et al., 2000) while non-lemniscal subdivisions receive more driver type projections (large synapses) (Llano and Sherman, 2008). As our experiments did not distinguish between subnuclei of the MGB our work could not disentangle the relative changes within the various subdivisions. Corticothalamic connections outnumber the thalamic inputs and dominate the synaptic background in thalamic neurons and thereby determine the thalamocortical transmission (Wolfart et al., 2005). For example, in mice moderate cooling (16–21°C) eliminates silent states in the somatosensory thalamus (Sheroziya and Timofeev, 2015). Silencing auditory cortex optogenetically leaves the MGB less excitable, with higher reliability and linearity but keeps general tuning stable (Lohse et al., 2020). Therefore, it is expected that not all aspects of thalamic sound processing can be influenced by cortex. In the current study with awake non-human primates we have documented that two important aspects of auditory processing, namely processing of spatial location for orientation to sounds and temporally modulated sounds relevant for example for speech comprehension (Ding et al., 2017), can be modulated by cortical control.

The majority of thalamic neurons respond in a synchronized manner at least to some temporal modulation frequencies (Bartlett and Wang, 2007, 2011). Former work has demonstrated that thalamocortical loops are involved in rhythmic activity (Llinás et al., 2005). Corticothalamic neurons have likewise been shown to affect fast-spiking interneurons in the cortex to directly reset slow rhythmic activity but not by changing activity of thalamic resetter neurons (Guo et al., 2017). Thus, corticothalamic feedback plays a decisive role in oscillatory activity. Therefore, we reasoned that manipulating precisely timed cortical feedback would influence thalamic processing of temporal modulations. Interestingly, while changes in temporal precision of responses were bidirectional, the largest changes were observed for low modulation frequencies in line with the abovementioned literature.

Effects of Cortical Feedback on Thalamic Processing of Spatial Locations

Our data are the first to describe tuning to spatial location in the MGB collected from awake common marmosets. All recordings were performed in the same setting described in an earlier study which investigated the representation of the full spatial field in the auditory cortex (Remington and Wang, 2019). While a detailed description of spatial receptive field (SRF) properties is outside of the scope of the current study, some comparisons seem noteworthy: in general thalamic SRFs were mostly larger than their counterparts in the auditory cortex with tuning areas of 0.36 ± 0.15 (mean ± STD) in the MGB and tuning areas of 0.14, 0.24, and 0.34 in field CM/CL, A1 and R/RT, respectively (Remington and Wang, 2019). Similar to observations in the auditory cortex the SRF of thalamic neurons could increase or shrink with increasing sound level. At the population level however, spatial selectivity was found to be level tolerant both for the auditory cortex (Remington and Wang, 2019) and the MGB.

In our experiments, we have further documented changes in tuning to spatial location in the MGB during altered cortical feedback. Processing of spatial location is based on three cues: interaural level and time differences as well as head related directional filtering (Grothe et al., 2010). While level and time differences are processed in brainstem nuclei, the inferior colliculus has been argued as being the first stage in which all three cues are combined (Slee and Young, 2011). Further, corticofugal modulation of sound processing or input selection of relevant stimuli or sound features is not only possible in the auditory thalamus (Guo et al., 2017) but has been shown throughout the auditory pathway (Malmierca et al., 2015; Suga, 2020; Asilador and Llano, 2021) including the cochlear nucleus (Luo et al., 2008) and the inferior colliculus (Nakamoto et al., 2008; Straka et al., 2015; Qi et al., 2020). Cooling of auditory cortex shifts the sensitivity of inferior colliculus neurons to interaural level cues (Nakamoto et al., 2008). However, corticothalamic and corticocollicular feedback arises from layer

6 or 5, respectively (Malmierca et al., 2015) and our data suggest that both cortical output layers are affected by cortical cooling. Therefore, it would be interesting to investigate the relative contributions of corticothalamic feedback vs. the possibly altered colliculothalamic input due to corticocollicular feedback.

Limitations of the Current Study

In our study we have used cooling to manipulate corticofugal feedback. As a technique cooling has its advantages in being flexible and quickly reversible. However, disadvantages include the relatively large affected region which is difficult to control and the lack of temporal specificity which might play a role especially during processing of temporally dynamic stimuli. The former point essentially precluded to investigate the relationship between the tonotopic position in AI being cooled and the tonotopic position in MGB being affected (see e.g., Suga, 2020) while the latter prevented an analysis of a potential time dependence of corticofugal feedback on thalamic processing.

Although the cortico-thalamic connection contains both excitatory (direct) as well as inhibitory influences (indirect *via* the thalamic reticular nucleus) it cannot be ruled out that the bidirectionality of changes we observed is due to the spatially relatively broad and cell type unspecific manipulation invoked *via* cortical cooling. Even the same corticofugal connection can have various effects on the target region based on how it is activated (Vila et al., 2019). Ideally, an optogenetic experiment with anterograde labeling of cortico-thalamic neurons and optical stimulation in the thalamus would be performed (Fenno et al., 2011; Yizhar et al., 2011; Vila et al., 2019; Williamson and Polley, 2019). If successful in primates, optogenetic experiments could selectively target layer 5 or layer 6 projection neurons to investigate their separate roles for adjusting thalamic processing.

Further experiments should delineate the respective role of subdivisions of the MGB as well as the role various circuit elements of the cortico-thalamo-cortical, cortico-colliculo-thalamo-cortical and various other corticofugal feedback loops (Winer, 2005; León et al., 2012; Saldaña, 2015; Lohse et al., 2021), e.g., the thalamic reticular nucleus, the inferior colliculus or even lower brainstem centers play in adjusting thalamic processing in awake primates. Toward this end, future studies should include many more neurons, confirm their anatomical locations and expand observations to the thalamic reticular nucleus as well as the shell and core of the inferior colliculus.

Future Directions

One function of corticofugal feedback might be to adjust thalamic processing to focus on relevant stimulus features in a given situation-dependent context (Guo et al., 2017). This idea is further supported by findings describing the activation of corticothalamic projection neurons during movement preparation (Clayton et al., 2021). In light of the available literature, our main finding of bidirectional changes for many parameters we investigated, suggests that the thalamus does act like a stimulus filter that can be adjusted according to behavioral needs. Future experiments should study thalamic processing of complex sounds during behavioral tasks and under conditions of manipulated corticofugal feedback in primates to investigate the flexibility of corticofugal influences.

DATA AVAILABILITY STATEMENT

The raw data supporting the conclusions of this article will be made available by the authors, without undue reservation.

ETHICS STATEMENT

The animal study was reviewed and approved by Institutional Animal Care and Use Committee of the Johns Hopkins University.

AUTHOR CONTRIBUTIONS

MJ, FO, and XW contributed to conception of the study, discussed, and interpreted the data. MJ and XW designed the study. MJ performed all experiments, data analysis, and wrote the first draft of the manuscript. FO and XW wrote sections of the manuscript. All authors contributed to manuscript revision, read, and approved the submitted version.

FUNDING

This work was supported by the National Institutes of Health grants DC003180 and DC005808 (XW) and a grant from the Deutsche Forschungsgemeinschaft (DFG, SFB-TRR 31, TP A03) to FO. The funders had no role in study design, data collection and analysis, decision to publish, or preparation of the manuscript.

ACKNOWLEDGMENTS

We thank J. Estes and N. Sotuyo for assistance with animal care.

REFERENCES

Aitkin, L. M., Merzenich, M. M., and Irvine, D. R. F. (1986). Frequency representation in auditory cortex of the common marmoset (Callithrix jacchus jacchus). *J. Comp. Neurol.* 252, 175–185. doi: 10.1002/cne.902520204

Alitto, H. J., and Usrey, W. M. (2003). Corticothalamic feedback and sensory processing. *Curr. Opin. Neurobiol.* 13, 440–445. doi: 10.1016/S0959-4388(03)00096-5

Anderson, L. A., and Malmierca, M. S. (2012). The effect of auditory cortex deactivation on stimulus-specific adaptation in the inferior colliculus of the rat. *Eur. J. Neurosci.* 37, 52–62. doi: 10.1111/ejn.12018

Asilador, A., and Llano, D. A. (2021). Top-down inference in the auditory system: potential roles for corticofugal projections. *Front. Neural Circuits* 14:615259. doi: 10.3389/fncir.2020.615259

Bartlett, E. L., Stark, J. M., Guillery, R. W., and Smith, P. H. (2000). Comparison of the fine structure of cortical and collicular terminals in the rat medial geniculate body. *Neuroscience* 100, 811–828. doi: 10.1016/S0306-4522(00)00340-7

Bartlett, E. L., and Wang, X. (2007). Neural representations of temporally modulated signals in the auditory thalamus of awake primates. *J. Neurophysiol.* 97, 1005–1017. doi: 10.1152/jn.00593.2006

Bartlett, E. L., and Wang, X. (2011). Correlation of neural response properties with auditory thalamus subdivisions in the awake marmoset. *J. Neurophysiol.* 105, 2647–2667. doi: 10.1152/jn.00238.2010

Bendor, D., and Wang, X. (2005). The neuronal representation of pitch in primate auditory cortex. *Nature* 436, 1161–1165. doi: 10.1038/nature 03867

Bruno, R. M., and Sakmann, B. (2006). Cortex is driven by weak but synchronously active thalamocortical synapses. *Science* 312, 1622–1627. doi: 10.1126/science.1124593

Burkhanova, G., Chernova, K., Khazipov, R., and Sheroziya, M. (2020). Effects of cortical cooling on activity across layers of the rat barrel cortex. *Front. Syst. Neurosci.* 14:52. doi: 10.3389/fnsys.2020.00052

Cappe, C., Morel, A., Barone, P., and Rouiller, E. M. (2009). The thalamocortical projection systems in primate: an anatomical support for multisensory and sensorimotor interplay. *Cereb. Cortex* 19, 2025–2037. doi: 10.1093/cercor/bhn228

Clayton, K. K., Williamson, R. S., Hancock, K. E., Tasaka, G., Mizrahi, A., Hackett, T. A., et al. (2021). Auditory corticothalamic neurons are recruited by motor preparatory inputs. *Curr. Biol.* 31, 310–321.e5. doi: 10.1016/j.cub.2020.10.027

Cooke, D. F., Goldring, A. B., Yamayoshi, I., Tsourkas, P., Recanzone, G. H., Tiriac, A., et al. (2012). Fabrication of an inexpensive, implantable cooling device for reversible brain deactivation in animals ranging from rodents to primates. *J. Neurophysiol.* 107, 3543–3558. doi: 10.1152/jn.01101.2011

Coomber, B., Edwards, D., Jones, S. J., Shackleton, T. M., Goldschmidt, J., Wallace, M. N., et al. (2011). Cortical inactivation by cooling in small animals. *Front. Syst. Neurosci.* 5:53. doi: 10.3389/fnsys.2011.00053

Crandall, S. R., Cruikshank, S. J., and Connors, B. W. (2015). A corticothalamic switch: controlling the thalamus with dynamic synapses. *Neuron* 86, 768–782. doi: 10.1016/j.neuron.2015.03.040

Cruikshank, S. J., Urabe, H., Nurmikko, A. V., and Connors, B. W. (2010). Pathway-specific feedforward circuits between thalamus and neocortex revealed by selective optical stimulation of axons. *Neuron* 65, 230–245. doi: 10.1016/j.neuron.2009.12.025

De La Mothe, L. A., Blumell, S., Kajikawa, Y., and Hackett, T. A. (2006). Thalamic connections of the auditory cortex in marmoset monkeys: Core and medial belt regions. *J. Comp. Neurol.* 496, 72–96. doi: 10.1002/cne.20924

de la Mothe, L. A., Blumell, S., Kajikawa, Y., and Hackett, T. A. (2012). Thalamic connections of auditory cortex in marmoset monkeys: lateral belt and parabelt regions. *Anat. Rec. Adv. Integr. Anat. Evol. Biol.* 295, 822–836. doi: 10.1002/ar.22454

Deschênes, M., Veinante, P., and Zhang, Z.-W. (1998). The organization of corticothalamic projections: reciprocity versus parity. *Brain Res. Rev.* 28, 286–308. doi: 10.1016/S0165-0173(98)00017-4

Ding, N., Patel, A. D., Chen, L., Butler, H., Luo, C., and Poeppel, D. (2017). Temporal modulations in speech and music. *Neurosci. Biobehav. Rev.* 81, 181–187. doi: 10.1016/j.neubiorev.2017.02.011

Dong, N., Berlinguer-Palmini, R., Soltan, A., Ponon, N., O'Neil, A., Travelyan, A., et al. (2018). Opto-electro-thermal optimization of photonic probes for optogenetic neural stimulation. *J. Biophotonics* 11:e201700358. doi: 10.1002/jbio.201700358

Fenno, L., Yizhar, O., and Deisseroth, K. (2011). The development and application of optogenetics. *Annu. Rev. Neurosci.* 34, 389–412. doi: 10.1146/annurev-neuro-061010-113817

Galvan, A., Hu, X., Smith, Y., and Wichmann, T. (2016). Effects of optogenetic activation of corticothalamic terminals in the motor thalamus of awake monkeys. *J. Neurosci.* 36, 3519–3530. doi: 10.1523/JNEUROSCI.4363-15.2016

Gao, L., and Wang, X. (2020). Intracellular neuronal recording in awake nonhuman primates. *Nat. Protoc.* 15, 3615–3631. doi: 10.1038/s41596-020-0388-3

Girardin, C. C., and Martin, K. A. C. (2009). Cooling in cat visual cortex: stability of orientation selectivity despite changes in responsiveness and spike width. *Neuroscience* 164, 777–787. doi: 10.1016/j.neuroscience.2009.07.064

Gold, C., Henze, D. A., Koch, C., and Buzsáki, G. (2006). On the origin of the extracellular action potential waveform: A modeling study. *J. Neurophysiol.* 95, 3113–3128. doi: 10.1152/jn.00979.2005

Goldberg, J. M., and Brown, P. B. (1969). Response of binaural neurons of dog superior olivary complex to dichotic tonal stimuli: some physiological mechanisms of sound localization. *J. Neurophysiol.* 32, 613–636. doi: 10.1152/jn.1969.32.4.613

Grothe, B., Pecka, M., and McAlpine, D. (2010). Mechanisms of sound localization in mammals. *Physiol. Rev.* 90, 983–1012. doi: 10.1152/physrev.00026.2009

Guo, W., Clause, A. R., Barth-Maron, A., and Polley, D. B. (2017). A corticothalamic circuit for dynamic switching between feature detection and discrimination. *Neuron* 95, 180–194.e5. doi: 10.1016/j.neuron.2017.05.019

Happel, M. F. K., Deliano, M., Handschuh, J., and Ohl, F. W. (2014). Dopamine-modulated recurrent corticoefferent feedback in primary sensory cortex promotes detection of behaviorally relevant stimuli. *J. Neurosci.* 34, 1234–1247. doi: 10.1523/JNEUROSCI.1990-13.2014

He, J. (2003). Corticofugal modulation of the auditory thalamus. *Exp. Brain Res.* 153, 579–590. doi: 10.1007/s00221-003-1680-5

Ibrahim, B. A., Murphy, C. A., Yudintsev, G., Shinagawa, Y., Banks, M. I., and Llano, D. A. (2021). Corticothalamic gating of population auditory thalamocortical transmission in mouse. *Elife* 10:e56645. doi: 10.7554/eLife.56645.sa2

Jüttner, J., Szabo, A., Gross-Scherf, B., Morikawa, R. K., Rompani, S. B., Hantz, P., et al. (2019). Targeting neuronal and glial cell types with synthetic promoter AAVs in mice, non-human primates and humans. *Nat. Neurosci.* 22, 1345–1356. doi: 10.1038/s41593-019-0431-2

León, A., Elgueda, D., Silva, M. A., Hamamé, C. M., and Delano, P. H. (2012). Auditory cortex basal activity modulates cochlear responses in chinchillas. *PLoS ONE* 7:e36203. doi: 10.1371/journal.pone.0036203

Llano, D. A., and Sherman, S. M. (2008). Evidence for nonreciprocal organization of the mouse auditory thalamocortical-corticothalamic projection systems. *J. Comp. Neurol.* 507, 1209–1227. doi: 10.1002/cne.21602

Llano, D. A., and Sherman, S. M. (2009). Differences in intrinsic properties and local network connectivity of identified layer 5 and layer 6 adult mouse auditory corticothalamic neurons support a dual corticothalamic projection hypothesis. *Cereb. Cortex* 19, 2810–2826. doi: 10.1093/cercor/bhp050

Llinás, R., Urbano, F. J., Leznik, E., Ramírez, R. R., and van Marle, H. J. F. (2005). Rhythmic and dysrhythmic thalamocortical dynamics: GABA systems and the edge effect. *Trends Neurosci.* 28, 325–333. doi: 10.1016/j.tins.2005.04.006

Lohse, M., Bajo, V. M., King, A. J., and Willmore, B. D. B. (2020). Neural circuits underlying auditory contrast gain control and their perceptual implications. *Nat. Commun.* 11:324. doi: 10.1038/s41467-019-14163-5

Lohse, M., Dahmen, J. C., Bajo, V. M., and King, A. J. (2021). Subcortical circuits mediate communication between primary sensory cortical areas in mice. *Nat. Commun.* 12:3916. doi: 10.1038/s41467-021-24200-x

Lomber, S. G., Payne, B. R., and Horel, J. A. (1999). The cryoloop: An adaptable reversible cooling deactivation method for behavioral or electrophysiological assessment of neural function. *J. Neurosci. Methods* 86, 179–194. doi: 10.1016/S0165-0270(98)00165-4

Lu, T., Liang, L., and Wang, X. (2001). Neural representations of temporally asymmetric stimuli in the auditory cortex of awake primates. *J. Neurophysiol.* 85, 2364–2380. doi: 10.1152/jn.2001.85.6.2364

Luo, F., Wang, Q., Kashani, A., and Yan, J. (2008). Corticofugal modulation of initial sound processing in the brain. *J. Neurosci.* 28, 11615–11621. doi: 10.1523/JNEUROSCI.3972-08.2008

Malhotra, S., Hall, A. J., and Lomber, S. G. (2004). Cortical control of sound localization in the cat: unilateral cooling deactivation of 19 cerebral areas. *J. Neurophysiol.* 92, 1625–1643. doi: 10.1152/jn.01205.2003

Malmierca, M. S., Anderson, L. A., and Antunes, F. M. (2015). The cortical modulation of stimulus-specific adaptation in the auditory midbrain and thalamus: a potential neuronal correlate for predictive coding. *Front. Syst. Neurosci.* 9:19. doi: 10.3389/fnsys.2015.00019

Miyashita, T., Shao, Y. R., Chung, J., Pourzia, O., and Feldman, D. E. (2013). Long-term channelrhodopsin-2 (ChR2) expression can induce abnormal axonal morphology and targeting in cerebral cortex. *Front. Neural Circuits* 7:8. doi: 10.3389/fncir.2013.00008

Mukherjee, A., Bajwa, N., Lam, N. H., Porrero, C., Clasca, F., and Halassa, M. M. (2020). Variation of connectivity across exemplar sensory and associative thalamocortical loops in the mouse. *Elife* 9:e62554. doi: 10.7554/eLife.62554.sa2

Nakamoto, K. T., Jones, S. J., and Palmer, A. R. (2008). Descending projections from auditory cortex modulate sensitivity in the midbrain to cues for spatial position. *J. Neurophysiol.* 99, 2347–2356. doi: 10.1152/jn.01326.2007

Payne, B. R., and Lomber, S. G. (1999). A method to assess the functional impact of cerebral connections on target populations of neurons. *J. Neurosci. Methods* 86, 195–208. doi: 10.1016/S0165-0270(98)00166-6

Peel, T. R., Dash, S., Lomber, S. G., and Corneil, B. D. (2020). Frontal eye field inactivation alters the readout of superior colliculus activity for saccade generation in a task-dependent manner. *J. Comput. Neurosci.* 49, 229–249. doi: 10.1101/646604

Qi, J., Zhang, Z., He, N., Liu, X., Zhang, C., and Yan, J. (2020). Cortical stimulation induces excitatory postsynaptic potentials of inferior colliculus neurons in a frequency-specific manner. *Front. Neural Circuits* 14:591986. doi: 10.3389/fncir.2020.591986

Remington, E. D., and Wang, X. (2019). Neural representations of the full spatial field in auditory cortex of awake marmoset (Callithrix jacchus). *Cereb. Cortex* 29, 1199–1216. doi: 10.1093/cercor/bhy025

Rouiller, E. M., and Durif, C. (2004). The dual pattern of corticothalamic projection of the primary auditory cortex in macaque monkey. *Neurosci. Lett.* 358, 49–52. doi: 10.1016/j.neulet.2004.01.008

Sadagopan, S., and Wang, X. (2008). Level invariant representation of sounds by populations of neurons in primary auditory cortex. *J. Neurosci.* 28, 3415–3426. doi: 10.1523/JNEUROSCI.2743-07.2008

Saldaña, E. (2015). All the way from the cortex: a review of auditory corticosubcollicular pathways. *Cerebellum* 14, 584–596. doi: 10.1007/s12311-015-0694-4

Saldeitis, K., Happel, M. F. K., Ohl, F. W., Scheich, H., and Budinger, E. (2014). Anatomy of the auditory thalamocortical system in the mongolian gerbil: Nuclear origins and cortical field-, layer-, and frequency-specificities: Auditory thalamocortical system in gerbils. *J. Comp. Neurol.* 522, 2397–2430. doi: 10.1002/cne.23540

Saldeitis, K., Jeschke, M., Budinger, E., Ohl, F. W., and Happel, M. F. K. (2021). Laser-induced apoptosis of corticothalamic neurons in layer VI of auditory cortex impact on cortical frequency processing. *Front. Neural Circuits* 15:659280. doi: 10.3389/fncir.2021.659280

Sherman, S. M., and Guillery, R. (2006). *Exploring the Thalamus and Its Role in Cortical Function*. 2. ed. Cambridge, MA: MIT Press.

Sheroziya, M., and Timofeev, I. (2015). Moderate cortical cooling eliminates thalamocortical silent states during slow oscillation. *J. Neurosci.* 35, 13006–13019. doi: 10.1523/JNEUROSCI.1359-15.2015

Slee, S. J., and Young, E. D. (2011). Information conveyed by inferior colliculus neurons about stimuli with aligned and misaligned sound localization cues. *J. Neurophysiol.* 106, 974–985. doi: 10.1152/jn.00384.2011

Spinks, R. L., Baker, S. N., Jackson, A., Khaw, P. T., and Lemon, R. N. (2003). Problem of dural scarring in recording from awake, behaving monkeys: a solution using 5-fluorouracil. *J. Neurophysiol.* 90, 1324–1332. doi: 10.1152/jn.00169.2003

Straka, M. M., Hughes, R., Lee, P., and Lim, H. H. (2015). Descending and tonotopic projection patterns from the auditory cortex to the inferior colliculus. *Neuroscience* 300, 325–337. doi: 10.1016/j.neuroscience.2015.05.032

Suga, N. (2020). Plasticity of the adult auditory system based on corticocortical and corticofugal modulations. *Neurosci. Biobehav. Rev.* 113, 461–478. doi: 10.1016/j.neubiorev.2020.03.021

Suzuki, T. W., Inoue, K.-I., Takada, M., and Tanaka, M. (2021). Effects of optogenetic suppression of cortical input on primate thalamic neuronal activity during goal-directed behavior. *eneuro* 8:ENEURO.0511-20.2021. doi: 10.1523/ENEURO.0511-20.2021

Takei, T., Lomber, S. G., Cook, D. J., and Scott, S. H. (2021). Transient deactivation of dorsal premotor cortex or parietal area 5 impairs feedback control of the limb in macaques. *Curr. Biol.* 31, 1476–1487.e5. doi: 10.1016/j.cub.2021.01.049

Taylor, J. A., Hasegawa, M., Benoit, C. M., Freire, J. A., Theodore, M., Ganea, D. A., et al. (2021). Single cell plasticity and population coding stability in auditory thalamus upon associative learning. *Nat. Commun.* 12:2438. doi: 10.1038/s41467-021-22421-8

Usrey, W. M., and Sherman, S. M. (2019). Corticofugal circuits: Communication lines from the cortex to the rest of the brain. *J. Comp. Neurol.* 527, 640–650. doi: 10.1002/cne.24423

Vila, C.-H., Williamson, R. S., Hancock, K. E., and Polley, D. B. (2019). Optimizing optogenetic stimulation protocols in auditory corticofugal neurons based on closed-loop spike feedback. *J. Neural Eng.* 16:066023. doi: 10.1088/1741-2552/ab39cf

Villa, A. E. P., Rouiller, E. M., Simm, G. M., Zurita, P., De Ribaupierre, Y., and De Ribaupierre, F. (1991). Corticofugal modulation of the information processing in the auditory thalamus of the cat. *Exp. Brain Res.* 86, 506–517. doi: 10.1007/BF00230524

Volgushev, M., Kudryashov, I., Chistiakova, M., Mukovski, M., Niesmann, J., and Eysel, U. T. (2004). Probability of transmitter release at neocortical synapses at different temperatures. *J. Neurophysiol.* 92, 212–220. doi: 10.1152/jn.01166.2003

Volgushev, M., Vidyasagar, T. R., Chistiakova, M., and Eysel, U. T. (2000a). Synaptic transmission in the neocortex during reversible cooling. *Neuroscience* 98, 9–22. doi: 10.1016/S0306-4522(00)00109-3

Volgushev, M., Vidyasagar, T. R., Chistiakova, M., Yousef, T., and Eysel, U. T. (2000b). Membrane properties and spike generation in rat visual cortical cells during reversible cooling. *J Physiol* 522, 59–76. doi: 10.1111/j.1469-7793.2000.0059m.x

Wang, Q., Webber, R. M., and Stanley, G. B. (2010). Thalamic synchrony and the adaptive gating of information flow to cortex. *Nat. Neurosci.* 13, 1534–1541. doi: 10.1038/nn.2670

Whitmire, C. J., Liew, Y. J., and Stanley, G. B. (2021). Thalamic state influences timing precision in the thalamocortical circuit. *J. Neurophysiol.* 125, 1833–1850. doi: 10.1152/jn.00261.2020

Williamson, R. S., and Polley, D. B. (2019). Parallel pathways for sound processing and functional connectivity among layer 5 and 6 auditory corticofugal neurons. *Elife* 8:e42974. doi: 10.7554/eLife.42974.023

Winer, J. A. (2005). Decoding the auditory corticofugal systems. *Hear. Res.* 207, 1–9. doi: 10.1016/j.heares.2005.06.007

Winer, J. A., and Larue, D. T. (1987). Patterns of reciprocity in auditory thalamocortical and corticothalamic connections: Study with horseradish peroxidase and autoradiographic methods in the rat medial geniculate body. *J. Comp. Neurol.* 257, 282–315. doi: 10.1002/cne.902570212

Wolfart, J., Debay, D., Le Masson, G., Destexhe, A., and Bal, T. (2005). Synaptic background activity controls spike transfer from thalamus to cortex. *Nat. Neurosci.* 8, 1760–1767. doi: 10.1038/nn1591

Wood, K. C., Town, S. M., Atilgan, H., Jones, G. P., and Bizley, J. K. (2017). Acute inactivation of primary auditory cortex causes a sound localisation deficit in ferrets. *PLoS ONE* 12:e0170264. doi: 10.1371/journal.pone.0170264

Yizhar, O., Fenno, L. E., Davidson, T. J., Mogri, M., and Deisseroth, K. (2011). Optogenetics in neural systems. *Neuron* 71, 9–34. doi: 10.1016/j.neuron.2011.06.004

Yu, Y. Q., Xiong, Y., Chan, Y. S., and He, J. (2004). Corticofugal gating of auditory information in the thalamus: an *in vivo* intracellular recording study. *J. Neurosci.* 24, 3060–3069. doi: 10.1523/JNEUROSCI.4897-03.2004

Yudintsev, G., Asilador, A., Sons, S., Sekaran, N. V. C., Coppinger, M., Nair, K., et al. (2021). Evidence for layer-specific connectional heterogeneity in the mouse auditory corticocollicular system. *J. Neurosci.* 41, 9906–9918. doi: 10.1523/JNEUROSCI.2624-20.2021

Conflict of Interest: The authors declare that the research was conducted in the absence of any commercial or financial relationships that could be construed as a potential conflict of interest.

Advantages of publishing in Frontiers

OPEN ACCESS
Articles are free to read for greatest visibility and readership

FAST PUBLICATION
Around 90 days from submission to decision

HIGH QUALITY PEER-REVIEW
Rigorous, collaborative, and constructive peer-review

TRANSPARENT PEER-REVIEW
Editors and reviewers acknowledged by name on published articles

Frontiers
Avenue du Tribunal-Fédéral 34
1005 Lausanne | Switzerland

Visit us: www.frontiersin.org
Contact us: frontiersin.org/about/contact

REPRODUCIBILITY OF RESEARCH
Support open data and methods to enhance research reproducibility

DIGITAL PUBLISHING
Articles designed for optimal readership across devices

FOLLOW US
@frontiersin

IMPACT METRICS
Advanced article metrics track visibility across digital media

EXTENSIVE PROMOTION
Marketing and promotion of impactful research

LOOP RESEARCH NETWORK
Our network increases your article's readership